

Electronic Thesis and Dissertation Repository

8-2-2018 10:30 AM

Design, Synthesis, and Oxidation Reactivity of Palladacyclic Complexes Containing N-donor Ligands

Ava Behnia, *The University of Western Ontario*

Supervisor: Richard Puddephatt, *The University of Western Ontario*

Joint Supervisor: Johanna Blacquiere, *The University of Western Ontario*

A thesis submitted in partial fulfillment of the requirements for the Doctor of Philosophy degree in Chemistry

© Ava Behnia 2018

Follow this and additional works at: <https://ir.lib.uwo.ca/etd>

 Part of the [Inorganic Chemistry Commons](#)

Recommended Citation

Behnia, Ava, "Design, Synthesis, and Oxidation Reactivity of Palladacyclic Complexes Containing N-donor Ligands" (2018). *Electronic Thesis and Dissertation Repository*. 5575.
<https://ir.lib.uwo.ca/etd/5575>

This Dissertation/Thesis is brought to you for free and open access by Scholarship@Western. It has been accepted for inclusion in Electronic Thesis and Dissertation Repository by an authorized administrator of Scholarship@Western. For more information, please contact wlsadmin@uwo.ca.

Abstract

This thesis describes the synthesis and reactivity of complexes containing the cycloneophyl-Pd(II) group, PdCH₂CMe₂C₆H₄, in combination with *N*-donor ligands. These compounds contain both alkyl- and arylpalladium bonds and the selectivity of bond cleavage in reactions with oxidants and protic reagents is studied, often involving oxidative addition and reductive elimination reaction sequences.

The diimine ligand in [Pd(CH₂CMe₂C₆H₄)(MesN=CH-CH=NMe₂)] does not support formation of stable palladium(IV) complexes, but reactions with Br₂ or I₂ lead to reductive elimination by C-C bond formation of 1,1-dimethylcyclobutabenzene while the reaction with H₂O₂ gives [Pd(CH₂CMe₂C₆H₄O)(MesN=CH-CH=NMe₂)] by overall selective oxygen atom insertion into the aryl-palladium bond.

Coordination of the ligand 2-C₅H₄NCH=N-2-C₆H₄OH, **3-L1H**, led to protonolysis of the arylpalladium bond to give a neophyl complex [Pd(CH₂CMe₂C₆H₅)(κ³-*N,N',O*-**3-L1**)], which then isomerized to [Pd(2-C₆H₄-*t*-Bu)(κ³-*N,N',O*-**3-L1**)], by a sequence of reactions that includes reversible C-H bond activation. The combination of a Pd(II) precursor with a diimine-phenol ligand and an oxidant (H₂O₂ or O₂) under different conditions has given both a molecular square and a molecular tetrahedron by self-assembly of building blocks comprising Pd(II) centres coordinated to oxidized forms of the ligand.

The complex [Pd(CH₂CMe₂C₆H₄){κ²-*N,N'*-N(CH₂-2-C₅H₄N)₂(CH₂CH₂CH₂OH)}] reacted with aqueous CO₂ and H₂O₂ to give complex [Pd(CO₃){κ³-*N,N',N''*-N(CH₂-2-C₅H₄N)₂(CH₂CH₂CH₂OH)}], and organic products resulting from a unique form of neophyl rearrangement. The complexes [Pd(CH₂CMe₂C₆H₄)(κ²-*N,N'*-**L**)], **L** = RO(CH₂)₃N(CH₂-2-C₅H₄N)₂, R = H or Me, react with Br₂, I₂, O₂ or H₂O₂ to give Pd(IV) complexes which are sufficiently stable to isolate or to detect spectroscopically, but which decompose slowly in solution by reductive elimination.

Keywords

Organometallic chemistry • Pd(II)/Pd(IV) catalysis • Palladium complexes • *N*-donor ligands • C-H activation • Oxidative addition • Reductive elimination • Oxidation chemistry • H/D exchange • Mechanistic studies • NMR spectroscopy • X-ray crystallography • Green oxidant

Co-Authorship Statement

This thesis includes work from four previously published manuscripts in Chapters 2, 3, 4 and 5. Chapter 6 is in preparation and will be submitted shortly.

The article presented in Chapter 2 was co-authored by: A. Behnia, P. D. Boyle, J. M. Blacquiere and R. J. Puddephatt, *Organometallics*, 2016, **35**, 2645–2654. AB performed all of the synthetic and characterization work. RJP performed the DFT calculations. PDB collected and solved the X-ray crystallographic data. The manuscript was prepared by AB and edited by JMB and RJP.

The article presented in Chapter 3 was co-authored by: A. Behnia, M. A. Fard, J. M. Blacquiere and R. J. Puddephatt, *Dalton Trans.*, 2018, **47**, 3538–3548. AB was responsible for all of the synthetic work for the article. X-ray crystallography data were collected and processed by AB, with significant input and assistance from MAF. The computational work was performed by RJP. AB prepared the manuscript, including all data interpretation and analysis, and the document was edited by JMB and RJP.

The article presented in Chapter 4 was co-authored by: A. Behnia, P. D. Boyle, M. A. Fard, J. M. Blacquiere and R. J. Puddephatt, *Dalton Trans.*, 2016, **45**, 19485–19490. AB performed all of the synthetic and characterization work. PDB and MAF collected and solved the X-ray crystallographic data. The manuscript was prepared by AB and edited by JMB and RJP.

The article presented in Chapter 5 was co-authored by: A. Behnia, M. A. Fard, J. M. Blacquiere and R. J. Puddephatt, *Organometallics*, 2017, **36**, 4759–4769. AB performed all of the synthetic and characterization work. X-ray crystallography data were collected and processed by AB, with assistance from MAF. The computational work was performed by RJP. AB prepared the manuscript, including all data interpretation and analysis, and edited by JMB and RJP.

Chapter 6 is co-authored by: A. Behnia, M. A. Fard, J. M. Blacquiere and R. J. Puddephatt. AB performed all of the synthetic and characterization work. X-ray crystallography data were collected and processed by AB, with assistance from MAF. The computational work was

performed by RJP. AB prepared the manuscript, including all data interpretation and analysis, and edited by JMB and RJP. The manuscript is complete and ready to be submitted.

Chapter 7 describes works performed by the author. All the syntheses, characterizations and analysis were performed by the author under the supervision of JMB and RJP.

Acknowledgments

I would like to express my gratitude to my supervisors, Dr. Johanna M. Blacquiere and Dr. Richard J. Puddephatt. I am truly grateful for such an amazing opportunity to be inspired everyday by these two great researchers. Being Johanna's first and Dick's last Ph.D. student is a great example of how lucky I am. They have constantly encouraged and supported me throughout my Ph.D. and without their guidance none of what is presented in this thesis would have been possible.

I would also like to thank my past and present lab mates that I have worked with during the past four years. I would especially like to thank James Stubbs for being my first friend in the lab and also in Canada! I would also like to thank Mahmood Fard for being a great lab-mate who is always ready to answer all of my questions about X-ray crystallography, and also for our collaborations. Many thanks to Richard Hazlehurst, Scott Hendriks, Lizzy Davenport, Kyle Jackman, Devon Chapple, and Benjamin Bridge for all the laughter, support, and fun in the lab.

I would also like to take this opportunity to thank the great research staff at Western University for their assistance throughout my Ph.D. Specifically, I would like to thank Dr. Mathew Willans (NMR), Doug Hairsine (mass spectrometry) Dr. Paul Boyle (X-ray), and Kristina Jurcic (MALDI).

I feel very lucky to have great friends from all over the world that have supported me during my Ph.D. journey. A big thank you to Leily, Parisa, Nazanin, Yasi, Tristan, Ben and Vanessa.

A great deal of gratitude goes to my parents, as they have always supported me and believed in me, as well as my brother, Izad, for encouraging me to apply to Western and helping me in the process.

Lastly, and most importantly, I have to thank my husband, Soheil, for all of his support throughout my Ph.D. I know starting a new life here in Canada and graduate school at the same time were not easy, but I have been so lucky to have you in my life and I couldn't do it without your kind and unconditional love and support.

Table of Contents

Abstract.....	i
Co-Authorship Statement.....	iii
Acknowledgments.....	v
Table of Contents.....	vi
List of Tables.....	xii
List of Figures.....	xiii
List of Charts.....	xix
List of Schemes.....	xx
List of Abbreviations.....	xxvi
List of Complexes.....	xxx
Dedication.....	xxxiv
1 Introduction.....	1
1.1 Palladium in Organometallic Chemistry and Catalysis.....	1
1.2 Common Models for Pd(IV) Stabilization.....	3
1.2.1 <i>N</i> -Donor ligands.....	3
1.2.2 <i>C</i> -Donor, Cycloneophyl-Type Ligands.....	6
1.3 Fundamental Reaction Steps Mediated by Pd(II) or Pd(IV).....	8
1.3.1 Redox Reactions.....	8
1.3.2 Redox Neutral Reactions.....	13
1.4 Pd(IV)-Catalyzed C-H Functionalization.....	18
1.4.1 Iodine(III)-based Oxidants in C-H Bond Activation Reactions.....	18
1.4.2 Halide-based Oxidants in C-H Bond Activation Reactions.....	19
1.4.3 Peroxide-based Oxidants in C-H Bond Activation Reactions.....	22
1.4.4 Green Oxidants in C-H Bond Activation Reactions.....	22

1.5	A Description of the Thesis	27
1.6	References	28
2	Selective Oxygen-Atom Insertion into an Aryl-Palladium Bond	36
2.1	Introduction.....	36
2.2	Result and Discussion.....	40
2.3	Conclusions.....	54
2.4	Experimental.....	55
2.4.1	Reagents and General Procedures.....	55
2.4.2	Synthesis of [Pd ^{II} (CH ₂ CMe ₂ C ₆ H ₄)(MesN=CH-CH=NMe _s)], 2-2	56
2.4.3	Synthesis of [PdBr ₂ (MesN=CH-CH=NMe _s)], 2-3	57
2.4.4	Synthesis of [PdI ₂ (MesN=CH-CH=NMe _s)], 2-4	57
2.4.5	Synthesis of [Pd(MesN=CH-CH=NMe _s)(CH ₂ CMe ₂ C ₆ H ₄ O)], 2-5	57
2.4.6	Reaction of Complex 2-2 with Halogens.....	58
2.4.7	Reaction of Complex 2-5 with Halogens.....	58
2.4.8	Reaction of Complex 2-2 with Excess H ₂ O ₂	59
2.4.9	Reaction of Complex 2-5 with CO.....	59
2.4.10	DFT Calculations.....	60
2.5	References.....	60
3	Mild and Selective Pd-Ar Protonolysis and C-H Activation Promoted by a Ligand Aryloxy Group	64
3.1	Introduction.....	64
3.2	Result and Discussion.....	67
3.2.1	Synthesis and Characterization of Pd-Alkyl (3-1) and Pd-Aryl (3-2) Complexes.....	67
3.2.2	Experimental and Computational Evolution of Protonolysis Selectivity.....	69
3.2.3	Role of the Pendent Phenol in the Formation of 3-1	73
3.2.4	Deuterium Labeling Studies in the Formation of 3-1 and 3-2	74

3.2.5	Isomerization of 3-1 to 3-2 , Solvent Study and Kinetic Experiments	78
3.2.6	Computational Analysis of Pd-Aryl and Pd-Alkyl Protonolysis	81
3.3	Conclusion	83
3.4	Experimental	84
3.4.1	Reagent and General Procedure	84
3.4.2	Synthesis of [Pd(CH ₂ CMe ₂ C ₆ H ₅)(κ ³ - <i>N,N'</i> , <i>O</i> -C ₆ H ₄ N=CH(2-C ₅ H ₄ N))] (3-1).	84
3.4.3	Synthesis of [Pd(C ₆ H ₄ (2- <i>t</i> -Bu))(κ ³ - <i>N,N'</i> , <i>O</i> -C ₆ H ₄ N=CH(2-C ₅ H ₄ N))] (3-2).	85
3.4.4	Synthesis of [Pd(CH ₂ CMe ₂ C ₆ H ₄)(C ₆ H ₄ N=CH(2-C ₅ H ₄ N))] (3-3a/3-3b).	85
3.5	References	86
4	Pincer-Plus-One Ligands in Self-Assembly with Palladium(II): A Molecular Square and a Molecular Tetrahedron	90
4.1	Introduction	90
4.2	Result and Discussion	91
4.3	Conclusion	97
4.4	Experimental	97
4.4.1	Reagents and General Procedures	97
4.4.2	Synthesis of complex 4-1	98
4.4.3	Synthesis of complexes 4-2 and 4-3	99
4.4.4	X-ray Structure Determination	99
4.5	References	100
5	Reactivity of a Palladacyclic Complex: A Monodentate Carbonate Complex and the Remarkable Selectivity and Mechanism of a Neophyl Rearrangement	102
5.1	Introduction	102
5.2	Result and Discussion	106
5.2.1	Computational Studies	118

5.3	Conclusions.....	121
5.4	Experimental.....	121
5.4.1	Reagents and General Procedures.....	121
5.4.2	Synthesis of $[\text{Pd}(\text{CH}_2\text{CMe}_2\text{C}_6\text{H}_4)(\kappa^2\text{-}N,N'\text{-}5\text{-L1})]$, 5-1	122
5.4.3	Synthesis of $[\text{Pd}(\text{CO}_3)(\kappa^3\text{-}N,N',N''\text{-}5\text{-L1})]$, 5-2	123
5.4.4	Synthesis of $[\text{PdCl}(\kappa^3\text{-}N,N',N''\text{-}5\text{-L1})]_2[\text{PdCl}_4]$, 5-3a	123
5.4.5	Synthesis of $[\text{Pd}(\text{OTf})(\kappa^3\text{-}N,N',N''\text{-}5\text{-L1})](\text{OTf})$, 5-4	124
5.4.6	Synthesis of $[\text{Pd}(\text{OH})(\kappa^3\text{-}N,N',N''\text{-}5\text{-L1})](\text{OH})$, 5-5	124
5.4.7	Synthesis of $[\text{Pd}(\text{CH}_2\text{CMe}_2\text{Ph})(\kappa^3\text{-}N,N',N''\text{-}5\text{-L1})][\text{HCO}_3]$, 5-6	125
5.4.8	Reaction of Complex 5-6 with H_2O_2	125
5.4.9	X-Ray Structure Determination.....	126
5.4.10	DFT Calculations.....	126
5.5	References.....	126
6	Cycloneophylpalladium(IV) Complexes by Oxidative Addition of Bromine, Iodine and Methyl Iodide and their Reductive Elimination Reactions.....	131
6.1	Introduction.....	131
6.2	Result and Discussion.....	133
6.2.1	The Cycloneophylpalladium(II) Complexes.....	133
6.2.2	Palladium Complexes from Reactions of 5-1 and 6-1 with Bromine and Iodine.....	135
6.2.3	Palladium Complexes from Reaction with Methyl Iodide.....	139
6.2.4	Organic Products from the Reductive Elimination Reactions of Complexes 6-2 , 6-3 , 6-4 and 6-5	141
6.2.5	Kinetic Studies.....	145
6.2.6	Computational Studies.....	148
6.3	Conclusion.....	152
6.4	Experimental.....	153

6.4.1	Reagents and General Procedure	153
6.4.2	Synthesis of $[\text{Pd}^{\text{II}}(\text{CH}_2\text{CMe}_2\text{C}_6\text{H}_4)(\kappa^2\text{-}N,N'\text{-}\mathbf{6-L1})]$, 6-1	154
6.4.3	Synthesis of $[\text{Pd}^{\text{IV}}(\text{CH}_2\text{CMe}_2\text{C}_6\text{H}_4)(\kappa^3\text{-}N,N',N''\text{-}\mathbf{5-L1}$ or $\mathbf{-6-L1})(\text{X})\text{X}]$ Complexes, X: I, Br, 6-2 , 6-3 , 6-4 and 6-5	155
6.4.4	Thermolysis Reactions from Pd(IV) Complexes:.....	157
6.4.5	Synthesis of $[\text{Pd}^{\text{II}}(\kappa^3\text{-}N,N',N''\text{-}\mathbf{5-L1})\text{I}][\text{I}]$, 6-6	158
6.4.6	Synthesis of $[\text{Pd}^{\text{II}}(\kappa^3\text{-}N,N',N''\text{-}\mathbf{6-L1})\text{I}][\text{I}]$, 6-7	159
6.4.7	Synthesis of $[\text{Pd}^{\text{II}}(\kappa^3\text{-}N,N',N''\text{-}\mathbf{6-L1})\text{I}][\text{BF}_4]$, 6-7a	159
6.4.8	Synthesis of $[\text{Pd}^{\text{II}}(\kappa^3\text{-}N,N',N''\text{-}\mathbf{5-L1})\text{Br}][\text{Br}]$, 6-8	159
6.4.9	Synthesis of $[\text{Pd}^{\text{II}}(\kappa^3\text{-}N,N',N''\text{-}\mathbf{6-L1})\text{Br}][\text{Br}]$, 6-9	160
6.4.10	Synthesis of $[\text{Pd}^{\text{IV}}(\text{CH}_2\text{CMe}_2\text{C}_6\text{H}_4)(\kappa^3\text{-}N,N',N''\text{-}\mathbf{5-L1})\text{Me}][\text{I}]$, 6-10	160
6.4.11	Synthesis of $[\text{Pd}^{\text{IV}}(\text{CH}_2\text{CMe}_2\text{C}_6\text{H}_4)(\kappa^3\text{-}N,N',N''\text{-}\mathbf{6-L1})\text{Me}][\text{I}]$, 6-11	161
6.4.12	Synthesis of $[\text{Pd}^{\text{II}}(\text{CH}_2\text{CMe}_2\text{C}_6\text{H}_4\text{-CH}_3)(\kappa^3\text{-}N,N',N''\text{-}\mathbf{5-L1})][\text{I}]$, 6-12	161
6.4.13	Synthesis of $[\text{Pd}^{\text{II}}(\text{CH}_2\text{CMe}_2\text{C}_6\text{H}_4\text{-CH}_3)(\kappa^3\text{-}N,N',N''\text{-}\mathbf{6-L1})][\text{I}]$, 6-13	162
6.4.14	UV-Visible Studies	162
6.4.15	X-Ray Structure Determinations.....	162
6.5	References.....	163
7	Reductive C-O Elimination from Stable Pd(IV)-OH Complexes Prepared Using O₂ or H₂O₂ as Oxidants	166
7.1	Introduction.....	166
7.2	Result and Discussion	169
7.3	Conclusion	171
7.4	Experimental	171
7.4.1	Synthesis of $[\text{Pd}^{\text{IV}}(\text{CH}_2\text{CMe}_2\text{C}_6\text{H}_4)(\kappa^3\text{-}N,N',N''\text{-}\mathbf{5-L1})\text{OH}][\text{PF}_6]$, 7-1	172
7.4.2	Synthesis of $[\text{Pd}^{\text{IV}}(\text{CH}_2\text{CMe}_2\text{C}_6\text{H}_4)(\kappa^3\text{-}N,N',N''\text{-}\mathbf{6-L1})\text{OH}][\text{PF}_6]$, 7-2	173
7.4.3	Synthesis of $[\text{Pd}^{\text{II}}(\kappa^3\text{-}N,N',N''\text{-}\mathbf{5-L1})\text{OH}][\text{PF}_6]$, 7-3	173
7.5	References.....	174

8 Summary, Conclusion and Future Work	176
8.1 Summary and Conclusion	176
8.2 Future Work	182
8.3 References	183
Appendices.....	185
Appendix A: Supplementary Information for Chapter 2	185
Appendix B: Supplementary Information for Chapter 3.....	222
Appendix C: Supplementary Information for Chapter 4.....	255
Appendix D. Supplementary Information for Chapter 5	280
Appendix E. Supplementary Information for Chapter 6.....	313
Appendix F. Supplementary Information for Chapter 7	376
Appendix G. Copyright Material and Permissions	389
Appendix H. Curriculum Vitae	391

List of Tables

Table 1-1. Bond dissociation energies (BDEs) and $pK_a(\text{aq})$ values of some common C-H bonds.	14
Table 2-1 Optimization of the formation of 2-5 from 2-2 at room temperature.	44
Table 3-1 Isomerization of 3-1 to 3-2 in various solvents.	79
Table 6-1 Observed products after reductive elimination from complexes 6-2, 6-3, 6-4 and 6-5 in CDCl_3 solution.	143
Table 6-2 Observed first-order rate constants for the reductive elimination reactions.	147

List of Figures

- Figure 2-1 The structures of the two independent molecules of complex 2-2, showing 30% probability ellipsoids. Selected bond parameters: Pd(1)C(1A) 1.994(4); Pd(1)C(8A) 2.018(4); Pd(1)N(1A) 2.170(3); Pd(1)N(2A) 2.119(3) Å; C(1A)Pd(1)C(8A) 79.42(16); N(2A)Pd(1)N(1A) 76.82(12)°; Pd(2)C(1B) 1.993(4); Pd(2)C(8B) 2.039(5); Pd(2)N(2B) 2.117(3); Pd(2)N(1B) 2.158(3) Å; C(1B)Pd(2)C(8B) 79.43(18); N(2B)Pd(2)N(1B) 76.57(13)° 42
- Figure 2-2 The structures of complexes 2-3 and 2-4, with ellipsoids shown at the 50% probability level. Selected bond parameters: 2-3, Pd(1)N(1) 2.023(3); Pd(1)Br(1) 2.4085(5) Å; N(1)Pd(1)N(1A) 79.92(14); Br(1)Pd(1)Br(1) 93.47(3)°; 2-4, Pd(1)N(1A) 2.065(2); Pd(1)N(2A) 2.069(2); Pd(1)I(2A) 2.5668(5); Pd(1)I(1A) 2.5700(5) Å; N(1A)Pd(1)N(2A) 79.03(9); I(2A)Pd(1)I(1A) 90.437(17)° 43
- Figure 2-3 ¹H NMR spectra in the region of the imine protons during reaction of complex 2-2 with 2 eq H₂O₂ in (CD₃)₂CO at room temperature to give complex 2-5. Spectra depict a) authentic 2-2; and the reaction mixture of 2-2 and H₂O₂ after (b) 10 min., (c) 2 h., and (d) 3 h..... 45
- Figure 2-4 A view of the structure of complex 2-5 (ellipsoids at 50% probability). Co-crystallized benzene and hydrogen atoms are not shown, for clarity. Selected bond parameters: Pd(1)O(1) 1.9900(10); Pd(1)C(1) 2.0124(12); Pd(1)N(2) 2.0187(11); Pd(1)N(1) 2.1685(10) Å; O(1)Pd(1)C(1) 92.45(4); N(2)Pd(1)N(1) 78.12(4)° 46
- Figure 2-5 Calculated structures and relative energies (kJ mol⁻¹) of complexes and intermediates in the reaction of 2-2 with H₂O₂ to give complex 2-5. *M* represents the proposed initial interaction between the 4d_{z²} HOMO of complex 2-2 and the σ* LUMO of H₂O₂. Selected calculated bond parameters: H₂O₂, O-O 1.59, O-H 1.01 Å; 2-13, Pd··O 2.47, O-O 1.72, PdO-H 1.00, PdOO-H 1.01 Å, Pd··O-O 177°; 2-14, Pd-O 1.98, O··O 2.57, PdO··H 1.54, PdOH-O 1.05, PdOHO-H 1.00 Å; 2-15, Pd-O 2.02, O··O 2.77, PdO··H 1.77, PdOH-O 1.01, PdOHO-H 0.99 Å; 2-5, Pd-O 2.02 Å..... 51

Figure 3-1 Thermal displacement plot of 3-1 (left) and 3-2 (right) with ellipsoids at 50% probability. Hydrogen atoms and a molecule of co-crystallized benzene in both are omitted for clarity. Selected bond distances (Å) and angles (deg): 3-1, Pd(1)O(1) 2.064(3); Pd(1)N(1) 2.031(3); Pd(1)N(2) 2.044(3); Pd(1)C(1) 2.046(4); N(1)Pd(1)N(2) 80.43(13); N(1)Pd(1)O(1) 81.49(11); O(1)Pd(1)C(1) 102.95(13). 3-2, Pd(1)O(1) 2.057(7); Pd(1)N(1) 2.018(8); Pd(1)N(2) 2.039(7); Pd(1)C(13) 2.019(8); N(1)Pd(1)N(2) 80.1(3); N(1)Pd(1)O(1) 83.20(3); O(1)Pd(1)C(13) 97.0(3). 68

Figure 3-2 Top: UV-Visible absorption spectra of 3-1 (8.58×10^{-5} M) in (a) C₆H₆, (b) CHCl₃; (c) CH₂Cl₂ and (e) CH₃OH. Bottom: photograph of solutions of 3-1 (8.58×10^{-5} M) in (a) C₆H₆; (b) CHCl₃; (c) CH₂Cl₂; (d) CH₃CN; (e) CH₃OH. 69

Figure 3-3 Thermal displacement plot of 3-3b with ellipsoids at 50% probability. Hydrogen atoms and a molecule of co-crystallized benzene are omitted for clarity. Selected bond distances (Å) and angles (deg): Pd(1)N(1) 2.135(1); Pd(1)N(2) 2.193(1); Pd(1)C(13) 2.024(1); Pd(1)C(18) 2.006(1); N(1)Pd(1)N(2) 77.32(4); C(18)Pd(1)C(13) 79.53(4); $\tau_4 = 0.05$ 72

Figure 3-4 Calculated structures and relative energies of complexes 3-1 and 3-2, and proposed intermediates 3-A and 3-B. The conversion of 3-1 to 3-2 is likely to occur via the reversible sequence 3-1 to 3-A to 3-B to 3-2..... 73

Figure 3-5 The aromatic regions of the ¹H NMR spectra (599.3 MHz, CD₂Cl₂) for: a) 3-1 b) 3-1-*d*₁ and c) 3-1-*d*₂. The integrations are relative to the imine backbone resonance *H*10, which is set to one..... 75

Figure 3-6 Conversion of 3-1 to 3-2 over time in protio (solid lines) and deuterio (dashed lines) solvents: Methanol (blue), chloroform (green) and dichloromethane (red)..... 80

Figure 3-7(a), (b), (c) Calculated structures of intermediate complexes 3-A, 3-B and 3-B.MeOH, as space-filling models with only the OH and closest CH protons included, for clarity; (d), (e), (f), the calculated HOMO, having Pd 4d_z² and Pd-C bonding character, for the protonolysis for complex 3-A, 3-B and 3-B.MeOH. 82

Figure 3-8 Calculated structures and relative energies of complexes 3-C and 3-D..... 83

Figure 4-1 The structure of complex 4-3 (previously reported as a CHCl ₃ solvate). Selected bond parameters: Pd(1)N(1) 1.951(2), Pd(1)N(2) 2.017(3), Pd(1)O(1) 2.011(2), Pd(1)Cl(1) 2.303(1) Å; N(1)Pd(1)Cl(1) 175.80(7), N(2)Pd(1)O(1) 165.60(9)°.	93
Figure 4-2 Simulated (top) and observed (bottom) MALDI MS isotope patterns for a) [4-1] ⁺ , and b) [4-2] ⁺ . Matrix = pyrene.	94
Figure 4-3 The building block and polyhedral structure in (a) 4-1 and (b) 4-2.	95
Figure 4-4 The structure of complex 4-1. Selected bond parameters: Pd(1)N(2) 1.957(3), Pd(1)O(1) 1.971(3), Pd(1)O(2) 1.977(3), Pd(1)N(3) 2.061(3) Å; O(1)Pd(1)O(2) 179.78(13), N(2)Pd(1)N(3) 173.59(14)°.	96
Figure 4-5 The structure of complex 4-2. Selected bond parameters: Pd(1)N(1) 1.977(1), Pd(1)N(2) 1.931(1), Pd(1)O(2) 2.033(1), Pd(1)O(6) 2.042(1), Pd(1)Pd(2) 3.238(1) Å; N(1)Pd(1)O(2) 166.43(5), N(2)Pd(1)O(6) 178.10(5)°.	96
Figure 5-1 ¹ H NMR spectra (600 MHz, acetone- <i>d</i> ₆ solution) of complex 5-1 at different temperatures.	108
Figure 5-2 Isotope patterns for [5-2+K] ⁺ : (a) simulated and (b) observed by MALDI MS using anthracene as the matrix.	110
Figure 5-3 The structure of complex 5-3b, showing 30% probability ellipsoids. Selected bond distances (Å): Pd(1)N(1) 2.0170(8); Pd(1)N(2) 2.0254(8); Pd(1)N(3) 2.0107(8); Pd(1)Cl(1) 2.3024(6).	111
Figure 5-4 The molecular structures of complexes (a) 5-2a and (b) 5-2b, showing 30% probability ellipsoids. Selected bond distances (Å) and angles (deg) for 5-2a, Pd(1)N(1) 2.003(9); Pd(1)N(2) 2.007(8); Pd(1)N(3) 2.007(9); Pd(1)O(2) 2.012(7); C(16)O(2) 1.221(13); C(16)O(4) 1.352(13); C(16)O(3) 1.258(12); N(1)Pd(1)N(2) 84.27(3); N(2)Pd(1)N(3) 82.99(3); N(3)Pd(1)O(2) 97.06(3); O(2)Pd(1)N(1) 95.52(3); and for 5-2b, Pd(1)N(1) 2.006(2); Pd(1)N(2) 2.017(2); Pd(1)N(3) 2.015(2); Pd(1)O(2) 2.020(2); C(16)O(2) 1.325(3); C(16)O(4) 1.285(3); C(16)O(3) 1.256(3); N(1)Pd(1)N(2) 83.46(9); N(2)Pd(1)N(3) 84.00(9); N(3)Pd(1)O(2) 96.49(8); O(2)Pd(1)N(1) 96.10(8).	112

Figure 5-5 The structures of dimer units of (above) complex 5-2a and (below) complex 5-2b formed by hydrogen bonding, showing 25% thermal ellipsoids.	113
Figure 5-6 NMR spectra of complex 5-6-d in D ₂ O solution: a) ² H NMR spectrum and b) ¹ H NMR spectrum.....	115
Figure 5-7 The calculated structures and relative energies of isomers 5-1a and 5-1b.....	118
Figure 5-8 The calculated structures and relative energies of 5-6, 5-M and 5-N.....	119
Figure 5-9 The predicted structures and relative energies of complexes 5-M, 5-Q, 5-Q* and 5-5.	120
Figure 5-10 Calculated hydrogen bonded structures for complex 5-2. In the O-H··O units, the shorter OH distance is to the oxygen of water or alcohol, and the longer distance is to the oxygen of carbonate.....	121
Figure 6-1 ¹ H NMR spectra (600 MHz, CD ₂ Cl ₂ solution) of complex 6-1 at different temperatures.....	135
Figure 6-2 Structure of complex 6-2, showing 30% probability ellipsoids. Selected bond distances: Pd(1A)–I(1A) 2.5785(9); Pd(1A)–N(1A) 2.150(4); Pd(1A)–N(2A) 2.197(4); Pd(1A)–N(3A) 2.229(5); Pd(1A)–C(1A) 2.072(5); Pd(1A)–C(6A) 1.994(6) Å; H-bond distance: O(1A)··I(2CA) 3.54(1) Å.	137
Figure 6-3 Structure of complex 6-4, showing 30% probability ellipsoids for the two independent molecules. Selected bond distances (Å): molecule A, Pd(1A)–I(1A) 2.420(2); Pd(1A)–N(1A) 2.171(12); Pd(1A)–N(2A) 2.121(12); Pd(1A)–N(3A) 2.203(12); Pd(1A)–C(1A) 2.075(13); Pd(1A)–C(6A) 1.985(15); molecule B, Pd(1B)–I(1B) 2.4272(19); Pd(1B)–N(1B) 2.154(12); Pd(1B)–N(2B) 2.147(12); Pd(1B)–N(3B) 2.206(12); Pd(1B)–C(1B) 2.049(12); Pd(1B)–C(6B) 1.996(15).	138
Figure 6-4 Structures of complexes 6-6, 6-7, 6-8 and 6-9. Selected distances: complex 6-6, Pd(1B)–I(1B) 2.5928(10); Pd(1B)–N(1B) 2.025(5); Pd(1B)–N(2B) 2.055(5); Pd(1B)–N(3B) 2.037(5) Å; complex 6-7, Pd(1)–I(1) 2.5911(19); Pd(1)–N(1) 2.028(2); Pd(1)–N(2) 2.041(2); Pd(1)–N(3) 2.017(2) Å; complex 6-8, Pd(1)–Br(1) 2.4101(8); Pd(1)–N(1) 2.026(5);	

Pd(1)–N(2) 2.014(5); Pd(1)–N(3) 2.034(5) Å; complex 6-9, Pd(1)–Br(1) 2.4282(12); Pd(1)–N(1) 2.024(5); Pd(1)–N(2) 2.038(5); Pd(1)–N(3) 1.993(5) Å.	139
Figure 6-5 NMR spectra of complex 6-12 and 6-12- <i>d</i> ₃ : (a) ¹ H NMR spectrum of 6-12 in CD ₂ Cl ₂ ; (b) ¹ H NMR spectrum of 6-12- <i>d</i> ₃ in CD ₂ Cl ₂ ; (c) ² H NMR spectrum of 6-12- <i>d</i> ₃ in CH ₂ Cl ₂	140
Figure 6-6 Above, UV-visible absorption spectra of complex 6-2 in chloroform (8.33 × 10 ⁻³ M, 50°C) during the reductive elimination reaction (absorbance at 425 nm decreases with time. Below, the corresponding first-order plot of ln[A-A _∞]/[A ₀ -A _∞] versus time for the initial part of the reaction.	147
Figure 6-7 The calculated structures of complexes shown in Scheme 6-8 (the iodide ion is not shown in the Pd(II) complexes for clarity), and the relative energies (kJ mol ⁻¹) with respect to 5-1a + MeI.	150
Figure 6-8 The calculated structures of cationic complexes shown in Scheme 6-7, and the relative energies (kJ mol ⁻¹) with respect to complex 6-2.....	151
Figure 6-9 The calculated structures of isomers of 6-2 and possible intermediate iodine complexes 6- <i>O</i> and 6- <i>P</i> , and their relative energies (kJ mol ⁻¹).....	152
Figure 7-1 Structure of complex 7-2, showing 30% probability ellipsoids. Selected bond distances: Pd(1)–O(1) 1.990(5); Pd(1)–N(1) 2.136(8); Pd(1)–N(2) 2.150(7); Pd(1)–N(3) 2.185(8); Pd(1)–C(1) 2.039(8); Pd(1)–C(6) 1.979(8) Å.	170
Figure 8-1 General mechanism for common Pd(II)/Pd(IV) catalysis that follow C-H activation at Pd(II) (X = C, O, N, F, Cl, Br, I).....	176
Figure 8-2 A summary of observed oxidative addition and reductive elimination reactions in Chapter 2.....	177
Figure 8-3 A summary of observed insertion, oxidative addition and reductive elimination reactions in Chapter 2.	178
Figure 8-4 The CMD-type C-H activation discussed in Chapter 3.	179

Figure 8-5 A summary of observed oxidative addition and reductive elimination reactions in Chapter 6.....	181
Figure 8-6 Proposed C(sp ²)-H bond hydroxylation reaction for future work.....	183

List of Charts

Chart 1-1 Examples of isolated Pd(IV) complexes containing: 1-1 ⁵² , bidentate bipy-type ligands; 1-2, ⁵³ 1-3, ³⁹ and 1-4, ⁵¹ tridentate <i>N</i> -donor ligands; 1-5 ⁵⁰ and 1-6, ⁵⁴ phpy-type ligands.	4
Chart 1-2 General structure for cycloneophyl-palladacycle, Pd(CH ₂ CMe ₂ - <i>o</i> -C ₆ H ₄)L ₂ (L = COD or PPh ₃).....	6
Chart 2-1 Atom labels for complexes 2-2 and 2-5 for NMR spectroscopy assignments	56
Chart 3-1 Activation of a generic C-H bond promoted by a carboxylate group.....	64
Chart 3-2 Proposed transition state structures for the S _E 2 protonolysis of the Pd-aryl bond in 3-1 (<i>3-E</i>) and the Pd-alkyl bond in 3-2, without (<i>3-F</i>) and with (<i>3-G</i>) a MeOH solvent bridge.	81
Chart 4-1 . NMR labeling scheme for complexes made in this study.	98
Chart 6-1 NMR labels for Pd(IV) complexes, 6-2, 6-3, 6-4 and 6-5.....	154
Chart 7-1 NMR labels for Pd(IV) complexes, 7-1 and 7-2.....	172

List of Schemes

Scheme 1-1 General mechanism for Pd-catalyzed coupling reactions (X = Cl, Br, I, OTf and R = aryl, benzyl, vinyl, allyl and M = Zn, Mg, B, Sn). ^{6,9,18-35}	2
Scheme 1-2 General mechanism for Pd(II)/Pd(IV) catalysis that follow either C-H activation at Pd(II) (red) or at Pd(IV) (blue) (X = C, O, N, F, Cl, Br, I).....	2
Scheme 1-3 Fluorination of arylboronic acids by (a) a Pd-pyridyl complex 1-7 and (b) a Pd-benzoquinoliny complex 1-8, (Ns = SO ₂ -(<i>p</i> -NO ₂ -C ₆ H ₄))......	5
Scheme 1-4 Ligand effect study on Pd(IV) stabilization.....	6
Scheme 1-5 Base-induced paladacyclometallation reaction.....	7
Scheme 1-6 C(sp ³)-O and C(sp ²)-O bond formation from Pd(IV) intermediates.....	8
Scheme 1-7 General schematic of the oxidative addition reaction.....	9
Scheme 1-8 General schematic of the three-centre concerted oxidative addition reaction.	9
Scheme 1-9 General schematic of the bimolecular S _N 2 oxidative addition reaction.....	10
Scheme 1-10 General schematic of the reductive elimination reaction.....	11
Scheme 1-11 Oxidative addition of methyl iodide to Pd(II), followed by C-C bond-forming reductive elimination.	11
Scheme 1-12 C-O bond forming reductive elimination reaction.....	12
Scheme 1-13 Proposed mechanisms for C-O bond-forming reductive elimination reaction.	12
Scheme 1-14 Directing group facilitating C-H activation.	14
Scheme 1-15 General mechanism of a C-H activation reaction via (a) oxidative addition, (b) σ-bond metathesis and c) CMD-type C-H activation mechanisms.....	15
Scheme 1-16 Proposed mechanism for Pd-catalyzed C-H activation of benzene.	15

Scheme 1-17 CO insertion into Pd-C bond in cycloneophyl-palladacycle.	16
Scheme 1-18 a) Pd(IV) chloromethyl formation through oxidative addition of dichloromethane to a palladacycle(II). b) six membered Pd(IV) iodide or bromide formation through methylene insertion into Pd-C(sp ²) bond.	17
Scheme 1-19 Protonolysis of (a) Pd-C(sp ²) bond, where X is a coordinating anion and (b) Pd-C(sp ³) bond, where X is a non-coordinating anion.	18
Scheme 1-20 Pd-catalyzed C(aryl)-H acetoxylation using PhI(OAc) ₂ as an oxidant.	19
Scheme 1-21 C-H bond halogenation in 3-methyl-2-phenylpyridine and the proposed mechanism for C-H bond halogenation.	20
Scheme 1-22 Pd(II) oxidation and study the C-H activation reaction verses C-Cl bond-forming reductive elimination (<i>N</i> - <i>N</i> ligand = 4,4'-Di- <i>tert</i> -butyl-2,2'-dipyridyl, dtbpy).	21
Scheme 1-23 Formation of a stable Pd(IV) complex and study of the C-H activation reaction versus C-Cl bond-forming reductive elimination (<i>N</i> - <i>N</i> ligand = 4,4'-Di- <i>tert</i> -butyl-2,2'-dipyridyl, dtbpy).	21
Scheme 1-24 Pd-catalyzed C(aryl)-H acetoxylation using K ₂ S ₂ O ₈ as an oxidant.	22
Scheme 1-25 Pd-catalyzed C-H bond oxygenation reaction using oxone as oxidant.	22
Scheme 1-26 Pd-catalyzed C-H activation using O ₂ as an oxidant.	23
Scheme 1-27 Pd-catalyzed C-H bond activation using H ₂ O ₂ as an oxidant.	24
Scheme 1-28 Reversible hydration of dpk in water.	24
Scheme 1-29 Proposed mechanism for C-O bond-forming reductive elimination reaction form a Pd(IV)-OH in water.	25
Scheme 1-30 Pd-catalyzed C-H bond activation using H ₂ O ₂ as an oxidant.	26
Scheme 1-31 Proposed mechanism for formation of 1-35 by aerobic oxidation of 1-34.	26

Scheme 1-32 Proposed mechanism for aerobic oxidation of 1-36.	27
Scheme 2-1 Competition between C-X (X = OR or NHR), C-F and C-C reductive elimination from the palladium(IV) complex 2-A.	37
Scheme 2-2 Reductive elimination with selective aryl C-O bond formation.	38
Scheme 2-3 Precedent for O-atom insertion into M-Ar from organonickel chemistry.	39
Scheme 2-4 Examples of oxygen atom insertion. Reagents: (i) MCPBA, C ₆ F ₅ IO or H ₂ O ₂ /Fe(III) catalyst; (ii) <i>t</i> -BuOOH/[V(O)(acac) ₂] catalyst.	39
Scheme 2-5 Ligand assisted reaction with H ₂ O ₂	40
Scheme 2-6 Synthesis of complex 2-2.	41
Scheme 2-7 The reaction of 2-2 with bromine or iodine.	42
Scheme 2-8 The reaction of complex 2-2 with hydrogen peroxide.	44
Scheme 2-9 The reaction of complex 2-5 with bromine or iodine.	46
Scheme 2-10 The reaction of 2-5 with CO.	47
Scheme 2-11 Above, some potential reactions of complex 2-2 with H ₂ O ₂ and, below, the calculated energies of reaction in kJ mol ⁻¹	49
Scheme 2-12 Some possible products, and their relative energies (kJ mol ⁻¹) from reaction of complex 2-2 with bromine or iodine.	52
Scheme 2-13 Potential products, and their relative energies from reactions of complex 2-5.	53
Scheme 2-14 A likely mechanism for reactions of complex 2-5 with oxidants X ₂ (X = Br, I, OH), and the relative energies (kJ mol ⁻¹) for the case with X = I.	54
Scheme 3-1 Concerted (S _E 2, top) and step-wise (S _E (OX), bottom) mechanistic routes for protonolysis (forward) or the microscopic reverse concerted or stepwise C-H activation reactions, respectively, at Pd(II) or Pt(II).	65

Scheme 3-2 First examples of reversible protonolysis/C-H bond activation on reaction of [Pd(CH ₂ CMe ₂ C ₆ H ₄)(PPh ₃) ₂] with acids HX that is proposed to follow an S _E (OX) mechanism. S = solvent.	66
Scheme 3-3 Metalation of 3-L1H to selectively give complex 3-1 and isomerization of 3-1 to 3-2. Conditions, (i) 3-L1H and [Pd(CH ₂ CMe ₂ (C ₆ H ₄))(COD)] (2-1), Method A: Et ₂ O, -70 °C to room temperature over 17 h, isolated yield 3-1, 80%. Method B: CD ₂ Cl ₂ , room temperature, 10 min; in situ yield 3-1, >95%; (ii) 1 in MeOH, room temperature, 5 days, 90% conversion to 3-2, 80% isolated yield.	67
Scheme 3-4 Expected intermediates in the formation of 3-1 and 3-2 following a) a concerted S _E 2; or b) stepwise S _E (OX) pathway.	70
Scheme 3-5 Coordination of ligand 3-L2 to give a mixture of isomers 3-3a and 3-3b. Conditions: (i) 3-L2 and [Pd(CH ₂ CMe ₂ (C ₆ H ₄))(COD)] (2-1), Et ₂ O, -65 °C to room temperature over 18 h, isolated yield 3-3a/3-3b, 73% as a 1:0.6 mixture.	71
Scheme 3-6 Attempted deuterolysis and C-H activation using exogenous phenol- <i>d</i> ₁ with a mixture of 3-3a/3-3b. The abbreviated <i>N-N</i> ligand represents ligand 3-L2.	74
Scheme 3-7 Metalation of 3-L1D to give 3-1- <i>d</i> ₁ or 3-1- <i>d</i> ₂	74
Scheme 3-8 Proposed route for deuterium incorporation into 3-1- <i>d</i> ₁ and 3-1- <i>d</i> ₂	76
Scheme 3-9 Isomerization of 3-1- <i>d</i> ₂ to give 3-2- <i>d</i> ₂ with deuterium incorporation in the <i>t</i> -Bu moiety.	78
Scheme 4-1 Self-assembly of a pincer-plus-one ligand and Pd(II) to give a hexamer.	90
Scheme 4-2 Synthesis of complexes 4-1, 4-2 and 4-3.	92
Scheme 5-1 Diverse oxidation reactivity achieved with a simple diimine ligand (2-2, 2-5), a ligand with pendent nitrogen donor group (5-A, 5-B), and ligands with a pendent alcohol or phenol group (5-C, 5-D, 5-E and 5-F).	103
Scheme 5-2 Some known carbonate and bicarbonate complexes of palladium(II).	104

Scheme 5-3 The neophyl carbocation rearrangement.....	105
Scheme 5-4 β -Phenyl or β -methyl elimination reactions at palladium(II).	106
Scheme 5-5 Synthesis of complex 5-1, and the proposed mechanism of interconversion of isomers 5-1a and 5-1b by way of 5-1*.....	107
Scheme 5-6 Two independent syntheses of the palladium(II) carbonate complex 5-2.	109
Scheme 5-7 The conversion of complex 5-1 to 5-2 by way of complex 5-6, and the distribution of organic products.	114
Scheme 5-8 Possible mechanisms of reaction of 5-6 with H ₂ O ₂ (the ligand 5-L1 is drawn as <i>NNN</i> for simplicity) to give 5-2. The favored mechanism involves concerted β -Me elimination and nucleophilic OH ⁻ attack followed by C-C reductive elimination (5- <i>M</i> \rightarrow 5- <i>Q</i> \rightarrow 5-5). The disfavored mechanism involves β -Me elimination, alkene insertion and C-O reductive elimination (5- <i>M</i> \rightarrow 5- <i>O</i> \rightarrow 5- <i>P</i> \rightarrow 5-5).	117
Scheme 6-1 Reductive elimination from Pd(IV) (a) with CH ₂ -X bond formation (X = OR or NR ₂); (b) with C ₆ H ₄ -X bond formation (X = OH, L = solvent dmsO).....	132
Scheme 6-2 Reductive coupling from proposed 5-coordinate intermediates 6- <i>G</i> , by either C-C reductive elimination to give the cyclobutane derivative CB or by oxygen-atom insertion to give 2-5.	133
Scheme 6-3 Synthesis of complexes 5-1 and 6-1, which are observed as a fluxional mixture assigned as 5-1a or 6-1a and 5-1b or 6-1b that likely interconvert via 5-1* or 6-1*, respectively.	134
Scheme 6-4 The oxidative addition reaction of complexes 5-1 and 6-1 with iodine and bromine to give complexes 6-2, 6-3, 6-4 and 6-5, and slower reductive elimination to give complexes 6-6, 6-7, 6-8 and 6-9.	136
Scheme 6-5 The reaction of complexes 5-1 and 6-1 with methyl iodide to give complexes 6-10, 6-11, 6-12 and 6-13.....	140

Scheme 6-6 The mixture of organic products detected from reductive elimination from complexes 6-2, 6-3, 6-4 and 6-5 (X = I from 6-2 and 6-3, X = Br from 6-4 and 6-5).....	142
Scheme 6-7 A simplified pathway for the reductive elimination reactions.....	145
Scheme 6-8 The three potential modes of reductive elimination from complex 6-10 with C-C bond formation.....	149
Scheme 7-1 Pd-catalyzed C-H functionalization reactions with O ₂ or H ₂ O ₂ as oxidants. (a) aerobic acetoxylation of C-H bonds; (b) aerobic hydroxylation of arenes; (c) hydroxylation of C-H bonds with H ₂ O ₂	167
Scheme 7-2 Oxygen-atom insertion into the Pd-C bond, using H ₂ O ₂ as the oxidant.....	167
Scheme 7-3 (a) oxidation of a Pd(II) complex in water; (b) oxidation of a palladacycloneophyl complex using green oxidants; (c) Pd-catalyzed C-H bond activation using H ₂ O ₂ as an oxidant.	168
Scheme 7-4 Pd(II) oxidation in the presence of dioxygen or hydrogen peroxide as an oxidant.	169
Scheme 7-5 Reductive elimination reaction from 7-2.....	171

List of Abbreviations

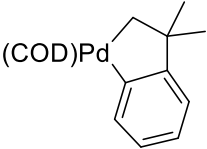
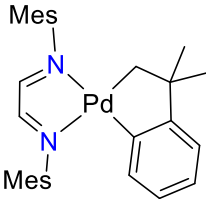
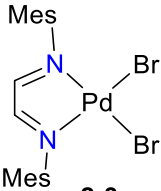
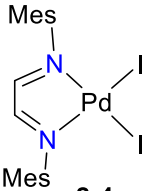
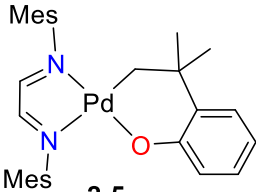
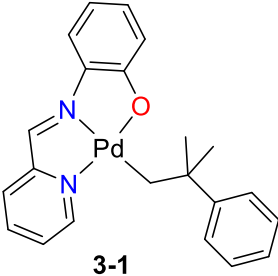
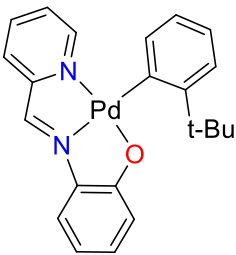
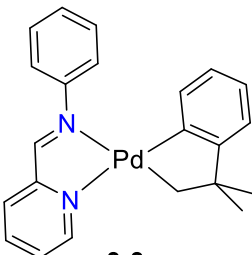
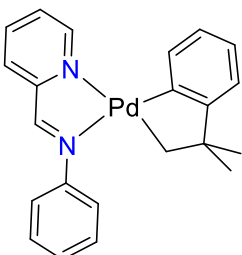
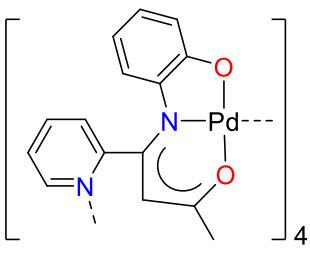
°	degrees
a, b, c, α , β , γ	unit cell parameters
Å	angstrom
acac	acetylacetonate
Anal. Calcd.	analysis calculated
Ar	Aryl group
BDE	bond dissociation energies
BF	3,3-dimethyl-2,3-dihydro-benzofuran
BP	4,4-dimethyl-2-oxo-2 <i>H</i> -1-benzopyran
bpy	bipyridine
br	broad
Bu	butyl
calcd	calculated
CB	1,1-dimethylcyclobutabenzene
CCDC	Cambridge Crystallographic Data Centre
COD	1,5-Cyclooctadiene
δ	chemical shift
d	doublet
dd	doublet of doublets
dt	doublet of triplets
DCM	dichloromethane
DFT	density functional theory
equiv.	molar equivalents
ESI-MS	Electrospray Ionization Mass Spectrometry

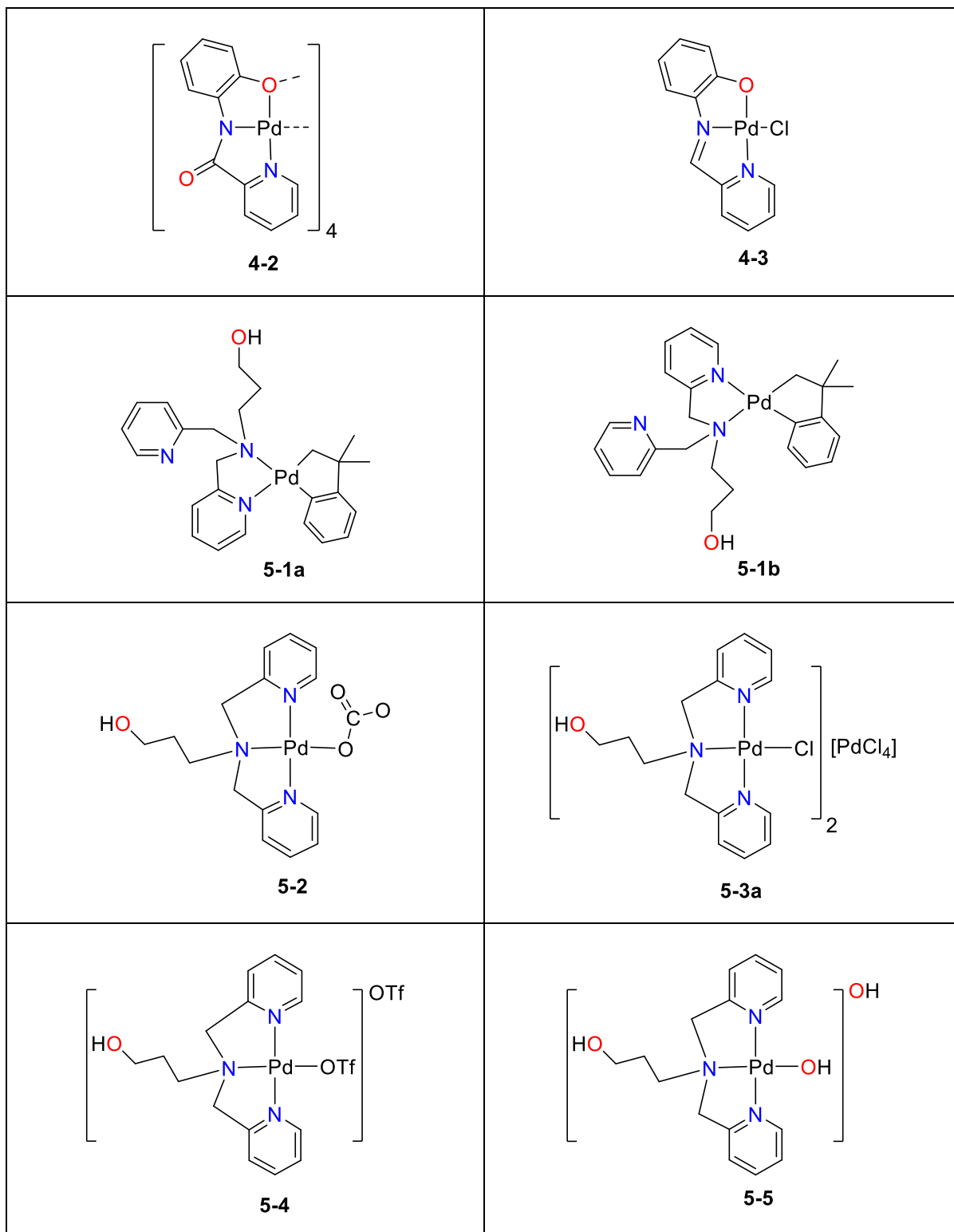
<i>fac</i>	facial
FT-IR	Fourier transform infrared
g	gram
ΔG	free energy activation
GC/MS	Gas Chromatography/Mass Spectroscopy
gCOSY	gradient homonuclear correlation spectroscopy
gHMBC	gradient heteronuclear multiple-bond correlation spectroscopy
gHSQC	gradient heteronuclear single-quantum correlation spectroscopy
GOF	goodness of fit
h	hour
<i>h</i>	Planck's constant
<i>h</i> ν	electromagnetic radiation
HOMO	highest occupied molecular orbital
IB	(2-Iodo-2-methylpropyl)benzene
IP	1-Iodo-2-methyl-2-phenylpropane
IR	infrared
<i>J</i>	coupling constant
λ	wavelength
L	ligand
LMCT	ligand to metal charge transfer
LUMO	lowest unoccupied molecular orbital
μL	microliter
<i>m/z</i>	mass to charge ratio

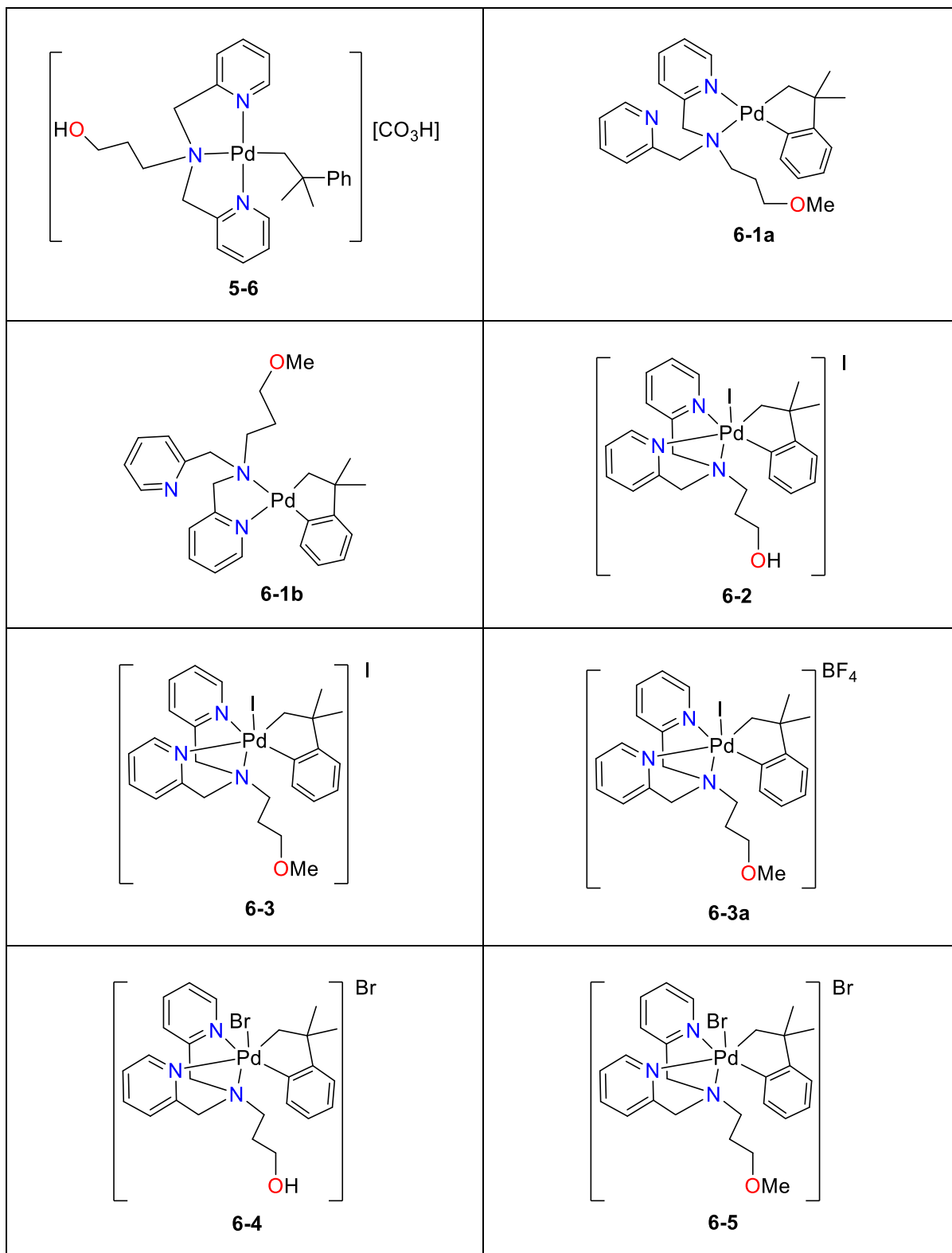
m	multiplet
M	metal
<i>m</i>	meta
MB	(2-Methylprop-1-en-1yl)benzene
Me	methyl
Me ₃ tacn	<i>N,N',N''</i> -trimethyl-1,4,7-triazacyclononane
Mes	mesityl, 2,4,6-trimethylphenyl
mg	milligram
MHz	megahertz
min	minute
mL	millilitre
MO	molecular orbital
mol	moles
MS	mass spectroscopy
nm	nanometer
NMR	nuclear magnetic resonance
ν	frequency
<i>o</i>	ortho
OTf	triflate, trifluoromethanesulfonate
<i>p</i>	para
Ph	phenyl
phen	phenanthroline
phpy	phenylpyridyl
ppm	parts per million
py	pyridyl

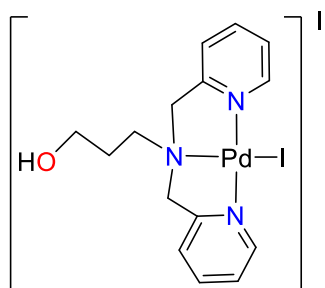
q	quartet
refinm	refinement
refl	reflections
RT	room temperature
s	singlet
S _N 2	bimolecular nucleophilic substitution reaction
solv	solvent
T	temperature
t	triplet
<i>t</i> Bu	<i>tert</i> -butyl
THF	tetrahydrofuran
TOF	time of flight
Tp	hydrotris(pyrazolyl)borate
UV/Vis	ultraviolet/visible
VT-NMR	variable temperature-NMR
X	halide, or halogen; anion
XRD	X-ray diffraction
Z	number of formula units

List of Complexes

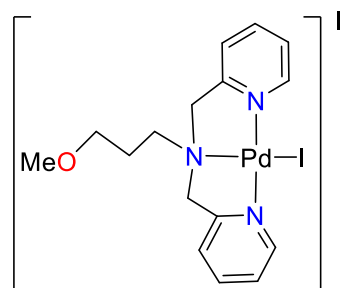
 <p>(COD)Pd</p> <p>2-1</p>	 <p>Mes</p> <p>Mes</p> <p>2-2</p>
 <p>Mes</p> <p>Br</p> <p>Br</p> <p>Mes</p> <p>2-3</p>	 <p>Mes</p> <p>I</p> <p>I</p> <p>Mes</p> <p>2-4</p>
 <p>Mes</p> <p>Mes</p> <p>2-5</p>	 <p>3-1</p>
 <p>t-Bu</p> <p>3-2</p>	 <p>3-3a</p>
 <p>3-3b</p>	 <p>4-1</p>



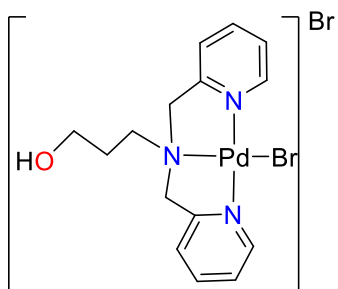




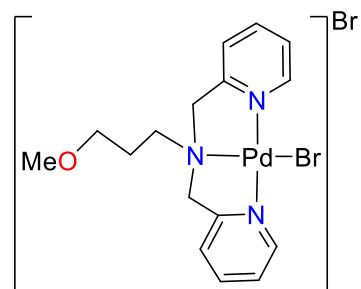
6-6



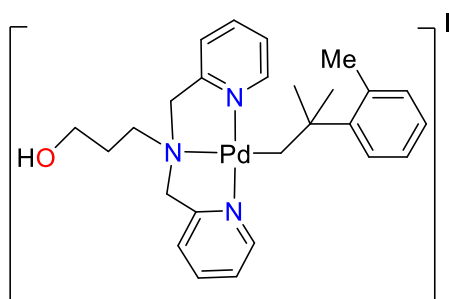
6-7



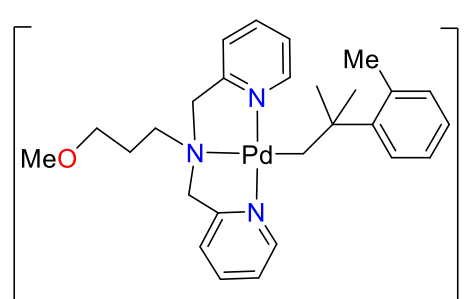
6-8



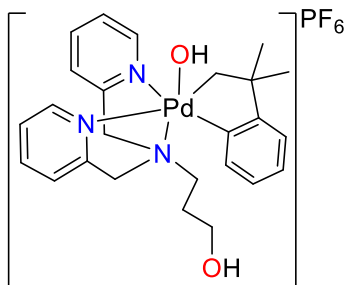
6-9



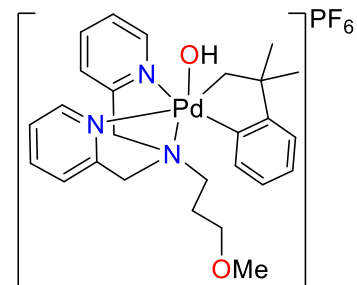
6-12



6-13



7-1



7-2

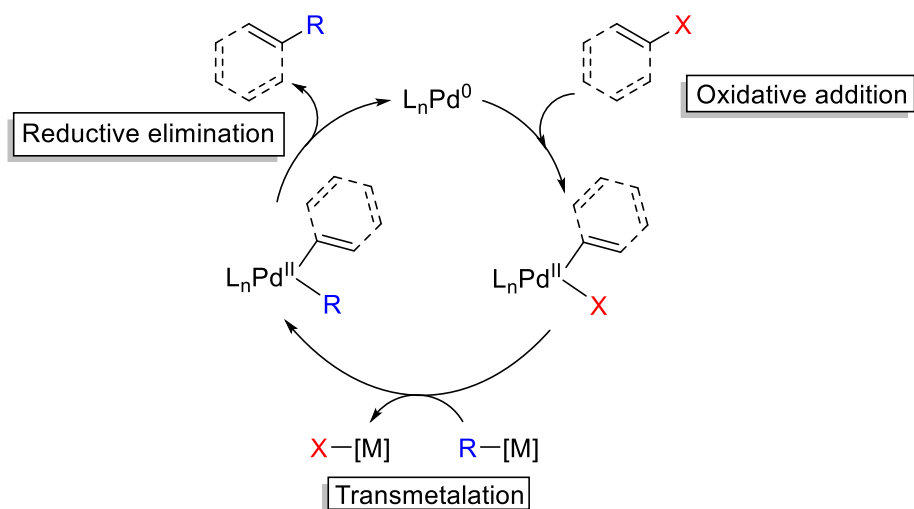
Dedication

To Soheil

1 Introduction

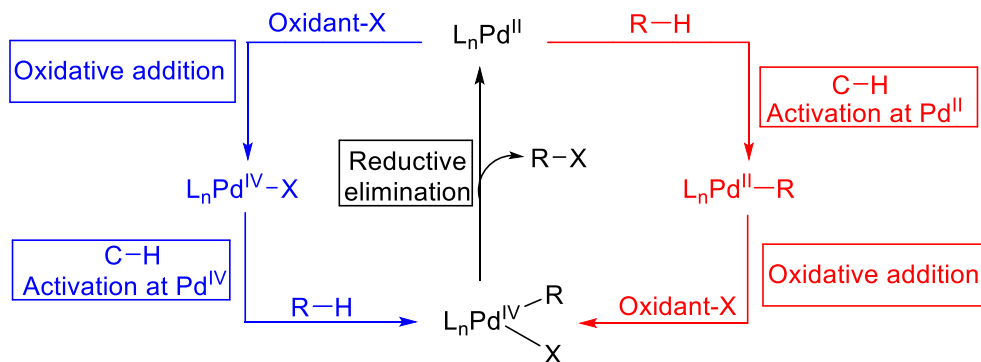
1.1 Palladium in Organometallic Chemistry and Catalysis

Organometallic chemistry is the chemistry of compounds that contain at least one chemical bond between a carbon atom and a metal atom.¹ The first organometallic compound, $\text{K}[\text{Pt}(\text{C}_2\text{H}_4)\text{Cl}_3]\cdot\text{H}_2\text{O}$, was made in 1827 by a Danish chemist, W.C. Zeise² and ever since, platinum and other group 10 metal complexes have played very significant roles in the development of organometallic chemistry and organic synthesis in both stoichiometric and catalytic processes.³ In 1802, William Hyde Wollaston isolated and characterized the metal palladium.^{4,5} Since then, palladium compounds have been widely used for a range of synthetically useful organic transformations such as C-C coupling, C-H functionalization, C-N and C-O bond formation, to afford pharmaceuticals, agrochemicals, and natural and commercial products.⁶⁻¹² Palladium can exist in five different oxidation states (0, +1, +2, +3, +4).^{3,13} The oxidation states of +1 or +3 are not common for palladium.¹⁴⁻¹⁷ The two-electron separation between the common oxidation states of palladium (0, +2, +4) highlights its high tendency to undergo two-electron oxidation or reduction reactions, which will be discussed in greater detail in sections 1.2.2. Moreover, the majority of Pd-catalyzed reactions, such as Negishi,^{18,19} Stille,^{20,21} Sonogashira,²²⁻²⁵ Kumada-Corriu,²⁶⁻²⁸ and Suzuki-Miyaura²⁹⁻³² coupling reactions involve Pd(0)/Pd(II) cycles, which have been intensely investigated over the past decades.^{29,33-35} All of the mentioned reactions start with an oxidative addition to a Pd(0) centre, followed by transmetalation with an organometallic reagent (Scheme 1-1). Finally, there is a reductive elimination from the Pd(II) centre, forming cross-coupled products, along with the regeneration of the Pd(0) catalyst. The year 2010 is remarkable for Pd(0)/Pd(II) catalysis, as the Nobel prize in Chemistry in that year was awarded jointly to Negishi, Suzuki, and Heck for “palladium-catalyzed cross coupling reactions in organic synthesis”.⁹



Scheme 1-1 General mechanism for Pd-catalyzed coupling reactions ($X = Cl, Br, I, OTf$ and $R = aryl, benzyl, vinyl, allyl$ and $M = Zn, Mg, B, Sn$).^{6,9,18-35}

In contrast to the extensive investigation of Pd(0)/Pd(II) catalysis, Pd(II)/Pd(IV) catalysis is less well known due to the long-standing difficulty in isolating and characterizing Pd(IV) complexes.³⁶ Pd(II)/Pd(IV) catalysis eliminates some problems associated with Pd(0)/Pd(II) catalysis such as challenging C(sp³)-C(sp³) coupling due to the β -hydride elimination, palladium-black or nanoparticle formation, and the necessity to conduct the reactions under air- and moisture-free conditions.³⁷⁻³⁹ In recent years, C-H bond functionalization reactions proceeding via Pd(II)/Pd(IV) catalysis have provided a lot of opportunities to access new C-C and C-E (E = N, O, F, Cl, Br, I) bonds that are not easily accessed by the Pd(0)/Pd(II) catalysis. Pd(II)/Pd(IV) catalyzed C-H functionalization reactions are proposed to proceed via either of catalytic cycles, red or blue, illustrated in Scheme 1-2.⁴⁰⁻⁴⁴



Scheme 1-2 General mechanism for Pd(II)/Pd(IV) catalysis that follow either C-H activation at Pd(II) (red) or at Pd(IV) (blue) ($X = C, O, N, F, Cl, Br, I$).

Both of the cycles involve three fundamental steps and the steps are the same, only the order differs. The red cycle starts with a C-H activation reaction at a Pd(II) centre, followed by oxidative addition of an appropriate oxidant to the Pd(II) centre to form a Pd(IV) complex. Finally, a C-X (X = C, N, O, F, Cl, Br, I) bond-forming reductive elimination step from the high-valent palladium centre releases the product and regenerates the Pd(II) catalyst. The vast majority of Pd(II)/Pd(IV)-catalyzed C-H bond functionalizations follow the red cycle;⁴⁵⁻⁴⁷ however, recently some reports have proposed that the C-H activation reaction can also occur at a Pd(IV) centre (Scheme 1-2, blue).^{48,49} Pd(IV) complexes are usually difficult to isolate. Within the past decade, there has been lots of research on the stability of these Pd(IV) intermediates to obtain detailed information about the process occurring at the Pd(IV) centre during catalysis. In both red and blue cycles in Scheme 1-2, additional steps, such as protonolysis or insertion reactions may also occur.⁴⁰⁻⁴⁴

1.2 Common Models for Pd(IV) Stabilization

In the previous section (Section 1.1), the importance of Pd(II)/Pd(IV) catalysis in organic synthesis to form variety of bonds from C-C to C-E (E = O, N, F, Cl, Br, I) was discussed. The bond formation process occurs during the reductive elimination step from a Pd(IV) complex. As mentioned in Section 1.1, Pd(IV) complexes are usually unstable and hard to isolate. Therefore, finding a way to stabilize high-valent palladium centers is helpful to study the bond-forming reductive elimination step in detail and optimize the catalytic reactivity. Ligands have a key role in stability and reactivity of Pd(IV) complexes. In the following sections, Section 1.2.1 and 1.2.2, the ligand design features that have been implicated for Pd(IV) stabilization will be discussed.

1.2.1 *N*-Donor ligands

To date, stable Pd(IV) complexes mainly involve electron-donating *N*-donor ligands that are usually multidentate and hemilabile. In Chart 1-1, some examples of isolated and well-studied Pd(IV) complexes, **1-1** to **1-6**, are shown.^{39,50-54}

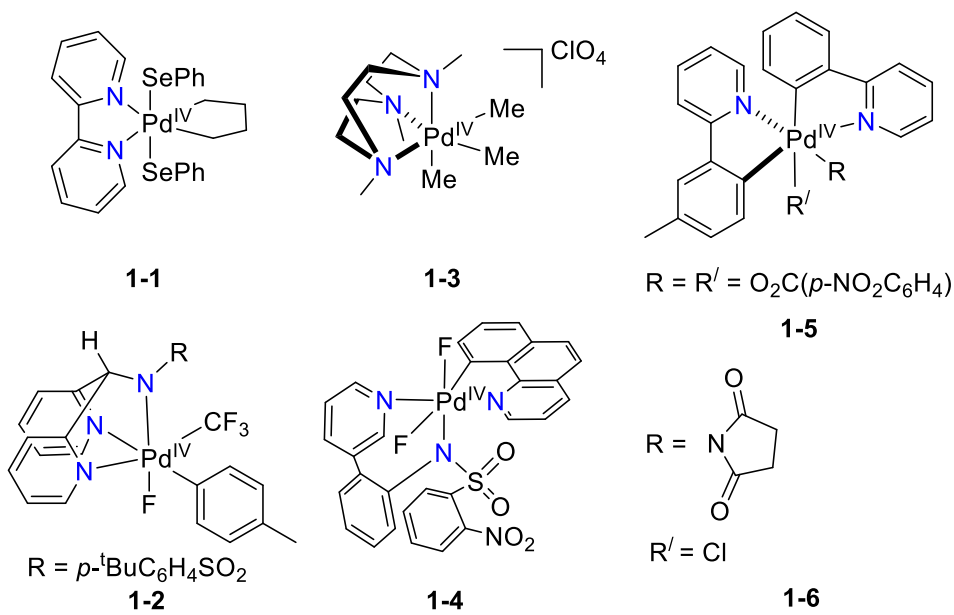
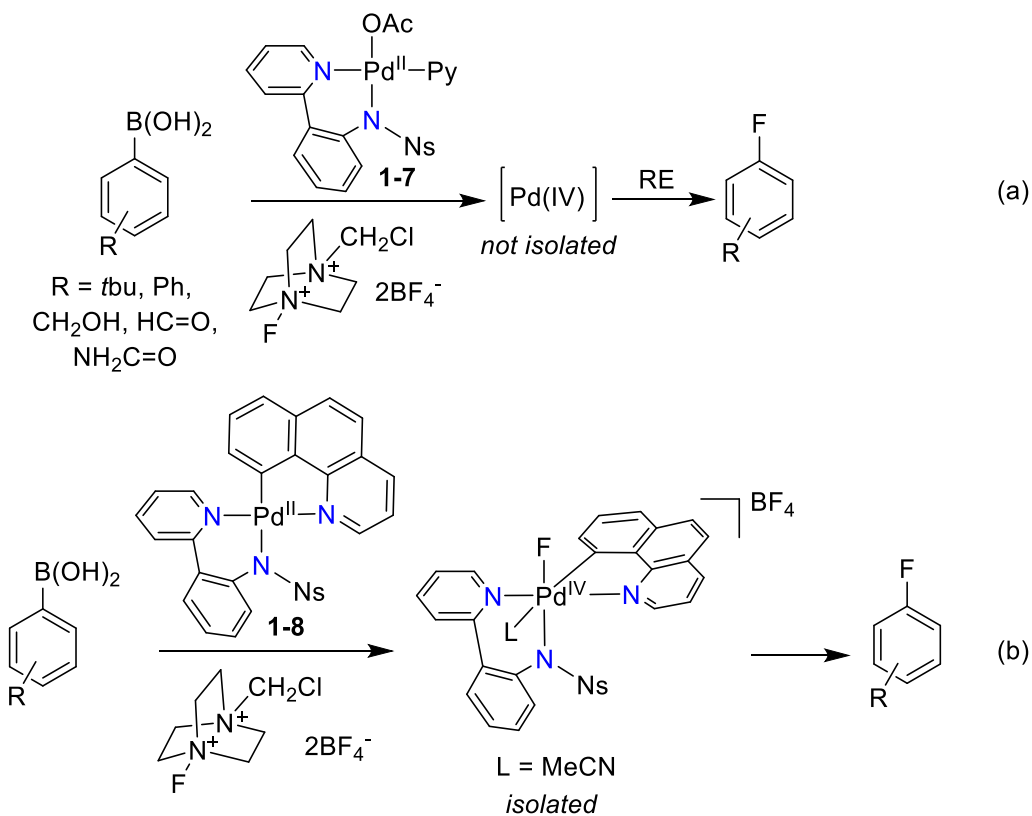


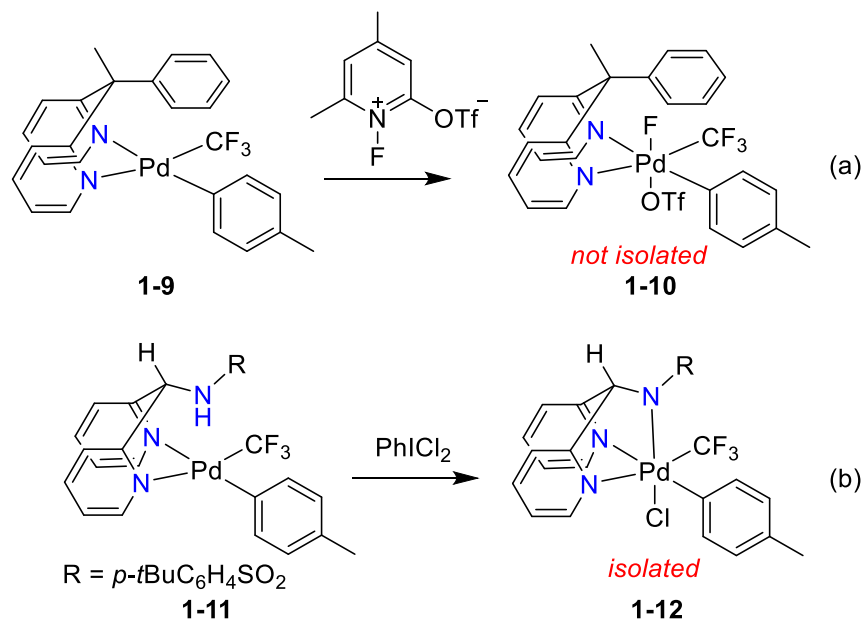
Chart 1-1 Examples of isolated Pd(IV) complexes containing: **1-1**⁵², bidentate bipy-type ligands; **1-2**,⁵³ **1-3**,³⁹ and **1-4**,⁵¹ tridentate *N*-donor ligands; **1-5**⁵⁰ and **1-6**,⁵⁴ phpy-type ligands.

The fluorination of arylboronic acid is an important example, highlighting the role of the ligand in stabilizing high-valent palladium centres (Scheme 1-3).^{51,55-58} It is proposed that the fluorination of arylboronic acids catalyzed by complex **1-7** proceeds via Pd(II)/Pd(IV) catalytic pathway (Scheme 1-3a).⁵¹ However, no Pd(IV) intermediate is isolated to confirm this suggested pathway. In 2010, the Ritter group altered the ligand design in **1-7** and synthesized an analogous complex to **1-7** that has a chelating benzoquinolinylligand (Scheme 1-3b, complex **1-8**).⁵⁸ The benzoquinolinylligand assisted in Pd(IV) isolation; therefore, it was confirmed that Pd(IV) species are involved in the oxidative fluorination of arylboronic acids catalyzed by **1-7**.



Scheme 1-3 Fluorination of arylboronic acids by (a) a Pd-pyridyl complex **1-7** and (b) a Pd-benzoquinolonyl complex **1-8**, (Ns = SO₂-(*p*-NO₂-C₆H₄)).

Another good example of the role of the ligand in Pd(IV) stabilization is reported by Sanford group (Scheme 1-4).⁵³ They determined that reacting the complex **1-9**, containing a *fac*-tridentate *NNC*-type ligand, with an oxidant did not form a stable Pd(IV) complex such as **1-10** (Scheme 1-4a). However, altering the ligand design to a *fac*-tridentate *NNN*-type (complex **1-11**) resulted in the successful isolation of a Pd(IV) complex, **1-12** (Scheme 1-4b).



Scheme 1-4 Ligand effect study on Pd(IV) stabilization.

1.2.2 C-Donor, Cycloneophyl-Type Ligands

Palladacycles containing a cycloneophyl ligand have been considered as good models to study C-C and C-X bond formation from Pd(IV) complexes.^{41,42,59-72} Palladacycles are defined as carbocyclic systems with two or more atoms replaced by a palladium metal.⁷³ Cycloneophyl derivatives of palladacycles in the form of Pd(CH₂CMe₂-*o*-C₆H₄)L₂ (L = COD or PPh₃) stand among the best studied palladacycles, due to their simple synthesis, high reactivity, and high thermal stability (Chart 1-2). Moreover, existence of two methyl groups on the β position limits undesired β-hydride elimination.⁷⁴⁻⁷⁷

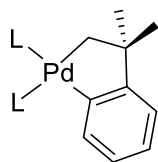
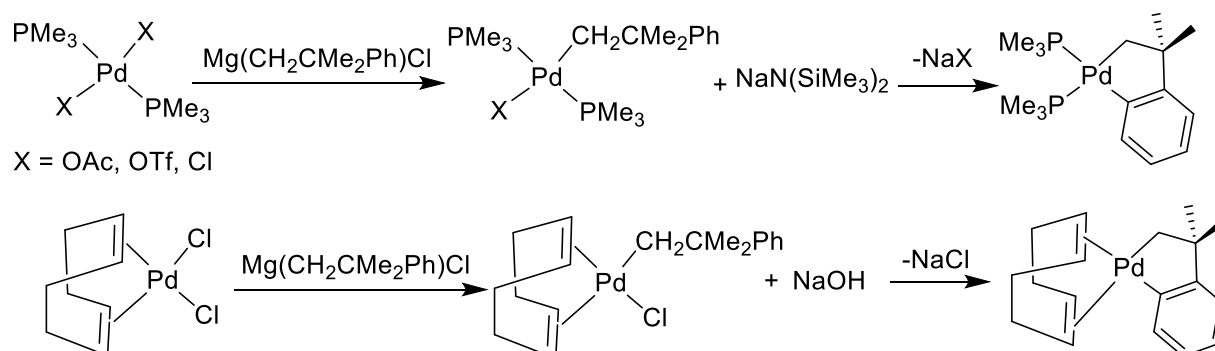


Chart 1-2 General structure for cycloneophyl-palladacycle, Pd(CH₂CMe₂-*o*-C₆H₄)L₂ (L = COD or PPh₃).

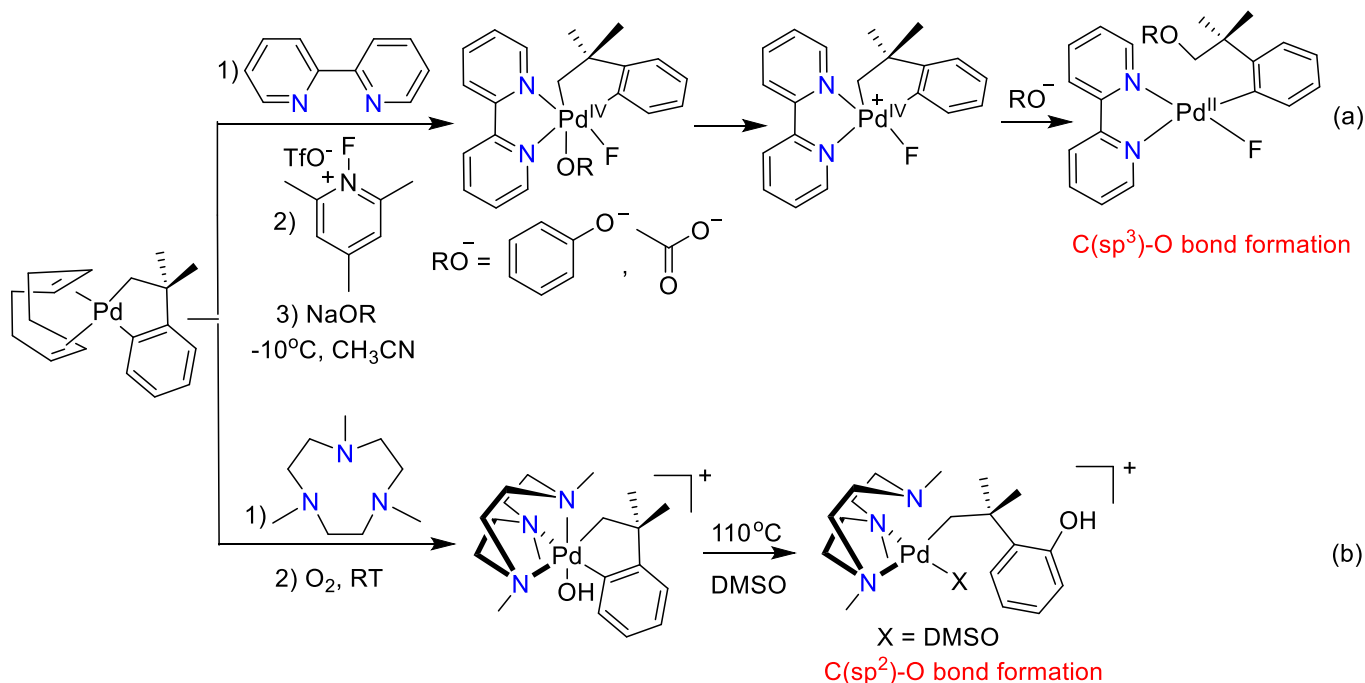
To synthesize a cycloneophyl-palladacycle complex, usually a Grignard reagent is treated with a dihalide complex, such as Pd(COD)Cl₂, to form a halo(alkyl)-Pd complex via a transmetalation step. A transmetalation reaction, which involves a metal-carbon bond activation is a typical method for the preparation of open-chain metal alkyl complexes that have been applied to metallacycle synthesis.¹

Next, the halo(alkyl)-Pd complex that contains a β -phenyl group undergoes cyclometallation by adding a suitable base to assist in an intramolecular C-H activation (Scheme 1-5).^{41,42,50,59,78-83}



Scheme 1-5 Base-induced paladacyclometallation reaction.

Cycloneophyl-palladacycles contain both a Pd-C(aryl) and a Pd-C(alkyl) bond; thus, they are excellent groups to study different reactivity of Pd-C(aryl) versus Pd-C(alkyl) bonds. The selectivity in reactions involving electrophilic Pd-C bond cleavage, reductive elimination with C-X (X = C or heteroatom) bond formation, and insertion reactions with unsaturated reagents has attracted considerable attention in recent years.^{42,59,78} For instance, in 2014, Sanford and Mirica groups separately studied the reductive elimination reaction from two stable palladacycles containing a bidentate and a tridentate ligand, respectively (Scheme 1-6a and 1-6b, respectively).^{42,59} They observed different selectivity in the C-O bond-formation step. Comparing these two studies confirms that the nature of the supporting *N*-donor ligand controls the selectivity of C(sp²)-O versus C-(sp³)-O bond formation; however, a systematic ligand effect study has yet to be completed.



Scheme 1-6 C(sp³)-O and C(sp²)-O bond formation from Pd(IV) intermediates.

1.3 Fundamental Reaction Steps Mediated by Pd(II) or Pd(IV)

As it was mentioned in Section 1.1, during the past two decades, numerous types of bonds are formed via C-H functionalization reactions catalyzed by Pd(II)/Pd(IV) systems. In this section, the fundamentals of each step of Pd(II)/Pd(IV) catalysis will be discussed in detail to optimize the catalytic reactivity.

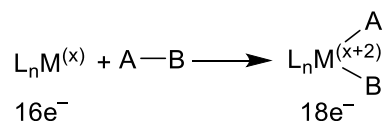
1.3.1 Redox Reactions

Oxidative addition and reductive elimination reactions are discussed in Section 1.3.1.1 and 1.3.1.2, respectively. These reactions, that involve a variation in the oxidation state of the metal centre, are very important in every catalytic and organometallic reactions involving Pd(II)/Pd(IV) cycles.

1.3.1.1 Oxidative Addition

The oxidative addition reaction is considered a very important process in chemistry and plays a major role in both catalysis to give functionalized organics, and the synthesis of organometallics.^{3,84} The oxidative addition reaction involves the oxidation of the metal centre, which is typically a transition metal with 16 or fewer electrons, via the addition of a substrate (A-B; Scheme 1-7). This is favored for reactions where the A-B bond is weaker than the sum of the resulting M-A and M-B bonds. ligands that

promote this reaction are strong donors in order to stabilize the oxidized metal centre. This reaction results in an increase in the coordination number and the formal oxidation state of the metal centre by two.^{2,3,84} Changes in the nature of the substrate (A-B) and the metal centre can alter the pathway for oxidative addition; thus, several types of mechanism have been proposed that are discussed in the subsequent sections.

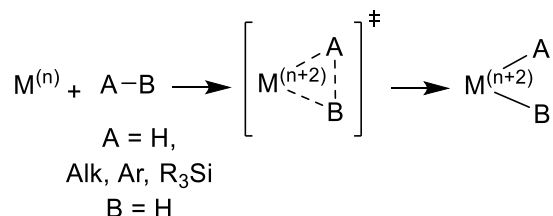


Scheme 1-7 General schematic of the oxidative addition reaction.

Oxidative addition at Pd(II) complexes generally follow the two-electron pathway, as Pd(II) complexes have 16 electrons, d^8 electronic configuration and square planar geometry, leaving two vacant coordination sites for the substrate to bond to the metal centre. This results in 18 electron Pd(IV) complexes that have a d^6 electronic configuration and adopt octahedral geometry.^{44,85,86} As discussed in Section 1.1, Pd(IV) complexes are not as stable as Pd(II) complexes. However, it has been shown recently that oxidative addition of appropriate oxidants to Pd(II) complexes containing *N*-donor ligands, stable Pd(IV) complexes can be successfully isolated (Section 1.2).^{41,59-61,87}

1.3.1.1.1 Three-Centre Concerted Mechanism

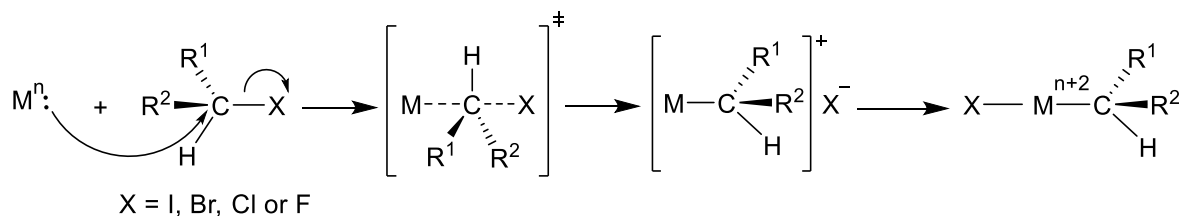
The three-centre concerted mechanism for oxidative addition reactions is usually observed for non-polar substrates such as H₂, alkanes (R-H), arenes (Ar-H), and silanes (R₃Si-H). These substrates are often difficult to activate; thus, the substrate first binds as a σ -complex, then, it undergoes R-H bond breaking due to strong back donation from the metal into the vacant R-H σ^* orbital (Scheme 1-8). This concerted mechanism results in a product with *cis* geometry.^{3,88,89}



Scheme 1-8 General schematic of the three-centre concerted oxidative addition reaction.

1.3.1.1.2 S_N2 Mechanism

The bimolecular S_N2 mechanism of oxidative addition reactions is typically observed for polar electrophilic substrates such as methyl, alkyl, and benzyl halides (R-X, X: F, Cl, Br or I).² In the S_N2 pathway, the nucleophilic attack of the metal centre at the least electronegative atom of the substrate form a five-coordinate intermediate, followed by breaking the C-X bond of the substrate and forming a cationic intermediate. Subsequently, the anionic ligand coordinates to the metal and forms a trans configuration at the metal centre (Scheme 1-9).^{2,73,84}



Scheme 1-9 General schematic of the bimolecular S_N2 oxidative addition reaction.

The bimolecular S_N2 oxidative addition mechanism displays all the characteristics and reactivity orders of a typical S_N2-type reaction as observed in organic chemistry.² The reactions follow second order kinetics and involves an inversion of configuration at a chiral carbon of the substrate. The rate of the reaction is accelerated in the presence of polar solvents. Moreover, the reactivity of the alkyl halides in this mechanism is as follows: Me > primary > secondary > tertiary and I > Br > Cl > F.^{2,73} In reactions with square planar complexes, trans oxidative addition is usually observed. The bimolecular S_N2 mechanism of the oxidative addition reactions is also observed for halogens (X₂, X = F, Cl, Br, I). Sometimes the product stereochemistry is determined by thermodynamics and products of trans addition (usually the kinetic product), cis addition or an equilibrium mixture of these compounds can be obtained.²

1.3.1.2 Reductive Elimination from Pd(IV)

Reductive elimination is the microscopic reverse of oxidative addition and is considered as the most important step in Pd(II)/Pd(IV) catalysis since it is the product forming step. The reductive elimination reaction involves the reduction in coordination number and oxidation state of the metal centre by two (Scheme 1-10). Two covalent substituents (A and B), where A and/or B is a carbon atom, break their bonds with the metal and form a new A-B bond.^{1,3,13} Steric properties play a significant role in the rate of the reductive elimination reaction. Sterically bulky ligands promote the reductive elimination

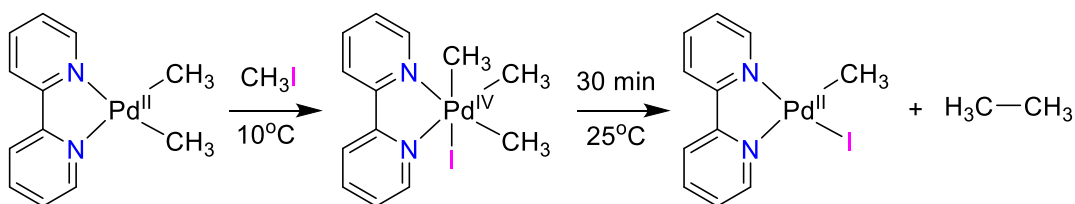
reaction. Generally, ligands which are to be lost must be *cis* to each other in order to eliminate by the concerted mechanism. Thus, the ligands that are in a *trans* arrangement undergo an isomerization reaction to form a *cis* isomer prior to the reductive elimination step. For the concerted mechanism, the stereochemistry at the leaving group ligands is retained.³



Scheme 1-10 General schematic of the reductive elimination reaction.

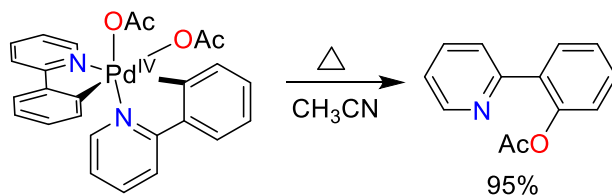
Pd(IV)RR' complexes readily undergo reductive elimination to form new types of C-C and C-heteroatom bonds, such as C(sp²)-C(sp³), C(sp³)-C(sp³), C(sp²)-E and C(sp³)-E (E = O, N, F, Cl, Br, I), which are difficult to form via traditional Pd(0)/Pd(II) catalysis. Isolating Pd(IV) complexes helps in understanding the details of the process that is occurring at the Pd(IV) complex during the bond-forming reductive elimination step.

The first example of C-C bond formation from a well-defined and crystallographically characterized Pd(IV) complex was reported by Canty in 1986. He has shown that the Pd(IV) complex, *fac*-[(bpy)Pd^{IV}(CH₃)₃(I)], undergoes a C-C bond-forming reductive elimination to form ethane (Scheme 1-11).⁹⁰



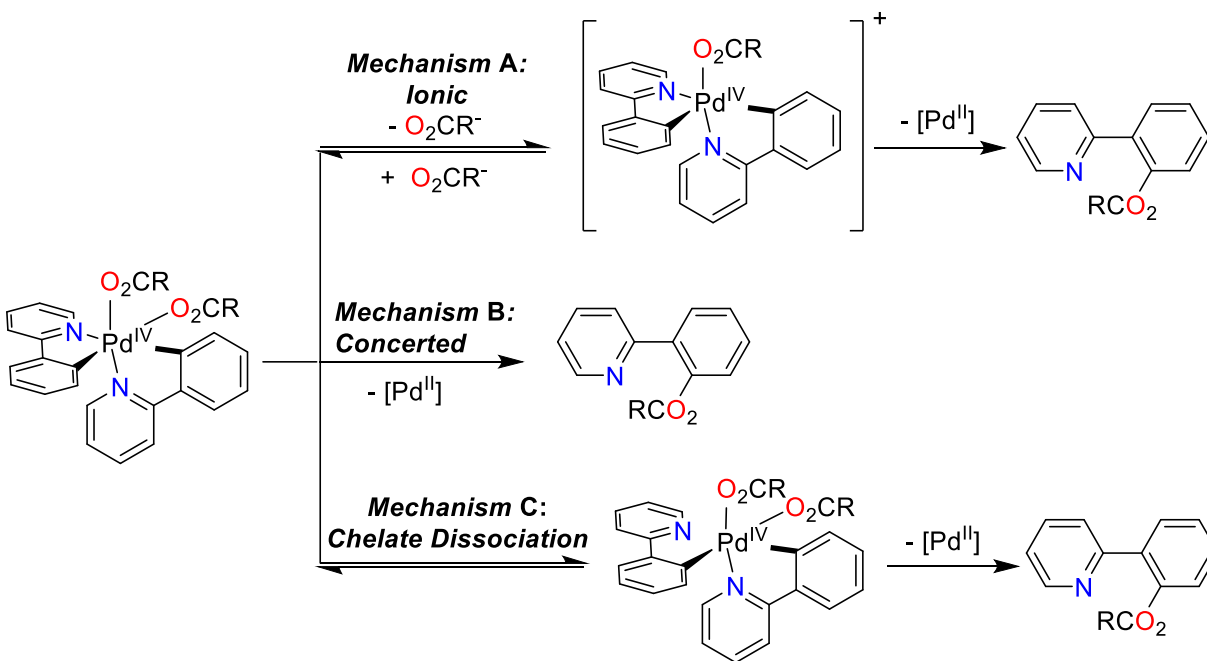
Scheme 1-11 Oxidative addition of methyl iodide to Pd(II), followed by C-C bond-forming reductive elimination.

In 2009 for the first time, Sanford *et. al* investigated the mechanistic details for a C-O bond-forming reductive elimination reaction from a stable Pd(IV) complex (Scheme 1-12).⁹¹



Scheme 1-12 C-O bond forming reductive elimination reaction.

Three mechanisms were considered for the C-O bond forming reductive elimination reaction (Scheme 1-13). The first possible route is an ionic mechanism (**A**), which involves carboxylate ligand dissociation to form a five-coordinated cationic palladium intermediate, followed by a reductive elimination reaction. The second possibility is a concerted-type mechanism (**B**), where a reductive elimination reaction occurs directly from the six-coordinated palladium complex. The third option is a chelate dissociation mechanism (**C**), which involves a chelate dissociation followed by a reductive elimination reaction from a five-coordinated palladium intermediate.



Scheme 1-13 Proposed mechanisms for C-O bond-forming reductive elimination reaction.

Based on the experimental observations, **C** was the initially proposed as the favored mechanism.⁵⁰ No dependence of the rate of the reductive elimination reaction on solvent polarity was observed. This observation is in contrast with an ionic-type mechanism. Therefore, they concluded that the reaction does not follow mechanism **A**. To differentiate between mechanisms **B** and **C**, they compared the rate

of reductive elimination reaction of two palladium complexes having two different NC-type ligands with different rigidities. Having a less rigid NC-type ligand, increased the overall rate of reductive elimination, which is consistent with the ease of nitrogen dissociation to form a neutral five-coordinated palladium complex and mechanism **C**. A few years later, Liu and co-workers based on theoretical studies, proposed that reductive elimination follows mechanism **B**.⁹² Mechanism **B** was supported with a close match between the calculated and experimental activation energy barriers. However, Sanford *et. al* in a more recent detailed study concluded that the reductive elimination reaction follows mechanism **A**.⁹¹ The Sanford group observed that the starting Pd(IV) complex undergoes rapid exchange between bound and free carboxylate group at low temperatures. The starting Pd(IV) is coordinatively saturated and a dissociation of a carboxylate ligand to form an ionic five-coordinated intermediate is necessary for the exchange. These studies indicate that the mechanism for C-heteroatom bond-forming reductive elimination reactions from Pd(IV) complexes is still not well understood.

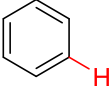
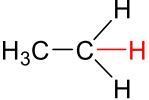
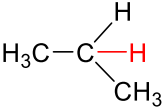
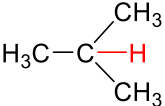
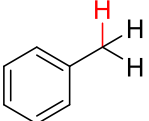
1.3.2 Redox Neutral Reactions

Pd(II)/Pd(IV) catalysis sometimes involves some additional steps during which the oxidation state of the palladium centre does not change. C-H activation, insertion and protonolysis reactions are considered as three major steps that will be discussed in Section 1.3.2.1, 1.3.2.2 and 1.3.2.3, respectively.

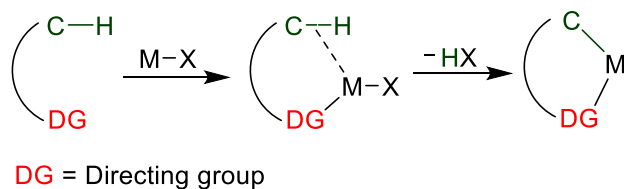
1.3.2.1 Activation of C-H Bonds

Alkanes or saturated hydrocarbons are the most abundant and least expensive chemical feedstock available.⁹³ Therefore, finding a way to cleave a C-H bond of the alkanes or arenes to transform them into more valuable compounds such as alcohols, aldehydes, ethers, and acids is worthwhile. This process is called C-H activation, and is considered as a challenging process due to inertness of C-H bonds,^{94,95} confirmed by the high bond dissociation energies (BDEs) and high pKa values (Table 1-1).⁹⁶ However, there have been several examples of catalytic C-H activation and functionalization in the literature utilizing a transition metal as a catalyst such as platinum, palladium, rhodium, and iridium. Transition metals react with a C-H bond of alkanes or arenes, forming M-C bonds that are far more reactive than C-H bonds. Therefore, in comparison with C-H bonds, C-M bonds can be converted to new functional groups under milder conditions.⁹⁴⁻¹⁰⁰

Table 1-1. Bond dissociation energies (BDEs) and $pK_a(\text{aq})$ values of some common C-H bonds.⁹⁶

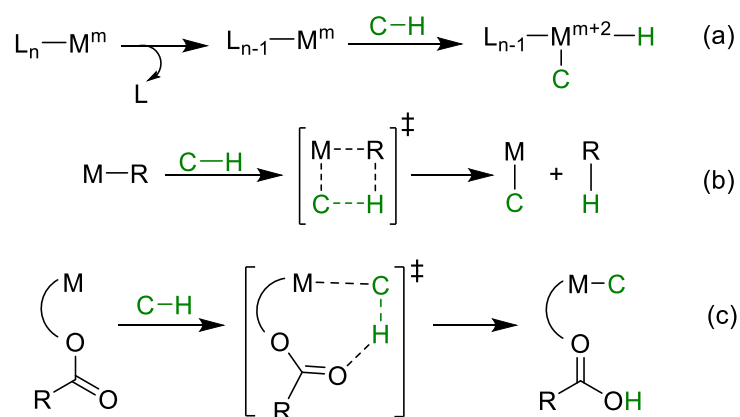
	BDE (kJ/mol)	pK_a value
	465	40
$\text{H}_3\text{C}-\text{H}$	440	56
	410	50
	400	
	390	71
	368	41

Another challenge in C-H activation is related to controlling the site selectivity in molecules that have various C-H bonds. Diverse strategies have been employed to improve this issue. In metal-mediated C-H activations, tuning the electronics and sterics of the ancillary ligand at the metal centre is among the strategies employed to overcome this issue. However, a clear trend in optimal ligand properties has not yet emerged. Using substrates that contain coordinating ligands as directing groups is also another approach to overcome the site selectivity challenge in C-H activation.¹⁰¹ These directing groups can be *N*-donor types such as pyridine, or *O*-donor types such as ketones and esters.^{102–104} The directing group binds to the metal centre as a ligand and therefore, it selectively brings a C-H bond close to the metal centre to increase the rate of an intramolecular C-H activation reaction (Scheme 1-14).

**Scheme 1-14** Directing group facilitating C-H activation.

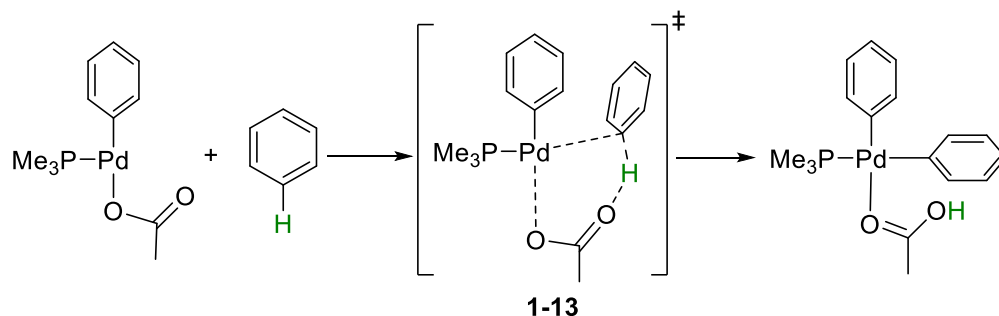
Several mechanisms are proposed for C-H activations such as oxidative addition and σ -bond metathesis (Scheme 1-15, a and b).^{105–107} In the oxidative addition mechanism, a ligand dissociates from a metal

complex to make an open coordination site (Scheme 1-15a). Then, the metal centre undergoes oxidative addition, forming a M-H and a M-C bond. The σ -bond metathesis mechanism, which is mostly common to d^0 metals, involves a four-centre transition state intermediate (Scheme 1-15b).



Scheme 1-15 General mechanism of a C-H activation reaction via (a) oxidative addition, (b) σ -bond metathesis and c) CMD-type C-H activation mechanisms.

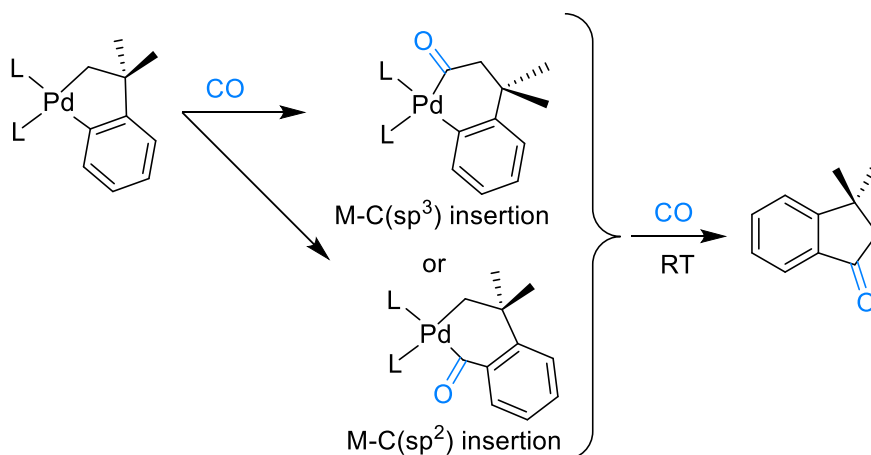
The concerted metallation-deprotonation (CMD), also known as internal electrophilic substitution (IES) and the ambiphilic metal-ligand activation (AMLA), reaction is the other proposed mechanism for C-H activation.¹⁰⁸⁻¹¹⁰ This type of C-H activation, which is assisted by an intramolecular base, has been considered as an efficient alternative to traditional activation methods over the past two decades (Scheme 1-15c).^{108,109} The CMD pathway occurs through a cyclic transition state, in which a basic ligand on the metal, typically a carboxylate, deprotonates the C-H bond with the formation of the M-C bond in a concerted manner. Based on the computational and experimental analysis, Gorelsky *et. al* proposed a CMD mechanism for a Pd-catalyzed C-H bond activation of benzene (Scheme 1-16).^{109,111} Based on the calculated activation barriers, it was concluded that the acetate ligand behaved as an internal base and assisted in binding of benzene at the Pd centre and the formation of intermediate **1-13**.



Scheme 1-16 Proposed mechanism for Pd-catalyzed C-H activation of benzene.

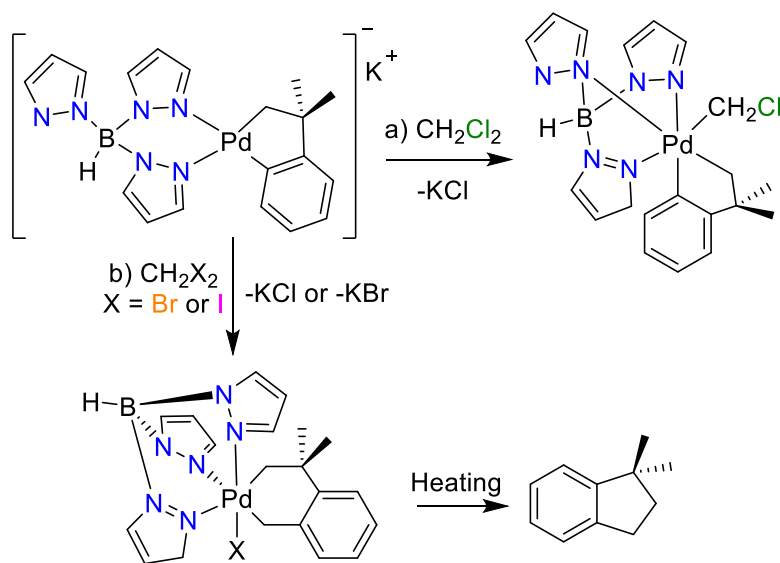
1.3.2.2 Insertion Reaction

The reaction of palladacycles with unsaturated organic and inorganic molecules, such as CO, CO₂, and SO₂ lead to their insertion into the Pd-C bonds and the expansion of the ring. Afterward, the reductive elimination reaction results in carbocyclic or heterocyclic product formation via C-C or C-heteroatom bond formation (Scheme 1-17).¹¹²⁻¹¹⁶ If the Pd-C bond belongs to a cycloneophyl-palladacycle complex with both Pd-C(sp²) and Pd-C(sp³) bonds, the reaction leads to selective insertion, which can be of high interest in selective catalysis.⁷⁸ Many factors affect the selective insertion of small molecules on Pd-C bonds in cycloneophyl-palladacycles, such as electronic and steric effects of the supporting ligand (Scheme 1-17, ligand L). However, systematic studies of the supporting ligand effect on selective insertion into a Pd-C bond are needed.



Scheme 1-17 CO insertion into Pd-C bond in cycloneophyl-palladacycle. ^{112,113}

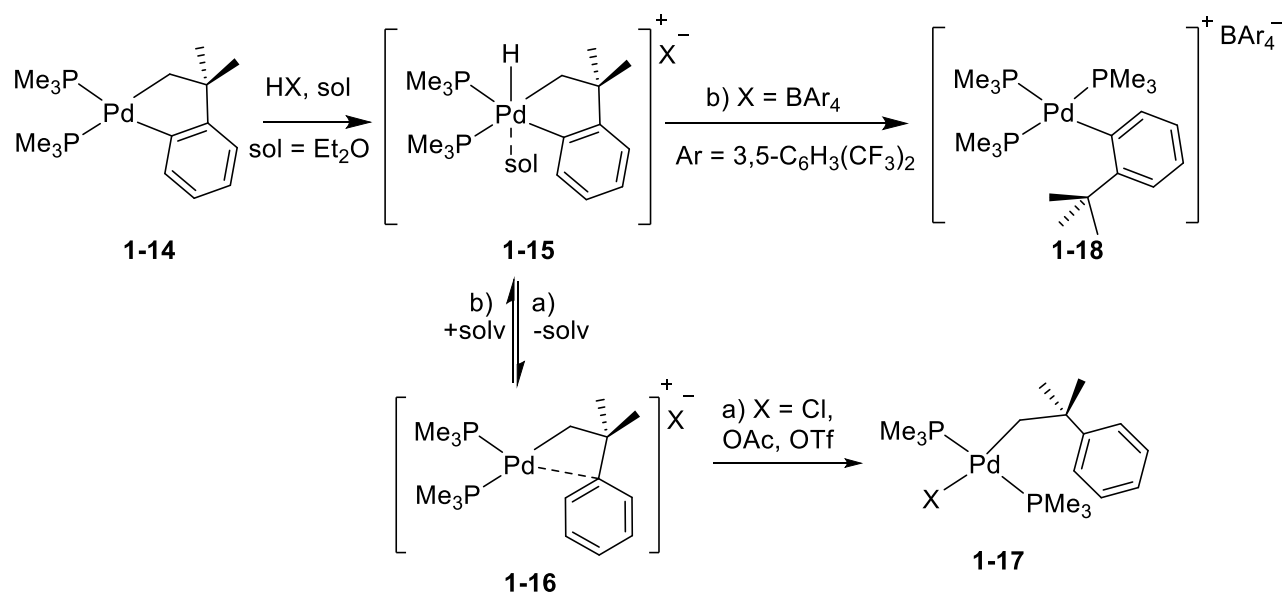
Palma *et. al* have studied cycloneophyl-palladacycle(II) complexes containing rigid hydrotrispyrazolylborate ligands.⁶³ They have reported that the reaction of CH₂Cl₂ with the cationic palladacycle gives rise to stable Pd(IV) formation via an oxidative addition reaction of a C-Cl bond (Scheme 1-18a). Meanwhile, the analogous reaction of the cycloneophyl-palladacycle(II) with CH₂I₂ or CH₂Br₂ results in the formation of a six membered palladacycle as a result of selective methylene-insertion into the Pd-C(sp²) bond (Scheme 1-18b). A C(sp³)-C(sp³) bond formation reductive elimination reaction from the six membered palladacycle complex forms 1,1-dimethyl-indane. The ability of CH₂-migration into the Pd-C(sp²) bonds has been attributed to the strength of the CH₂-X bonds, which can be anticipated considering the electronegativity and the size of the halomethyl ligand.



Scheme 1-18 a) Pd(IV) chloromethyl formation through oxidative addition of dichloromethane to a palladacycle(II). b) six membered Pd(IV) iodide or bromide formation through methylene insertion into Pd-C(sp²) bond.

1.3.2.3 Protonolysis Reaction

The cleavage of a Pd-C σ -bond in a reaction of palladacycles with a Bronsted acid is called protonolysis. The protonolysis of one Pd-C bond of a palladacycle is the reverse of the concerted C-H activation reaction, by which a palladacycle is formed. The protonolysis reactions usually happen selectively in neophyl-type compounds, where there is an option between C(sp³) and C(sp²) protonolysis. The steric and electronic effects of the ancillary ligand affect the selectivity of C(sp³) versus C(sp²) protonolysis.^{61,62,64,65,78,82,117} For instance, Campora *et. al* reported Pd-C(sp²) bond protonolysis by the reaction of one equivalent of HX (X = Cl, OAc or OTf) with a cycloneophyl-Pd(II) complex **1-14** (Scheme 1-19, path a).⁸² For the mechanism, they suggested that first, a Pd(IV)-hydride intermediate, **1-15**, is formed.¹¹⁸ They hypothesised that there is a higher kinetic barrier to the reorientation of the orbital of Pd-C(sp³), relative to C(sp²), to form the C-H bond. Therefore, **1-15** is expected to have a hydrogen transfer to C(sp²) to form the cationic intermediate **1-16**. The highly electrophilic palladium centre in **1-16** is stabilized by π -bonding interactions with the C_{ipso} of the phenyl group.^{119,120} Afterwards, X, which is a coordinating-anion, coordinates to form **1-17**. However, if X is a noncoordinating-anion such as $\text{BAr}^{\text{F}}_4^-$ ($\text{Ar}^{\text{F}} = 3,5\text{-C}_6\text{H}_3(\text{CF}_3)_2$), the reaction will be reversed to give **1-15** (Scheme 1-19, path b). Eventually, **1-15** undergoes the kinetically less-favourable hydrogen transfer to C(sp³), followed by phosphane substitution to form **1-18** via Pd-C(sp³) bond protonolysis.



Scheme 1-19 Protonolysis of (a) Pd-C(sp²) bond, where X is a coordinating anion and (b) Pd-C(sp³) bond, where X is a non-coordinating anion.

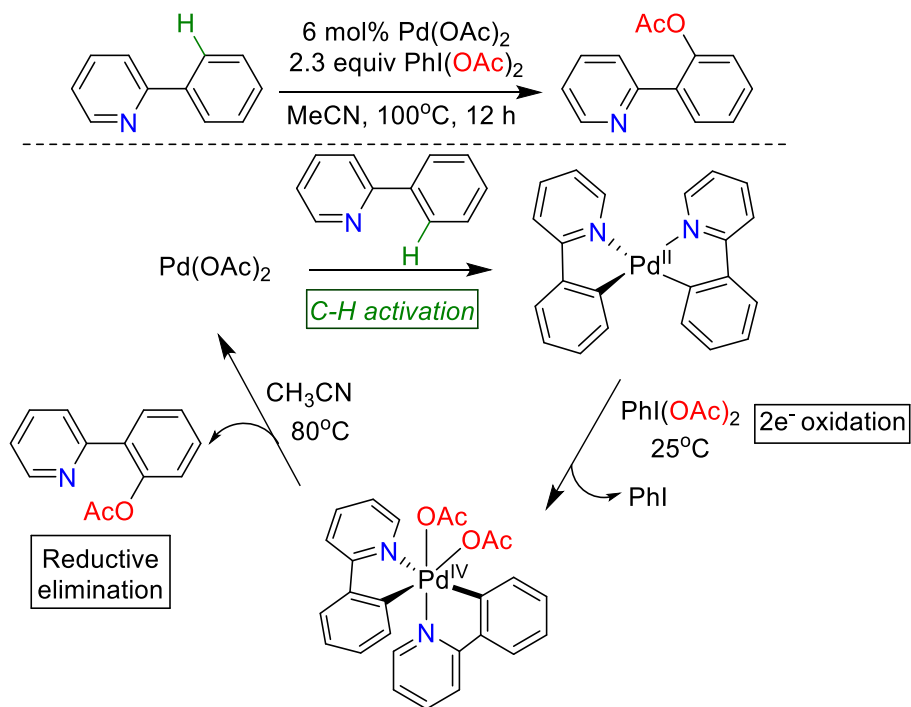
1.4 Pd(IV)-Catalyzed C-H Functionalization

In recent years, Pd(II)/Pd(IV) catalysis has been used in numerous studies for C-H bond oxidative functionalization reactions in organic synthesis. Pd(II) complexes are compatible with diverse types of oxidants, such as PhI(OAc)₂,¹²¹ N-chlorosuccinimide (NCS),¹²² oxone,¹²³ O₂, and H₂O₂,⁵⁹ for easy oxidation to Pd(IV) intermediates. Afterward, in the reductive elimination step, new types of bonds, such as C-E (E = C, O, N, S, halogens) are made. Formation of these bonds were difficult via traditional Pd(0)/Pd(II) catalysis.^{43,100,122,124–127} Below, the effect of different types of oxidants on C-H bond functionalization reactions will be discussed.

1.4.1 Iodine(III)-based Oxidants in C-H Bond Activation Reactions

After the success in using hypervalent iodine reagents in Pd-catalyzed cross-coupling reactions, researchers focused on using I^{III} reagents, especially PhI(OAc)₂, as in oxidative C-H activation reactions.^{91,121,125,127–129} For instance, Sanford *et. al* reported a Pd-catalyzed acetoxylation of C(aryl)-H bonds, using PhI(OAc)₂ as an oxidant (Scheme 1-20).^{91,128} Various pyridine derivatives acted as directing groups to form *ortho*-acetoxyated products. To probe the mechanism for this C-H functionalization reaction, Sanford *et. al* studied the stoichiometric reaction. They suggested that the functionalization reaction starts with C-H activation of the substrate to form cyclopalladated

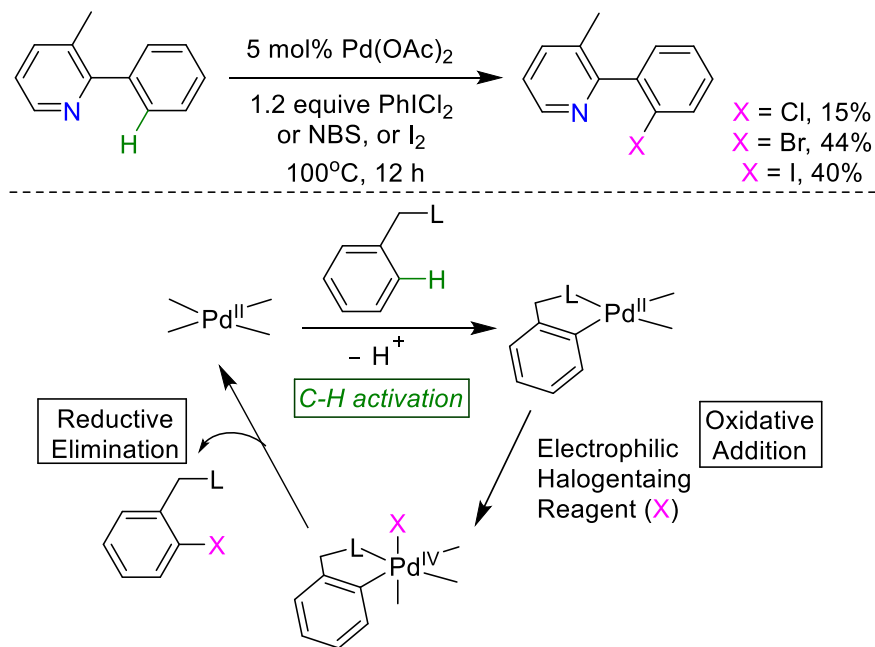
intermediate. Afterward, by adding an oxidant, Pd(II) is oxidized to Pd(IV), which is stable at -35°C . In the final step, the C(aryl)-O bond-forming reductive elimination reaction affords the product. The formation of toxic PhI along with the high price of hypervalent iodine reagents can be counted as the disadvantages of using these compounds.



Scheme 1-20 Pd-catalyzed C(aryl)-H acetoxylation using $\text{PhI}(\text{OAc})_2$ as an oxidant.

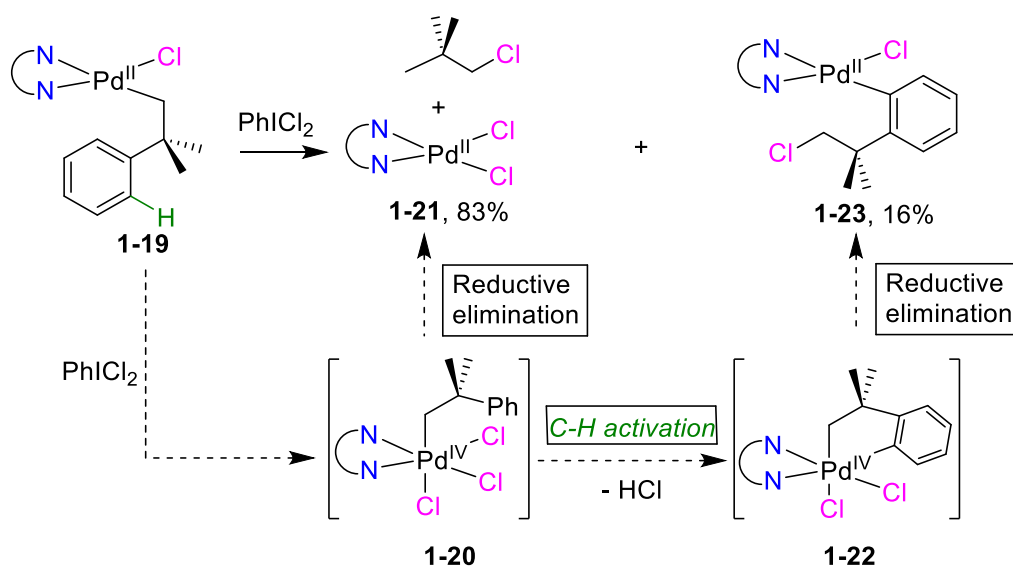
1.4.2 Halide-based Oxidants in C-H Bond Activation Reactions

Halogenated compounds are very important components of biologically active molecules and pharmaceuticals in general,¹³⁰ as well as reagents for synthesis, such as Grignard reagents.¹³¹ *N*-chlorosuccinimide (NCS),^{54,132} *N*-bromosuccinimide (NBS),^{122,132} PhICl_2 ¹²⁵ and molecular halogens, X_2 ($\text{X} = \text{Cl}, \text{Br}, \text{I}$)^{133,134} have been used in all types of C-C cross coupling reactions. Sanford *et. al* proposed a mechanism for Pd-catalyzed ligand-directed oxidative C-H bond halogenation reactions.¹²² The proposed catalytic cycle starts with a ligand-directed C-H activation at the Pd(II) centre to form a palladacycle. The resulting palladacycle is then oxidized to Pd(IV) by an X_2 oxidant, and this is followed by C-X bond forming to form the halogenated organics (Scheme 1-21). The C-halogen bond formation proceeds either by intramolecular C-X bond elimination from the metal centre,¹³⁵ or by the attack of an external nucleophile (X) in an $\text{S}_{\text{N}}2$ -like reaction.¹³⁶



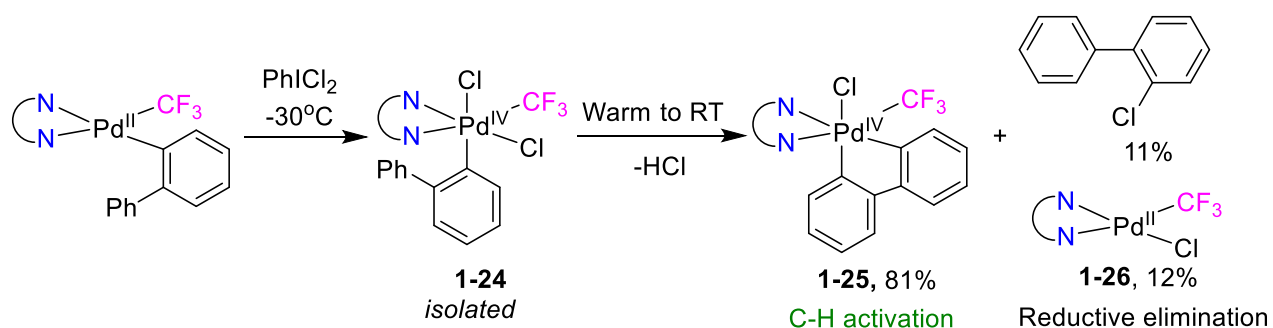
Scheme 1-21 C-H bond halogenation in 3-methyl-2-phenylpyridine and the proposed mechanism for C-H bond halogenation.

Sanford *et. al* reported an oxidation of a Pd(II) complex **1-19** with PhICl₂, resulting in C-Cl bond formation (Scheme 1-22).¹²⁵ The addition of the oxidant resulted in the formation of two new Pd(II) complexes, **1-21** and **1-23**, rather than a Pd(IV) complex. For the formation of **1-21**, they hypothesized a reductive elimination C(aryl)-Cl bond formation from a Pd(IV) intermediate **1-20**. Meanwhile, in order to make **1-23**, a C-H bond activation from **1-20** forms **1-22**, followed by C(aryl)-Cl bond-forming reductive elimination. Complex **1-23**, which is the result of a C-H activation process, was a minor product. Sanford decided to design a new system to increase the rate of C-H activation and slow down the competing reductive elimination process to elucidate the mechanism for C-H activation at Pd(IV) centres.



Scheme 1-22 Pd(II) oxidation and study the C-H activation reaction versus C-Cl bond-forming reductive elimination (*N*-*N* ligand = 4,4'-Di-*tert*-butyl-2,2'-dipyridyl, dtbpy).

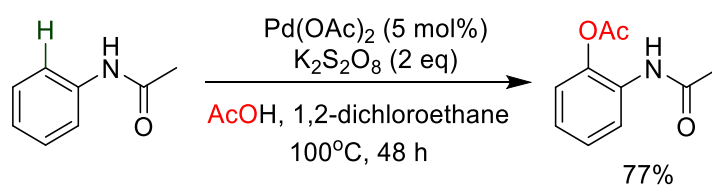
In the new system, chloride was replaced with CF₃, which is less prone to reductive elimination,⁵³ and a biphenyl ligand was placed as a substrate to limit the conformational flexibility of the C-H bond in the substrate (Scheme 1-23).¹²⁵ The major product of the oxidation reaction was complex **1-25**, which is the result of C-H activation from the isolated intermediate **1-24**. Complex **1-26**, which is the result of C(aryl)-Cl bond-forming reductive elimination, is the minor product (12%). These observations demonstrated that high oxidation state Pd can mediate the C-H activation.



Scheme 1-23 Formation of a stable Pd(IV) complex and study of the C-H activation reaction versus C-Cl bond-forming reductive elimination (*N*-*N* ligand = 4,4'-Di-*tert*-butyl-2,2'-dipyridyl, dtbpy).

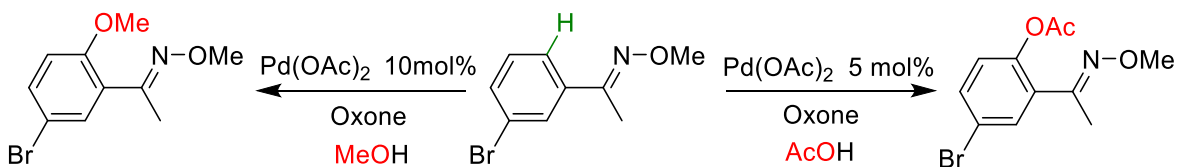
1.4.3 Peroxide-based Oxidants in C-H Bond Activation Reactions

Peroxide-based oxidants, such as *meta*-chloroperoxybenzoic acid (mCPBA),^{137–139} *tert*-butyl hydroperoxide (*t*-BuOOH),¹³⁴ potassium persulfate (K₂S₂O₈),^{123,140,141} and potassium peroxymonosulfate (oxone)^{123,142,143} are much less expensive than hypervalent iodine oxidants. The Pd-catalyzed oxygenation of C(aryl)-H bonds has been performed using peroxide-based oxidants in acetic acid or methanol as the solvent.^{122,141} It is proposed that oxidants promote the oxidative addition reaction to form a Pd(IV) intermediate, while the solvent acts as the nucleophile for C-O bond formation. For instance, Wang *et. al* reported a Pd-catalyzed *ortho*-acetoxylation using K₂S₂O₈ as an oxidant in acetic acid (Scheme 1-24).¹⁴¹



Scheme 1-24 Pd-catalyzed C(aryl)-H acetoxylation using K₂S₂O₈ as an oxidant

Sanford *et.al* also reported a Pd(II)-catalyzed acetoxylation of C(aryl)-H bonds using oxone as an oxidant in acetic acid or methanol as the solvent.¹²³ Substrates with a variety of directing groups including oxime ethers, amides, and isoxazolines reacted in acetic acid solvent to afford aryl esters, and in alcohol solvents to afford aryl ethers (Scheme 1-25). For the mechanism, Sanford proposed the formation of a Pd(IV) alkoxide intermediate by the addition of oxone, which could undergo C-O bond-forming reductive elimination, based on analogous stable Pt(IV) intermediate.^{144,145}

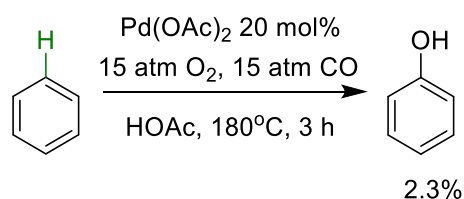


Scheme 1-25 Pd-catalyzed C-H bond oxygenation reaction using oxone as oxidant.

1.4.4 Green Oxidants in C-H Bond Activation Reactions

The development of efficient oxidative C-H functionalization reactions using inexpensive, environmentally benign, and green oxidants, such as hydrogen peroxide (H₂O₂) and dioxygen (O₂) remains a significant challenge in modern chemistry.^{37,146–150} The mechanisms of the Pd-catalyzed

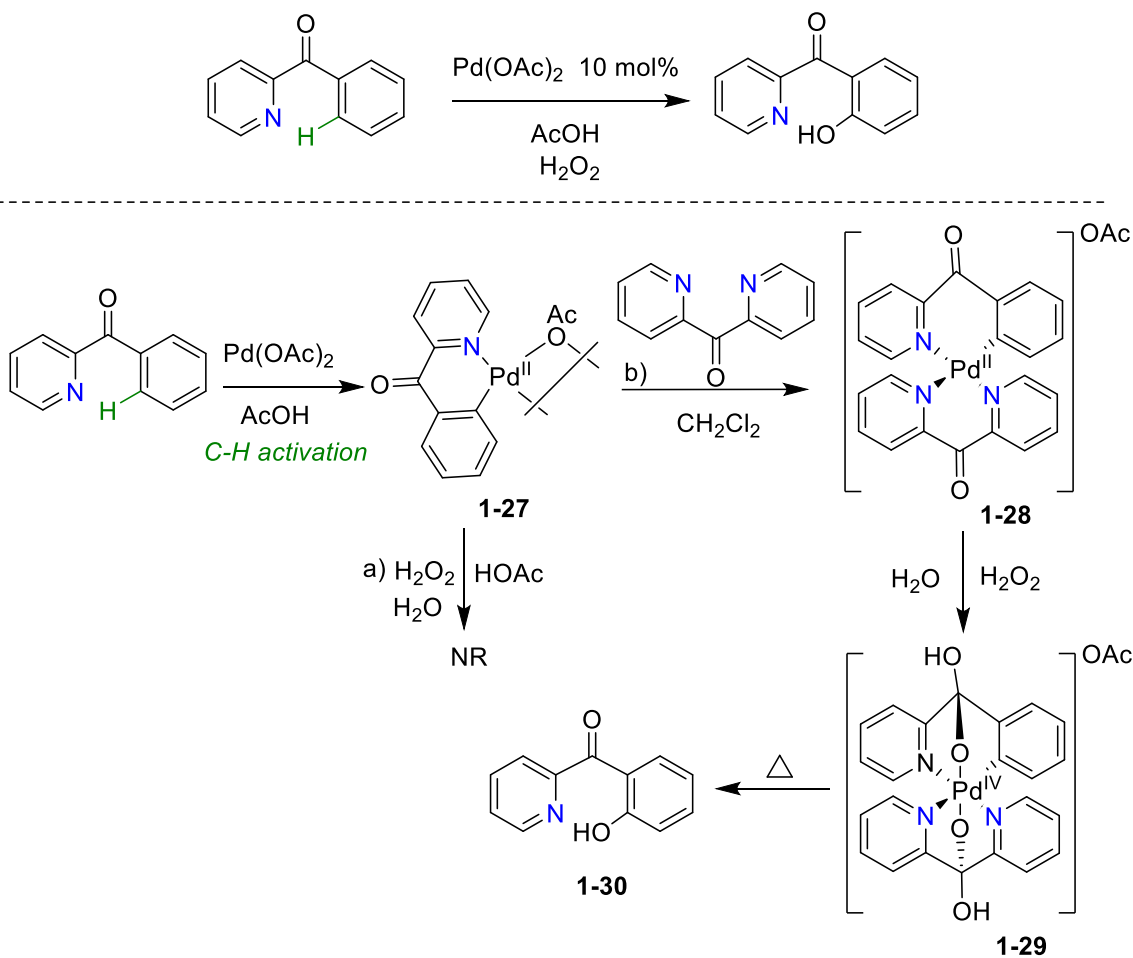
oxidative C-H functionalization reactions using $\text{PhI}(\text{OAc})_2$, PhICl_2 , and *N*-halosuccinimides as oxidants have been studied in great detail; nevertheless, little is known about Pd-catalyzed C-H oxidation with H_2O_2 ^{97,151–157} and O_2 ,^{149,150,153,158–160} which can offer the potential of transforming hydrocarbons into more valuable products such as alcohols, with water as the only by-product. Fujiwara *et. al* designed a catalytic system using $\text{Pd}(\text{OAc})_2$ and dioxygen as the oxidant for the first time in 1990 to convert benzene into phenol.¹⁶¹ However, their system required harsh conditions, the reported yield was low and they did not study the mechanism (Scheme 1-26).



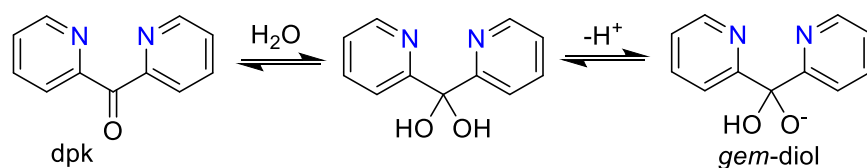
Scheme 1-26 Pd-catalyzed C-H activation using O_2 as an oxidant.

Since then, the Vedernikov, Liu, Yu and Mirica groups have tried to isolate stable Pd(IV) complexes using O_2 and H_2O_2 as oxidants. These Pd(IV) complexes have been proposed as key intermediates in oxidative Pd(II)-catalyzed C-H activation using O_2 or H_2O_2 as oxidants, such as hydroxylations.

Vedernikov *et. al* reported the first mechanistic study on the C-O bond-forming reductive elimination reaction from an isolated Pd(IV)-C(aryl) complex, to form an aryl alcohol product in water. This study is useful for the design of systems for Pd-catalyzed C-H functionalization using green oxidants (Scheme 1-27).^{152,162} In their reaction, first the substrate was added to $\text{Pd}(\text{OAc})_2$ to form the complex **1-27** via a C-H bond activation step. Then a ligand exchange reaction between the labile acetate and di-2-pyridyl ketone (dpk) ligand, which had been used before to support Pt(IV) complexes,¹⁶³ occurred to form the isolated complex **1-28** (Scheme 1-27a). Upon addition of H_2O_2 as oxidant, complex **1-28** was oxidized to a Pd(IV) complex **1-29**, which was stable enough to be isolated and characterized. Finally, **1-30** was made through a direct C-O bond-forming reductive elimination reaction from the six-coordinated complex **1-29**. In order to propose a mechanism for C-O bond formation, first the necessity of the dpk ligand as a supporting ligand was studied. Oxidation of complex **1-28**, without the supporting dpk ligand, did not provide a Pd(IV) complex (Scheme 1-27b). Therefore, they proposed that the dpk ligand was necessary for oxidation of the Pd(II) to Pd(IV). It was confirmed that the dpk ligand in free and coordinated mode, undergoes reversible hydration in water (Scheme 1-28).¹⁶⁴ Deprotonation of the *gem*-diol makes a κ^3 -*NNO* chelating ligand that can stabilize the Pd(IV) centre.



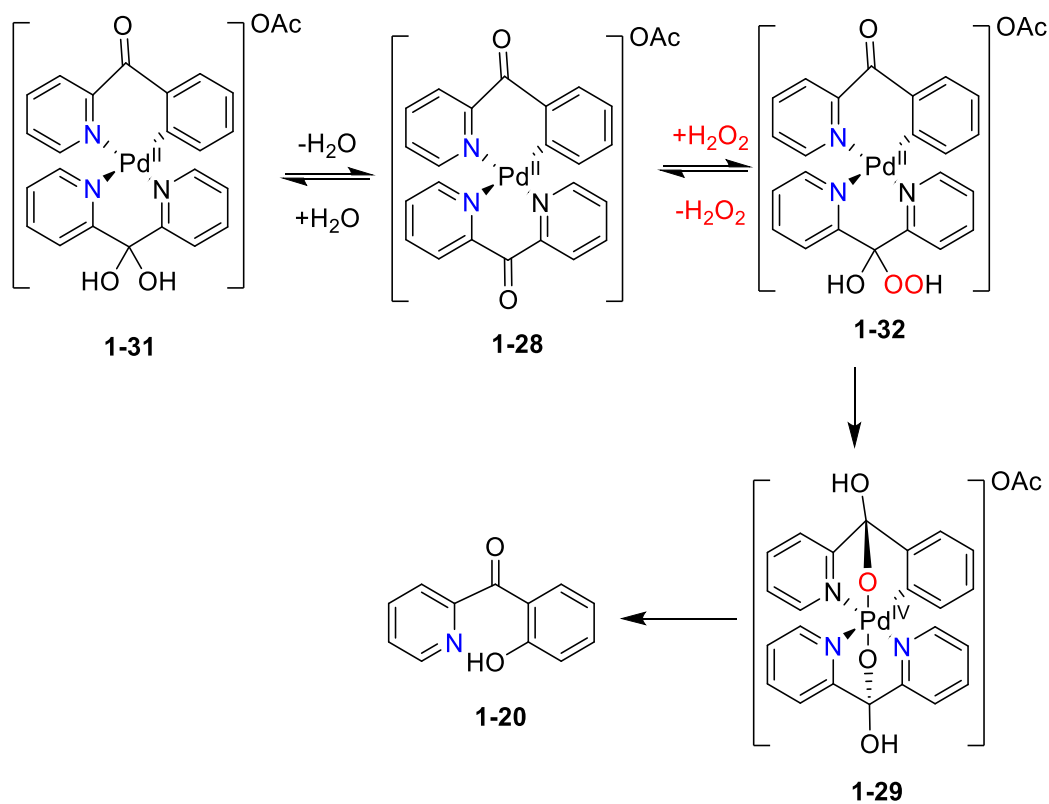
Scheme 1-27 Pd-catalyzed C-H bond activation using H_2O_2 as an oxidant.¹⁵²



Scheme 1-28 Reversible hydration of dpk in water.¹⁶³

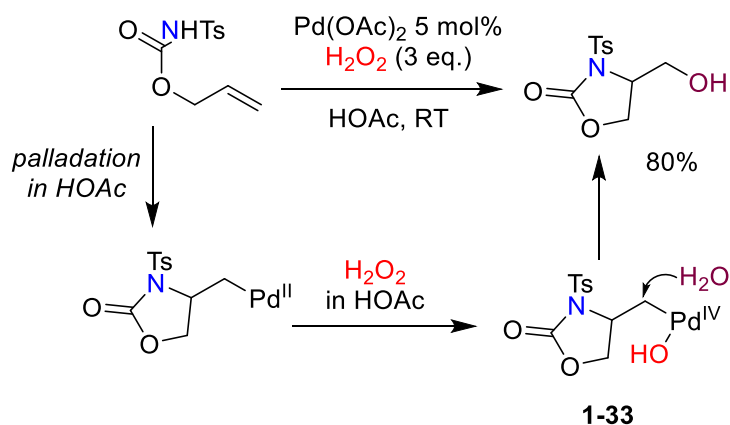
The oxidation reaction of **1-28** in hydrogen peroxide was monitored by mass spectrometry as well as ^1H NMR spectroscopy. Formation of three complexes, **1-29**, **1-31** and **1-32** was confirmed (Scheme 1-29). In the ^1H NMR spectrum, signals for **1-31** were predominant at first but disappeared gradually. However, signals for **1-29** grew over time. Also, signals for **1-32** appeared upon addition of H_2O_2 , persisted at the middle stage and disappeared at the end of the reaction. Based on these results and

computational studies, kinetic studies and isotope labeling experiments, the following mechanism was proposed. First, the coordinated dpk ligand undergoes a reversible hydration reaction to form **1-31** in water. Subsequently, a nucleophilic attack of H₂O₂ across C=O bond of the coordinated dpk ligand of **1-31** occurs to form **1-32**. In the complex *exo*-**1-32**, the Pd(II) centre and the OOH group are close enough to each other to form the Pd(IV) complex **1-29** in an intramolecular fashion and by heterolytic cleavage of the O-O bond in **1-32** via nucleophilic attack of Pd(II) onto the hydroperoxide adduct. Finally, a direct C-O bond-forming reductive elimination reaction from the six-coordinated Pd(IV) complex **1-29**, releases the organic molecule.



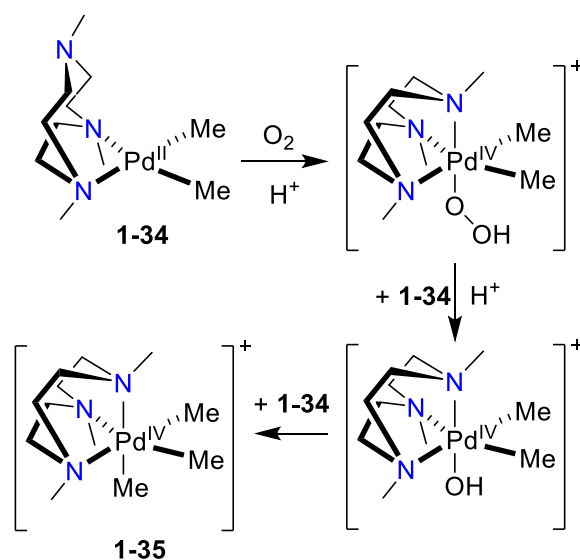
Scheme 1-29 Proposed mechanism for C-O bond-forming reductive elimination reaction from a Pd(IV)-OH in water.

Liu *et. al* have developed a new system for ligand-assisted intramolecular Pd-catalyzed C(alkyl)-H activation reactions, using H₂O₂ as the oxidant.¹⁵⁵ In their system, it is proposed that H₂O₂ oxidized a Pd(II)-C(alkyl) complex **1-33** to form a Pd(IV)-hydroxo complex (Scheme 1-30). Subsequently, water attacked the carbon centre of Pd(IV)-C(alkyl) complex as a nucleophile and in a S_N2 manner to form a C-O bond.^{165,166}



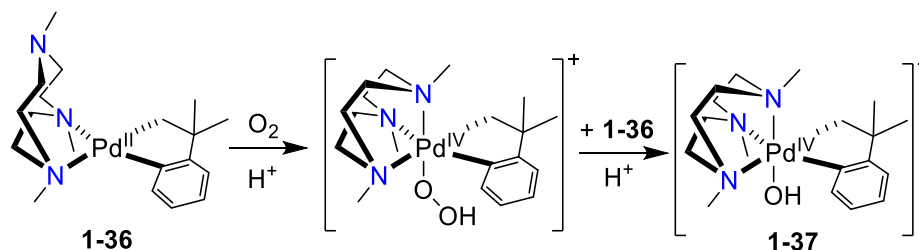
Scheme 1-30 Pd-catalyzed C-H bond activation using H_2O_2 as an oxidant.

For the first time, Mirica *et. al* isolated a Pd(IV) complex by aerobic oxidation of a Pd(II) precursor and supported the role of Pd(IV) species as viable intermediates in Pd-mediated catalytic aerobic transformation (Scheme 1-31).³⁹ They reported that $(\text{Me}_3\text{tacn})\text{Pd}^{\text{II}}\text{Me}_2$ (**1-34**) undergoes inner-sphere oxidation by O_2 followed by protonation to form the Pd(IV)-hydroperoxide species, which are observed by mass spectroscopy. Then, Pd(IV)-OOH oxidized another molecule of **1-34**, assisted by protons to form two molecules of Pd(IV)-OH intermediates. Formation of Pd(IV)-OOH and Pd(IV)-OH in water were confirmed by mass spectrometry. Next, the electrophilic Pd(IV)-OH undergoes a Me-transfer to the nucleophilic **1-34** complex to afford isolable $[(\text{Me}_3\text{tacn})\text{Pd}^{\text{IV}}\text{Me}_3]^+$ (**1-35**).



Scheme 1-31 Proposed mechanism for formation of **1-35** by aerobic oxidation of **1-34**.

Two years later, Mirica *et. al* reported another study on aerobic oxidation of $(\text{Me}_3\text{tacn})\text{Pd}^{\text{II}}(\text{CH}_2\text{CMe}_2\text{C}_6\text{H}_4)$ (**1-36**) to directly form isolable $[(\text{Me}_3\text{tacn})\text{Pd}^{\text{IV}}(\text{OH})(\text{CH}_2\text{CMe}_2\text{C}_6\text{H}_4)]^+$ (**1-37**) without the need for an alkyl-transfer reaction (Scheme 1-32).⁵⁹ Therefore, it was concluded that a methyl group is not necessary for aerobic oxidation of the Pd(II) centre.



Scheme 1-32 Proposed mechanism for aerobic oxidation of **1-36**.

1.5 A Description of the Thesis

This thesis describes the synthesis, reactivity and spectroscopic analysis of cycloneophyl-Pd(II) complexes containing *N*-donor ligands. The synthesis and challenges faced in the preparation and design of these complexes and their reactivities towards oxidative addition reactions followed by reductive elimination is discussed. Efforts in isolating stable Pd(IV) complexes and mechanistic studies using various techniques such as ^1H NMR, ^2H NMR and UV-Vis spectroscopies are also outlined.

Chapter 2 outlines the synthesis and characterization of a new cycloneophyl-palladacycle(II) complex containing a bidentate *N*-donor ligand. Efforts towards isolating a stable Pd(IV) complex through the oxidative addition reaction to the palladacycle, using bromine or iodine as oxidants, was not successful. However, the C-C bond-forming reductive elimination step from the unstable Pd(IV) was studied, using experimental techniques and computational analyses. The oxidative addition reaction to the palladacycle(II), using hydrogen peroxide lead to the selective oxygen-atom insertion into the aryl-palladium bond. The mechanism for the O-atom insertion and basis for selectivity were discussed. Chapter 3 outlines that a bidentate *N*-donor ligand having an appended phenol group assisted the Pd-aryl bond protonolysis reaction through the deprotonation of the phenol group. Deuterium labelling experiments confirmed that the ligand phenol promotes protonolysis and that the reverse, aryl C-H activation, occurs under very mild reaction conditions (within 10 min at room temperature). Furthermore, an unusual isomerization of a Pd-alkyl complex to a Pd-aryl complex, was observed. Isotope effect studies assisted in mechanistic studies for the observed isomerization reaction.

Chapter 4 describes the oxidation of the *N*-donor ligand containing an appended phenol group using green oxidants, such as H₂O₂ or O₂. The ligand oxidation afforded a molecular square and a molecular tetrahedron by self-assembly of building blocks comprising Pd(II) centres coordinated to the oxidized forms of the ligand. The synthesis of these tetramers was modified and the pincer-plus one ligand design was proposed as a great potential candidate for the designed synthesis of oligomeric and polymeric complexes with unusual structures, properties and potential uses.

Chapter 5 describes the synthesis and characterization of a new fluxional palladacycle(II) complex containing a tridentate *N*-donor ligand. CO₂ fixation reaction from air, afforded the first monodentate Pd-bicarbonate complex and a mixture of organic products. A mechanism for these reactions was proposed.

Chapter 6 deals with the oxidation of a palladacycle (II) containing a tridentate *N*-donor ligand, with dihalides that afforded stable Pd(IV) complexes. All Pd(IV) complexes were isolated and fully characterized. The reductive elimination reactions to form C-C or C-X (X = Br or I) and the mechanisms of these reactions were elucidated by kinetic studies.

Chapter 7 describes the synthesis of two unique Pd(IV)-OH complexes, using O₂ or H₂O₂ as oxidant.

Chapter 8 in this thesis provides a summary of the work and gives some general conclusions. Future work and considerations are also provided here.

1.6 References

1. G. O. Spessard and G. L. Miessler, *Organometallic Chemistry*, Oxford University Press, 2010.
2. L. M. Rendina and R. J. Puddephatt, *Chem. Rev.*, 1997, **97**, 1735–1754.
3. R. H. Crabtree, *The Organometallic Chemistry of the Transition Metals*, John Wiley & Sons, 2014.
4. M. C. Usselman, *Ann. Sci.*, 1978, **35**, 551–579.
5. M. C. Usselman, *Pure Intelligence: The Life of William Hyde Wollaston*, University of Chicago Press, 2015.
6. E. Negishi, *Handbook of Organopalladium Chemistry for Organic Synthesis*, John Wiley & Sons, Hoboken, NJ, 2002.
7. P. Henry, *Palladium Catalyzed Oxidation of Hydrocarbons*, Springer Netherlands, 1980.
8. H. -U. Blase, A. Indolese, F. Naud, U. Nettekoven and A. Schnyder, *Adv. Synth. Catal.*, 2004, **346**, 1583–1598.

9. The Nobel Prize in Chemistry 2010 - Press Release, https://www.nobelprize.org/nobel_prizes/chemistry/laureates/2010/press.html, (accessed May 9, 2018).
10. C. C. Johansson Seechurn, M. O. Kitching, T. J. Colacot and V. Snieckus, *Angew. Chem. Int. Ed.*, 2012, **51**, 5062–5085.
11. J. Yamaguchi, A. D. Yamaguchi and K. Itami, *Angew. Chem. Int. Ed.*, 2012, **51**, 8960–9009.
12. C. Liu, H. Zhang, W. Shi and A. Lei, *Chem. Rev.*, 2011, **111**, 1780–1824.
13. F. A. Cotton, G. Wilkinson, C. A. Murillo and M. Bochmann, *Advanced Inorganic Chemistry*, John Wiley & Sons, Toronto, 6th edn., 1999.
14. J. R. Khusnutdinova, N. P. Rath and L. M. Mirica, *J. Am. Chem. Soc.*, 2010, **132**, 7303–7305.
15. D. C. Powers, D. Benitez, E. Tkatchouk, W. A. Goddard and T. Ritter, *J. Am. Chem. Soc.*, 2010, **132**, 14092–14103.
16. D. C. Powers, M. A. L. Geibel, J. E. M. N. Klein and T. Ritter, *J. Am. Chem. Soc.*, 2009, **131**, 17050–17051.
17. G. A. Lane, W. E. Geiger and N. G. Connelly, *J. Am. Chem. Soc.*, 1987, **109**, 402–407.
18. E. Negishi, *Acc. Chem. Res.*, 1982, **15**, 340–348.
19. A. B. González-Pérez, R. Álvarez, O. N. Faza, Á. R. de Lera and J. M. Aurrecoechea, *Organometallics.*, 2012, **31**, 2053–2058.
20. P. Espinet and A. M. Echavarren, *Angew. Chem. Int. Ed.*, 2004, **43**, 4704–4734.
21. D. Milstein and J. K. Stille, *J. Am. Chem. Soc.*, 1979, **101**, 4981–4991.
22. K. Sonogashira, *J. Organomet. Chem.*, 2002, **653**, 46–49.
23. R. Chinchilla and C. Nájera, *Chem. Soc. Rev.*, 2011, **40**, 5084–5121.
24. M. Schilz and H. Plenio, *J. Org. Chem.*, 2012, **77**, 2798–2807.
25. R. Chinchilla and C. Nájera, *Chem. Rev.*, 2007, **107**, 874–922.
26. C. E. I. Knappke and A. J. von Wangelin, *Chem. Soc. Rev.*, 2011, **40**, 4948–4962.
27. R. J. P. Corriu and J. P. Masse, *J. Chem. Soc. Chem. Commun.*, 1972, **0**, 144a-144a.
28. K. Tamao, K. Sumitani and M. Kumada, *J. Am. Chem. Soc.*, 1972, **94**, 4374–4376.
29. N. Miyaoura and A. Suzuki, *Chem. Rev.*, 1995, **95**, 2457–2483.
30. A. Suzuki, *Angew. Chem. Int. Ed.*, 2011, **50**, 6722–6737.
31. A. A. C. Braga, N. H. Morgon, G. Ujaque and F. Maseras, *J. Am. Chem. Soc.*, 2005, **127**, 9298–9307.
32. A. A. C. Braga, G. Ujaque and F. Maseras, *Organometallics*, 2006, **25**, 3647–3658.

33. S. S. Stahl, *Angew. Chem. Int. Ed.*, 2004, **43**, 3400–3420.
34. K. M. Gligorich and M. S. Sigman, *Chem. Commun.*, 2009, 3854–3867.
35. S. S. Stahl, *Science*, 2005, **309**, 1824–1826.
36. J. E. Huheey, E. A. Keiter and R. L. Keiter, *Inorganic Chemistry: Principles of Structure and Reactivity*, Prentice Hall, New York, NY, 4th ed., 1997.
37. A. N. Campbell and S. S. Stahl, *Acc. Chem. Res.*, 2012, **45**, 851–863.
38. N. Selander and K. J. Szabó, *Chem. Rev.*, 2011, **111**, 2048–2076.
39. J. R. Khusnutdinova, F. Qu, Y. Zhang, N. P. Rath and L. M. Mirica, *Organometallics.*, 2012, **31**, 4627–4630.
40. N. D. Ball, J. W. Kampf and M. S. Sanford, *J. Am. Chem. Soc.*, 2010, **132**, 2878–2879.
41. J. M. Racowski, J. B. Gary and M. S. Sanford, *Angew. Chem. Int. Ed.*, 2012, **51**, 3414–3417.
42. N. M. Camasso, M. H. Pérez-Temprano and M. S. Sanford, *J. Am. Chem. Soc.*, 2014, **136**, 12771–12775.
43. D. Kalyani, N. R. Deprez, L. V. Desai and M. S. Sanford, *J. Am. Chem. Soc.*, 2005, **127**, 7330–7331.
44. L.-M. Xu, B.-J. Li, Z. Yang and Z.-J. Shi, *Chem. Soc. Rev.*, 2010, **39**, 712–733.
45. T. W. Lyons and M. S. Sanford, *Chem. Rev.*, 2010, **110**, 1147–1169.
46. S. R. Neufeldt and M. S. Sanford, *Acc. Chem. Res.*, 2012, **45**, 936–946.
47. X. Chen, K. M. Engle, D.-H. Wang and J.-Q. Yu, *Angew. Chem. Int. Ed.*, 2009, **48**, 5094–5115.
48. R. Alam, L. T. Pilarski, E. Pershagen and K. J. Szabó, *J. Am. Chem. Soc.*, 2012, **134**, 8778–8781.
49. N. Selander, B. Willy and K. J. Szabó, *Angew. Chem. Int. Ed.*, 2010, **49**, 4051–4053.
50. A. R. Dick, J. W. Kampf and M. S. Sanford, *J. Am. Chem. Soc.*, 2005, **127**, 12790–12791.
51. T. Furuya and T. Ritter, *J. Am. Chem. Soc.*, 2008, **130**, 10060–10061.
52. A. J. Canty, H. Jin, B. W. Skelton and A. H. White, *Inorg. Chem.*, 1998, **37**, 3975–3981.
53. A. Maleckis and M. S. Sanford, *Organometallics.*, 2011, **30**, 6617–6627.
54. S. R. Whitfield and M. S. Sanford, *J. Am. Chem. Soc.*, 2007, **129**, 15142–15143.
55. A. W. Kaspi, A. Yahav-Levi, I. Goldberg and A. Vigalok, *Inorg. Chem.*, 2008, **47**, 5–7.
56. K. L. Hull, W. Q. Anani and M. S. Sanford, *J. Am. Chem. Soc.*, 2006, **128**, 7134–7135.
57. T. Furuya, H. M. Kaiser and T. Ritter, *Angew. Chem. Int. Ed.*, 2008, **47**, 5993–5996.
58. T. Furuya, D. Benitez, E. Tkatchouk, A. E. Strom, P. Tang, W. A. Goddard and T. Ritter, *J. Am. Chem. Soc.*, 2010, **132**, 3793–3807.
59. F. Qu, J. R. Khusnutdinova, N. P. Rath and L. M. Mirica, *Chem. Commun.*, 2014, **50**, 3036–3039.

60. N. M. Camasso, A. J. Canty, A. Ariaferd and M. S. Sanford, *Organometallics*, 2017, **36**, 4382–4393.
61. M. H. Pérez-Temprano, J. M. Racowski, J. W. Kampf and M. S. Sanford, *J. Am. Chem. Soc.*, 2014, **136**, 4097–4100.
62. J. Cámpora, M. del Mar Conejo, K. Mereiter, P. Palma, C. Pérez, M. L. Reyes and C. Ruiz, *J. Organomet. Chem.*, 2003, **683**, 220–239.
63. J. Cámpora, P. Palma, D. del Río, J. A. López and P. Valerga, *Chem. Commun.*, 2004, 1490–1491.
64. A. J. Canty, A. Ariaferd, N. M. Camasso, A. T. Higgs, B. F. Yates and M. S. Sanford, *Dalton Trans.*, 2017, **46**, 3742–3748.
65. I. M. Pendleton, M. H. Pérez-Temprano, M. S. Sanford and P. M. Zimmerman, *J. Am. Chem. Soc.*, 2016, **138**, 6049–6060.
66. J. Cámpora, P. Palma, D. del Río, J. A. López, E. Álvarez and N. G. Connelly, *Organometallics*, 2005, **24**, 3624–3628.
67. J. J. Sandoval, C. Melero, P. Palma, E. Álvarez, A. Rodríguez-Delgado and J. Cámpora, *Organometallics*, 2016, **35**, 3336–3343.
68. X. Mu, T. Wu, H. Wang, Y. Guo and G. Liu, *J. Am. Chem. Soc.*, 2012, **134**, 878–881.
69. T. Wu, G. Yin and G. Liu, *J. Am. Chem. Soc.*, 2009, **131**, 16354–16355.
70. J. Nicasio-Collazo, E. Álvarez, J. C. Alvarado-Monzón, G. Andreu-de-Riquer, J. O. C. Jimenez-Halla, L. M. D. León-Rodríguez, G. Merino, U. Morales, O. Serrano and J. A. López, *Dalton Trans.*, 2011, **40**, 12450–12453.
71. Á. Gutiérrez-Bonet, F. Juliá-Hernández, B. de Luis and R. Martin, *J. Am. Chem. Soc.*, 2016, **138**, 6384–6387.
72. J. Nicasio-Collazo, K. Wrobel, K. Wrobel and O. Serrano, *New J. Chem.*, 2017, **41**, 8729–8733.
73. J. P. Collman, *Principles and applications of organotransition metal chemistry*, University Science Books, 1987.
74. E. Carmona, M. Paneque, M. L. Poveda, E. Gutierrez-Puebla and A. Monge, *Polyhedron*, 1989, **8**, 1069–1075.
75. J. X. McDermott, J. F. White and G. M. Whitesides, *J. Am. Chem. Soc.*, 1976, **98**, 6521–6528.
76. T. J. McCarthy, R. G. Nuzzo and G. M. Whitesides, *J. Am. Chem. Soc.*, 1981, **103**, 3396–3403.
77. S. Komiya, Y. Morimoto, A. Yamamoto and T. Yamamoto, *Organometallics*, 1982, **1**, 1528–1536.
78. A. Behnia, P. D. Boyle, J. M. Blacquiere and R. J. Puddephatt, *Organometallics*, 2016, **35**, 2645–2654.

79. A. Behnia, P. D. Boyle, M. A. Fard, J. M. Blacquiere and R. J. Puddephatt, *Dalton Trans.*, 2016, **45**, 19485–19490.
80. A. Behnia, M. A. Fard, J. M. Blacquiere and R. J. Puddephatt, *Dalton Trans.*, 2018, **47**, 3538–3548.
81. A. Behnia, M. A. Fard, J. M. Blacquiere and R. J. Puddephatt, *Organometallics*, 2017, **36**, 4759–4769.
82. J. Cámpora, J. A. López, P. Palma, P. Valerga, E. Spillner and E. Carmona, *Angew. Chem. Int. Ed.*, 1999, **38**, 147–151.
83. N. D. Ball and M. S. Sanford, *J. Am. Chem. Soc.*, 2009, **131**, 3796–3797.
84. D. F. Shriver and P. W. Atkins, *Inorganic chemistry*, New York W.H. Freeman and Co, 3rd ed., 1999.
85. A. Canty, Ed., *Higher Oxidation State Organopalladium and Platinum Chemistry*, Springer-Verlag, Berlin Heidelberg, 2011.
86. K. Muñiz, *Angew. Chem. Int. Ed.*, 2009, **48**, 9412–9423.
87. E. Abada, P. Y. Zavalij and A. N. Vedernikov, *J. Am. Chem. Soc.*, 2017, **139**, 643–646.
88. J. F. Hartwig, *Organotransition metal chemistry: from bonding to catalysis*, 2010.
89. R. H. Crabtree, *Angew. Chem. Int. Ed.*, 2003, **32**, 789–805.
90. P. K. Byers, A. J. Canty, B. W. Skelton and A. H. White, *J. Chem. Soc. Chem. Commun.*, 1986, 1722–1724.
91. J. M. Racowski, A. R. Dick and M. S. Sanford, *J. Am. Chem. Soc.*, 2009, **131**, 10974–10983.
92. Y. Fu, Z. Li, S. Liang, Q.-X. Guo and L. Liu, *Organometallics*, 2008, **27**, 3736–3742.
93. S. S. Stahl, J. A. Labinger and J. E. Bercaw, *Angew. Chem. Int. Ed.*, 1998, **37**, 2180–2192.
94. J. A. Labinger and J. E. Bercaw, *Nature*, 2002, **417**, 507–514.
95. H. Chen, S. Schlecht, T. C. Semple and J. F. Hartwig, *Science.*, 2000, **287**, 1995–1997.
96. D. A. D. Eric V. Anslyn, *Anslyn, E. V.; Dougherty, D. A. Modern Physical Organic Chemistry*, University Science Books, 2006.
97. A. E. Shilov and G. B. Shul'pin, *Chem. Rev.*, 1997, **97**, 2879–2932.
98. A. S. Goldman and K. I. Goldberg, in *Activation and Functionalization of C–H Bonds*, American Chemical Society, 2004, vol. 885, pp. 1–43.
99. B. A. Arndtsen, R. G. Bergman, T. A. Mobley and T. H. Peterson, *Acc. Chem. Res.*, 1995, **28**, 154–162.
100. A. R. Dick and M. S. Sanford, *Tetrahedron*, 2006, **62**, 2439–2463.
101. A. J. Hickman and M. S. Sanford, *ACS Catal.*, 2011, **1**, 170–174.

102. A. D. Ryabov, *Chem. Rev.*, 1990, **90**, 403–424.
103. J. Dupont, C. S. Consorti and J. Spencer, *Chem. Rev.*, 2005, **105**, 2527–2572.
104. A. C. Cope and R. W. Siekman, *J. Am. Chem. Soc.*, 1965, **87**, 3272–3273.
105. R. N. Perutz and S. Sabo-Etienne, *Angew. Chem. Int. Ed.*, 2007, **46**, 2578–2592.
106. R. Waterman, *Organometallics*, 2013, **32**, 7249–7263.
107. D. Balcells, E. Clot and O. Eisenstein, *Chem. Rev.*, 2010, **110**, 749–823.
108. Y. Boutadla, D. L. Davies, S. A. Macgregor and A. I. Poblador-Bahamonde, *Dalton Trans.*, 2009, 5820–5831.
109. S. I. Gorelsky, D. Lapointe and K. Fagnou, *J. Am. Chem. Soc.*, 2008, **130**, 10848–10849.
110. J. Oxgaard, W. J. Tenn, R. J. Nielsen, R. A. Periana and W. A. Goddard, *Organometallics*, 2007, **26**, 1565–1567.
111. D. L. Davies, S. A. Macgregor and C. L. McMullin, *Chem. Rev.*, 2017, **117**, 8649–8709.
112. E. Carmona, P. Palma, M. Paneque, M. L. Poveda, E. Gutierrez-Puebla and A. Monge, *J. Am. Chem. Soc.*, 1986, **108**, 6424–6425.
113. E. Carmona, E. Gutierrez-Puebla, J. M. Marin, A. Monge, M. Paneque, M. L. Poveda and C. Ruiz, *J. Am. Chem. Soc.*, 1989, **111**, 2883–2891.
114. K. -R. Pörschke, *Angew. Chem. Int. Ed.*, 2003, **26**, 1288–1290.
115. P. T. Matsunaga, J. C. Mavropoulos and G. L. Hillhouse, *Polyhedron*, 1995, **14**, 175–185.
116. P. Diversi, G. Ingrosso, A. Lucherini, T. Lumini, F. Marchetti, S. Merlino, V. Adovasio and M. Nardelli, *J. Chem. Soc. Dalton Trans.*, 1988, 461–467.
117. J. Cámpora, P. Palma and E. Carmona, *Coord. Chem. Rev.*, 1999, **193**, 207–281.
118. A. J. Canty, in *Comprehensive Organometallic Chemistry II*, eds. E. W. Abel, F. G. A. Stone and G. Wilkinson, Elsevier, Oxford, 1995, pp. 225–290.
119. J. Fornies, B. Menjon, N. Gomez and M. Tomas, *Organometallics*, 1992, **11**, 1187–1193.
120. C.-S. Li, C.-H. Cheng, F.-L. Liao and S.-L. Wang, *J. Chem. Soc. Chem. Commun.*, 1991, 710–712.
121. N. R. Deprez and M. S. Sanford, *Inorg. Chem.*, 2007, **46**, 1924–1935.
122. D. Kalyani, A. R. Dick, W. Q. Anani and M. S. Sanford, *Org. Lett.*, 2006, **8**, 2523–2526.
123. L. V. Desai, H. A. Malik and M. S. Sanford, *Org. Lett.*, 2006, **8**, 1141–1144.
124. K. L. Hull, E. L. Lanni and M. S. Sanford, *J. Am. Chem. Soc.*, 2006, **128**, 14047–14049.
125. J. M. Racowski, N. D. Ball and M. S. Sanford, *J. Am. Chem. Soc.*, 2011, **133**, 18022–18025.
126. P. L. Arnold, M. S. Sanford and S. M. Pearson, *J. Am. Chem. Soc.*, 2009, **131**, 13912–13913.

127. L. V. Desai, K. J. Stowers and M. S. Sanford, *J. Am. Chem. Soc.*, 2008, **130**, 13285–13293.
128. A. R. Dick, K. L. Hull and M. S. Sanford, *J. Am. Chem. Soc.*, 2004, **126**, 2300–2301.
129. L. V. Desai, K. L. Hull and M. S. Sanford, *J. Am. Chem. Soc.*, 2004, **126**, 9542–9543.
130. A. Butler and J. V. Walker, *Chem. Rev.*, 1993, **93**, 1937–1944.
131. G. S. Silverman and P. E. Rakita, *Handbook of Grignard reagents*, New York: Marcel Dekker/CRC Press, 1996.
132. K. J. Stowers and M. S. Sanford, *Org. Lett.*, 2009, **11**, 4584–4587.
133. R. van Belzen, C. J. Elsevier, A. Dedieu, N. Veldman and A. L. Spek, *Organometallics*, 2003, **22**, 722–736.
134. P. L. Alsters, P. F. Engel, M. P. Hogerheide, M. Copijn, A. L. Spek and G. van Koten, *Organometallics.*, 1993, **12**, 1831–1844.
135. J. F. Hartwig, *Acc. Chem. Res.*, 1998, **31**, 852–860.
136. B. S. Williams and K. I. Goldberg, *J. Am. Chem. Soc.*, 2001, **123**, 2576–2587.
137. C. R. Sinha, D. Bandyopadhyay and A. Chakravorty, *J. Chem. Soc. Chem. Commun.*, 1988, 468–470.
138. C. Sinha, D. Bandyopadhyay and A. Chakravorty, *Inorg. Chem.*, 1988, **27**, 1173–1178.
139. A. K. Mahapatra, D. Bandyopadhyay, P. Bandyopadhyay and A. Chakravorty, *Inorg. Chem.*, 1986, **25**, 2214–2221.
140. M. Muehlhofer, T. Strassner and W. A. Herrmann, *Angew. Chem. Int. Ed.*, 2002, **41**, 1745–1747.
141. G.-W. Wang, T.-T. Yuan and X.-L. Wu, *J. Org. Chem.*, 2008, **73**, 4717–4720.
142. D. Yang, *Acc. Chem. Res.*, 2004, **37**, 497–505.
143. J. M. Schomaker, B. R. Travis and B. Borhan, *Org. Lett.*, 2003, **5**, 3089–3092.
144. Y.-A. Lee and O.-S. Jung, *Bull. Chem. Soc. Jpn.*, 2002, **75**, 1533–1537.
145. A. R. Dick, J. W. Kampf and M. S. Sanford, *Organometallics.*, 2005, **24**, 482–485.
146. B. G. Hashiguchi, S. M. Bischof, M. M. Konnick and R. A. Periana, *Acc. Chem. Res.*, 2012, **45**, 885–898.
147. L. Boisvert and K. I. Goldberg, *Acc. Chem. Res.*, 2012, **45**, 899–910.
148. A. N. Vedernikov, *Acc. Chem. Res.*, 2012, **45**, 803–813.
149. J. Zhang, E. Khaskin, N. P. Anderson, P. Y. Zavalij and A. N. Vedernikov, *Chem. Commun.*, 2008, 3625–3627.
150. Y.-H. Zhang and J.-Q. Yu, *J. Am. Chem. Soc.*, 2009, **131**, 14654–14655.
151. P. Wadhvani and D. Bandyopadhyay, *Organometallics.*, 2000, **19**, 4435–4436.

152. W. Oloo, P. Y. Zavalij, J. Zhang, E. Khaskin and A. N. Vedernikov, *J. Am. Chem. Soc.*, 2010, **132**, 14400–14402.
153. J. R. Khusnutdinova, N. P. Rath and L. M. Mirica, *J. Am. Chem. Soc.*, 2012, **134**, 2414–2422.
154. S. Pal and A. N. Vedernikov, *Dalton Trans.*, 2012, **41**, 8116–8122.
155. H. Zhu, P. Chen and G. Liu, *J. Am. Chem. Soc.*, 2014, **136**, 1766–1769.
156. G. Yin, T. Wu and G. Liu, *Chem. Eur. J.*, 2011, **18**, 451–455.
157. B. Lücke, K. V. Narayana, A. Martin and K. Jähnisch, *Adv. Synth. Catal.*, 2004, **346**, 1407–1424.
158. K. J. Stowers, K. C. Fortner and M. S. Sanford, *J. Am. Chem. Soc.*, 2011, **133**, 6541–6544.
159. K. J. Stowers, A. Kubota and M. S. Sanford, *Chem. Sci.*, 2012, **3**, 3192–3195.
160. A. V. Sberegaeva, P. Y. Zavalij and A. N. Vedernikov, *J. Am. Chem. Soc.*, 2016, **138**, 1446–1455.
161. T. Jintoku, K. Nishimura, K. Takaki and Y. Fujiwara, *Chem. Lett.*, 1990, **19**, 1687–1688.
162. W. N. Oloo, P. Y. Zavalij and A. N. Vedernikov, *Organometallics*, 2013, **32**, 5601–5614.
163. A. N. Vedernikov, *Chem. Commun.*, 2009, 4781–4790.
164. J. R. Khusnutdinova, L. L. Newman and A. N. Vedernikov, *J. Organomet. Chem.*, 2011, **696**, 3998–4006.
165. N. Kanbayashi and K. Onitsuka, *Angew. Chem. Int. Ed.*, 2011, **50**, 5197–5199.
166. M. Gärtner, S. Mader, K. Seehafer and G. Helmchen, *J. Am. Chem. Soc.*, 2011, **133**, 2072–2075.

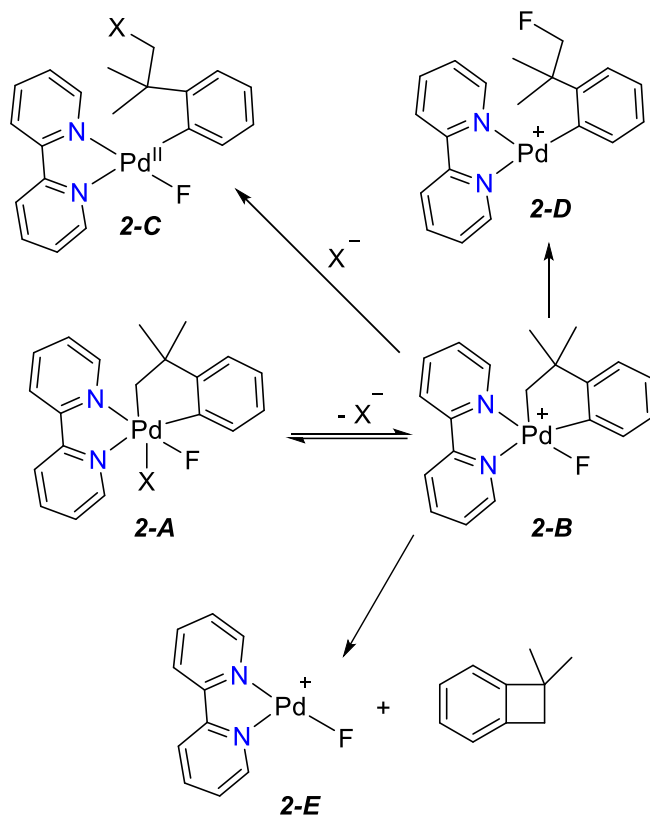
2 Selective Oxygen-Atom Insertion into an Aryl-Palladium Bond

(A. Behnia, J. M. Blacquiere and R. J. Puddepaht, *Organometallics*, 2016, **35**, 2645-2654.)

2.1 Introduction

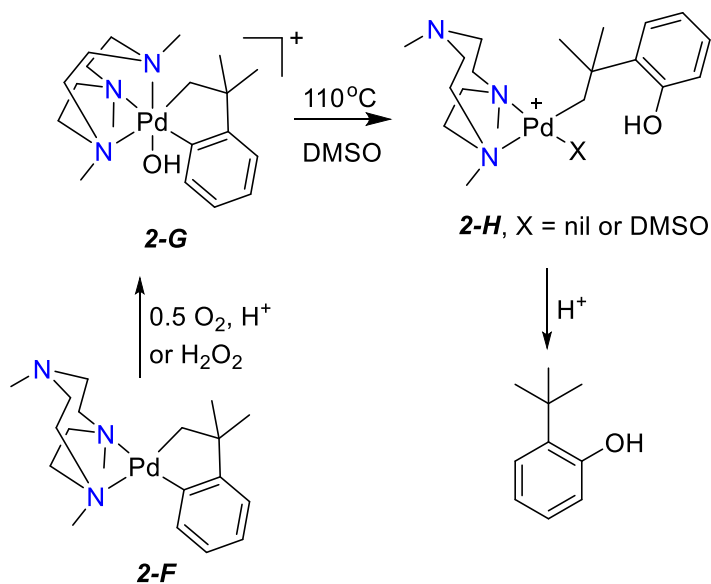
The development of organopalladium(IV) chemistry in recent years has been impressive, and has stimulated research into catalysis involving Pd(II)/Pd(IV) cycles to complement the many important catalytic reactions involving Pd(0)/Pd(II) cycles.¹⁻¹³ The higher oxidation state catalysis has greatest potential in reactions carried out under oxidizing conditions, including the functionalization of hydrocarbons to form oxygenated or halogenated derivatives.¹⁻²⁴ These catalytic reactions typically contain steps involving oxidation of palladium(II) to palladium(IV) by oxygen, halogen or their equivalents (i.e. peroxide or hypervalent halide oxidants), followed by reductive elimination involving C-O or C-X (X= halogen) bond formation. It is therefore important to understand the factors that influence reactivity and selectivity in these reactions.¹⁻²⁴

Palladium(IV) complexes containing both Pd-C(sp³) and Pd-C(sp²) bonds, such as **2-A** (Scheme 2-1), allow a direct study of selectivity in reductive elimination.²⁵⁻³¹ The Sanford group has shown that the first step in the reductive elimination from **2-A** is dissociation of the ligand X⁻ (e.g. X⁻ = PhO⁻, NO₃⁻, OTs⁻, NHTs⁻) to give a 16-electron 5-coordinate intermediate **2-B**. This Pd(IV) intermediate can undergo reduction to Pd(II) through three possible routes: 1) nucleophilic attack by X⁻ gives **2-C** with CH₂-X bond formation; 2) concerted intramolecular reductive elimination with CH₂-F bond formation gives **2-D**; or 3) reductive elimination of C-C gives 1,1-dimethylcyclobutabenzene and **2-E**. The 14-electron complexes **2-D** or **2-E** undergo further coordination with X⁻ to give square planar 16-electron palladium(II) complexes. The selectivity in the reductive elimination is dependent on the nature of the anion X⁻.²⁵⁻²⁷



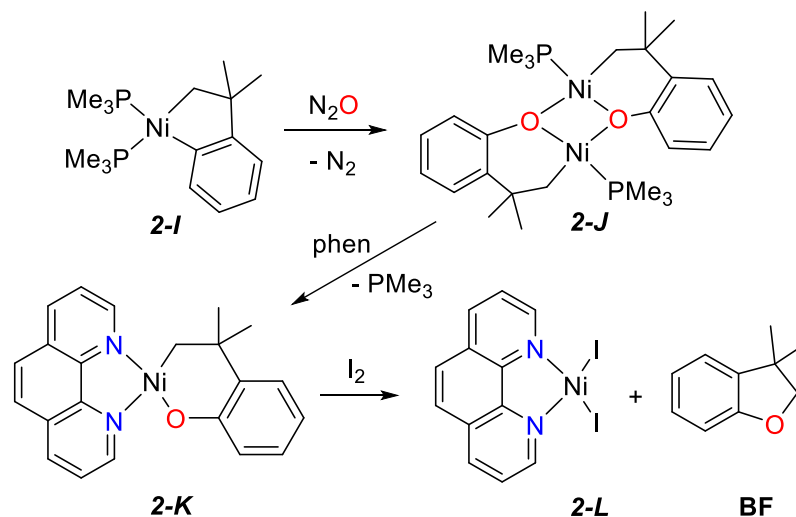
Scheme 2-1 Competition between C-X (X = OR or NHR), C-F and C-C reductive elimination from the palladium(IV) complex **2-A**.²⁵⁻²⁷

The Mirica group showed that the palladium(II) complex **2-F** (Scheme 2-2) was easily oxidized by oxygen or hydrogen peroxide to give the stable hydroxopalladium(IV) complex **2-G**, from which, on heating to 110°C in dimethylsulfoxide solution, reductive elimination occurred to give a complex which was formulated as **2-H**.²⁸ In contrast to the Sanford complexes of Scheme 2-1,²⁵⁻²⁷ the reductive elimination from **2-G** involves selective C(sp²)-O rather than C(sp³)-O bond formation, probably by a concerted intramolecular mechanism.²⁸ The tentatively assigned intermediate **2-H** subsequently reacts with acid to give 2-*t*-butylphenol. Protonolysis of a metal-carbon bond in the related compound [Pd(CH₂CMe₂C₆H₄)(PMe₃)₂] with phosphine instead of amine donor ligands is proposed to occur through a transient hydridopalladium(IV) intermediate and can lead to cleavage of either the Pd-C(sp³) or Pd-C(sp²) bond, though the latter is favored kinetically.²⁹



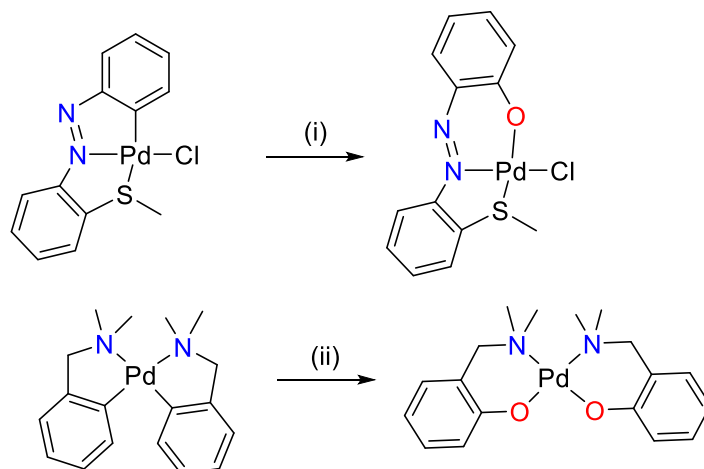
Scheme 2-2 Reductive elimination with selective aryl C-O bond formation.²⁸

These observations show that the nature of the supporting ligands play a key role in controlling selectivity of sp^2 or sp^3 C-X bond formation. The Me_3TACN and hydroxo ligands in **2-G** (Scheme 2-2) do not easily dissociate so reaction is proposed to occur directly from the 6-coordinate 18-electron complex.²⁸ However, the X^- ligand in **2-A** (Scheme 1-2), which is *trans* to a high *trans*-influence alkyl group, dissociates reversibly and, as is established for several related palladium(IV) and platinum(IV) complexes,^{1-6,32-34} the reductive elimination occurs more easily from the 16-electron intermediate **2-B**.²⁵⁻²⁷ The commonly acknowledged pathways for reductive C-O bond formation include a step-wise nucleophilic attack (i.e. Scheme 2-1) or a concerted pathway. A third, less well studied, pathway involves overall oxygen-atom insertion into a Pd-C bond. Hillhouse found that treatment of the nickel(II) complex **2-I** with nitrous oxide afforded a Ni(II) dimer **2-J** with an oxygen atom inserted selectively into the Ni-C(sp^2) bond (Scheme 2-3).³⁵ Oxidation of the monomer **2-K** with iodine leads to formation of the diiodonickel(II) complex **2-L** and the benzofuran derivative **BF**, through C(sp^3)-O reductive elimination.



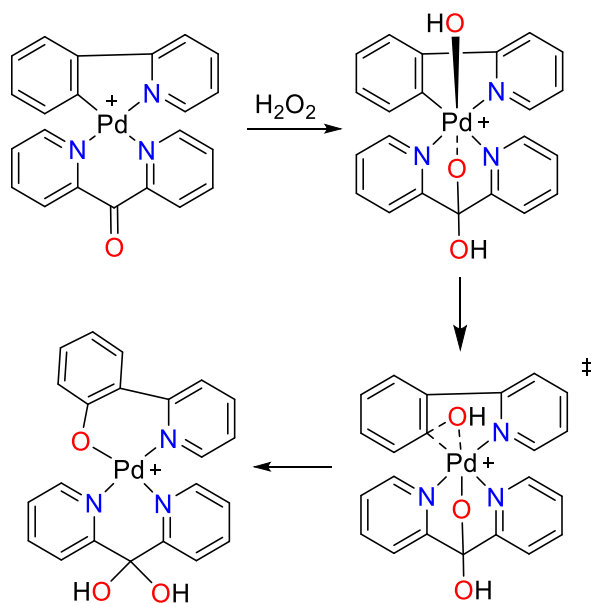
Scheme 2-3 Precedent for O-atom insertion into M-Ar from organonickel chemistry.³⁵

Oxygen atom insertion into arylpalladium or arylrhodium bonds has also been established in complexes where no alkylpalladium bond is present (Scheme 2-4). Several oxygen atom donors could be used but, in most cases, oxidation with hydrogen peroxide or *t*-butyl hydroperoxide required an iron(III) or vanadium(IV) catalyst (Scheme 2-4).³⁶⁻⁴¹



Scheme 2-4 Examples of oxygen atom insertion. Reagents: (i) MCPBA, C₆F₅IO or H₂O₂/Fe(III) catalyst; (ii) *t*-BuOOH/[V(O)(acac)₂] catalyst.³⁶⁻⁴¹

The mechanism was proposed to involve a transient oxopalladium(IV) intermediate, whose possible nature has recently been probed theoretically.⁴² Only with ligand assistance has the direct reaction with hydrogen peroxide in water been observed (Scheme 2-5).¹⁴



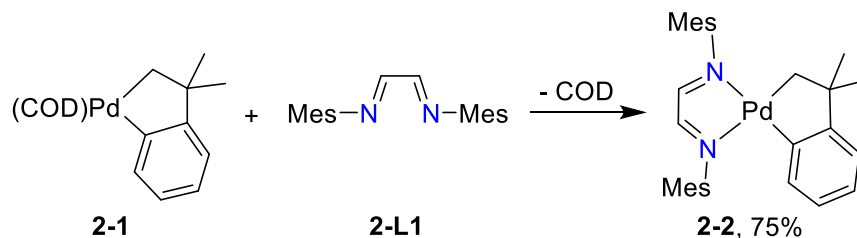
Scheme 2-5 Ligand assisted reaction with H₂O₂.¹⁴

Recently, the hydroxylation of arenes using O₂ or H₂O₂ as the environmentally benign oxidant and O-atom source has been achieved, with some examples using palladium(II) catalysts.⁴³⁻⁴⁵ The identification of the operative pathway for C-O bond formation is critical for the continued optimization of catalytic functionalization of both arenes and alkanes.¹⁻²⁴ Herein, we study the reactions of a palladium(II) complex [Pd(CH₂CMe₂C₆H₄)(MesN=CH-CH=NMe₃)] (**2-2**) with the oxidants H₂O₂ and halogens. We chose the diimine ligand MesN=CH-CH=NMe₃⁴⁶ (**2-L1**) on the basis that the nitrogen donors will allow oxidation to the Pd(IV) state (compare Schemes 2-1 and 2-2),²⁵⁻²⁸ while the steric bulk of the *N*-mesityl substituents will promote reductive elimination. The reactions lead to C-O and C-C bond formation from the palladacycle, including selective oxygen-atom insertion from the hydrogen peroxide oxidant.

2.2 Result and Discussion

The complex [Pd(CH₂CMe₂C₆H₄)(MesN=CH-CH=NMe₃)] (**2-2**) was prepared by ligand exchange from the corresponding 1,5-cyclooctadiene complex [Pd(CH₂CMe₂C₆H₄)(COD)]²⁸⁻³¹ (**2-1**) and MesN=CH-CH=NMe₃⁴⁶ (**2-L1**) according to Scheme 2-6. The best yield of 75% was obtained by carrying out the reaction in ether solution at -65 °C for 17 hours. Once obtained in pure form, complex **2-2** was thermally stable and could be stored at room temperature in air for extended periods. In order to facilitate subsequent reaction monitoring of **2-2**, a complete assignment of the ¹H and ¹³C NMR spectra of the complex was made by using a combination of correlated ¹H-¹H COSY and ¹H-¹³C HSQC

and HMBC NMR spectra. Complex **2-2** has effective C_s symmetry and its ^1H NMR spectrum contained two singlet imine resonances at δ 7.06 and 7.05 and two sets of mesityl resonances. The CH_2 and CMe_2 resonances of the hydrocarbon ligand appeared at δ 2.48 and 1.49 respectively.



Scheme 2-6 Synthesis of complex **2-2**.

The structure of complex **2-2** was determined and is shown in Figure 2-1. Along with a molecule of ether, there are two independent but similar molecules of **2-2** found in the unit cell, designated by Pd(1) and Pd(2). Both molecules are square planar with very small values of Houser's τ_4 parameter of 0.053 and 0.042 ($\tau_4 = 0$ for an ideal square planar complex).⁴⁷ A significant difference between the two molecules is in the degree of non-planarity of the metallacycle formed with the hydrocarbon ligand. In the Pd(2) molecule C(6B) and C(7B) are displaced out of the square plane by 0.33 and 0.77 Å, respectively. In Pd(1), a higher degree of distortion by 0.10 Å is observed for both C(6A) and C(7A). A difference in the twist angles of the mesityl groups with respect to the square plane of the palladium centre is also observed between Pd(1) and Pd(2). The angle between the square plane and the two mesityl planes are 77 and 91° for the Pd(1) molecule and 79 and 78° for the Pd(2) molecule.

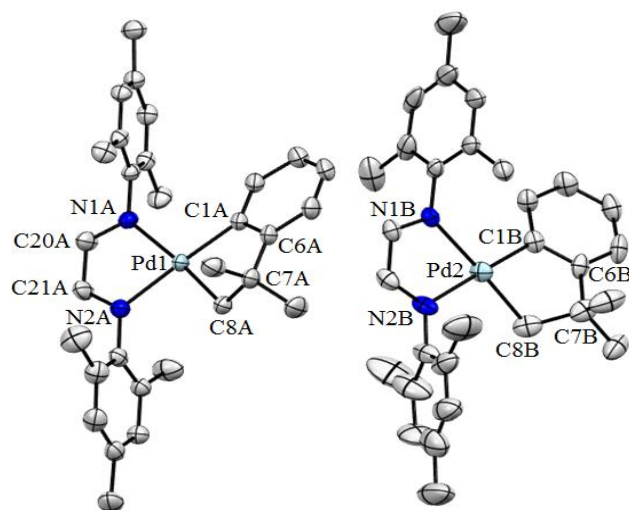
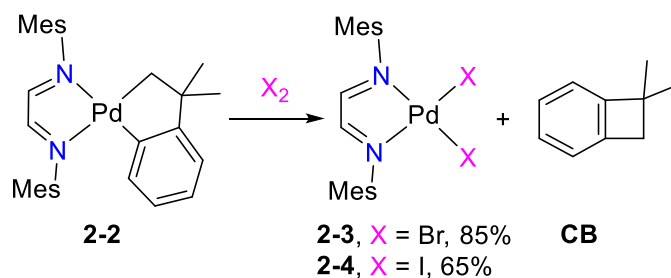


Figure 2-1 The structures of the two independent molecules of complex **2-2**, showing 30% probability ellipsoids. Selected bond parameters: Pd(1)C(1A) 1.994(4); Pd(1)C(8A) 2.018(4); Pd(1)N(1A) 2.170(3); Pd(1)N(2A) 2.119(3) Å; C(1A)Pd(1)C(8A) 79.42(16); N(2A)Pd(1)N(1A) 76.82(12)°; Pd(2)C(1B) 1.993(4); Pd(2)C(8B) 2.039(5); Pd(2)N(2B) 2.117(3); Pd(2)N(1B) 2.158(3) Å; C(1B)Pd(2)C(8B) 79.43(18); N(2B)Pd(2)N(1B) 76.57(13)°.

The reaction of complex **2-2** with bromine or iodine occurred largely according to Scheme 2-7 to give 1,1-dimethylcyclobutabenzene (**CB**) and the corresponding palladium(II) complex [PdX₂(MesN=CH-CH=NMe)], **2-3**, X = Br, or **2-4**, X = I. The 1,1-dimethylcyclobutabenzene, which was characterized by its ¹H NMR and mass spectra,^{26,48-49} is presumed to be formed by reductive elimination, with C-C bond formation, from a palladium(IV) intermediate by analogy with the mechanism of Scheme 2-1.²⁵⁻²⁷ However, when the reaction was monitored by ¹H NMR spectroscopy, no palladium(IV) complex was detected so this presumed intermediate is transient. The complexes **2-3/2-4** have effective C_{2v} symmetry and, in contrast to **2-2**, the ¹H NMR spectra contained only one imine resonance and one set of mesityl resonances.



Scheme 2-7 The reaction of **2-2** with bromine or iodine.

The structures of **2-3** and **2-4** were determined and are shown in Figure 2-2. Both structures are square planar (τ_4 : **2-3** = 0.00, **2-4** = 0.079). In the structure of **2-3** the molecule contains a crystallographic 2-fold rotation axis. The structure of **2-4** is more complex and the repeat unit has the formula $(\mathbf{2-4})_3 \cdot (\text{acetone})_2$, with three independent but similar molecules of **2-4**, of which only the Pd(1) molecule is shown in Figure 2-2.

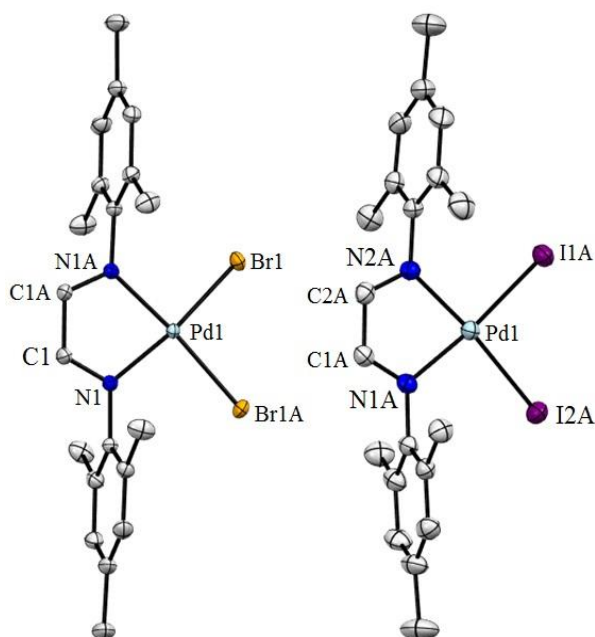
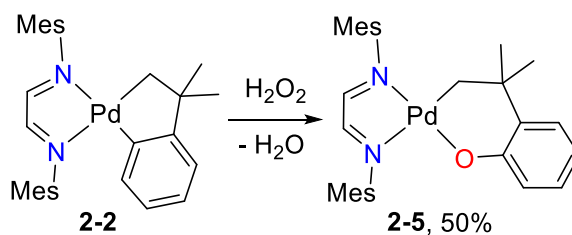


Figure 2-2 The structures of complexes **2-3** and **2-4**, with ellipsoids shown at the 50% probability level. Selected bond parameters: **2-3**, Pd(1)N(1) 2.023(3); Pd(1)Br(1) 2.4085(5) Å; N(1)Pd(1)N(1A) 79.92(14); Br(1)Pd(1)Br(1) 93.47(3)°; **2-4**, Pd(1)N(1A) 2.065(2); Pd(1)N(2A) 2.069(2); Pd(1)I(2A) 2.5668(5); Pd(1)I(1A) 2.5700(5) Å; N(1A)Pd(1)N(2A) 79.03(9); I(2A)Pd(1)I(1A) 90.437(17)°.

The reaction of complex **2-2** with hydrogen peroxide occurred, with different selectivity from the reactions with halogens, according to Scheme 2-8. The reaction to give the product $[\text{Pd}(\text{CH}_2\text{CMe}_2\text{C}_6\text{H}_4\text{O})(\text{MesN}=\text{CH}-\text{CH}=\text{NMes})]$ (**2-5**) occurs by selective oxygen-atom insertion into the arylpalladium bond. The product is analogous to that observed previously by Hillhouse³⁵ on oxidation of Ni(II) complexes with N_2O (Scheme 2-3).



Scheme 2-8 The reaction of complex **2-2** with hydrogen peroxide.

To identify the optimal reaction conditions the conversion was monitored by ^1H NMR spectroscopy by following the diagnostic imine singlets of **2-2** and **2-5** (Table 2-1 and Figure 2-3). The conversion to **2-5** is highest in more polar solvents (Table 2-1, Entries 1-4), suggesting a charge-separated species is important in the formation of **2-5**. Alternatively, the more polar solvent may promote miscibility of the H_2O_2 solution (30% in H_2O). Using acetone as the optimal solvent the reaction time was increased from 1 to 3 h, giving a maximum conversion of 82% (Entry 5). The formation of **2-5** is thus considerably slower than reaction of **2-2** with the halogens to give **2-3/2-4** (Scheme 2-7), in which a dramatic colour change is observed within minutes. Different equivalents of H_2O_2 in the range of 1 to 4 were tested (Entries 5-9), revealing that two equivalents are optimal. The decrease in observed yield of **2-5** with greater equivalents is notable in the context of catalytic applications where an oxidant is used in considerable excess to the catalyst. Here, the low conversion with higher equivalents is, at least in part, due to subsequent reactivity of **2-5** to release the organic ligand as a benzofuran product (*vide infra*). The optimization reveals that the maximum conversion to **2-5** (82%) is achieved in acetone with 2 equivalents of H_2O_2 in a reaction time of three hours, and the isolated yield was 50% under these conditions.

Table 2-1 Optimization of the formation of **2-5** from **2-2** at room temperature.^a

Entry	Solvent	ϵ^b	Time (h)	2-2 : H_2O_2	2-5 (%) ^c
1	$(\text{CD}_3)_2\text{CO}$	20.7	1	1:2	67
2	CD_2Cl_2	8.9	1	1:2	33
3	CDCl_3	4.8	1	1:2	40
4	C_6D_6	2.2	1	1:2	21

5	(CD ₃) ₂ CO	20.7	3	1:2	82
6	(CD ₃) ₂ CO	20.7	3	1:1	43
7	(CD ₃) ₂ CO	20.7	3	1:1.5	62
8	(CD ₃) ₂ CO	20.7	3	1:3	40
9	(CD ₃) ₂ CO	20.7	3	1:4	37

^a All reactions were carried out under air and at room temperature (see experimental for details). ^b Dielectric constant of solvent; ^c The yield of **2-5** was calculated by integration of its imine resonances relative to the internal standard 1,3,5-trimethoxybenzene.

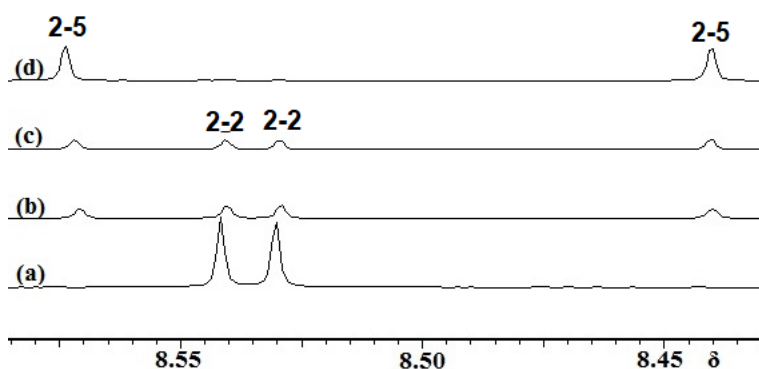


Figure 2-3 ¹H NMR spectra in the region of the imine protons during reaction of complex **2-2** with 2 eq H₂O₂ in (CD₃)₂CO at room temperature to give complex **2-5**. Spectra depict a) authentic **2-2**; and the reaction mixture of **2-2** and H₂O₂ after (b) 10 min., (c) 2 h., and (d) 3 h.

Compound **2-5** was fully characterized by ¹H and ¹³C NMR and IR spectroscopies, mass spectrometry, elemental analysis and X-ray crystallography. The ¹H NMR spectrum gives two sets of imine and mesityl resonances indicating that **2-5** has C_s symmetry (Figure 2-3). The singlet resonances for CH₂ and CMe₂ are found at δ 1.73 and 1.10, respectively, upfield of those found for **2-2**.

The structure of complex **2-5** was determined as the benzene solvate and is shown in Figure 2-4. The structure confirms the selectivity for O-atom insertion is for the Pd-C(sp²) bond. The 6-membered PdC₄O ring adopts a twist chair conformation, with the atom C(6) having the highest displacement of

0.64 Å from the palladium square plane. The two mesityl rings are twisted out of the square plane of the palladium diimine ring by 67 and 79°.

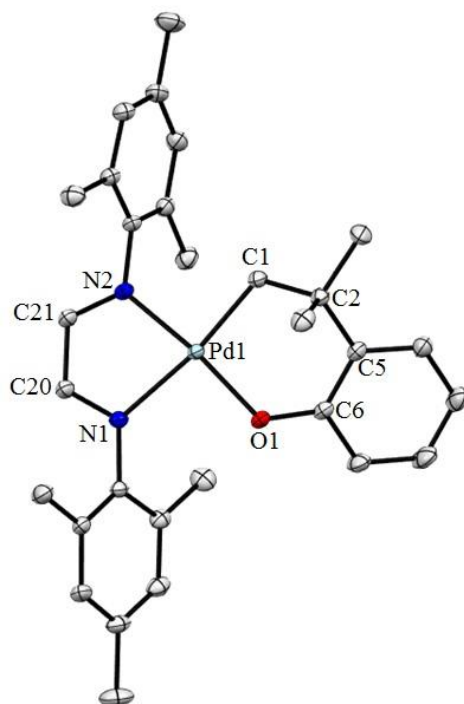
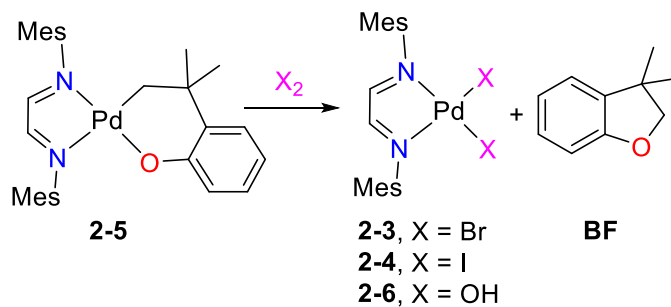


Figure 2-4 A view of the structure of complex **2-5** (ellipsoids at 50% probability). Co-crystallized benzene and hydrogen atoms are not shown, for clarity. Selected bond parameters: Pd(1)O(1) 1.9900(10); Pd(1)C(1) 2.0124(12); Pd(1)N(2) 2.0187(11); Pd(1)N(1) 2.1685(10) Å; O(1)Pd(1)C(1) 92.45(4); N(2)Pd(1)N(1) 78.12(4)°.

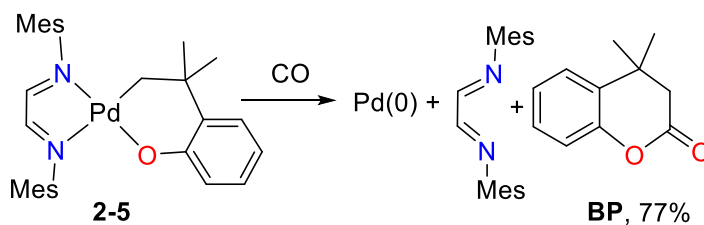
The complex **2-5** reacted with bromine or iodine oxidants to give the corresponding complex **2-3** or **2-4** and 3,3-dimethyl-2,3-dihydro-benzofuran (**BF**) according to Scheme 2-9.



Scheme 2-9 The reaction of complex **2-5** with bromine or iodine.

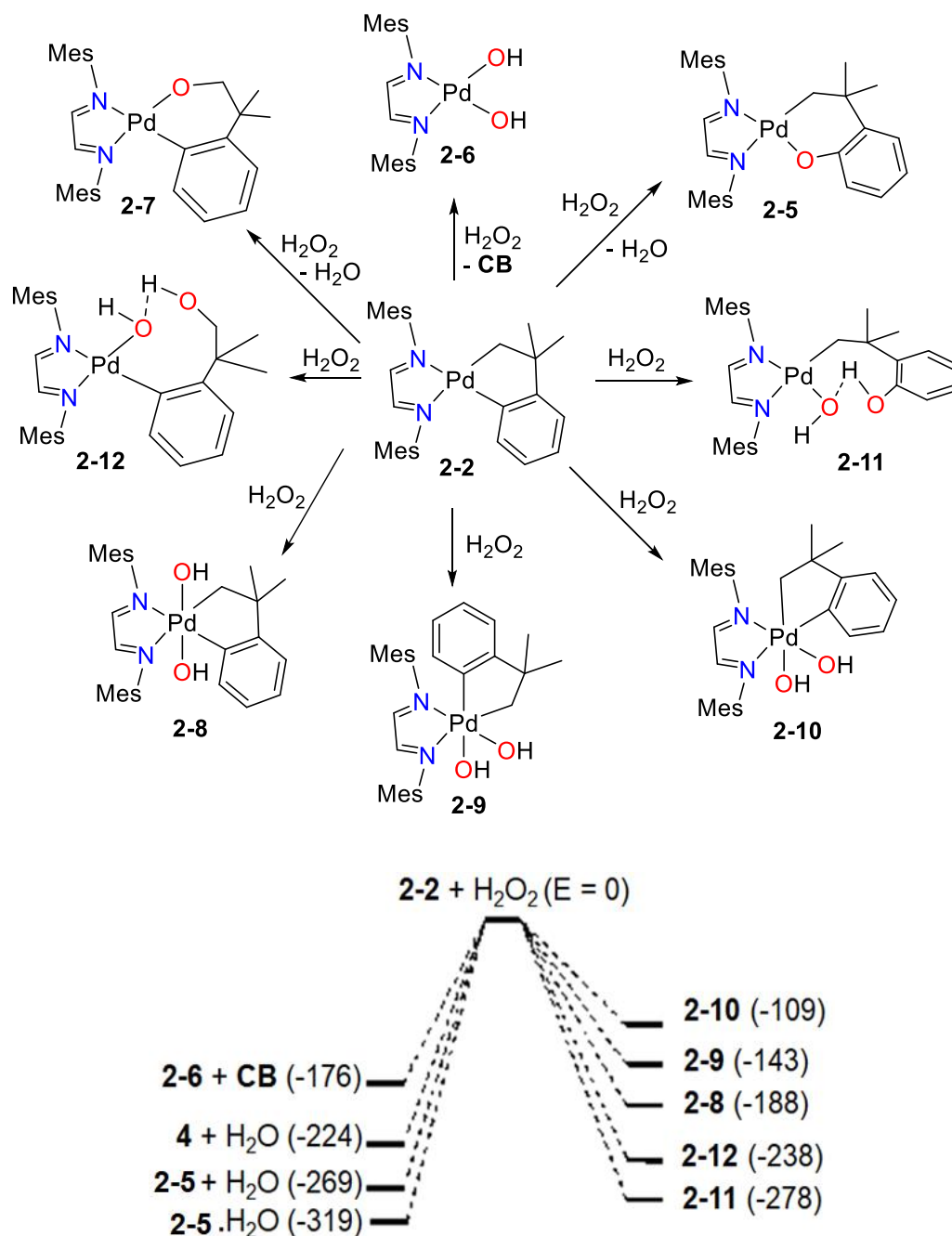
Complexes **2-3** and **2-4** were characterized as described above, while the organic product 3,3-dimethyl-2,3-dihydro-benzofuran was identified by its NMR and mass spectra, and isolated in 27% yield from the reaction with iodine.⁵⁰⁻⁵² The reaction is expected to occur by an oxidative addition-reductive elimination sequence, but no palladium(IV) intermediate was detected. The presumed reductive elimination step occurs selectively by C(sp³)-O bond formation, rather than C(sp³)-X bond formation. The formation of **2-3**, **2-4** and **BF** is consistent with halide oxidation of the analogous O-atom inserted nickel complex studied by Hillhouse³⁵ (Scheme 2-3). The reaction of **2-2** with excess hydrogen peroxide occurs to give **2-5** (Scheme 2-8) and then further reaction occurs with release of 3,3-dimethyl-2,3-dihydro-benzofuran (Scheme 2-9). In this case the expected dihydroxopalladium(II) complex **2-6** has not been obtained in pure form. When the reaction with H₂O₂ was monitored by ¹H NMR spectroscopy, imine resonances for a symmetrical complex, suggested to be **2-6**, were observed but they decayed over a period of hours. It is well known that hydroxopalladium(II) complexes tend to form dimers or oligomers by forming bridging hydroxide or oxide groups, and this may occur with the proposed complex **2-6**.⁵³⁻⁵⁸ However, we have not been able to isolate pure products or to identify them by NMR spectroscopy or ESI-MS or MALDI-MS, and the characterization of **2-6** remains tentative. The requirement for excess hydrogen peroxide in this case suggests that a parallel palladium catalyzed decomposition of hydrogen peroxide may occur.⁵⁸

A solution of complex **2-5** in acetone-*d*₆ reacted quickly with CO (1 atm) to give a precipitate of palladium black. After 15 minutes, the solution was filtered to remove the Pd and the organic products were identified as the free diimine ligand and 4,4-dimethyl-2-oxo-2H-1-benzopyran (**BP**) by their ¹H NMR spectra (Scheme 2-10). The formation of the benzopyran derivative **BP** was confirmed by GC-MS, and was the only product derived from the palladacycle unit of **2-5** that was detected. In this case, the product is suggested to form by CO insertion followed by reductive elimination from a palladium(II) complex intermediate. The nickel(II) complex **J** (Scheme 2-3) gives a similar reaction with carbon monoxide to form **BP**.³⁵



Scheme 2-10 The reaction of **2-5** with CO.

To gain more insight into the selective oxygen-atom insertion reaction to give complex **2-5**, DFT calculations were carried out (see experimental section for details). Some of the potential reactions of complex **2-2** with hydrogen peroxide are shown in Scheme 2-11, and calculations of the energies of reaction were carried out for each case. The simplest reactions considered were *trans* or *cis* oxidative addition to give the palladium(IV) complexes **2-8**, **2-9** or **2-10**. More complex reactions involve oxidative addition followed either by reductive elimination with C-O bond formation to give **2-5** or **2-7** and water or **2-11** or **2-12**, or reductive elimination with C-C bond formation to give **2-6** and **CB**. Of the palladium(IV) isomers **2-8**, **2-9** and **2-10**, the product of *trans* oxidative addition, **2-8**, is calculated to be most stable and, in related platinum(II) chemistry, *trans* oxidative addition is also preferred kinetically in the polar mechanism of oxidative addition of O-O bonds.⁵⁹⁻⁶⁰ Formation of complex **2-5** or **2-7** involves overall oxygen-atom insertion into the Pd-C(sp²) or Pd-C(sp³) bond, respectively, and formation of **2-5** is favoured by 45 kJ mol⁻¹ over **2-7**. Similarly, the complex **2-11** or **2-12** would be formed by formal C(sp²)-O or C(sp³)-O reductive elimination from **2-8**, **2-9** and **2-10**. Product **2-11** (which is analogous to complex **2-H** in Scheme 2-2) is calculated to be at lower energy than **2-12** by 45 kJ mol⁻¹. The theory thus indicates that the products of aryl-oxygen bond formation, **2-5** or **2-11**, which are related by addition or loss of water, are thermodynamically most stable. Simple calculated bond energies favor **2-11** over **2-5** + H₂O by 9 kJ mol⁻¹ but, if the water remains hydrogen bonded to **2-5**, then **2-5**•H₂O is more stable than **2-11** by 41 kJ mol⁻¹. Of course, entropy effects favor **2-5** + H₂O over **2-11**. The products will, of course, be controlled by kinetic factors but the selective formation of complex **2-5** (Scheme 2-11) is consistent with there being a lower activation energy for formation of a more stable product.



Scheme 2-11 Above, some potential reactions of complex **2-2** with H_2O_2 and, below, the calculated energies of reaction in kJ mol^{-1} .

A suggested mechanism of reaction to give complex **2-5** is shown in Figure 2-5. An initial encounter complex **2-13** is formed between complex **2-2** and H_2O_2 , involving donation from the filled $4d_{z^2}$ orbital of **2-2** to the vacant $\sigma^*(\text{OO})$ orbital of H_2O_2 , indicated by **2-M** in Figure 2-5, leading to an increase in the calculated O-O bond distance from 1.59 Å to 1.72 Å. The rate determining step is likely to involve

further charge transfer to H₂O₂ with cleavage of the O-O bond to give the proposed palladium(IV) complex intermediate **2-14**. Complex **2-14** can be considered to contain a Pd⁺OH group hydrogen bonded to hydroxide or an oxopalladium (Pd⁺O⁻) group hydrogen bonded to water. The importance of such an intermediate is consistent with the experimental observation that polar solvents are preferable for this reaction. Since the reagent used was 30% aqueous H₂O₂, it is likely that additional water molecules may be involved in stabilizing **2-14**, and so its structure is tentative.⁶¹ With this proviso, the calculation suggests that it should be considered primarily as an oxo complex, with the significant hydrogen bonding to water (Figure 2-5) providing a mechanism to avoid the “oxo wall”.^{42,62-66} Once C-O bond formation begins, the formation of complex **2-15**, which is just complex **2-5** hydrogen bonded to water, is very favorable, and then dissociation of water gives the observed product **2-5**. The mechanism (Figure 2-5) can be considered to combine the deprotonation and bond formation steps of the proposed Mirica mechanism²⁸ of Scheme 2-2. Generation of **2-5** via the latter, stepwise, path cannot be conclusively discarded. In such a process, complex **2-15** could be considered to be an intermediate on the way to a phenol derivative along with hydroxide, and this step could be followed by deprotonation of the phenol to give **2-5**. Deprotonation would be disfavored in the Mirica system since such a step would generate the strong acid HClO₄ rather than the equivalent of H₂O produced here.

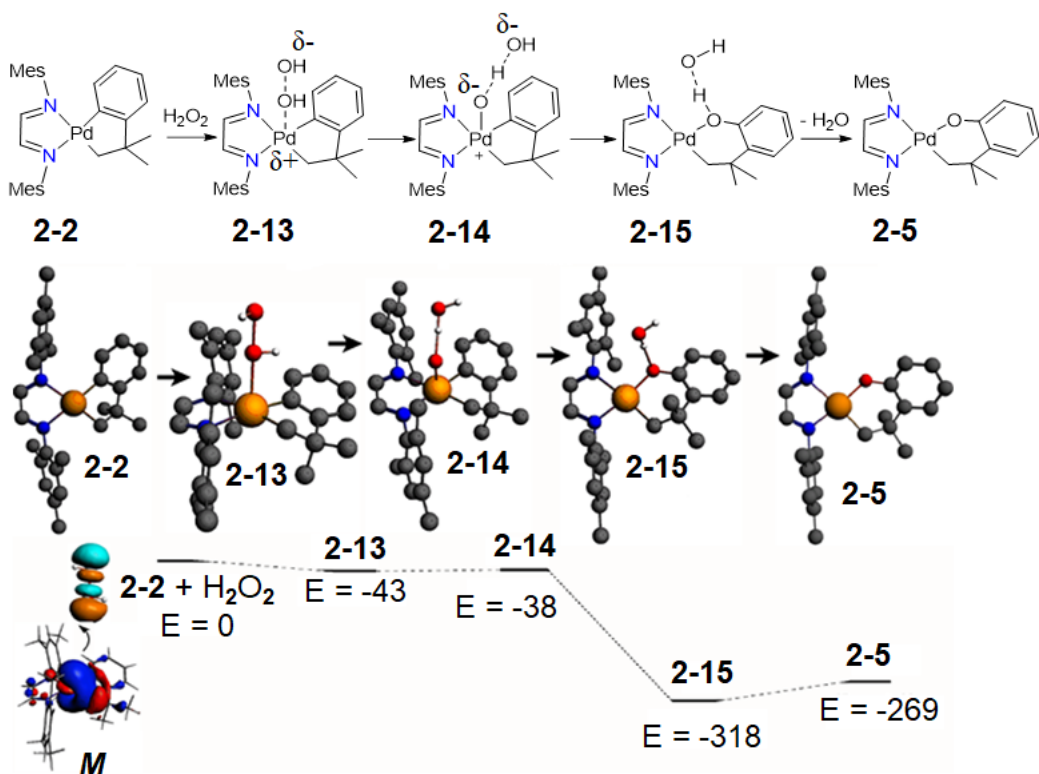
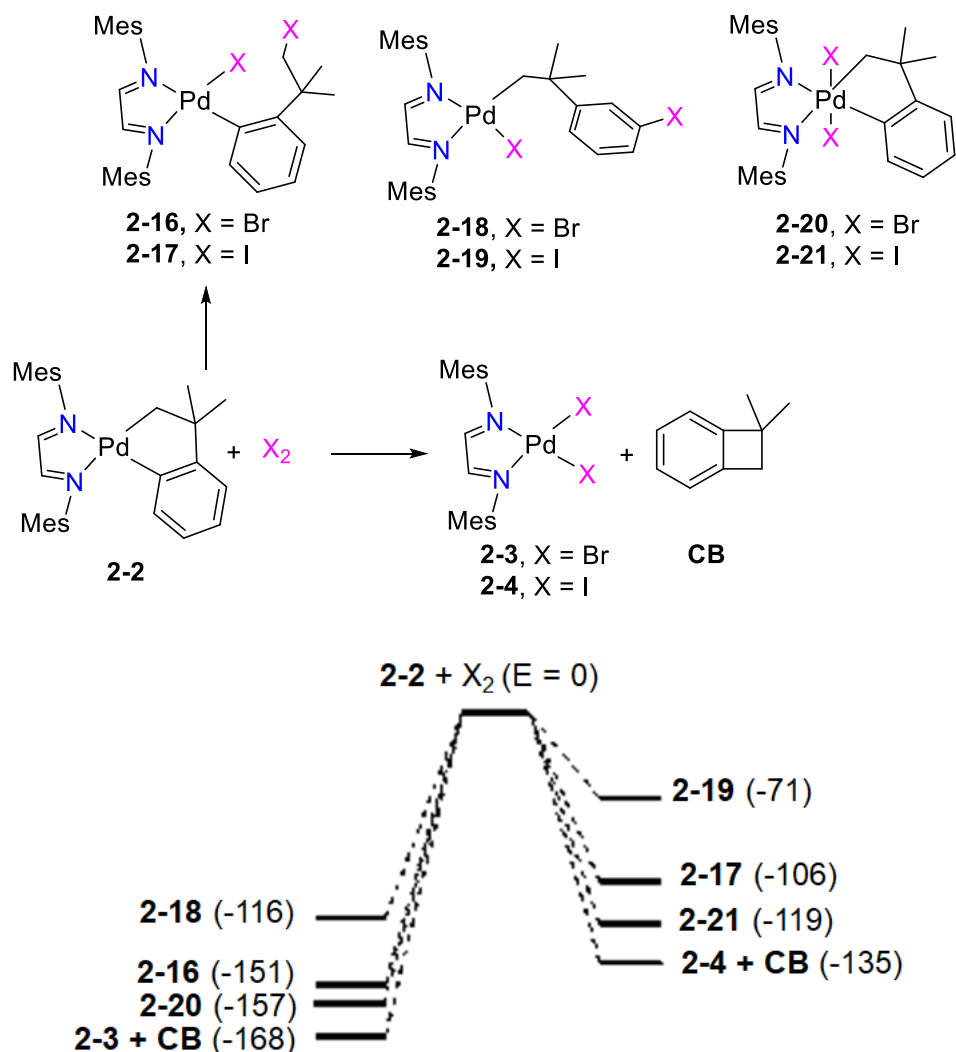


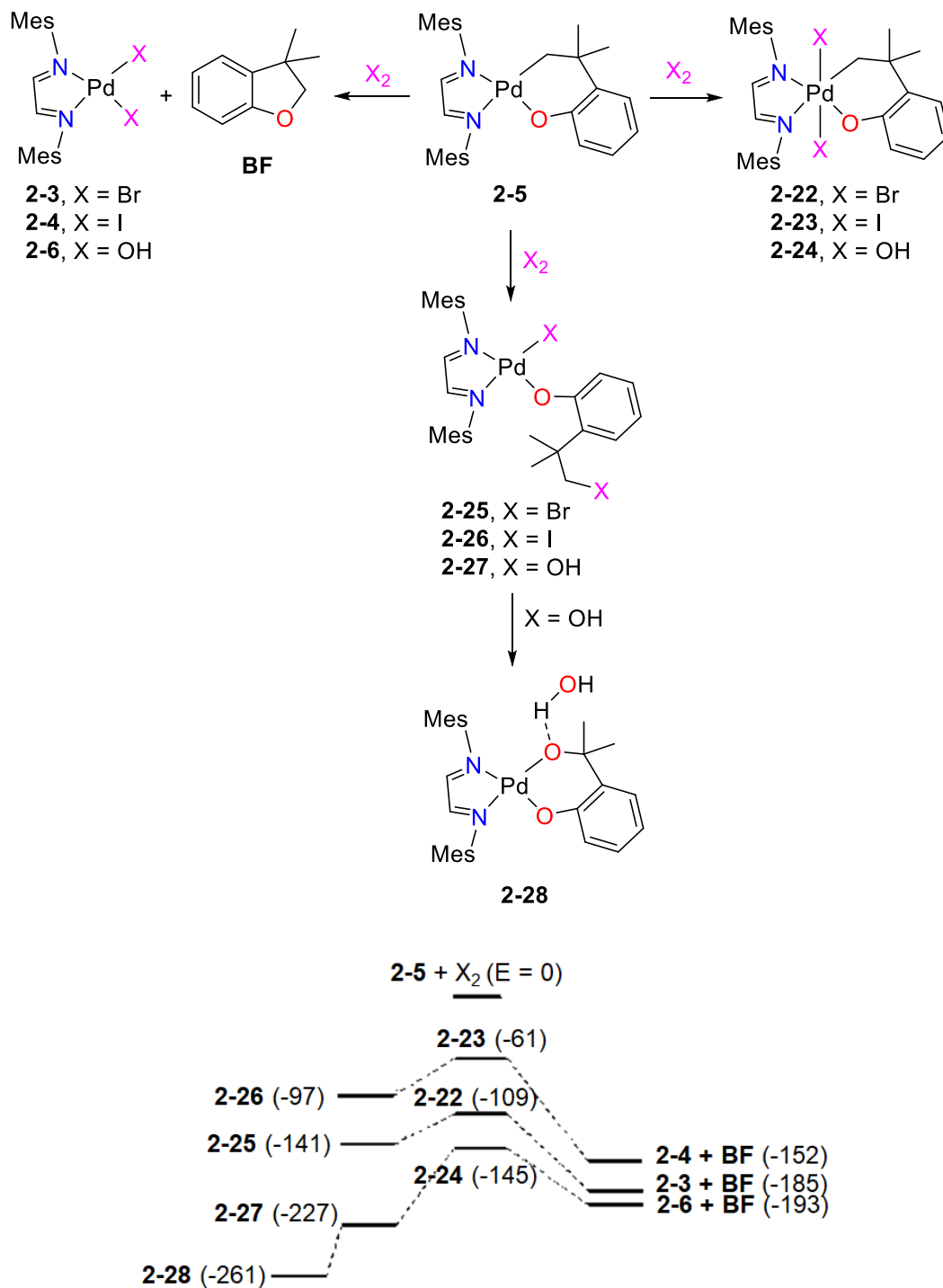
Figure 2-5 Calculated structures and relative energies (kJ mol^{-1}) of complexes and intermediates in the reaction of **2-2** with H_2O_2 to give complex **2-5**. **2-M** represents the proposed initial interaction between the $4d_{z^2}$ HOMO of complex **2-2** and the σ^* LUMO of H_2O_2 . Selected calculated bond parameters: H_2O_2 , O-O 1.59, O-H 1.01 Å; **2-13**, Pd \cdots O 2.47, O-O 1.72, PdO-H 1.00, PdOO-H 1.01 Å, Pd \cdots O-O 177°; **2-14**, Pd-O 1.98, O \cdots O 2.57, PdO \cdots H 1.54, PdOH-O 1.05, PdOHO-H 1.00 Å; **2-15**, Pd-O 2.02, O \cdots O 2.77, PdO \cdots H 1.77, PdOH-O 1.01, PdOHO-H 0.99 Å; **2-5**, Pd-O 2.02 Å.

Scheme 2-12 shows the potential products and their relative energies from reaction of complex **2-2** with bromine and iodine. In this case the reaction to give **2-3** and **CB** is calculated to be most favorable, again consistent with the experimental observations. The preference for C-C over C-X reductive elimination is calculated to follow the sequence $X = \text{I} > \text{Br} > \text{OH}$ (Schemes 2-11 and 2-12) and can be rationalized by the relative Pd-X and C-X bond dissociation energies, with $D(\text{C-X}) - D(\text{Pd-X})$ following the ligand hardness sequence $X = \text{OH} > \text{Br} > \text{I}$. In contrast to the case with $X = \text{OH}$ (Scheme 2-11), the theory predicts that for C-X bond formation, reaction at $\text{C}(\text{sp}^3)$ is preferred over $\text{C}(\text{sp}^2)$, with **2-16** being lower in energy than **2-18** (Scheme 2-12).



Scheme 2-12 Some possible products, and their relative energies (kJ mol⁻¹) from reaction of complex **2-2** with bromine or iodine.

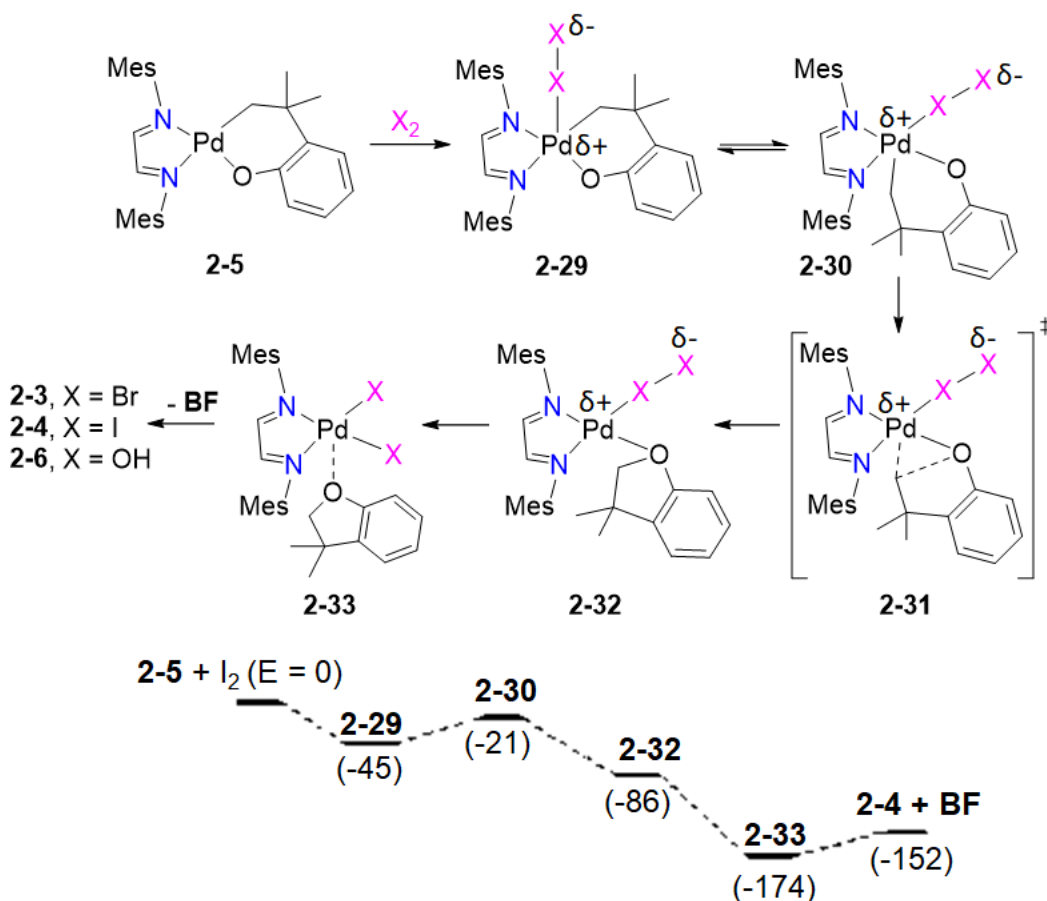
In the above examples, the thermodynamically more stable products are also favored kinetically as they are the experimentally observed products. This is also the case for the reactions of **2-5** with Br₂ and I₂ (Scheme 2-13). The calculations show that oxidation followed by intramolecular C(sp³)-O reductive elimination to give **BF** and **2-3,2-4** is more favorable than reductive elimination to give **2-25,2-26** that contains a new C(sp³)-X bond (X = Br, I). In contrast, **2-6** and **BF** are not the most favourable products for oxidation of **2-5** with H₂O₂. Instead, the more stable product is expected to be **2-27** or the cyclic derivative **2-28**. Experimentally **BF** is observed as a product of oxidation of **2-5** with H₂O₂ (Scheme 2-9). It is expected that the products in all of the reactions are determined by kinetic control and this is the only case in which the product is not also the most thermodynamically stable, as calculated by DFT.



Scheme 2-13 Potential products, and their relative energies from reactions of complex **2-5**.

From a mechanistic point of view, the reductive elimination following oxidation of **2-5** with Br₂, I₂ or H₂O₂ is likely to occur from a 5-coordinate Pd(IV) intermediate (Scheme 2-14 for the representative example with I₂). Initial attack by the electrophilic iodine is likely to give the diiodine complex **2-29**, for which several precedents are known.⁶⁷⁻⁶⁹ Complete I-I bond cleavage from **2-29** followed by attack

of the iodide ion at palladium or at the CH₂ group would give **2-23** or **2-26** respectively (Scheme 2-13). However, intramolecular C-O reductive elimination to give **2-4** is evidently preferred, perhaps after pseudorotation of **2-29** to give the isomer **2-30** so that the initial benzofuran (**BF**) palladium(II) complex **2-32** is formed in its most stable form by way of transition state **2-31**. Then displacement of **BF** by iodide via complex **2-33** completes the reaction.



Scheme 2-14 A likely mechanism for reactions of complex **2-5** with oxidants X₂ (X = Br, I, OH), and the relative energies (kJ mol⁻¹) for the case with X = I.

2.3 Conclusions

The initial reaction of complex **2-2** with hydrogen peroxide occurs to give selective oxygen-atom insertion into the arylpalladium bond to give complex **2-5** (Scheme 2-8), while the reactions with bromine and iodine lead to intramolecular C-C bond formation to give 1,1-dimethylcyclobutabenzene and **2-3** or **2-4** (Scheme 2-7). Complex **2-5** reacts with all three oxidants by intramolecular C-O bond formation to give 3,3-dimethyl-2,3-dihydro-benzofuran and **2-3**, **2-4** or **2-6** (Scheme 2-9). In most cases,

experimentally observed oxidation products were calculated to be the most thermodynamically stable products. This suggests that, in similar systems, thermodynamic stability can act as a good guide for kinetically controlled oxidation selectivity. The observed oxygen-atom insertion may be an operative process in C-O bond forming reactions catalyzed by Pd with H₂O₂ as the oxidant. The selectivity observed here is promising for a greater development in catalytic oxidations of hydrocarbons.

2.4 Experimental

2.4.1 Reagents and General Procedures

All reactions were carried out under air, unless otherwise specified. For those reactions that were conducted under nitrogen atmosphere, standard Schlenk techniques were used. All solvents used for air- and moisture-sensitive reactions were purified using an Innovative Technologies 400-5 Solvent Purification System (SPS) and were stored over activated 4 Å molecular sieves. NMR spectra were recorded at 298 K using Varian INOVA 400 or 600 MHz spectrometers. ¹H and ¹³C chemical shifts were referenced internally to solvent (residual signal for ¹H) where the chemical shift was set to appropriate values relative to TMS at 0.00 ppm. Complete assignment of each compound was aided by the use of ¹H-¹H gCOSY, ¹H-¹³C{¹H} HSQC and ¹H-¹³C{¹H} HMBC experiments and are reported using the labeling scheme in Chart 2-1. Commercial reagents and aqueous 30% H₂O₂ were used without further purification. The complex [PdCl₂(COD)]²⁸⁻²⁹, and the diimine ligand, 1,2-bis(mesitylimino)ethane (**2-L1**),⁴⁶ were synthesized according to the literature procedures. The complex [PdCl(CH₂CMe₂C₆H₅)(COD)]²⁸⁻²⁹ was prepared under N₂ following the procedure reported by Mirica *et al.*²⁸ with the following slight modification: after addition of the Grignard reagent at -70°C, the solution was stirred at low temperature and allowed to slowly reach room temperature over 17 h. Complex [Pd(CH₂CMe₂C₆H₄)(COD)]²⁸⁻²⁹ (**2-1**) was also prepared under N₂ following a procedure from Mirica *et al.*²⁸ with the following minor modification: the reaction was carried out using an ice bath, and a degassed water solution was used to dissolve the base. In both modified syntheses, ¹H NMR spectra matched literature values and yields were improved by 30% and 10%, respectively. Elemental analyses were performed by Laboratoire d'Analyse Élémentaire de l'Université de Montréal. Organic products were analyzed using a Shimadzu GCMS-QP2010 Ultra GC with a DB-5 column. MALDI-TOF mass spectra were collected using an AB Sciex 5800 TOF/TOF mass spectrometer using anthracene as the matrix in a 20:1 matrix:substrate molar ratio.

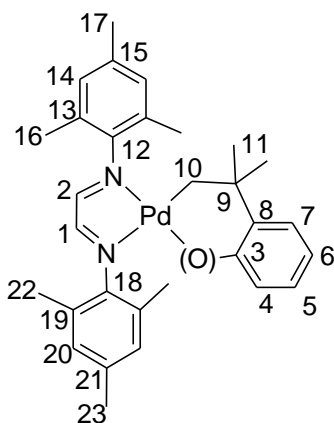


Chart 2-1 Atom labels for complexes **2-2** and **2-5** for NMR spectroscopy assignments

2.4.2 Synthesis of $[\text{Pd}^{\text{II}}(\text{CH}_2\text{CMe}_2\text{C}_6\text{H}_4)(\text{MesN}=\text{CH}-\text{CH}=\text{NMe})]$, **2-2**.

To a stirred solution of $[\text{Pd}(\text{CH}_2\text{CMe}_2\text{C}_6\text{H}_4)(\text{COD})]$, **2-1**, (0.907 g, 2.00 mmol in ether (50 mL) cooled to -65°C was added a solution of $\text{MesN}=\text{CH}-\text{CH}=\text{NMe}$, **2-L1**, (0.764 g, 2.00 mmol) in ether (20 mL). The mixture was allowed to stir and slowly reach room temperature over 17 h, during which time the color of the solution changed from yellow to red. Upon removal of the solvent under reduced pressure, a red solid was formed, which was reprecipitated from ether (5 mL) with hexanes (30 mL). The solid was collected by filtration and dried under vacuum, to give **2-2** as an air-stable product (0.841 g, 1.58 mmol, 75 %). ^1H NMR (C_6D_6 , 600 MHz, 25°C) δ : 7.06 (s, *H1*, 1H), 7.05 (s, *H2*, 1H), 7.00 (t, $J = 7$ Hz, *H5*, 1H), 6.94 (d, $J = 7$ Hz, *H4*, 1H), 6.86 (m, *H6*, 1H), 6.77 (s, *H20*, 2H), 6.75 (s, *H14*, 2H), 6.65 (d, $J = 8$ Hz, *H7*, 1H), 2.48 (s, *H10*, 2H), 2.17 (s, *H16* and *H17*, 9H), 2.12 (s, *H22*, 6H), 2.10 (s, *H23*, 3H), 1.49 (s, *H11*, 6H.) $^{13}\text{C}\{^1\text{H}\}$ NMR (C_6D_6 , 151 MHz, 25°C) δ : 170.19 (*C8*), 161.64 (*C1*), 161.45 (*C2*), 158.71 (*C3*), 147.44 (*C18*), 146.66 (*C12*), 136.36 (*C15*), 136.26 (*C21*), 134.85 (*C7*), 129.61 (*C14*), 129.47 (*C20*), 128.93 (*C13* and *C19*), 124.76 (*C5*), 124.40 (*C6*), 122.61 (*C4*), 48.00 (*C9*), 47.58 (*C10*), 34.68 (*C11*), 21.40 (*C23*), 21.32 (*C17*), 18.85 (*C22*), 18.45 (*C16*). Note that the correlations do not identify specific rings, so assignments for the *C12-C17* and *C18-C23* rings, and for imine groups *C1* and *C2*, are arbitrary and could be inverted. MALDI MS (anthracene matrix): Calcd. m/z 530.2 $[\text{Pd}(\text{MesN}=\text{CH}-\text{CH}=\text{NMe})(\text{CH}_2\text{CMe}_2\text{C}_6\text{H}_4)]^{\bullet+}$, Obs. m/z 530.2. Anal. Calcd. for $\text{C}_{30}\text{H}_{36}\text{N}_2\text{Pd}$: C, 67.85; H, 6.83; N, 5.28. Found: C, 67.81; H, 7.00; N, 5.14. Red crystals suitable for single crystal X-ray crystallographic analysis were grown by the slow evaporation of a solution of **2-2** in ether at room temperature.

2.4.3 Synthesis of [PdBr₂(MesN=CH-CH=NMe_s)], **2-3**.

To a solution of complex **2-2** (0.020 g, 0.037 mmol) in acetone (2 mL) was added excess Br₂ (10.4 μL, 0.203 mmol) whilst stirring. After 5 min the reaction mixture became a bright orange color. After 2 h the volume of solvent was reduced to ~1 mL and pentane (4 mL) was added to precipitate the product as an orange powder, which was separated by filtration, washed with pentane (3 × 2 mL) and hexanes (3 × 2 mL), and dried under high vacuum (0.021 g, 0.031 mmol, 85%). ¹H NMR (DMSO-*d*₆, 600 MHz, 25°C) δ: 8.27 (s, 2H, CH=N), 6.97 (s, 4H, mes-*H*), 2.29 (s, 18H, 6Me). Anal. Calcd. for C₂₀H₂₄Br₂N₂Pd: C, 43.00; H, 4.33; N, 5.01. Found: C, 43.35; H, 4.42; N, 4.85. Orange crystals suitable for single crystal X-ray crystallographic analysis were grown from the slow vapor diffusion of methanol into a DMSO solution of **2-3**.

2.4.4 Synthesis of [PdI₂(MesN=CH-CH=NMe_s)], **2-4**.

Compound **2-4** was synthesized in a similar way to **2-3**, but using I₂ (0.027 g, 0.092 mmol, 2.5 equiv) instead of Br₂. The dark red solid was formed in 65% yield (0.028 g, 0.036 mmol). ¹H NMR ((CD₃)₂CO, 600 MHz, 25°C) δ: 8.51 (s, 2H, CH=N), 6.95 (s, 4H, mes-*H*), 2.30 (m, 18H, 6Me). Anal. Calcd. for C₂₀H₂₄I₂N₂Pd: C, 36.81; H, 3.71. Found: C, 36.90; H, 3.71. Orange crystals suitable for single crystal X-ray crystallographic analysis were grown by the slow evaporation of acetone solution of **2-4** in the room temperature.

2.4.5 Synthesis of [Pd(MesN=CH-CH=NMe_s)(CH₂CMe₂C₆H₄O)], **2-5**.

A vial was charged with a stir bar, **2-2** (0.040 g, 0.072 mmol) and acetone (4 mL). The H₂O₂ solution (7.5 μL, 2 equiv, 0.14 mmol) was added to the vial via a microliter syringe while stirring. The solution was stirred for 3 h. and then the solvent was evaporated to dryness and residue was washed with hexanes (3 × 3 mL). The crude product was isolated by silica gel column chromatography (9:1 ethyl acetate:pentane) (R_f = 0.087). The product was observed as a dark green band and fractions of this colour were combined and the solvent was removed under vacuum to give **2-5** as a dark-green solid in 50% yield (0.019 mg, 0.036 mmol). ¹H NMR ((CD₃)₂CO, 600 MHz, 25°C) δ: 8.57 (s, *H*1, 1H), 8.44 (s, *H*2, 1H), 7.01 (s, *H*14, 2H), 6.98 (s, *H*20, 2H), 6.78 (d, 1H, *J* = 8 Hz, *H*4), 6.63 (m, 1H, *H*5), 6.25 (d, 1H, *J* = 8 Hz, *H*7), 6.19 (t, *J* = 8 Hz, *H*6, 1H), 2.38 (s, *H*22, 6H), 2.32 (s, *H*17, 3H), 2.32 (s, *H*23, 3H), 2.25 (s, *H*16, 6H), 1.73 (s, *H*10, 2H), 1.10 (s, *H*11, 6H); ¹³C{¹H} NMR ((CD₃)₂CO, 151 MHz, 25°C) δ: 167.14 (*C*1), 164.40 (*C*3), 162.85 (*C*2), 145.26 (*C*12), 145.09 (*C*18), 138.85 (*C*8), 136.85 (*C*21), 136.30 (*C*15), 129.54 (*C*19), 129.38 (*C*13), 129.25 (*C*20), 129.11 (*C*14), 126.12 (*C*5), 124.89 (*C*4), 118.98

(C7), 113.44 (C6), 47.58 (C10), 34.50 (C9), 30.84 (C11), 20.76 (C23), 20.69 (C17), 18.39 (C22), 17.67 (C16). Note that the correlations do not identify specific rings, so assignments for the C12-C17 and C18-C23 rings, and for imine groups C1 and C2, are arbitrary and could be inverted. MALDI MS (Anthracene matrix): Calcd. m/z 546.2 [Pd(MesN=CH-CH=NMe)(CH₂CMe₂OC₆H₄)]⁺, Obs. m/z 546.2. Anal. Calcd. for C₃₀H₃₆N₂OPd.H₂O: C, 63.77; H, 6.78; N, 4.96. Found: C, 64.03; H, 6.67; N, 4.79. Single crystals suitable for X-ray crystallographic analysis were grown by the slow evaporation of a benzene solution of **2-5** at room temperature.

2.4.6 Reaction of Complex **2-2** with Halogens.

A 1:1 solution of iodine and complex **2-2** in CDCl₃ was monitored by ¹H NMR spectroscopy. The resonances for complex **2-4** and 1,1-dimethyl-1,2-dihydrocyclobutabenzene were observed and complex **2-2** was completely consumed.^{26,48-49} After 2 h., the volume of solution was reduced, and pentane was added to precipitate complex **2-4**. The solid was filtered, washed with pentane, and the solvent was removed from the filtrate to give 1,1-dimethyl-1,2-dihydrocyclobutabenzene **CB** as a yellow oil, which was redissolved in CDCl₃ and characterized by ¹H NMR spectroscopy and GC-MS. Yield of **CB** 37%, calculated using dimethyl terephthalate as internal standard. ¹H NMR for **CB** (CDCl₃, 600 MHz, 25°C) δ: 8.01 (m, 1H, C₆H₄), 7.17 (m, 1H, C₆H₄), 7.07 (m, 1H, C₆H₄), 7.01 (m, 1H, C₆H₄), 2.95 (s, 2H, CH₂), 1.42 (s, 6H, CH₃). LR-MS: Found: m/z = 132.15. Calcd. for C₁₀H₁₂: m/z = 132.2. The reaction of **2-2** with bromine was carried out in a similar way.

2.4.7 Reaction of Complex **2-5** with Halogens.

A solution of **2-5** (0.020 g, 0.036 mmol) and the internal standard dimethyl terephthalate (0.001 g, 0.009 mmol) was prepared in acetone-*d*₆ (0.7 mL). A ¹H NMR spectrum was obtained to determine the initial ratio of **2-5** to the internal standard. To this was added a solution of iodine (0.009 g, 0.036 mmol) in acetone-*d*₆ (0.7 mL) and the reaction was monitored by ¹H NMR spectroscopy. The resonances for complex **2-4** and 3,3-dimethyl-2,3-dihydro-benzofuran, **BF**, were observed; complex **2-5** was completely consumed after 2 h.⁵⁰⁻⁵² The in-situ yield of **BF** was calculated to be 27% relative to the internal standard. Pentane (2 mL) was added to the reaction solution to precipitate complex **2-4**. The mixture was filtered, and the filtrate was evaporated to give a crude sample of 3,3-dimethyl-2,3-dihydro-benzofuran, **BF**, as a pale brown oil. The oil was dissolved in CDCl₃ and characterized by ¹H NMR spectroscopy and GC-MS. ¹H NMR (CDCl₃, 600 MHz, 25°C) δ: 4.22 (s, 2H, OCH₂), 1.33 (s, 6H, CH₃), in agreement with the literature values.⁵⁰ The aromatic signals are obscured due to the presence

of other signals there. The sample was dissolved in acetone- d_6 to facilitate identification of **BF** in other reactions. ^1H NMR for **BF** ($(\text{CD}_3)_2\text{CO}$, 600 MHz, 25°C) δ : 6.64 - 6.66 (m, 4H, C_6H_4), 4.19 (s, 2H, OCH_2), 1.31 (s, 6H, CH_3). GC-MS for **BF**, Found: $m/z = 148.2$. Calcd. for $\text{C}_{10}\text{H}_{12}\text{O}$: $m/z = 148.1$. The reaction with bromine was carried out in a similar way.

2.4.8 Reaction of Complex **2-2** with Excess H_2O_2 .

A vial was charged with a stir bar, complex **2-2** (0.020 g, 0.036 mmol) and d_6 -acetone (2 mL). A solution of H_2O_2 (7.5 μL , 4 equiv, 0.14 mmol) was added to the vial via a microliter syringe while stirring. The reaction was monitored by ^1H NMR spectroscopy, as conversion to **2-5**, **2-6** and **BF** occurred. After 10 min. relative integration revealed the following species: **2-2** (6%), **2-5** (60%), **2-6** (34%). Within 2 h signals for **2-6** had completely disappeared, but **2-5** persisted. Formation of the organic product **BF** was confirmed by comparison to the ^1H NMR spectrum of isolated **BF** in acetone- d_6 (see above). ^1H NMR in $(\text{CD}_3)_2\text{CO}$ at 600 MHz, 25°C resonances tentatively assigned to **2-6**: $\delta(^1\text{H}) = 8.10$ (s, 2H, $\text{CH}=\text{N}$), 6.91 (s, 4H, mes- CH), 2.11 (s, 18H, CH_3).

2.4.9 Reaction of Complex **2-5** with CO.

A solution of complex **2-5** (0.016 g, 0.030 mmol) in acetone- d_6 (3 mL) was stirred under CO atmosphere at room temperature for 15 min. The solution was filtered to remove the precipitated palladium black and then monitored by ^1H NMR spectroscopy. Complex **2-5** was completely consumed and resonances for MesN=CH-CH=NMe and 4,4-dimethyl-2-oxo-2H-1-benzopyran, **BP** (77% yield), were observed.^{35,46} ^1H NMR for **BP** (CD_2Cl_2 , 600 MHz, 25°C) δ : 7.36 (dd, 1H, aryl), 7.27 (m, 1H, aryl), 7.18 (m, 1H, aryl), 7.05 (dd, 1H, aryl), 2.62 (s, 2H, CH_2), 1.35 (s, 6H, 2 CH_3). LR-MS for **BP**: Found: $m/z = 176.15$. Calcd. for $\text{C}_{11}\text{H}_{12}\text{O}_2$: $m/z = 176.21$.

2.4.9.1 X-Ray Structure Determinations⁷⁰⁻⁷³

Data Collection and Processing. A crystal was mounted on a Mitegen polyimide micromount with a small amount of Paratone N oil. All X-ray measurements were made using a Bruker Kappa Axis Apex2 diffractometer at a temperature of 110 K. The frame integration was performed using SAINT, and the resulting raw data was scaled and absorption corrected using a multi-scan averaging of symmetry equivalent data using SADABS.

Structure Solution and Refinement. The structures were solved by using the SHELXT program. All non-hydrogen atoms were obtained from the initial solution. The hydrogen atoms were introduced at idealized positions and were allowed to ride on the parent atom. The structural model was fit to the

data using full matrix least-squares based on F^2 . The calculated structure factors included corrections for anomalous dispersion from the usual tabulation. The structure was refined using the SHELXL-2014 program from the SHELX suite of crystallographic software.⁷⁰⁻⁷³ Details are given in Table A2.1 and in the CIF files.

2.4.10 DFT Calculations

DFT calculations were carried out for gas phase structures by using the Amsterdam Density Functional program based on the **BP** functional, with double-zeta basis set and first-order scalar relativistic corrections.⁷⁴⁻⁷⁵ Minima were confirmed by vibrational analysis; transition states were not determined.

2.5 References

1. A. J. Canty, *Acc. Chem. Res.*, 1992, **25**, 83-90.
2. A. J. Canty, *Dalton Trans.*, 2009, 10409-10417.
3. P. Sehnal, R. J. K. Taylor and I. J. S. Fairlamb, *Chem. Rev.*, 2010, **110**, 824-889.
4. L. -M. Xu, B. -J. Li, Z. Yang and S. -J. Shi, *Chem. Soc. Rev.*, 2010, **39**, 712-733.
5. K. J. Bonney and F. Schoenebeck, *Chem. Soc. Rev.*, 2014, **43**, 6609-6638.
6. I. Vicente-Hernandez, M. -T. Chicote, J. Vicente and D. Bautista, *Chem. Commun.*, 2016, **52**, 594-596.
7. B. E. Haines, H. Xu, P. Verma, C. -C. Wang, J. -Q. Yu and D. G. Musaev, *J. Am. Chem. Soc.*, 2015, **137**, 9022-9031.
8. J. Hu, T. Lan, Y. Sun, H. Chen, J. Yao and Y. Rao, *Chem. Commun.*, 2015, **51**, 14929-14932.
9. J. J. Topczewski and M. S. Sanford, *Chem. Sci.*, 2015, **6**, 70-76.
10. Y. Li, Y. Wu, G. -S. Li and X. -S. Wang, *Adv. Synth. Catal.*, 2014, **356**, 1412-1418.
11. M. G. Campbell and T. Ritter, *Chem. Record.*, 2014, **14**, 482-491.
12. K. Muniz, *Angew. Chem., Int. Ed.*, 2009, **48**, 9412-9423.
13. A. J. Canty, M. C. Denney, G. van Koten, B. W. Skelton and A. H. White, *Organometallics.*, 2004, **23**, 5432-5439.
14. W. N. Oloo, P. Y. Zavalij and A. M. Vedernikov, *Organometallics.*, 2013, **32**, 5601-5614.
15. A. N. Campbell and S. S. Stahl, *Acc. Chem. Res.*, 2012, **45**, 851-863.
16. L. Boisvert, M. C. Denney, S. K. Hanson and K. I. Goldberg, *J. Am. Chem. Soc.*, 2009, **131**, 15802-15814.
17. M. L. Scheuermann and K. I. Goldberg, *Chem. Eur. J.*, 2014, **20**, 14556-14568.
18. A. K. Cook and M. S. Sanford, *J. Am. Chem. Soc.*, 2015, **137**, 3109-3118.

19. T. W. Lyons and M. S. Sanford, *Chem. Rev.*, 2010, **110**, 1147-1169.
20. A. Vigalok, *Acc. Chem. Res.*, 2015, **48**, 238-247.
21. M. J. Geier, M. D. Aseman and M. R. Gagné, *Organometallics.*, 2014, **33**, 4353-4356.
22. A. V. Sbergaeva, P. Y. Zavalij and A. N. Vedernikov, *J. Am. Chem. Soc.*, 2016, **138**, 1446-1455.
23. T. Furuya, D. Benitez, E. Tkatchouk, A. E. Strom, P. Tang, W. A. Goddard and T. Ritter, *J. Am. Chem. Soc.*, 2010, **132**, 3793-3807.
24. J. M. Racowski, A. R. Dick and M. S. Sanford, *J. Am. Chem. Soc.*, 2009, **131**, 10974-10983.
25. M. H. Pérez-Temprano, J. M. Racowski, J. W. Kampf and M. S. Sanford, *J. Am. Chem. Soc.*, 2014, **136**, 4097-4100.
26. N. M. Camasso, M. H. Pérez-Temprano and M. S. Sanford, *J. Am. Chem. Soc.*, 2014, **136**, 12771-12775.
27. N. M. Camasso and M. S. Sanford, *Science.*, 2015, **347**, 1218-1220.
28. F. Qu, J. R. Khusnutdinova, N. P. Rath and L. M. Mirica, *Chem. Commun.*, 2014, **50**, 3036-3039.
29. J. Campora, J. A. Lopez, P. Palma, P. Valerga, E. Spillner and E. Carmona, *Angew. Chem. Int. Ed.*, 1999, **38**, 147-151.
30. J. Campora, E. Gutierrez-Puebla, J. A. Lopez, A. Monge, P. Palma, D. del Rio and E. Carmona, *Angew. Chem. Int. Ed.*, 2001, **40**, 3641-3644.
31. J. Campora, P. Palma and E. Carmona, *Coord. Chem. Rev.*, 1999, **193**, 207-281.
32. K. A. Grice, M. L. Scheuermann and K. I. Goldberg, *Top. Organomet. Chem.*, 2011, **35**, 1-28.
33. R. J. Puddephatt, *Angew. Chem. Int. Ed.*, 2002, **41**, 261-263.
34. E. G. Bowes, S. Pal and J. A. Love, *J. Am. Chem. Soc.*, 2015, **137**, 16004-16007.
35. K. Koo, G. L. Hillhouse and A. L. Rheingold, *Organometallics.*, 1995, **14**, 456-460.
36. P. L. Alsters, H. T. Teunissen, J. Boersma, A. L. Spek and G. van Koten, *Organometallics.*, 1993, **12**, 4691-4696.
37. K. Kamaraj and D. Bandyopadhyay, *Organometallics.*, 1999, **18**, 438-446.
38. P. Wadhvani and D. Bandyopadhyay, *Organometallics.*, 2000, **19**, 4435-4436.
39. R. Bhawmick, P. Das, D. N. Neogi, P. Bandyopadhyay, *Polyhedron.*, 2006, **25**, 1177-1181.
40. J. E. Kukowski, K. J. Keuseman and I. P. Smoliakova, *Trans. Met. Chem.*, 2015, **40**, 877-884.

41. C. R. Turlington, J. Morris, P. S. White, W. W. Brennessel, W. D. Jones, M. Brookhart and J. L. Templeton, *Organometallics* 2014, **33**, 4442-4448.
42. T. M. Figg, G. Schoendorff, B. Chilukuri and T. R. Cundari, *Organometallics*, 2013, **32**, 4993-4996.
43. Y. Yan, P. Feng, Q. -Z. Zheng, Y. -F. Liang, J. -F. Lu, Y. Cui and N. Jiao, *Angew. Chem. Int. Ed.*, 2013, **52**, 5827-5831.
44. T. Yamaguchi, E. Yamaguchi, N. Tada and A. Itoh, *Adv. Synth. Catal.*, 2015, **357**, 2017-2021.
45. W. Oloo, P. Y. Zavalij, J. Zhang, E. Khaskin and A. N. Vedernikov, *J. Am. Chem. Soc.*, 2010, **132**, 14400-14402.
46. A. J. Arduengo, R. Krafczyk and R. Schmutzler, *Tetrahedron*, 1999, **55**, 14523-14534.
47. L. Yang, D. R. Powell and R. P. Houser, *Dalton Trans.*, 2007, 955-964.
48. M. Chaumontet, R. Piccardi, N. Audic, J. Hitce, J. -L. Peglion, E. Clot and O. Baudoin, *J. Am. Chem. Soc.*, 2008, **130**, 15157-15166.
49. J. W. Wilt and W. W. Pawlikowski, *J. Org. Chem.*, 1975, **40**, 3641-3644.
50. W. Wang, R. Zhou, Z. -J. Jiang, X. Wang, H. -Y. Fu, X. -L. Zheng, H. Chen, H and R. -X. Li, *Eur. J. Org. Chem.*, 2015, 2579-2584.
51. C. Gervais, D. Anker, G. Carret and H. Pacheco, *Tetrahedron*, 1979, **35**, 745-752.
52. R. Heck, J. Corse, E. Grunwald and S. Winstein, *J. Am. Chem. Soc.*, 1957, **79**, 3278-3284.
53. A. Singh, U. Anandhi, M. A. Cinellu and P. R. Sharp, *Dalton Trans.*, 2008, 2314-2327.
54. R. B. Bedford, J. G. Bowen, R. B. Davidson, M. F. Haddow, A. E. Seymour-Julen, H. A. Sparkes and R. L. Webster, *Angew. Chem. Int. Ed.*, 2015, **54**, 6591-6594.
55. T. Allscher and P. Klufers, *Chem. Eur. J.*, 2012, **18**, 10571-10584.
56. Y. Zhang, R. J. Puddephatt, L. Manojlovic-Muir and K. W. Muir, *Chem. Commun.*, 1996, 2599-2600.
57. W. D. Bailey, L. Luconi, A. Rossin, D. Yakhvarov, S. E. Flowers, W. Kaminsky, R. A. Kemp, G. Giamastiani and K. I. Goldberg, *Organometallics*, 2015, **34**, 3998-4010.
58. A. J. Ingram, K. L. Walker, R. N. Zare and R. M. Waymouth, *J. Am. Chem. Soc.*, 2015, **137**, 13632-13646.

59. K. R. Pellarin, M. S. McCready, T. I. Sutherland and R. J. Puddephatt, *Organometallics.*, 2012, **31**, 8291-8300.
60. R. J. Hazlehurst, K. R. Pellarin, M. S. McCready and R. J. Puddephatt, *Can. J. Chem.*, 2015, **93**, 74-81.
61. For example, an isomer of **2-14** with the PdOHOH group equatorial and aryl group axial, **2-14a**, is calculated to be lower in energy (by 28 kJ mol⁻¹) than **2-14** and would be accessible by pseudorotation. The oxygen-atom insertion could occur in a similar way by C-O reductive elimination from **2-14a**.
62. J. R. Winkler and H. B. Gray, *Struct. Bonding (Berlin)* 2011, **142**, 17-28.
63. J. M. Mayer, *Comments. Inorg. Chem.*, 1988, **8**, 125-135.
64. C. J. Ballhausen and H. B. Gray, *Inorg. Chem.*, 1962, **1**, 111-122.
65. J. R. Winkler and H. B. Gray, In *Molecular Electronic Structures of Transition Metal Complexes I*; P. D. M. Mingos, P. Day, P. J. Dahl, Eds.; Springer Berlin Heidelberg: Berlin, Heidelberg, 2012, p 17.
66. K. R. Pellarin, M. S. McCready and R. J. Puddephatt, *Organometallics.*, 2012, **31**, 6388-6394.
67. A. Y. Rogachev and R. Hoffmann, *J. Am. Chem. Soc.*, 2013, **135**, 3262-3275.
68. R. A. Gossage, A. D. Ryabov, A. L. Spek, D. J. Stufkens, J. A. M. van Beek, R. van Eldik and G. van Koten, *J. Am. Chem. Soc.*, 1999, **121**, 2488-2497.
69. S. M. Nabavizadeh, H. Amini, M. Rashidi, K. R. Pellarin, M. S. McCready, B. F.T. Cooper and R. J. Puddephatt, *J. Organomet. Chem.*, 2012, **713**, 60-67.
70. Bruker-AXS, SAINT version 2013.8, 2013, Bruker-AXS, Madison, WI 53711, USA.
71. Bruker-AXS, SADABS version 2012.1, 2012, Bruker-AXS, Madison, WI 53711, USA.
72. G. M. Sheldrick, *Acta Cryst.*, 2015, **A71**, 3-8.
73. G. M. Sheldrick, *Acta Cryst.*, 2015, **C71**, 3-8.
74. G. Te Velde, F. M. Bickelhaupt, E. J. Baerends, van Gisbergen. S, C. F. Guerra, J G. Snijders and T. Ziegler, *J. Comput. Chem.*, 2001, **22**, 931-967.
75. A. Becke, *Phys. Rev. A.*, 1988, **38**, 3098-3100.

3 Mild and Selective Pd-Ar Protonolysis and C-H Activation Promoted by a Ligand Aryloxy Group

(A. Behnia, M. A. Fard, J. M. Blacquiere and R. J. Puddephatt, *Dalton Trans.*, 2018, **47**, 3538-3548.)

3.1 Introduction

The activation of a C-H bond is a fundamental step required in catalytic upgrading of hydrocarbons and in functionalization of arenes and alkenes for synthesis.¹⁻⁶ Advances in palladium promoted C-H bond activation strategies have afforded many catalytic routes to the direct arylation of aromatic and heteroaromatic substrates,⁷ and oxidative coupling^{8, 9} of two unactivated arenes. A dominant feature that characterizes the difficulty of these transformations is the strong bond strengths and high pK_a values of the C-H bonds to be functionalized. For example, benzene, as a representative arene, has a C-H bond dissociation energy of 473 kJ mol⁻¹ and pK_a of 43.³ A key advance to achieving catalytic C-H activation included the use of directing groups on the substrate to bring the C-H bond into close proximity of the metal centre.^{6, 10} A second major advance for C-H activation catalysis was the use of carboxylate-type ligands (Chart 3-1), specifically trifluoroacetate.^{11, 12} The weak σ -donor ligand gives an electron-poor palladium centre that is needed to promote electrophilic activation of the C-H bond. Additionally, the carboxylate ligand works in concert with the metal centre to deprotonate the activated C-H bond through a ligand assisted C-H activation mechanism. This route to C-H activation is a variation of the σ -complex assisted metathesis (σ -CAM) mechanism¹³ and is often referred to as AMLA = ambiphilic metal ligand activation¹⁴ or CMD = concerted metallation deprotonation¹⁵ in the catalysis literature. Despite the above advances, mild catalytic C-H activation reactions remain challenging.⁴

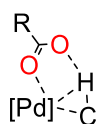
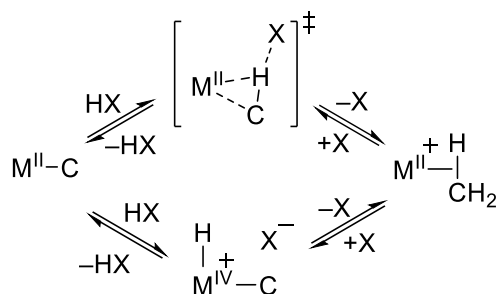


Chart 3-1 Activation of a generic C-H bond promoted by a carboxylate group.

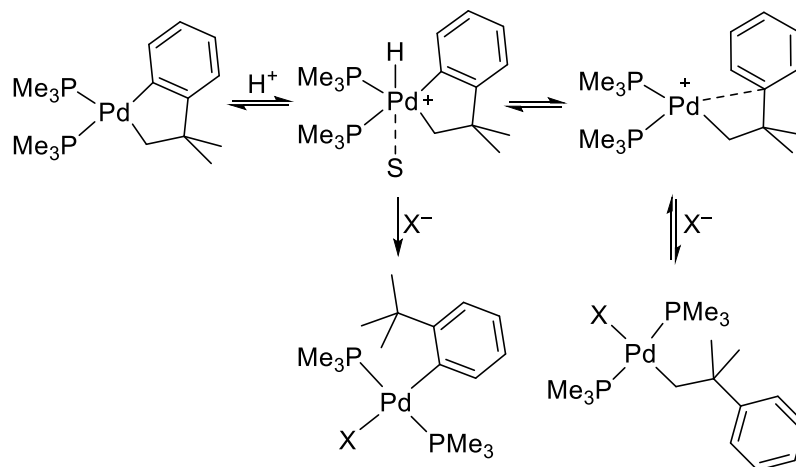
Fundamental studies of C-H activation at metal centres often target the reverse reaction, namely the protonolysis of a metal-carbon σ -bond. Studies with Pt and Pd complexes have revealed two common mechanistic routes for C-H activation/protonolysis (Scheme 3-1).¹⁶ In the protonolysis direction, the concerted S_E2 reaction involves Pd-C cleavage that is assisted by an external acid (HX) and does not involve formal oxidation of the metal centre. The reverse C-H activation is

analogous to the ligand assisted C-H activation that is prevalent in the catalysis literature, in which the base (X^-) is intramolecular. The alternative protonolysis mechanism is a stepwise $S_E(\text{OX})$ pathway that involves oxidative addition of HX to give a high energy Pd(IV)/Pt(IV) intermediate. This is followed by rapid formal C-H reductive elimination. Experimental distinction between these two mechanisms can be challenging. Bercaw originally proposed that a primary kinetic isotope effect (KIE) that is consistent with a tunneling mechanism (i.e. $k_H/k_D > 10$) is indicative of an S_E2 route.¹⁷ While a subsequent study urged caution with such an analysis,¹⁸ a recent computational study¹⁹ suggested that a large KIE supports an S_E2 pathway, but that a small KIE could be due to either the S_E2 or $S_E(\text{OX})$ routes. The high values of k_H/k_D are expected for the S_E2 mechanism when there is a steep barrier to the reaction.



Scheme 3-1 Concerted (S_E2 , top) and step-wise ($S_E(\text{OX})$, bottom) mechanistic routes for protonolysis (forward) or the microscopic reverse concerted or stepwise C-H activation reactions, respectively, at Pd(II) or Pt(II).

The $S_E(\text{OX})$ mechanism has been proposed for protonolysis of platinum-carbon bonds, when the supporting ligands promote formation of the higher oxidation state platinum(IV) hydride intermediate. The hydridoplatinum(IV) complexes can often be detected in such reactions. However, protonolysis of platinum-carbon bonds in complexes with weaker donor ligands, such as 1,5-cyclooctadiene (COD), are thought to occur by the concerted S_E2 mechanism.²⁰⁻²⁴ Recent precedents favour the S_E2 mechanism of protonolysis of palladium(II)-carbon bonds.²⁵⁻²⁷ In contrast, in pioneering studies by Cámpora, Palma and Carmona, the reversible protonolysis of cycloneophylpalladium(II) complexes was proposed to occur by way of a hydridopalladium(IV) intermediate (the $S_E(\text{OX})$ mechanism, Scheme 3-1).²⁸ They showed that the kinetically controlled neophylpalladium(II) product was formed by selective cleavage of the arylpalladium bond, but that rearrangement to a 2-*t*-butylphenylpalladium(II) complex could occur on heating (Scheme 3-2).



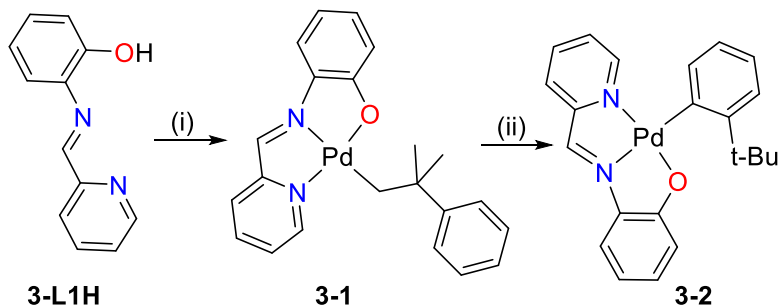
Scheme 3-2 First examples of reversible protonolysis/C-H bond activation on reaction of $[\text{Pd}(\text{CH}_2\text{CMe}_2\text{C}_6\text{H}_4)(\text{PPh}_3)_2]$ with acids HX that is proposed to follow an $\text{S}_{\text{E}}(\text{ox})$ mechanism. S = solvent.²⁸

Unlike many other areas of transition metal catalysis, ancillary ligand design has received relatively minor attention in C-H activation catalyst development. Notable exceptions include ligands employed by Yu, Stahl, and others.²⁹⁻³⁶ Phenoxide has been utilized as an additive in catalytic C-C coupling of aryl halides and ketones^{37, 38} and it was postulated that it could coordinate to the palladium centre and act as an intramolecular base to assist in C-H activation.³⁷ A more recent computational analysis suggests that the phenoxide does indeed act as an intramolecular base, but that it does not assist in the C-H activation step.³⁹ Despite this, the potential for steric and electronic tuning of a ligand appended aryloxy functionality makes it an attractive candidate as an intramolecular base for C-H activation. Additionally, the success of multi-dentate metal-ligand cooperative ligands that shuttle protons in hydrogenation/dehydrogenation catalysis suggests that a pincer manifold is an important feature to impart stability.^{40, 41} Indeed, a pendent hydroxide in an N-N'-bidentate ligand is implicated in proton shuttling during aerobic oxidation of platinum complexes.^{42, 43} Herein, we demonstrate that a pincer ligand with an aryloxy moiety promotes very mild C(sp²)-H bond activation. Additionally, the relative rates of Pd-C(sp²) vs Pd-C(sp³) protonolysis are probed, in part by study of an unusual reversible Pd-alkyl to Pd-aryl isomerization reaction.

3.2 Result and Discussion

3.2.1 Synthesis and Characterization of Pd-Alkyl (**3-1**) and Pd-Aryl (**3-2**) Complexes

The known⁴³ ligand C₅H₄NCH=N-2-C₆H₄OH (**3-L1H**) was treated with the palladium precursor [Pd(CH₂CMe₂C₆H₄)(COD)]^{44, 45} (**2-1**) in cold ether to give a single product identified as Pd-alkyl complex **3-1** (Scheme 3-3). This complex is also formed as the exclusive product within 10 minutes in a small-scale reaction in CD₂Cl₂ at room temperature. Isomer **3-2**, with a Pd-aryl bond, is not observed under either of these conditions. However, stirring **3-1** in methanol for several days results in conversion of **3-1** to **3-2**. Complex **3-2** was isolated in good yield (80%). However, complex **3-1** was consistently present and it was subsequently shown that **3-1** and **3-2** form an equilibrium mixture with $K_{eq} = [\mathbf{3-2}]/[\mathbf{3-1}] = 9$. This observed reaction selectivity is consistent with the above described study²⁸ where isomerization of [PdX(CH₂C(Me)₂Ph)(PMe₃)₂] was promoted by exogenous acid (Scheme 3-2).



Scheme 3-3 Metalation of **3-L1H** to selectively give complex **3-1** and isomerization of **3-1** to **3-2**.

Conditions, (i) **3-L1H** and [Pd(CH₂CMe₂(C₆H₄))(COD)] (**2-1**), Method A: Et₂O, -70°C to room temperature over 17 h, isolated yield **3-1**, 80%. Method B: CD₂Cl₂, room temperature, 10 min; in situ yield **3-1**, >95%; (ii) **1** in MeOH, room temperature, 5 days, 90% conversion to **3-2**, 80% isolated yield.

Complexes **3-1** and **3-2** are air stable and both were fully characterized by ¹H, ¹³C and a combination of correlated ¹H-¹H COSY, ¹H-¹³C HSQC, HMBC NMR spectra, mass spectrometry, IR spectroscopy, and X-ray crystallography. A diagnostic OH stretch was not found in the IR spectrum of either **3-1** or **3-2**, which is expected for the κ^3 -N,N',O-coordination mode for the deprotonated ligand **3-L1**. MALDI mass spectrometry also showed the same signal for samples of **3-1** and **3-2** at an *m/z* value of 436.8. The location and isotope pattern were consistent with the simulation for the common composition of **3-1** and **3-2** (Figure A3.24),

confirming the assignment as structural isomers. The hydrocarbon ^1H NMR resonances are distinct and diagnostic for the two different complexes. The spectrum for **3-1** showed three resonances in a 2:2:1 ratio for the phenyl group of the hydrocarbon ligand. Additionally, two singlets in a 2:6 ratio were observed for the methylene and methyl protons, respectively. Alternatively, the spectrum for **3-2** showed a single peak in the alkyl region for the *t*-Bu moiety of the hydrocarbon ligand, along with four distinct aryl resonances for the 2-*t*-BuC₆H₄ group. The solid-state structures of **3-1** and **3-2** confirm the connectivity assigned spectroscopically (Figure 3-1). In both cases, the ligand is bound in a $\kappa^3\text{-}N,N',O$ mode giving a square planar geometry with a Houser's τ_4 parameter⁴⁶ of 0.16. While, the ideal τ_4 parameter for square planar structures is zero, the deviation from the ideal is likely due to the tight N(1)-Pd(1)-O(1) bite angle of 81.49(11)° and 83.20(3)° for **3-1** and **3-2**, respectively. The rest of the bonding parameters are unexceptional.

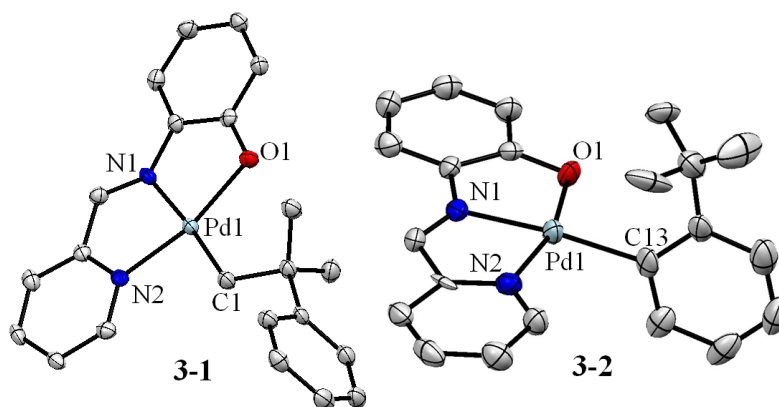


Figure 3-1 Thermal displacement plot of **3-1** (left) and **3-2** (right) with ellipsoids at 50% probability. Hydrogen atoms and a molecule of co-crystallized benzene in both are omitted for clarity. Selected bond distances (Å) and angles (deg): **3-1**, Pd(1)O(1) 2.064(3); Pd(1)N(1) 2.031(3); Pd(1)N(2) 2.044(3); Pd(1)C(1) 2.046(4); N(1)Pd(1)N(2) 80.43(13); N(1)Pd(1)O(1) 81.49(11); O(1)Pd(1)C(1) 102.95(13). **3-2**, Pd(1)O(1) 2.057(7); Pd(1)N(1) 2.018(8); Pd(1)N(2) 2.039(7); Pd(1)C(13) 2.019(8); N(1)Pd(1)N(2) 80.1(3); N(1)Pd(1)O(1) 83.20(3); O(1)Pd(1)C(13) 97.0(3).

While **3-1** is very dark grey in the solid state, it shows solvatochromic⁴⁷ behaviour in solution. The λ_{max} for **1** red shifted as the complex was dissolved in successively less polar solvents (Figure 3-2 and Table A3.1). The solvatochromism of **3-1** is explained by the calculated HOMO, HOMO–1 and LUMO frontier molecular orbitals (Figure A3.28). The LUMO has mostly π^* character of the pincer ligand, while the HOMO has mixed Pd 4d(π) and ligand π character and the HOMO–1 has mostly Pd 4d₂₂

character. The lowest energy transitions are calculated to have both metal-to-ligand charge transfer and intraligand charge transfer character. In square planar complexes, such transitions often lead to the observation of solvatochromism,⁴⁸⁻⁵¹ but the color changes for **3-1** are particularly striking. Qualitatively, **3-2** is also solvatochromic, but quantitative absorption data was not acquired due to persistent minor contamination by **3-1**.

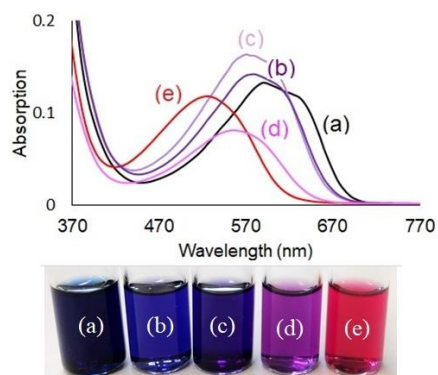
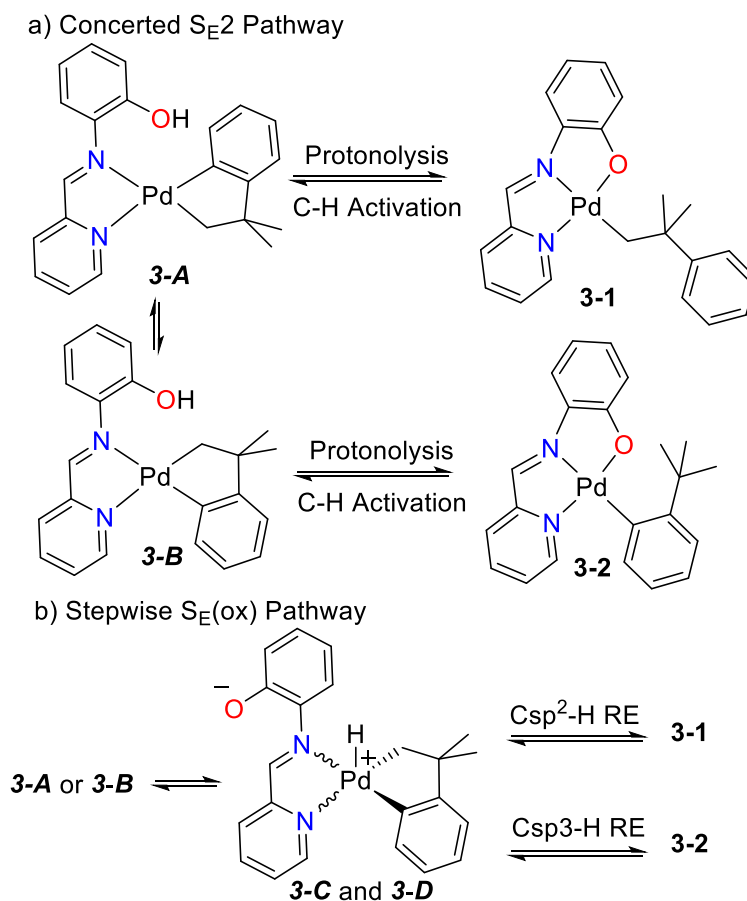


Figure 3-2 Top: UV-Visible absorption spectra of **3-1** (8.58×10^{-5} M) in (a) C₆H₆, (b) CHCl₃; (c) CH₂Cl₂ and (e) CH₃OH. Bottom: photograph of solutions of **3-1** (8.58×10^{-5} M) in (a) C₆H₆; (b) CHCl₃; (c) CH₂Cl₂; (d) CH₃CN; (e) CH₃OH.

3.2.2 Experimental and Computational Evolution of Protonolysis Selectivity

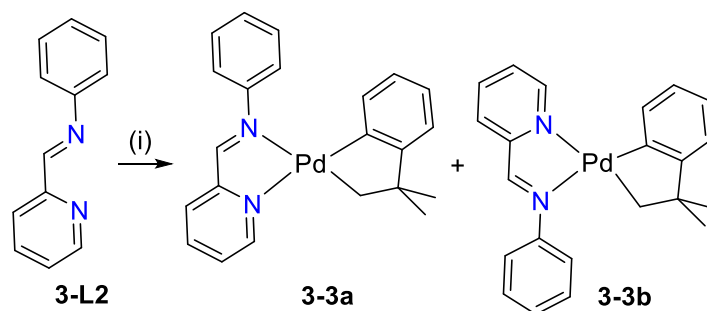
Initial coordination of ligand **3-L1H** is expected to give intermediate **3-A** or **3-B** (Scheme 3-4). Concerted protonolysis, through an S_E2 mechanism, of the Pd-aryl bond in **3-A** or the Pd-alkyl bond in **3-B** would give the products **3-1** and **3-2**, respectively (Scheme 3-4a). Complex **3-A** cannot give **3-2** directly by the intramolecular S_E2 mechanism, because of geometrical constraints, so an isomerization step to give **3-B**, in which the OH and PdCH₂ groups are adjacent, is needed before protonolysis of the Pd-CH₂ bond can occur to give **3-2**. The conversion between regioisomers **3-A** and **3-B** is expected to proceed via a trigonal bipyramidal intermediate in which the hydroxyl oxygen acts as the fifth donor group. There are good precedents for facile *cis-trans* isomerization in complexes analogous to **3-A** and **3-B**. For example, the complex [Pd(CH₂CMe₂C₆H₄)(κ²-N,N'-HO(CH₂)₃N(CH₂-2-C₅H₄N)₂)] undergoes similar *cis-trans* isomerization on the NMR time scale.⁵² Alternatively, an S_E(ox) pathway for the protonolysis would involve oxidative addition from **3-A** or **3-B** to give a Pd(IV) hydride intermediate (**3-C** or **3-D**, Scheme 3-4b). Reductive elimination with C(sp²)-H or Csp³-H bond formation would then give products **3-1** and **3-2**, respectively. In an attempt to observe the

possible intermediates **3-A**, **3-B**, **3-C** and **3-D** we conducted a low temperature (-20°C) addition of ligand **3-L1H** to $[\text{Pd}(\text{CH}_2\text{CMe}_2\text{C}_6\text{H}_4)(\text{COD})]$ (**2-1**) (Figure A3.23). A mixture of ligand and product **3-1** was observed on mixing and the reaction was complete on raising the temperature to 0°C . No intermediates were detected, indicating that the ligand substitution to form **3-A** or **3-B** is slower than the subsequent protonolysis of the arylpalladium bond to form **3-1**.



Scheme 3-4 Expected intermediates in the formation of **3-1** and **3-2** following a) a concerted $\text{S}_{\text{E}2}$; or b) stepwise $\text{S}_{\text{E}(\text{ox})}$ pathway.

Several potential mechanisms were considered to explain the initial selectivity for formation of **3-1** over **3-2**. It could be due to a preference for the ligand **3-L1H** to bind to give intermediate **3-A** followed by $\text{S}_{\text{E}2}$ Pd-aryl protonolysis that is more rapid than the **3-A** to **3-B** isomerization. If such a preference existed we expected that the same steric preference would be true for the known⁴³ ligand **3-L2**, which does not contain a pendent hydroxyl group (Scheme 3-5).



Scheme 3-5 Coordination of ligand **3-L2** to give a mixture of isomers **3-3a** and **3-3b**. Conditions: (i) **3-L2** and $[\text{Pd}(\text{CH}_2\text{CMe}_2\text{C}_6\text{H}_4)(\text{COD})]$ (**2-1**), Et_2O , -65°C to room temperature over 18 h, isolated yield **3-3a/3-3b**, 73% as a 1:0.6 mixture.

Reaction of **3-L2** with $[\text{Pd}(\text{CH}_2\text{CMe}_2\text{C}_6\text{H}_4)(\text{COD})]$ (**2-1**) gave a 1:0.6 mixture of air stable isomers (**3-3a** and **3-3b**) in a good yield (73%). The mixture of the two isomers suggests that minimal steric preference for ligand coordination exists. Complexes **3-3a** and **3-3b** were fully characterized by ^1H , ^{13}C and a combination of correlated $^1\text{H}-^1\text{H}$ COSY, $^1\text{H}-^{13}\text{C}$ HSQC, HMBC NMR spectra, mass spectrometry, IR spectroscopy, elemental analysis and X-ray crystallography. The hydrocarbon aryl signals of the major isomer are more shielded than those for the minor isomer. The greater shielding is attributed to the adjacent *N*-phenyl substituent of **3-L1** leading to the assignment as **3-3a**. The minor isomer **3-3b** selectively crystallized and the solid-state structure confirms the expected square planar geometry (Figure 3-3). A fast isomerization rate between **3-3a** and **3-3b** is evidenced by a ^1H NMR spectrum of crystalline **3-3b**, which revealed a mixture of the two isomers in the same ratio as the powder sample described above. This suggests that *cis-trans* isomerization (i.e. conversion from **3-A** to **3-B**) is not a rate-limiting step in the formation of **3-2**. If the expected $\text{S}_{\text{E}}2$ mechanism is followed, the selectivity of **3-1** over **3-2** is therefore likely due to a difference in the relative rates of $\text{Pd-C}(\text{sp}^2)$ vs $\text{Pd-C}(\text{sp}^3)$ protonolysis.

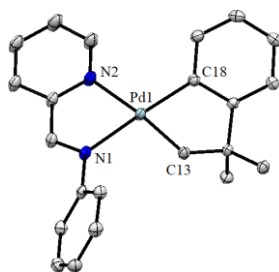


Figure 3-3 Thermal displacement plot of **3-3b** with ellipsoids at 50% probability. Hydrogen atoms and a molecule of co-crystallized benzene are omitted for clarity. Selected bond distances (Å) and angles (deg): Pd(1)N(1) 2.135(1); Pd(1)N(2) 2.193(1); Pd(1)C(13) 2.024(1); Pd(1)C(18) 2.006(1); N(1)Pd(1)N(2) 77.32(4); C(18)Pd(1)C(13) 79.53(4); $\tau_4 = 0.05$.

Thermodynamic calculations of isomers **3-3a** and **3-3b** revealed that the former is more stable by 8 kJ mol⁻¹. This is in line with the observed equilibrium mixture of **3-3a** and **3-3b**, which would give a difference in free energy of about 1 kJ mol⁻¹. A slightly larger difference in energies is calculated for the proposed intermediates **3-A** and **3-B**, with **3-A** being 13 kJ mol⁻¹ more stable (Figure 3-4). For both complexes, the phenol group is directed towards the palladium center, forming a weak hydrogen bond with OH...Pd = 2.40 and 2.64 Å in **3-A** and **3-B** respectively.⁵³ Calculations predict that **3-1** and **3-2** are more stable than **3-A** and **3-B**, as required by the observed chemistry, and that **3-1** is more stable than **3-2** by 3 kJ mol⁻¹. The experimentally determined equilibrium constant, $K_{eq} = [\mathbf{3-2}]/[\mathbf{3-1}] = 9$, instead shows that complex **3-2** is more stable than **3-1** by about 5 kJ mol⁻¹. The difference between theory and experiment is minor given the small energy differences. The similar thermodynamic energies for the pairs of **3-A/3-B** and **3-1/3-2** strongly suggests that the observed selectivity for the initial reaction is primarily due to the relative kinetic barriers for Pd-C(sp²) vs Pd-C(sp³) protonolysis. The complex **3-2** gives an intense resonance in the ¹H NMR spectrum due to the *t*-butyl protons and could be detected readily if formed in 1% or greater yield, so the initial selectivity of protonolysis is at least 99%.

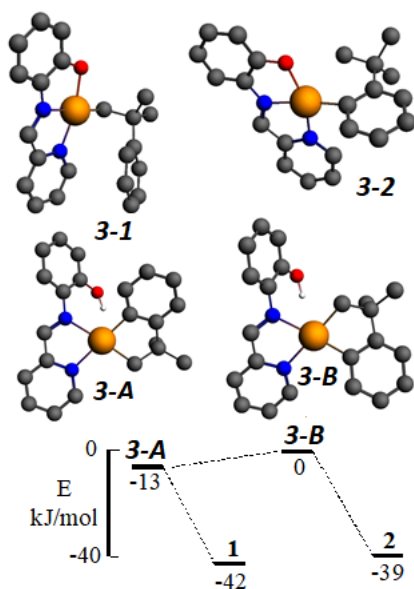
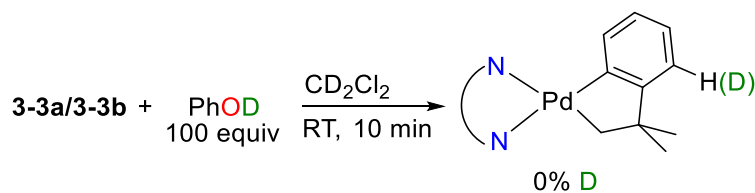


Figure 3-4 Calculated structures and relative energies of complexes **3-1** and **3-2**, and proposed intermediates **3-A** and **3-B**. The conversion of **3-1** to **3-2** is likely to occur via the reversible sequence **3-1** to **3-A** to **3-B** to **3-2**.

3.2.3 Role of the Pendent Phenol in the Formation of **3-1**

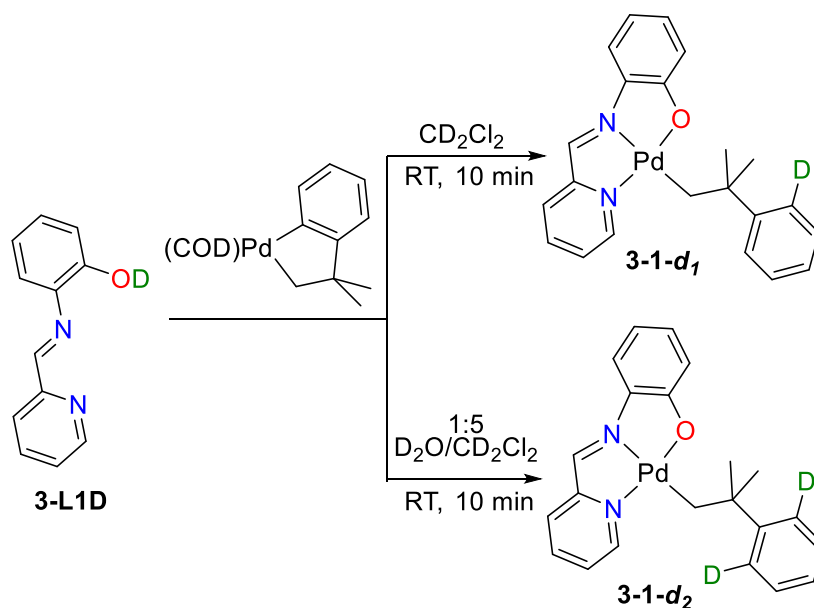
Deprotonation of the phenol group of the ligand **3-L1H** occurs for the formation of both **3-1** and **3-2**. With the control complexes **3-3a/3-3b** on hand, we sought to determine if it is necessary that the phenol group is intramolecular, and positioned close to the Pd-C bond to be cleaved, in order for the protonolysis to occur. The mixture of **3-3a/3-3b** was treated with 100 equiv of PhOD and the reaction mixture was analyzed by ^2H NMR spectroscopy after 10 min (Scheme 3-6). Under these conditions, no deuterium incorporation into the hydrocarbon moiety was observed. The exogenous phenol is insufficient to promote deuterolysis (or protonolysis) and the intramolecular nature of the phenol group in **3-L1H** is essential to the observed formation of **3-1**. This is consistent with either a concerted $\text{S}_{\text{E}2}$ mechanism for protonolysis of the Pd-C_{Ar} bond or for an $\text{S}_{\text{E}}(\text{OX})$ mechanism with formation of hydride **3-C** or **3-D**.



Scheme 3-6 Attempted deuteration and C-H activation using exogenous phenol- d_1 with a mixture of **3-3a/3-3b**. The abbreviated *N-N* ligand represents ligand **3-L2**.

3.2.4 Deuterium Labeling Studies in the Formation of **3-1** and **3-2**

A low barrier for either Pd-aryl protonolysis ($\text{S}_{\text{E}2}$ pathway), or O-H oxidative addition and $\text{C}(\text{sp}^2)\text{-H}$ reductive elimination ($\text{S}_{\text{E}(\text{OX})}$ pathway), is inferred from the rapid formation of **3-1** at room temperature (within 10 min). Deuterium labelling studies were undertaken to gain a clearer mechanistic picture of the formation of **3-1**. Treatment of the palladium precursor $[\text{Pd}(\text{CH}_2\text{CMe}_2\text{C}_6\text{H}_4)(\text{COD})]$ (**2-1**) with **3-L1D** in CD_2Cl_2 gave quantitative conversion to the Pd-alkyl complex **3-1- d_1** within 10 min (Scheme 3-7).



Scheme 3-7 Metalation of **3-L1D** to give **3-1- d_1** or **3-1- d_2** .

The pattern of the methylene and methyl signals in **3-1- d_1** is very similar to that found in **3-1**. The aryl region is also similar, but with a few key differences. In **3-1**, the signals for the equivalent protons H5 and H9 along with H18 are found as an overlapping signal around 7.7 ppm that integrates to three

protons (Figure 3-5). In **3-1-d₁**, this signal only integrates to two protons and the pattern of the overlapping multiplet has changed. This shows that deuterium is incorporated at the 5 (or 9) position of the hydrocarbon aryl moiety. Deuteration at this site breaks the symmetry of the hydrocarbon aryl protons and this is evidenced by the unresolved multiplet for H6 and H8 that was previously a virtual triplet in **3-1**. Analysis of **3-1-d₁** by ²H NMR spectroscopy revealed only one aromatic signal at 7.66 ppm (Figure A3.6), which is in the expected location for deuterium incorporation at position 5 (or 9) of the hydrocarbon aryl moiety.

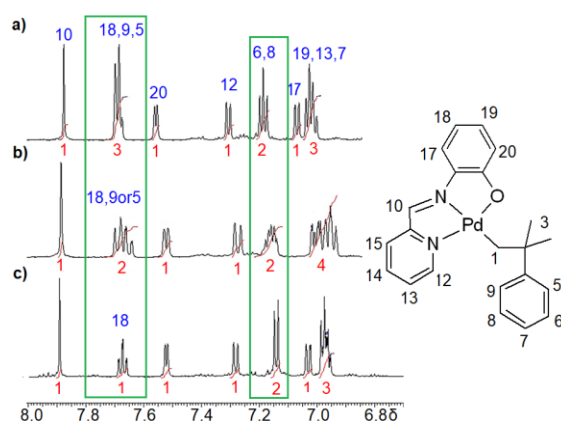
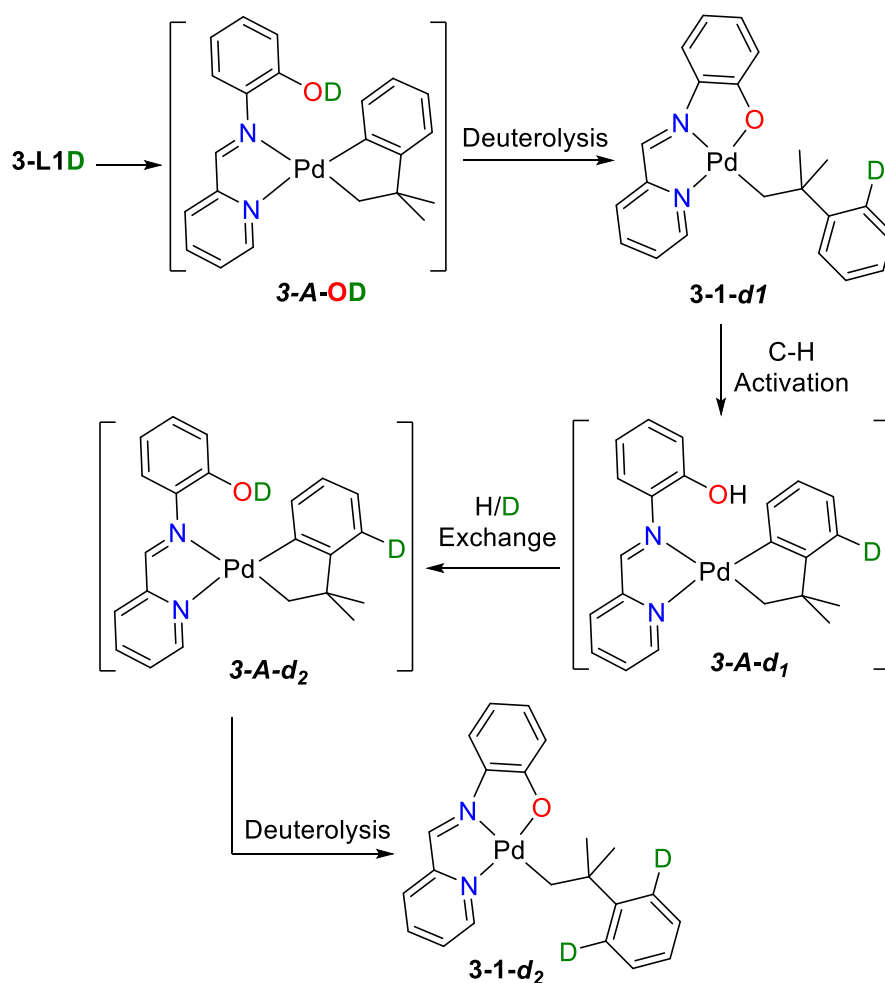


Figure 3-5 The aromatic regions of the ¹H NMR spectra (599.3 MHz, CD₂Cl₂) for: a) **3-1** b) **3-1-d₁** and c) **3-1-d₂**. The integrations are relative to the imine backbone resonance *H*10, which is set to one.

Mechanistically, **3-1-d₁** is likely formed from intermediate **3-A-OD**, which is the expected product from coordination of the ligand **3-L1D** to the Pd precursor (Scheme 3-8, top). Incorporation of deuterium into the hydrocarbon group in **3-1-d₁** confirms that the proton of the formed Ar-H bond in **3-1** originates from the phenol group of **3-L1H**. This could be consistent with either a concerted or step-wise pathway for protonolysis.



Scheme 3-8 Proposed route for deuterium incorporation into **3-1-d₁** and **3-1-d₂**.

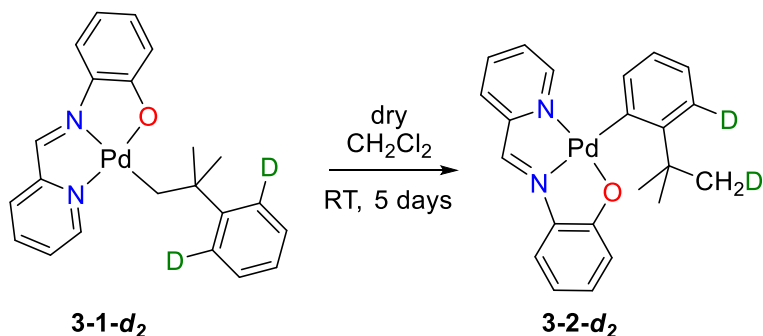
Metalation of **3-L1D** in a mixture of D_2O and CD_2Cl_2 quantitatively afforded the bis-deuterated product **3-1-d₂** within 10 min, rather than the mono-deuterated **3-1-d₁** (Scheme 3-7). A triplet is now found at ca. 7.7 ppm in the 1H NMR spectrum that integrates to one proton for H18 (Figure 3-5c). This suggests that deuterium is incorporated at both the 5 and 9 positions of the hydrocarbon aryl moiety. Moreover, a doublet is observed for H6 and H8 that integrates to two. This suggests that H6 and H8 are equivalent and that they have only one proton neighbour (i.e. H7).

The incorporation of two deuterium atoms into **3-1-d₂** indicates that a C-H activation step must occur on route to **3-1-d₂**. We propose that the first deuterium atom is incorporated through deuterolysis of the Pd-aryl bond, thus the same route that gives **3-1-d₁** (Scheme 3-8). The mono-deuterated species would then undergo a concerted C-H activation at the hydrocarbon aryl ortho

position. This would give intermediate **3-A-d₁**, in which the aryloxy ligand moiety is re-protonated. Protonolysis of the Pd-aryl bond by the ligand functionality would give back **3-1-d₁** through a non-productive pathway. Alternatively, in the presence of D₂O the pendent ligand OH will undergo H/D exchange to give intermediate **3-A-d₂**. Deuterolysis of the adjacent Pd-aryl bond in **3-A-d₂** will give the bis-deuterated product **3-1-d₂**. Such a pathway would imply that both the protonolysis and the C-H activation steps are facile and rapid since **3-1-d₂** is the only observed product within 10 min at room temperature. The ease of reaction is, in part, due to the fact that the Pd-alkyl linkage in **3-1-d₁** serves the role of a non-labile directing group. The positioned ligand aryloxy is likely important in promoting a concerted ligand promoted C_{Ar}-H activation.

The isolated mono-deuterated complex **3-1-d₁** was dissolved in wet-CD₂Cl₂ and the sample was analyzed by ¹H and ²H NMR spectroscopy. At early time points, the pattern of signals for **3-1-d₁** converted to the expected pattern for **3-1**, which then reacted over a period of days to give **3-2**, also containing no deuterium. Activation of the Ar-D bond should generate intermediate **3-A-OD**, that is depicted in Scheme 3-8, and would readily undergo H/D exchange with H₂O in the wet solvent to give **3-A** and hence **3-1**. The washing out of the deuterium atom is further evidence for the reversibility between compounds **3-A** and **3-1**, which is a required feature for the isomerization of **3-1** to **3-2**.

It was postulated that the Ar-D bonds in **3-1-d₂** would activate to give intermediate **3-A-d₂**. In dry solvent over prolonged time the deuterium atom of the ligand phenol should be incorporated into the *t*-butyl group of the Pd-aryl isomer. To probe this, the bis-deuterated Pd-alkyl complex **3-1-d₂** was left in dry CH₂Cl₂ for 5 days (Scheme 3-9). The ¹H NMR spectrum of the product mixture indicated the presence of both **3-1** and **3-2**, but the location of the deuterium atoms was not apparent. However, the ²H NMR spectrum revealed only two signals, at 7.17 and 1.69 ppm, which are assigned to the C-D aryl and *t*-butyl groups of **3-2-d₂**, respectively, as expected according to Scheme 3-9.



Scheme 3-9 Isomerization of **3-1-*d*₂** to give **3-2-*d*₂** with deuterium incorporation in the *t*-Bu moiety.

3.2.5 Isomerization of **3-1** to **3-2**, Solvent Study and Kinetic Experiments

A number of control reactions were conducted to attempt to clarify the mechanism for the isomerization of **3-1** to **3-2**. In each case compound **3-1** was stirred in CDCl₃ and the conversion to **3-2** was monitored over time by ¹H NMR spectroscopy, by following the diagnostic imine singlets of **3-1** and **3-2**, and integration relative to an internal standard. No observable changes in rate were observed on conducting the reaction in the light or in the dark, suggesting a radical mechanism is not operative. The reaction rate was independent of palladium concentration, which excludes a bimolecular pathway. Expectedly, heating accelerates the reaction, but it also promotes side reactions and the formation of by-products. By-product formation is also observed on leaving **3-1** in solution at room temperature for prolonged periods (>6 days in CHCl₃, >14 days in MeOH). A likely by-product includes a Pd tetramer, that we have previously characterized from reactions under similar prolonged reactions,⁵⁴ in which **3-L1** is oxidized by O₂.

There is no clear relationship between the conversion to **3-2** and the polarity of a selection of protio-solvents (Table 3-1, Entries 1-6). While reaction in non-polar benzene is negligible, very similar conversion values are observed in MeCN, CH₂Cl₂ and CHCl₃ despite their different polarities. The highest conversion is observed in methanol where 58% **3-2** is generated after 22 h and this value increases to an equilibrium value of 90% by 5 days (cf. 55% **3-2** in CH₂Cl₂ after 5 days). The acceleration of isomerization in MeOH may suggest that the solvent enables a distinct mechanistic path to the one that is operative in chlorinated solvents. Prior computational studies of C-H activation by palladium acetate complexes have shown that protic solvents, such as MeOH, can form a hydrogen-bonded bridge between the non-coordinated acetate oxygen and

the C-H bond to be cleaved.⁵⁵ This ‘relay’ deprotonation of the carbon atom was more energetically feasible than the more typical deprotonation via the acetate oxygen.

Table 3-1 Isomerization of **3-1** to **3-2** in various solvents^a

Entry	Solvent	ϵ^b	3-1 (%) ^c	3-2 (%) ^c
1	CH ₃ CN	37.5	66	34
2 ^d	CH ₃ OH	33.6	42	58
3 ^{d,e}	CH ₃ OH	33.6	10	90
4 ^d	CH ₂ Cl ₂	8.9	61	39
5 ^d	CHCl ₃	4.8	62	38
6 ^d	C ₆ H ₆	2.2	97	3
7	CD ₃ CN	37.5	60	40
8	CD ₃ OD	33.6	97	3
9	CD ₂ Cl ₂	8.9	70	30
10	CDCl ₃	4.8	68	32
11	C ₆ D ₆	2.2	98	2

^a Conditions: [**3-1**] = 0.72 mM, 22 h, RT, under air. ^b Dielectric constant of solvent. ^c The yield of **3-1** and **3-2** was calculated by integration of the ligand imine resonance relative to the internal standard 1,3,5-trimethoxybenzene. ^d The reaction was conducted in the listed solvent, but the ¹H NMR spectra (including the time = 0 sample) were acquired in CDCl₃. ^e Reaction time = 5 days.

The deuterio solvents CDCl₃ and CD₂Cl₂ gave very similar yields of **3-2** as compared to their protio analogues (Table 3-1, Figure 3-6). However, the yield of **3-2** was dramatically suppressed in MeOD where only 3% product was observed by 22 h. The suppressed isomerization is attributed to the competing H/D exchange of the hydroxide moiety in intermediates **3-A** and **3-B**. Deuterolysis in **3-A** is expected to be rapid (*vide supra*) and indeed **3-1** is rapidly converted to **3-1-d₂** as judged by ¹H NMR spectroscopy. We ascribe the very slow rate for the formation of **3-2** to the slow deuterolysis of the palladium alkyl bond in **3-B**. The observed rates of

formation of **3-2** in MeOH and MeOD give a very large kinetic isotope effect of ca. 40 (first order rate constants approximately 4×10^{-4} and $2 \times 10^{-5} \text{ min}^{-1}$ at 298K in MeOH and CD₃OD respectively, see Figure A3.29). While both equilibrium and kinetic isotope effects may be important in the conversion of **3-1** to **3-2**, the magnitude of the observed KIE is consistent with tunneling and current theory¹⁹ would predict an S_E2 mechanism for reactions in MeOH. As noted, isomerization of **3-1** in MeOD, is effectively the isomerization of **3-1-d₂** due to rapid H-D exchange of the ortho aryl protons. Thus, the KIE reflects the differing rates for isomerization of **3-1** vs. **3-1-d₂**, and incorporates components due to both the CH(D) activation and the slow protonolysis (deuterolysis) steps. Qualitatively, the isomerization of isolated **3-1-d₂** also occurs more slowly than that of **3-1** in CH₂Cl₂. Quantitative rate comparisons were not determined due to the slow initial rates for isomerization of the protio complex **3-1** in CH₂Cl₂ (see Figure 3-6). Over prolonged reaction times (5 days) solutions of both *in situ* generated **3-1-d₂** (i.e. **3-1** in MeOD) and isolated **3-1-d₂** in CH₂Cl₂ gave complex mixtures.

We hypothesized that H₂O in the as-received chlorinated solvents is responsible for promoting isomerization of **3-1** to **3-2**, also through a solvent bridge mechanism. Surprisingly, the yield of **3-2** in dry CDCl₃ or CD₂Cl₂ is higher than in the as-received solvents by 20 and 14%, respectively. The solvent effects on the protonolysis of **3-B** to give **3-2** are thus inconclusive and do not clearly point toward an S_E2 solvent bridge mechanism. This clearly shows that the presence of an external hydroxylic reagent is not a necessary prerequisite for the isomerization reaction, while it does not exclude the possibility that a methanol bridge could accelerate the reaction.

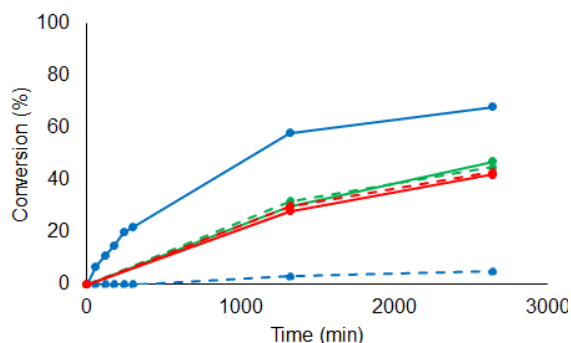


Figure 3-6 Conversion of **3-1** to **3-2** over time in protio (solid lines) and deuterio (dashed lines) solvents: Methanol (blue), chloroform (green) and dichloromethane (red).

3.2.6 Computational Analysis of Pd-Aryl and Pd-Alkyl Protonolysis

The experimental evidence above suggests that the interconversion between **3-A** and **3-1** follows an S_E2 mechanism. The likely transition state **3-E** for the forward, Pd-Aryl protonolysis, and reverse, Ar-H activation, shows concerted bond cleavage and formation (Chart 3-2).

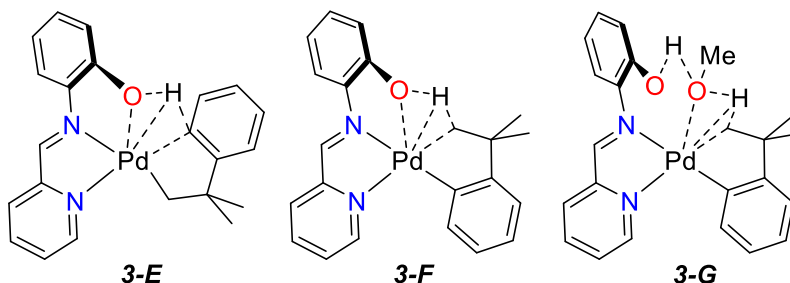


Chart 3-2 Proposed transition state structures for the S_E2 protonolysis of the Pd-aryl bond in **3-1** (**3-E**) and the Pd-alkyl bond in **3-2**, without (**3-F**) and with (**3-G**) a MeOH solvent bridge.

To gain some perspective on the geometric feasibility of the possible transition state **3-E**, intermediate **3-A** is depicted as a space-filling structure (Figure 3-7b). In order to form the new C-H bond in the reaction of **3-A** to give **3-1**, rotation about the phenol-imine C-N bond is needed to bring the proton and the Pd-aryl carbon atom closer together (this H...C distance is calculated as 2.64 Å in **3-A**). There is no great steric hindrance to this and so a smooth transition to complex **3-1** is possible by way of **3-E**. The calculated HOMO for **3-A** has components of Pd 4d_{z²} and Pd-Ar and Pd-CH₂ bonding character (Figure 3-7d). On rotation of the phenol group, the proton interacts more with the electron density on the adjacent sp² carbon and less with the electron density of the Pd 4d_{z²} orbital to give transition state **3-E**.

The isomerization of **3-1** to **3-2** in MeOH likely also proceeds via S_E2 protonolysis of the Pd-CH₂ bond, based on the very large KIE value in that solvent. The expected transition state **3-F** for the protonolysis of **3-B** to **3-2**, without a methanol solvent bridge, is depicted in Chart 3-2. An analogous reaction to that described for **3-A**→**3-E**→**3-1** is expected to be more difficult for **3-B**. This is in part due to the lower reactivity of alkyl groups towards electrophilic attack but also because the phenol group rotation is blocked by steric interactions between the OH group and the Pd-CH₂ protons (Figure 3-7b). The CH₂ group cannot easily rock away from the hydroxyl group because it is part of a relatively rigid chelate group, and so a significant geometrical distortion is needed to allow the phenol proton to approach the carbon atom of the CH₂ group. This latter effect is not present when attack by an external proton occurs, as is the case in the Campora, Palma and Carmona chemistry²⁸ described above (Scheme 3-2). Here, it

is expected that the geometric constraints lead to particularly high selectivity for the intramolecular reaction to give **3-1** from **3-A** rather than **3-2** from **3-B**, and also to the very high value of the KIE for the overall isomerization reaction.

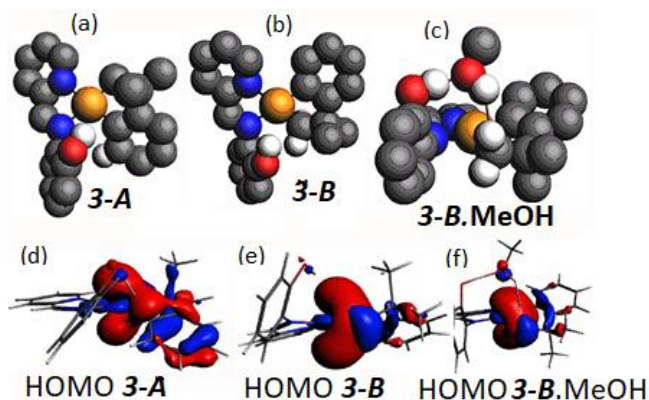


Figure 3-7(a), (b), (c) Calculated structures of intermediate complexes **3-A**, **3-B** and **3-B.MeOH**, as space-filling models with only the OH and closest CH protons included, for clarity; (d), (e), (f), the calculated HOMO, having Pd $4d_{z^2}$ and Pd-C bonding character, for the protonolysis for complex **3-A**, **3-B** and **3-B.MeOH**.

Despite the inconclusive experimental evidence regarding the role of solvent in the Pd-CH₂ bond protonolysis, the HOMO of **3-B** was also calculated with a molecule of MeOH in the coordination environment, **3-B.MeOH** (Figure 3-7c). Methanol is depicted in a hydrogen bonding interaction with the phenol proton of ligand **3-L1**, leaving the proton of the solvent molecule to be positioned appropriately to attack the Pd-CH₂ group to give **3-2** through a concerted solvent-bridged intermediate **3-G** (Chart 3-2). The proton approach angle is much more favourable than in the structure without the solvent bridge. However, the importance of such a path may be minor given the lack of clear experimental support for solvent bridging.

The third possible mechanism for the formation of **3-2** is the stepwise S_E(ox) mechanism, with palladium(IV) hydride intermediates **3-C** or **3-D** (Scheme 3-4b). Many isomers are possible and were considered, but the structures and energetics of two likely 5-coordinate complexes, **3-C** and **3-D**, formed by proton transfer to palladium without ligand rearrangement are shown in Figure 3-8. The possible Pd-H intermediate **3-D** would be formed from **3-B** while **3-C** would be formed from **3-A**. An attractive feature of this mechanism is that C-H reductive elimination from either **3-C** or **3-D** could occur by coupling of the hydride with either the sp² or sp³ carbon

to give **3-1** or **3-2**, respectively. Formation of **3-1** is expected to be much faster in either case since the aryl group is in the optimum conformation for C-H coupling in the cyclometalated derivative.^{28, 56, 57} However, both hydride complexes **3-C** and **3-D** are at high energy (Figure 3-8). This result is in line with the experimental evidence for the reversible protonolysis/C-H activation between **3-A** and **3-1** that rather suggests an S_E2 mechanism. For these reasons, the hydride S_E(ox) mechanism is considered improbable. Nevertheless, as is evident from the structures of the proposed intermediates **3-E** and **3-F** and from the nature of the HOMO (Figure 3-7d and e), some degree of Pd···H bonding is expected along the reaction coordinate for either protonolysis or C-H bond activation, and the appended phenol group plays a crucial role.

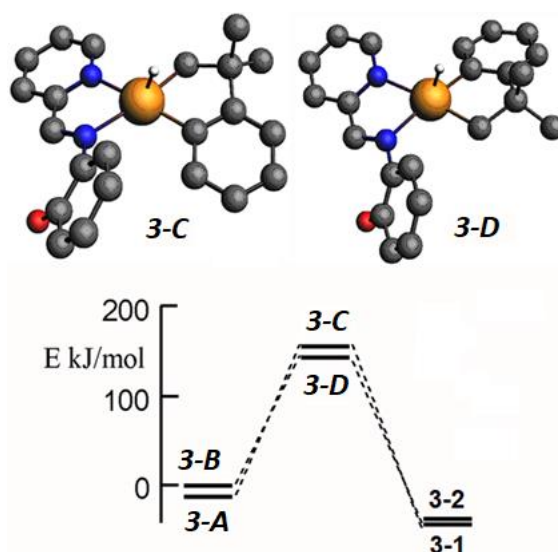


Figure 3-8 Calculated structures and relative energies of complexes **3-C** and **3-D**.

3.3 Conclusion

Herein, the ligand **3-L1H**, with two nitrogen donors and a phenol group, was used to evaluate protonolysis and C-H activation reactions in a palladium cycloneophyl structure. Coordination of **3-L1H** to [Pd(CH₂CMe₂C₆H₄)(COD)], (**2-1**), gives the Pd-alkyl complex **3-1** as a result of selective Pd-Ar bond protonolysis. In the presence of D₂O, rapid deuterium incorporation into both ortho positions of the released aryl group suggests that both Pd-Ar protonolysis and C_{Ar}-H activation are facile reactions under mild conditions. Deuterium labeling, and computational studies suggest that a concerted protonolysis/C-H activation mechanism is operative and is promoted by the phenol/phenoxide group of the **3-L1H** or **3-L1** ligand, respectively. In contrast, protonolysis of the Pd-alkyl bond is much slower than that of the Pd-aryl bond. While slow, the reaction does occur and leads to isomerization of **3-1** to

give an equilibrium mixture with the more stable arylpalladium complex **3-2**. The formation of **3-2** exhibits a very large KIE value (k_H/k_D ca. 40) that is consistent with proton tunneling and is suggestive of a concerted S_E2 mechanism in the slow protonolysis step to form **3-2**. In this reaction system, there is a relatively low barrier for Pd-Ar protonolysis and Ar-H activation, while the barrier for Pd-alkyl protonolysis is significantly greater. We are currently evaluating the capacity of complexes with ligand **3-L1** to coordinate and promote intermolecular C-H activation reactions on reagents bearing directing groups.

3.4 Experimental

3.4.1 Reagent and General Procedure

All reactions were carried out in air. The complex $[\text{Pd}(\text{CH}_2\text{CMe}_2\text{C}_6\text{H}_4)(\text{COD})]$ ^{44, 45}, **2-1**, and the diimine ligands, 2-(pyridin-2-ylmethyleneimino)phenol⁴³, **3-L1H**, and pyridin-2-ylmethyleneiminobenzene,⁴³ **3-L2**, were synthesized according to the literature procedures. NMR spectra were recorded at 298 K using a Varian 600 MHz spectrometer. ¹H and ¹³C chemical shifts were referenced internally to solvent (residual signal for ¹H) where the chemical shift was set to appropriate values relative to TMS at 0.00 ppm. Complete assignments of each compound were aided by the use of ¹H-¹H gCOSY, ¹H-¹H NOESY, ¹H-¹³C HSQC, and ¹H-¹³C HMBC experiments and are reported using the labelling scheme in Chart A3.1. For ²H NMR experiment, ²H chemical shift was referenced externally to the ²H peak of (CD₃)₂CO ($\delta(^2\text{H}) = 2.05$ ppm). Commercial reagents were used without further purification. Elemental analyses were performed by Laboratoire d'Analyse Élémentaire de l'Université de Montréal. MALDI-TOF mass spectra were collected using an AB Sciex 5800 TOF/TOF mass spectrometer using anthracene as the matrix in a 20:1 matrix:substrate molar ratio. DFT calculations were conducted using a B1LYP functional, double-zeta force field, scalar correction for relativity and methanol solvation by using COSMO.^{58, 59}

3.4.2 Synthesis of $[\text{Pd}(\text{CH}_2\text{CMe}_2\text{C}_6\text{H}_5)(\kappa^3\text{-}N,N',O\text{-C}_6\text{H}_4\text{N}=\text{CH}(2\text{-C}_5\text{H}_4\text{N}))]$ (**3-1**).

To a cooled (-65 °C) and stirred solution of $[\text{Pd}(\text{CH}_2\text{CMe}_2\text{C}_6\text{H}_4)(\text{COD})]$, (**2-1**) (0.30 g, 0.86 mmol) in ether (50 mL) was added a solution of 2-C₅H₄NCH=N-2-C₆H₄OH, **3-L1H**, (0.17 g, 0.86 mmol) in ether (30 mL). The mixture was slowly warmed to room temperature over 17 h while stirring, during which time the color of the solution changed from yellow to dark gray. Upon removal of the solvent under reduced pressure, a gray solid was formed, which was washed with hexanes (2 × 30 mL) and dried

under vacuum, to give **3-1** as an air-stable gray product (0.30 g, 0.68 mmol, 80 %). ^1H NMR (CDCl_3 , 600 MHz, 25°C) δ : 7.81 (s, *H*10, 1H), 7.71 (d, $J = 8$ Hz, *H*5 and *H*9, 2H), 7.57 (m, *H*18, 1H), 7.33 (d, $J = 5$ Hz, *H*20, 1H), 7.23 (d, $J = 8$ Hz, *H*17, 1H), 7.16 (t, $J = 8$ Hz, *H*6 and *H*8, 2H), 6.98-7.01 (m, *H*7, *H*12 and *H*13, 3H), 6.86 (t, $J = 6$ Hz, *H*19, 1H), 6.71 (d, $J = 9$ Hz, *H*15, 1H), 6.31 (t, $J = 7$ Hz, *H*14, 1H), 1.83 (s, *H*1, 2H), 1.60 (s, *H*3, 6H); ^1H NMR (CD_2Cl_2 , 600 MHz, 25°C) δ : 7.88 (s, *H*10, 1H), 7.70-7.67 (m, *H*18, *H*5, *H*9, 3H), 7.56 (d, $J = 5$ Hz, *H*20, 1H), 7.30 (d, $J = 8$ Hz, *H*12, 1H), 7.19 (m, *H*6 and *H*8, 2H), 7.06-6.97 (m, *H*17, *H*7, *H*13 and *H*19, 4H), 6.58 (d, $J = 8$ Hz, *H*15, 1H), 6.35 (t, $J = 8$ Hz, *H*14, 1H), 1.82 (s, *H*1, 2H), 1.58 (s, *H*3, 6H). $^{13}\text{C}\{^1\text{H}\}$ NMR (CDCl_3 , 151 MHz, 25°C) δ : 178.39 (*C*16), 161.91 (*C*21), 153.51 (*C*4), 150.94 (*C*20), 139.80 (*C*10), 138.48 (*C*18), 134.62 (*C*12), 132.65 (*C*11), 127.78 (*C*6 and *C*8), 126.53 (*C*5 and *C*9), 125.60 (*C*19), 125.34 (*C*17), 125.08 (*C*7), 122.85 (*C*15), 118.23 (*C*13), 114.54 (*C*14), 42.12 (*C*2) 37.98 (*C*1), 30.89 (*C*3). MALDI MS (anthracene matrix): calcd m/z 436.84 [**3-1**] $^{\bullet+}$, obsd m/z 436.84. Elemental Analysis: calcd for $\text{C}_{22}\text{H}_{22}\text{N}_2\text{OPd}$: C, 60.49; H, 5.08; N, 6.41; found: C, 60.86; H, 5.30; N, 6.44. Single crystals suitable for X-ray crystallographic analysis were grown by the slow evaporation of a benzene solution of **3-1** at room temperature.

3.4.3 Synthesis of $[\text{Pd}(\text{C}_6\text{H}_4(2-t\text{-Bu}))(\kappa^3\text{-}N,N',O\text{-C}_6\text{H}_4\text{N}=\text{CH}(2\text{-C}_5\text{H}_4\text{N}))]$ (**3-2**).

A dilute solution of **3-1** (0.10 g, 0.23 mmol) in methanol (400 mL) was stirred in room temperature for 7 days. Upon removal of the solvent under reduced pressure a gray solid was obtained, which was washed with hexanes (3×30 mL) and dried under vacuum to give **3-2** as an air-stable product in 80% yield (0.08 g, 0.18 mmol). ^1H NMR ($\text{CO}(\text{CD}_3)_2$, 600 MHz, 25°C) δ : 8.37 (s, *H*9, 1H), 8.04 (m, *H*13, 1H), 7.76 (m, , *H*7 and *H*14, 2H), 7.50 (m, *H*11, 1H), 7.37 (m, *H*12, 1H), 7.27 (m, *H*16, 1H), 7.12 (dd, $J = 8$ Hz, *H*4, 1H), 6.98 (m, *H*18, 1H), 6.85 (dd, $J = 8$ Hz, *H*5, 1H), 6.78 (m, *H*6, 1H), 6.45 (dd, $J = 8$ Hz, *H*19, 1H), 6.34 (m, *H*17, 1H), 1.68 (s, *H*1, 9H). $^{13}\text{C}\{^1\text{H}\}$ NMR ($\text{CO}(\text{CD}_3)_2$, 151 MHz, 25°C) δ : 178.64 (*C*20), 161.92 (*C*10), 155.10 (*C*3), 152.25 (*C*11), 151.71 (*C*8), 143.20 (*C*9), 140.03 (*C*13), 134.09 (*C*7), 133.90 (*C*18), 132.82 (*C*15), 126.79 (*C*12), 126.34 (*C*14), 123.89 (*C*4), 122.98 (*C*6) 122.95 (*C*5), 121.60 (*C*19), 118.30 (*C*16), 113.83 (*C*17), 36.25 (*C*2), 32.74 (*C*1). MALDI MS (anthracene matrix): calcd m/z 436.84 [**3-2**] $^{\bullet+}$, obsd m/z 436.84. Single crystals suitable for X-ray crystallographic analysis were grown by the slow evaporation of a benzene solution of **3-2** at room temperature.

3.4.4 Synthesis of $[\text{Pd}(\text{CH}_2\text{CMe}_2\text{C}_6\text{H}_4)(\text{C}_6\text{H}_4\text{N}=\text{CH}(2\text{-C}_5\text{H}_4\text{N}))]$ (**3-3a/3-3b**).

To a cooled (-65 °C) stirred solution of $[\text{Pd}(\text{CH}_2\text{CMe}_2\text{C}_6\text{H}_4)(\text{COD})]$, (**2-1**) (0.30 g, 0.86 mmol) in ether (50 mL) was added a solution of 2- $\text{C}_5\text{H}_4\text{NCH}=\text{NPh}$, **3-L2**, (0.15 g, 0.86 mmol) in ether (20 mL). The

solution was stirred at low temperature (1 h) and then allowed to slowly reach room temperature over 17 h. A color change from yellow to orange was observed over time. Upon removal of the solvent under reduced pressure, an oily orange product was formed, which was precipitated from ether (5 mL) with hexanes (30 mL). The solid was collected by filtration and dried under vacuum, to give **3-3a/3-3b** as an air-stable orange powder product (0.26 g, 0.62 mmol, 73%). Integration of comparative peaks in different deuterated solvents indicates that **3-3a** is formed with a 1:0.6 preference over **3-3b**. Characterization for **3-3a**: ^1H NMR (CDCl_3 , 600 MHz, 25°C) δ : 8.81 (d, $J = 5$ Hz, H_{15} , 1H), 8.53 (s, H_{10} , 1H), 7.96-8.00 (m, H_{14} , 1H), 7.72-7.74 (m, H_{12} , 1H), 7.55-7.59 (m, H_{13} , 1H), 7.34-7.46 (m, H_{17-21} , 5H), 6.82-6.85 (m, H_7 , 1H), 6.76 (dd, $J = 7, 1.4$ Hz, H_8 , 1H), 6.52 (td, $J = 7$ Hz, H_6 , 1H), 6.39 (dd, $J = 7$ Hz, H_5 , 1H), 2.65 (s, H_2 , 2H), 1.41 (s, H_1 , 6H). $^{13}\text{C}\{^1\text{H}\}$ NMR (CDCl_3 , 151 MHz, 25°C) δ : 161.11 (C_4), 162.36 (C_{10}), 157.07 (C_9), 153.59 (C_{11}), 149.78 (C_{15}), 149.57 (C_{16}), 137.88 or 137.84 (C_{14}), 136.62 (C_5), 128.99 (C_{17-21}), 128.98 (C_{17-21}), 127.98 (C_{17-21}), 127.59 (C_{13}), 127.09 (C_{12}), 123.26 (C_6), 123.08 (C_7), 122.58 (C_{17-21}), 121.38 (C_8), 47.23 (C_3), 46.26 (C_2), 33.75 (C_1). Characterization for **3-3b**: ^1H NMR (CDCl_3 , 600 MHz, 25°C) δ : 9.21 (d, $J = 5$ Hz, H_{15} , 1H), 8.48 (s, H_{10} , 1H), 7.96-8.00 (m, H_{15} , 1H), 7.72-7.74 (m, H_{12} , 1H), 7.64-7.67 (m, H_{13} , 1H), 7.55-7.59 (m, H_{5-8} , 1H), 7.34-7.46 (m, H_{17-21} , 3H), 7.27-7.29 (m, H_{17-21} , 2H), 6.99-7.00 (m, H_{5-8} , 2H), 6.82-6.85 (m, H_{5-8} , 1H), 2.15 (s, H_2 , 2H), 1.28 (s, H_1 , 6H). $^{13}\text{C}\{^1\text{H}\}$ NMR (CDCl_3 , 151 MHz, 25°C) δ : 161.15 (C_4), 163.00 (C_{10}), 158.80 (C_9), 153.75 (C_{11}), 150.83 (C_{14}), 149.41 (C_{16}), 137.88 or 137.84 (C_{15}), 134.78 (C_{5-8}), 127.76 (C_{13}), 127.04 (C_{12}), 124.17 (C_{5-8}), 123.40 (C_{5-8}), 122.10 (C_{17-21}), 121.88 (C_{5-8}), 47.95 (C_3), 46.70 (C_2), 33.57 (C_1). MALDI MS (anthracene matrix): calcd m/z 420.8 [**3-3a** or **3-3b**] $^{+}$, obs'd m/z 420.8. Elemental Analysis: calcd for $\text{C}_{22}\text{H}_{22}\text{N}_2\text{Pd}$: C, 62.78; H, 5.27; N, 6.65. Found: C, 62.71; H, 5.60; N, 6.39. Single crystals of **3-3b** suitable for X-ray crystallographic analysis were grown by the slow diffusion of pentane into a THF solution of the complex at room temperature.

3.5 References

1. A. E. Shilov and G. B. Shul'pin, *Chem. Rev.*, 1997, **97**, 2879-2932.
2. R. G. Bergman, *Nature*, 2007, **446**, 391.
3. F. Roudesly, J. Oble and G. Poli, *J. Mol. Catal. A: Chem.*, 2017, **426**, 275-296.
4. T. Gensch, M. N. Hopkinson, F. Glorius and J. Wencel-Delord, *Chem. Soc. Rev.*, 2016, **45**, 2900-2936.
5. J. Wencel-Delord, T. Droge, F. Liu and F. Glorius, *Chem. Soc. Rev.*, 2011, **40**, 4740-4761.

6. T. W. Lyons and M. S. Sanford, *Chem. Rev.*, 2010, **110**, 1147-1169.
7. C. B. Bheeter, L. Chen, J.-F. Soule and H. Doucet, *Cat. Sci. Tech.*, 2016, **6**, 2005-2049.
8. Y. Yang, J. Lan and J. You, *Chem. Rev.*, 2017, **117**, 8787-8863.
9. C. Liu, J. Yuan, M. Gao, S. Tang, W. Li, R. Shi and A. Lei, *Chem. Rev.*, 2015, **115**, 12138-12204.
10. Z. Chen, B. Wang, J. Zhang, W. Yu, Z. Liu and Y. Zhang, *Org. Chem. Front.*, 2015, **2**, 1107-1295.
11. D. L. Davies, S. A. Macgregor and C. L. McMullin, *Chem. Rev.*, 2017, **117**, 8649-8709.
12. L. Ackermann, *Chem. Rev.*, 2011, **111**, 1315-1345.
13. R. N. Perutz and S. Sabo-Etienne, *Angew. Chem. Int. Ed.*, 2007, **46**, 2578-2592.
14. Y. Boutadla, D. L. Davies, S. A. Macgregor and A. I. Poblador-Bahamonde, *Dalton Trans.*, 2009, 5820-5831.
15. S. I. Gorelsky, D. Lapointe and K. Fagnou, *J. Am. Chem. Soc.*, 2008, **130**, 10848-10849.
16. M. Lersch and M. Tilset, *Chem. Rev.*, 2005, **105**, 2471-2526.
17. J. E. Bercaw, G. S. Chen, J. A. Labinger and B.-L. Lin, *J. Am. Chem. Soc.*, 2008, **130**, 17654-17655.
18. V. J. Scott, J. A. Labinger and J. E. Bercaw, *Organometallics*, 2011, **30**, 4374-4378.
19. B. K. Mai and Y. Kim, *Inorg. Chem.*, 2016, **55**, 9822-9829.
20. S. S. Stahl, J. A. Labinger and J. E. Bercaw, *J. Am. Chem. Soc.*, 1995, **117**, 9371-9372.
21. G. S. Hill, L. M. Rendina and R. J. Puddephatt, *Organometallics*, 1995, **14**, 4966-4968.
22. R. Romeo, M. R. Plutino and L. I. Elding, *Inorg. Chem.*, 1997, **36**, 5909-5916.
23. U. Belluco, M. Giustiniani and M. Graziani, *J. Am. Chem. Soc.*, 1967, **89**, 6494-6500.
24. J. K. Jawad, R. J. Puddephatt and M. A. Stalteri, *Inorg. Chem.*, 1982, **21**, 332-337.
25. M. J. Woolley, G. N. Khairallah, G. da Silva, P. S. Donnelly, B. F. Yates and R. A. J. O'Hair, *Organometallics*, 2013, **32**, 6931-6944.
26. J. E. Bercaw, G. S. Chen, J. A. Labinger and B.-L. Lin, *Organometallics*, 2010, **29**, 4354-4359.
27. B. M. Cochran and F. E. Michael, *J. Am. Chem. Soc.*, 2008, **130**, 2786-2792.
28. J. Cámpora, J. A. López, P. Palma, P. Valerga, E. Spillner and E. Carmona, *Angew. Chem. Int. Ed.*, 1999, **38**, 147-151.
29. Y.-F. Yang, G. Chen, X. Hong, J.-Q. Yu and K. N. Houk, *J. Am. Chem. Soc.*, 2017, **139**, 8514-8521.
30. D. G. Musaev, A. Kaledin, B.-F. Shi and J.-Q. Yu, *J. Am. Chem. Soc.*, 2012, **134**, 1690-1698.
31. B.-F. Shi, N. Maugel, Y.-H. Zhang and J.-Q. Yu, *Angew. Chem. Int. Ed.*, 2008, **47**, 4882-4886.
32. Y. Izawa and S. S. Stahl, *Adv. Synth. Catal.*, 2010, **352**, 3223-3229.
33. E. Larionov, M. Nakanishi, D. Katayev, C. Besnard and E. P. Kundig, *Chem. Sci.*, 2013, **4**, 1995-2005.

34. A. Renaudat, L. Jean-Gérard, R. Jazzar, C. E. Kefalidis, E. Clot and O. Baudoin, *Angew. Chem. Int. Ed.*, 2010, **49**, 7261-7265.
35. S. Anas, A. Cordi and H. B. Kagan, *Chem. Commun.*, 2011, **47**, 11483-11485.
36. T. Saget, S. J. Lemouzy and N. Cramer, *Angew. Chem. Int. Ed.*, 2012, **51**, 2238-2242.
37. J. L. Rutherford, M. P. Rainka and S. L. Buchwald, *J. Am. Chem. Soc.*, 2002, **124**, 15168-15169.
38. D. Solé, X. Urbaneja and J. Bonjoch, *Adv. Synth. Catal.*, 2004, **346**, 1646-1650.
39. D. Solé, I. Fernández and M. A. Sierra, *Chem. Eur. J.*, 2012, **18**, 6950-6958.
40. J. R. Khusnutdinova and D. Milstein, *Angew. Chem. Int. Ed.*, 2015, **54**, 12236-12273.
41. C. Gunanathan and D. Milstein, *Chem. Rev.*, 2014, **114**, 12024-12087.
42. K. A. Thompson, C. Kadwell, P. D. Boyle and R. J. Puddephatt, *J. Organomet. Chem.*, 2017, **829**, 22-30.
43. M. E. Moustafa, P. D. Boyle and R. J. Puddephatt, *Chem. Commun.*, 2015, **51**, 10334-10336.
44. A. Behnia, P. D. Boyle, J. M. Blacquiere and R. J. Puddephatt, *Organometallics*, 2016, **35**, 2645-2654.
45. F. Qu, J. R. Khusnutdinova, N. P. Rath and L. M. Mirica, *Chem. Commun.*, 2014, **50**, 3036-3039.
46. L. Yang, D. R. Powell and R. P. Houser, *Dalton Trans.*, 2007, 955-964.
47. A. Marini, A. Muñoz-Losa, A. Biancardi and B. Mennucci, *J. Phys. Chem. B*, 2010, **114**, 17128-17135.
48. C. Gourlaouen and C. Daniel, *Dalton Trans.*, 2014, **43**, 17806-17819.
49. T. Hashimoto, K. Fukumoto, N. H.-T. Le, T. Matsuoka, S. Kawamorita, N. Komiya and T. Naota, *Dalton Trans.*, 2016, **45**, 19257-19268.
50. N. Chaudhury and R. J. Puddephatt, *J. Organomet. Chem.*, 1975, **84**, 105-115.
51. T. Yamamoto, A. Yamamoto and S. Ikeda, *J. Am. Chem. Soc.*, 1971, **93**, 3350-3359.
52. A. Behnia, M. A. Fard, J. M. Blacquiere and R. J. Puddephatt, *Organometallics*, 2017, **36**, 4759-4769.
53. Similar OH...M hydrogen bonds to electron rich platinum(II) centers have been observed previously, and discussed in terms of bonding. M. Baya, U. Belio, A. Martin, *Inorg. Chem.* 2014, **53**, 189-200.
54. A. Behnia, P. D. Boyle, M. A. Fard, J. M. Blacquiere and R. J. Puddephatt, *Dalton Trans.*, 2016, **45**, 19485-19490.
55. M. Anand and R. B. Sunoj, *Organometallics*, 2012, **31**, 6466-6481.
56. P. A. Shaw and J. P. Rourke, *Dalton Trans.*, 2017, **46**, 4768-4776.

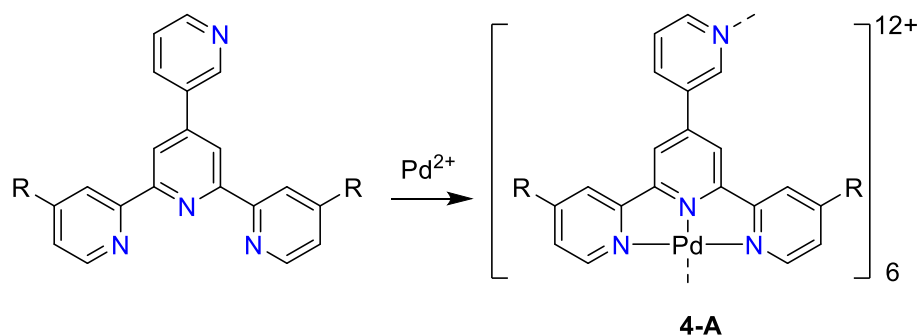
57. H. R. Thomas, R. J. Deeth, G. J. Clarkson and J. P. Rourke, *Organometallics*, 2011, **30**, 5641-5648.
58. G. te Velde, F. M. Bickelhaupt, E. J. Baerends, C. Fonseca Guerra, S. J. A. van Gisbergen, J. G. Snijders and T. Ziegler, *J. Comput. Chem.*, 2001, **22**, 931-967.
59. A. D. Becke, *Phys. Rev. A*, 1988, **38**, 3098-3100.

4 Pincer-Plus-One Ligands in Self-Assembly with Palladium(II): A Molecular Square and a Molecular Tetrahedron

(A. Behnia, P. D. Boyle, M. A. Fard, J. M. Blacquiere and R. J. Puddephatt, *Dalton Trans.*, 2016, **45**, 19485-19490.)

4.1 Introduction

The application of chemical principles in combination with symmetry considerations has allowed the rational design of hundreds of nanoscale compounds of palladium(II) through self-assembly by dynamic coordination chemistry or by secondary bonding forces, such as hydrogen bonds or metallophilic attractions.¹⁻⁶ Most two-component systems have used *cis*-blocked palladium(II) complexes as acceptors and bidentate or polydentate bridging ligands as donors.¹⁻⁶ Palladium(II) complexes with tridentate ligands, usually terpyridine-based, have been used less often as acceptors in combination with bridging ligands as donors, and pincer ligands with appended hydrogen bonding groups for self-assembly have also given interesting oligomers and polymers.⁷⁻¹¹ An intriguing ligand design for self-assembly involves both a mer-tridentate (i.e. pincer) component for coordination to one metal and a monodentate (i.e. pincer-plus-one) donor for coordination to a second metal. However, a recent comprehensive review⁶ cited only one example of such a ligand with a terpyridine portion and an additional 3-pyridyl substituent that self-assembles with palladium(II) to give a cyclic hexamer (Scheme 4-1), having a 12+ charge, as shown by TWIM-MS.¹² This article reports two examples of unexpected ligand oxidation that converts a tridentate Schiff-base ligand to two different pincer-plus-one ligand structures. These architectures promote the self-assembly of two different palladium(II) tetramers that are arranged in a molecular square or tetrahedron shape.

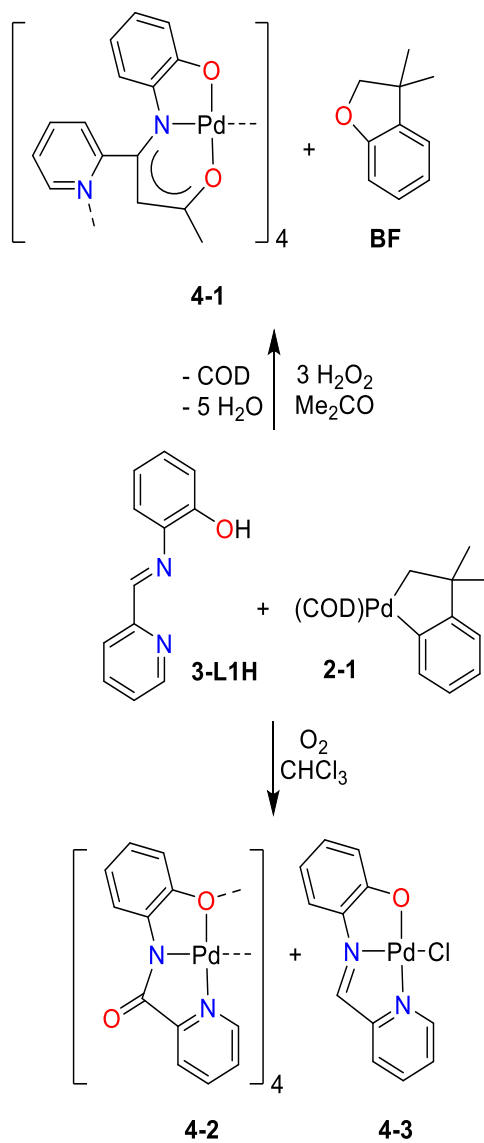


Scheme 4-1 Self-assembly of a pincer-plus-one ligand and Pd(II) to give a hexamer.¹²

4.2 Result and Discussion

The new tetramers were obtained serendipitously while studying the reaction of the diimine-phenol ligand, **3-L1H**,¹³ with the organopalladium complex, **2-1**,¹⁴⁻¹⁵ in the presence of oxidants hydrogen peroxide or dioxygen (Scheme 4-2). The original intention being that the diimine group would displace the COD ligand from **2-1** and that the phenol substituent would facilitate subsequent biomimetic oxidation chemistry. Rather, two tetramers, **4-1** and **4-2**, were obtained, with both reactions involving ligand oxidation and loss of the hydrocarbon moiety present in precursor **2-1**.

In the first reaction, an acetone solution of complex **2-1** was treated with hydrogen peroxide, followed by addition of ligand **3-L1H**, to give tetramer **4-1**, as a red solid. Characterization of **4-1** (*vide infra*) indicates that the building block unit in **4-1** is a neutral palladium(II) fragment with a tetradentate dianionic N₂O₂-donor ligand, formed by oxidative coupling of an acetone molecule with the imine group of the parent ligand **3-L1H**. The pincer component of **4-1** contains both a 6-membered acnac ring and a 5-membered amidophenoxide ring, with the pyridyl group bridging to the neighboring palladium atom.



Scheme 4-2 Synthesis of complexes **4-1**, **4-2** and **4-3**.

Small-scale ^1H NMR experiments were conducted in an attempt to optimize the reaction conditions and to reveal characteristics of the reaction pathway. Following the same conditions to those above, **4-1** is formed in 57% yield and this is accompanied by benzofuran (**BF**) in a 30% yield. We have shown previously that oxidation of Pd(II) complexes related to **2-1** with excess H_2O_2 likewise affords **BF**.¹⁵ The reaction involves oxidation-promoted oxygen-atom insertion into a Pd-aryl bond, followed by palladium oxidation and reductive elimination to release **BF**. While a similar process appears to be operative in the formation of **4-1**, the mechanistic details are not yet determined. Critical to the reproducible formation of **4-1** is the described order of addition of reaction components. If metallation (**3-L1H** + **2-1**) precedes oxidation (addition of H_2O_2), numerous products are formed with no evidence for **4-1**.

Alternatively, if H₂O₂ was added to ligand **3-L1H**, followed by addition of **2-1**, the tetramer **4-1** was not formed. As expected, a switch in solvent to CHCl₃ does not afford **4-1**, nor does a switch in oxidant to O₂.

The second tetramer **4-2** is obtained by reaction of a chloroform solution of **3-L1H** and **2-1** in the presence of dioxygen. Ligand **3-L1H** is again oxidized, but in this case an amido moiety is generated, with the incorporated oxygen atom likely originating from the O₂ oxidant. This is supported by the fact that tetramer **4-2** is not formed on conducting the reaction under N₂. Characterization (*vide infra*) reveals that the pincer component of the ligand is comprised of the pyridyl, amido and phenoxide donors. The phenoxide bridges to a second metal to act also as the plus-one portion of the ligand. This reaction is complex and gave a mixture of several palladium complexes and organic compounds, including BF. The green complex **4-2** was the principal product that was insoluble in acetone. The purple monometallic complex **4-3** was isolated from the acetone-soluble fraction, crystallized and analysed by X-ray diffraction (Figure 4-1). The complex has been prepared previously, and the structure reported as a chloroform solvate.¹⁷⁻¹⁸ The bond parameters for the unsolvated form (Figure 4-1) are unexceptional, but they serve to illustrate the structure of the deprotonated ligand **3-L1H** in its expected simple pincer binding mode.¹⁷⁻¹⁸ Presumably the chloro ligand derives from the CHCl₃ solvent used for the reaction.

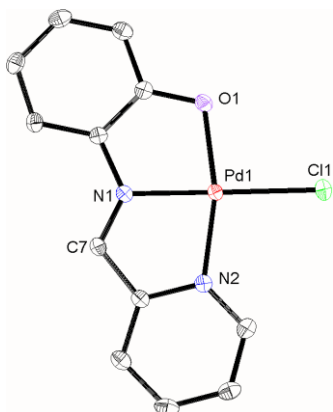


Figure 4-1 The structure of complex **4-3** (previously reported¹⁷⁻¹⁸ as a CHCl₃ solvate). Selected bond parameters: Pd(1)N(1) 1.951(2), Pd(1)N(2) 2.017(3), Pd(1)O(1) 2.011(2), Pd(1)Cl(1) 2.303(1) Å; N(1)Pd(1)Cl(1) 175.80(7), N(2)Pd(1)O(1) 165.60(9)°.

Both reactions to give **4-1** and **4-2** (Scheme 4-2) clearly involve multiple steps and intermediates, and the mechanisms are not yet understood. We note that the addition of deprotonated acetone to imine complexes¹³ and the oxidation of imines to amides mediated by

Pd(II)¹⁶ are well established reactions. These transformations are needed for the formation of **4-1** and **4-2**, respectively.

Tetramers **4-1** and **4-2** were isolated and characterized by NMR and IR spectroscopy, MALDI mass spectrometry and elemental analysis. ¹H NMR spectra of **4-1** and **4-2** both reveal one set of ligand resonances that indicates the tetramers have four-fold symmetry in the solution state. The hydrocarbon ligand of the precursor **2-1** is not part of the structures and this is supported by the absence of signals in the aliphatic region that would be diagnostic for the methyl and methylene groups. For complex **4-1**, ligand oxidation and acetone coupling is evident from the absence of the imine singlet of **3-L1H** and the appearance of singlets for the acnac CH and methyl moieties at 5.92 and 1.64 ppm, respectively. The downfield location of the former is typical for this site in other M(acnac) complexes.¹⁹ The imine resonance is likewise absent in the ¹H spectrum for **4-2** consistent with oxidation to an amide moiety. The tetrameric nature of both **4-1** and **4-2** was confirmed by charge-transfer MALDI MS analysis in which the molecular cation is observed at *m/z* 1433.8 and 1273.9, respectively (Figure 4-2). Small deviations between the observed and simulated isotope patterns may be due to the contribution of an ionization pathway involving protonation to give an overlapping signal for [M+H]⁺. The molecular square (**4-1**) fragments in the gas phase to give signals for both the loss of one ligand and one Pd-L unit at *m/z* = 1181.8 and 1075.9, respectively. In contrast, the molecular tetrahedron **4-2** fragments to give a dimer. The different fragmentation pathways may reflect the potential for metallophilic interactions in **4-2**, but not **4-1**.

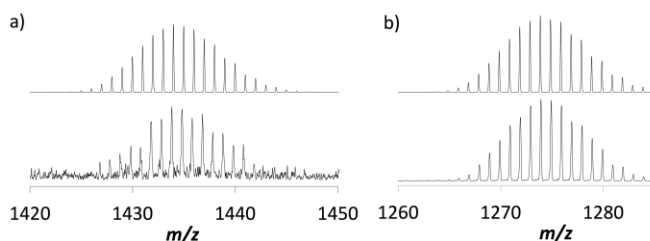


Figure 4-2 Simulated (top) and observed (bottom) MALDI MS isotope patterns for a) [**4-1**]⁺, and b) [**4-2**]⁺. Matrix = pyrene.

Both complexes **4-1** and **4-2** are neutral and amenable to crystallization, in contrast to the highly charged complex **A**, their only analog. Figure 4-3 shows a single building block, with pincer-plus-one ligation, and the shape of the molecular tetramer for each **4-1** and **4-2**. In both cases, loss of the hydrocarbon ligand and oxidation of the imine fragment is evident from the

structures. In each case, the palladium(II) centre has distorted square planar stereochemistry with *trans,trans*-PdN₂O₂ and *cis,cis*-PdN₂O₂ coordination in **4-1** and **4-2**, respectively. Compound **4-1** shows the most significant distortion of the pincer moiety with an angle of 6.7° found between a plane defined by the carbon atoms of the acnac ring and the Pd square plane.

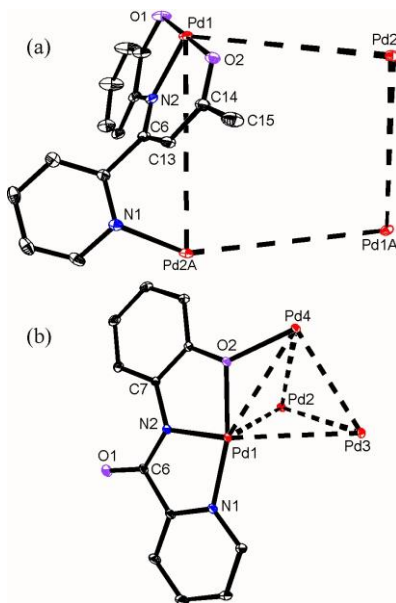


Figure 4-3 The building block and polyhedral structure in (a) **4-1** and (b) **4-2**.

The four palladium atoms in **4-1** have the shape of a distorted square, with edge distances 5.61 and 5.78 Å, longer diagonal distances of 7.62 and 7.72 Å, and internal angles of 84 and 85°. In contrast, the palladium atoms in **4-2** define a distorted tetrahedron, with all six Pd...Pd distances in the range 3.24–3.58 Å and with internal angles in the range 56–64°. The shorter Pd...Pd distances in **4-2** are consistent with the presence of weak metallophilic bonding, but there are clearly no metal-metal interactions in **4-1**.

The full structures of **4-1** and **4-2** are shown in Figures 4-4 and 4-5, respectively. The Pd...Pd separations are controlled mostly by the nature of the bridging between Pd(pincer ligand) units and are naturally longer in **4-1** than in **4-2**. This extra bridging can occur on either side of the roughly planar Pd(pincer ligand) unit and so each building block can have either *P* or *M* conformational chirality.²⁰ The self-assembly to give tetramers, in which the stereochemistry is locked in, can then occur by: 1) self-recognition to give racemic *PPPP/MMMM* isomers, 2) self-discrimination to give the achiral *PMPM* isomer, or 3) a more random way to include the racemic *PPPM/PMMM* isomers. In both **4-1** and **4-2** the self-assembly occurs by self-discrimination. In the solid state, **4-1** and **4-2** have crystallographically imposed *C*₂ and *C*₁ symmetry respectively, but both have approximate *S*₄ symmetry and this is consistent with the

highly symmetric ^1H NMR spectra discussed above. Most known molecular tetrahedra contain octahedrally coordinated metal ions and usually self-assemble by self-recognition.^{1-5,21-24} There are only a few examples of molecular tetrahedra with square planar metal centres and they all have much longer Pd...Pd separations than in **4-2**.^{1-6,25-27} The shortest Pd...Pd separations in **4-2** may result from a combination of π -stacking and metallophilic bonding effects (Figure 4-5).

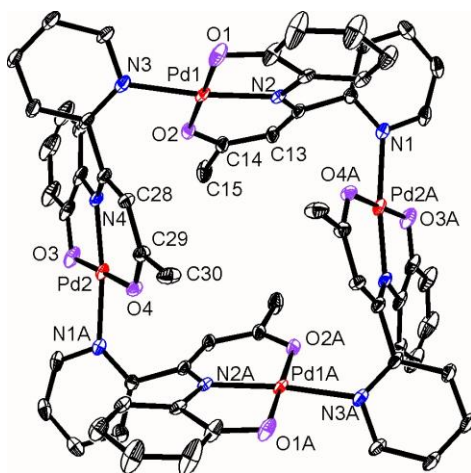


Figure 4-4 The structure of complex **4-1**. Selected bond parameters: Pd(1)N(2) 1.957(3), Pd(1)O(1) 1.971(3), Pd(1)O(2) 1.977(3), Pd(1)N(3) 2.061(3) Å; O(1)Pd(1)O(2) 179.78(13), N(2)Pd(1)N(3) 173.59(14)°.

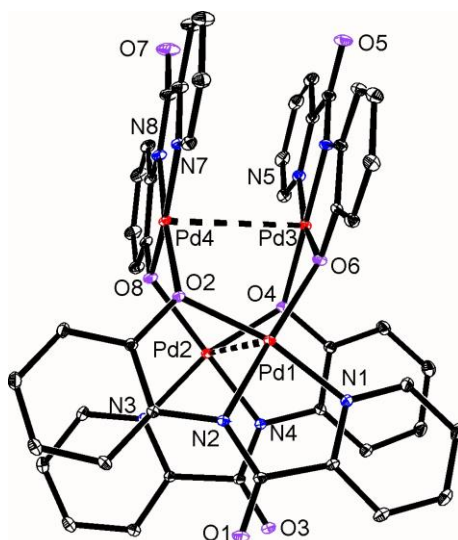


Figure 4-5 The structure of complex **4-2**. Selected bond parameters: Pd(1)N(1) 1.977(1), Pd(1)N(2) 1.931(1), Pd(1)O(2) 2.033(1), Pd(1)O(6) 2.042(1), Pd(1)Pd(2) 3.238(1) Å; N(1)Pd(1)O(2) 166.43(5), N(2)Pd(1)O(6) 178.10(5)°.

4.3 Conclusion

The structures of two interesting tetramers are described. Several degrees of serendipity are involved in their synthesis. The ligand **3-L1H** is oxidised in both cases, but in very different ways to form dianionic pincer ligands in the complexes **4-1** and **4-2**. The neutral palladium(II)-pincer ligand fragments have an additional donor group and a vacant site at palladium(II) and they self-assemble to give tetramers in both cases. Both the molecular square in **4-1** and tetrahedron in **4-2** are new structural types, each having the unusual *S4* symmetry.^{1-9,20-24} None of this unprecedented chemistry was predicted in advance, but it is important to recognise that the pincer-plus-one ligand design has great potential for the designed synthesis of oligomeric and polymeric complexes with unusual structures, properties and potential uses. The syntheses of **4-1** and **4-2** presented here are reproducible under the defined experimental conditions, but given the long reaction times (and low yields in the case of **4-2**) we suggest the formation of **4-1** and **4-2** serve to inspire intentional synthesis of the oxidized ligands²⁸ for the purposes of self-assembly of nanoscale structures.

4.4 Experimental

4.4.1 Reagents and General Procedures

NMR spectra were recorded at 298 K using a Varian Inova 600 MHz spectrometer. ¹H and ¹³C chemical shifts are reported relative to tetramethylsilane. Complete assignments of each compound were aided by the use of ¹H-¹H gCOSY, ¹H-¹³C HSQC, and ¹H-¹³C HMBC experiments and are reported using the labeling scheme in Chart 4-1. Commercial reagents and aqueous 30% H₂O₂ were used without further purification. The complex [Pd(CH₂CMe₂C₆H₄)(COD)]¹⁴⁻¹⁵ (**2-1**), and the diimine ligand, 2-(pyridin-2-ylmethyleneimino)phenol¹³ (**3-L1H**) were synthesized according to the literature procedures. Elemental analyses were performed by Laboratoire d'Analyse Élémentaire del'Université de Montréal. Organic products were analyzed using a Shimadzu GCMS-QP2010 Ultra GC with a DB-5 column. MALDI-TOF mass spectra were collected using an AB Sciex 5800 TOF/TOF mass spectrometer using pyrene as the matrix in a 20:1 matrix:substrate molar ratio.

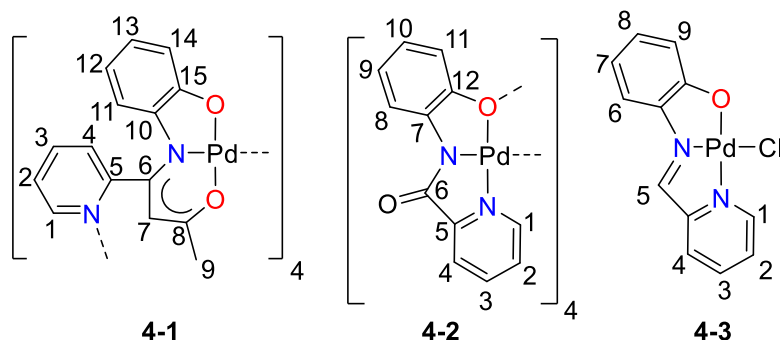


Chart 4-1 . NMR labeling scheme for complexes made in this study.

4.4.2 Synthesis of complex **4-1**

To a stirred solution of $[\text{Pd}(\text{CH}_2\text{CMe}_2\text{C}_6\text{H}_4)(\text{COD})]$, **2-1**, (0.090 g, 0.26 mmol) in acetone (5 mL) was added a 30% H_2O_2 solution (79.5 μL , 3 equiv) via a micropipette syringe at room temperature. An immediate color change from yellow to sharp orange was observed. The mixture was allowed to stir for 2 h. Then, the reaction flask was transferred to a -65°C cold bath. Once the mixture cooled, a solution of 2- $\text{C}_5\text{H}_4\text{NCH}=\text{N}-2-\text{C}_6\text{H}_4\text{OH}$, **3-L1H**, (0.05 g, 0.26 mmol) in acetone (5 mL) was added to the flask via syringe. The solution was stirred at low temperature and allowed to slowly reach room temperature over 6 h. A color change from orange to dark red was observed over time. Next, the reaction flask was left for a night and bright red crystals were grown by slow evaporation of the solvent. Crystals were washed with hexane (3×2 mL) and dried under high vacuum, to give **4-1** as an air-stable product (0.03 g, 0.02 mmol, 35%). ^1H NMR (CDCl_3 , 600 MHz, 25°C) δ : 9.26 (d, 1H, $J = 6$ Hz, H_1), 7.82 (t, 1H, $J = 8$ Hz, H_3), 7.52 (dd, 1H, $J = 8$ Hz, 6Hz, H_2), 7.32 (d, 1H, $J = 8$ Hz, H_4), 6.87 (d, 1H, $J = 8$ Hz, H_{11}), 6.78 (t, 1H, $J = 8$ Hz, H_{12}), 6.09 (t, 2H, $J = 8$ Hz, H_{13}), 5.95 (d, 1H, $J = 8$ Hz, H_{14}), 5.92 (s, 1H, H_7), 1.64 (s, 3H, H_9); $^{13}\text{C}\{^1\text{H}\}$ NMR (CDCl_3 , 600 MHz, 25°C) δ : 176.99 (C8), 165.91 (C10), 159.09 (C6), 153.19 (C1 or C5), 153.11 (C1 or C5), 141.35 (C15), 139.25 (C3), 127.13 (C4), 125.97 (C12), 124.90 (C2), 121.92 (C11), 117.71 (C14), 112.70 (C13), 102.88 (C7), 23.85 (C9). MALDI MS (Pyrene matrix): Calcd. m/z 1434.7 [**4-1**] $^{+}$, Obs. m/z 1434.7. Anal. Calcd for $\text{C}_{60}\text{H}_{48}\text{N}_8\text{O}_8\text{Pd}_4 \cdot (\text{CH}_3)_2\text{CO}$: C, 50.53; H, 3.54. Found: C, 50.67; H, 3.94. Single crystals suitable for X-ray crystallographic analysis were grown by the slow evaporation of an acetone solution of the complex at room temperature. In a separate experiment, the similar reaction was carried out in acetone- d_6 containing dimethyl terephthalate as internal NMR standard. The yield of **4-1**

in solution was determined to be 57%, and the yield of the organic benzofuran product **BF**, identified by its ^1H NMR spectrum,¹⁻⁵ was 30%.

4.4.3 Synthesis of complexes **4-2** and **4-3**

A dilute solution of 2-C₅H₄NCH=N-2-C₆H₄OH, **3-L1H**, (0.17 g, 0.86 mmol) in chloroform (500 mL) was added to a stirred dilute chloroform solution (500 mL) of [Pd(CH₂CMe₂C₆H₄)(COD)], **2-1**, (0.30 g, 0.86 mmol) cooled to -65 °C. The mixture was allowed to stir and slowly reach room temperature and stirring was continued for 4 weeks, during which time O₂ gas was bubbled through the solution for 15 minutes every three days and the color of the solution changed from yellow to dark grey. Upon removal of the solvent under reduced pressure, a grey solid was formed. This solid was extracted with acetone (3x30mL). The insoluble fraction was identified as complex **4-2**, which was isolated as a green powder (0.06 g, 0.05 mmol, 22%). ^1H NMR (CDCl₃, 600 MHz, 25°C) δ : 7.80-7.74 (m, 3H, *H3*, *H4*, *H8*), 7.54 (d, 1H, *J* = 8 Hz, *H11*), 7.31 (d, 1H, *J* = 6 Hz, *H1*), 6.79 - 6.75 (m, 2H, *H2*, *H9*), 6.40 (m, 1H, *H10*); $^{13}\text{C}\{^1\text{H}\}$ NMR (CDCl₃, 600 MHz, 25°C) δ : 164.50 (*C6*), 162.88 (*C12*), 157.36 (*C5*), 145.71 (*C1*), 139.30 (*C7*), 139.17 (*C3*), 126.17 (*C2*), 125.89 (*C8*), 123.39 (*C9*), 120.76 (*C11*), 120.20 (*C10*), 119.16 (*C4*). MALDI MS (Anthracene matrix): Calcd. *m/z* 1274.4 [**4-2**]^{•+}, Obs. *m/z* 1274.4. Anal. Calcd. for C₄₈H₃₂N₈O₈Pd₄.3CHCl₃: C, 37.52; H, 2.16; N, 6.86. Found: C, 37.86; H, 2.98; N, 6.39%. Single crystals suitable for X-ray crystallographic analysis were grown by slow diffusion of cyclohexane into a solution of **4-2** in CHCl₃. The acetone extracts were evaporated under vacuum to give complex **4-3** as a purple powder (0.04 g, 0.13 mmol, 15%). ^1H NMR ((CD₃)₂CO, 600 MHz, 25°C) δ : 8.51 (d, 1H, *J* = 5 Hz, *H1*), 8.31 (s, 1H, *H5*), 8.17 (t, 1H, *J* = 8 Hz, *H3*), 7.84 (d, 1H, *J* = 8 Hz, *H4*), 7.62 (dd, 1H, *J* = 8 Hz, 6 Hz, *H2*), 7.33 (d, 1H, *J* = 8 Hz, *H6*), 7.03 (t, 1H, *J* = 8 Hz, *H8*), 6.48 (d, 1H, *J* = 8 Hz, *H9*), 6.41 (t, 1H, *J* = 8 Hz, *H7*) in agreement with literature values.¹⁷⁻¹⁸ Single crystals suitable for X-ray crystallographic analysis were grown by dissolving the product in chloroform, followed by slow evaporation of the solvent.

4.4.4 X-ray Structure Determination²⁹⁻³³

In a typical experiment, the selected crystal was mounted on a Mitegen polyimide micromount with a small amount of Paratone N oil. All X-ray measurements were made using a Bruker Kappa Axis Apex2 diffractometer at a temperature of 110 K. The frame integration was performed using SAINT, and the resulting raw data were scaled and absorption corrected using a multi-scan averaging of symmetry equivalent data using SADABS. The structure was solved

by using a dual space methodology using the SHELXT program. All non-hydrogen atoms were obtained from the initial solution. The hydrogen atoms were introduced at idealized positions and were allowed to ride on the parent atom. The structural model was fit to the data using full matrix least-squares based on F^2 . The calculated structure factors included corrections for anomalous dispersion from the usual tabulation. The structure was refined using the SHELXL-2014 program from the SHELX suite of crystallographic software. Details are given in Table A4-1. In complex **4-2**, the lattice contained two CHCl_3 molecules of solvation. One of the CHCl_3 molecules was highly disordered and could not be fit to a chemically sensible model. The electron density associated with this moiety was masked out of the refinement using the SQUEEZE algorithm as implemented in PLATON. The other CHCl_3 had a Cl atom disordered over two sites. The occupancy of the predominant orientation refined to a normalized value of 0.532(9).

4.5 References

1. T. R. Cook and P. J. Stang, *Chem. Rev.*, 2015, **115**, 7001.
2. S. Mukherjee and P. S. Mukherjee, *Chem. Commun.*, 2014, **50**, 2239.
3. M.D. Ward and P. R. Raithby, *Chem. Soc. Rev.*, 2013, **42**, 1619.
4. T. R. Cook, Y. R. Zheng and P. J. Stang, *Chem. Rev.*, 2013, **113**, 734.
5. R. Chakrabarty, P. S. Mukherjee and P. J. Stang, *Chem. Rev.*, 2011, **111**, 6810.
6. N. B. Debata, D. Tripathy and D. K. Chand, *Coord. Chem. Rev.*, 2012, **256**, 1831.
7. S. Perera, X. Li, M. Soler, A. Schultz, C. Wesdemiotis, C. N. Moorefield and G. R. Newkome, *Angew. Chem. Int. Ed.*, 2010, **49**, 6539.
8. E.C. Constable, C. E. Housecroft and C. B. Smith, *Inorg. Chem. Comm.*, 2003, **6**, 1011.
9. R. D. Sommer, A. L. Rheingold, A. J. Goshe and B. Bosnich, *J. Am. Chem. Soc.*, 2001, **123**, 3940.
10. N. C. Mehendale, M. Lutz, A. L. Spek, R. J. M. Klein Gebbink and G. van Koten, *J. Organomet. Chem.*, 2008, **693**, 2971.
11. O. Adeyi, W. B. Cross, G. Forrest, L. Godfrey, E. G. Hope, A. McLeod, A. Singh, K. Singh, G. A. Solan, Y. Wang and L. A. Wright, *Dalton Trans.*, 2013, **42**, 7710.
12. S. Perea, X. Li, M. Guo, C. Wesdemiotis, C. N. Moorefield and G. R. Newkome, *Chem. Commun.*, 2011, **47**, 4658.
13. M. E. Moustafa, P. D. Boyle and R. J. Puddephatt, *Chem. Commun.*, 2015, **51**, 10334.

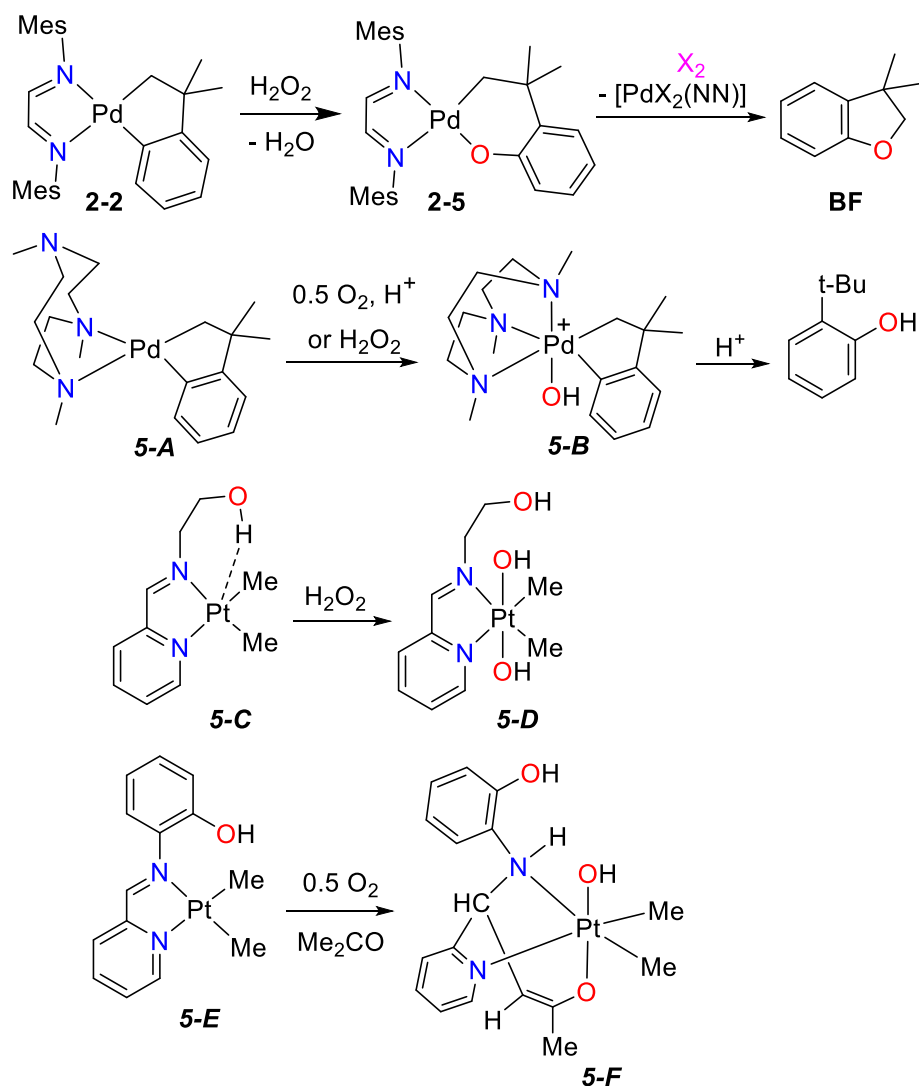
14. F. Qu, J. R. Khusnutdinova, N. P. Rath and L. M. Mirica, *Chem. Commun.*, 2014, **50**, 3036.
15. A. Behnia, P. D. Boyle, J. M. Blacquiere and R. J. Puddephatt, *Organometallics*, 2016, **35**, 2645.
16. Y. Suto, N. Yamagiwa and Y. Torisawa, *Tetrahedron Lett.*, 2008, **49**, 5732.
17. I. Angurell, I. Martinez-Ruiz, O. Rossell, M. Seco, P. Gomez-Sal, A. Martin, M. Font-Bardia and X. Solans, *J. Organomet. Chem.*, 2007, **692**, 3882.
18. N. Gomez-Blanco, J. J. Fernandez, A. Fernandez, D. Vazquez-Garcia, M. Lopez-Torres and J.M. Vila, *Eur. J. Inorg. Chem.*, 2009, 3071.
19. J. D. Crowley, A. J. Goshe, I. M. Steele and B. Bosnich, *Chem. Eur. J.* 2004, 1944.
20. G. Bringmann, A. J. Price Mortimer, P.A. Keller, M. J. Dresser, J. Garner and M. Breuning *Angew. Chem. Int. Ed.*, 2005, **44**, 5584.
21. D. L. Caulder, R. E. Powers, T. N. Parac and K. N. Raymond, *Angew. Chem. Int. Ed.*, 1998, **37**, 1840.
22. J. S. Fleming, K. L. V. Mann, C.-A. Carraz, E. Psillakis, J. C. Jefferey, J. A. McCleverty and M. D. Ward, *Angew. Chem. Int. Ed.*, 1998, **37**, 1279.
23. W. Meng, T. K. Ronson and J. R. Nitschke, *Proc. Nat. Acad. Sci.*, 2013, **110**, 10531.
24. C. Giri, F. Topic, P. Mal and K. Rissanen, *Dalton Trans.*, 2014, **43**, 17889.
25. S. M. Jansze, G. Cecot, M. D. Wise, K. O. Zhurov, T. K. Ronson, A. M. Castilla, A. Finelli, P. Pattison, E. Solari, R. Scopelliti, G. E. Zelinskii, A. V. Vologzhanina, Y. Z. Voloshin, J. R. Nitschke and K. Severin, *J. Am. Chem. Soc.*, 2016, **138**, 2046.
26. C. Klein, C. Gutz, M. Bogner, F. Topic, K. Rissanen and A. Lutzen, *Angew. Chem. Int. Ed.*, 2014, **53**, 3739.
27. D. K. Chand, K. Biradha, M. Kawano, S. Sakamoto, K. Yamaguchi and M. Fujita, *Chem. Asian J.*, 2006, **1**, 82.
28. The free ligand in **4-3** appears to be unknown but the ligand in **4-4** is known, though the binding mode in **4-4** is not. D. S. Marlin, M. M. Olmstead and P. K. Mascharak, *Eur. J. Inorg. Chem.* 2002, 859.
29. *APEX 2, Crystallography software package*; Bruker AXS: Madison, WI, 2005.
30. *SAINT, Data Reduction Software*; Bruker AXS: Madison, WI, 1999.
31. G.M. Sheldrick, *SADABS v.2.01*, Bruker AXS: Madison, WI, 2006.
32. G.M. Sheldrick, *Acta Cryst. A*, 2008, **64A**, 112.
33. A. L. Spek, *Acta Cryst.*, 2015, **C71**, 9

5 Reactivity of a Palladacyclic Complex: A Monodentate Carbonate Complex and the Remarkable Selectivity and Mechanism of a Neophyl Rearrangement

(A. Behnia, M. A. Fard, J. M. Blacquiere and R. J. Puddephatt, *Organometallics.*, 2017, **36**, 4759-4769.)

5.1 Introduction

Catalytic oxidation of organic compounds using plentiful and environmentally benign oxidants, such as H₂O₂ and O₂, is highly desirable.¹⁻¹³ A major ongoing challenge in this field is to improve oxidation selectivity and this is driving many fundamental studies into the reactivity and mechanism of key oxidation steps.¹⁻¹⁶ Specifically, organopalladium(II) complexes with hard nitrogen-donor ligands oxidize with H₂O₂ to give reactive palladium(IV) intermediates that can undergo reductive elimination with C-O bond formation.¹⁴⁻¹⁶ For example, complex **2-2**, with the bulky MesN=CC=NMe₂ (**2-L1**) ligand, reacts with hydrogen peroxide to give the product of oxygen-atom insertion, **2-5**, probably by an oxidative addition-reductive elimination sequence, whereas complex **5-A**, with a potentially tridentate triazacyclononane ligand, gives a stable palladium(IV) complex **5-B** (Scheme 5-1).¹⁴⁻¹⁶ In related organoplatinum chemistry, ligands with pendent hydroxyl groups enhance reactivity towards oxidation by H₂O₂ or O₂. Thus, the dimethylplatinum(II) complexes **5-C** and **5-E** are oxidized by hydrogen peroxide and dioxygen, respectively, to give **5-D** and **5-F** (Scheme 5-1).¹⁷⁻¹⁸ The proton coupled electron transfer reactions, which are possible with ligands of the type shown in Scheme 5-1, have general significance in several areas of chemistry.¹⁹⁻²²

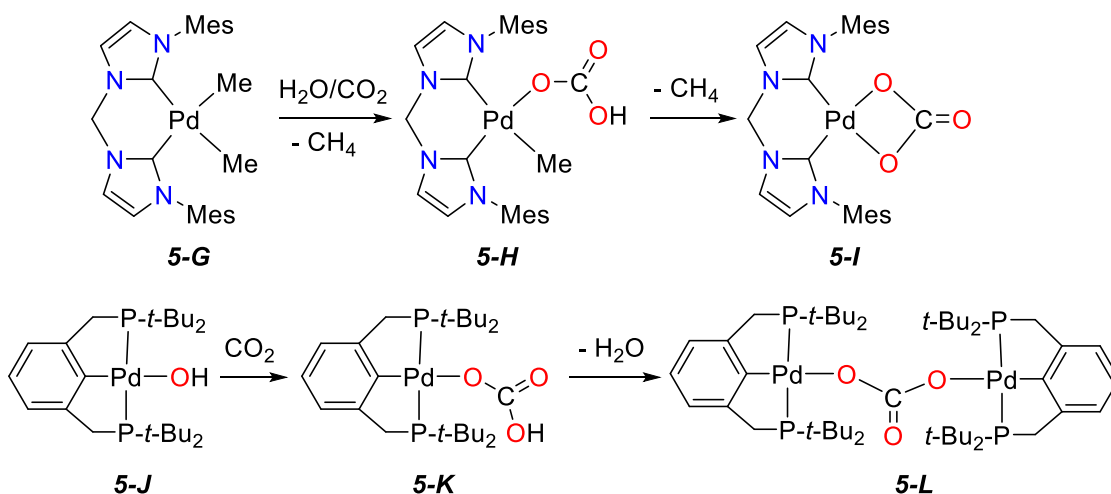


Scheme 5-1 Diverse oxidation reactivity achieved with a simple diimine ligand (**2-2**, **2-5**), a ligand with pendent nitrogen donor group (**5-A**, **5-B**), and ligands with a pendent alcohol or phenol group (**5-C**, **5-D**, **5-E** and **5-F**).

The ‘cycloneophyl’, $\text{CH}_2\text{CMe}_2\text{C}_6\text{H}_4$, group (**2-2**, **2-5**, **5-A** and **5-B** Scheme 5-1) has proven to be particularly valuable in studies of reactivity and selectivity in organopalladium chemistry.^{14-16,23-29} The group is ideally suited to assess selectivity as it contains both $\text{Pd-C}(\text{sp}^3)$ and $\text{Pd-C}(\text{sp}^2)$ bonds, and the $\text{C}(\text{Me})_2$ group prevents any complicating β -hydride elimination pathways. In order to further increase the reactivity of palladium(II) complexes towards oxidation by dioxygen or hydrogen peroxide, we have studied the cycloneophylpalladium(II) complex with the ligand $\text{HO}(\text{CH}_2)_3\text{N}(\text{CH}_2\text{-2-py})_2$, **5-L1**, py = pyridyl.³⁰ The ligand is expected to bind to give $[\text{Pd}(\text{CH}_2\text{CMe}_2\text{C}_6\text{H}_4)(\kappa^2\text{-N,N}'\text{-5-L1})]$, **5-1**, in which **5-L1** binds through the amine and one pyridyl group, leaving one free pyridyl group to act in an

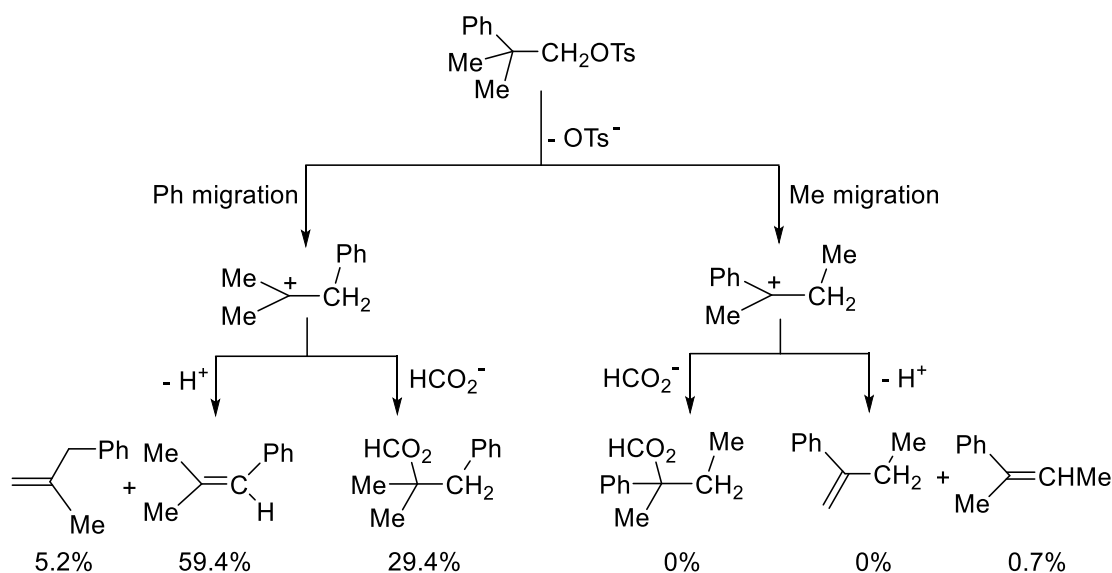
analogous way as the free nitrogen donor in **5-A** and a free hydroxyl group to act in an analogous way as those in **5-C** and **5-E** (Scheme 5-1). Efforts to isolate palladium(IV) complexes are ongoing, but this paper reports two unexpected and interesting observations. The first is that complex **5-1** can fix carbon dioxide from the air to give the first example of a monodentate carbonate complex of palladium(II), $[\text{Pd}(\kappa^1\text{-CO}_3)(\kappa^3\text{-N,N',N''-5-L1})]$, and the second is that the reaction involves a unique type of the “neophyl rearrangement.” Some background information to place these observations in context is given below.

The fixation of CO_2 from the air and conversion to useful organic products are considerable challenges and the subjects of much current research.³¹⁻³⁶ One approach is to trap CO_2 by complexes of catalytically active metals, often to give carbonate or carboxylate derivatives, followed by conversion to organic derivatives. In this context, several carbonate and bicarbonate complexes of palladium(II) are known and they can often be prepared by reactions involving $\text{CO}_2/\text{H}_2\text{O}$ or carbonic acid.³⁷⁻⁴⁷ For example, **5-H** (Scheme 5-2) can be prepared from the corresponding dimethylpalladium(II) complex, **5-G**, by protonolysis with $\text{CO}_2/\text{H}_2\text{O}$ and can then undergo further loss of methane to give the bidentate carbonate complex **5-I**.³⁷ The hydroxopalladium(II) complex **5-J** reacts with CO_2 to give the monodentate bicarbonate complex **5-K**, which can eliminate water to give the binuclear bridging carbonate complex **5-L**.³⁸⁻⁴⁰ However, to the best of our knowledge, no monodentate carbonate complexes of palladium have been reported.



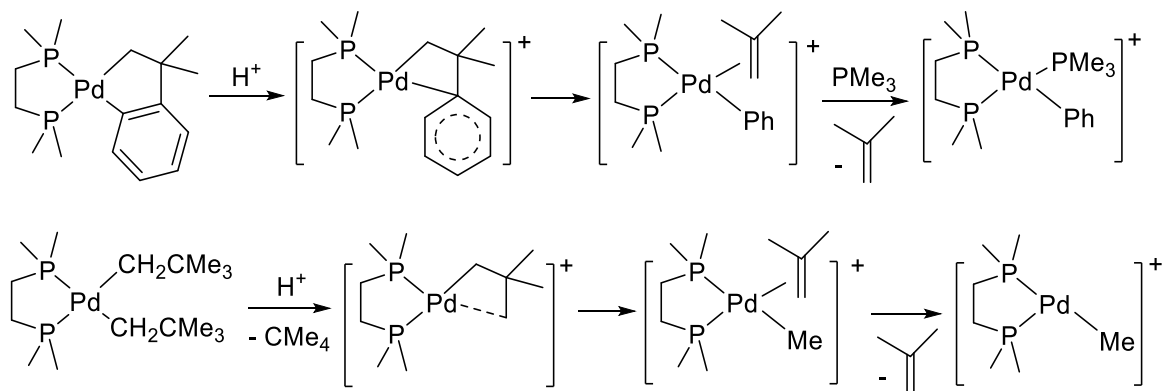
Scheme 5-2 Some known carbonate and bicarbonate complexes of palladium(II).

The neophyl rearrangement can be observed in reactions involving either free radical or carbocation intermediates. In free radical reactions there is often a competition between hydrogen abstraction by the primary radical $\text{PhCMe}_2\text{CH}_2^\bullet$ to give *t*-butylbenzene or rearrangement by phenyl group migration to give $\text{PhCH}_2\text{CMe}_2^\bullet$, followed by disproportionation or dimerization of this rearranged radical.⁴⁸⁻⁵³ No products that would arise from the radical $\text{MeCH}_2\text{CMePh}^\bullet$, which would be formed by methyl group migration in the primary neophyl radical, were observed in this or subsequent studies.⁴⁸⁻⁵³ Similarly, in neophyl cations or incipient cations formed in solvolysis reactions, phenyl migration always occurs to a greater extent than methyl migration.⁵⁴⁻⁵⁶ For example, formolysis of neophyl tosylate occurred only 0.7% by methyl migration (Scheme 5-3).⁵⁵ Mechanisms involving radical or cationic intermediates can be distinguished by the characteristic product mixtures formed.⁴⁸⁻⁵⁶



Scheme 5-3 The neophyl carbocation rearrangement.

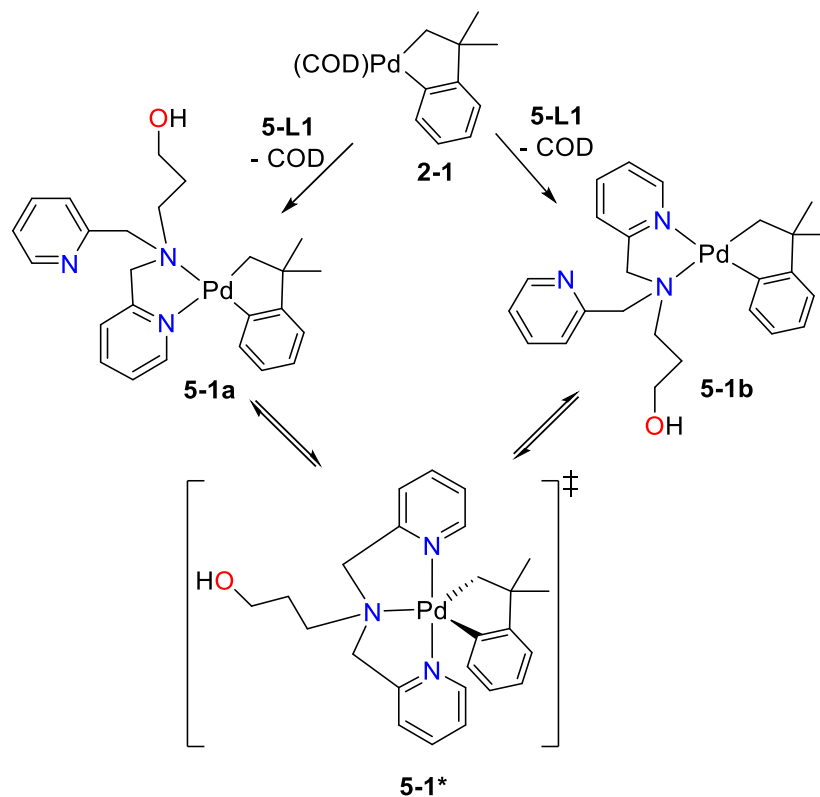
Selective phenyl migration also occurs in the β -carbon elimination from a cationic neophylpalladium(II) complex,⁵⁷ though methyl migration can occur in neopentyl complexes, as determined by mass spectrometry (Scheme 5-4).⁵⁸⁻⁵⁹ In contrast to all of the above examples, the reactions reported in this paper give organic products that are formed mostly by methyl migration in the neophyl rearrangement, and the mechanistic basis for this unique selectivity will be discussed.



Scheme 5-4 β -Phenyl or β -methyl elimination reactions at palladium(II).

5.2 Result and Discussion

The complex $[\text{Pd}(\text{CH}_2\text{CMe}_2\text{C}_6\text{H}_4)(\kappa^2\text{-}N,N'\text{-}\mathbf{5}\text{-L1})]$, **5-1**, was prepared by ligand exchange from the corresponding 1,5-cyclooctadiene complex $[\text{Pd}(\text{CH}_2\text{CMe}_2\text{C}_6\text{H}_4)(\text{COD})]$ ^{14-16,23-29}, **2-1**, and the known ligand *N,N*-bis(pyrid-2-ylmethyl)-*N*-(3-hydroxypropyl)amine, **5-L1** (Scheme 5-5).³⁰ Complex **5-1** was thermally stable under dinitrogen atmosphere and it was fully characterized by ¹H and ¹³C NMR spectroscopy, including correlated ¹H–¹H COSY, ¹H–¹H NOESY, and ¹H–¹³C HSQC and HMBC NMR spectroscopy at both room temperature and -30°C, and also by mass spectrometry and IR spectroscopy. The IR spectra of the free ligand **5-L1** and complex **5-1** show peaks due to $\nu(\text{OH})$ centred at 3304 and 3285 cm^{-1} , respectively. The MALDI-MS of **5-1** gave a parent ion peak at $m/z = 495.9$, that matches well with the simulated m/z value and isotope pattern for $[\mathbf{5}\text{-1}+\text{H}]^+$.



Scheme 5-5 Synthesis of complex **5-1**, and the proposed mechanism of interconversion of isomers **5-1a** and **5-1b** by way of **5-1***.

It should be noted that complex **5-1** is asymmetric and so there are two potential isomers **5-1a** and **5-1b** with the CH₂Pd group *trans* to the pyridine or amine donor, respectively. However, at room temperature, the ¹H NMR spectrum of **5-1** in (CD₃)₂CO solution gave only singlet resonances for the CH₂ and CMe₂ groups of the organic CH₂CMe₂C₆H₄ ligand, while four resonances for the C₆H₄ group were observed (Figure 5-1). Only a single set of broad resonances was observed for the two pyridylmethyl groups of the coordinated ligand **5-L1**, suggesting that the complex might exhibit fluxionality, and this was confirmed by the NMR spectra at lower temperatures. At -30°C, each broad pyridyl resonance had split into two equal resonances. Additionally, the broad CH₂N resonance that integrates to four protons (for H7a and H7b) had split into four overlapping doublets in the region δ 4.1-4.4 (Figure 5-1). Similarly, the CMe₂ resonance of the organic ligand had split into two equal resonances, while the CH₂ resonance did not give resolved separate peaks. Following precedents on the mechanisms of substitution at palladium(II),⁶⁰⁻⁶¹ it is likely that the exchange between free and coordinated pyridyl groups occurs by way of square pyramidal and trigonal bipyramidal intermediates, and the trigonal bipyramidal intermediate **5-1*** (which contains an effective plane of symmetry) is able

to collapse to **5-1a** or **5-1b** by dissociation of one of the two pyridyl groups (Scheme 5-5). The activation energy for fluxionality is estimated, using the Eyring equation, as $\Delta G^\ddagger = 58 \text{ kJ mol}^{-1}$ at 297 K.⁶²

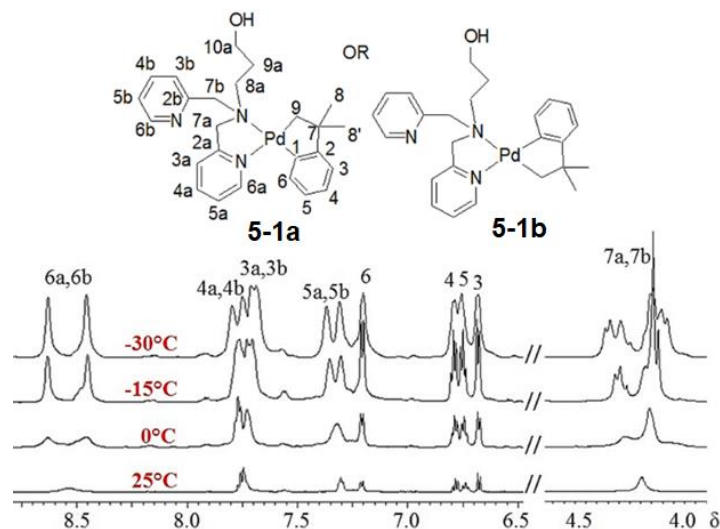
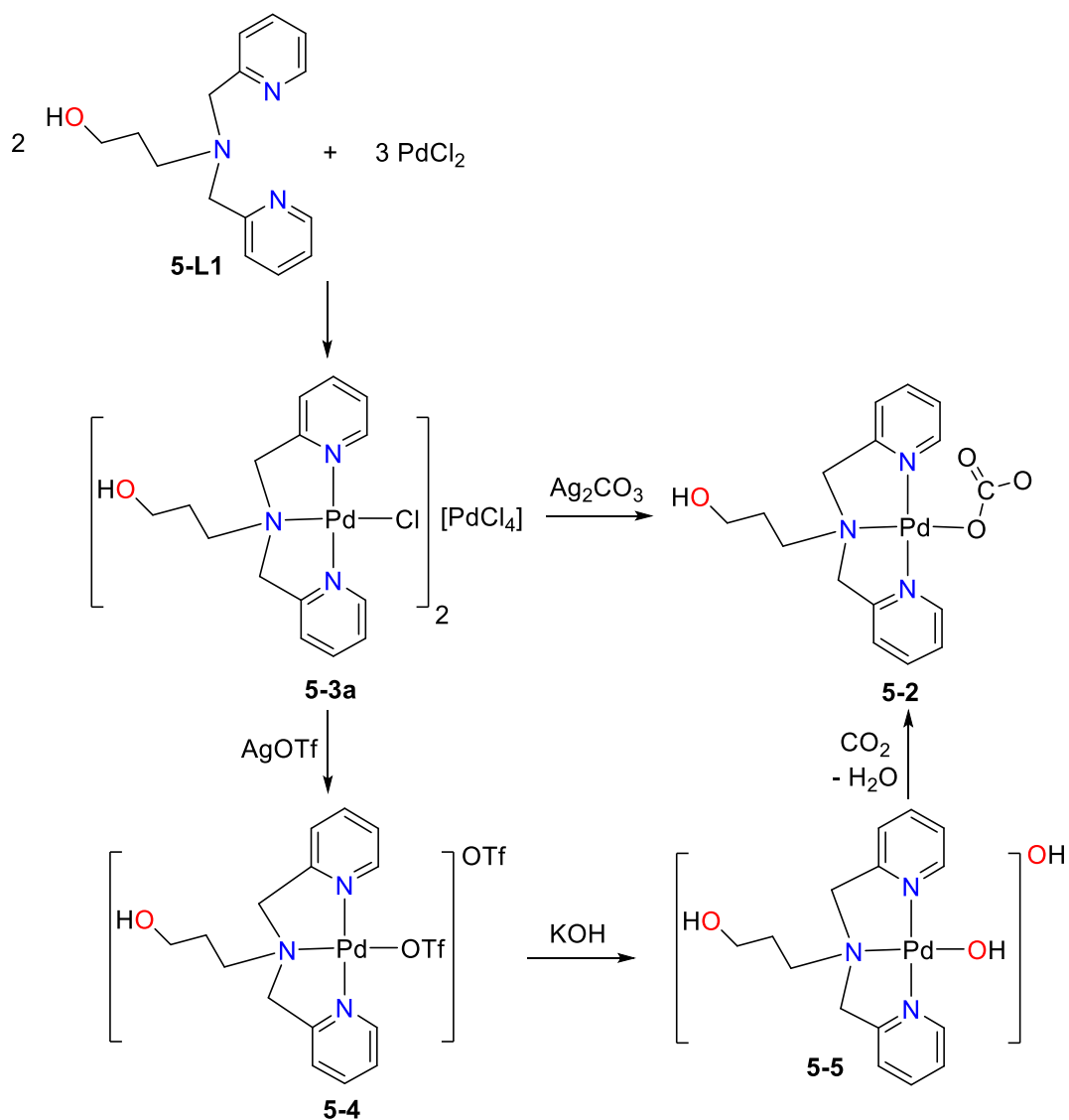


Figure 5-1 ^1H NMR spectra (600 MHz, acetone- d_6 solution) of complex **5-1** at different temperatures.

In solution, complex **5-1** exists largely as one isomer, though minor peaks in the low temperature NMR spectra might be due to a minor isomer. A ^1H - ^1H NOESY experiment was carried out at -30°C , to check for the close interligand contacts expected between H^{6a} and H^6 for isomer **5-1a** or H^{6a} and H^9 for isomer **5-1b**. However, no interligand correlations were observed, perhaps as a result of the fluxionality, so it is uncertain if the major isomer is **5-1a** or **5-1b**.

All attempts to crystallize **5-1** (dry solvent, inert atmosphere, various solvents and temperatures) were unsuccessful. However, in one attempt, a solution of complex **5-1** in tetrahydrofuran, which had not been dried or distilled, was allowed to evaporate slowly in air, and gave good crystals of a compound which was structurally characterized as the carbonate complex $[\text{Pd}(\kappa^1\text{-O-CO}_3)(\kappa^3\text{-N,N',N''-5-L1})]$, **5-2**, in the hydrated form $[\text{Pd}(\kappa^1\text{-O-CO}_3)(\kappa^3\text{-N,N',N''-5-L1})] \cdot 6\text{H}_2\text{O}$, **5-2a**. There were enough single crystals to obtain a ^1H NMR spectrum of complex **5-2**, which was soluble in D_2O . The NMR spectrum was consistent with the observed structure, in which both pyridyl groups are coordinated and the complex has approximate C_s symmetry. However, there was insufficient material to allow full characterization and the mechanism by which the organic $\text{CH}_2\text{CMe}_2\text{C}_6\text{H}_4$ ligand was replaced by carbonate was obscure, so further research was clearly necessary. In the first step, the independent synthesis of complex **5-2** was carried out, as illustrated in Scheme 5-6. The reaction of ligand **5-L1** with palladium(II) chloride

gave the cationic chloropalladium(II) complex $[\text{PdCl}(\kappa^3\text{-}N,N',N''\text{-}5\text{-L1})]^+$, **5-3**, which was isolated as the tetrachloropalladate(II) salt $[\text{PdCl}(\kappa^3\text{-}N,N',N''\text{-}5\text{-L1})][\text{PdCl}_4]$, **5-3a**. The chloride salt $[\text{PdCl}(\kappa^3\text{-}N,N',N''\text{-}5\text{-L1})]\text{Cl}$, **5-3b**, was prepared later. Complex **5-3a** reacted with excess silver carbonate to give complex **5-2** in good yield. Alternatively, complex **5-3a** reacted with silver triflate to give the triflate complex **5-4**, which reacted with potassium hydroxide to give the hydroxopalladium(II) complex **5-5**, which could then undergo further reaction with carbon dioxide to give **5-2**. This last synthesis is analogous to the route used to make other bicarbonate or carbonate complexes of palladium(II), Scheme 5-2,³⁷⁻⁴⁷ and provides a potential step in which CO_2 from air could give complex **5-2**.



Scheme 5-6 Two independent syntheses of the palladium(II) carbonate complex **5-2**.

Complexes **5-2** (both **5-2a** and a different crystalline form $[\text{Pd}(\kappa^1\text{-O-CO}_3)(\kappa^3\text{-N,N',N''-5-L1})\cdot 5\text{H}_2\text{O}\cdot \text{MeOH}$, **5-2b**) and **5-3b** were characterized by structure determination and all complexes **5-2**, **5-3**, **5-4** and **5-5** were characterized spectroscopically. The ^1H and ^{13}C NMR spectra were consistent with the complexes having C_s symmetry, with equivalent 2-pyridylmethyl groups, for which each CH^aH^b group appeared as an AB multiplet in the ^1H NMR spectra. The ^{13}C NMR spectrum of complex **5-2** contained a resonance at $\delta = 166$ for the carbonate carbon atom, just outside the range $\delta = 159\text{-}164$ reported for η^2 -carbonate or η^1 -bicarbonate complexes of palladium(II).³⁷⁻⁴⁷ The infrared spectrum of complex **5-2** contained a strong band at 1316 cm^{-1} , assigned to $\nu(\text{CO})$ of the η^1 -carbonate ligand, at considerably lower energy than the range of $1655\text{-}1700\text{ cm}^{-1}$ found for η^2 -carbonate complexes,^{37-47,63} or $1600\text{-}1650\text{ cm}^{-1}$ found for η^1 -bicarbonate complexes,³⁷⁻⁴⁰ indicating that this could be a useful criterion to distinguish between these bonding modes. In the MALDI-MS of **5-2**, using an anthracene matrix containing KCl to aid ionization, the most abundant ion was observed at m/z 462.8, corresponding to $[\mathbf{5-2}+\text{K}]^+$ (Figure 5-2).

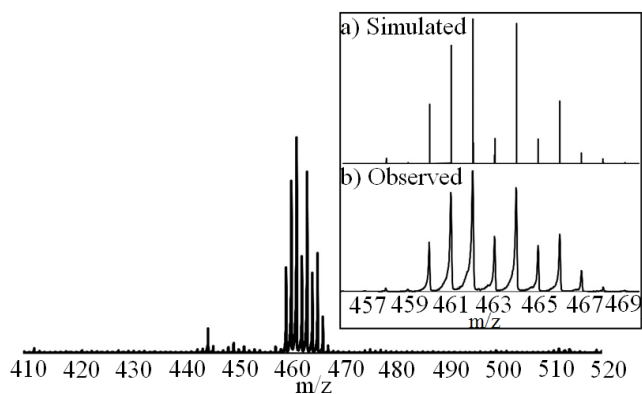


Figure 5-2 Isotope patterns for $[\mathbf{5-2}+\text{K}]^+$: (a) simulated and (b) observed by MALDI MS using anthracene as the matrix.

The structure of complex **5-3b** is shown in Figure 5-3, and confirms that **5-L1** acts as a tridentate ligand binding through the three nitrogen donors, to give a square planar cationic palladium(II) complex. The bond length Pd-N(2) for the amine donor is slightly longer than those to the pyridine donors, and the distances are unexceptional.⁶⁴⁻⁶⁹ The hydroxyl group is not coordinated but is hydrogen bonded to both the chloride anion and a water molecule in **5-3b**. Complex **5-3b** forms an interesting supramolecular polymeric structure formed by hydrogen bonding between the CH_2OH group, chloride anion and two water molecules, as illustrated in Figure A5.40.

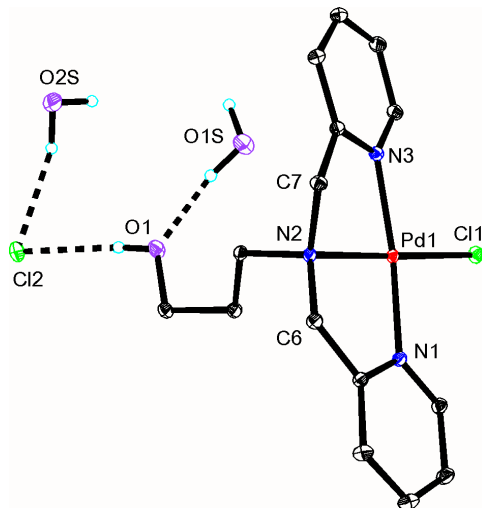


Figure 5-3 The structure of complex **5-3b**, showing 30% probability ellipsoids. Selected bond distances (Å): Pd(1)N(1) 2.0170(8); Pd(1)N(2) 2.0254(8); Pd(1)N(3) 2.0107(8); Pd(1)Cl(1) 2.3024(6).

The molecular structures of complex **5-2** in the solvates **5-2a** and **5-2b** are shown in Figure 5-4. The ligand is bound in a similar way as in complex **5-3**, and all contain slightly distorted square planar palladium(II) centers, with Houser's parameter $\tau_4 = 0.10$, 0.09 and 0.13 in **5-2a**, **5-2b** and **5-3** respectively.⁷⁰ The carbonate ligand is oriented roughly perpendicular to the square plane of the palladium(II) center and *syn* to the 3-hydroxypropyl group in each case. The carbonate is clearly monodentate and, to the best of our knowledge, this is the first example of a palladium complex containing a carbonate ligand bound in this form. The key to its formation is likely to be the use of a neutral pincer ligand that both prevents carbonate chelation and gives a neutral complex. With monodentate or bidentate co-ligands, bidentate carbonate is usually preferred (**5-I**, Scheme 5-2) while, with anionic pincer ligands, the monodentate bicarbonate or bridging carbonate (**5-K**, **5-L**, Scheme 5-2) is preferred.³⁷⁻⁴⁷ The main difference between the molecular structures of **5-2a** and **5-2b** is in the conformation of the 3-hydroxypropyl substituents, and this is attributed to different hydrogen bonding in the two solvates.

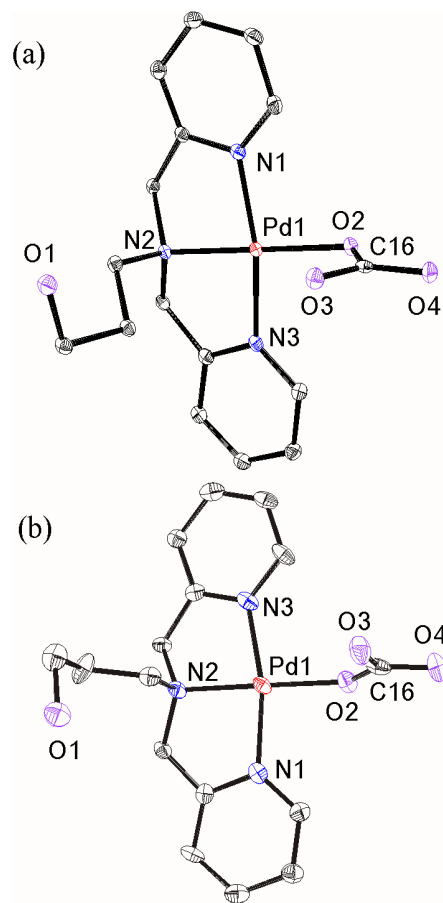


Figure 5-4 The molecular structures of complexes (a) **5-2a** and (b) **5-2b**, showing 30% probability ellipsoids. Selected bond distances (Å) and angles (deg) for **5-2a**, Pd(1)N(1) 2.003(9); Pd(1)N(2) 2.007(8); Pd(1)N(3) 2.007(9); Pd(1)O(2) 2.012(7); C(16)O(2) 1.221(13); C(16)O(4) 1.352(13); C(16)O(3) 1.258(12); N(1)Pd(1)N(2) 84.27(3); N(2)Pd(1)N(3) 82.99(3); N(3)Pd(1)O(2) 97.06(3); O(2)Pd(1)N(1) 95.52(3); and for **5-2b**, Pd(1)N(1) 2.006(2); Pd(1)N(2) 2.017(2); Pd(1)N(3) 2.015(2); Pd(1)O(2) 2.020(2); C(16)O(2) 1.325(3); C(16)O(4) 1.285(3); C(16)O(3) 1.256(3); N(1)Pd(1)N(2) 83.46(9); N(2)Pd(1)N(3) 84.00(9); N(3)Pd(1)O(2) 96.49(8); O(2)Pd(1)N(1) 96.10(8).

Both complexes **5-2a** and **5-2b** give complex three-dimensional network structures by hydrogen bonding involving the carbonate ligands, the 3-hydroxypropyl groups and water molecules. Figure 5-5 shows a small part of these networks in which dimer units can be identified. In complex **5-2a** there is direct pairwise intermolecular H-bonding between the carbonate and alcohol groups, with $O(1)\cdots O(4A) = O(1A)\cdots O(4) = 2.67$ Å, while pairs of water molecules also bridge between carbonate ligands, with $O(3)\cdots O(5) = O(3A)\cdots O(5A) = 2.71$ Å and $O(3)\cdots O(5a) = O(3a)\cdots O(5) = 2.80$ Å. In complex **5-2b**, a

water molecule, O(2W), bridges between each carbonate and alcohol group, with $O(1)\cdots O(2WA) = O(1A)\cdots O(2W) = 2.74 \text{ \AA}$ and $O(3)\cdots O(2W) = O(3a)\cdots O(2WA) = 2.70 \text{ \AA}$.

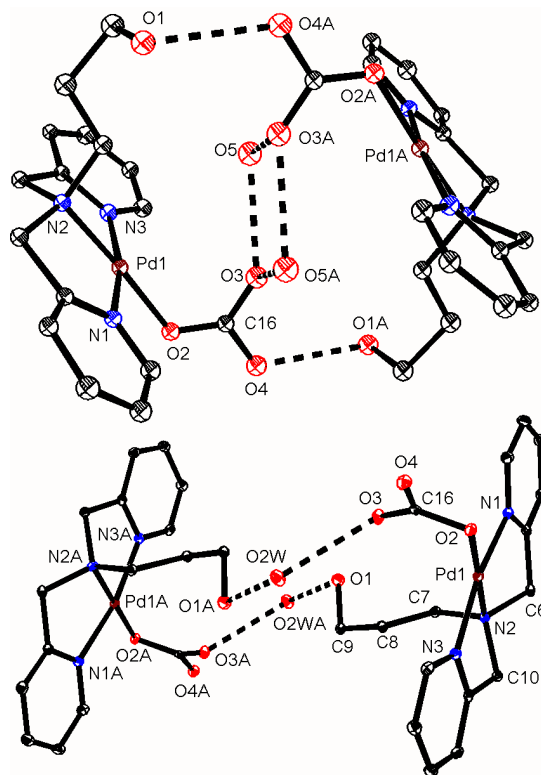
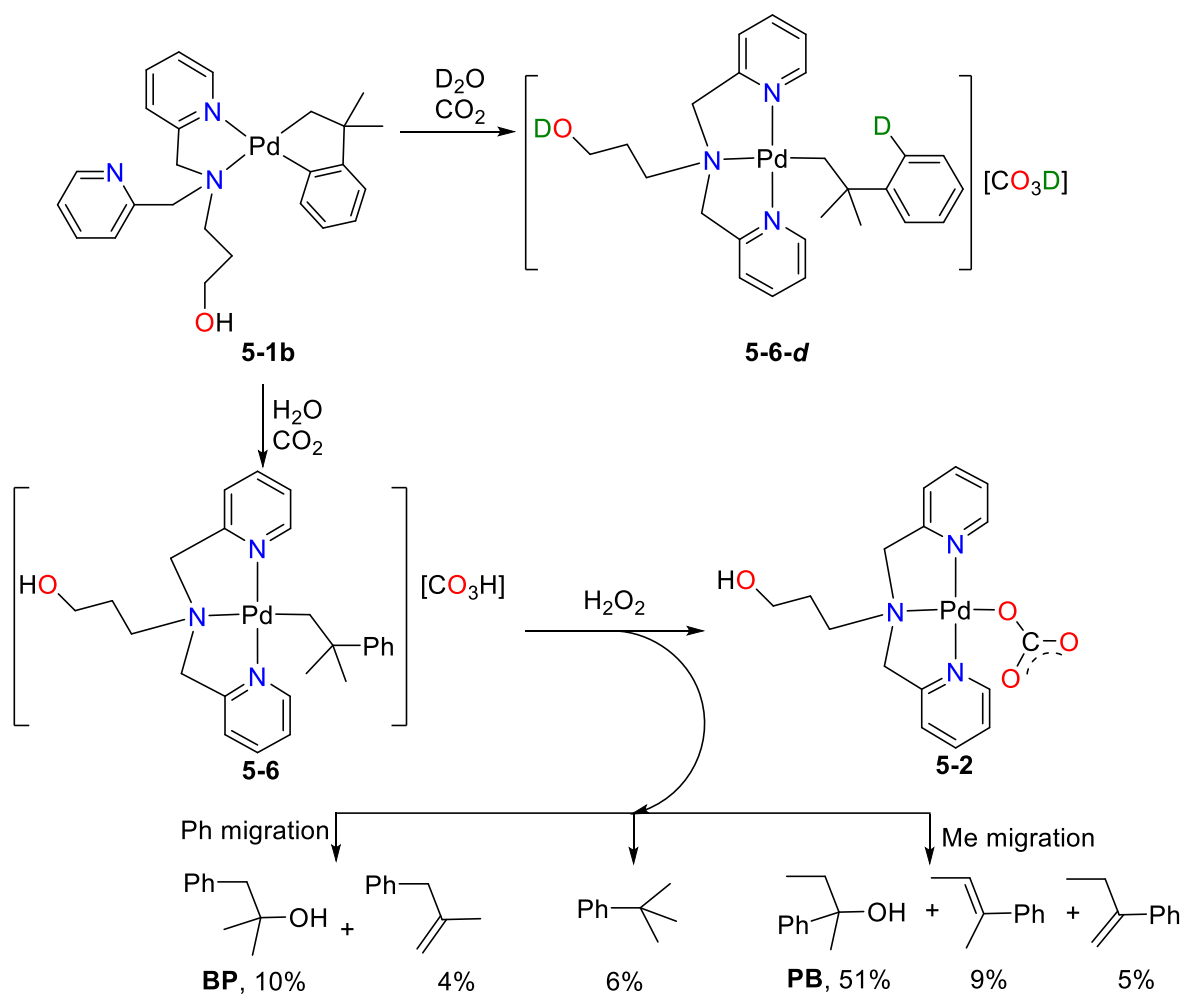


Figure 5-5 The structures of dimer units of (above) complex **5-2a** and (below) complex **5-2b** formed by hydrogen bonding, showing 25% thermal ellipsoids.

Having proved the structure of the unusual carbonate complex **5-2**, the remaining challenge was to determine how it was formed from complex **5-1**. It seemed possible that this could involve reaction of **5-1** with some combination of water, dioxygen and carbon dioxide. No reaction occurred when a solution of complex **5-1** in dry tetrahydrofuran was stirred under CO_2 , O_2 or a combination of the two. However, a reaction did occur when a solution of **5-1** in wet tetrahydrofuran was stirred under an atmosphere of CO_2 to give the cationic neophylpalladium(II) complex **5-6** as the bicarbonate salt (Scheme 5-7). The ^1H NMR spectrum of **5-6** showed the resonances expected for the ligand in κ^3 - N,N',N'' -**5-L1** bonding mode, similar to those for complexes **5-2**, **5-3**, **5-4** and **5-5** and also peaks typical for the neophylpalladium group.^{14-16,23-39} In particular, the phenyl group gave three resonances in a 2:2:1 intensity ratio for the *o*-, *m*- and *p*-H atoms. When the similar reaction was carried out in D_2O , the corresponding complex **5-6-d** was formed (Scheme 5-7), in which the phenyl group contained one deuterium atom in the ortho position, as shown by the ^1H and ^2H NMR spectra (Figure 5-6). In particular, the *ortho* resonance in the ^1H NMR integrated as a single proton, and the ^2H NMR showed

the presence of an *ortho*-D atom. In the infrared spectrum of complex **5-6**, a strong band was observed at $\nu(\text{CO}) = 1611 \text{ cm}^{-1}$, which is in the range for the bicarbonate ion ($1610\text{-}1655 \text{ cm}^{-1}$).⁶³ The formation of **5-6** from **5-1** involves selective protonolysis of the aryl-palladium bond by carbonic acid,²³⁻³⁹ but further protonolysis of the Pd-neophyl group from **5-6** did not occur under these conditions. An attempt to recrystallize complex **5-6** from chloroform led to decomposition to give chloro complex **5-3b** (Figure 5-3). The reaction of **5-6** with DCl in D₂O solution also gave complex **5-3b** along with PhCMe₂CH₂D. Finally, it was hypothesized that peroxide impurity in the tetrahydrofuran solvent might have been involved in the original synthesis of complex **5-2**, and so a reaction of complex **5-6** in aqueous solution with hydrogen peroxide was carried out. This reaction did indeed give complex **5-2** in good yield.



Scheme 5-7 The conversion of complex **5-1** to **5-2** by way of complex **5-6**, and the distribution of organic products.

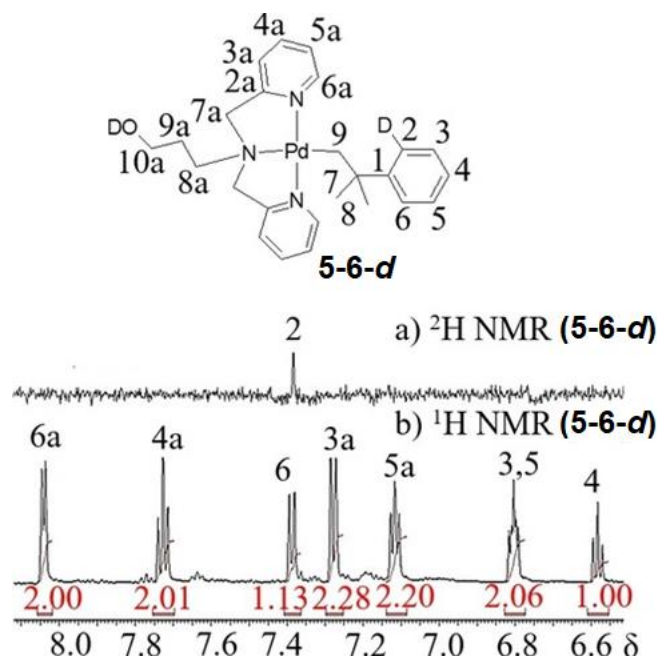
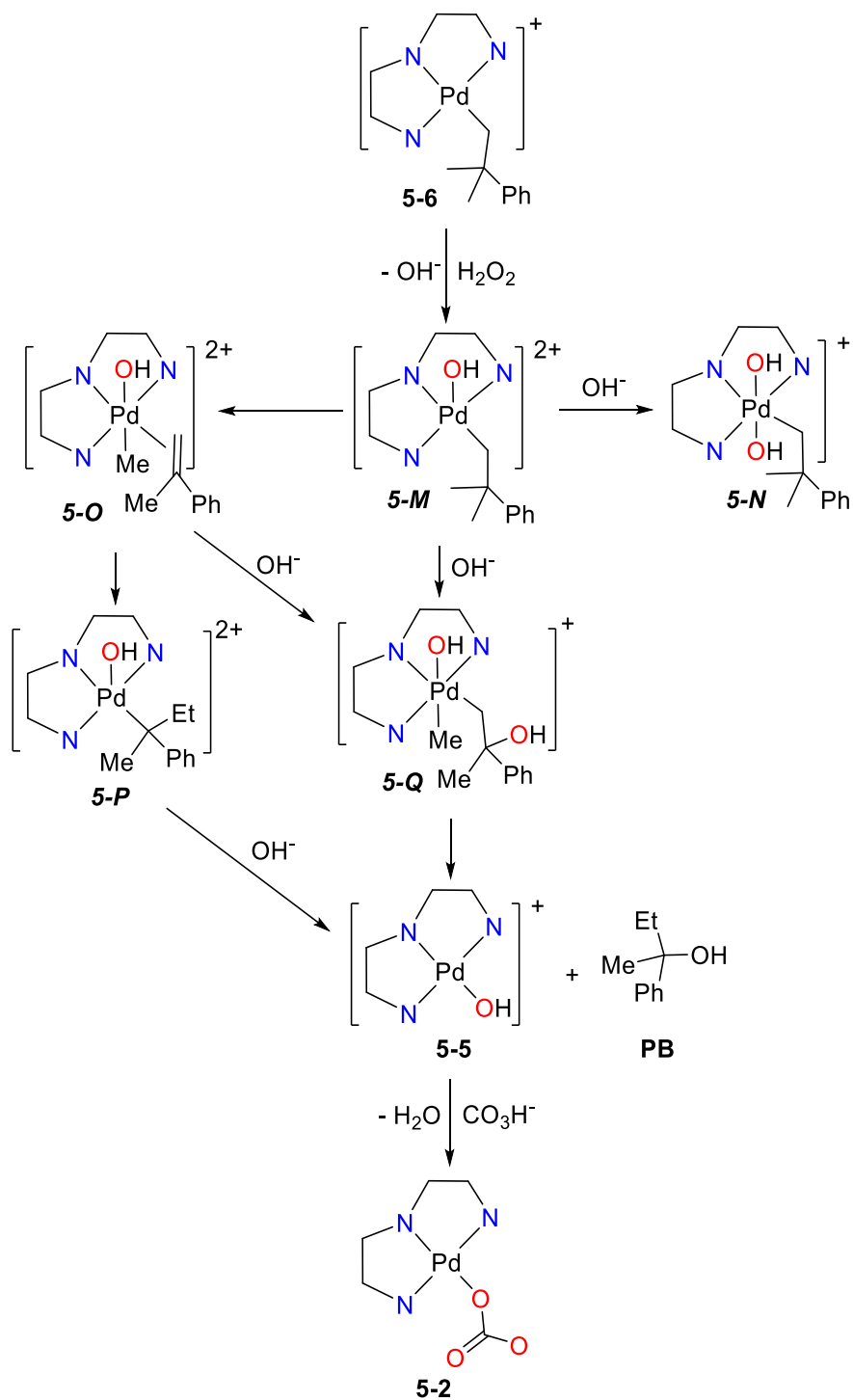


Figure 5-6 NMR spectra of complex **5-6-d** in D_2O solution: a) ^2H NMR spectrum and b) ^1H NMR spectrum.

The complex mixture of organic products from the reaction of complex **5-6** in D_2O solution with H_2O_2 was analyzed after extraction into CDCl_3 by a combination of GC-MS and ^1H NMR spectroscopy.⁷¹⁻⁷⁶ The major organic products were identified as PhMeEtCOH (2-phenyl-2-butanol, **PB**, 51%), *trans*-PhMeC=CHMe (*trans*-2-phenyl-2-butene, 9%) and PhEtC=CH₂ (2-phenyl-1-butene, 5%), which are products expected for hydrolysis of a neophyl cation after methyl group migration (compare Schemes 5-3 and 5-7),⁵⁴⁻⁵⁶ PhCH₂CMe₂OH (2-benzyl-2-propanol, **BP**, 10%) and PhCH₂MeC=CH₂ (2-benzyl-1-propene, 4%), which are products expected for hydrolysis of a neophyl cation after phenyl group migration (Schemes 5-3, 5-7),⁵⁴⁻⁵⁶ and *t*-BuPh (*t*-butylbenzene, 6%), which is the product expected from protonolysis of the neophyl group from **5-6** without rearrangement. Together, these products account for 85% of the neophyl groups originally present in the reagent **5-6**. No neophyl dimers were detected, which would be expected if neophyl radical intermediates were involved.⁴⁸⁻⁵³ Also absent was the alcohol PhMe₂CCH₂OH, which would be formed by hydrolysis of the neophyl cation without rearrangement. Although the nature of the products is as expected for a neophyl cation intermediate, the selectivity is dramatically different. Thus, the reaction of Scheme 5-3, with neophyl rearrangement, occurs with <1% methyl migration and >99% phenyl migration, but the present reaction occurs with 65% methyl migration and only 14% phenyl migration. A mechanism involving either a free neophyl carbocation or radical intermediate can therefore be eliminated based on the observed organic product

distribution.⁴⁸⁻⁵⁶ The rearrangement is therefore proposed to occur within the coordination sphere of the palladium center, probably after oxidation of complex **5-6** by hydrogen peroxide.

Two possible routes to the major products **5-2** and PhMeEtCOH, **PB**, are shown in Scheme 5-8, both involving β -methyl elimination as a key step. Hydrogen peroxide often gives *trans* oxidative addition by a polar mechanism.^{1-13,17-18,77-78} In reaction with complex **5-6** this would give the dicationic hydroxopalladium(IV) intermediate **5-M**,^{1-13,17-18} and then the octahedral palladium(IV) complex **5-N**. However, if hydroxide coordination to give **5-N** does not occur, β -methyl elimination from **5-M** might occur to give the alkene complex **5-O**,⁵⁷⁻⁵⁹ which could undergo alkene insertion in the opposite sense to give the PhMeEtCPd(IV) intermediate **5-P**. Reductive elimination with C-OH bond formation could then give the organic product **PB** and complex **5-5**, which would be expected to react easily with the bicarbonate anion to give the observed product **5-2**. There are several difficulties with this mechanism. Alkene complexes of palladium(IV) are unknown, and the dicationic complex **5-O** is likely to be at high energy. Isomerization of primary alkyl complex **5-M** to tertiary alkyl complex **5-P** is also likely to be unfavorable. Finally, reductive elimination with alkyl C-O bond formation usually occurs by external nucleophilic attack at carbon, and this will be difficult with a bulky tertiary alkyl group, as in **5-P**.^{19-22,79-84} Perhaps more likely is that the β -methyl elimination occurs in concert with hydroxide addition to give **5-Q**, and that **5-Q** undergoes reductive elimination with C-C bond formation to give **5-5** and **PB** (Scheme 5-8). The minor alcohol product PhCH₂CMe₂OH, 2-benzyl-2-propanol, **BP**, would be formed by an analogous sequence of reactions if the first intermediate **5-M** underwent β -phenyl instead of β -methyl elimination. The challenge is to understand why β -methyl elimination is dominant, when the closest precedent from palladium(II) chemistry would predict selective β -phenyl elimination (Scheme 5-4).^{19-22,79-84}



Scheme 5-8 Possible mechanisms of reaction of **5-6** with H_2O_2 (the ligand **5-L1** is drawn as *NNN* for simplicity) to give **5-2**. The favored mechanism involves concerted β -Me elimination and nucleophilic OH^- attack followed by C-C reductive elimination ($\text{5-M} \rightarrow \text{5-Q} \rightarrow \text{5-5}$). The disfavored mechanism involves β -Me elimination, alkene insertion and C-O reductive elimination ($\text{5-M} \rightarrow \text{5-O} \rightarrow \text{5-P} \rightarrow \text{5-5}$).

5.2.1 Computational Studies

Several problems in the above study could not be solved experimentally, so DFT calculations (BP functional, scalar correction for relativity) were carried out to provide additional insight. The calculated structures for complexes **5-1a** and **5-1b** are shown in Figure 5-7. Complex **5-1b** is calculated to be more stable than **5-1a** by 7 kJ mol^{-1} , so it is tentatively assigned as the dominant isomer of complex **5-1** (Scheme 5-5).

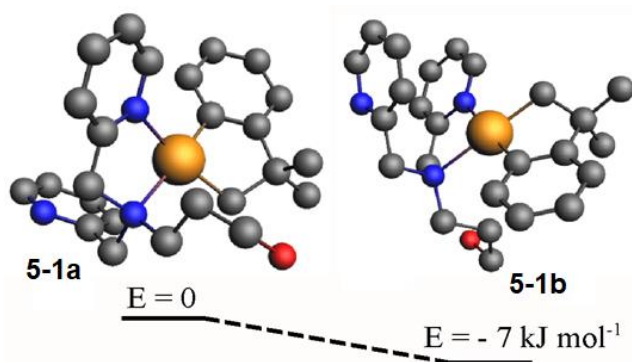


Figure 5-7 The calculated structures and relative energies of isomers **5-1a** and **5-1b**.

The modelling of the potential oxidative addition of hydrogen peroxide to complex **5-6** is shown in Figure 5-8. Complex **5-M** contains PdOH, CH₂OH and OH⁻ groups but the structure is predicted to have hydrogen bonding involving all of them.⁸⁵ As expected, the octahedral palladium(IV) complex **5-N**, which is predicted to have hydrogen bonding between the CH₂OH and adjacent PdOH group, is calculated to be most stable, though it was not observed. One feature that may be particularly significant is that the predicted conformation of the neophyl group in **5-6** and **5-M** has π -stacking between the phenyl group and one of the 2-pyridyl groups with one methyl group oriented towards the palladium center. In order to form the potential product **5-N**, the neophyl group has to reorient in order to allow access of the hydroxide ion to palladium (Figure 5-8).

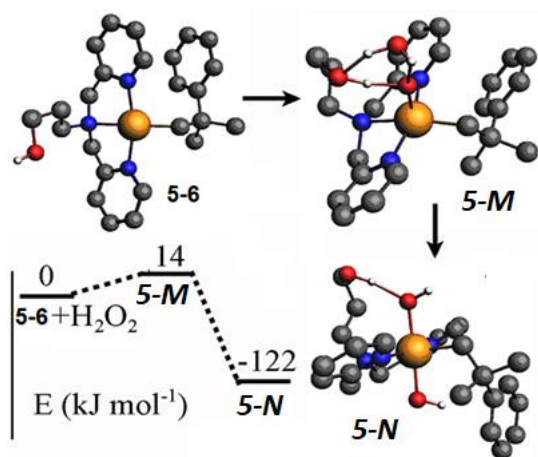


Figure 5-8 The calculated structures and relative energies of **5-6**, **5-M** and **5-N**.

We have attempted to model the potential intermediates and products arising from the unique neophyl rearrangement (Scheme 5-8). No minimum could be found for the potential alkene intermediate $[\text{Pd}(\text{OH})\text{Me}(\text{CH}_2=\text{CMePh})\mathbf{5-L1}]^{2+}\text{OH}^-$, **5-O**, or the analogous product of β -phenyl elimination, $[\text{Pd}(\text{OH})\text{Ph}(\text{CH}_2=\text{CMe}_2)\mathbf{5-L1}]^{2+}\text{OH}^-$, **5-O***. The best structures found resembled carbocations containing the $\text{Pd-CH}_2\text{-CMePh}^+$ or $\text{Pd-CH}_2\text{-CMe}_2^+$ units in **5-O** and **5-O***, respectively, and were at high energy. Consistent with the arguments above, the potential route involving β -methyl elimination and alkene insertion to give intermediates **5-O** and **5-P** is considered to be improbable. Figure 5-9 shows the calculated structures of the potential intermediates $[\text{Pd}(\text{OH})\text{Me}(\text{CH}_2\text{-CMePhOH})\mathbf{5-L1}]^+$, **5-Q**, and the analogous product of β -phenyl elimination, $[\text{Pd}(\text{OH})\text{Ph}(\text{CH}_2\text{-CMe}_2\text{OH})\mathbf{5-L1}]^+$, **5-Q***, for the alternative mechanism involving concerted β -carbon elimination/hydroxide addition. The formation of **5-Q** or **5-Q*** and subsequent reductive elimination with C-C bond formation (probably after a ligand dissociation step)^{14-16,86-90} to form the alcohol **PB** (Scheme 5-8) or **BP** are favorable, so this route is considered likely. However, these limited calculations do not explain the observed selectivity since the product of phenyl migration **5-Q*** is calculated to be more stable than that of methyl migration **5-Q**, and so the usual dominance of phenyl migration in neophyl rearrangements or β -carbon elimination, based on the better bridging ability of the phenyl group, might be predicted.⁵⁴⁻⁵⁷ A possible explanation is that the initial oxidation step to give **5-M**, in which a methyl group is oriented close to palladium (Figure 5-9), is rate determining and that methyl group migration occurs somewhat faster than the rotation about the neophyl-palladium bond that is needed to orient the phenyl group close to the vacant site, as required for phenyl group migration. Rotation of the neophyl group will be slowed by steric effects and also electronic effects, since the phenyl/pyridine π -stacking attraction will be lost on

rotation. We know of no precedents for β -elimination at palladium(IV) but there are examples of remote methyl group migration to platinum(IV) from methylboron or methylsilicon groups, often initiated by nucleophilic attack by hydroxide at boron or silicon.^{59,79-84}

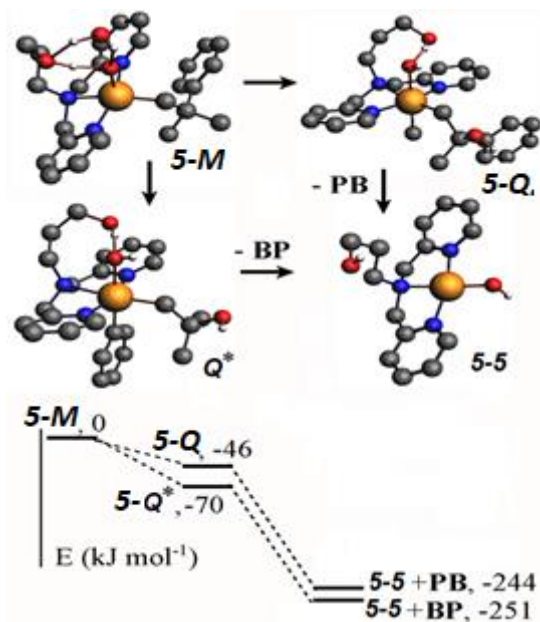


Figure 5-9 The predicted structures and relative energies of complexes **5-M**, **5-Q**, **5-Q*** and **5-5**.

The observed structures of complex **5-2** exhibit complex hydrogen bonding motifs (Figure 5-5). The complex is formulated as a neutral carbonate complex, in which the carbonate group is hydrogen bonded to water and, in **5-2a**, to the alcohol substituent. The hydrogen atoms were not refined in the structure determinations, and calculations on some model compounds were carried out to probe the nature of these hydrogen bonding interactions. In the three cases studied (Figure 5-10), an unsymmetrical hydrogen bond O-H \cdots O is predicted with the longer distance to the carbonate oxygen atom. This is the expected pattern given the relative base strengths of RO⁻, OH⁻ and CO₃²⁻, and supports the proposed formulation of complex **5-2** as the first monodentate carbonate complex of palladium(II).

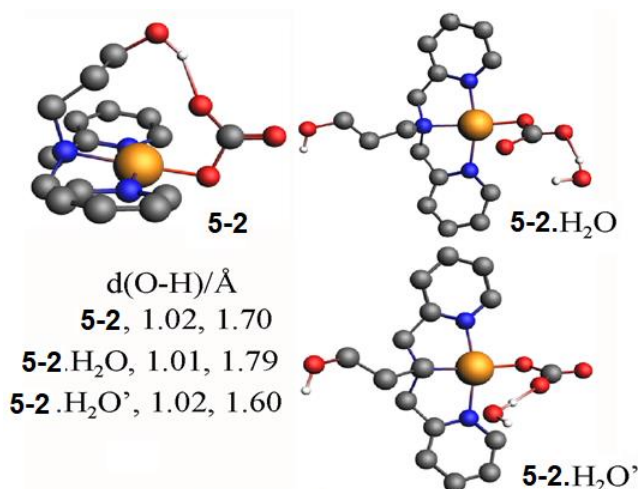


Figure 5-10 Calculated hydrogen bonded structures for complex **5-2**. In the O-H···O units, the shorter OH distance is to the oxygen of water or alcohol, and the longer distance is to the oxygen of carbonate.

5.3 Conclusions

A palladium(II) complex **5-2** containing a monodentate carbonate ligand was first prepared serendipitously, by fixation of carbon dioxide from air during an attempt to recrystallize a new fluxional “cycloneophyl” complex **5-1**.¹⁻²² The reaction is shown to occur in two steps. The first involves protonolysis by H₂O/CO₂ of the arylpalladium bond of **5-1** to give a cationic neophylpalladium complex with a bicarbonate anion. The second step involves oxidation of this complex by peroxide (perhaps present in the original synthesis as an impurity in the tetrahydrofuran solvent). This oxidation step is followed rapidly by formation of complex **5-2** with release of a mixture of organic products, the major one being 2-phenyl-2-butanol, **PB**. The formation of **PB** involves a neophyl rearrangement with the unprecedented preference for methyl over phenyl migration. A possible mechanistic basis for this unexpected reaction is proposed, involving β-carbon elimination at a palladium(IV) center.

5.4 Experimental

5.4.1 Reagents and General Procedures

Reactions were carried out in air, unless otherwise specified. For those reactions that were conducted under a nitrogen atmosphere, standard Schlenk or glove box techniques were used. All solvents used for air- and moisture-sensitive reactions were purified using an Innovative Technologies 400-5 Solvent Purification System (SPS) and were stored over activated 4 Å molecular sieves. NMR spectra were

recorded at 298 K using a Varian 600 MHz spectrometer (^{13}C at 150.7 MHz). ^1H and ^{13}C chemical shifts are reported relative to TMS. Complete assignments were aided by the use of ^1H - ^1H gCOSY, ^1H - ^1H NOESY, ^1H - $^{13}\text{C}\{^1\text{H}\}$ HSQC, and ^1H - $^{13}\text{C}\{^1\text{H}\}$ HMBC experiments and are reported using the labeling scheme in Figures 5-1 and 5-6 and in the SI. For ^2H NMR experiments, ^2H chemical shifts were referenced externally to the ^2H peak of D_2O ($\delta(^2\text{H}) = 4.63$ ppm). Aqueous 30% H_2O_2 was degassed by bubbling N_2 through for 10 minutes. The complexes $[\text{PdCl}_2(\text{COD})]$, $[\text{Pd}(\text{CH}_2\text{CMe}_2\text{C}_6\text{H}_4)(\text{COD})]$, **2-1**, and the ligand, *N,N*-bis(pyrid-2-ylmethyl)-*N*-(2-hydroxyethyl)amine, **5-L1**, were synthesized according to the literature procedures.^{14-16,23-30} NMR for **5-L1**: ^1H NMR (CDCl_3 , 600 MHz, 25°C) δ : 8.55 (d, 2H, $^3J(\text{H5H6}) = 5$ Hz, *H6*), 7.63 (t, 2H, $^3J(\text{H3H4}) = ^3J(\text{H4H5}) = 8$ Hz, *H4*), 7.40 (d, 2H, $^3J(\text{H3H4}) = 8$ Hz, *H3*), 7.16 (dd, 2H, $^3J(\text{H4H5}) = 8$ Hz, 5 Hz, *H5*), 3.81 (s, 4H, *CH}_2\text{N}*), 3.73 (t, 2H, $^3J(\text{HH}) = 6$ Hz, *CH}_2\text{O}*), 2.76 (t, 2H, $^3J(\text{HH}) = 6$ Hz, *CH}_2\text{N}*), 1.79 (quin, 2H, $^3J(\text{HH}) = 6$ Hz, *CH}_2*). The chemical shifts reported for **5-L1** in ref. 30 are correct but many of the coupling constants are not. Elemental analyses were performed by Laboratoire d'Analyse Élémentaire de l'Université de Montréal and Canadian Microanalytical Service Ltd. MALDI-TOF mass spectra were collected using an AB Sciex 5800 TOF/TOF mass spectrometer using pyrene or anthracene as the matrix in a 20:1 matrix:substrate molar ratio. Organic products were analyzed using a Shimadzu GCMS-QP2010 Ultra GC with a DB-5 column. Infrared spectra were collected by using a PerkinElmer UATR TWO FTIR spectrometer.

5.4.2 Synthesis of $[\text{Pd}(\text{CH}_2\text{CMe}_2\text{C}_6\text{H}_4)(\kappa^2\text{-N,N'-5-L1})]$, **5-1**

Under N_2 , a solution of *N,N*-bis(pyrid-2-ylmethyl)-*N*-(2-hydroxypropyl)amine, **5-L1**, (0.148 g, 0.577 mmol) in dry THF (15 mL) was added to a stirred solution of $[\text{Pd}(\text{CH}_2\text{CMe}_2\text{C}_6\text{H}_4)(\text{COD})]$, **2-1**, (0.200 g, 0.577 mmol) in dry THF (50 mL) cooled to -65°C . The mixture was stirred and slowly warmed to room temperature over 4 h. Upon removal of the solvent under reduced pressure, a brown oil was formed which was washed with hexane (20 mL) and cold ether (10 mL). The oil was dried under vacuum, to give **5-1** (0.237 g, 0.477 mmol, 83%). ^1H NMR ($(\text{CD}_3)_2\text{CO}$, 600 MHz, 25°C) δ : 8.50 (br, 2H, *H6a,H6b*), 7.7-7.8 (m, 4H, *H3a,H3b,H4a,H4b*), 7.29 (m, 2H, *H5a,H5b*), 7.19 (m, 1H, *H6*), 6.78 (m, 1H, *H4*), 6.73 (m, 1H, *H5*), 6.67 (d, 1H, $^3J(\text{H3H4}) = 7$ Hz, *H3*), 4.18 (br, 4H, *H7a,H7b*), 3.53 (t, 2H, $^3J(\text{H8aH9a}) = 5$ Hz, *H8a*), 2.88 (t, 2H, $^3J(\text{H9aH10a}) = 8$ Hz, *H10a*), 2.31 (m, 2H, *H9a*), 2.02 (s, 2H, *H9*), 1.31 (s, 6H, *H8,H8'*); $^{13}\text{C}\{^1\text{H}\}$ NMR ($(\text{CD}_3)_2\text{CO}$, 151 MHz, 25°C) δ : 167.89 (C2), 159.62 (C1), 157.46 (C2a,C2b), 148.81 (C6a,C6b), 136.71 (C4a,C4b), 134.44 (C5), 124.87 (C3a,C3b), 123.31 (C6), 123.06 (C5a,C5b), 121.97 (C4), 121.10 (C3), 62.71 (C7a,C7b), 59.89 (C10a), 55.32 (C8a), 47.11

(C7), 43.59 (C9), 33.42 (C8,C8'), 30.70 (C9a). ^1H NMR ($(\text{CD}_3)_2\text{CO}$, 600 MHz, -20°C) δ : 8.64 (1H, *H6a* or *H6b*), 8.46 (1H, *H6a* or *H6b*), 7.78 (1H, *H4a* or *H4b*), 7.75 (1H, *H4a* or *H4b*), 7.67-7.66 (2H, *H3a* and *H3b*), 7.36 (1H, *H5a* or *H5b*), 7.31 (1H, *H5a* or *H5b*), 7.19 (1H, *H6*), 6.78 (1H, *H4*), 6.73 (1H, *H5*), 6.67 (1H, *H3*), 4.11-4.32 (4H, *H7a,H7a',H7b,H7b'*), 3.4-3.6 (2H, *H8a,H8a'*), 2.7-2.8 (2H, *H10a,H10a'*), 2.36 (1H, *H9a* or *H9a'*), 2.31 (1H, *H9a* or *H9a'*), 2.05 (1H, *H9* or *H9'*), 1.96 (1H, *H9* or *H9'*), 1.31 (3H, *H8* or *H8'*), 1.27 (3H, *H8* or *H8'*). MALDI MS (pyrene matrix): Calcd for $[\text{Pd}(\text{CH}_2\text{CMe}_2\text{C}_6\text{H}_4)(\kappa^2\text{-}N,N'\text{-}\mathbf{5-L1})]^{*+}$: m/z 495.9. Obsd: m/z 495.9. IR: $\nu(\text{O-H})$ 3285 cm^{-1} . Recrystallization from unpurified THF led to decomposition, with formation of crystals of **5-2a**, whose ^1H NMR spectrum was identical to that of **5-2**, reported below.

5.4.3 Synthesis of $[\text{Pd}(\text{CO}_3)(\kappa^3\text{-}N,N',N''\text{-}\mathbf{5-L1})]$, **5-2**

In a darkened flask, to an aqueous solution (3 mL) of **5-3** (0.040 mg, 0.038 mmol) was added silver carbonate (0.031 mg, 0.11 mmol) in water (4 mL) with stirring. After 17 h, the reaction mixture was centrifuged to separate silver chloride and palladium salt as precipitates. The solvent was evaporated from the resultant yellow solution under vacuum to give **5-2** as an air-stable, yellow solid (0.040 mg, 0.094 mmol, 83%). ^1H NMR (D_2O , 600 MHz, 25°C) δ : 8.17 (d, 2H, $^3J(\text{H5aH6a}) = 6$ Hz, *H6a*), 8.13 (dd, 2H, $^3J(\text{H5aH6a}) = 6$ Hz, $^3J(\text{H4aH5a}) = 7$ Hz, *H5a*), 7.63 (d, 2H, $^3J(\text{H3aH4a}) = 7$ Hz, *H3a*), 7.58 (t, 2H, $^3J(\text{H3aH4a}) = ^3J(\text{H4aH5a}) = 7$ Hz, *H4a*), 5.30 (d, 2H, $^2J(\text{H7aH7a}') = 16$ Hz, *H7a* or *H7a'*), 4.43 (d, 2H, $^2J(\text{H7aH7a}') = 16$ Hz, *H7a* or *H7a'*), 3.55 (m, 2H, *H10a*), 3.09 (m, 2H, *H8a*), 2.02 (m, 2H, *H9a*); $^{13}\text{C}\{^1\text{H}\}$ NMR (D_2O , 151 MHz, 25°C) δ : 166.85 (carbonate), 163.26 (C2a), 148.50 (C6a), 141.41 (C5a), 124.80 (C4a), 122.86 (C3a), 67.50 (C7a), 60.47 (C10a), 58.57 (C8a), 30.20 (C9a). MALDI MS (Anthracene matrix): Calcd for $[\text{Pd}(\text{CO}_3)\mathbf{5-L1} + \text{K}]^{*+}$: $m/z = 462.8$. Obsd: $m/z = 462.8$. IR $\nu(\text{O-H})$ 3341 cm^{-1} , $\nu(\text{C-O})$ 1316 cm^{-1} . Anal. Calcd for $\text{C}_{32}\text{H}_{40}\text{N}_6\text{O}_8\text{Pd}_2 \cdot 5\text{H}_2\text{O}$: C, 40.90; H, 5.36; N, 8.94. Found: C, 41.07; H, 5.07; N 8.92. Yellow crystals suitable for single-crystal X-ray crystallographic analysis were grown by the slow evaporation of an aqueous solution of **5-2** at room temperature.

5.4.4 Synthesis of $[\text{PdCl}(\kappa^3\text{-}N,N',N''\text{-}\mathbf{5-L1})]_2[\text{PdCl}_4]$, **5-3a**

To a stirred solution of $[\text{PdCl}_2(\text{COD})]$ (0.300 g, 1.05 mmol) in acetone (50 mL) was added an acetone solution (20 mL) of **5-L1** (0.180 g, 0.700 mmol). A brown precipitate was observed after 15 minutes. The mixture was stirred for 2 more hours. The precipitate was then collected by vacuum filtration and washed with acetone (3×5 mL) and dried under vacuum, to give **5-3** as an air-stable solid (0.322 g, 0.307 mmol, 88%). ^1H NMR (D_2O , 600 MHz, 25°C) δ : 8.72 (d, 2H, $^3J(\text{HH}) = 6$ Hz, *H6a*), 8.15 (dd, 2H,

$^3J(\text{HH}) = 6 \text{ Hz}$, 7 Hz , $H5a$), 7.69 (d, 2H, $^3J(\text{HH}) = 7 \text{ Hz}$, $H3a$), 7.57 (t, 2H, $^3J(\text{HH}) = 7 \text{ Hz}$, $H4a$), 5.42 (d, 2H, $^2J(\text{HH}) = 15 \text{ Hz}$, $H7a$ or $H7a'$), 4.52 (d, 2H, $^2J(\text{HH}) = 15 \text{ Hz}$, $H7a$ or $H7a'$), 3.52 (t, 2H, $^3J(\text{HH}) = 5 \text{ Hz}$, $H10a$), 3.17 (m, 2H, $H8a$), 1.92 (m, 2H, $H9a$); $^{13}\text{C}\{^1\text{H}\}$ NMR (CD_3OD , 151 MHz, 25°C) δ : 164.86 (C2a), 150.58 (C6a), 141.32 (C5a), 124.73 (C4a), 122.93 (C3a), 67.30 (C7a), 60.92 (C8a), 58.22 (C10a), 30.70 (C9a). HR ESI-TOF MS: Calcd for $[\text{C}_{15}\text{H}_{19}\text{ClN}_3\text{OPd}]^+$: $m/z = 398.0251$. Obsd $m/z = 398.0250$. IR: $\nu(\text{O-H}) 3380 \text{ cm}^{-1}$. Anal. Calcd for $\text{C}_{30}\text{H}_{38}\text{Cl}_6\text{N}_6\text{O}_2\text{Pd}_3$: C, 34.43; H, 3.66; N, 8.03. Found: C, 34.03; H, 3.70; N 7.79. Crystals by slow evaporation of a solution of **5-3** in methanol at room temperature and the connectivity was established (Figure A5.39) though disorder of the $[\text{PdCl}_4]^{2-}$ unit and associated water solvate molecules did not allow full refinement.

5.4.5 Synthesis of $[\text{Pd}(\text{OTf})(\kappa^3\text{-N,N',N''-5-L1})](\text{OTf})$, **5-4**

In a darkened flask, an aqueous solution (2 mL) of silver triflate (0.058 mg, 0.228 mmol) was added to a solution of **5-3** (0.040 mg, 0.038 mmol) in water (5 mL). The mixture was stirred for 20 min., then it was centrifuged to separate insoluble material. The solvent was evaporated under vacuum from the light brown solution to give **5-4** in 82% yield (0.083 mg, 0.062 mmol). ^1H NMR (D_2O , 600 MHz, 25°C) δ : 8.04 (m, 4H, $H5a, H6a$), 7.53 (d, 2H, $^3J(\text{HH}) = 8 \text{ Hz}$, $H3a$), 7.47 (t, 2H, $^3J(\text{HH}) = 8 \text{ Hz}$, $H4a$), 5.52 (d, 2H, $^3J(\text{HH}) = 15 \text{ Hz}$, $H7a$ or $H7a'$), 4.32 (d, 2H, $^3J(\text{HH}) = 15 \text{ Hz}$, $H7a$ or $H7a'$), 3.41 (t, $^3J(\text{HH}) = 6 \text{ Hz}$, 2H, $H10a$), 3.00 (m, 2H, $H8a$), 1.87 (m, 2H, $H9a$); $^{13}\text{C}\{^1\text{H}\}$ NMR (D_2O , 151 MHz, 25°C) δ : 163.13 (C2a), 148.70 (C5a), 142.18 (C6a), 124.96 (C4a), 123.07 (C3a), 118.49 (CF_3), 68.61 (C7a), 61.53 (C8a), 58.33 (C10a), 30.15 (C9a); ^{19}F NMR (D_2O , 564 MHz, 25°C) δ : -78.96. HR ESI-TOF MS: Calcd for $[\text{C}_{16}\text{H}_{19}\text{F}_3\text{N}_3\text{O}_4\text{PdS}]^+$: $m/z = 512.0083$. Obsd: $m/z = 512.0085$. IR: $\nu(\text{O-H}) 3303 \text{ cm}^{-1}$.

5.4.6 Synthesis of $[\text{Pd}(\text{OH})(\kappa^3\text{-N,N',N''-5-L1})](\text{OH})$, **5-5**

To a solution of **5-4** (0.05 mg, 0.037 mmol) in water (10 mL) was added an aqueous solution (3 mL) of KOH (0.008 mg, 0.151 mmol) whilst stirring. After 20 min., the reaction mixture was centrifuged. The light brown solution was dried under vacuum to give a brown powder in 85% yield (0.025 mg, 0.060 mmol). ^1H NMR (D_2O , 600 MHz, 25°C) δ : 8.13 (m, 2H, $H3a$), 8.00 (t, 2H, $^3J(\text{H4aH5a}) = ^3J(\text{H5aH6a}) = 7 \text{ Hz}$, $H5a$), 7.50 (d, 2H, $^3J(\text{H5aH6a}) = 7 \text{ Hz}$, $H6a$), 7.46 (m, 2H, $H4a$), 5.12 (m, 2H, $H7a$ or $H7a'$), 4.28 (m, 2H, $H7a$ or $H7a'$), 3.39 (t, $^3J(\text{H9aH10a}) = 6 \text{ Hz}$, 2H, $H10a$), 2.88 (m, 2H, $H8a$), 1.79 (m, 2H, $H9a$); $^{13}\text{C}\{^1\text{H}\}$ NMR (D_2O , 151 MHz, 25°C) δ : 163.48 (C2a), 148.51 (C3a), 141.56 (C5a), 124.59 (C4a), 124.80 (C6a), 67.35 (C7a), 60.14 (C8a), 58.50 (C10a), 30.20 (C9a). MALDI MS (Pyrene matrix): Calcd for $[\text{Pd5-L1}]^+$, $m/z 363.75$. Obsd, $m/z 363.75$. IR $\nu(\text{O-H}) 3533 \text{ cm}^{-1}$.

5.4.7 Synthesis of [Pd(CH₂CMe₂Ph)(κ³-N,N',N''-5-L1)][HCO₃], **5-6**

Under N₂, degassed water (1.90 mL) was added to a dry and degassed THF solution (3 mL) of complex **5-1** (0.055 g, 0.11 mmol). The solution was stirred under an atmosphere of carbon dioxide for 2 h., then the solvent was evaporated under vacuum to give **5-2** as a yellow powder (0.053 g, 0.096 mmol, 88%). ¹H NMR (D₂O, 600 MHz, 25°C) δ: 8.04 (d, 2H, ³J(H5aH6a) = 5 Hz, H6a), 7.73 (t, 2H, ³J(H3aH4a) = ³J(H4aH5a) = 8 Hz, H4a), 7.38 (d, 2H, ³J(HH) = 8 Hz, H2, H6), 7.27 (d, 2H, ³J(H3aH4a) = 8 Hz, H3a), 7.12 (dd, 2H, ³J(H5aH6a) = 5 Hz, ³J(H4aH5a) = 8 Hz, H5a), 6.80 (m, 2H, H3, H5), 6.58 (t, 1H, ³J(H3H4) = ³J(H4H5) = 7 Hz, H4), 4.52 (d, 2H, ²J(H7aH7a') = 15 Hz, H7a or H7a'), 4.02 (d, 2H, ²J(H7aH7a') = 15 Hz, H7a or H7a'), 3.15 (t, 2H, ³J(H9aH10a) = 6 Hz, H10a), 2.49 (m, 2H, H8a), 1.82 (s, 2H, H9), 1.29 (m, 2H, H9a), 1.19 (s, 6H, H8); ¹³C{¹H} NMR (D₂O, 151 MHz, 25°C) δ: 163.84 (C2a), 160.08 (bicarbonate), 151.11 (C1), 149.33 (C6a), 139.52 (C4a), 127.66 (C3, C5), 125.70 (C2, C6), 125.28 (C4), 124.12 (C5a), 123.22 (C3a), 63.71 (C7a), 58.88 (C10a), 54.62 (C8a), 48.91 (C9), 41.46 (C7), 29.92 (C8), 29.25 (C9a). HR ESI-TOF MS: Calcd for [Pd(CH₂CMe₂Ph)(κ³-N,N',N''-5-L1)]: m/z 496.1580. Obsd: m/z 496.1628. IR: ν(O-H) 3209 cm⁻¹, ν(C-O) 1606 cm⁻¹. Anal. Calcd for C₂₆H₃₃N₃O₄Pd: C, 55.97; H, 5.96; N, 7.53. Found: C, 55.62; H, 5.93; N, 7.03. For the sample used for the ²H NMR experiment, degassed water was replaced with degassed D₂O, while the rest of the reaction conditions were unchanged. NMR in H₂O: δ(²H) = 7.4 (br, D2). Attempted recrystallization of **5-6** from CHCl₃ gave crystals of [PdCl(κ³-N,N',N''-5-L1)]Cl·2H₂O, **5-3b**, identified by structure determination.

5.4.8 Reaction of Complex **5-6** with H₂O₂

H₂O₂ (0.137 mL, 30% aqueous solution, 15 eq) was added to a solution of complex **5-6** (0.055 g, 0.098 mmol) in D₂O (1.2 mL) while vigorously stirring. The solution was stirred for 3 min., then it was extracted with CDCl₃ (1.5 mL). The D₂O layer was shown to contain complex **5-2** (84%) by ¹H NMR spectroscopy. The organic layer was analyzed by GC-MS and by ¹H NMR, using 1,3,5-trimethoxybenzene as internal standard. The major product was identified as PhMeEtCOH, **PB**. Yield 51%. ¹H NMR (CDCl₃, 600 MHz, 25°C) δ: 7.43 (2H, H^o), 7.32 (2H, H^m), 7.25 (1H, H^p), 1.75-1.85 (m, 2H, MeCH^aH^b), 1.50 (s, 3H, CCH₃), 0.75 (t, 3H, J = 7 Hz, CH₂CH₃).⁷¹ MS: Calcd for C₁₀H₁₄O: m/z = 150.11. Found: m/z = 150.10. Other organic products were identified and analyzed similarly. All yields are an average of two runs. *trans*-**2-phenyl-2-butene** (9%); ¹H NMR (CDCl₃, 600 MHz, 25°C) δ: 7.41-7.20 (m, 5H, ArH); 5.90 (br, 1H, C=CH); 2.06 (br, 3H, Ar-C-CH₃); 1.82 (br, 3H, C=CCH₃).⁷² MS: Calcd for C₁₀H₁₂: m/z = 132.20. Found: m/z = 132.10. **2-phenyl-1-butene** (5%); ¹H NMR (CDCl₃, 600 MHz, 25°C) δ: 7.41 – 7.22 (m, 5H, ArH), 5.26 (br, 1H, =CH₂), 5.04 (br, 1H, =CH₂), 2.50 (q, 2H, CH₂),

1.09 (t, 3H, CH₃).⁷³ MS: Calcd for C₁₀H₁₂: m/z = 132.20. Found: m/z = 132.24. **2-benzyl-2-propanol** (10%); ¹H NMR (CDCl₃, 600 MHz, 25°C) δ: 7.45 – 7.03 (m, 5H, ArH), 2.74 (s, 2H, CH₂), 1.2 (s, 6H, CH₃).⁷⁴ MS: Calcd for C₁₀H₁₄O: m/z = 150.11. Found: m/z = 150.05. **2-benzyl-1-propene** (4%); ¹H NMR (CDCl₃, 600 MHz, 25°C) δ: 7.28-7.16 (m, 5H, ArH), 4.80 (s, 1H, =CHH), 4.72 (s, 1H, =CHH), 3.30 (s, 2H, CH₂), 1.66 (s, 3H, CH₃).⁷⁵ MS: Calcd for C₁₀H₁₂: m/z = 132.20. Found: m/z = 132.10. ***t*-butylbenzene** (6%); ¹H NMR (CDCl₃, 600 MHz, 25°C) δ: 7.01-7.46 (m, ArH), 1.31 (s, (CH₃)₃).⁷⁶ MS: Calcd for C₁₀H₁₄: m/z = 134.21. Found: m/z = 134.17. The *t*-butylbenzene-d₁ formed from **5-6** and DCl in D₂O gave MS: Calcd. for C₁₀H₁₃D: m/z = 135.12. Found: m/z = 135.10.

5.4.9 X-Ray Structure Determination⁹¹⁻⁹⁴

Data Collection and Processing. A crystal was mounted on a Mitegen polyimide micromount with a small amount of Paratone N oil. All X-ray measurements were made using a Bruker Kappa Axis Apex2 diffractometer at a temperature of 110 K. The frame integration was performed using SAINT, and the resulting raw data was scaled and absorption corrected using a multi-scan averaging of symmetry equivalent data using SADABS.

Structure Solution and Refinement. The structures were solved by using the SHELXT program. All non-hydrogen atoms were obtained from the initial solution. The hydrogen atoms were introduced at idealized positions and were allowed to ride on the parent atom. The structural model was fit to the data using full matrix least-squares based on F^2 . The calculated structure factors included corrections for anomalous dispersion from the usual tabulation. The structure was refined using the SHELXL-2014 program from the SHELX suite of crystallographic software.⁹¹⁻⁹⁴ Details are given in Table A5.1 and in the CIF files.

5.4.10 DFT Calculations

DFT calculations were carried out for gas phase structures by using the Amsterdam Density Functional program based on the BP functional, with double-zeta basis set and first-order scalar relativistic corrections.⁹⁵⁻⁹⁶ Minima were confirmed by vibrational analysis; transition states were not determined. Details are given in the Appendix section, A5.

5.5 References

1. T. Punniyamurthy, S. Velusamy and J. Iqbal, *Chem. Rev.*, 2005, **105**, 2329-2364.
2. Z. Shi, C. Zhang, C. Tang and N. Jiao, *Chem. Soc. Rev.*, 2012, **41**, 3381-3430.
3. S. S. Stahl, *Science.*, 2005, **309**, 1824-1826.

4. A. A. Shteinman, *J. Mol. Catal. A.*, 2017, **426**, 305-315.
5. N. J. Gunsalus, A. Koppaka, S. H. Park, S. M. Bischof, B. G. Hashiguchi and R. A. Periana, *Chem. Rev.*, 2017, **117**, 8521-8573.
6. W. Wu and H. Jiang, *Acc. Chem. Res.*, 2012, **45**, 1736-1748.
7. A. N. Campbell and S. S. Stahl, *Acc. Chem. Res.*, 2012, **45**, 851-863.
8. K. M. Gligorich and M. S. Sigman, *Chem. Commun.*, 2009, 3854-3867.
9. M. S. Sigman and D. R. Jensen, *Acc. Chem. Res.*, 2006, **39**, 221-229.
10. Y. -H. Zhang and J. -Q. Yu, *J. Am. Chem. Soc.*, 2009, **131**, 14654-14655.
11. J. Huang, J. Li, J. Zheng, W. Wu, W. Hu, L. Ouyang and H. Jiang, *Org. Lett.*, 2017, **19**, 3354-3357.
12. M. L. Scheuermann and K. I. Goldberg, *Chem. Eur. J.*, 2014, **20**, 14556-14568.
13. A. N. Vedernikov, *Acc. Chem. Res.*, 2012, **45**, 803-813.
14. J. R. Khusnutdinova, N. P. Rath and L. M. Mirica, *J. Am. Chem. Soc.*, 2012, **134**, 2414-2422.
15. F. Qu, J. R. Khusnutdinova, N. P. Rath and L. M. Mirica, *Chem. Commun.*, 2014, **50**, 3036-3039.
16. A. Behnia, P. D. Boyle, J. M. Blacquiere and R. J. Puddephatt, *Organometallics.*, 2016, **35**, 2645-2654.
17. K. A. Thompson, C. Kadwell, P. D. Boyle and R. J. Puddephatt, *J. Organomet. Chem.* 2017, **829**, 22-30.
18. M. E. Moustafa, P. D. Boyle and R. J. Puddephatt, *Chem. Commun.*, 2015, **51**, 10334-10336.
19. J. J. Warren, T. A. Tronic and J. M. Mayer, *Chem. Rev.* 2010, **110**, 6961-7001.
20. D. R. Weinberg, C. J. Gagliardi, J. F. Hull, C. F. Murphy, C. A. Kent, B. C. Westlake, A. Paul, D. H. Ess, D. G. McCafferty and T. J. Meyer, *Chem. Rev.*, 2012, **112**, 4016-4093.
21. S. Hammes-Schiffer, *J. Am. Chem. Soc.*, 2015, **137**, 8860-8871.
22. W. Lubitz, H. Ogata, O. Rudiger and E. Reijerse, *Chem. Rev.*, 2014, **114**, 4081-4148.
23. J. Cámpora, J. A. López, P. Palma, P. Valerga, E. Spillner and E. Carmona, *Angew. Chem. Int. Ed.*, 1999, **38**, 147-151.
24. J. Cámpora, P. Palma and E. Carmona, *Coord. Chem. Rev.*, 1999, **193-195**, 207-281.
25. J. Cámpora, P. Palma, D. del Río, E. Carmona, C. Graiff and A. Tiripicchio, *Organometallics.*, 2003, **22**, 3345-3347.
26. A. Behnia, P. D. Boyle, M. A. Fard, J. M. Blacquiere and R. J. Puddephatt, *Dalton Trans.*, 2016, **45**, 19485-19490.
27. I. M. Pendleton, M. H. Pérez-Temprano, M. S. Sanford and P. M. Zimmerman, *J. Am. Chem. Soc.*, 2016, **138**, 6049-6060.

28. M. H. Pérez-Temprano, J. M. Racowski, J. W. Kampf and M. S. Sanford, *J. Am. Chem. Soc.*, 2014, **136**, 4097-4100.
29. A. J. Canty, A. Ariaferd, N. M. Camasso, A. T. Higgs, B. F. Yates and M. S. Sanford, *Dalton Trans.*, 2017, **46**, 3742-3748.
30. K. Sundaravel, M. Sankaralingam, E. Suresh and M. Palaniandavar, *Dalton Trans.*, 2011, **40**, 8444-8458.
31. A. M. Appel, J. E. Bercaw, A. B. Bocarsly, H. Dobbek, D. L. DuBois, M. Dupuis, J. G. Ferry, E. Fujita, R. Hille, P. J. A. Kenis, C. A. Kerfeld, R. H. Morris, C. H. F. Pede, A. R. Portis, S. W. Ragsdale, T. B. Rauchfuss, J. N. H. Reek, L. C. Seefeldt, R. K. Thauer and G. L. Waldrop, *Chem. Rev.*, 2013, **113**, 6621-6658.
32. I. Omae, *Current Org. Chem.*, 2016, **20**, 953-962.
33. I. Omae, *Coord. Chem. Rev.*, 2012, **256**, 1384-1405.
34. D. Yu, S. P. Teong and Y. Zhang, *Coord. Chem. Rev.*, 2015, **293-294**, 279-291.
35. M. T. Johnson, O. F. Wendt, *J. Organomet. Chem.*, 2014, **751**, 213-220.
36. K. -C. Lau, B. J. Petro, S. Bontemps and R. F. Jordan, *Organometallics.*, 2013, **32**, 6895-6898.
37. P. W. G. Ariyananda, G. P. A. Yap and J. Rosenthal, *Dalton Trans.*, 2012, **41**, 7977-7983.
38. J. Pushkar and O. F. Wendt, *Inorg. Chim. Acta.*, 2004, **357**, 1295-1298.
39. R. Johansson and O. F. Wendt, *Organometallics.*, 2007, **26**, 2426-2430.
40. A. H. Mousa, A. Fleckhaus, M. Kondrashov and O. F. Wendt, *J. Organomet. Chem.*, 2017, **845**, 157-164.
41. G. R. Fulmer, W. Kaminsky, R. A. Kemp and K. I. Goldberg, *Organometallics.*, 2011, **30**, 1627-1636.
42. K. A. Smoll, W. Kaminsky and K. I. Goldberg, *Organometallics.*, 2017, **36**, 1213-1216.
43. D. Ortiz, M. Blug, X. -F. Le Goff, P. Le Floch, N. Mezailles and P. Maitre, *Organometallics.*, 2012, **31**, 5975-5978.
44. J. Ruiz, M. T. Martinez, F. Florenciano, V. Rodriguez, G. Lopez, J. Perez, P. A. Chaloner and P. B. Hitchcock, *Inorg. Chem.*, 2003, **42**, 3650-3661.
45. R. J. Crutchley, J. Powell, R. Faggiano and C.J. L. Lock, *Inorg. Chim. Acta.*, 1977, **24**, L15-L16.
46. F. Ozawa, T. Son, S. Ebina, K. Osakada and A. Yamamoto, *Organometallics.*, 1992, **11**, 171-176.
47. C. Amatore, S. Gamez, A. Jutand, G. Meyer, M. Moreno-Manas, L. Morral and R. Pleixats, *Chem. Eur. J.*, 2000, **6**, 3372-3376.
48. W. H. Urry and M. S. Kharasch, *J. Am. Chem. Soc.*, 1944, **66**, 1438-1440.

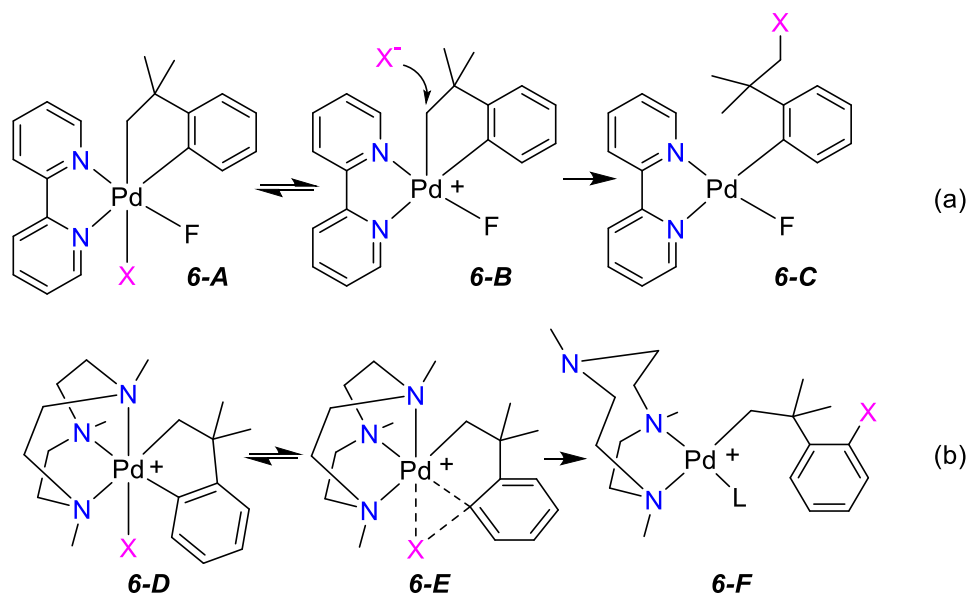
49. F. H. Seubold, *J. Am. Chem. Soc.*, 1953, **75**, 2532-2533.
50. J. W. Wilt and W. W. Pawlikowski, *J. Org. Chem.*, 1975, **40**, 3641-3644.
51. A. Burton, K. U. Ingold and J. C. Walton, *J. Org. Chem.*, 1996, **61**, 3778-3782.
52. M. Weber and H. Fischer, *J. Am. Chem. Soc.*, 1999, **121**, 7381-7388.
53. Z. -M. Chen, X. -M. Zhang and Y. -Q. Tu, *Chem. Soc. Rev.*, 2015, **44**, 5220-5245.
54. R. Heck and S. Winstein, *J. Am. Chem. Soc.*, 1957, **79**, 3432-3438.
55. W. H. Saunders and R. H. Paine, *J. Am. Chem. Soc.*, 1961, **83**, 882.
56. V. G. Shubin, *Top. Curr. Chem.*, 1984, **116**, 267-341.
57. J. Campora, E. Gutierrez-Puebla, J. A. Lopez, A. Monge, P. Palma, D. del Rio and E. Carmona, *Angew. Chem. Int. Ed.*, 2001, **40**, 3641.
58. A. R. Zhugralin, I. J. Koblyanskii and P. Chen, *Organometallics.*, 2015, **34**, 1301-1306.
59. M. E. O'Reilly, S. Dutta and A. S. Veige, *Chem. Rev.*, 2016, **116**, 8105-8145.
60. C. H. Langford and H. B. Gray, *Ligand Substitution Processes*, Benjamin, New York, 1965.
61. P. Banerjee, *Coord. Chem. Rev.* 1999, **190**, 19-28.
62. J. Sandstrom, *Dynamic NMR Spectroscopy*, Academic Press, London, 1982.
63. K. Nakamoto, *Infrared and Raman Spectra of Inorganic and Coordination Compounds*, 5th ed.; Wiley-Interscience: New York, 1997.
64. K. Seubert, D. Bohme, J. Kusters, W. -Z. Shen, E. Freisinger and J. Z. Muller, *Anorg. Allg. Chem.*, 2012, **638**, 1761-1767.
65. Z. Nagy, I. Fabian, A. Benyei and I. Sovago, *J. Inorg. Biochem.*, 2003, **94**, 291-299.
66. S. Kim, D. Kim, Y. Song, H. -J. Lee and H. Lee, *Aust. J. Chem.*, 2014, **67**, 953-961.
67. A. R. Petersen, A. J. P. White and G. J. P. Britovsek, *Dalton Trans.* 2016, **45**, 14520-14523.
68. A. McSkimming, V. Diachenko, R. London, K. Olrich, C. J. Onie, M. M. Bhadbhade, M. P. Bucknall, R. W. Read and S. B. Colbran, *Chem. Eur. J.*, 2014, **20**, 11445-11456.
69. P. Mandapati, P. K. Giesbrecht, R. L. Davis and D. E. Herbert, *Inorg. Chem.*, 2017, **56**, 3674-3685.
70. L. Yang, D. R. Powell and R. P. Houser, *Dalton Trans.*, 2007, 955-964.
71. J. E. Lynch and E. L. Eliel, *J. Am. Chem. Soc.*, 1984, **106**, 2943-2948.
72. S. Nave, R. P. Sonawane, T. G. Elford and V. K. Aggarwal, *J. Am. Chem. Soc.*, 2010, **132**, 17096-17098.
73. S. Movahhed, J. Westphal, M. Dindaroğlu, A. Falk and H. -G. Schmalz, *Chem. Eur. J.*, 2016, **22**, 7381-7384.

74. A. Fernández-Mateos, S. E. Madrazo, P. H. Teijón and R. R. González, *J. Org. Chem.*, 2009, **74**, 3913-3918.
75. E. Alacid and C. Nájera, *Org. Lett.*, 2008, **10**, 5011-5014.
76. J. Terao, M. Nakamura and N. Kambe, *Chem. Commun.*, 2009, 6011-6013.
77. K. Thorshaug, I. Fjeldahl, C. Romming and M. Tilset, *Dalton Trans.*, 2003, 4051-4056.
78. K. -T. Aye, J. J. Vittal and R. J. Puddephatt, *J. Chem. Soc. Dalton Trans.*, 1993, 1835-1839.
79. N. A. Smythe, K. A. Grice, B. S. Williams and K. I. Goldberg, *Organometallics.*, 2009, **28**, 277-288.
80. A. N. Desnoyer and J. A. Love, *Chem. Soc. Rev.*, 2017, **46**, 197-238.
81. A. V. Sberegaeva, P. Y. Zavalij and A. N. Vedernikov, *J. Am. Chem. Soc.*, 2016, **138**, 1446-1455.
82. S. Pal and A. N. Vedernikov, *Dalton Trans.*, 2012, **41**, 8116-8122.
83. M. Safa, M. C. Jennings and R. J. Puddephatt, *Organometallics.*, 2012, **31**, 3539-3550.
84. S. J. Mitton, R. McDonald and L. Turculet, *Polyhedron.*, 2013, **52**, 750-754.
85. The structures of **5-6**, **O** and **P** in the presence of aqueous hydrogen peroxide will certainly involve hydrogen bonding to solvent molecules, and the structures and relative energies shown in Figure 5-8 will consequently be modified. We do not claim that the 3-hydroxypropyl group plays a critical role in this reaction and preliminary results indicate that the chemistry is similar with the corresponding ligand having a 3-methoxypropyl substituent.
86. P. K. Byers, A. J. Canty, M. Crespo, R. J. Puddephatt and J. D. Scott, *Organometallics.*, 1988, **7**, 1363-1367.
87. J. Hyvl and J. Roithova, *Org. Lett.*, 2014, **16**, 200-203.
88. F. Z. Tang, Y. Zhang, N. P. Rath and L. M. Mirica, *Organometallics.*, 2012, **31**, 6690-6696.
89. L. -M. Xu, B. -J. Li, Z. Yang and Z. -J. Shi, *Chem. Soc. Rev.*, 2010, **39**, 712-733.
90. J. M. Racowski, A. R. Dick and M. S. Sanford, *J. Am. Chem. Soc.*, 2009, **131**, 10974-10983.
91. Bruker-AXS, SAINT version 2013.8, 2013, Bruker-AXS, Madison, WI 53711, USA.
92. Bruker-AXS, SADABS version 2012.1, **2012**, Bruker-AXS, Madison, WI 53711, USA.
93. G. M. Sheldrick, *Acta Cryst.*, 2015, **A71**, 3-8.
94. G. M. Sheldrick, *Acta Cryst.*, 2015, **C71**, 3-8.
95. G. Te Velde, F. M. Bickelhaupt, E. J. Baerends, S. van Gisbergen, C. F. Guerra, J. G. Snijders and T. Ziegler, *J. Comput. Chem.*, 2001, **22**, 931-967.
96. A. Becke, *Phys. Rev. A.*, 1988, **38**, 3098-3100.

6 Cycloneophylpalladium(IV) Complexes by Oxidative Addition of Bromine, Iodine and Methyl Iodide and their Reductive Elimination Reactions

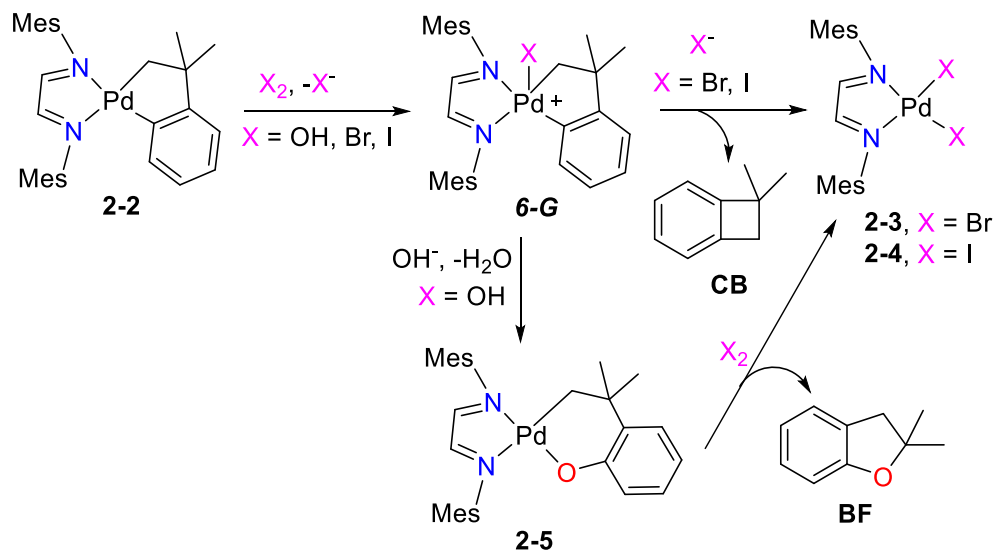
6.1 Introduction

It is now well established that Pd(II)/Pd(IV) cycles may be important in catalysis by palladium complexes, especially in reactions involving strong oxidants like halogens, dioxygen and peroxides.¹⁻² For example, the catalytic reaction of iodine with alkanes to form iodoalkanes is thought to involve alkane C-H bond activation to form an alkylpalladium(II) complex, followed by oxidative addition of iodine and then reductive elimination of the product iodoalkane.³⁻⁵ These impressive advances have stimulated further efforts to understand the factors that affect reactivity and selectivity in oxidative addition to palladium(II) and reductive elimination from palladium(IV) complexes.⁶⁻¹⁴ In studies of selectivity in reductive elimination, the cycloneophylpalladium(IV) complexes have played an important role.¹⁻²⁷ When the palladium(IV) complexes are sufficiently stable to be isolated, the mechanisms of reductive elimination have been studied and, in most cases, have been shown to involve 5-coordinate intermediates such as **6-B**. External nucleophilic attack on such intermediates occurs selectively at the CH₂ group and can lead, for example, to C-O or C-N bond formation (Scheme 6-1a).¹⁵⁻¹⁹ If the supporting ligand is tridentate, as in **6-D**, intramolecular reductive elimination from the 6-coordinate complex is proposed to give **6-F** (Scheme 6-1b).²⁰⁻²¹



Scheme 6-1 Reductive elimination from Pd(IV) (a) with CH₂-X bond formation (X = OR or NR₂); (b) with C₆H₄-X bond formation (X = OH, L = solvent dmsO)

With cycloneophylpalladium complexes, there have been few studies of oxidative addition-reductive elimination by reaction with bromine, iodine or methyl iodide. The complex **6-D** (X = I) may be formed by oxidative addition of iodine, but it is stable to reductive elimination.²⁰⁻²¹ On the other hand, the diimine complex, [Pd(CH₂CMe₂C₆H₄)(MesN=CHCH=NMe_s)], **2-2**, reacts with bromine or iodine to give [PdX₂(MesN=CHCH=NMe_s)], X = Br or I, and the cyclobutane derivative **CB**, probably by way of a palladium(IV) intermediate **6-G** that could not be detected (Scheme 6-2). With hydrogen peroxide, the oxygen-atom insertion product **2-5** was formed and further reaction with bromine or iodine gave the benzofuran derivative **BF** and the palladium(II) complex **2-3**, X = Br or **2-4**, X = I, but again no palladium(IV) intermediate could be detected.²⁵⁻²⁷ The present article reports related chemistry in which palladium(IV) intermediates can be isolated, or at least detected, but which also undergo facile reductive elimination. This allows study of the mechanism and selectivity of the reductive elimination steps.



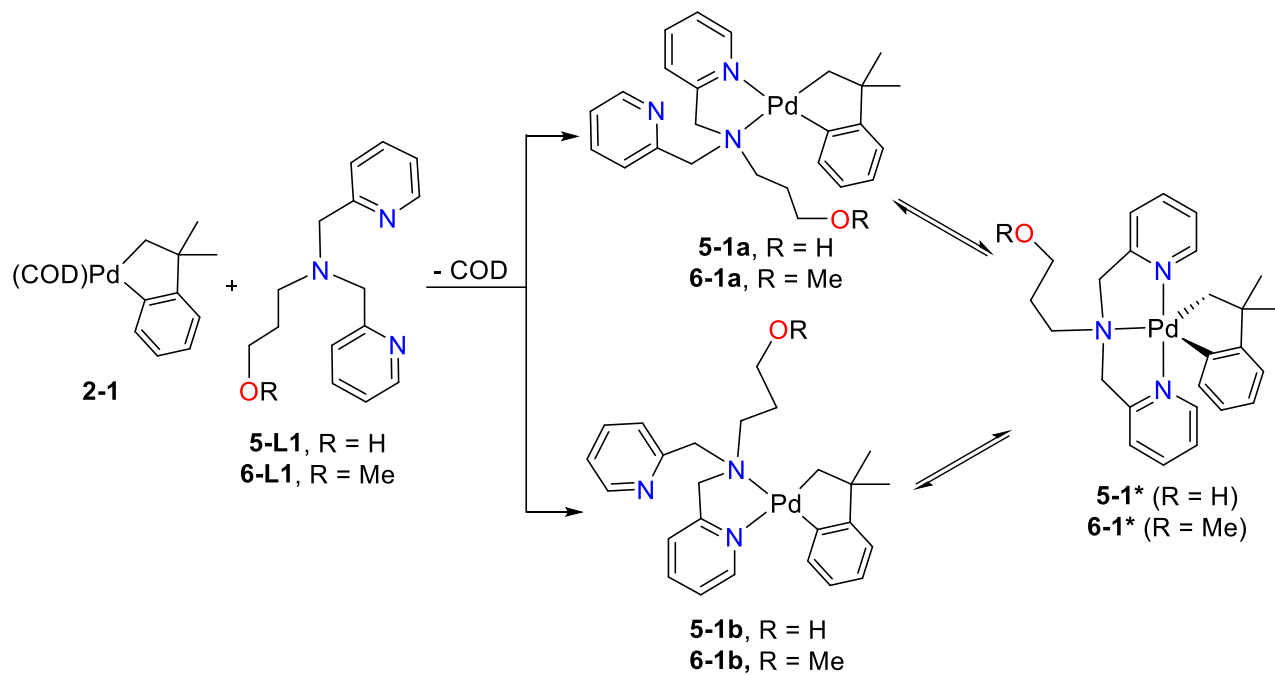
Scheme 6-2 Reductive coupling from proposed 5-coordinate intermediates **6-G**, by either C-C reductive elimination to give the cyclobutane derivative **CB** or by oxygen-atom insertion to give **2-5**.

6.2 Result and Discussion

6.2.1 The Cycloneophylpalladium(II) Complexes

The cycloneophylpalladium(II) complexes used in this work are shown in Scheme 6-3 and are based on the ligands $HO(CH_2)_3N(CH_2-2-C_5H_4N)_2$, **5-L1**, and $(CH_3)O(CH_2)_3N(CH_2-2-C_5H_4N)_2$, **6-L1**.²⁵⁻²⁹ These ligands are potentially tridentate, which should stabilise the palladium(IV) oxidation state. They also carry a 3-hydroxypropyl (**5-L1**) or 3-methoxypropyl substituent (**6-L1**), with the possibility that **5-L1** might take part in hydrogen-bonding interactions.²⁷ The complex $[Pd(CH_2CMe_2C_6H_4)(\kappa^2-N,N'-5-L1)]$, **5-1**, Scheme 6-3, was reported previously and shown to be fluxional.²⁷ The ligand binds through the central amine donor and one of the 2-pyridyl groups, and might exist primarily as either isomer **5-1a** or **5-1b**, which interconvert rapidly through the intermediate **5-1*** (Scheme 6-3). The new complex **6-1** behaves similarly, as shown by the variable temperature 1H NMR spectra in Figure 6-1. At room temperature, the 1H NMR spectrum of **6-1** in CD_2Cl_2 gave a single broad resonance at δ 8.49 for the H6a and H6b protons of the two 2-pyridyl groups and another broad resonance at δ 4.13 for the methylene protons of the two pyridylmethyl groups of coordinated **6-L1**. Each of these broad signals split at $-30^\circ C$, to give separate resonances for H6b and H6a (δ 8.63 and 8.43) and to give four overlapping resonances for the non-equivalent $pyCH_2N$ methylene protons (δ 4.06-4.17). A $^1H-^1H$ NOESY experiment at $-30^\circ C$ did not give any correlations between the hydrocarbon ligand and **6-L1**,

so it is uncertain if the major isomer is **6-1a** or **6-1b**. The complexes will be referred to as **5-1** and **6-1** in discussion below, but the isomeric structure shown will be arbitrary.



Scheme 6-3 Synthesis of complexes **5-1** and **6-1**, which are observed as a fluxional mixture assigned as **5-1a** or **6-1a** and **5-1b** or **6-1b** that likely interconvert via **5-1*** or **6-1***, respectively.

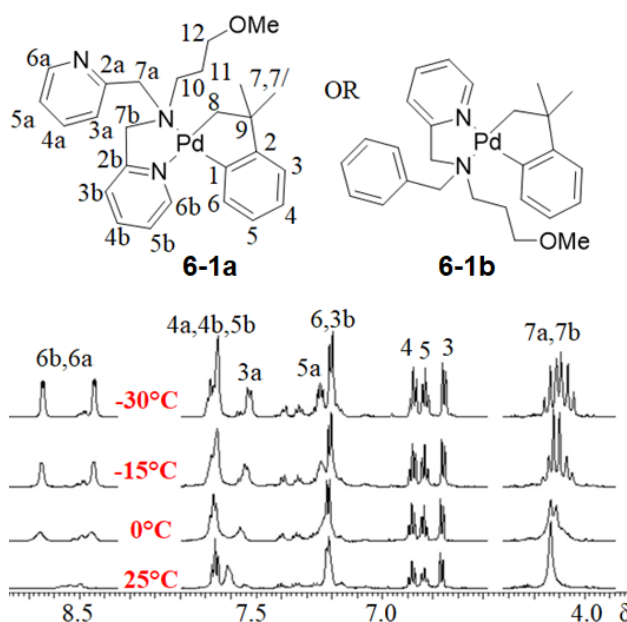
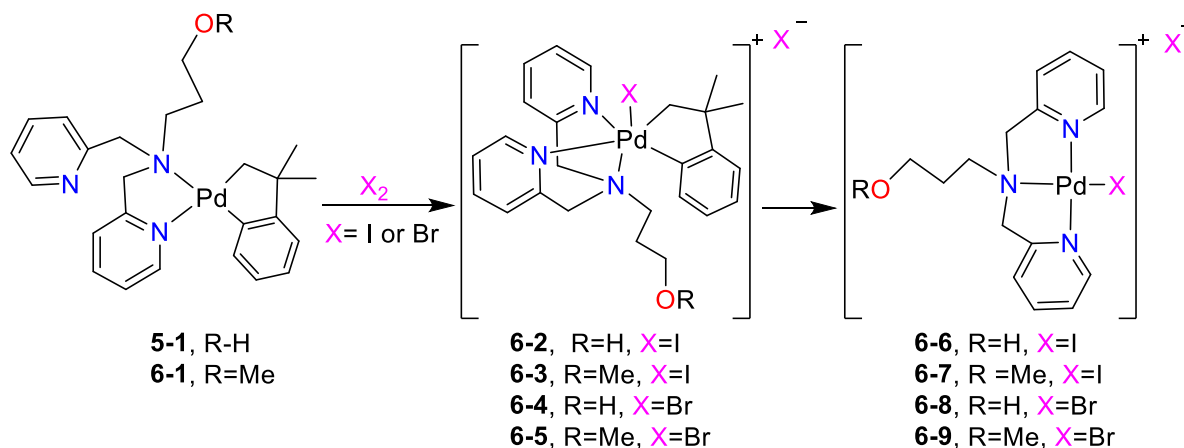


Figure 6-1 ^1H NMR spectra (600 MHz, CD_2Cl_2 solution) of complex **6-1** at different temperatures.

6.2.2 Palladium Complexes from Reactions of **5-1** and **6-1** with Bromine and Iodine

The complexes **5-1** and **6-1** reacted rapidly with iodine or bromine in chloroform solution at room temperature to give the corresponding cationic palladium(IV) complexes $[\text{PdX}(\text{CH}_2\text{CMe}_2\text{C}_6\text{H}_4)(\kappa^3\text{-}N,N',N''\text{-L})][\text{X}]$, **6-2**, $\text{X} = \text{I}$, $\text{L} = \mathbf{5-L1}$; **6-3**, $\text{X} = \text{I}$, $\text{L} = \mathbf{6-L1}$; **6-4**, $\text{X} = \text{Br}$, $\text{L} = \mathbf{5-L1}$; **6-5**, $\text{X} = \text{Br}$, $\text{L} = \mathbf{6-L1}$ (Scheme 6-4). The complexes have no symmetry and many isomers are possible, but they were formed as single stereoisomers, as indicated by their ^1H NMR spectra. The new palladium(IV) complexes **6-2**, **6-3**, **6-4** and **6-5** (78-90%) were isolated in pure form and could be stored at -5°C as solid samples for several weeks without noticeable decomposition. However, they decomposed slowly in solution at room temperature, and more rapidly at 50°C , to give the corresponding palladium(II) complexes **6-6**, **6-7**, **6-8** and **6-9** (84-91%), with loss of the cycloneophyl group (Scheme 6-4). The cationic complex **6-3** was also prepared as the tetrafluoroborate salt $[\text{PdI}(\text{CH}_2\text{CMe}_2\text{C}_6\text{H}_4)(\kappa^3\text{-}N,N',N''\text{-} \mathbf{6-L1})][\text{BF}_4]$, **6-3a**, by reaction of complex **6-1** with the oxidant *bis*(pyridine)iodonium tetrafluoroborate. Complex **6-3a** was significantly more stable than the corresponding iodide salt, **6-3**.



Scheme 6-4 The oxidative addition reaction of complexes **5-1** and **6-1** with iodine and bromine to give complexes **6-2**, **6-3**, **6-4** and **6-5**, and slower reductive elimination to give complexes **6-6**, **6-7**, **6-8** and **6-9**.

The new complexes were fully characterized by ^1H and ^{13}C NMR spectroscopy, including correlated ^1H - ^1H COSY, ^1H - ^1H NOESY, and ^1H - ^{13}C HSQC and HMBC NMR spectroscopy, as well as by ESI mass spectrometry and IR spectroscopy. For example, the IR spectrum of complex **6-2** showed a peak due to $\nu(\text{OH})$ centered at 3103 cm^{-1} . The ^1H NMR spectrum of **6-2** in CDCl_3 showed 12 distinct aromatic signals in the range δ 6.49 - 9.38 and four different doublet CH_2N resonances at δ 4.20, 4.97, 5.35 and 5.49. For the cycloneophyl group, the CMe_2 and CH_2 groups each gave two distinct resonances. These NMR data, which were similar for the other complexes **6-3**, **6-4** and **6-5**, indicate a single octahedral palladium(IV) complex with no symmetry, but the stereochemistry is not defined. The stereochemistry was determined by structure determinations on complexes **6-2** and **6-4**. Based on the usual polar mechanism of oxidative addition of halogens,³⁰⁻³³ we had expected the palladium(IV) product to be formed from **5-1** by formal addition of I^+ above the plane with coordination of the free pyridyl group below the plane to give an isomer with mutually *trans* iodide and pyridyl groups, but the products are formed selectively with iodide *trans* to the amine donor (Scheme 6-4).

Crystallization of complex **6-2** from acetone/pentane at room temperature occurred with partial decomposition to **6-6** to give co-crystals of **6-2** and **6-6** as the acetone solvate **6-2.6-6.Me₂CO**. The structure of complex **6-2** is shown in Figure 6-2. It confirms that **5-L1** acts as a *fac*-tridentate ligand and shows that the iodide ligand is *trans* to the amine donor while the two pyridyl donors are *trans* to carbon donors of the cycloneophyl group. The ligand hydroxyl group in **6-2** is not coordinated but is hydrogen bonded to an iodide anion.

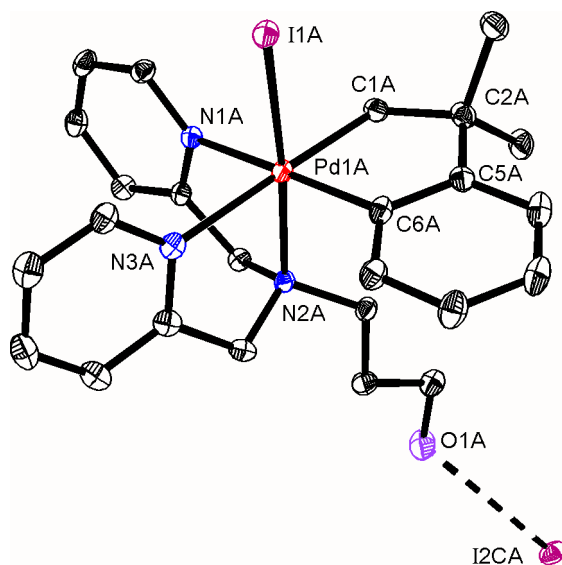


Figure 6-2 Structure of complex **6-2**, showing 30% probability ellipsoids. Selected bond distances:
 Pd(1A)–I(1A) 2.5785(9); Pd(1A)–N(1A) 2.150(4); Pd(1A)–N(2A) 2.197(4); Pd(1A)–N(3A)
 2.229(5); Pd(1A)–C(1A) 2.072(5); Pd(1A)–C(6A) 1.994(6) Å; H-bond distance: O(1A)···I(2CA)
 3.54(1) Å.

Crystals of complex **6-4**, as the acetone solvate, were grown from acetone/acetonitrile, at low temperature (-15°C) to avoid decomposition, and the structure is shown in Figure 6-3. There were two independent molecules in the lattice, which both have the same stereochemistry as complex **6-2** (amine

donor *trans* to halide, compare Figure 6-2), but were refined as enantiomers. Again, the ligand hydroxyl group was hydrogen bonded to a halide (bromide in this case) anion.

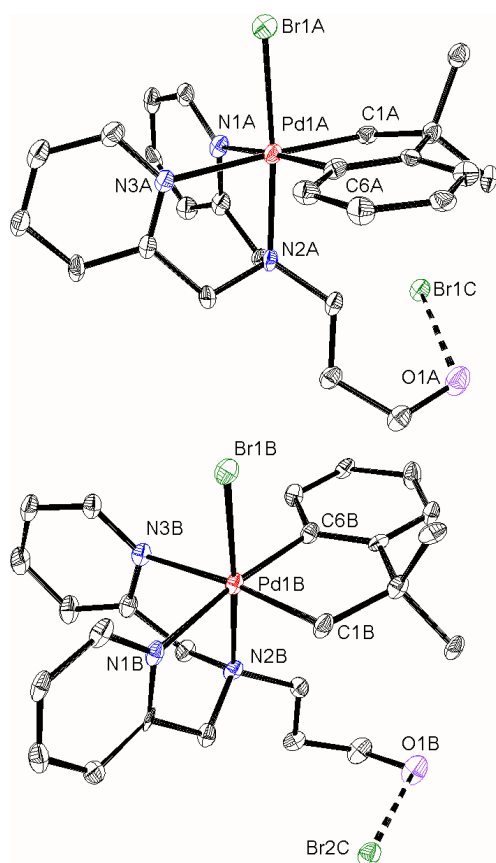


Figure 6-3 Structure of complex **6-4**, showing 30% probability ellipsoids for the two independent molecules. Selected bond distances (Å): molecule **A**, Pd(1A)–I(1A) 2.420(2); Pd(1A)–N(1A) 2.171(12); Pd(1A)–N(2A) 2.121(12); Pd(1A)–N(3A) 2.203(12); Pd(1A)–C(1A) 2.075(13); Pd(1A)–C(6A) 1.985(15); molecule **B**, Pd(1B)–I(1B) 2.4272(19); Pd(1B)–N(1B) 2.154(12); Pd(1B)–N(2B) 2.147(12); Pd(1B)–N(3B) 2.206(12); Pd(1B)–C(1B) 2.049(12); Pd(1B)–C(6B) 1.996(15).

The square planar palladium(II) complexes **6-6**, **6-7**, **6-8** and **6-9** are more symmetrical than their precursor complexes **6-2**, **6-3**, **6-4** and **6-5** and so they give simpler NMR spectra. For example, complex **6-6** gave only one set of pyridyl resonances, as expected for a complex having C_s symmetry, with equivalent 2-pyridylmethyl groups. The similar structures of the iodopalladium(II) complexes **6-6** and **6-7** and the bromopalladium(II) complexes **6-8** and **6-9** are shown in Figure 6-4. In complexes **6-6** (a component of the co-crystal **6-2.6-6.acetone**) and **6-8**, the ligand hydroxyl group is hydrogen bonded to

an iodide or bromide anion, respectively. In all complexes, the ligand **5-L1** or **6-L1** acts as a *mer*-tridentate ligand, binding through the three nitrogen atoms.

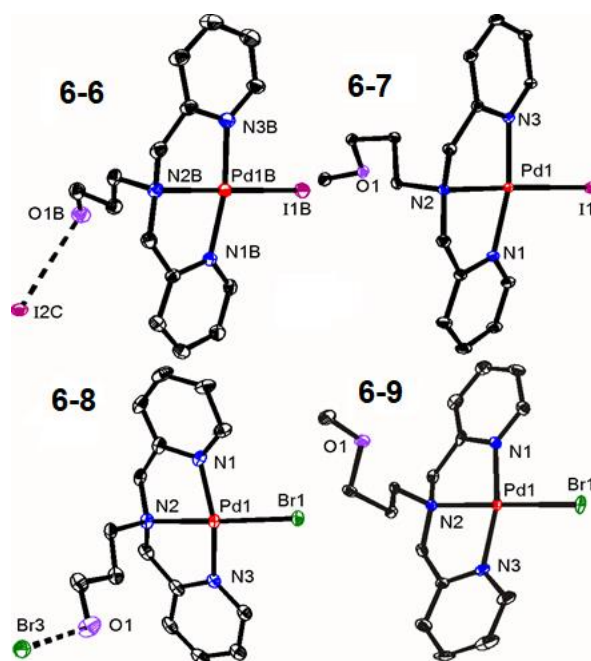
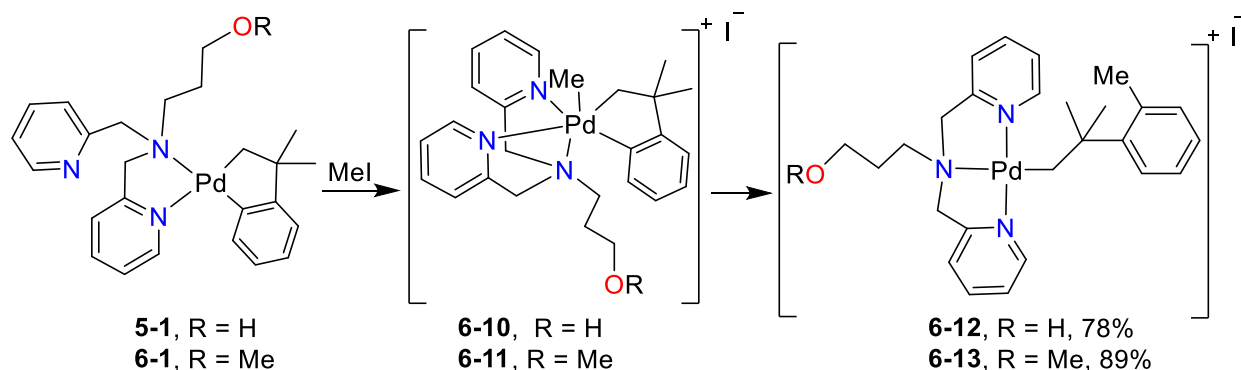


Figure 6-4 Structures of complexes **6-6**, **6-7**, **6-8** and **6-9**. Selected distances: complex **6-6**, Pd(1B)–I(1B) 2.5928(10); Pd(1B)–N(1B) 2.025(5); Pd(1B)–N(2B) 2.055(5); Pd(1B)–N(3B) 2.037(5) Å; complex **6-7**, Pd(1)–I(1) 2.5911(19); Pd(1)–N(1) 2.028(2); Pd(1)–N(2) 2.041(2); Pd(1)–N(3) 2.017(2) Å; complex **6-8**, Pd(1)–Br(1) 2.4101(8); Pd(1)–N(1) 2.026(5); Pd(1)–N(2) 2.014(5); Pd(1)–N(3) 2.034(5) Å; complex **6-9**, Pd(1)–Br(1) 2.4282(12); Pd(1)–N(1) 2.024(5); Pd(1)–N(2) 2.038(5); Pd(1)–N(3) 1.993(5) Å.

6.2.3 Palladium Complexes from Reaction with Methyl Iodide

The reaction of methyl iodide with complex **5-1** at room temperature gave the palladium(II) complex **6-12** (Scheme 6-5). This is the expected product if an initial product **6-10** of oxidative addition undergoes reductive elimination by selective coupling of the methyl and aryl group (sp^3 - sp^2 coupling). Complex **6-10** was identified later as a reaction intermediate by low temperature NMR spectroscopy. The ^1H NMR spectrum of **6-12** (Figure 6-5) contained only one set of resonances for the pyridyl groups, and gave singlet resonances for the PdCH_2 , CMe_2 and $\text{Me-C}_6\text{H}_4$ groups with relative intensities 2:6:3, as expected for a complex with C_s symmetry. These data are clearly not consistent with the palladium(IV) complex **6-10** or with potential products of reductive elimination by coupling of methyl and CH_2 groups (sp^3 - sp^3 coupling) or by coupling of the CH_2 and aryl groups which would give the

benzocyclobutane derivative **CB** (compare Scheme 6-2) and a methylpalladium(II) complex. The reaction of complex **5-1** with CD_3I gave the corresponding complex **6-12-*d*₃** (Figure 6-5). The reaction of methyl iodide with complex **6-1** occurred similarly to give complex **6-13**, Scheme 6-5, which was characterized in the same way.



Scheme 6-5 The reaction of complexes **5-1** and **6-1** with methyl iodide to give complexes **6-10**, **6-11**, **6-12** and **6-13**.

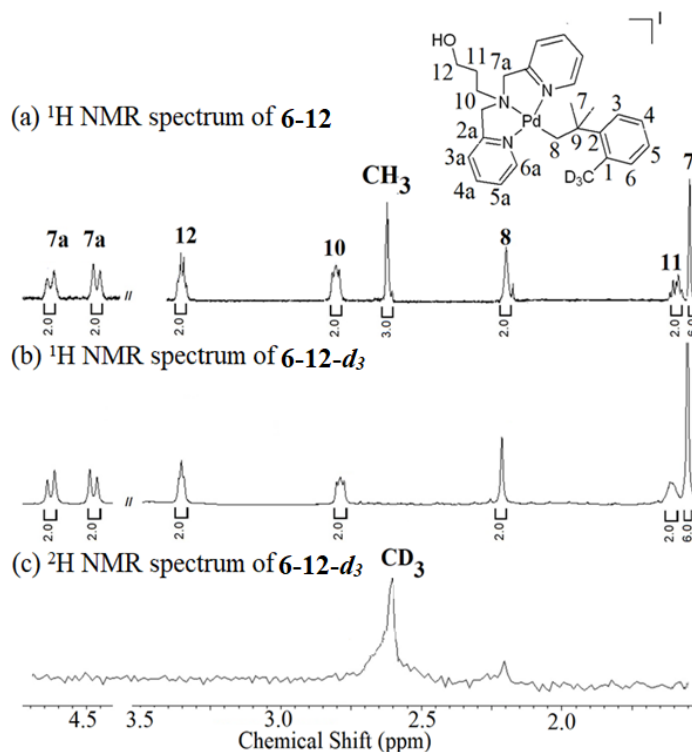


Figure 6-5 NMR spectra of complex **6-12** and **6-12-*d*₃**: (a) ^1H NMR spectrum of **6-12** in CD_2Cl_2 ; (b) ^1H NMR spectrum of **6-12-*d*₃** in CD_2Cl_2 ; (c) ^2H NMR spectrum of **6-12-*d*₃** in CH_2Cl_2 .

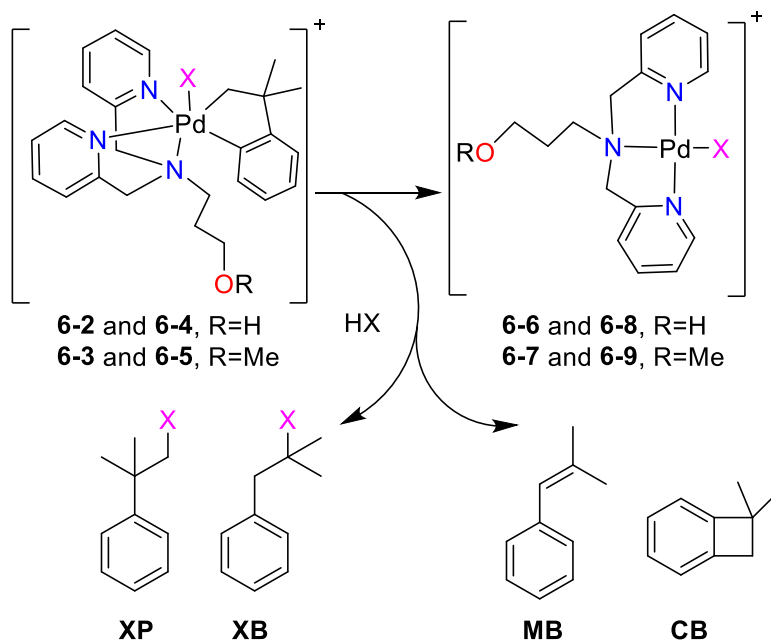
The reaction of complex **5-1** with MeI or CD₃I was also carried out at low temperature in order to detect the potential palladium(IV) intermediate. The reagents were mixed at -30°C and NMR spectra were recorded from -30°C to room temperature. The reaction was slow at -30°C but peaks for complex **5-1** had decayed and were replaced by peaks characteristic of a palladium(IV) complex at 0°C. The ligand and cycloneophyl resonances were similar to those for **6-2** and **6-4** so, although the data do not unambiguously define the stereochemistry, the related structure **6-10** is suggested for this intermediate. The methylpalladium resonance of the intermediate complex **6-10** was observed as a singlet at δ 1.91. At temperatures above 0°C, reductive elimination occurred selectively and the peaks for **6-10** were replaced by those for the palladium(II) product **6-12**. The similar reaction at low temperature of complex **6-1** gave the palladium(IV) intermediate **6-11**, which had similar thermal stability as **6-10** and which decomposed by warming to room temperature to give **6-13** (Scheme 6-5).

There have been several studies of selectivity in C-C coupling reactions at palladium(IV) or platinum(IV) centres, though we are not aware of any involving the cycloneophyl group.^{6-14,30-43} Most of the known reactions proceed after dissociation of a ligand to give a 5-coordinate intermediate.^{30-33,39-43} In simple dimethyl(aryl) derivatives, there is a preference for C(sp³)-C(sp³) coupling to give ethane rather than C(sp³)-C(sp²) coupling to give the corresponding methylarene.³⁴⁻³⁵ However, if the aryl group is part of a cyclometallated chelate group, there is usually a kinetic preference for C(sp³)-C(sp²) coupling.³⁶⁻³⁸ The reactivity of **6-10** and **6-11** falls into this pattern, with the selectivity for C(sp³)-C(sp²) coupling rationalised in terms of the favourable orientation of the plane of the aryl group roughly orthogonal to the methylpalladium(IV) bond, which allows facile access to the transition state for methyl-aryl group coupling.³⁴⁻³⁸

6.2.4 Organic Products from the Reductive Elimination Reactions of Complexes **6-2**, **6-3**, **6-4** and **6-5**.

Previous studies of reductive elimination from cycloneophylpalladium(IV) complexes have shown a high degree of selectivity, though the reactions may occur by C-C coupling to give the cyclobutane derivative **CB**, or by CH₂-X or aryl C-X coupling to give organopalladium(II) products (Schemes 6-1, 6-2).¹⁵⁻²⁷ However, the reductive elimination reactions from the palladium(IV) complexes, **6-2**, **6-3**, **6-4** and **6-5**, were not very selective (Scheme 6-6, Table 6-1). The decomposition of **6-2**, **6-3**, **6-4** and **6-5** in CDCl₃ solution gave the cyclobutane derivative **CB** by C-C coupling in yields ranging from 5 – 30% (Table 6-1). However, the other observed products are less easily explained. The neophyl halide product, **XP** (Scheme 6-6), is expected to be formed by X-CH₂ coupling but also with protonolysis of

the arylpalladium bond. This unanticipated protonolysis step is also required in formation of the products **XB** and **MB** (Scheme 6-6), but with an additional step involving a “cation-like” neophyl rearrangement with phenyl group migration.⁴⁴ The neophyl halides are stable to substitution under the mild conditions used in this work (most studies have involved the more reactive triflates or tosylates),⁴⁴ so the neophyl rearrangement must occur while the organic group is still bound to palladium.^{22-23,27} The reaction of complex **6-3** in CDCl₃ saturated with D₂O gave the expected products **XP-d₁**, **XB-d₁** (X = I) and **MB-d₁**. In the ²H NMR spectrum, two resonances were resolved at δ 7.37 and 7.25. The aryl resonances for **XP**, **XB** and **MB** all overlap in the narrow range δ 7.14-7.35 in the ¹H NMR spectrum so it was only possible to confirm the incorporation of deuterium atoms but not to confirm their expected *ortho* positions. The product ratios (Table 6-1, Figure A6.67) are affected by both the ligand (**5-L1** vs **6-L1**) and by the halide (Br vs I). **XP** is the major product in R = H complexes **6-2** and **6-4** (ligand **5-L1**). However, **MB** has higher yields in R = Me complexes **6-3** and **6-5** (ligand **6-L1**). R = Me complexes **6-3** and **6-5** (halide Br) show a similar selectivity trend to **6-3** and **6-5** (halide I). This confirms that the ligand (**5-L1** vs **6-L1**) has a stronger role in the selectivity of bond formations than the halides. The tetrafluoroborate salt **6-3a** gave a higher yield of **CB** compared to the corresponding iodide salt **6-3**.



Scheme 6-6 The mixture of organic products detected from reductive elimination from complexes **6-2**, **6-3**, **6-4** and **6-5** (X = I from **6-2** and **6-3**, X = Br from **6-4** and **6-5**)

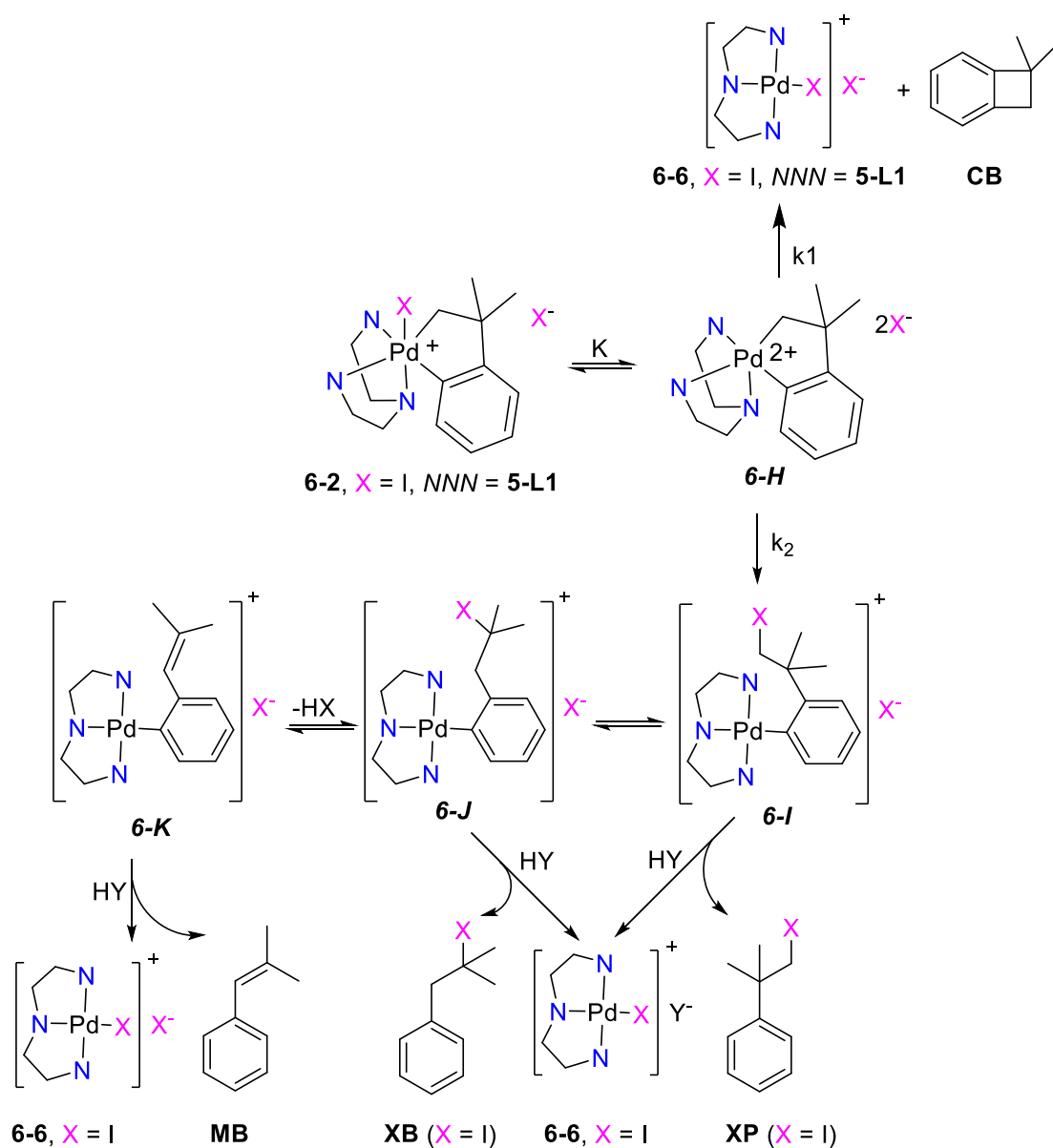
Table 6-1 Observed products after reductive elimination from complexes **6-2**, **6-3**, **6-4** and **6-5** in CDCl₃ solution.^a

Complex	Pd Prod. (% yield) ^b	X	XP %	XB %	MB %	CB %
6-2	6-6 (87)	I	37	28	20	5
6-3	6-7 (93)	I	25	8	48	5
6-3a^c	6-7a (80)	I	13	-	25	30
6-4	6-8 (90)	Br	50	-	9	28
6-5	6-9 (84)	Br	24	-	50	10

^a Conditions: 50°C, 7.5 h; yields are in situ NMR yields relative to an internal standard (1,3,5-trimethoxybenzene). ^b Isolated yield. ^c 60 h reaction time.

From the initial product analyses (Table 6-1), and from literature precedents,^{15-19,25-27,39-43} the reaction sequence shown in Scheme 6-7 (*NNN* = **5-L1** or **6-L1**, X = Br or I) was considered as a working hypothesis. The reductive elimination steps are likely to occur by way of a 5-coordinate intermediate formed by ligand dissociation from the palladium(IV) complex **6-2** (used as an example of **6-2**, **6-3**, **6-4** and **6-5**). If the dissociating ligand is iodide, this 5-coordinate intermediate is the dication **6-H** (Scheme 6-7). Complex **6-H** can undergo reductive elimination with C-C coupling to give **CB**, followed by rapid coordination of iodide to give **6-6**, or it can undergo nucleophilic attack by iodide at the CH₂ group to give **6-I**. Complex **6-I** can undergo protonolysis of the aryl-palladium bond to give **XP** (X = I) or it can undergo the neophyl rearrangement, with phenyl group migration,⁴⁴ to give **6-J** and **6-K** and protonolysis can then give **6-6** and **XB** (X = I) and **MB** respectively. One unresolved issue is that, when the product is **XP** or **XB**, there is not enough halide to give **6-6** as the halide salt. In all of the isolated crystals of **6-6**, **6-7**, **6-8** and **6-9** (Figure 6-4) the anion was iodide or bromide. It is unlikely that water is sufficiently acidic to act as HY in the protonolysis steps of Scheme 6-7. Several further experiments were carried out to test the validity of Scheme 6-7. The decomposition of complex **6-2** in CDCl₃ solution was monitored by ¹H NMR spectroscopy in order to attempt to detect the proposed intermediates **6-I**, **6-J** and **6-K**. One intermediate was detected at intermediate stages of reaction; its concentration was always low but it was tentatively identified as **6-J** by its ¹H NMR spectrum. The 2-pyridylmethyl groups were equivalent [e.g. δ(CH^aH^b) = 5.10, 4.47, each 2H, ²J(HH) = 15 Hz, H7a and H7b] while the organic group gave the expected singlet resonances for the CH₂ and CMe₂ groups [δ(CMe₂) = 1.63, 6H; δ(CH₂)

= 1.96, 2H; note that the CH₂I resonance for **6-I** would be expected at higher δ). If Scheme 6-7 is correct, the ratio of **CB** to the sum of the other products (**XP**, **XB**, **MB**) should be given by the ratio $k_1/k_2[X^-]$, where k_1 is the first order rate constant for reductive elimination from **6-H** to give **CB** and k_2 is the second order rate constant for formation of intermediate **6-I** by halide attack on **6-H**. This ratio was approximately 1:7, 1:16 and 1:6 for reactions of **6-3** in benzene, chloroform and methanol, respectively, showing no correlation with solvent polarity.⁴⁵ In methanol saturated with sodium iodide, the formation of **CB** was suppressed, as expected from Scheme 6-7. There is an analogy with the mechanistic study by the Goldberg group on the decomposition of [PtIMe₃(dppe)], dppe = Ph₂PCH₂CH₂PPh₂.⁴² This reductive elimination reaction was shown to occur from a 5-coordinate intermediate [PtMe₃(dppe)]⁺I⁻ by competitive C-C coupling, to give ethane and [PtIMe(dppe)], and C-I coupling, to give methyl iodide and [PtMe₂(dppe)] and the ethane formation was suppressed in the presence of excess iodide. In addition, the ratio **CB**:(**XP**, **XB**, **MB**) for decomposition in CDCl₃ solution was 1:16 for complex **6-3**, which has the iodide anion, but 1:2.3 for complex **6-3a**, which has the tetrafluoroborate anion (Table 6-1), again indicating that free iodide favors formation of **XP**, **XB**, **MB** over **CB**. Qualitatively, the rate of reductive elimination in chloroform solution from **6-3a** is much slower than from **6-3** (Table 6-1). All of these data are at least consistent with the mechanism of Scheme 6-7.



Scheme 6-7 A simplified pathway for the reductive elimination reactions.

6.2.5 Kinetic Studies

Kinetic studies of the reductive elimination reactions were carried out using UV-visible spectroscopy to monitor the rates. The proposed mechanism of Scheme 6-7 is complex but the relevant parts of the UV-visible spectra are dominated by the palladium cations (reagent **6-2** and product **6-6** in Scheme 6-7) so the overall rate of reductive elimination can be measured. Under conditions where there is a pre-equilibrium between **6-2** and **6-H** (Scheme 6-7), the overall rate is expected to be given by $-d(\mathbf{6-2})/dt = (k_1 + k_2[X^-])[\mathbf{6-H}] = K(k_1 + k_2[X^-])[\mathbf{6-2}]/[X^-] = k_{\text{obs}}[\mathbf{6-2}]$, where $k_{\text{obs}} = Kk_1/[X^-] + Kk_2$. The halide concentration is expected to decrease during the reaction as the products **XP** and **XB** are formed, so

good first-order kinetics cannot be expected. Nevertheless, first-order plots of $\ln[A-A_\infty]/[A_0-A_\infty]$ vs. time were approximately linear at early time points and the values of k_{obs} can at least be taken as a measure of reactivity.

A series of spectra obtained for reductive elimination from complex **6-2** in chloroform solution at 50°C, along with the first-order plot using changes in the absorbance at 425 nm, is shown in Figure 6-6 and a summary of the values of k_{obs} is given in Table 6-2. The reactions using **6-2** and **6-3** were each carried out in three solvents benzene, chloroform and methanol of different polarity (dielectric constant $\epsilon = 2.2, 4.8, 33.6$ respectively). The values of k_{obs} in benzene, chloroform, methanol were for **6-2** 0.0162(5), 0.0211(2), 0.020(1) min^{-1} and for **6-3** 0.017(1), 0.019(1), 0.019(1) min^{-1} , respectively. There is very little difference in these values, so clearly the effect of solvent polarity is small and the different ligand substituents (OH in **6-2** and OMe in **6-3**) also have very little effect on the overall rate of reductive elimination. Similarly, the bromide derivative **6-4** reacts at a similar rate as the iodide derivative **6-2**, with $k_{\text{obs}} = 0.016(2)$ and $0.0211(2) \text{ min}^{-1}$, respectively, at 50°C in chloroform solution. The reaction of complex **6-2** in methanol solution at 50°C was also monitored in the presence of excess sodium iodide or free pyridine, with initial $[\mathbf{6-2}] = 8.33 \times 10^{-3} \text{ M}$ and $[\text{NaI}]$ or $[\text{py}] = 8.33 \times 10^{-2} \text{ M}$, but neither free iodide or pyridine had a significant effect on the rate of reaction (Table 6-2). The only case in which a major difference in rate was observed was in the decomposition of **6-3** and **6-3a** in chloroform at 50°C, with $k_{\text{obs}} = 0.0211(2)$ and $0.0028(3) \text{ min}^{-1}$, respectively, with **6-3** reacting about seven times faster than **6-3a**. The kinetic data are in accord with qualitative observations made when similar reactions were monitored by ^1H NMR spectroscopy (Tables 6-1 and 6-2).

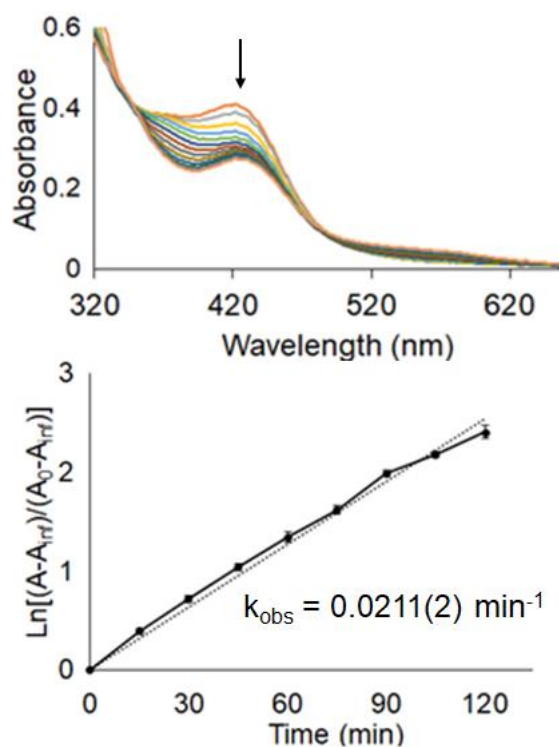


Figure 6-6 Above, UV-visible absorption spectra of complex **6-2** in chloroform (8.33×10^{-3} M, 50°C) during the reductive elimination reaction (absorbance at 425 nm decreases with time). Below, the corresponding first-order plot of $\ln[A-A_\infty]/[A_0-A_\infty]$ versus time for the initial part of the reaction.

Table 6-2 Observed first-order rate constants for the reductive elimination reactions.^a

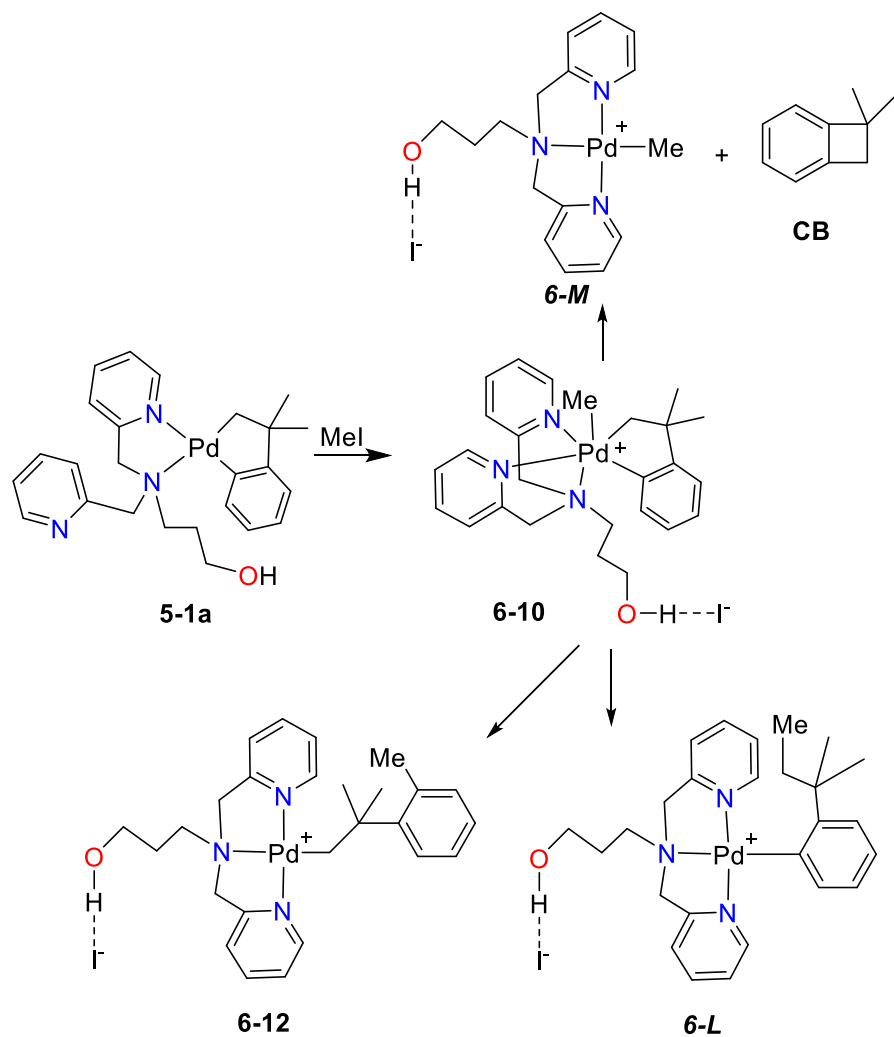
Complex	Additive ^a	Solvent	ϵ^b	k_{obs} (min^{-1})
6-2	None	C_6H_6	2.2	0.0162(5)
6-2	None	CHCl_3	4.8	0.0211(2)
6-2	None	CH_3OH	33.6	0.0200(1)
6-2	NaI^c	CH_3OH	33.6	0.0199(1)
6-2	Pyridine ^c	CH_3OH	33.6	0.0212(1)
6-3	None	C_6H_6	2.2	0.0170(1)
6-3	None	CHCl_3	4.8	0.0190(1)

6-3	None	CH ₃ OH	33.6	0.0190(1)
6-3A	None	CHCl ₃	4.8	0.0028(3)
6-4	None	CHCl ₃	4.8	0.0158(2)

^aSee experimental section for details. ^bDielectric constant. ^c[NaI] or [py] = 8.33 × 10⁻² M.

6.2.6 Computational Studies

In order to gain more insight into the selectivity of the reactions, some calculations were carried out using Density Functional Theory (BLYP functional, scalar correction for relativity). One limitation is that the reactions begin with neutral reagents but give ionic products and, given the complexity of the compounds, we have not attempted to model the resulting changes in solvation effects. Instead we have generally made only gas phase calculations with complex **5-1** as reagent, and have modeled the ionic products as zwitterions, with the iodide ion hydrogen bonded to the hydroxyl substituent of the ligand. Naturally, this methodology will not give accurate data for the step in which the ionic compounds are first formed, but it should give more reliable data for compounds with like charges. As an example, the potential products from reactions of complex **5-1** with methyl iodide are shown in Scheme 6-8, while calculated structures and relative energies with respect to **5-1a** and MeI are shown in Figure 6-7. The initial reaction of **5-1a** with methyl iodide is calculated to be unfavorable (ΔE +30 kJ mol⁻¹), no doubt because of the poor modeling of the solvation of the ions. The three potential routes for reductive elimination from **6-10** with C-C bond formation occur with no change in charges and so the relative energies with respect to **6-10** should be more reliable. The potential products are **6-12** formed by methyl-aryl coupling, **6-L** formed by methyl-alkyl coupling and **6-M** and **CB** formed by alkyl-aryl coupling (alkyl represents the Pd-CH₂ group of the metallacycle) (Scheme 6-8). Formation of **6-M** and **CB** is clearly least favorable (ΔE -54 kJ mol⁻¹, Figure 6-7), as expected in view of the ring strain of the **CB** product. The calculations predict that formation of **6-L** (ΔE -123 kJ mol⁻¹) is more favorable than formation of the observed product **6-12** (ΔE -106 kJ mol⁻¹). We have not calculated transition states, but the calculation is fully consistent with the selective formation of **6-12** being determined by kinetic and not by thermodynamic control.³⁶⁻³⁸



Scheme 6-8 The three potential modes of reductive elimination from complex **6-10** with C-C bond formation.

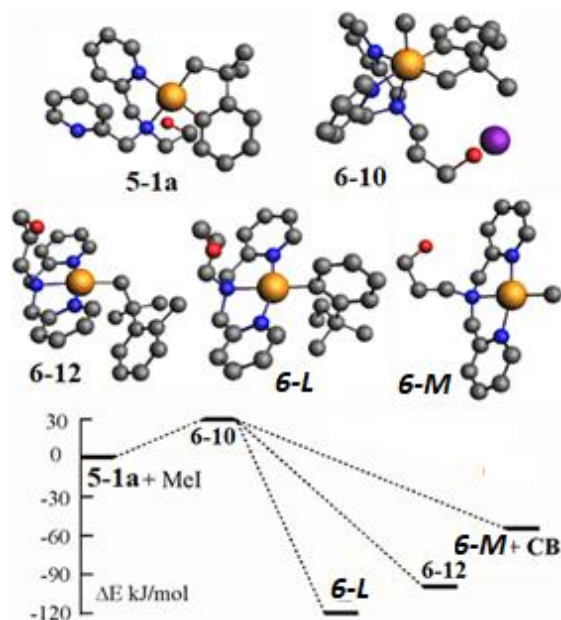


Figure 6-7 The calculated structures of complexes shown in Scheme 6-8 (the iodide ion is not shown in the Pd(II) complexes for clarity), and the relative energies (kJ mol⁻¹) with respect to **5-1a** + MeI.

Figure 6-8 shows the calculated structures and relative energies for products and potential products from reductive elimination from the iodopalladium(IV) complex **6-2** (Scheme 6-7). This reaction could occur initially by: C-C coupling to form **6-6** and **CB**; I-CH₂ coupling to form **6-I**; or I-C₆H₄ coupling to form **6-N**. The aryl-iodide coupling to give complex **6-N** (Figure 6-7) is calculated to be unfavorable and **6-N** is not observed experimentally, but the other two routes are favorable and the ¹H NMR spectroscopy evidence indicates that they both occur. The organic products **XP**, **XB** and **MB** are expected to be formed by protonolysis of **6-I** or the products of its neophyl rearrangement **6-J** and **6-K**. These products are at considerably lower energy than the cyclobutane derivative **CB**, but the ratio of **CB** to the combined products **XP**, **XB** and **MB** will be controlled by the initial reductive elimination steps to form **6-6** and **CB** or to form **6-I**, and these are competitive (Figure 6-8). However, the experimental results suggest that for **6-2** reductive elimination to give **6-I** is far preferred. These data suggest that the selectivity is more likely to be under kinetic rather than thermodynamic control.

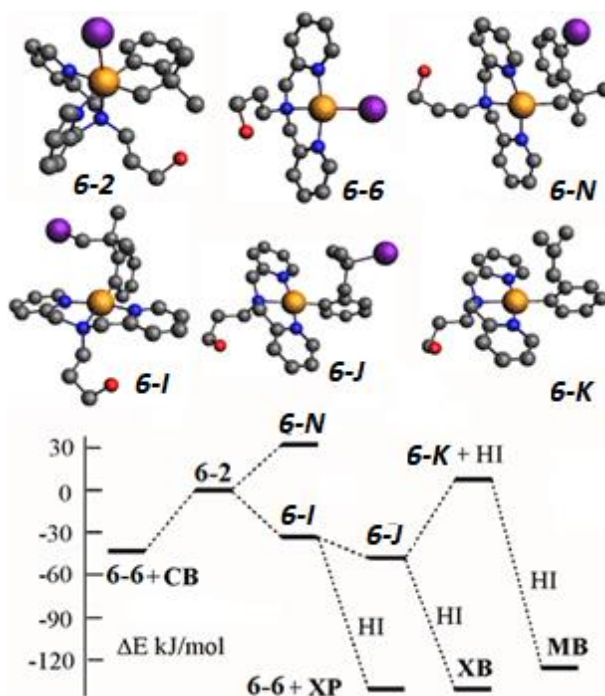


Figure 6-8 The calculated structures of cationic complexes shown in Scheme 6-7, and the relative energies (kJ mol^{-1}) with respect to complex **6-2**.

One remaining puzzle is why the oxidative addition of iodine occurs selectively to form the complex **6-2** rather than its isomers **6-2a** and **6-2b** (Figure 6-9). The palladium(II) complexes **5-1a** and **5-1b** (Scheme 6-3) are chiral and attack by iodine could occur on either side of each. Attack by iodine on **5-1a** could initially give the iodine complex **6-O** by attack *syn* to the 3-hydroxypropyl group or **6-P** by attack *syn* to the free 2-pyridylmethyl group, and **6-O** is at lower energy.³⁰⁻³³ If the final product was formed by kinetic control, **6-O** would be expected to give isomer **6-2a**. Similarly, addition to **5-1b** would be expected to give **6-2b**. Complex **6-2** is calculated to be more stable than either **6-2a** or **6-2b**, though the differences are small (Figure 6-9), so the data suggest that **6-2** is formed selectively through thermodynamic control.

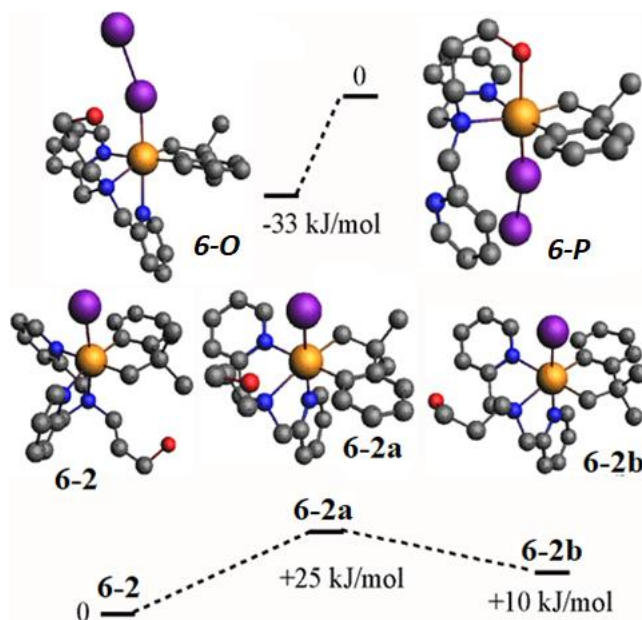


Figure 6-9 The calculated structures of isomers of **6-2** and possible intermediate iodine complexes **6-O** and **6-P**, and their relative energies (kJ mol^{-1}).

6.3 Conclusion

The cycloneophylpalladium(IV) complexes reported above contain flexible tridentate ligands that stabilise the Pd(IV) oxidation state to an extent that allows their isolation (or characterization at reduced temperature for the methylpalladium(IV) complexes) but not so much that the compounds require forcing conditions to initiate reductive elimination. The most selective reductive elimination is observed for the methylpalladium(IV) complexes **6-10** and **6-11**, which give only $\text{C}(\text{sp}^3)\text{-C}(\text{sp}^2)$ coupling with $\text{Me-C}_6\text{H}_4$ bond formation at about 0°C in solution (Scheme 6-5). The halogenopalladium(IV) complexes **6-2**, **6-3**, **6-4** and **6-5** are sufficiently stable to be isolated but they decompose slowly in solution by reductive elimination, in which there is competition between coupling by $\text{CH}_2\text{-X}$ ($\text{X} = \text{Br}$ or I) or $\text{CH}_2\text{-C}_6\text{H}_4$ bond formation (Scheme 6-7). The palladium(II) products of these reactions are $[\text{PdX}(\kappa^3\text{-N,N',N''-5-L1 or 6-L1})]\text{X}$, $\text{X} = \text{Br}$ or I , and a mixture of organic products is formed in steps subsequent to the major reductive elimination with $\text{CH}_2\text{-X}$ bond formation, involving both neophyl rearrangement and protonolysis. The slow reductive elimination reaction of **6-3a** (BF_4^- counter-anion) as compared to **6-3** (I^- counter-anion) suggests that the reductive elimination occurs by a mechanism in which $[\text{PdX}(\text{CH}_2\text{CMe}_2\text{C}_6\text{H}_4)(\kappa^3\text{-N,N',N''-5-L1 or 6-L1})]^+$, $\text{X} = \text{Br}$ or I , undergoes reversible halide dissociation to give a 5-coordinate intermediate $[\text{Pd}(\text{CH}_2\text{CMe}_2\text{C}_6\text{H}_4)(\kappa^3\text{-N,N',N''-5-L1 or 6-L1})]^{2+}$. This intermediate can then undergo intramolecular reductive elimination with $\text{CH}_2\text{-C}_6\text{H}_4$ bond formation, to

give the cyclobutane derivative **CB** and $[\text{PdX}(\kappa^3\text{-}N,N',N''\text{-}\mathbf{5}\text{-}\mathbf{L1}$ or $\mathbf{6}\text{-}\mathbf{L1})]^+$, or by halide attack on the Pd-CH₂ group to give initially $[\text{Pd}(2\text{-C}_6\text{H}_4\text{CMe}_2\text{CH}_2\text{X})(\kappa^3\text{-}N,N',N''\text{-}\mathbf{5}\text{-}\mathbf{L1}$ or $\mathbf{6}\text{-}\mathbf{L1})]^+$, which then undergoes the neophyl rearrangement and protonolysis of the aryl-palladium(II) bond to give a mixture of organic products. The complexes with ligands **5-L1** and **6-L1** have similar reactivity in these reactions, indicating that the hydroxyl substituent in **5-L1** plays only a minor role in the rate-determining steps. The work is significant in giving new insights into reactivity and mechanism in palladium(II)-palladium(IV) cycles that are important in several catalytic reactions.

6.4 Experimental

6.4.1 Reagents and General Procedure

All reactions were carried out in air, unless otherwise noted. For those reactions that were conducted under a nitrogen atmosphere, standard Schlenk or glove box techniques were used. All solvents used for air- and moisture-sensitive reactions were purified using an Innovative Technologies 400-5 Solvent Purification System (SPS) and were stored over activated 4 Å molecular sieves. NMR spectra were recorded using Varian 600 spectrometer. ¹H and ¹³C chemical shifts were referenced internally to solvent (residual signal for ¹H) where the chemical shift was set to appropriate values relative to TMS at 0.00 ppm. Chemical shifts are reported relative to trifluorotoluene for ¹⁹F NMR. Complete assignments of each compound were aided by the use of ¹H-¹H gCOSY, ¹H-¹³C{¹H} HSQC, and ¹H-¹³C{¹H} HMBC experiments and are reported using the labeling scheme in Chart 6-1 and Figures 6-1 and 6-4. For ²H NMR experiments, the ²H chemical shift was referenced externally to the ²H peak of CD₂Cl₂ (δ(²H) = 5.34 ppm). Commercial reagents were used without further purification. Complexes [PdCl₂(COD)], [Pd(CH₂CMe₂C₆H₄)(COD)], **2-1**, [Pd(CH₂CMe₂C₆H₄)(κ²-*N,N'*-**5-L1**)], **5-1**, and ligands, *N,N*-bis(pyrid-2-ylmethyl)-*N*-(2-hydroxyethyl)amine, **5-L1** and *N,N*-bis(pyrid-2-ylmethyl)-*N*-(2-methoxyethyl)amine, **6-L1**, were synthesized according to the literature procedures.^{20-21,25-29} Elemental analyses were performed by Laboratoire d'Analyse Élémentaire de l'Université de Montréal. Organic products were analyzed using a Shimadzu GCMS-QP2010 Ultra GC with a DB-5 column. Infrared spectra were collected on solid samples using a PerkinElmer UATR TWO FT-IR spectrometer. UV-Visible spectra were collected using an Agilent Technologies Cary 8454 UV-Visible spectrometer. MALDI-TOF mass spectra were collected using an AB Sciex 5800 TOF/TOF mass spectrometer using anthracene as the matrix in a 20:1 matrix:substrate molar ratio.

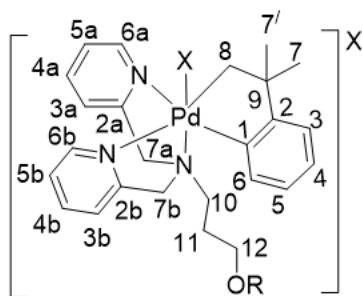


Chart 6-1 NMR labels for Pd(IV) complexes, **6-2**, **6-3**, **6-4** and **6-5**.

6.4.2 Synthesis of $[\text{Pd}^{\text{II}}(\text{CH}_2\text{CMe}_2\text{C}_6\text{H}_4)(\kappa^2\text{-}N,N'\text{-6-L1})]$, **6-1**.

Under N_2 , a solution of 3-methoxy-*N,N*-bis(pyridin-2-ylmethyl)propan-1-amine, **6-L1**, (0.117 g, 0.432 mmol) in dry THF (15 mL) was added to a stirred solution of $[\text{Pd}(\text{CH}_2\text{CMe}_2\text{C}_6\text{H}_4)(\text{COD})]$ (0.150 g, 0.432 mmol) in dry THF (25 mL) cooled to -65°C . The mixture was stirred and slowly warmed to room temperature over 4 h. Upon removal of the solvent under reduced pressure, a brown oil was formed which was washed with hexane (20 mL) and ether (10 mL). The oil was dried under vacuum, to give **6-1** (0.164 g, 0.328 mmol, 76%). ^1H NMR (CD_2Cl_2 , 600MHz, 25°C) δ : 8.45-8.55 (m, 2H, *H6b* and *H6a*), 7.64-7.68 (m, 3H, *H4a*, *H5b* and *H4b*), 7.50-7.53 (m, 1H, *H3a*), 7.21-7.24 (m, 1H, *H5a*), 7.24-7.18 (m, 2H, *H6* and *H3b*), 6.87 (t, 1H, $J = 7$ Hz, *H4*), 6.82 (t, 1H, $J = 7$ Hz, *H5*), 6.74 (d, 1H, $J = 7$ Hz, *H3*), 4.13-4.06 (m, 4H, *H7b* and *H7a*), 3.36 (t, 2H, $J = 6$ Hz, *H12*), 3.22 (s, 3H, OCH_3), 2.79 (t, 2H, $J = 8$ Hz, *H10*), 2.40-2.36 (m, 2H, *H11*), 2.02-1.97 (m, 2H, *H8*), 1.34 (s, 6H, *H7* and *H7'*); ^1H NMR (CD_2Cl_2 , 600MHz, -30°C) δ : 8.63 (d, 1H, $J = 4$ Hz, *H6a*), 8.43 (d, 1H, $J = 4$ Hz, *H6b*), 7.64-7.68 (m, 3H, *H4a*, *H5b* and *H4b*), 7.52 (d, 1H, $J = 7$ Hz, *H3a*), 7.24-7.18 (m, 1H, *H5a*), 7.20-7.17 (m, 2H, *H6* and *H3b*), 6.87 (t, 1H, $J = 7$ Hz, *H4*), 6.82 (t, 1H, $J = 7$ Hz, *H5*), 6.74 (d, 1H, $J = 7$ Hz, *H3*), 4.17-4.06 (m, 4H, *H7a*, *H7b*), 3.36 (t, 2H, $J = 6$ Hz, *H12*), 3.22 (s, 3H, OCH_3), 2.79 (t, 2H, $J = 8$ Hz, *H10*), 2.40-2.38 (m, 2H, *H11*), 2.01-1.97 (m, 2H, *H8*), 1.34 (s, 3H, *H7*), 1.33 (s, 3H, *H7'*); $^{13}\text{C}\{^1\text{H}\}$ NMR (CD_2Cl_2 , 151 MHz, -30°C) δ : 168.31 (C1), 159.56 (C2), 157.70 (C2b), 156.09 (C2a), 149.63 (C6a), 148.89 (C6b), 136.85 (C5b), 136.58 (C4b), 134.59 (C3b), 126.34 (C4a), 125.29 (C3a), 123.88 (C5), 123.28 (C5a), 122.98 (C6), 122.46 (C4), 121.57 (C3), 70.67 (C12), 63.03 (C7b), 62.77 (C7a), 58.34 (OCH_3), 55.44 (C10), 47.36 (C9), 43.84 (C8), 33.74 (C7), 33.17 (C7'), 27.70 (C11). MALDI MS (anthracene matrix): Calcd for $[\text{Pd}(\text{CH}_2\text{CMe}_2\text{C}_6\text{H}_4)\text{6-L1}]^+$: m/z 509.9. Observed: m/z 509.9.

6.4.3 Synthesis of $[\text{Pd}^{\text{IV}}(\text{CH}_2\text{CMe}_2\text{C}_6\text{H}_4)(\kappa^3\text{-}N,N',N''\text{-}5\text{-L1 or -6-L1})(\text{X})]\text{X}$ Complexes, X: I, Br, **6-2**, **6-3**, **6-4** and **6-5**.

6.4.3.1 General Procedure.

Under air, to the solution of $[\text{Pd}^{\text{II}}(\text{CH}_2\text{CMe}_2\text{C}_6\text{H}_4)(\kappa^2\text{-}N,N'\text{-}5\text{-L1})]$, **5-1**, (0.019 g, 0.040 mmol) or $[\text{Pd}^{\text{II}}(\text{CH}_2\text{CMe}_2\text{C}_6\text{H}_4)(\kappa^2\text{-}N,N'\text{-}6\text{-L1})]$, **6-1**, (0.020 g, 0.040 mmol) in chloroform (2 mL) was added the appropriate oxidant (1 equiv) while stirring vigorously. After 5 minutes the solvent was evaporated, and the resulting powder was washed with ether (10 mL) and hexane (5 mL) to remove residual impurities, then dried under reduced pressure. All Pd^{IV} complexes were characterized and then stored as solids at -5°C .

6.4.3.2 Synthesis of $[\text{Pd}^{\text{IV}}(\text{CH}_2\text{CMe}_2\text{C}_6\text{H}_4)(\kappa^3\text{-}N,N',N''\text{-}5\text{-L1})\text{I}][\text{I}]$, **6-2**.

Upon addition of iodine (0.010 g, 0.040 mmol) a color change from light orange to dark red was observed. Yield: 0.023 g, 0.031 mmol, 78%. ^1H NMR (CDCl_3 , 600 MHz, 25°C) δ : 9.38 (d, 1H, $J = 4$ Hz, *H6b*), 9.11 (d, 1H, $J = 4$ Hz, *H6a*), 8.02 (d, 1H, $J = 8$ Hz, *H3b*), 7.88 (d, 1H, $J = 8$ Hz, *H3a*), 7.83 (t, 1H, $J = 7$ Hz, *H4b*), 7.73 (t, 1H, $J = 7$ Hz, *H4a*), 7.33 (t, 1H, $J = 7$ Hz, *H5b*), 7.29 (t, 1H, $J = 7$ Hz, *H5a*), 7.08 (t, 1H, $J = 7$ Hz, *H5*), 6.98 (dd, 1H, $J = 8$ Hz, *H6*), 6.85 (t, $J = 7$ Hz, 1H, *H4*), 6.49 (d, 1H, $J = 8$ Hz, *H3*), 5.49 (d, 1H, $J = 17$ Hz, *H7a*), 5.35 (d, 1H, $J = 16$ Hz, *H7b*), 4.97 (d, 1H, $J = 17$ Hz, *H7a'*), 4.92 (d, 1H, $J = 7$ Hz, *H8*), 4.20 (d, 1H, $J = 16$ Hz, *H7b'*), 3.83-3.79 (m, 1H, *H12*), 3.74 (d, 1H, $J = 7$ Hz, *H8'*), 3.59 (m, 1H, *H10*), 3.45-3.41 (m, 1H, *H12*), 2.70 (br, 1H, *OH*), 2.59-2.54 (m, 1H, *H10*), 2.38-2.34 (m, 1H, *H11*), 2.07-2.02 (m, 1H, *H11*), 1.53 (s, 3H, *H7'*), 1.48 (s, 3H, *H7*); $^{13}\text{C}\{^1\text{H}\}$ NMR (CDCl_3 , 151 MHz, 25°C) δ : 160.19 (C2), 158.07 (C2a), 156.27 (C2b), 147.99 (C6b), 147.83 (C6a), 142.78 (C1), 139.86 (C4b), 139.66 (C4a), 131.57 (C3), 128.18 (C4), 126.98 (C5), 126.63 (C6), 125.60 (C3b), 125.30 (C5b), 124.97 (C5a), 124.45 (C3a), 65.35 (C7a), 65.11 (C7b), 61.91 (C8), 60.04 (C10), 59.72 (C12), 46.89 (C9), 32.20 (C7), 30.48 (C7'), 25.99 (C11). HR ESI-TOF MS: Calcd for $[\text{C}_{25}\text{H}_{31}\text{IN}_3\text{OPd}]^+$: $m/z = 622.0546$. Obsd $m/z = 622.0562$. IR: $\nu(\text{O-H})$ 3103 cm^{-1} . Orange crystals suitable for single-crystal X-ray crystallographic analysis were grown by the slow diffusion of pentane into an acetone solution of **6-2** at room temperature.

6.4.3.3 Synthesis of $[\text{Pd}^{\text{IV}}(\text{CH}_2\text{CMe}_2\text{C}_6\text{H}_4)(\kappa^3\text{-}N,N',N''\text{-}6\text{-L1})\text{I}][\text{I}]$, **6-3**.

Upon addition of iodine (0.010 g, 0.040 mmol) a color change from light orange to dark brown was observed. Yield: 0.026 g, 0.034 mmol, 90%. ^1H NMR (CDCl_3 , 600 MHz, 25°C) δ : 9.31 (d, 1H, $J = 5$ Hz, *H6b*), 9.07 (d, 1H, $J = 5$ Hz, *H6a*), 8.08 (d, 1H, $J = 8$ Hz, *H3b*), 7.84 (d, 1H, $J = 8$ Hz, *H3a*), 7.76

(t, 1H, J (HH) = 8 Hz, $H4b$), 7.68 (t, 1H, J = 8 Hz, $H4a$), 7.27 (dd, 1H, J = 5 Hz, 8 Hz, $H5b$), 7.24-7.19 (m, 1H, $H5a$), 7.06 (t, 1H, J = 7 Hz, $H5$), 6.96 (d, 1H, J = 7 Hz, $H6$), 6.83 (t, 1H, J = 7 Hz, $H4$), 6.53 (d, 1H, J = 7 Hz, $H3$), 5.85 (d, 1H, J = 17 Hz, $H7a'$), 5.62 (d, 1H, J = 15 Hz, $H7b'$), 4.93 (d, 1H, J = 7 Hz, $H8'$), 4.53 (d, 1H, J = 17 Hz, $H7a$), 4.08 (d, 1H, J = 15 Hz, $H7b$), 3.62 (d, J = 7 Hz, 1H, $H8$), 3.43 (m, 1H, $H12$), 3.36-3.32 (m, 1H, $H10$), 3.17 (s, 3H, OCH_3), 3.18-3.13 (m, 1H, $H12'$), 2.43-2.39 (m, 1H, $H11$), 2.26-2.23 (m, 1H, $H10'$), 2.06-2.01 (m, 1H, $H11'$), 1.48 (s, 3H, $H7'$), 1.47 (s, 3H, $H7$); $^{13}C\{^1H\}$ NMR ($CDCl_3$, 151 MHz, 25°C) δ : 160.04 (C2), 157.79 (C2a), 156.32 (C2b), 147.72 (C6b), 147.60 (C6a), 143.07 (C1), 139.84 (C4b), 139.69 (C4a), 131.59 (C3), 128.18 (C4), 126.90 (C5), 126.51 (C6), 125.23 (C5b,C3b), 124.93 (C5a), 124.52 (C3a), 69.70 (C12), 65.09 (C7a), 64.82 (C7b), 61.23 (C10 and C8), 58.48 (OCH_3), 46.75 (C9), 32.23 (C7), 30.01 (C7'), 23.03 (C11). HR ESI-TOF MS: Calcd for $[C_{26}H_{33}IN_3OPd]^+$: m/z = 636.0703. Obsd m/z = 636.0729. IR ν (methyl in O- CH_3) 2912 cm^{-1} .

6.4.3.4 Synthesis of $[Pd^{IV}(CH_2CMe_2C_6H_4)(\kappa^3-N,N',N''-6-L1)I][BF_4]$, **6-3a**.

Upon addition of bis(pyridine)iodonium(I) tetrafluoroborate (0.014 g, 0.040 mmol), in dark, a color change from light orange to dark brown was observed. (0.024 g, 0.033 mmol, 80%). 1H NMR ($CDCl_3$, 600 MHz, 25°C) δ : 9.34 (d, 1H, J = 5 Hz, $H6b$), 9.09 (d, 1H, J = 5 Hz, $H6a$), 7.81-2.78 (m, 1H, $H3b$), 7.73 (d, 1H, J = 8 Hz, $H3a$), 7.60 (d, 1H, J = 8 Hz, $H4b$), 7.75-7.70 (m, 1H, $H4a$), 7.25-7.20 (m, 1H, $H5b$), 7.19-7.14 (m, 1H, $H5a$), 7.08 (d, 1H, J = 7 Hz, $H5$), 6.99 (d, J = 7 Hz, $H6$), 6.85 (t, 1H, J = 7 Hz, $H4$), 6.53 (d, 1H, J = 7 Hz, $H3$), 4.94 (d, 1H, J = 17 Hz, $H7a$), 4.77 (d, 1H, J = 15 Hz, $H7b$), 4.61 (d, 1H, J = 7 Hz, $H8$), 4.22 (d, 1H, J = 17 Hz, $H7a$), 3.65 (d, 1H, J = 15 Hz, $H7b$), 3.46 (d, J = 7 Hz, 1H, $H8'$), 3.42-3.39 (m, 1H, $H12$), 3.37-3.33 (m, 1H, $H10$), 3.18 (s, 3H, OCH_3), 3.17-3.14 (m, 1H, $H12$), 2.30-2.27 (m, 1H, $H11$), 2.26-2.22 (m, 1H, $H10$), 1.98-1.94 (m, 1H, $H11$), 1.50 (s, 3H, $H7'$), 1.49 (s, 3H, $H7$); ^{19}F NMR ($CDCl_3$, 564, 25°C) δ : -151.23. HR ESI-TOF MS: Calcd for $[C_{25}H_{31}IN_3OPd]^+$: m/z = 636.0703. Obsd m/z = 636.0562.

6.4.3.5 Synthesis of $[Pd^{IV}(CH_2CMe_2C_6H_4)(\kappa^3-N,N',N''-5-L1)Br][Br]$, **6-4**.

Upon addition of bromine (2.06 μ L, 0.040 mmol), an immediate color change from orange to light green was observed. (0.022 mg, 0.034 mmol, 85%). 1H NMR ($CDCl_3$, 600MHz, 25°C) δ : 9.04 (d, 1H, J = 4 Hz, $H6b$), 8.85 (d, 1H, J = 4 Hz, $H6a$), 7.94 (d, 1H, J = 8 Hz, $H3b$), 7.79-7.77 (m, 1H, $H3a$), 7.76-7.74 (m, 1H, $H4b$), 7.68 (t, 1H, J = 7 Hz, $H4a$), 7.30-7.28 (m, 1H, $H5b$), 7.21-7.19 (m, 1H, $H5a$), 7.07-7.04 (m, 1H, $H5$), 6.96 (d, 1H, J = 7 Hz, $H6$), 6.83 (t, 1H, J = 8 Hz, $H4$), 6.50 (d, 1H, J = 8 Hz, $H3$), 5.52 (d, 1H, J = 17 Hz, $H7a$), 5.47 (d, 1H, J = 16 Hz, $H7b$), 5.14 (d, 1H, J = 17 Hz, $H7a'$), 4.77 (d, 1H, J = 7

Hz, H8), (d, 1H, $J = 16$ Hz, $H7b'$), 4.03 (d, 1H, $J = 7$ Hz, $H8'$), 3.67-3.62 (m, 1H, $H10$), 3.70-3.66 (m, 1H, $H12$), 3.34-3.31 (m, 1H, $H12'$), 2.56-2.53 (m, 1H, $H11$), 2.39-2.36 (m, 1H, $H10'$), 2.07-2.03 (m, 1H, $H11'$), 1.51 (s, 3H, $H7'$), 1.48 (s, 1H, $H7$); $^{13}\text{C}\{^1\text{H}\}$ NMR (CDCl_3 , 151 MHz, 25°C) δ : 158.79 (C1), 157.92 (C2b), 156.06 (C2a), 149.86 (C2), 146.73 (C6b), 146.46 (C6a), 139.95 (C4b), 139.81 (C4a), 129.48 (C3), 128.32 (C4), 126.93 (C6), 126.83 (C5), 125.02 (C5b), 124.95 (C3b), 124.55 (C5a), 124.03 (C3a), 67.73 (C8), 66.60 (C7a), 66.43 (C7b), 61.47 (C12), 59.51 (C10), 47.32 (C9), 33.10 (C7), 33.20 (C7'), 26.47 (C11). HR ESI-TOF MS: Calcd for $[\text{C}_{25}\text{H}_{31}\text{BrN}_3\text{OPd}]^+$: $m/z = 574.0685$. Obsd $m/z = 574.0706$. IR: $\nu(\text{O-H})$ 3103 cm^{-1} . IR: $\nu(\text{O-H})$ 3361 cm^{-1} . Clear crystals suitable for single-crystal X-ray crystallographic analysis were grown by the slow diffusion of acetone into an acetonitrile solution of **6-4** at -15°C.

6.4.3.6 Synthesis of $[\text{Pd}^{\text{IV}}(\text{CH}_2\text{CMe}_2\text{C}_6\text{H}_4)(\kappa^3\text{-N,N',N''-6-L1})\text{Br}][\text{Br}]$, **6-5**.

Upon addition of bromine (2.06 μL , 0.040 mmol), an immediate color change from orange to green was observed. (0.021 mg, 0.031 mmol, 80%). ^1H NMR (CD_2Cl_2 , 600MHz, -8°C) δ : 9.04 (d, 1H, $J = 4$ Hz, $H6b$), 8.86 (d, 1H, $J = 4$ Hz, $H6a$), 7.91 (d, 1H, $J = 8$ Hz, $H3b$), 7.82-7.79 (m, 1H, $H3a$), 7.75-7.72 (m, 1H, $H4b$), 7.39-7.354 (m, 1H, $H4a$), 7.26-7.23 (m, 1H, $H5b$), 7.17-7.15 (m, 1H, $H5a$), 7.14-7.11 (m, 1H, $H5$), 7.03 (d, 1H, $J = 8$ Hz, $H6$), 6.90 (t, 1H, $J = 8$ Hz, $H4$), 6.62 (d, 1H, $J = 8$ Hz, $H3$), 5.93 (d, 1H, $J = 17$ Hz, $H7a$), 5.74 (d, 1H, $J = 16$ Hz, $H7b$), 4.65 (d, 1H, $J = 17$ Hz, $H7a'$), 4.80 (d, 1H, $J = 6$ Hz, H8), 4.25 (d, 1H, $J = 16$ Hz, $H7b'$), 3.88 (d, 1H, $J = 6$ Hz, $H8'$), 3.46-3.42 (m, 1H, $H10$), 3.40-3.37 (m, 1H, $H12$), 3.31-3.27 (m, 1H, $H12$), 3.17 (s, 3H, OCH_3), 2.33-2.37 (m, 2H, $H11, H10$), 2.07-2.02 (m, 1H, $H11$), 1.51 (s, 3H, $H7'$), 1.50 (s, 3H, $H7$); $^{13}\text{C}\{^1\text{H}\}$ NMR (CD_2Cl_2 , 600MHz, -8°C) δ : 158.72 (C1), 157.30 (C2b), 155.91 (C2a), 150.19 (C2), 146.67 (C6b), 146.65 (C6a), 139.97 (C4b), 139.98 (C4a), 129.71 (C3), 128.57 (C4), 127.89 (C6), 126.83 (C5), 125.21 (C5b), 125.85 (C5a), 124.90 (C3b), 123.92 (C3a), 69.64 (C12), 66.89 (C8), 66.21 (C7a), 66.02 (C7b), 62.49 (C10), , 58.48 (OCH_3), 47.12 (C9), 32.83 (C7), 28.86 (C7'), 23.42 (C11). HR ESI-TOF MS: Calcd for $[\text{C}_{26}\text{H}_{33}\text{BrN}_3\text{OPd}]^+$: $m/z = 588.0841$. Obsd $m/z = 588.0468$. IR $\nu(\text{methyl in O-CH}_3)$ 2894 cm^{-1} .

6.4.4 Thermolysis Reactions from Pd(IV) Complexes:

6.4.4.1 General Synthesis of $[\text{Pd}^{\text{II}}(\kappa^3\text{-N,N',N''-5-L1 or -6-L1})(\text{X})]\text{X}$ Complexes, X: I, Br, **6-6**, **6-7**, **6-8** and **6-9**.

A solution of a Pd(IV) complex **6-2**, **6-3**, **6-4** or **6-5** (0.070 mmol) was dissolved in CHCl_3 (4 mL) and heated at 50°C in an oil bath for 7.5 h. The solvent was removed under reduced pressure and the residue

was washed with ether (3 × 5 mL) and hexane (3 × 5 mL), then dried under vacuum (Thermolysis of complex **6-3a** was conducted following the same procedure, except heated at 50°C for 60 h).

6.4.4.2 General Procedure for the Analysis of Organic Products from Thermolysis

To a solution of a Pd(IV) complex **6-2**, **6-3**, **6-4** and **6-5** (0.070 mmol) in CDCl₃ (2 mL), was added 1,3,5-trimethoxybenzene as internal standard (0.023 mmol). A ¹H NMR spectrum was collected of the solution. The solution was stirred at 50°C for 7.5 h. (except for **6-3a** that was stirred for 72 h). Then solutions were monitored by ¹H and ¹H-¹H gCOSY NMR spectroscopy to identify and quantified the organics and calculate their yields relative to the internal standard. In order to isolate the organics, the solutions were filtered through a plug of silica to separate the metal complexes, the silica was washed with CHCl₃ (3 × 5 mL) and the solvents were evaporated by rotary evaporation. The organic products were then dissolved in chloroform for analysis by GC-MS.

6.4.5 Synthesis of [Pd^{II}(κ³-N,N',N''-**5-L1**)I][I], **6-6**.

A chloroform solution of **6-2** (0.042 g, 0.070 mmol) was dissolved in chloroform and heated to form **6-6** (0.036 g, 0.058 mmol, 87%). ¹H NMR (CDCl₃:CD₃OD, 600MHz, 25°C) δ: 9.28 (d, 2H, *J* = 5 Hz, *H6a*), 7.96 (m, 2H, *H4a*), 7.74 (d, 2H, *J* = 7 Hz, *H3a*), 7.31 (t, 2H, *J* = 6 Hz, *H5a*), 5.24 (d, 2H, *J* = 16 Hz, *H7a*), 4.89 (d, 2H, *J* = 16 Hz, *H7a'*), 3.49-3.45 (m, 2H, *H10*), 3.21-3.16 (m, 2H, *H12*), 1.87-1.83 (m, 2H, *H11*); ¹³C{¹H} NMR (CDCl₃:CD₃OD, 1:0.3, 151 MHz, 25°C) δ: 164.74 (C2a), 156.47 (C6a), 140.77 (C4a), 125.61 (C3a), 123.85 (C5a), 67.89 (C7a, C7a'), 60.21 (C12), 58.55 (C10), 30.18 (C11). HR ESI-TOF MS: Calcd for [C₁₅H₁₉IN₃OPd]⁺: m/z = 489.960. Obsd m/z = 489.958. Anal. Calcd for C₁₅H₁₉I₂N₃OPd: C, 29.17; H, 3.10; N, 6.80. Found: C, 29.10; H, 3.05; N 6.59 %. *Organic release step*: 1-Iodo-2-methyl-2-phenylpropane (**IP**): Yield 37%. ¹H NMR (CDCl₃, 600 MHz, 25°C) δ: 7.27-7.33 (m, 5H, C₆H₅), 3.43 (s, 2H, CH₂), 1.50 (s, 6H, 2CH₃).¹⁸ LR-MS: Calcd for C₁₀H₁₃I: m/z = 260.12. Found: m/z = 260.15. (2-Iodo-2-methylpropyl)benzene (**IB**): Yield 28%. ¹H NMR (CDCl₃, 600 MHz, 25°C) δ: 7.21-7.35 (m, 5H, C₆H₅), 3.22 (s, 2H, CH₂), 1.96 (s, 6H, 2CH₃).⁴⁹ LR-MS: Calcd for C₁₀H₁₃I: m/z = 260.12. Found: m/z = 260.10. (2-Methylprop-1-en-1yl)benzene (**MB**): Yield 20%. ¹H NMR (CDCl₃, 600 MHz, 25°C) δ: 7.27-7.35 (m, 2H, C₆H₅), 7.14-7.24 (m, 3H, C₆H₅), 6.27 (s, 1H, Ph-CH=), 1.90 (s, 3H, CH₃), 1.86 (s, 3H, CH₃).⁵⁰ LR-MS: Calcd for C₁₀H₁₂: m/z = 132.21. Found: m/z = 132.20. Dimethyl-1,2-dihydrocyclobutabenzene (**CB**): Yield 5%. ¹H NMR (CDCl₃, 600 MHz, 25°C) δ: 8.01 (m, 1H, C₆H₄), 7.17 (m, 1H, C₆H₄), 7.07 (m, 1H, C₆H₄), 7.01 (m, 1H, C₆H₄), 2.99 (s, 2H, CH₂), 1.46 (s, 6H, Me).^{15,25} LR-MS: Calcd for C₁₀H₁₂: m/z = 132.21. Found: m/z = 132.20.

6.4.6 Synthesis of [Pd^{II}(κ³-N,N',N''-6-L1)I][I], **6-7**.

A chloroform solution of **6-3** (0.044 g, 0.070 mmol) was dissolved in chloroform and heated to form **6-7** (0.040 g, 0.061 mmol, 91%). ¹H NMR (CDCl₃, 600 MHz, 25°C) δ: 9.32 (d, 2H, *J* = 5 Hz, *H6a*), 7.98-7.95 (m, 2H, *H5a*), 7.90 (d, 2H, *J* = 8 Hz, *H3a*), 7.32 (t, 2H, *J* = 7 Hz, *H4a*), 5.62 (d, 2H, *J* = 16 Hz, *H7a*), 5.45 (d, 2H, *J* = 16 Hz, *H7a'*), 3.39-3.43 (m, 4H, *H12*, *H10*), 3.23 (s, 3H, CH₃), 2.00-2.05 (m, 2H, *H11*); ¹³C{¹H} NMR (CDCl₃, 151 MHz, 25°C) δ: 165.15 (C2a), 156.53 (C6a), 140.95 (C5a), 125.60 (C4a), 124.24 (C3a), 69.17 (C7a, C7a'), 69.08 (C12), 60.82 (C10), 58.77 (CH₃), 28.50 (C11). HR ESI-TOF MS: Calcd for [C₁₆H₂₁IN₃OPd]⁺: *m/z* = 503.9764. Obsd *m/z* = 503.9658. Anal. Calcd for C₁₆H₂₁I₂N₃OPd: C, 30.43; H, 3.35; N, 6.65. Found: C, 30.57; H, 3.73; N 6.48. Orange crystals suitable for single-crystal X-ray crystallographic analysis were grown by the slow diffusion of pentane into a dichloromethane solution of **6-7** at room temperature. *Organic release step*: **MB**: 48%. **IP**: 25%. **IB**: 8%. **CB**: 5%.

6.4.7 Synthesis of [Pd^{II}(κ³-N,N',N''-6-L1)I][BF₄], **6-7a**.

A chloroform solution of **6-3a** (0.050, 0.070 mmol) was dissolved in chloroform and heated for 60 h to form **6-7a** (0.034 g, 0.058 mmol, 80%). ¹H NMR (CDCl₃, 600 MHz, 25°C) δ: 9.30 (d, 2H, *J* = 5 Hz, *H6a*), 8.01-7.96 (m, 2H, *H5a*), 7.71 (d, 2H, *J* = 8 Hz, *H3a*), 7.34 (t, 2H, *J* = 8 Hz, *H4a*), 5.30 (d, 2H, *J* = 16 Hz, *H7a*), 4.66 (d, 2H, *J* = 16 Hz, *H7a'*), 3.34-3.39 (m, 2H, *H12*), 3.18 (s, 3H, CH₃), 3.13-3.15 (m, 2H, *H10*), 2.00-2.05 (m, 2H, *H11*); ¹³C{¹H} NMR (CDCl₃, 151 MHz, 25°C) δ: 165.15 (C2a), 156.53 (C6a), 140.95 (C5a), 125.60 (C4a), 124.24 (C3a), 69.17 (C7a), 69.08 (C12), 60.82 (C10), 58.77 (CH₃), 28.50 (C11). HR ESI-TOF MS: Calcd for [C₁₆H₂₁IN₃OPd]⁺: *m/z* = 503.9764. Obsd *m/z* = 503.9658. *Organic release step*: **IP**: 13%. **MB**: 25%. **CB**: 30%.

6.4.8 Synthesis of [Pd^{II}(κ³-N,N',N''-5-L1)Br][Br], **6-8**.

A chloroform solution of **6-4** (0.040 g, 0.070 mmol) was dissolved in chloroform and heated to form **6-8** (0.031 g, 0.059 mmol, 90%). ¹H NMR ((CD₃)₂SO, 600 MHz, 25°C) δ: 8.86 (d, 2H, *J* = 5 Hz, *H6a*), 8.27-8.23 (m, 2H, *H4a*), 7.78 (d, 2H, *J* = 8 Hz, *H3a*), 7.67 (t, 2H, *J* = 7 Hz, *H5a*), 5.06 (d, 2H, *J* = 16 Hz, *H7a*), 4.56 (d, 2H, *J* = 16 Hz, *H7a'*), 3.39 (t, 2H, *J* = 6 Hz, *H12*), 3.13-3.10 (m, 2H, *H10*), 1.77-1.72 (m, 2H, *H11*). ¹³C{¹H} NMR ((CD₃)₂SO, 151 MHz, 25°C) 165.21 (C2a), 152.03 (C6a), 141.50 (C4a), 125.38 (C5a), 123.42 (C3a), 66.94 (C7a, C7a'), 60.55 (C10), 57.82 (C12), 30.83 (C11). HR ESI-TOF MS: Calcd for [C₁₅H₁₉BrN₃OPd]⁺: *m/z* = 441.9746. Obsd *m/z* = 441.9732. Yellow crystals suitable for single-crystal X-ray crystallographic analysis were grown by the slow diffusion of cyclohexane into a

chloroform solution of **6-4** at room temperature. *Organic release step*: 1-Bromo-2-methyl-2-phenylpropane (**BP**): 50%. ^1H NMR for **BP** (CDCl_3): $\delta(^1\text{H})$ 7.27-7.33 (m, 5H, C_6H_5), 3.59 (s, 2H, CH_2), 1.48 (s, 6H, 2CH_3). ^{13}C MS: Calcd for $\text{C}_{10}\text{H}_{13}\text{Br}$: $m/z = 213.12$. Found: $m/z = 213.15$. **CB**: 28%. **MB**: 9%.

6.4.9 Synthesis of $[\text{Pd}^{\text{II}}(\kappa^3\text{-N,N',N''-6-L1})\text{Br}][\text{Br}]$, **6-9**.

A chloroform solution of **6-5** (0.040 g, 0.070 mmol) was heated to form **6-9** (0.038 g, 0.056 mmol, 84%). ^1H NMR ($(\text{CD}_3)_2\text{SO}$, 600 MHz, 25°C) 8.80 (d, 2H, $J = 5$ Hz, $H6a$), 8.21-8.16 (m, 2H, $H4a$), 7.74 (d, 2H, $J = 8$ Hz, $H3a$), 7.62 (t, 2H, $J = 7$ Hz, $H5a$), 5.51 (d, 2H, $J = 16$ Hz, $H7a$), 4.50 (d, 2H, $J = 16$ Hz, $H7a'$), 3.11 (s, 3H, OCH_3), 2.67-2.70 (m, 2H, $H12$), 2.34-2.30 (m, 2H, $H10$), 1.49-1.45 (m, 2H, $H11$). HR ESI-TOF MS: Calcd for $[\text{C}_{16}\text{H}_{21}\text{BrN}_3\text{OPd}]^+$: $m/z = 455.9902$. Obsd $m/z = 455.9732$. Anal. Calcd for $\text{C}_{16}\text{H}_{21}\text{Br}_2\text{N}_3\text{OPd}$: C, 35.75; H, 3.94; N, 7.82. Found: C, 35.81; H, 4.01; N 7.59. Yellow crystals suitable for single-crystal X-ray crystallographic analysis were grown by the slow diffusion of cyclohexane into a dichloromethane solution of **6-5** at room temperature. *Organic release step*: **BP**: 24%. **CB**: 10%. **MB**: 50%.

6.4.10 Synthesis of $[\text{Pd}^{\text{IV}}(\text{CH}_2\text{CMe}_2\text{C}_6\text{H}_4)(\kappa^3\text{-N,N',N''-5-L1})\text{Me}][\text{I}]$, **6-10**.

An NMR tube containing a CD_2Cl_2 solution (1.5 mL) of $[\text{Pd}^{\text{II}}(\text{CH}_2\text{CMe}_2\text{C}_6\text{H}_4)(\kappa^2\text{-N,N''-5-L1})]$ (0.028 g, 0.056 mmol) was inserted into the NMR instrument and the probe was cooled to -30°C . The NMR tube was ejected, pre-cooled (-5°C) CD_3I (10.5 μL , 0.169 mmol, 3 eq) was added to it, and the tube was re-inserted into the probe. The temperature was slowly increased to -10°C when reaction to give **6-10** was complete. ^1H NMR (CD_2Cl_2 , 600 MHz, -10°C) 8.50 (d, 1H, $J = 6$ Hz, $H6b$), 8.32 (d, 1H, $J = 6$ Hz, $H6a$), 7.93 (t, 1H, $J = 8$ Hz, $H4b$), 7.81-7.75 (m, 1H, $H4a$), 7.70 (m, 2H, $H3a$ and $H3b$), 7.48 (dd, 1H, $J = 8$ Hz, 6 Hz, $H5b$), 7.40 (dd, 1H, $J = 8$ Hz, 6 Hz, $H5a$), 7.01 (t, 1H, $J = 7$ Hz, $H5$), 6.84 (d, 1H, $J = 7$ Hz, $H6$), 6.74 (t, 1H, $J = 7$ Hz, $H4$), 6.08 (d, $J = 7$ Hz, 1H, $H3$), 4.82 (d, 1H, $J = 17$ Hz, $H7a$), 4.48 (d, 1H, $J = 16$ Hz, $H7b$), 4.19 (d, 1H, $J = 17$ Hz, $H7a'$), 4.13 (d, 1H, $J = 16$ Hz, $H7b'$), 3.64-3.60 (m, 1H, $H12$), 3.30 (m, 1H, $H12$), 3.27 (m, 1H, $H8$), 3.05 (d, 1H, $J = 9$ Hz, $H8'$), 2.74 (m, 1H, $H10$), 2.63 (m, 1H, $H10$), 1.81-1.76 (m, 1H, $H11$), 1.57-1.51 (m, 1H, $H11'$), 1.32 (s, 3H, $H7$), 1.27 (s, 3H, $H7'$). An analogous experiment was done, except for adding CH_3I instead of CD_3I to characterize the Pd- CH_3 chemical shift: ^1H NMR (CD_2Cl_2 , 600 MHz, -10°C) 1.91 (s, 3H, Pd- CH_3). Reductive elimination to give **6-12** was observed at temperatures higher than 0°C .

6.4.11 Synthesis of $[\text{Pd}^{\text{IV}}(\text{CH}_2\text{CMe}_2\text{C}_6\text{H}_4)(\kappa^3\text{-}N,N',N''\text{-6-L1})\text{Me}][\text{I}]$, **6-11**.

Complex **6-11** was made and characterized in an analogous manner as complex **6-10**. ^1H NMR (CD_2Cl_2 , 600 MHz, -10°C) 8.48 (d, 1H, $J = 5$ Hz, $H6b$), 8.34 (d, 1H, $J = 5$ Hz, $H6a$), 7.93 (t, 1H, $J = 7$ Hz, $H4b$), 7.80-7.75 (m, 1H, $H4a$), 7.65-7.71 (m, 2H, $H3a, H3b$), 7.48-7.42 (m, 1H, $H5b$), 7.41 (dd, 1H, $J = 6$ Hz, 8 Hz, $H5a$), 7.05 (t, 1H, $J = 7$ Hz, $H5$), 6.88 (d, 1H, $J = 7$ Hz, $H6$), 6.76-6.72 (m, 1H, $H4$), 6.21 (d, $J = 8$ Hz, 1H, $H3$), 4.78 (d, 1H, $J = 16$ Hz, $H7a$), 4.61 (d, 1H, $J = 16$ Hz, $H7b$), 4.49 (d, 1H, $J = 16$ Hz, $H7a'$), 4.40 (d, 1H, $J = 16$ Hz, $H7b'$), 3.50-3.54 (m, 1H, $H12$), 3.30-3.32 (m, 1H, $H12'$), 3.29-3.25 (m, 1H, $H8$), 3.14 (d, 1H, $J = 9$ Hz, $H8'$), 2.75-2.70 (m, 1H, $H10$), 2.66-2.62 (m, 1H, $H10'$), 1.85-1.80 (m, 1H, $H11$), 1.47-1.50 (m, 1H, $H11'$), 1.34 (s, 3H, $H7$), 1.31 (s, 3H, $H7'$). An analogous experiment was done, except for adding CH_3I instead of CD_3I to characterize the Pd- CH_3 chemical shift: ^1H NMR (CD_2Cl_2 , 600 MHz, -10°C) 1.95 (s, 3H, Pd- CH_3). Reduction of Pd(IV) was observed at temperatures higher than 0°C .

6.4.12 Synthesis of $[\text{Pd}^{\text{II}}(\text{CH}_2\text{CMe}_2\text{C}_6\text{H}_4\text{-CH}_3)(\kappa^2\text{-}N,N'\text{-5-L1})][\text{I}]$, **6-12**.

To a solution of $[\text{Pd}^{\text{II}}(\text{CH}_2\text{CMe}_2\text{C}_6\text{H}_4)(\kappa^2\text{-}N,N'\text{-5-L1})]$ (0.028 g, 0.056 mmol) in dichloromethane (2 mL) was added excess MeI (10.5 μL , 0.169 mmol, 3 eq) whilst stirring. An immediate color change from orange to deep brown was observed. After the solvent was removed under reduced pressure, the orange product was washed with pentane (3×2 mL) and ether (3×2 mL) and dried on high vacuum (0.027 g, 0.043 mmol, 78%). ^1H NMR (CD_2Cl_2 , 600 MHz, 25°C) 8.26 (d, 2H, $J = 5$ Hz, $H6a$), 7.88 (t, 2H, $J = 7$ Hz, $H4a$), 7.61 (d, 2H, $J = 7$ Hz, $H3a$), 7.51 (d, 2H, $J = 8$ Hz, $H3$), 7.32 (t, 1H, $J = 5$ Hz, 7 Hz, $H5a$), 6.95-6.90 (m, 1H, $H4$), 6.77-6.72 (m, 2H, $H6$ and $H5$), 4.65 (d, 2H, $J = 15$ Hz, $H7a$), 4.50 (d, 2H, $J = 15$ Hz, $H7a'$), 3.37 (t, 2H, $J = 5$ Hz, $H12$), 2.82-2.78 (m, 2H, $H10$), 2.66 (s, 3H, CH_3), 2.23 (s, 2H, $H8$), 1.66-1.61 (m, 2H, $H11$), 1.57 (s, 6H, $H7$); $^{13}\text{C}\{^1\text{H}\}$ NMR (CD_2Cl_2 , 151 MHz, 25°C) 177.5 (C1), 163.93 (C2a), 149.29 (C6a), 148.20 (C2), 139.40 (C4a), 135.72 (C1), 132.64 (C5), 125.62 (C3), 125.60 (C6), 124.19 (C5a), 124.05 (C3a), 63.66 (C7a), 59.00 (C12), 54.53 (C10), 44.95 (C9), 43.56 (C8), 32.68 (C7), 29.4 (C11), 24.67 (CH_3). HR ESI-TOF MS: Calcd for $[\text{C}_{26}\text{H}_{34}\text{N}_3\text{OPd}]^+$: $m/z = 510.1736$. Obsd $m/z = 510.1946$. IR: $\nu(\text{O-H})$ 3337 cm^{-1} . For the sample used for the ^2H NMR experiment, CD_3I was used instead of CH_3I , while the rest of the reaction conditions were unchanged. ^2H NMR (CH_2Cl_2 , 600 MHz, 25°C): δ 2.66 (br, CD_3).

6.4.13 Synthesis of $[\text{Pd}^{\text{II}}(\text{CH}_2\text{CMe}_2\text{C}_6\text{H}_4\text{-CH}_3)(\kappa^3\text{-N,N',N''-6-L1})][\text{I}]$, **6-13**.

Complex **6-13** was made in an analogous manner as complex **6-12** in 89% yield (0.032 g, 0.049 mmol). ^1H NMR (CD_2Cl_2 , 600 MHz, 25°C) 8.25 (d, 2H, $J = 5$ Hz, $H6a$), 7.89 (t, 2H, $J = 7$ Hz, $H4a$), 7.56 (d, 2H, $J = 7$ Hz, $H3a$), 7.53 (d, 1H, $J = 8$ Hz, $H3$), 7.32 (dd, 2H, $J = 5$ Hz, 7 Hz, $H5a$), 6.95-6.91 (m, 1H, $H4$), 6.76-6.72 (m, 2H, $H6$ and $H5$), 4.83 (d, 2H, $J = 15$ Hz, $H7a$), 4.48 (d, 2H, $J = 15$ Hz, $H7a'$), 3.17 (t, 2H, $J = 6$ Hz, $H12$), 3.10 (s, 3H, OCH_3), 2.76 (t, 2H, $J = 8$ Hz, $H10$), 2.66 (s, 3H, OCH_3), 2.25 (s, 2H, $H8$), 1.81 (br, 2H, $H11$), 1.57 (s, 6H, $H7,7'$); $^{13}\text{C}\{^1\text{H}\}$ NMR (CD_2Cl_2 , 151 MHz, 25°C) 164.06 (C1), 149.31 (C2a), 148.13 (C6a), 139.48 (C2), 135.73 (C4a), 132.68 (C1), 125.75 (C5 and C3), 124.24 (C6), 123.80 (C5a), 69.58 (C3a), 64.42 (C7a), 58.33 (C12), 55.48 (C10), 43.62 (C9), 40.75 (C8, $C8'$), 32.74 ($C7, C7'$), 27.50 (C11). ^2H experiment: ^2H NMR (CH_2Cl_2 , 600 MHz, 25°C) 3.10 (br, DX). HR ESI-TOF MS: Calcd for $[\text{C}_{27}\text{H}_{36}\text{N}_3\text{OPd}]^+$: $m/z = 524.1893$. Obsd $m/z = 524.1945$. Anal. Calcd for $\text{C}_{27}\text{H}_{36}\text{IN}_3\text{OPd}$: C, 49.74; H, 5.56; N, 6.44. Found: C, 49.91; H, 5.28; N 6.23. IR: $\nu(\text{methyl in O-CH}_3)$ 2868 cm^{-1} .

6.4.14 UV-Visible Studies

Complex **6-2** (0.017 g, 0.023 mmol) was dissolved in chloroform (2.8 mL) to give an 8.33×10^{-3} M solution. This solution was placed into a 4 mL cuvette (optical path length 1 cm) at room temperature then heated to 50°C . A UV-vis spectrum was recorded every 15 minutes for 7.5 hours. The experiment was repeated twice to confirm the reproducibility. The observed rate constant, k_{obs} , was calculated by measuring the slope of the linear relationship between $\ln[A-A_\infty]/[A_0-A_\infty]$ and time, for the first 2 h of heating (Table 6-2 and Figure 6-6). Data for **6-3**, **6-4** and **6-5**, and in solvents methanol or benzene were obtained in a similar way. For studying the effect of free pyridine or sodium iodide on the rate, a solution in methanol of complex **6-2** (8.33×10^{-3} M) and pyridine or NaI (8.33×10^{-2} M) was prepared, and the rate of reductive elimination was determined as above (see Appendix A6).

6.4.15 X-Ray Structure Determinations.⁵¹⁻⁵⁴

Data Collection and Processing. A crystal was mounted on a Mitegen polyimide micromount with a small amount of Paratone N oil. All X-ray measurements were made using a Bruker Kappa Axis Apex2 diffractometer at a temperature of 110 K. The frame integration was performed using SAINT, and the resulting raw data was scaled and absorption corrected using a multiscan averaging of symmetry equivalent data using SADABS.

Structure Solution and Refinement. The structures were solved by using the SHELXT program. All non-hydrogen atoms were obtained from the initial solution. The hydrogen atoms were introduced at idealized positions and were allowed to ride on the parent atom. The structural model was fit to the data using full matrix least-squares based on F2. The calculated structure factors included corrections for anomalous dispersion from the usual tabulation. The structure was refined using the SHELXL-2014 program from the SHELX suite of crystallographic software.⁵¹⁻⁵⁴ Details are given in Table A6.1-A6.14.

6.5 References

1. P. Sehnal, R. J. K. Taylor and I. J. S. Fairlamb, *Chem. Rev.*, 2010, **110**, 824-889.
2. G. Yin, X. Mu and G. Liu, *Acc. Chem. Res.*, 2016, **49**, 2413-2423.
3. D. A. Petrone, J. T. Ye and M. Lautens, *Chem. Rev.*, 2016, **116**, 8003-8104.
4. R. Giri, X. Chen and J. -Q. Yu, *Angew. Chem. Int. Ed.*, 2005, **44**, 2112-2115.
5. M. -J. Zhou, T. -L. Yang and L. Dang, *J. Org. Chem.*, 2016, **81**, 1006-1020.
6. A. J. Canty, *Acc. Chem. Res.*, 1992, **25**, 83-90.
7. J. Cámpora, P. Palma and E. Carmona, *Coord. Chem. Rev.* 1999, **193**, 207-281.
8. A. J. Canty and G. van Koten, *Acc. Chem. Res.*, 1995, **28**, 406-413.
9. A. Vigalok, *Acc. Chem. Res.*, 2015, **28**, 238-247.
10. A. J. Canty, *Dalton Trans.*, 2009, 10409-10417.
11. L. -M. Xu, B. -J. Li, Z. Yang and Z. -J. Shi, *Chem. Soc. Rev.*, 2010, **39**, 712-733.
12. J. M. Racowski and M. S. Sanford, *Top. Organomet. Chem.*, 2011, **35**, 61-84.
13. K. J. Bonney and F. Schoenebeck, *Chem. Soc. Rev.* 2014, **43**, 6609-6638.
14. A. V. Sberegaeva, D. Watts and A. N. Vedernikov, *Adv. Organomet. Chem.* 2017, **67**, 221-297.
15. M. H. Pérez-Temprano, J. M. Racowski, W. J. Kampf and M. S. Sanford, *J. Am. Chem. Soc.*, 2014, **136**, 4097-4100.
16. I. M. Pendleton, M. H. Pérez-Temprano, M. S. Sanford and P. M. Zimmerman, *J. Am. Chem. Soc.*, 2016, **138**, 6049-6060.
17. J. M. Racowski, J. B. Gary and M. S. Sanford, *Angew. Chem. Int. Ed.*, 2012, **51**, 3414.
18. A. J. Canty, A. Ariafard, N. M. Camasso, A. T. Higgs, B. F. Yates and M. S. Sanford, *Dalton Trans.*, 2017, **46**, 3742-3748.
19. N. M. Camasso, A. J. Canty, A. Ariafard and M. S. Sanford, *Organometallics.*, 2017, **36**, 4382-4393.
20. J. R. Khusnutdinova, N. P. Rath and L. M. Mirica, *J. Am. Chem. Soc.*, 2012, **134**, 2414-2422.

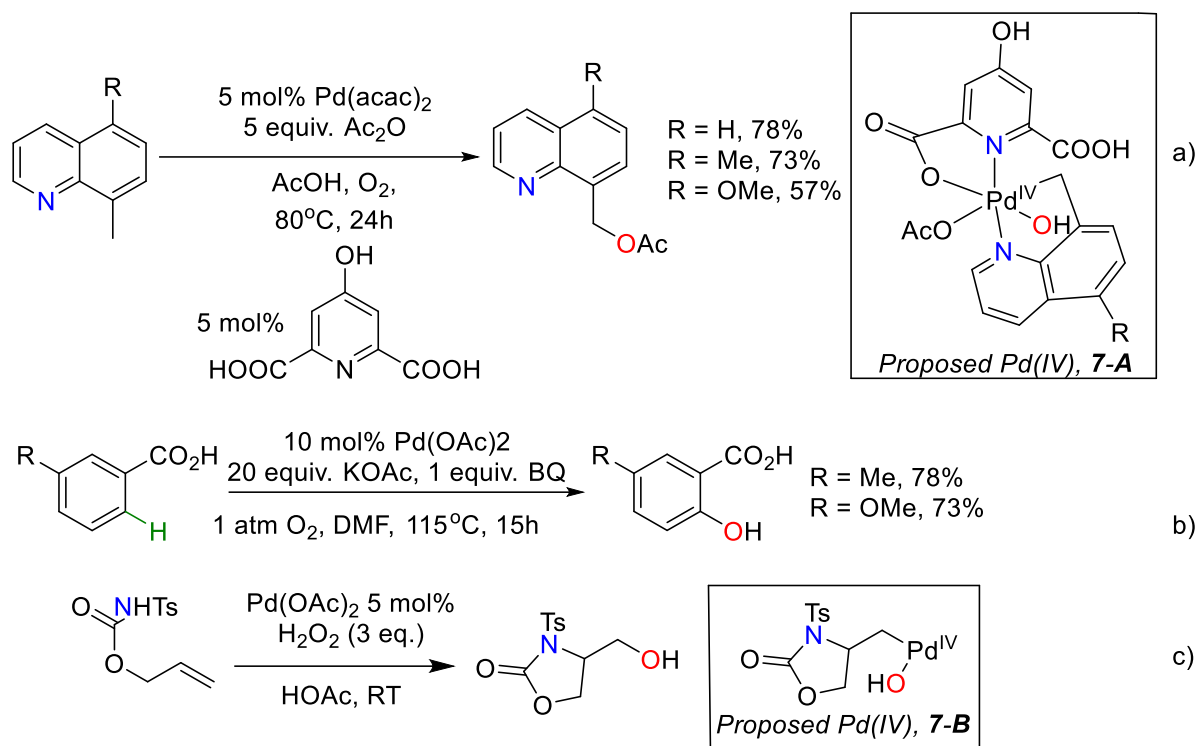
21. F. Qu, J. R. Khusnutdinova, N. P. Rath and L. M. Mirica, *Chem. Commun.*, 2014, **50**, 3036-3039.
22. J. Cámpora, J. A. López, P. Palma, P. Valerga, E. Spillner and E. Carmona, *Angew. Chem. Int. Ed.*, 1999, **38**, 147.
23. J. Cámpora, P. Palma, D. del Río, E. Carmona, C. Graiff, A. Tiripicchio, *Organometallics.*, 2003, **22**, 3345.
24. J. Nicasio-Collazo, K. Wrobel and O. Serrano, *New J. Chem.*, 2017, **41**, 8729-8733.
25. A. Behnia, P. D. Boyle, J. M. Blacquiere and R. J. J. M.; Puddephatt, *Organometallics.*, 2016, **35**, 2645-2654.
26. A. Behnia, P. D. Boyle, M. A. Fard, J. M. Blacquiere and R. J. Puddephatt, *Dalton Trans.*, 2016, **45**, 19485.
27. A. Behnia, M. A. Fard, J. M. Blacquiere and R. J. Puddephatt, *Organometallics.*, 2017, **36**, 4759-4769.
28. K. Sundaravel, M. Sankaralingam, E. Suresh and M. Palaniandavar, *Dalton Trans.*, 2011, **40**, 8444-8458.
29. J. -Z. Wu, E. Bouwman, A. M. Mills, A. L. Spek, J. Reedijk, *Inorg. Chim. Acta.*, 2004, **357**, 2694-2702.
30. J. M. Goldberg, J. L. Berman, W. Kaminsky, K. I. Goldberg and D. M. Heinekey, *J. Organomet. Chem.* 2017, **845**, 171-176.
31. A. Y. Rogachev and R. Hoffmann, *J. Am. Chem. Soc.*, 2013, **135**, 3262-3275.
32. M. Nabavizadeh, H. Amini, M. Rashidi, K. R. Pellarin, M. S. McCreedy, B. F. T. Cooper and R. J. Puddephatt, *J. Organomet. Chem.*, 2012, **713**, 60-67.
33. L. M. Rendina and R. J. Puddephatt, *Chem. Rev.*, 1997, **97**, 1735-1754.
34. B. A. Markies, A. J. Canty, J. Boersma, G. van Koten, *Organometallics.*, 1994, **13**, 2053-2058.
35. J. K. Jawad, R. J. Puddephatt and M. A. Stalteri, *Inorg. Chem.*, 1982, **21**, 332-337.
36. P. A. Shaw and J. P. Rourke, *Dalton Trans.*, 2017, **46**, 4768-4776.
37. E. G. Bowes, S. Pal and J. A. Love, *J. Am. Chem. Soc.*, 2015, **137**, 16004-16007.
38. C. M. Anderson, M. Crespo, N. Kfoury, M. A. Weinstein and J. M. Tanski, *Organometallics.*, 2013, **32**, 4199-4207.
39. P. A. Shaw, G. J. Clarkson and J. P. Rourke, *Organometallics.*, 2016, **35**, 3751-3762.
40. K. A. Grice, M. L. Scheuermann and K. I. Goldberg, *Organomet. Chem.*, 2011, **35**, 1-27.
41. R. J. Puddephatt, *Angew. Chem. Int. Ed.*, 2002, **41**, 261-263.
42. K. I. Goldberg, J. Y. Yan and E. M. Breitung, *J. Am. Chem. Soc.*, 1995, **117**, 6889-6896.

43. M. P. Brown, R. J. Puddephatt and C. E. E. Upton, *J. Chem. Soc. Dalton Trans.*, 1974, 2457.
44. Review: V. G. Shubin, *Top. Curr. Chem.*, 1984, 116/117, 267-341.
45. In methanol, complex **6-3** gave about equal amounts of **XP** and **XB** with X = I or OMe, the latter involving solvolysis by methanol.
46. G. Te Velde, F. M. Bickelhaupt, E. J. Baerends, S. van Gisbergen, C. F. Guerra, J. G. Snijders and T. Ziegler, *J. Comput. Chem.*, 2001, **22**, 931-967.
47. A. Becke, *Phys. Rev. A.*, 1988, **38**, 3098-3100.
48. J. P. Collman, J. I. Brauman and A. M. Madonik, *Organometallics.*, 1986, **5**, 310-322.
49. K. Kiyokawa, T. Watanabe, F. Fra, T. Kojima and S. Minakata, *J. Org. Chem.*, 2017, **82**, 11711–11720.
50. R. Frlan, M. Sova, S. Gobec, G. Stavber and Z. Casar, *J. Org. Chem.* **2015**, *80*, 7803–7809.
51. Bruker-AXS, SAINT version 2013.8, 2013, Bruker-AXS, Madison, WI 53711, USA.
52. Bruker-AXS, SADABS version 2012.1, **2012**, Bruker-AXS, Madison, WI 53711, USA.
53. G. M. Sheldrick, *Acta Cryst.*, 2015, **A71**, 3-8.
54. G. M. Sheldrick, *Acta Cryst.*, 2015, **C71**, 3-8.

7 Reductive C-O Elimination from Stable Pd(IV)-OH Complexes Prepared Using O₂ or H₂O₂ as Oxidants

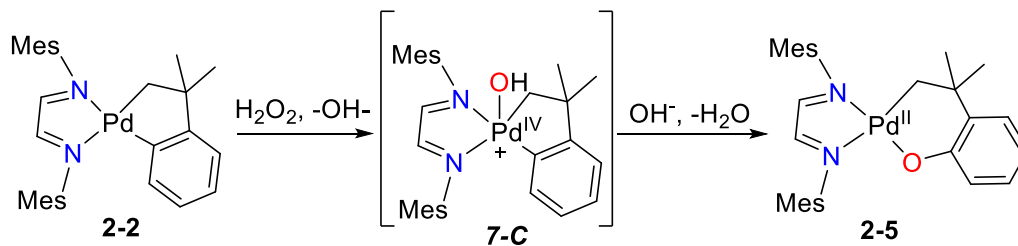
7.1 Introduction

Pd-catalyzed C-H bond functionalization reactions have been developed over the past two decades as an important tool in organic synthesis.¹⁻⁶ Despite the wide range of such synthetic methods, the use of inexpensive, abundant and environmentally friendly oxidants in oxidative C-H bond functionalization reactions remains challenging.⁷⁻⁹ O₂ and hydrogen peroxide are extremely attractive oxidants for C-H functionalization reactions as they are green and practical for large-scale synthesis. The mechanisms of Pd-catalyzed oxidative C-H bond functionalization reactions using non-green oxidants, such as PhI(OAc)₂, IOAc and K₂S₂O₈, to achieve C-H bond acetoxylation, hydroxylation and alkoxylation have been intensely investigated.^{2,10-13} However, much less is known about Pd-catalyzed C-H bond oxidation with O₂ or H₂O₂.¹⁴⁻¹⁸ Some recent studies on Pd(II)/Pd(IV) catalysis have proposed high-valent Pd(IV) species as active intermediates in Pd-catalyzed C-H bond functionalization reactions using O₂ or H₂O₂ as an oxidant.^{14,16,19} For instance, Vedernikov *et. al* proposed the intermediacy of a Pd(IV)-OH complex (**7-A**) in the acetoxylation of C(sp³)-H bonds using O₂ as the terminal oxidant in AcOH/Ac₂O (Scheme 7-1, a).¹⁶ Additionally, Yu *et.al* studied the Pd-catalyzed *ortho*-hydroxylation of potassium benzoates with dioxygen as the terminal oxidant in DMF (Scheme 7-1, b).¹⁹ Yu *et.al* proposed that the C-H oxidation reaction could follow a Pd(II)/Pd(IV) pathway, where dioxygen could function as the terminal oxidant to oxidize Pd(II) to Pd(IV). In addition, labeling studies revealed that the oxygen atom in the product is derived from O₂. Likewise, Liu *et. al* proposed the formation of Pd(IV)-OH intermediate (**7-B**) in a Pd-catalyzed C-H activation reaction, using H₂O₂ as the oxidant (Scheme 7-1, c).¹⁴



Scheme 7-1 Pd-catalyzed C-H functionalization reactions with O_2 or H_2O_2 as oxidants. (a) aerobic acetoxylation of C-H bonds;¹⁶ (b) aerobic hydroxylation of arenes;¹⁹ (c) hydroxylation of C-H bonds with H_2O_2 .¹⁴

We have recently reported that the stoichiometric reaction between a palladacycloneophyl complex and H_2O_2 as an oxidant leads to the selective oxygen-atom insertion into a Pd-C bond (Scheme 7-2, complex **2-5**).²⁰ The mechanism of this reaction was proposed to involve a Pd(IV)-OH intermediate that we were not able to observe or isolate (Scheme 7-2, **7-C**).

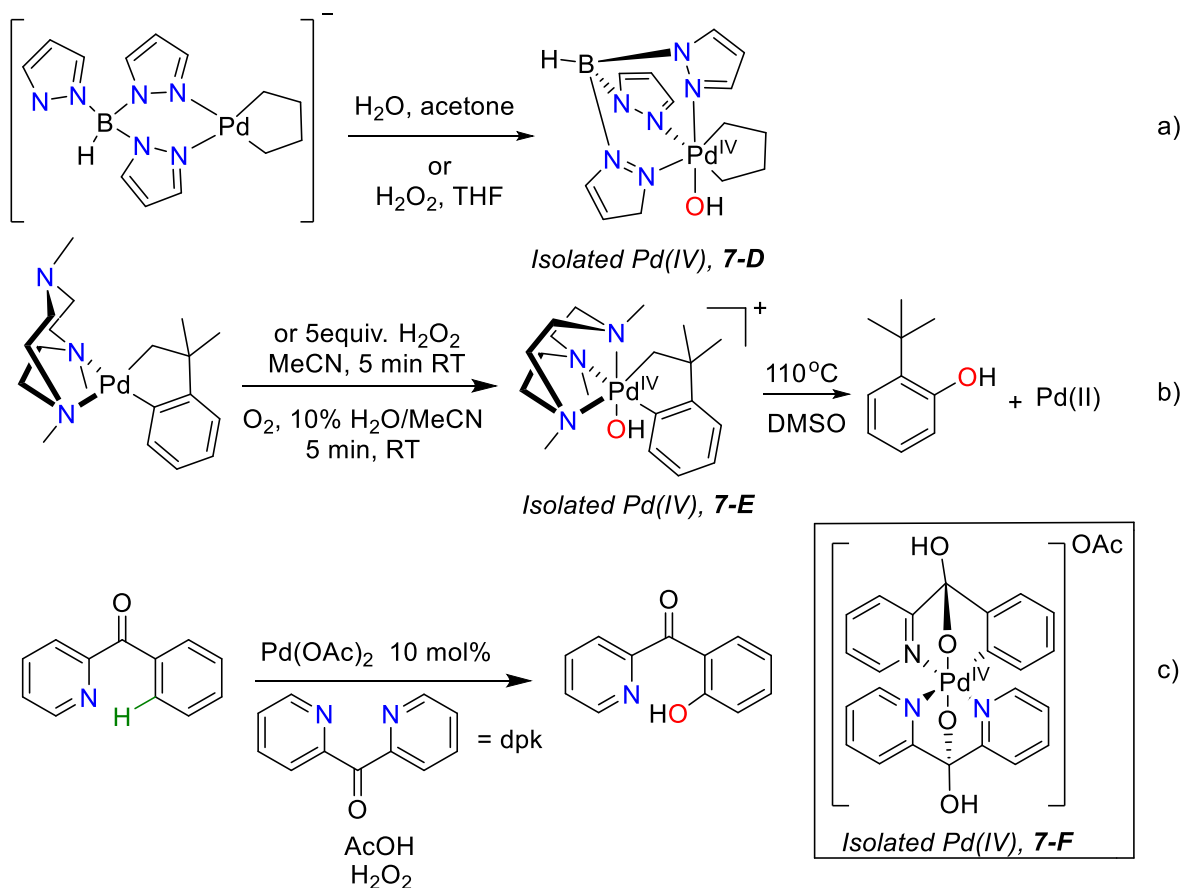


Scheme 7-2 Oxygen-atom insertion into the Pd-C bond, using H_2O_2 as the oxidant.²⁰

Although H_2O_2 can also oxidize Pd(II) complexes to form Pd(IV)-OH complexes, only a few isolated and characterized Pd(IV)-OH complexes have been reported so far.²¹⁻²³ Canty *et. al* for the first time could isolate a Pd(IV) complex (**7-D**), which resulted from an oxidation reaction of a Pd(II) complex

with H₂O₂ (Scheme 7-3, a).²¹ Mirica *et. al* also reported a facile aerobic oxidation to form a stable and isolated Pd(IV)-OH complex (**7-E**) (Scheme 7-3, b).²² For both of the studies in Scheme 7-3a and 7-3b it was proposed that the multidentate N-donor ligands, TP (hydrotris(pyrazolyl)borate) and Me₃tacn (*N,N,N'*-trimethyl-1,4,7-triazacyclononane) support the isolation of **7-D** and **7-E**, respectively. Mirica *et. al* studied the reductive elimination reaction from **7-E**. They reported a rare example of selective C(sp²)-O reductive elimination from a Pd(IV)-OH complex to form 1-tert-butylphenol.

It was only in 2010 that the first Pd(IV) intermediate from a catalytic reaction was isolated.²³ Vedernikov *et. al* isolated and characterized Pd(IV) intermediate (**7-F**) in the Pd-catalyzed C-H oxidative functionalization reaction with a green oxidant, H₂O₂ (Scheme 7-3, c). In this study it was confirmed that the dpk ligand is involved in the oxidation of Pd(II) to Pd(IV).

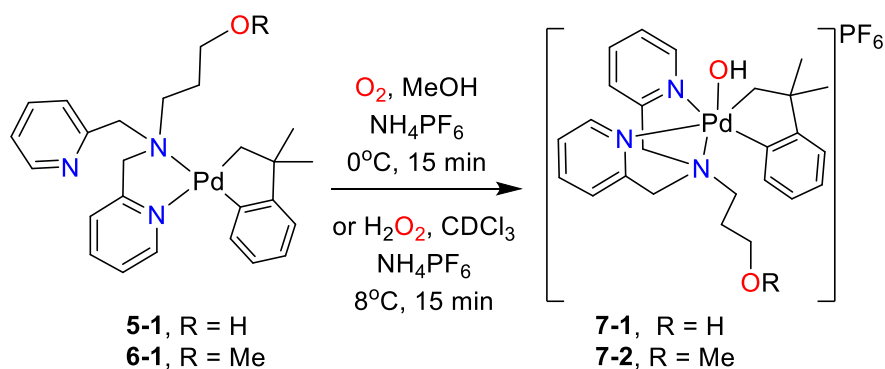


Scheme 7-3 (a) oxidation of a Pd(II) complex in water;²¹ (b) oxidation of a palladacycloneophyl complex using green oxidants;²² (c) Pd-catalyzed C-H bond activation using H₂O₂ as an oxidant.²³

Expanding the chemistry of Pd-catalyzed C-H bond functionalization reactions using green oxidants is challenging for two main reasons. First, the oxidation of Pd(II) complexes to isolable Pd(IV) utilizing O₂ or H₂O₂ is extremely rare. Therefore, we decided to utilize simply-synthesized tridentate *N*-donor ligands to aid in this transformation. These types of *N*-donor ligands were introduced in Chapter 6 as good candidates to assist in Pd(IV) isolation. The second challenge is that very few examples of Pd-catalyzed C-H functionalization using O₂ or H₂O₂ have been reported so far, and there is little mechanistic information.^{16–19,23,24} Herein, we report the palladacycloneophyl complexes **5-1** and **6-1** that undergo rapid oxidation with O₂ or H₂O₂ to form isolable Pd(IV)-OH complexes.

7.2 Result and Discussion

Exposure of an orange solution of [Pd(CH₂CMe₂C₆H₄)(κ²-*N,N'*-**5-L1**)] (**5-1**) or [Pd(CH₂CMe₂C₆H₄)(κ²-*N,N'*-**6-L1**)] (**6-1**) in methanol to O₂ in the presence of NH₄PF₆ rapidly generates a yellow precipitate. ¹H NMR analysis reveals the formation of new Pd(IV) complexes, [Pd(OH)(CH₂CMe₂C₆H₄)(κ³-*N,N',N''*-**L**)] [PF₆] (**7-1**, **L** = **5-L1**; **7-2**, **L** = **6-L1**) (Scheme 7-4). In addition, complexes **7-1** and **7-2** can also be generated upon addition of 6 equiv of H₂O₂ in the presence of NH₄PF₆. Complexes **7-1** and **7-2** could be stored at -5°C as solid samples for over a month.



Scheme 7-4 Pd(II) oxidation in the presence of dioxygen or hydrogen peroxide as an oxidant.

The complexes **7-1** and **7-2** were formed as single stereoisomers, as indicated by their ¹H NMR spectra. **7-1** and **7-2** were fully characterized by ¹H and ¹³C NMR spectroscopy, including correlated ¹H–¹H COSY, and ¹H–¹³C HSQC and HMBC NMR spectroscopy. The ¹H NMR spectrum of **7-1** in DMSO-*d*₆ showed 12 distinct aromatic signals in the range δ 6.61–8.71 and four different doublet resonances at δ 4.92, 4.62, 4.58 and 4.52 for methylene protons of the pyCH₂N groups. For the cycloneophyl group, the CMe₂ and CH₂ groups each gave two distinct resonances. These NMR data, which were similar for

7-2, indicate a single octahedral palladium(IV) complex with no symmetry, but the stereochemistry is not defined. Crystallization of **7-2** (as the hexafluorophosphate salt) from acetone/pentane was successful at -15°C . The structure of complex **7-2** is shown in Figure 7-1. X-ray analysis reveals an octahedral palladium centre with two C atoms and two pyridyl donors in the equatorial plane, while the amine donor and the hydroxide ligand occupy the axial positions (Scheme 7-4 and Figure 7-1). The Pd-C distances (2.039 and 1.979 Å) are similar to other cycloneophylpalladium(IV) complexes reported in Chapter 6, while the Pd-OH distance (1.990 Å) is similar to those of other palladacycle Pd(IV)-OH complexes.^{21,22}

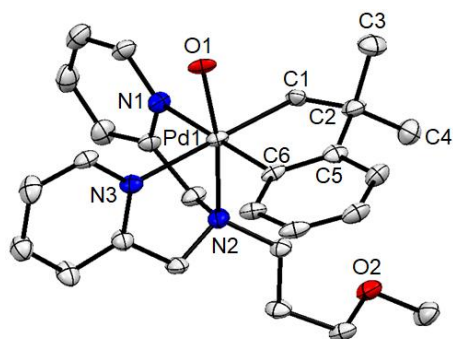
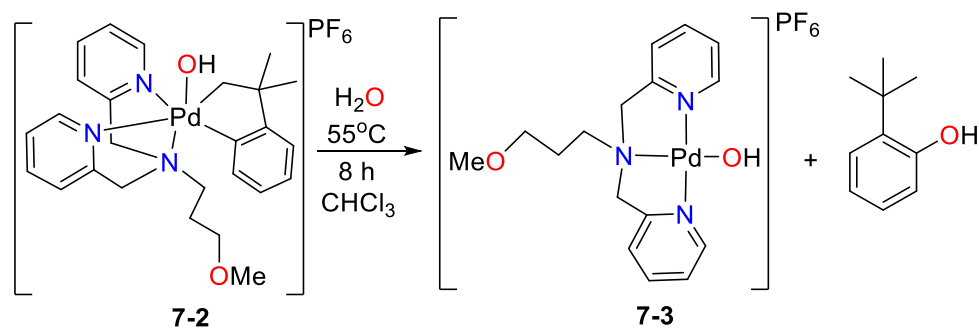


Figure 7-1 Structure of complex **7-2**, showing 30% probability ellipsoids. Selected bond distances: Pd(1)–O(1) 1.990(5); Pd(1)–N(1) 2.136(8); Pd(1)–N(2) 2.150(7); Pd(1)–N(3) 2.185(8); Pd(1)–C(1) 2.039(8); Pd(1)–C(6) 1.979(8) Å.

Complex **7-1** was only soluble in solvents with high polarity such as DMSO and DMF, while **7-2** was more soluble and so was considered as a good candidate to study the reductive elimination step. Complex **7-2** was dissolved in chloroform and heated at 55°C for 8 hours to give the corresponding Pd(II) complex **7-3**, with loss of the cycloneophyl group (Scheme 7-5). The reductive elimination reaction from **7-2** has qualitatively the same rate as the reductive elimination reaction from halide complexes in Chapter 6 (Scheme 6-4, complexes **6-2**, **6-3**, **6-4** and **6-5**). ^1H NMR of complex **7-3** gave only one set of pyridyl resonances that confirms the C_s symmetry of the structure with equivalent 2-pyridylmethyl groups. The preliminary results of the organic-release step show that the reductive elimination reaction from **7-2** was very selective, unlike similar reactions with halide oxidants studied in Chapter 6. The product of the reductive elimination reaction from **7-2** was 2-tert-butylphenol as determined by GC-MS (Scheme 7-5). Interestingly, the formation of $\text{PhCMe}_2\text{CH}_2\text{OH}$, that would be formed as a result of $\text{C}(\text{sp}^3)\text{-O}$ reductive elimination was not observed. Selectivity optimization and yield determination for the organic products is currently ongoing.



Scheme 7-5 Reductive elimination reaction from **7-2**.

7.3 Conclusion

Palladacycloneophyl complexes, **5-1** and **6-1** undergo facile oxidation with green oxidants such as O₂ and H₂O₂ to form stable Pd(IV)–OH complexes, **7-1** and **7-2**, respectively. The Pd(IV) complexes were isolated and fully characterized. The tridentate NNN-donor ligands, **5-L1** and **6-L1** can effectively stabilize the octahedral geometry of the generated Pd(IV) centres. Interestingly, thermolysis of Pd(IV)–OH complex **7-2** leads to selective C(sp²)–O vs. C(sp³)–O bond formation giving 2-tert-butylphenol as the organic product. This result in complete contrast to the reactions in Chapter 6 with halides (but similar to reactions with MeI). The isolated Pd(IV)-OH complexes and the observed selective C-O bond formation could be suitable candidate to study the selective aerobic C-H bond functionalization reactions catalyzed by Pd(II)/Pd(IV).

7.4 Experimental

All reactions were carried out under air. NMR spectra were recorded at 298 K using Varian INOVA 600 MHz spectrometers. ¹H and ¹³C chemical shifts were referenced internally to solvent (residual signal for ¹H) where the chemical shift was set to appropriate values relative to TMS at 0.00 ppm. Complete assignment of each compound was aided by the use of ¹H–¹H gCOSY, ¹H–¹³C{¹H} HSQC and ¹H–¹³C{¹H} HMBC experiments and are reported using the labeling scheme in Chart 7-1. Commercial reagents and aqueous 30% H₂O₂ were used without further purification. Complexes [PdCl₂(COD)],^{20,22} [Pd(CH₂CMe₂C₆H₄)(COD)] (**2-1**),^{20,22} [Pd(CH₂CMe₂C₆H₄)(κ²-N,N'-**5-L1**)] (**5-1**),^{20,22} and ligands, *N,N*-bis(pyrid-2-ylmethyl)-*N*-(2-hydroxyethyl)amine (**5-L1**)²⁵ and *N,N*-bis(pyrid-2-ylmethyl)-*N*-(2-methoxyethyl)amine (**6-L1**)²⁶ were synthesized according to the literature procedures. Dioxygen (99%) was purchased from Praxair and passed through a drying tube containing calcium sulphate and a cold ice trap to remove water prior to use. The crystal sample of **7-2** was mounted

on a Mitegen polyimide micromount with a small amount of Paratone N oil. All X-ray measurements were made on a Bruker Kappa Axis Apex2 diffractometer at a temperature of 110 K.²⁷⁻³⁰

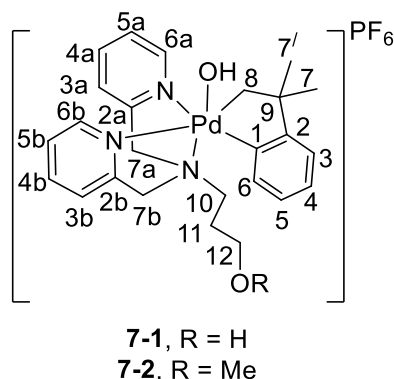


Chart 7-1 NMR labels for Pd(IV) complexes, **7-1** and **7-2**.

7.4.1 Synthesis of $[\text{Pd}^{\text{IV}}(\text{CH}_2\text{CMe}_2\text{C}_6\text{H}_4)(\kappa^3\text{-}N,N',N''\text{-5-L1})\text{OH}][\text{PF}_6]$, **7-1**.

Method A. Under air, a 25 mL round bottom flask was charged with $\text{Pd}^{\text{II}}(\text{CH}_2\text{CMe}_2\text{C}_6\text{H}_4)(\kappa^2\text{-}N,N'\text{-5-L1})$, **5-1**, (0.300 g, 0.631 mmol), 10 mL cold methanol (0 °C) and a stir bar, which was placed into an ice bath. The flask was capped with a septum. O_2 was bubbled through a stainless-steel needle for 5 minutes into the flask, equipped with a bleed needle. The septum was removed and excess NH_4PF_6 (0.308 g, 1.89 mmol) was added to the solution. The flask was capped again with the septum and stirred under O_2 pressure for 10 more minutes, during which time a yellow precipitate was formed. The precipitate was filtered and washed with cold methanol (10 mL) and cold ether (20 mL) to give **7-1** in pure form. Yield: 0.282 g, 0.428 mmol, 71%. *Method B.* To a stirred solution of **5-1**, (0.060 g, 0.126 mmol) in CDCl_3 (3 mL) cooled to 8 °C was added excess amount of NH_4PF_6 (0.061 g, 0.378 mmol). Then H_2O_2 (11.6 μL , 6 equiv) was added to the solution and stirred for 15 min, during which time the precipitate was formed. The mixture was filtered to separate the yellow precipitate, which was washed with cooled (0 °C) ether (10 mL) and the solid was dried under vacuum, to give **7-2**. Yield: 0.033 g, 0.050 mmol, 40%. ^1H NMR ($(\text{CD}_3)_2\text{SO}$, 600MHz, 25°C) δ : 8.72 (d, 1H, $J = 4$ Hz, $H6b$), 8.57 (d, 1H, $J = 4$ Hz, $H6a$), 7.56-7.52 (m, 2H, $H3b$ and $H5b$), 7.46 (d, 1H, $J = 8$ Hz, $H3a$), 7.98 (t, 1H, $J = 7$ Hz, $H4b$), 7.94 (t, 1H, $J = 8$ Hz, $H4a$), 7.50 (t, 1H, $J = 6$ Hz, $H5a$), 7.11 (t, 1H, $J = 7$ Hz, $H5$), 7.05 (dd, 1H, $J = 8$ Hz, $H6$), 6.90 (t, $J = 7$ Hz, 1H, $H4$), 6.63 (d, 1H, $J = 8$ Hz, $H3$), 4.92 (d, 1H, $J = 17$ Hz, $H7a$), 4.58-4.62 (m, 2H, $H7a'$ and $H7b'$), 4.52 (d, 1H, $J = 16$ Hz, $H7b$), 4.04 (d, 1H, $J = 7$ Hz, $H8'$), 4.01 (d, 1H, $J = 7$ Hz, $H8$), 3.33-3.38 (m, 1H, $H12$), 3.32-3.35 (m, 1H, $H10$), 3.27-3.31 (m, 1H, $H10$), 2.43-2.48 (m, 1H, $H12$), 1.83-1.88 (m, 1H, $H11$), 1.76-1.81 (m, 1H, $H11$), 1.43 (s, 6H, $H7$ and $H7'$); $^{13}\text{C}\{^1\text{H}\}$ NMR

((CD₃)₂SO, 151 MHz, 25°C) δ: 160.56 (C2), 156.99 (C2a), 155.66 (C2b), 153.46 (C1), 145.45 (C6b), 145.10 (C6a), 140.04 (C4b), 139.93 (C4a), 129.95 (C3), 126.96 (C4), 126.02 (C5), 125.58 (C6), 124.67 (C3b and C5b), 124.32 (C5a), 123.03 (C3b and C5b), 122.24 (C3a), 66.13 (C7b), 65.77 (C7a), 65.37 (C8), 61.68 (C12), 58.16 (C10), 53.50 (C11), 47.11 (C9), 34.67 (C7'), 31.13 (C7).

7.4.2 Synthesis of [Pd^{IV}(CH₂CMe₂C₆H₄)(κ³-N,N',N''-6-L1)OH][PF₆], **7-2**.

Complex **7-2** was made in the similar way to 7-1. Yield of Method A: 0.024 g, 0.036 mmol, 62%. Yield of Method B: 0.011 g, 0.017 mmol, 30%. ¹H NMR (CD₂Cl₂, 600MHz, -10°C) δ: 8.75 (d, 1H, *J* = 5 Hz, *H6b*), 8.58 (d, 1H, *J* = 5 Hz, *H6a*), 7.79 (t, 1H, *J* = 8 Hz, *H4a*), 7.58 (t, 1H, *J* = 8 Hz, *H4b*), 7.54 (d, 1H, *J* = 8 Hz, *H3b*), 7.43-7.39 (m, 2H, *H5b* and *H3a*), 7.39 (t, 1H, *J* = 7 Hz, *H5a*), 7.17 (t, 1H, *J* = 7 Hz, *H4*), 7.04 (t, 1H, *J* = 7 Hz, *H6*), 6.92 (t, 1H, *J* = 8 Hz, *H5*), 6.67 (d, *J* = 8 Hz, 1H, *H3*), 4.60-4.50 (m, 3H, *H7a*, *H7a'* and *H7b'*), 4.58-4.62 (m, 2H, *H7a'* and *H7b'*), 4.42 (d, 1H, *J* = 16 Hz, *H7b*), 4.24 (d, 1H, *J* = 7 Hz, *H8'*), 3.90 (d, 1H, *J* = 7 Hz, *H8*), 3.35-3.42 (m, 1H, *H12*), 3.32-3.35 (m, 1H, *H10*), 3.17 (s, 3H, *CH*₃), 3.13-3.15 (m, 1H, *H10*), 2.55-2.60 (m, 1H, *H12*), 2.07-2.03 (m, 1H, *H11*), 1.90-1.85 (m, 1H, *H11*), 1.48 (s, 3H, *H7*), 1.46 (s, 3H, *H7'*); ¹³C{¹H} NMR (CD₂Cl₂, 151 MHz, -10°C) δ: 160.73 (C2), 156.08 (C2a) 154.78 (C2b), 152.93 (C1), 145.91 (C6b), 145.67 (C6a), 140.24 (C4a), 140.21 (C4b), 130.04 (C3), 127.81 (C5), 127.06 (C4), 126.48 (C6), 125.16 (C3a and C5b), 124.84 (C5a), 123.57 (C3b), 122.81 (C3a and C5b), 69.29 (C10), 67.34 (C8), 66.63 (C7a), 66.50 (C7b), 63.15 (C12), 58.51 (CH₃), 46.98 (C9), 31.16 (C7'), 31.10 (C7), 22.90 (C11). HR ESI-TOF MS: Calcd for [C₂₆H₃₄N₃O₂Pd]⁺: *m/z* = 526.1685 Obsd *m/z* = 526.1690. Crystals suitable for single-crystal X-ray crystallographic analysis were grown by the slow diffusion of acetone into an ether solution of **7-2** at -15°C.

7.4.3 Synthesis of [Pd^{II}(κ³-N,N',N''-5-L1)OH][PF₆], **7-3**.

Complex **7-2** (0.060 g 0.089 mmol) was dissolved in CHCl₃ (5 mL) and heated at 55 °C for 8 h, during which time a yellow precipitate was formed. The precipitate was collected by filtration and washed with ether (3 × 5 mL) and hexane (3 × 5mL) to give **7-3**. Yield: 0.026 g, 0.048 mmol, 54%. ¹H NMR ((CD₃)₂SO, 600 MHz, 25°C) δ: 8.59 (d, 2H, *J* = 5 Hz, *H6a*), 8.22 (m, 2H, *H4a*), 7.75 (d, 2H, *J* = 7 Hz, *H3a*), 7.65 (t, 2H, *J* = 6 Hz, *H5a*), 5.50 (d, 2H, *J* = 15 Hz, *H7a*), 4.50 (d, 2H, *J* = 15 Hz, *H7a'*), 3.29 (m, 2H, *H10*), 3.07 (m, 2H, *H12*), 1.83 (m, 2H, *H11*); ¹³C{¹H} NMR ((CD₃)₂SO, 151 MHz, 25°C) δ: 165.41 (C2a), 150.71 (C6a), 124.09 (C4a), 125.58 (C3a), 123.84 (C5a), 69.18 (C7a), 67.29 (C7a'), 60.86 (C12), 58.33 (C10), 28.14 (C11). To characterize the organics, an analogous reaction was filtered

through a plug of silica to remove the palladium complexes. The filtrate was dried then it was diluted in an appropriate solvent for GC-MS analysis.

7.5 References

1. D. Kalyani, N. R. Deprez, L. V. Desai and M. S. Sanford, *J. Am. Chem. Soc.*, 2005, **127**, 7330–7331.
2. A. R. Dick and M. S. Sanford, *Tetrahedron*, 2006, **62**, 2439–2463.
3. D. Kalyani, A. R. Dick, W. Q. Anani and M. S. Sanford, *Org. Lett.*, 2006, **8**, 2523–2526.
4. K. L. Hull, E. L. Lanni and M. S. Sanford, *J. Am. Chem. Soc.*, 2006, **128**, 14047–14049.
5. J. M. Racowski, N. D. Ball and M. S. Sanford, *J. Am. Chem. Soc.*, 2011, **133**, 18022–18025.
6. L. V. Desai, K. J. Stowers and M. S. Sanford, *J. Am. Chem. Soc.*, 2008, **130**, 13285–13293.
7. S. S. Stahl, *Angew. Chem. Int. Ed.*, 2004, **43**, 3400–3420.
8. M. C. Denney, N. A. Smythe, K. L. Cetto, R. A. Kemp and K. I. Goldberg, *J. Am. Chem. Soc.*, 2006, **128**, 2508–2509.
9. B. V. Popp and S. S. Stahl, *J. Am. Chem. Soc.*, 2007, **129**, 4410–4422.
10. N. R. Deprez and M. S. Sanford, *Inorg. Chem.*, 2007, **46**, 1924–1935.
11. L. V. Desai, H. A. Malik and M. S. Sanford, *Org. Lett.*, 2006, **8**, 1141–1144.
12. G.-W. Wang, T.-T. Yuan and X.-L. Wu, *J. Org. Chem.*, 2008, **73**, 4717–4720.
13. M. Muehlhofer, T. Strassner and W. A. Herrmann, *Angew. Chem. Int. Ed.*, 2002, **41**, 1745–1747.
14. H. Zhu, P. Chen and G. Liu, *J. Am. Chem. Soc.*, 2014, **136**, 1766–1769.
15. Y. Guoyin, W. Tao and L. Guosheng, *Chem. Eur. J.*, 2011, **18**, 451–455.
16. J. Zhang, E. Khaskin, N. P. Anderson, P. Y. Zavalij and A. N. Vedernikov, *Chem. Commun.*, 2008, 3625–3627.
17. K. J. Stowers, A. Kubota and M. S. Sanford, *Chem. Sci.*, 2012, **3**, 3192–3195.
18. K. J. Stowers, K. C. Fortner and M. S. Sanford, *J. Am. Chem. Soc.*, 2011, **133**, 6541–6544.
19. Y.-H. Zhang and J.-Q. Yu, *J. Am. Chem. Soc.*, 2009, **131**, 14654–14655.
20. A. Behnia, P. D. Boyle, J. M. Blacquiere and R. J. Puddephatt, *Organometallics.*, 2016, **35**, 2645–2654.
21. A. J. Canty, H. Jin, A. S. Roberts, B. W. Skelton and A. H. White, *Organometallics.*, 1996, **15**, 5713–5722.
22. F. Qu, J. R. Khusnutdinova, N. P. Rath and L. M. Mirica, *Chem. Commun.*, 2014, **50**, 3036–3039.
23. W. Oloo, P. Y. Zavalij, J. Zhang, E. Khaskin and A. N. Vedernikov, *J. Am. Chem. Soc.*, 2010, **132**, 14400–14402.

24. W. N. Oloo, P. Y. Zavalij and A. N. Vedernikov, *Organometallics.*, 2013, **32**, 5601–5614.
25. K. Sundaravel, M. Sankaralingam, E. Suresh and M. Palaniandavar, *Dalton Trans.*, 2011, **40**, 8444–8458.
26. J.-Z. Wu, E. Bouwman, A. M. Mills, A. L. Spek and J. Reedijk, *Inorg. Chim. Acta.*, 2004, **357**, 2694–2702.
27. Bruker-AXS, SAINT version 2013.8, 2013, Bruker-AXS, Madison, WI 53711, USA.
28. Bruker-AXS, SADABS version 2012.1, **2012**, Bruker-AXS, Madison, WI 53711, USA.
29. G. M. Sheldrick, *Acta Cryst.*, 2015, **A71**, 3-8.
30. G. M. Sheldrick, *Acta Cryst.*, 2015, **C71**, 3-8.

8 Summary, Conclusion and Future Work

8.1 Summary and Conclusion

The research presented herein addressed the primary goals of the thesis: The isolation of stable Pd(IV) complexes and the study of each step of a Pd-catalyzed C-H functionalization mechanism, from C-H activation to oxidative addition and reductive elimination (Figure 8-1).

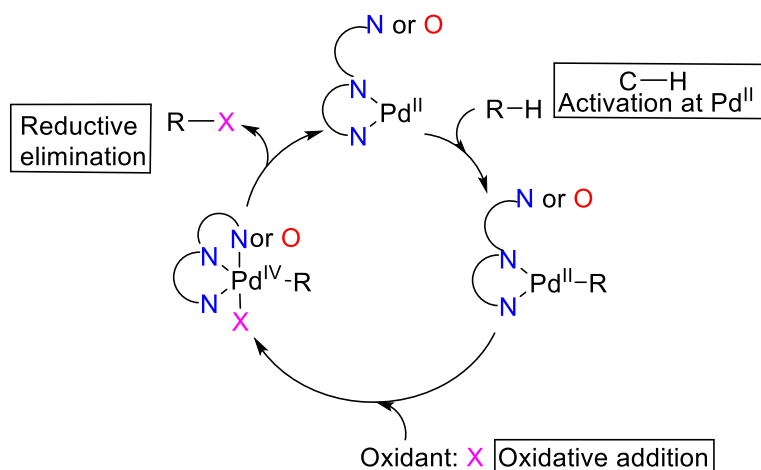


Figure 8-1 General mechanism for common Pd(II)/Pd(IV) catalysis that follow C-H activation at Pd(II) (X = C, O, N, F, Cl, Br, I).

Our first ligand design in Chapter 2 was a bidentate diimine ligand, $\text{MesN}=\text{CH}-\text{CH}=\text{NMes}^1$ (**2-L1**).² Oxidation reactions of a Pd(II) complex containing **2-L1**, $[\text{Pd}(\text{CH}_2\text{CMe}_2\text{C}_6\text{H}_4)(\text{2-L1})]$ (**2-2**), by addition of Br_2 or I_2 formed $[\text{PdX}_2(\text{2-L1})]$ (**2-3**, X = Br and **2-4**, X = I) complexes and 1,1-dimethylcyclobutabenzene (**CB**) as the organic product (Figure 8-2).

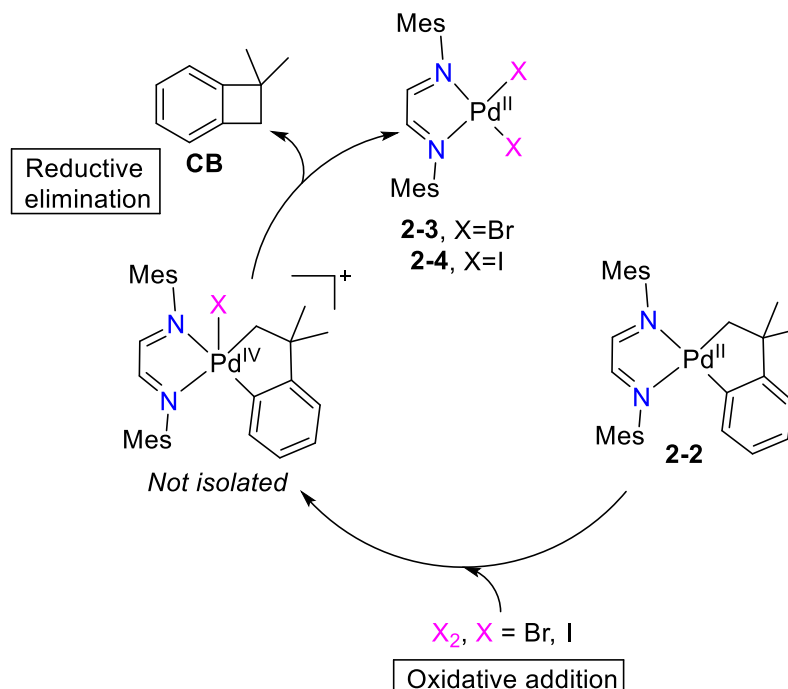


Figure 8-2 A summary of observed oxidative addition and reductive elimination reactions in Chapter 2.

These results suggest that the bidentate *N*-donor ligand (**2-L1**) is not able to assist in Pd(IV) isolation. However, based on computational studies we suggested that the reductive elimination following oxidation of **2-2** with Br₂ or I₂ is likely to occur from a five-coordinate Pd(IV) intermediate. By adding H₂O₂ as a green oxidant to **2-2**, we observed different reactivity. H₂O₂ addition resulted in selective functionalization of the Pd-C(sp²) bond to form [Pd(CH₂CMe₂C₆H₄O)(MesN=CH-CH=NMe)] (**2-5**) via O-atom insertion (Figure 8-3). Pd(II)/Pd(IV) catalysis sometimes involves some additional steps during which the oxidation state of the palladium centre does not change. The insertion reaction is considered as a major step. This unique insertion reaction was optimized experimentally, and the mechanism was studied computationally. Like in Figure 8-2, it is proposed that the insertion reaction takes place via a Pd(IV) intermediate, that was not stable enough to be detected in solution. The oxidative addition reaction to **2-5** was followed by rapid formation of [PdX₂(**2-L1**)] (**2-3**, X = Br and **2-4**, X = I, **2-6**, X = OH) and release of **BF** as the organic product via C(sp³)-O bond formation.

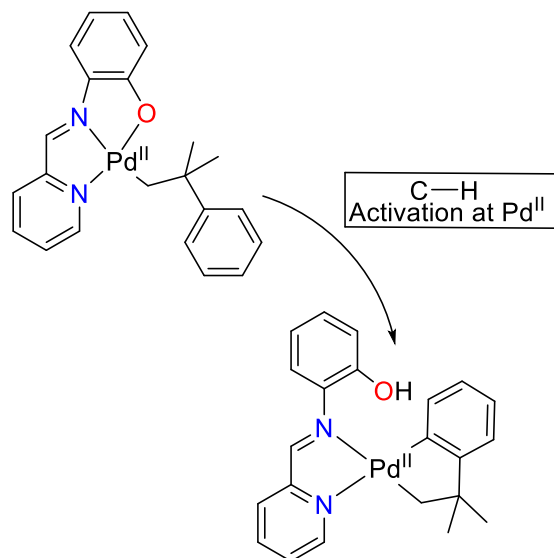


Figure 8-4 The CMD-type C-H activation discussed in Chapter 3.

An excess amount of phenol as an intermolecular base was added to a control Pd(II) complex having no aryl oxide moiety, $[\text{Pd}(\text{CH}_2\text{CMe}_2\text{C}_6\text{H}_4)(\text{C}_6\text{H}_4\text{N}=\text{CH}(2\text{-C}_5\text{H}_4\text{N}))]$ (**3-3**). No C-H activation was observed, that confirms the role of phenol group in **3-L1H** in assisting in the C-H activation step as an intramolecular base. The mechanism of the protonolysis and the C-H activation reactions were studied in detail both experimentally and computationally. A concerted $\text{S}_{\text{E}2}$ type mechanism was suggested for both reactions. To study the second step of a common Pd(II)/Pd(IV) catalysis, which is an oxidative addition step we added H_2O_2 as the oxidant to **3-1**. We were not able to observe or isolate any Pd(IV) intermediate and concluded that the **3-L1H** ligand design was not amenable to Pd(IV) isolation.

In Chapter 4 we presented that oxidation of a mixture of **2-1** and **3-L1H** with H_2O_2 and O_2 resulted in oxidation of the ligand **3-L1H** rather than the metal centre. The products were two different pincer-plus-one ligand structures.⁶ These pincer-plus-one ligand structures promoted the self-assembly of two new tetrameric palladium structures, **4-1** and **4-2**. The ligand oxidation reaction like insertion reaction is not a part of common Pd(II)/Pd(IV) catalysis, but it is a very important side reaction step that needs to be considered for any type of catalysis. Oxidative decomposition of ligands is considered as a deactivation pathway in catalysis. Deactivation leads to loss of the catalyst reactivity.⁷ Therefore, exploring the deactivation pathways is important to improve the catalyst performance.

In Chapter 5, an alternate tridentate *N*-donor ligand $\text{HO}(\text{CH}_2)_3\text{N}(\text{CH}_2\text{-2-py})_2$ ⁸ (**5-L1**) that contains an alcoholic chain was studied.⁹ We proposed that **5-L1** is less acidic than **3-L1** that contains an appended

phenolic group. Therefore, the protonolysis reaction was less probable to occur and we could study other steps of common Pd(II)/Pd(IV) catalysis such as oxidative addition and reductive elimination. The metalation reaction between **5-L1** and **2-1** formed the desired Pd(II) complex, [Pd(CH₂CMe₂C₆H₄)(κ²-N,N'-**5-L1**)] (**5-1**). In an attempt to crystallize **5-1** in a THF solution under air during 14 days, we observed an unexpected result by crystallizing [Pd(κ¹-O-CO₃)(κ³-N,N',N''-**5-L1**)], **5-2**, as the first monodentate carbonate complex of Pd(II). We studied the reason of this unexpected result experimentally and computationally. First, **5-1** undergoes a Pd-C(sp²) protonolysis by carbonic acid to form of [Pd(CH₂CMe₂Ph)(κ³-N,N',N''-**5-L1**)] [HCO₃] (**5-6**). Then, **5-6** undergoes oxidation by peroxide to form **5-2**. The oxidation step also released a mixture of organic products. The major product was 2-phenyl-2-butanol (**PB**) that is a result of neophyl rearrangement with the unprecedented preference for methyl over phenyl migration. A possible mechanistic basis for this unexpected reaction is proposed, involving β-carbon elimination at a palladium(IV) center.

In Chapter 6 and 7, we studied the potential of **5-L1** and (CH₃)O(CH₂)₃N(CH₂-2-C₅H₄N)₂ (**6-L1**) ligand structures in supporting Pd(IV) isolation through the oxidation reaction. Moreover, **5-L1** containing a hydroxyl group and **6-L1** containing a methoxyl group could help us to study the ligand effect on the bond-forming reductive elimination step.

In Chapter 6, the tridentate N-donor ligands (**5-L1** and **6-L1**) assisted in stabilization of the high-valent palladium centre. We could successfully isolate stable Pd(IV) complexes by adding Br₂ or I₂ as oxidants to palladacycloneophyl complexes **5-1** and [Pd(CH₂CMe₂C₆H₄)(κ²-N,N'-**6-L1**)] (**6-1**) (Figure 8-5). This was a remarkable result for us since it let us study the two main steps of common Pd(II)/Pd(IV) catalysis, oxidative addition and reductive elimination in great detail. The reductive elimination step was studied by thermolysis of the isolated Pd(IV) complexes. A mixture of organic products was formed that is a result of C-C and C-X (X = Br or I) bond formation. Reductive elimination from Pd(IV) complexes containing the **5-L1** ligand formed the same organics as Pd(IV) complexes having **6-L1** as the ligand. The ratio of the organics was different in systems with **5-L1** and **6-L1**, which confirms that the supporting N-donor ligand has a role in the selectivity of bond-forming reductive elimination step. A mechanism was proposed for the formation of each organic product. On the other hand, the kinetic study of the reductive elimination step from Pd(IV) complexes with **5-L1** and **5-L2** ligands revealed the same rate. Therefore, the hydroxyl moiety in **5-L1** has a minor role in the rate-determining step.

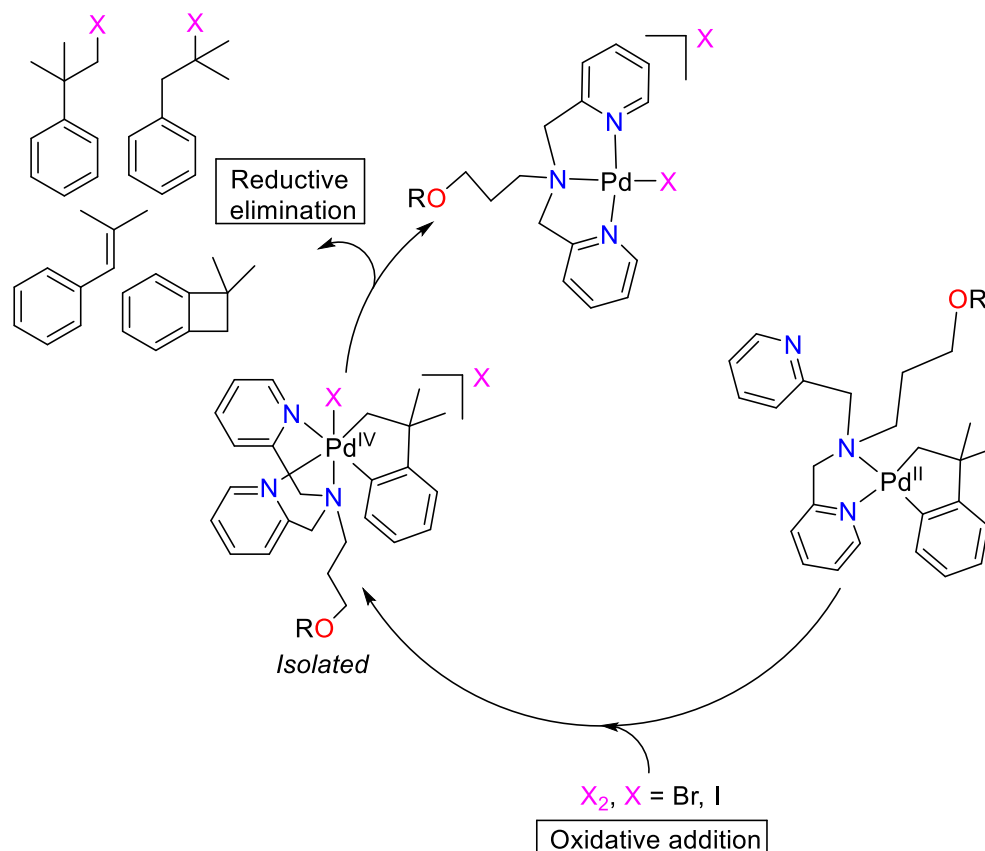


Figure 8-5 A summary of observed oxidative addition and reductive elimination reactions in Chapter 6.

In Chapter 7, stable Pd(IV)-OH complexes ($[Pd(OH)(CH_2CMe_2C_6H_4)(\kappa^3-N,N',N''-5-L1)][PF_6]$, **7-1** and $[Pd(OH)(CH_2CMe_2C_6H_4)(\kappa^3-N,N',N''-6-L1)][PF_6]$, **7-2**) were made through the oxidation of **5-1** or **6-1** with the green oxidants O_2 and H_2O_2 . Complexes **7-1** and **7-2** are among only a very small group of Pd(IV)-OH complexes. There are more discussions about these interesting Pd(IV)-OH structures (**7-1** and **7-2**) in the future work section.

Consequently, each step in the oxidative Pd-catalyzed C-H bond functionalization reactions depicted in Figure 8-1, including C-H bond activation, oxidation of Pd(II) complexes using dihalides (Br_2 and I_2) and green oxidants (O_2 and H_2O_2), and C-E (E = C, Br, I, O) reductive elimination, has been separately demonstrated under mild reaction conditions. Tridentate N-donor ligand structures (**5-L1** and **6-L1**) are important to isolate Pd(IV) intermediates in Pd(II)/Pd(IV) catalysis. On the other hand, bidentate N-donor ligands such as **2-L1** and **3-L1H** are not able to assist in Pd(IV) intermediate isolation. However, they promote important reactions such as insertion and C-H activation.

8.2 Future Work

The reductive elimination reaction from **7-1** and **7-2** will be studied in more detail in order to characterize and quantify all organic products formed in this step. In Chapter 6, we observed that the supporting *N*-donor ligand (**5-L1** and **6-L1**) has a role in selectivity of C-C and C-X (X = Br, I) bond formation reactions. We observed some trends of the ligand effect on selectivity; however, the reason for the observed trend was not clear. The results from the organic release step from **7-1** and **7-2** would help us to define the supporting ligand role in the selectivity of bond formations. The observed O₂ activation reactivity of **5-1** and **6-1** under mild reaction conditions is very interesting to us and we will apply this potential in some Pd-catalyzed aerobic hydroxylation or epoxidation reactions.

Based on the observed interesting C-H activation chemistry in Chapter 3, it is worthwhile to study the **3-L1H** ligand design effect on some possible Pd-catalyzed C-H functionalization reactions, such as hydroxylation of 2-phenylpyridine (Figure 8-6).

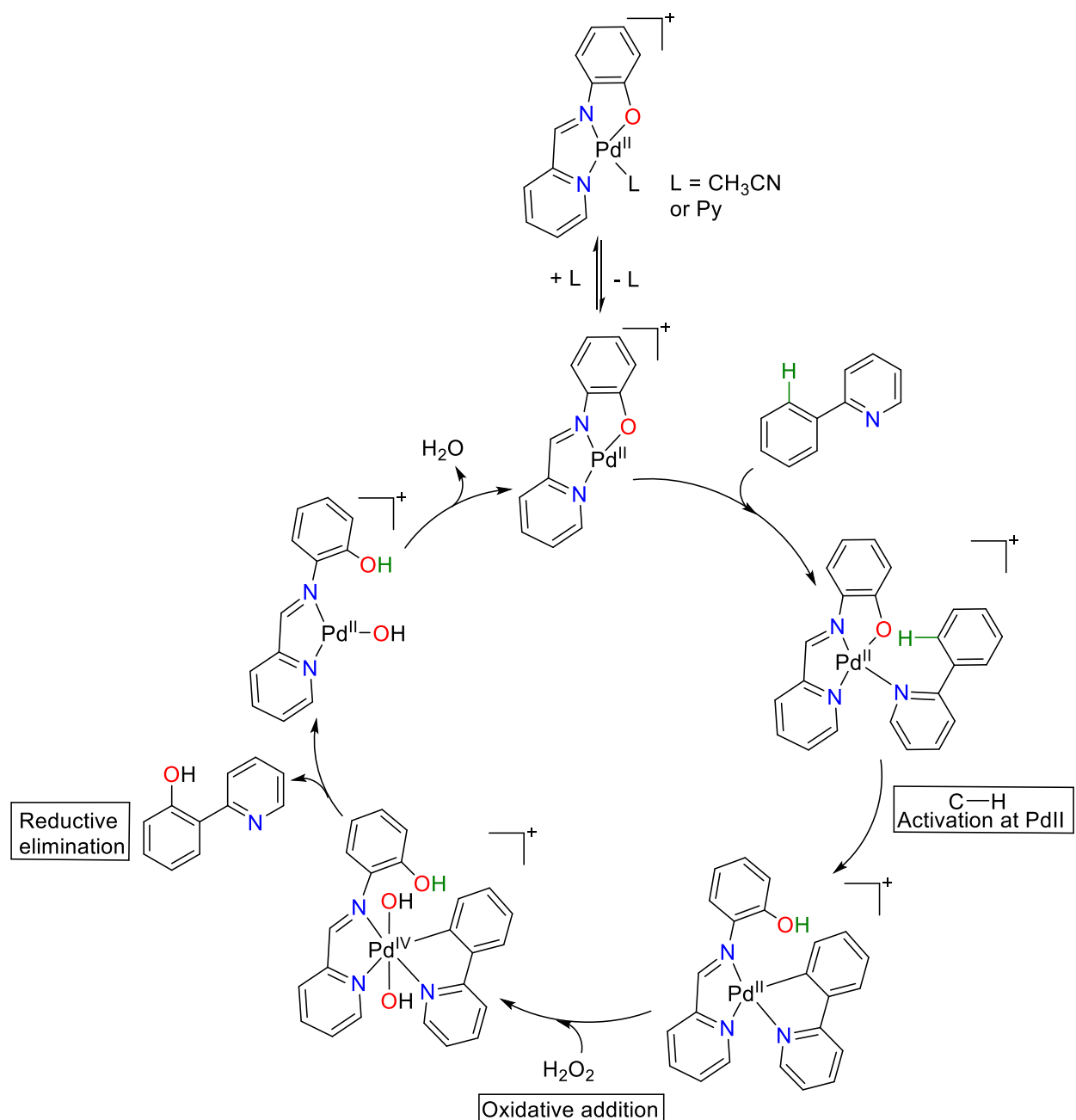


Figure 8-6 Proposed C(sp²)-H bond hydroxylation reaction for future work.

8.3 References

1. A. J. Arduengo, R. Krafczyk, R. Schmutzler, H. A. Craig, J. R. Goerlich, W. J. Marshall and M. Unverzagt, *Tetrahedron*, 1999, **55**, 14523–14534.
2. A. Behnia, P. D. Boyle, J. M. Blacquiere and R. J. Puddephatt, *Organometallics.*, 2016, **35**, 2645–2654.
3. M. E. Moustafa, P. D. Boyle and R. J. Puddephatt, *Chem. Commun.*, 2015, **51**, 10334–10336.

4. A. Behnia, M. A. Fard, J. M. Blacquiere and R. J. Puddephatt, *Dalton Trans.*, 2018, **47**, 3538–3548.
5. F. Qu, J. R. Khusnutdinova, N. P. Rath and L. M. Mirica, *Chem. Commun.*, 2014, **50**, 3036–3039.
6. A. Behnia, P. D. Boyle, M. A. Fard, J. M. Blacquiere and R. J. Puddephatt, *Dalton Trans.*, 2016, **45**, 19485–19490.
7. R. H. Crabtree, *Chem. Rev.*, 2015, **115**, 127–150.
8. K. Sundaravel, M. Sankaralingam, E. Suresh and M. Palaniandavar, *Dalton Trans.*, 2011, **40**, 8444–8458.
9. A. Behnia, M. A. Fard, J. M. Blacquiere and R. J. Puddephatt, *Organometallics.*, 2017, **36**, 4759–4769.

Appendices

Appendix A: Supplementary Information for Chapter 2

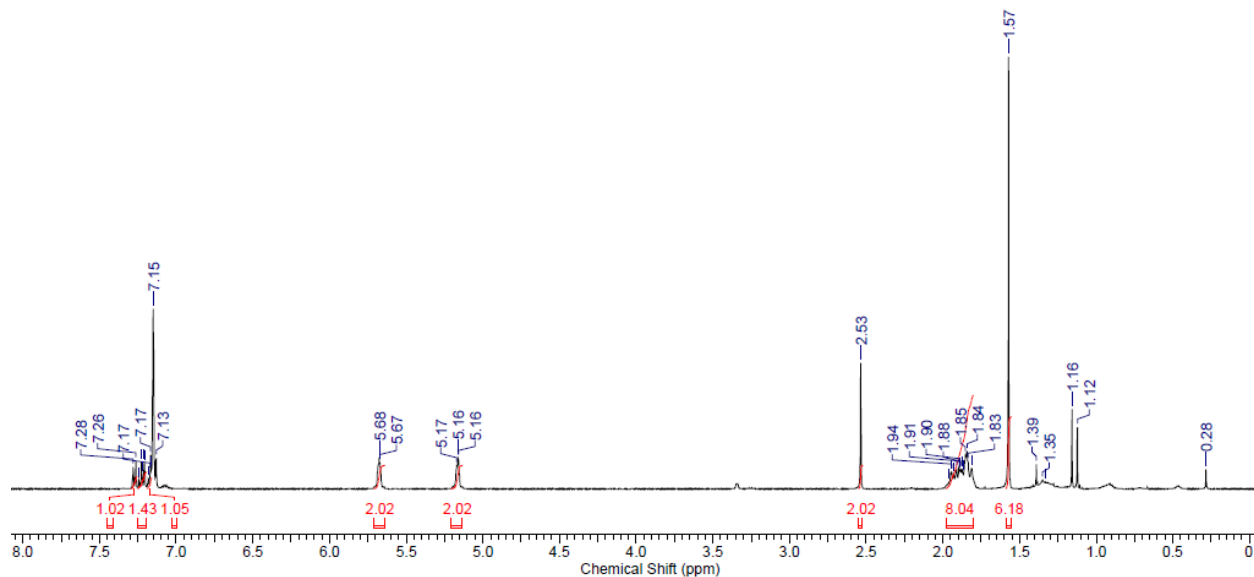


Figure A2.1 ^1H NMR spectrum of **2-1** in C_6D_6 at 600 MHz.

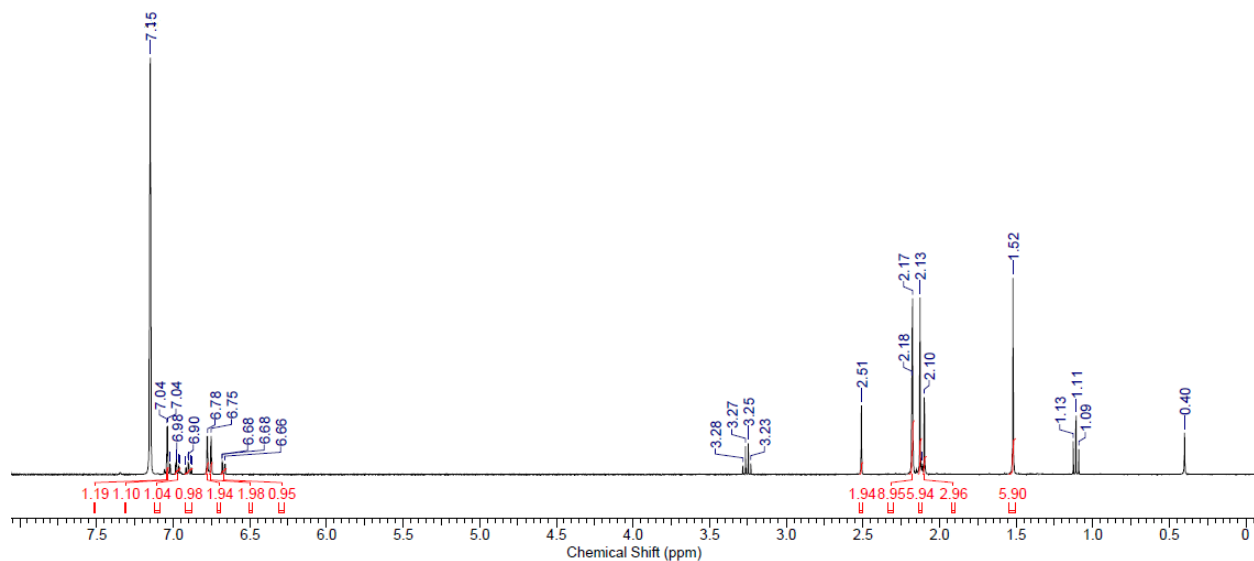


Figure A2.2 ^1H NMR spectrum of **2-2** in C_6D_6 at 600 MHz.

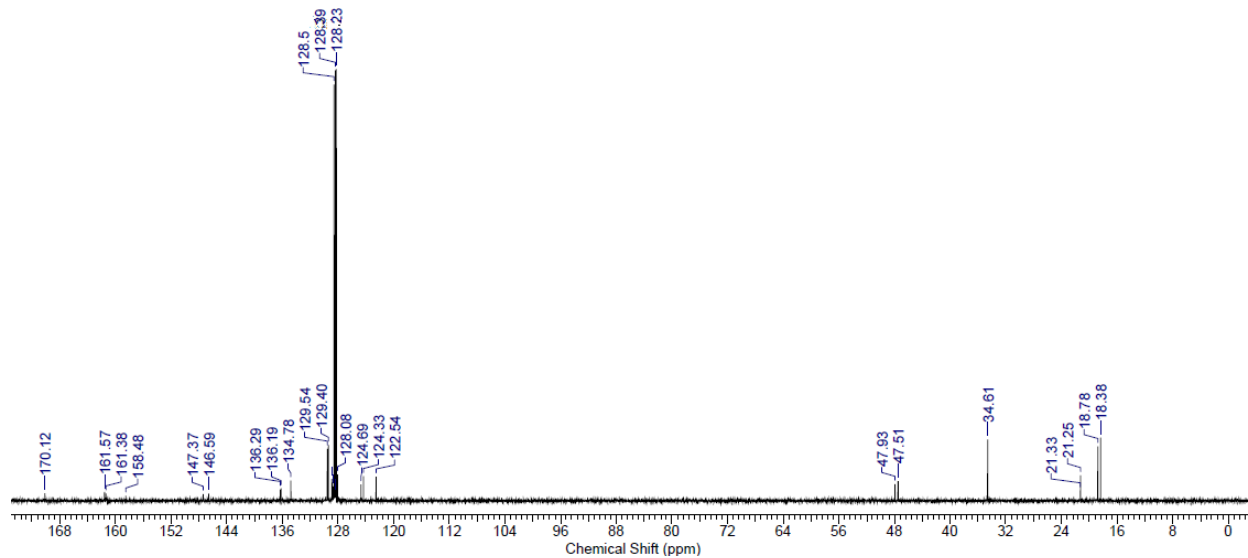


Figure A2.3 $^{13}\text{C}\{^1\text{H}\}$ NMR spectrum of **2-2** in C_6D_6 at 151 MHz.

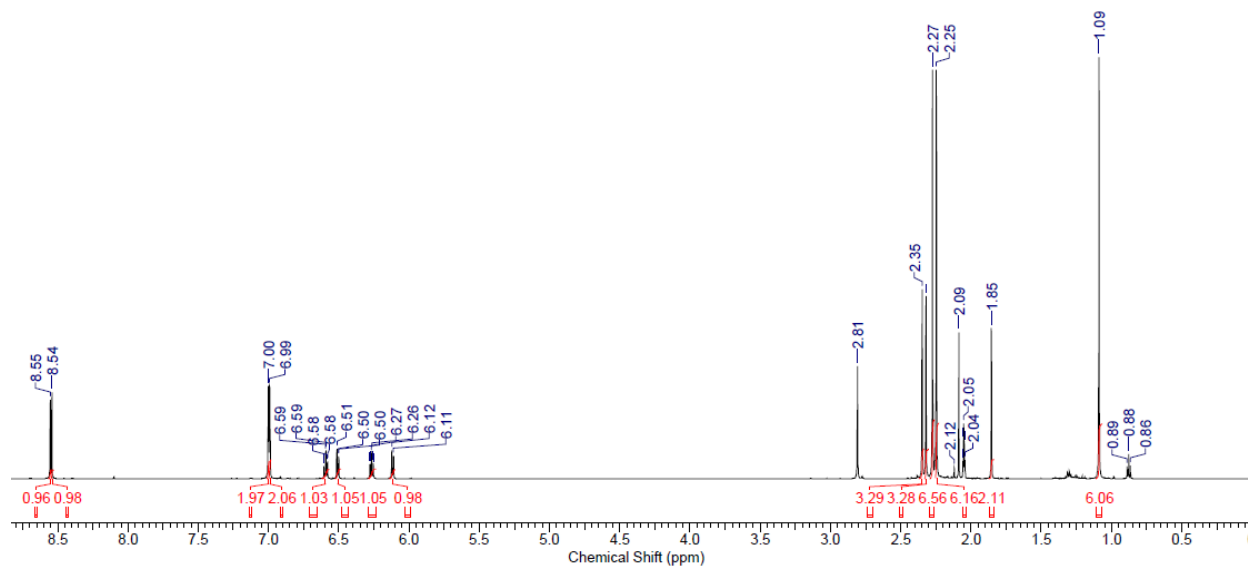


Figure A2.4 ^1H NMR spectrum of **2-2** in $(\text{CD}_3)_2\text{CO}$ at 600 MHz.

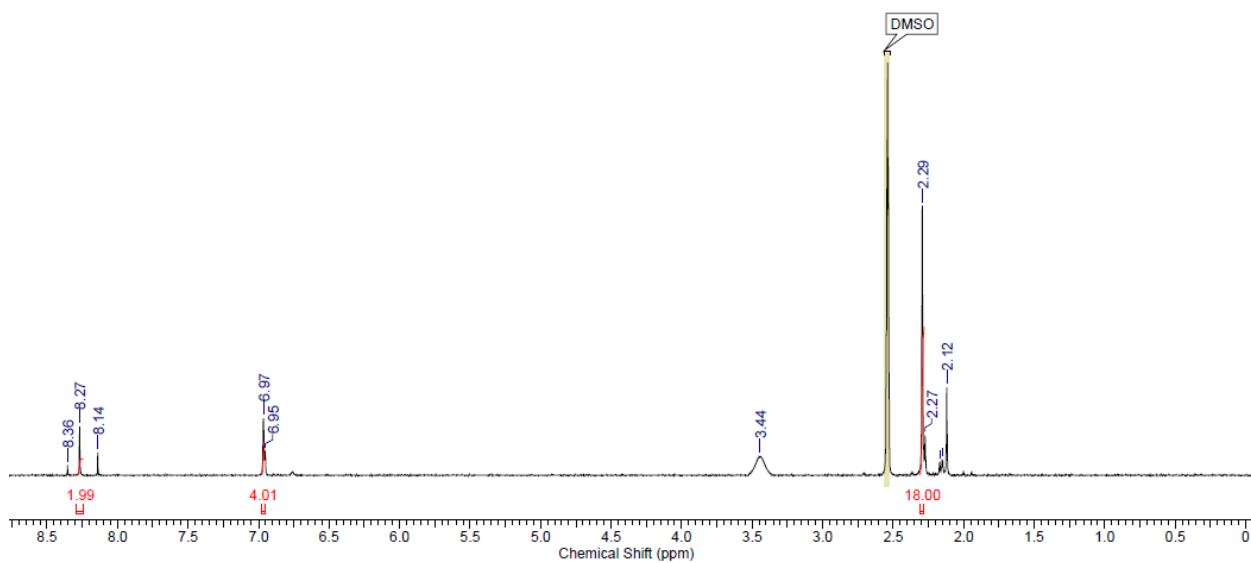


Figure A2.5 ^1H NMR spectrum of **2-3** in $(\text{CD}_3)_2\text{SO}$ at 600 MHz.

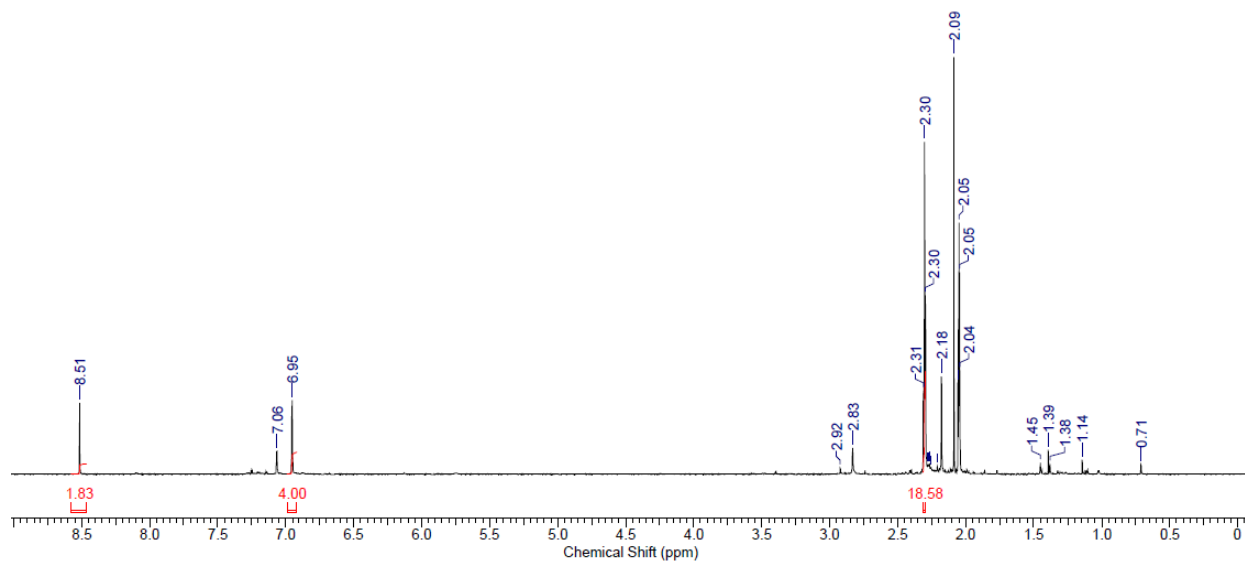


Figure A2.6 ^1H NMR of complex **2-4** in $(\text{CD}_3)_2\text{CO}$ at 600 MHz.

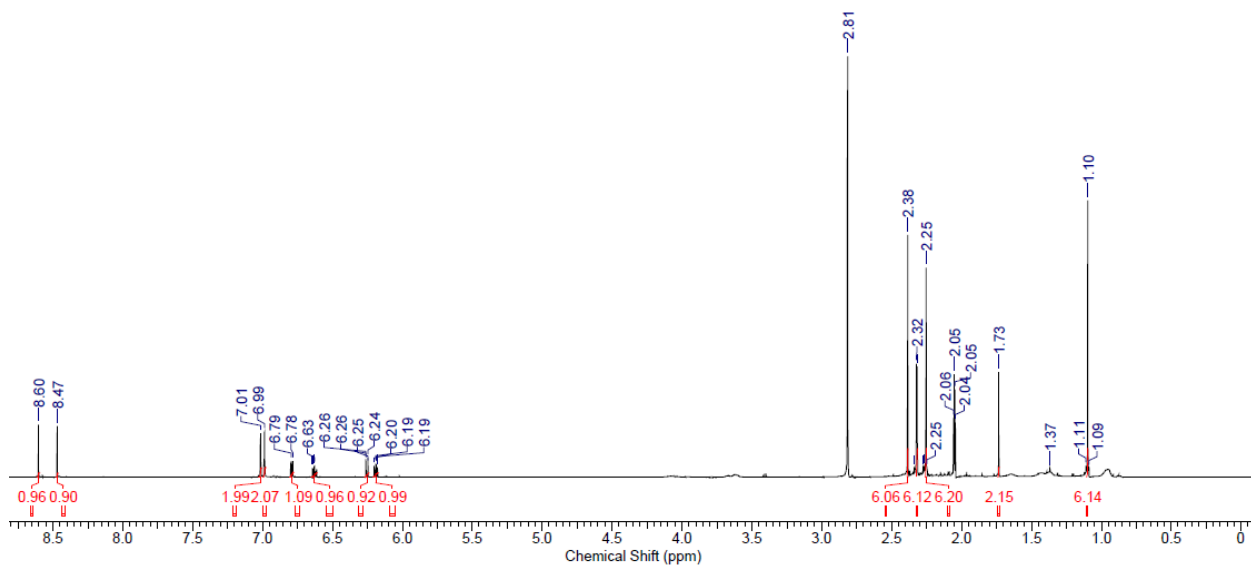


Figure A2.7 ^1H NMR of complex **2-5** in $(\text{CD}_3)_2\text{CO}$ at 600 MHz.

Table A2.1 Summary of crystallographic data for complexes **2-2**, **2-3**, **2-4** and **2-5**.

	2-2	2-3	2-4	2-5
Formula	$\text{C}_{30}\text{H}_{36}\text{N}_2\text{Pd} \cdot 0.5(\text{C}_4\text{H}_{10}\text{O})$	$\text{C}_{20}\text{H}_{24}\text{Br}_2\text{N}_2\text{Pd}$	$\text{C}_{20}\text{H}_{24}\text{I}_2\text{N}_2\text{Pd} \cdot (\text{CO}(\text{CH}_3)_2)$	$\text{C}_{30}\text{H}_{36}\text{N}_2\text{OPd} \cdot (\text{C}_6\text{H}_6)$
Formula weight	568.07	558.63	710.69	625.11
Crystal system	orthorhombic	tetragonal	Monoclinic	Monoclinic
Space group	$P b c a$	$I 4_1 c d$	$C 2/c$	$P 2_1/c$
a [Å]	22.239(9)	17.252(4)	19.207(4)	9.8813(19)
b [Å]	21.009(7)	17.252	19.213(4)	22.647(7)
c [Å]	25.246(8)	14.344(4)	29.230(6)	13.939(4)
α [°]	90	90	90	90
β [°]	90	90	100.070(10)	95.725(9)
γ [°]	90	90	90	90
V [Å ³]	11795(7)	4269(2)	10620(4)	3103.8(13)

<i>Z</i>	16	8	16	4
ρ_{cal} [g cm ⁻³]	1.280	1.738	1.778	1.338
λ , Å, (MoK α)	0.71073	0.71073	0.71073	0.628
<i>F</i> (000)	4752	2192	5472	1304
<i>T</i> [K]	110	110	173	110
$\theta_{\text{min}}, \theta_{\text{max}}$ [°]	3.331, 28.349	3.295, 42.573	3.357, 32.599	3.208, 40.312
Total reflns	216309	106381	114328	156470
Unique reflns	14656	7246	19308	19217
<i>R</i> ₁	0.0540	0.0321	0.0342	0.0369
w <i>R</i> ₂ [<i>I</i> ≥ 2σ(<i>I</i>)]	0.1141	0.0789	0.0585	0.0763
<i>R</i> ₁ (all data)	0.0866	0.0606	0.0680	0.0638
w <i>R</i> ₂ (all data)	0.1305	0.1162	0.0676	0.0850
GOF	1.037	1.069	1.038	1.026
Maximum shift/error	0.0003	0.000	0.004	0.003
Min & Max peak heights on final ΔF Map (e ⁻ /Å)	-1.557, 2.084	-0.656, 2.952	-0.982, 0.638	-1.226, 0.871

Where: $R_1 = \sum(|F_o| - |F_c|) / \sum F_o$; $wR_2 = [\sum(w(F_o^2 - F_c^2)^2) / \sum(wF_o^4)]^{1/2}$; $GOF = [\sum(w(F_o^2 - F_c^2)^2) / (\text{No. of reflns.} - \text{No. of params.})]^{1/2}$

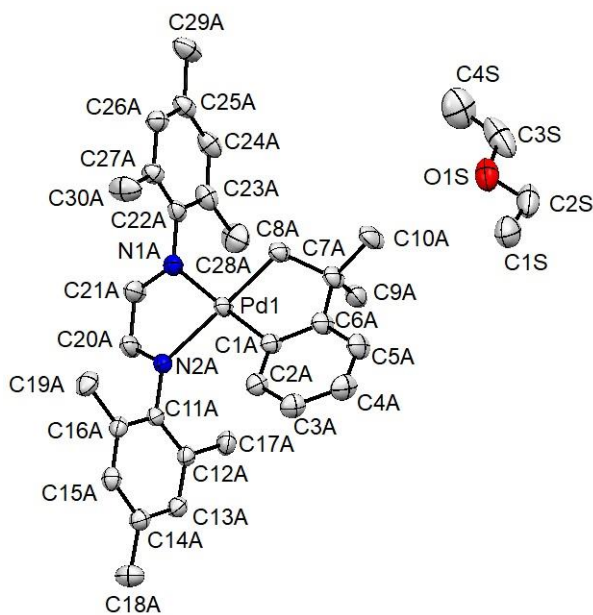


Figure A2.8 Displacement ellipsoid plot of **2-2** co-crystallized with an ether molecule showing naming and numbering scheme. Ellipsoids are drawn at the 50% probability level and hydrogen atoms are omitted for clarity.

Table A2.2 Atomic coordinates for **2-2**.

Atom	x	y	z	$U_{\text{iso/equiv}}$
Pd1	0.40603(2)	0.76475(2)	0.57024(2)	0.02810(8)
N1A	0.48686(14)	0.81675(16)	0.59131(12)	0.0292(7)
N2A	0.41719(15)	0.74336(17)	0.65170(12)	0.0315(7)
C1A	0.39215(17)	0.7849(2)	0.49404(14)	0.0302(8)
C2A	0.41130(18)	0.8399(2)	0.46810(15)	0.0333(9)
C3A	0.3966(2)	0.8510(2)	0.41501(16)	0.0399(10)
C4A	0.3638(2)	0.8065(3)	0.38709(16)	0.0454(11)
C5A	0.3435(2)	0.7520(3)	0.41203(16)	0.0447(12)
C6A	0.35631(18)	0.7410(2)	0.46575(15)	0.0357(9)
C7A	0.33473(18)	0.6846(2)	0.49765(15)	0.0362(10)
C8A	0.33400(18)	0.7092(2)	0.55507(15)	0.0339(9)
C9A	0.3789(2)	0.6293(2)	0.49242(17)	0.0424(11)
C10A	0.2712(2)	0.6626(3)	0.48130(18)	0.0535(14)
C11A	0.52564(16)	0.85674(19)	0.56036(13)	0.0271(8)
C12A	0.56627(17)	0.82852(19)	0.52524(14)	0.0288(8)

C13A	0.60404(18)	0.8687(2)	0.49657(14)	0.0315(8)
C14A	0.60244(18)	0.9346(2)	0.50196(15)	0.0323(8)
C15A	0.55973(18)	0.9604(2)	0.53608(15)	0.0317(8)
C16A	0.52091(17)	0.9225(2)	0.56575(14)	0.0296(8)
C17A	0.5699(2)	0.7570(2)	0.52007(16)	0.0380(9)
C18A	0.6458(2)	0.9764(2)	0.47202(18)	0.0437(11)
C19A	0.4753(2)	0.9520(2)	0.60254(17)	0.0435(11)
C20A	0.5036(2)	0.8056(2)	0.63913(15)	0.0409(11)
C21A	0.4642(2)	0.7672(2)	0.67266(15)	0.0408(11)
C22A	0.37663(18)	0.7078(2)	0.68459(14)	0.0306(8)
C23A	0.3837(2)	0.6423(2)	0.68846(18)	0.0409(10)
C24A	0.3440(2)	0.6092(2)	0.72102(19)	0.0437(10)
C25A	0.29860(19)	0.6392(2)	0.74836(16)	0.0370(9)
C26A	0.29117(19)	0.7038(2)	0.74193(15)	0.0345(9)
C27A	0.32957(18)	0.7397(2)	0.70974(15)	0.0323(8)
C28A	0.4323(3)	0.6079(3)	0.6578(2)	0.0601(14)
C29A	0.2577(2)	0.6018(3)	0.78485(19)	0.0513(13)
C30A	0.3197(3)	0.8095(2)	0.7014(2)	0.0549(13)
Pd2	0.56230(2)	0.69091(2)	0.29654(2)	0.03245(9)
N1B	0.55637(14)	0.77860(16)	0.34077(12)	0.0293(7)
N2B	0.50880(16)	0.66606(18)	0.36274(12)	0.0369(8)
C1B	0.61096(18)	0.7128(2)	0.23279(14)	0.0315(9)
C2B	0.61716(19)	0.7734(2)	0.21105(15)	0.0354(9)
C3B	0.6491(2)	0.7829(2)	0.16414(16)	0.0418(11)
C4B	0.6758(2)	0.7318(3)	0.13881(16)	0.0466(12)
C5B	0.6700(2)	0.6710(3)	0.15947(17)	0.0466(12)
C6B	0.63691(18)	0.6609(2)	0.20574(15)	0.0349(9)
C7B	0.6264(2)	0.5971(2)	0.23049(18)	0.0432(11)
C8B	0.5668(2)	0.6044(2)	0.26025(16)	0.0427(11)
C9B	0.6778(3)	0.5836(2)	0.2704(2)	0.0615(16)
C10B	0.6228(2)	0.5429(3)	0.1894(2)	0.0534(13)
C11B	0.58656(19)	0.83828(19)	0.33183(15)	0.0329(9)
C12B	0.6471(2)	0.8420(2)	0.34493(16)	0.0373(9)
C13B	0.6758(3)	0.8995(2)	0.3367(2)	0.0542(13)

C14B	0.6463(3)	0.9515(3)	0.3150(2)	0.0659(15)
C15B	0.5875(3)	0.9452(2)	0.3010(2)	0.0621(14)
C16B	0.5552(2)	0.8883(2)	0.30875(17)	0.0478(11)
C17B	0.6801(2)	0.7855(2)	0.36649(17)	0.0414(10)
C18B	0.6784(4)	1.0151(3)	0.3087(3)	0.107(3)
C19B	0.4912(3)	0.8811(3)	0.2915(2)	0.0695(17)
C20B	0.52351(18)	0.7746(2)	0.38231(14)	0.0337(9)
C21B	0.49598(19)	0.7129(2)	0.39376(15)	0.0367(10)
C22B	0.4892(2)	0.6019(3)	0.37705(17)	0.0510(12)
C23B	0.5226(3)	0.5681(2)	0.41436(19)	0.0584(13)
C24B	0.5043(3)	0.5058(3)	0.4277(2)	0.0695(16)
C25B	0.4590(3)	0.4783(4)	0.4049(3)	0.0758(17)
C26B	0.4251(3)	0.5098(3)	0.3681(3)	0.0823(19)
C27B	0.4409(3)	0.5755(4)	0.3507(2)	0.0848(19)
C28B	0.5749(3)	0.5952(3)	0.4399(3)	0.088(2)
C29B	0.4375(4)	0.4100(3)	0.4191(3)	0.114(3)
C30B	0.4070(4)	0.6164(5)	0.3106(3)	0.126(3)
C1S	0.2669(4)	0.5001(5)	0.4101(3)	0.071(3)
C2S	0.2630(4)	0.4334(5)	0.4314(3)	0.070(3)
O1S	0.2684(2)	0.4333(3)	0.4867(2)	0.0597(17)
C3S	0.2595(3)	0.3717(3)	0.5163(3)	0.087(2)
C4S	0.2555(5)	0.3792(6)	0.5687(4)	0.087(3)
C1S'	0.3052(8)	0.5087(8)	0.6016(6)	0.059(5)
C2S'	0.2756(8)	0.4447(7)	0.5929(5)	0.054(4)
O1S'	0.2810(4)	0.4292(5)	0.5393(4)	0.048(3)
C3S'	0.2595(3)	0.3717(3)	0.5163(3)	0.087(2)
C4S'	0.2629(10)	0.3527(10)	0.4697(7)	0.084(7)
H2A	0.4347	0.8703	0.4868	0.040
H3A	0.4091	0.8893	0.3982	0.048
H4A	0.3552	0.8133	0.3507	0.055
H5A	0.3207	0.7218	0.3927	0.054
H8A1	0.3339	0.6726	0.5797	0.041
H8A2	0.2967	0.7340	0.5611	0.041
H9A1	0.3807	0.6156	0.4554	0.064

H9A2	0.3653	0.5937	0.5145	0.064
H9A3	0.4189	0.6430	0.5040	0.064
H10A	0.2432	0.6986	0.4837	0.080
H10B	0.2578	0.6285	0.5050	0.080
H10C	0.2721	0.6468	0.4448	0.080
H13A	0.6319	0.8504	0.4725	0.038
H15A	0.5570	1.0054	0.5392	0.038
H17A	0.5855	0.7388	0.5530	0.057
H17B	0.5968	0.7459	0.4907	0.057
H17C	0.5297	0.7398	0.5131	0.057
H18A	0.6342	1.0211	0.4764	0.066
H18B	0.6450	0.9652	0.4344	0.066
H18C	0.6865	0.9702	0.4859	0.066
H19A	0.4879	0.9455	0.6393	0.065
H19B	0.4360	0.9319	0.5969	0.065
H19C	0.4722	0.9977	0.5953	0.065
H20A	0.5405	0.8219	0.6523	0.049
H21A	0.4734	0.7601	0.7089	0.049
H24A	0.3484	0.5644	0.7245	0.052
H26A	0.2591	0.7246	0.7598	0.041
H28A	0.4276	0.5619	0.6626	0.090
H28B	0.4719	0.6211	0.6709	0.090
H28C	0.4289	0.6184	0.6201	0.090
H29A	0.2670	0.5563	0.7819	0.077
H29B	0.2157	0.6091	0.7748	0.077
H29C	0.2640	0.6158	0.8215	0.077
H30A	0.3559	0.8329	0.7119	0.082
H30B	0.2856	0.8237	0.7229	0.082
H30C	0.3112	0.8176	0.6639	0.082
H2B	0.5994	0.8088	0.2284	0.042
H3B	0.6524	0.8244	0.1496	0.050
H4B	0.6982	0.7384	0.1072	0.056
H5B	0.6886	0.6361	0.1421	0.056
H8B1	0.5632	0.5702	0.2871	0.051

H8B2	0.5329	0.6000	0.2351	0.051
H9B1	0.7160	0.5803	0.2513	0.092
H9B2	0.6697	0.5436	0.2889	0.092
H9B3	0.6801	0.6184	0.2961	0.092
H10D	0.5970	0.5560	0.1599	0.080
H10E	0.6059	0.5048	0.2062	0.080
H10F	0.6632	0.5334	0.1761	0.080
H13B	0.7170	0.9035	0.3462	0.065
H15B	0.5675	0.9805	0.2853	0.074
H17D	0.7227	0.7960	0.3706	0.062
H17E	0.6759	0.7496	0.3420	0.062
H17F	0.6631	0.7738	0.4010	0.062
H18D	0.7196	1.0114	0.3220	0.161
H18E	0.6569	1.0479	0.3288	0.161
H18F	0.6793	1.0269	0.2712	0.161
H19D	0.4873	0.8431	0.2692	0.104
H19E	0.4790	0.9187	0.2711	0.104
H19F	0.4653	0.8768	0.3227	0.104
H20B	0.5173	0.8103	0.4048	0.040
H21B	0.4696	0.7075	0.4230	0.044
H24B	0.5259	0.4833	0.4542	0.083
H26B	0.3909	0.4894	0.3534	0.099
H28D	0.5961	0.5620	0.4598	0.133
H28E	0.5623	0.6291	0.4641	0.133
H28F	0.6019	0.6130	0.4130	0.133
H29D	0.4280	0.3868	0.3865	0.172
H29E	0.4016	0.4125	0.4415	0.172
H29F	0.4695	0.3876	0.4383	0.172
H30D	0.3928	0.6553	0.3280	0.189
H30E	0.3726	0.5925	0.2968	0.189
H30F	0.4340	0.6276	0.2814	0.189
H1S1	0.2631	0.4992	0.3714	0.106
H1S2	0.2344	0.5258	0.4251	0.106
H1S3	0.3058	0.5187	0.4198	0.106

H2S1	0.2240	0.4143	0.4211	0.084
H2S2	0.2955	0.4072	0.4158	0.084
H3S1	0.2223	0.3510	0.5034	0.104
H3S2	0.2936	0.3430	0.5084	0.104
H4S1	0.2498	0.3375	0.5855	0.130
H4S2	0.2926	0.3987	0.5820	0.130
H4S3	0.2212	0.4067	0.5770	0.130
H1S4	0.3019	0.5206	0.6391	0.089
H1S5	0.3477	0.5062	0.5916	0.089
H1S6	0.2850	0.5409	0.5798	0.089
H2S3	0.2955	0.4119	0.6149	0.065
H2S4	0.2327	0.4468	0.6031	0.065
H3S3	0.2779	0.3374	0.5377	0.104
H3S4	0.2160	0.3708	0.5248	0.104
H4S4	0.2435	0.3109	0.4668	0.126
H4S5	0.2425	0.3830	0.4463	0.126
H4S6	0.3052	0.3492	0.4594	0.126

Table A2.3 Bond lengths for **2-2**.

Pd1-C1A	1.994(4)	C4B-C5B	1.385(7)
Pd1-C8A	2.018(4)	C4B-H4B	0.9500
Pd1-N2A	2.119(3)	C5B-C6B	1.397(6)
Pd1-N1A	2.170(3)	C5B-H5B	0.9500
N1A-C20A	1.285(5)	C6B-C7B	1.496(6)
N1A-C11A	1.435(5)	C7B-C8B	1.532(7)
N2A-C21A	1.274(5)	C7B-C10B	1.542(6)
N2A-C22A	1.435(5)	C7B-C9B	1.549(6)
C1A-C2A	1.395(6)	C8B-H8B1	0.9900
C1A-C6A	1.412(6)	C8B-H8B2	0.9900
C2A-C3A	1.400(5)	C9B-H9B1	0.9800
C2A-H2A	0.9500	C9B-H9B2	0.9800
C3A-C4A	1.380(7)	C9B-H9B3	0.9800
C3A-H3A	0.9500	C10B-H10D	0.9800
C4A-C5A	1.382(7)	C10B-H10E	0.9800

C4A-H4A	0.9500	C10B-H10F	0.9800
C5A-C6A	1.405(5)	C11B-C12B	1.388(6)
C5A-H5A	0.9500	C11B-C16B	1.390(6)
C6A-C7A	1.511(6)	C12B-C13B	1.382(6)
C7A-C9A	1.527(7)	C12B-C17B	1.498(6)
C7A-C8A	1.539(5)	C13B-C14B	1.388(8)
C7A-C10A	1.544(6)	C13B-H13B	0.9500
C8A-H8A1	0.9900	C14B-C15B	1.361(9)
C8A-H8A2	0.9900	C14B-C18B	1.523(8)
C9A-H9A1	0.9800	C15B-C16B	1.407(7)
C9A-H9A2	0.9800	C15B-H15B	0.9500
C9A-H9A3	0.9800	C16B-C19B	1.496(8)
C10A-H10A	0.9800	C17B-H17D	0.9800
C10A-H10B	0.9800	C17B-H17E	0.9800
C10A-H10C	0.9800	C17B-H17F	0.9800
C11A-C16A	1.393(6)	C18B-H18D	0.9800
C11A-C12A	1.398(5)	C18B-H18E	0.9800
C12A-C13A	1.393(6)	C18B-H18F	0.9800
C12A-C17A	1.511(6)	C19B-H19D	0.9800
C13A-C14A	1.391(6)	C19B-H19E	0.9800
C13A-H13A	0.9500	C19B-H19F	0.9800
C14A-C15A	1.392(5)	C20B-C21B	1.463(6)
C14A-C18A	1.509(6)	C20B-H20B	0.9500
C15A-C16A	1.392(6)	C21B-H21B	0.9500
C15A-H15A	0.9500	C22B-C27B	1.381(7)
C16A-C19A	1.508(5)	C22B-C23B	1.394(8)
C17A-H17A	0.9800	C23B-C24B	1.411(8)
C17A-H17B	0.9800	C23B-C28B	1.448(9)
C17A-H17C	0.9800	C24B-C25B	1.294(9)
C18A-H18A	0.9800	C24B-H24B	0.9500
C18A-H18B	0.9800	C25B-C26B	1.367(10)
C18A-H18C	0.9800	C25B-C29B	1.555(9)
C19A-H19A	0.9800	C26B-C27B	1.491(10)
C19A-H19B	0.9800	C26B-H26B	0.9500
C19A-H19C	0.9800	C27B-C30B	1.525(11)
C20A-C21A	1.460(6)	C28B-H28D	0.9800

C20A-H20A	0.9500	C28B-H28E	0.9800
C21A-H21A	0.9500	C28B-H28F	0.9800
C22A-C23A	1.389(6)	C29B-H29D	0.9800
C22A-C27A	1.395(6)	C29B-H29E	0.9800
C23A-C24A	1.393(6)	C29B-H29F	0.9800
C23A-C28A	1.513(7)	C30B-H30D	0.9800
C24A-C25A	1.376(7)	C30B-H30E	0.9800
C24A-H24A	0.9500	C30B-H30F	0.9800
C25A-C26A	1.378(6)	C1S-C2S	1.503(12)
C25A-C29A	1.514(6)	C1S-H1S1	0.9800
C26A-C27A	1.399(5)	C1S-H1S2	0.9800
C26A-H26A	0.9500	C1S-H1S3	0.9800
C27A-C30A	1.499(6)	C2S-O1S	1.403(9)
C28A-H28A	0.9800	C2S-H2S1	0.9900
C28A-H28B	0.9800	C2S-H2S2	0.9900
C28A-H28C	0.9800	O1S-C3S	1.506(9)
C29A-H29A	0.9800	C3S-C4S	1.334(11)
C29A-H29B	0.9800	C3S-H3S1	0.9900
C29A-H29C	0.9800	C3S-H3S2	0.9900
C30A-H30A	0.9800	C4S-H4S1	0.9800
C30A-H30B	0.9800	C4S-H4S2	0.9800
C30A-H30C	0.9800	C4S-H4S3	0.9800
Pd2-C1B	1.993(4)	C1S'-C2S'	1.513(17)
Pd2-C8B	2.039(5)	C1S'-H1S4	0.9800
Pd2-N2B	2.117(3)	C1S'-H1S5	0.9800
Pd2-N1B	2.158(3)	C1S'-H1S6	0.9800
N1B-C20B	1.281(5)	C2S'-O1S'	1.398(14)
N1B-C11B	1.440(5)	C2S'-H2S3	0.9900
N2B-C21B	1.289(5)	C2S'-H2S4	0.9900
N2B-C22B	1.462(6)	O1S'-C3S'	1.422(10)
C1B-C2B	1.393(6)	C3S'-C4S'	1.244(15)
C1B-C6B	1.411(6)	C3S'-H3S3	0.9900
C2B-C3B	1.395(5)	C3S'-H3S4	0.9900
C2B-H2B	0.9500	C4S'-H4S4	0.9800
C3B-C4B	1.383(7)	C4S'-H4S5	0.9800
C3B-H3B	0.9500	C4S'-H4S6	0.9800

Table A2.4 Bond angles for **2-2**.

C1A-Pd1-C8A	79.42(16)	C4B-C5B-H5B	119.8
C1A-Pd1-N2A	177.82(14)	C6B-C5B-H5B	119.8
C8A-Pd1-N2A	98.89(14)	C5B-C6B-C1B	120.1(4)
C1A-Pd1-N1A	104.96(14)	C5B-C6B-C7B	124.6(4)
C8A-Pd1-N1A	174.33(15)	C1B-C6B-C7B	115.2(4)
N2A-Pd1-N1A	76.82(12)	C6B-C7B-C8B	104.5(4)
C20A-N1A-C11A	116.4(3)	C6B-C7B-C10B	112.9(4)
C20A-N1A-Pd1	112.2(3)	C8B-C7B-C10B	111.0(4)
C11A-N1A-Pd1	131.2(2)	C6B-C7B-C9B	108.7(4)
C21A-N2A-C22A	118.7(3)	C8B-C7B-C9B	109.8(4)
C21A-N2A-Pd1	114.6(3)	C10B-C7B-C9B	109.9(4)
C22A-N2A-Pd1	126.7(2)	C7B-C8B-Pd2	110.6(3)
C2A-C1A-C6A	118.4(3)	C7B-C8B-H8B1	109.5
C2A-C1A-Pd1	125.5(3)	Pd2-C8B-H8B1	109.5
C6A-C1A-Pd1	115.9(3)	C7B-C8B-H8B2	109.5
C1A-C2A-C3A	121.1(4)	Pd2-C8B-H8B2	109.5
C1A-C2A-H2A	119.5	H8B1-C8B-H8B2	108.1
C3A-C2A-H2A	119.5	C7B-C9B-H9B1	109.5
C4A-C3A-C2A	120.0(4)	C7B-C9B-H9B2	109.5
C4A-C3A-H3A	120.0	H9B1-C9B-H9B2	109.5
C2A-C3A-H3A	120.0	C7B-C9B-H9B3	109.5
C3A-C4A-C5A	120.1(4)	H9B1-C9B-H9B3	109.5
C3A-C4A-H4A	120.0	H9B2-C9B-H9B3	109.5
C5A-C4A-H4A	120.0	C7B-C10B-H10D	109.5
C4A-C5A-C6A	120.7(4)	C7B-C10B-H10E	109.5
C4A-C5A-H5A	119.7	H10D-C10B-H10E	109.5
C6A-C5A-H5A	119.7	C7B-C10B-H10F	109.5
C5A-C6A-C1A	119.7(4)	H10D-C10B-H10F	109.5
C5A-C6A-C7A	125.4(4)	H10E-C10B-H10F	109.5
C1A-C6A-C7A	114.9(3)	C12B-C11B-C16B	122.9(4)
C6A-C7A-C9A	110.3(4)	C12B-C11B-N1B	117.6(4)

C6A-C7A-C8A	104.0(3)	C16B-C11B-N1B	119.4(4)
C9A-C7A-C8A	110.1(3)	C13B-C12B-C11B	117.5(5)
C6A-C7A-C10A	112.5(4)	C13B-C12B-C17B	121.4(5)
C9A-C7A-C10A	109.7(4)	C11B-C12B-C17B	121.1(4)
C8A-C7A-C10A	110.1(4)	C12B-C13B-C14B	121.9(6)
C7A-C8A-Pd1	111.4(3)	C12B-C13B-H13B	119.0
C7A-C8A-H8A1	109.4	C14B-C13B-H13B	119.0
Pd1-C8A-H8A1	109.4	C15B-C14B-C13B	118.7(5)
C7A-C8A-H8A2	109.4	C15B-C14B-C18B	120.6(6)
Pd1-C8A-H8A2	109.4	C13B-C14B-C18B	120.7(7)
H8A1-C8A-H8A2	108.0	C14B-C15B-C16B	122.5(5)
C7A-C9A-H9A1	109.5	C14B-C15B-H15B	118.8
C7A-C9A-H9A2	109.5	C16B-C15B-H15B	118.8
H9A1-C9A-H9A2	109.5	C11B-C16B-C15B	116.4(5)
C7A-C9A-H9A3	109.5	C11B-C16B-C19B	121.5(5)
H9A1-C9A-H9A3	109.5	C15B-C16B-C19B	122.1(5)
H9A2-C9A-H9A3	109.5	C12B-C17B-H17D	109.5
C7A-C10A-H10A	109.5	C12B-C17B-H17E	109.5
C7A-C10A-H10B	109.5	H17D-C17B-H17E	109.5
H10A-C10A-H10B	109.5	C12B-C17B-H17F	109.5
C7A-C10A-H10C	109.5	H17D-C17B-H17F	109.5
H10A-C10A-H10C	109.5	H17E-C17B-H17F	109.5
H10B-C10A-H10C	109.5	C14B-C18B-H18D	109.5
C16A-C11A-C12A	122.1(4)	C14B-C18B-H18E	109.5
C16A-C11A-N1A	118.8(3)	H18D-C18B-H18E	109.5
C12A-C11A-N1A	119.0(4)	C14B-C18B-H18F	109.5
C13A-C12A-C11A	117.5(4)	H18D-C18B-H18F	109.5
C13A-C12A-C17A	121.7(4)	H18E-C18B-H18F	109.5
C11A-C12A-C17A	120.7(4)	C16B-C19B-H19D	109.5
C14A-C13A-C12A	122.4(4)	C16B-C19B-H19E	109.5
C14A-C13A-H13A	118.8	H19D-C19B-H19E	109.5
C12A-C13A-H13A	118.8	C16B-C19B-H19F	109.5
C13A-C14A-C15A	117.7(4)	H19D-C19B-H19F	109.5
C13A-C14A-C18A	121.0(4)	H19E-C19B-H19F	109.5

C15A-C14A-C18A	121.3(4)	N1B-C20B-C21B	117.3(4)
C14A-C15A-C16A	122.2(4)	N1B-C20B-H20B	121.4
C14A-C15A-H15A	118.9	C21B-C20B-H20B	121.4
C16A-C15A-H15A	118.9	N2B-C21B-C20B	117.6(4)
C15A-C16A-C11A	117.9(3)	N2B-C21B-H21B	121.2
C15A-C16A-C19A	120.9(4)	C20B-C21B-H21B	121.2
C11A-C16A-C19A	121.2(4)	C27B-C22B-C23B	122.3(6)
C12A-C17A-H17A	109.5	C27B-C22B-N2B	118.9(6)
C12A-C17A-H17B	109.5	C23B-C22B-N2B	118.6(4)
H17A-C17A-H17B	109.5	C22B-C23B-C24B	118.7(6)
C12A-C17A-H17C	109.5	C22B-C23B-C28B	121.8(5)
H17A-C17A-H17C	109.5	C24B-C23B-C28B	119.5(6)
H17B-C17A-H17C	109.5	C25B-C24B-C23B	122.2(7)
C14A-C18A-H18A	109.5	C25B-C24B-H24B	118.9
C14A-C18A-H18B	109.5	C23B-C24B-H24B	118.9
H18A-C18A-H18B	109.5	C24B-C25B-C26B	121.0(7)
C14A-C18A-H18C	109.5	C24B-C25B-C29B	123.3(8)
H18A-C18A-H18C	109.5	C26B-C25B-C29B	115.7(7)
H18B-C18A-H18C	109.5	C25B-C26B-C27B	121.2(6)
C16A-C19A-H19A	109.5	C25B-C26B-H26B	119.4
C16A-C19A-H19B	109.5	C27B-C26B-H26B	119.4
H19A-C19A-H19B	109.5	C22B-C27B-C26B	114.4(7)
C16A-C19A-H19C	109.5	C22B-C27B-C30B	118.5(6)
H19A-C19A-H19C	109.5	C26B-C27B-C30B	127.0(6)
H19B-C19A-H19C	109.5	C23B-C28B-H28D	109.5
N1A-C20A-C21A	118.2(4)	C23B-C28B-H28E	109.5
N1A-C20A-H20A	120.9	H28D-C28B-H28E	109.5
C21A-C20A-H20A	120.9	C23B-C28B-H28F	109.5
N2A-C21A-C20A	117.9(3)	H28D-C28B-H28F	109.5
N2A-C21A-H21A	121.1	H28E-C28B-H28F	109.5
C20A-C21A-H21A	121.1	C25B-C29B-H29D	109.5
C23A-C22A-C27A	121.9(4)	C25B-C29B-H29E	109.5
C23A-C22A-N2A	119.0(4)	H29D-C29B-H29E	109.5
C27A-C22A-N2A	119.1(4)	C25B-C29B-H29F	109.5

C22A-C23A-C24A	117.7(4)	H29D-C29B-H29F	109.5
C22A-C23A-C28A	121.3(4)	H29E-C29B-H29F	109.5
C24A-C23A-C28A	121.0(4)	C27B-C30B-H30D	109.5
C25A-C24A-C23A	122.1(4)	C27B-C30B-H30E	109.5
C25A-C24A-H24A	118.9	H30D-C30B-H30E	109.5
C23A-C24A-H24A	118.9	C27B-C30B-H30F	109.5
C24A-C25A-C26A	118.7(4)	H30D-C30B-H30F	109.5
C24A-C25A-C29A	120.5(4)	H30E-C30B-H30F	109.5
C26A-C25A-C29A	120.7(4)	C2S-C1S-H1S1	109.5
C25A-C26A-C27A	121.7(4)	C2S-C1S-H1S2	109.5
C25A-C26A-H26A	119.1	H1S1-C1S-H1S2	109.5
C27A-C26A-H26A	119.1	C2S-C1S-H1S3	109.5
C22A-C27A-C26A	117.7(4)	H1S1-C1S-H1S3	109.5
C22A-C27A-C30A	121.0(4)	H1S2-C1S-H1S3	109.5
C26A-C27A-C30A	121.3(4)	O1S-C2S-C1S	110.7(7)
C23A-C28A-H28A	109.5	O1S-C2S-H2S1	109.5
C23A-C28A-H28B	109.5	C1S-C2S-H2S1	109.5
H28A-C28A-H28B	109.5	O1S-C2S-H2S2	109.5
C23A-C28A-H28C	109.5	C1S-C2S-H2S2	109.5
H28A-C28A-H28C	109.5	H2S1-C2S-H2S2	108.1
H28B-C28A-H28C	109.5	C2S-O1S-C3S	118.9(6)
C25A-C29A-H29A	109.5	C4S-C3S-O1S	113.5(7)
C25A-C29A-H29B	109.5	C4S-C3S-H3S1	108.9
H29A-C29A-H29B	109.5	O1S-C3S-H3S1	108.9
C25A-C29A-H29C	109.5	C4S-C3S-H3S2	108.9
H29A-C29A-H29C	109.5	O1S-C3S-H3S2	108.9
H29B-C29A-H29C	109.5	H3S1-C3S-H3S2	107.7
C27A-C30A-H30A	109.5	C3S-C4S-H4S1	109.5
C27A-C30A-H30B	109.5	C3S-C4S-H4S2	109.5
H30A-C30A-H30B	109.5	H4S1-C4S-H4S2	109.5
C27A-C30A-H30C	109.5	C3S-C4S-H4S3	109.5
H30A-C30A-H30C	109.5	H4S1-C4S-H4S3	109.5
H30B-C30A-H30C	109.5	H4S2-C4S-H4S3	109.5
C1B-Pd2-C8B	79.43(18)	C2S'-C1S'-H1S4	109.5

C1B-Pd2-N2B	178.25(15)	C2S'-C1S'-H1S5	109.5
C8B-Pd2-N2B	99.34(17)	H1S4-C1S'-H1S5	109.5
C1B-Pd2-N1B	104.69(15)	C2S'-C1S'-H1S6	109.5
C8B-Pd2-N1B	175.48(15)	H1S4-C1S'-H1S6	109.5
N2B-Pd2-N1B	76.57(13)	H1S5-C1S'-H1S6	109.5
C20B-N1B-C11B	116.8(3)	O1S'-C2S'-C1S'	108.2(11)
C20B-N1B-Pd2	113.7(3)	O1S'-C2S'-H2S3	110.1
C11B-N1B-Pd2	129.3(2)	C1S'-C2S'-H2S3	110.1
C21B-N2B-C22B	119.1(3)	O1S'-C2S'-H2S4	110.1
C21B-N2B-Pd2	114.6(3)	C1S'-C2S'-H2S4	110.1
C22B-N2B-Pd2	126.2(3)	H2S3-C2S'-H2S4	108.4
C2B-C1B-C6B	118.4(4)	C2S'-O1S'-C3S'	124.4(10)
C2B-C1B-Pd2	125.7(3)	C4S'-C3S'-O1S'	129.6(12)
C6B-C1B-Pd2	115.7(3)	C4S'-C3S'-H3S3	104.9
C1B-C2B-C3B	121.0(4)	O1S'-C3S'-H3S3	104.9
C1B-C2B-H2B	119.5	C4S'-C3S'-H3S4	104.9
C3B-C2B-H2B	119.5	O1S'-C3S'-H3S4	104.9
C4B-C3B-C2B	120.0(4)	H3S3-C3S'-H3S4	105.8
C4B-C3B-H3B	120.0	C3S'-C4S'-H4S4	109.5
C2B-C3B-H3B	120.0	C3S'-C4S'-H4S5	109.5
C3B-C4B-C5B	120.0(4)	H4S4-C4S'-H4S5	109.5
C3B-C4B-H4B	120.0	C3S'-C4S'-H4S6	109.5
C5B-C4B-H4B	120.0	H4S4-C4S'-H4S6	109.5
C4B-C5B-C6B	120.3(4)	H4S5-C4S'-H4S6	109.5

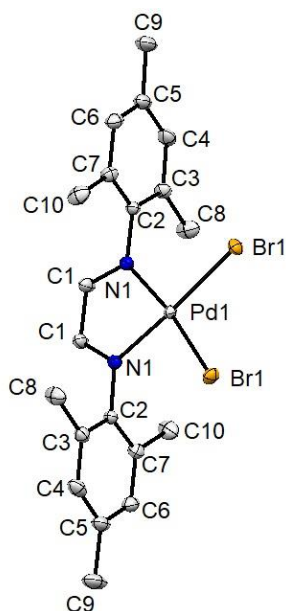


Figure A2.9 Displacement ellipsoid plot of **2-3** showing naming and numbering scheme. Ellipsoids are drawn at the 50% probability level and hydrogen atoms are omitted for clarity.

Table A2.5 Atomic coordinates for **2-3**.

Atom	x	y	z	$U_{\text{iso/equiv}}$
Pd1	0.5000	0.5000	0.46336(2)	0.01203(4)
Br1	0.42702(2)	0.42922(2)	0.34829(2)	0.01988(6)
N1	0.55959(13)	0.54605(13)	0.57146(18)	0.0150(4)
C1	0.53397(18)	0.52572(19)	0.6521(2)	0.0201(5)
C2	0.62788(15)	0.59379(16)	0.5689(2)	0.0148(4)
C3	0.61878(17)	0.67456(16)	0.5676(2)	0.0186(5)
C4	0.6856(2)	0.71933(19)	0.5688(3)	0.0241(5)
C5	0.75952(18)	0.6858(2)	0.5687(3)	0.0239(6)
C6	0.76536(17)	0.60485(19)	0.5676(3)	0.0223(5)
C7	0.69999(17)	0.55770(17)	0.5672(2)	0.0194(5)
C8	0.53889(19)	0.70971(18)	0.5690(4)	0.0287(7)
C9	0.8316(2)	0.7351(2)	0.5722(3)	0.0351(8)
C10	0.7065(2)	0.47025(19)	0.5649(3)	0.0287(7)
H1	0.5576	0.5429	0.7083	0.024
H4	0.6811	0.7742	0.5696	0.029

H6	0.8153	0.5816	0.5670	0.027
H8A	0.5095	0.6885	0.6216	0.043
H8B	0.5121	0.6974	0.5106	0.043
H8C	0.5431	0.7661	0.5757	0.043
H9A	0.8406	0.7524	0.6363	0.053
H9B	0.8250	0.7803	0.5316	0.053
H9C	0.8761	0.7046	0.5508	0.053
H10A	0.6835	0.4485	0.6217	0.043
H10B	0.7612	0.4554	0.5614	0.043
H10C	0.6789	0.4502	0.5102	0.043

Table A2.6 Bond lengths for **2-3**.

Pd1-N1	2.023(3)	C5-C6	1.400(5)
Pd1-N1	2.023(3)	C5-C9	1.507(5)
Pd1-Br1	2.4085(5)	C6-C7	1.390(4)
Pd1-Br1	2.4085(5)	C6-H6	0.9500
N1-C1	1.287(4)	C7-C10	1.513(4)
N1-C2	1.438(3)	C8-H8A	0.9800
C1-C1	1.470(6)	C8-H8B	0.9800
C1-H1	0.9500	C8-H8C	0.9800
C2-C7	1.391(4)	C9-H9A	0.9800
C2-C3	1.402(4)	C9-H9B	0.9800
C3-C4	1.387(4)	C9-H9C	0.9800
C3-C8	1.506(4)	C10-H10A	0.9800
C4-C5	1.400(5)	C10-H10B	0.9800
C4-H4	0.9500	C10-H10C	0.9800

Table A2.7 Bond angles for **2-3**.

N1-Pd1-N1	79.92(14)	C7-C6-C5	121.7(3)
N1-Pd1-Br1	171.92(7)	C7-C6-H6	119.2
N1-Pd1-Br1	93.47(7)	C5-C6-H6	119.2
N1-Pd1-Br1	93.47(7)	C6-C7-C2	117.6(3)
N1-Pd1-Br1	171.92(7)	C6-C7-C10	121.6(3)
Br1-Pd1-Br1	93.47(3)	C2-C7-C10	120.8(3)
C1-N1-C2	117.4(3)	C3-C8-H8A	109.5

C1-N1-Pd1	114.1(2)	C3-C8-H8B	109.5
C2-N1-Pd1	128.46(19)	H8A-C8-H8B	109.5
N1-C1-C1	115.98(17)	C3-C8-H8C	109.5
N1-C1-H1	122.0	H8A-C8-H8C	109.5
C1-C1-H1	122.0	H8B-C8-H8C	109.5
C7-C2-C3	123.0(3)	C5-C9-H9A	109.5
C7-C2-N1	118.5(2)	C5-C9-H9B	109.5
C3-C2-N1	118.5(2)	H9A-C9-H9B	109.5
C4-C3-C2	117.4(3)	C5-C9-H9C	109.5
C4-C3-C8	122.4(3)	H9A-C9-H9C	109.5
C2-C3-C8	120.2(3)	H9B-C9-H9C	109.5
C3-C4-C5	121.8(3)	C7-C10-H10A	109.5
C3-C4-H4	119.1	C7-C10-H10B	109.5
C5-C4-H4	119.1	H10A-C10-H10B	109.5
C6-C5-C4	118.5(3)	C7-C10-H10C	109.5
C6-C5-C9	120.2(3)	H10A-C10-H10C	109.5
C4-C5-C9	121.2(3)	H10B-C10-H10C	109.5

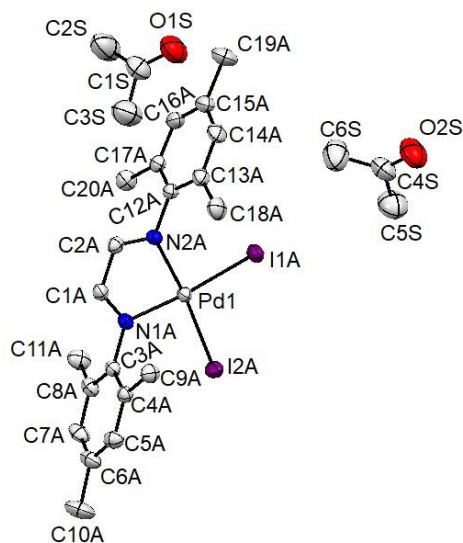


Figure A2.10 Displacement ellipsoid plot of **2-4** co-crystalized with an acetone molecule showing naming and numbering scheme. Ellipsoids are drawn at the 50% probability level and hydrogen atoms are omitted for clarity.

Table A2.8 Atomic coordinates for **2-4**.

Atom	x	y	z	U _{iso} /equiv
Pd1	0.72530(2)	0.43470(2)	0.75091(2)	0.02389(5)
I1A	0.61558(2)	0.46923(2)	0.69166(2)	0.03335(5)
I2A	0.64651(2)	0.40030(2)	0.80969(2)	0.03475(5)
N1A	0.81927(11)	0.40826(12)	0.79320(8)	0.0243(5)
N2A	0.79743(11)	0.46126(12)	0.70894(8)	0.0246(5)
C1A	0.87365(14)	0.41949(14)	0.77452(9)	0.0265(6)
C2A	0.86185(14)	0.45070(14)	0.72831(9)	0.0263(6)
C3A	0.82855(13)	0.37519(15)	0.83822(9)	0.0250(5)
C4A	0.83088(13)	0.30267(15)	0.84061(9)	0.0267(6)
C5A	0.83713(14)	0.27185(16)	0.88395(10)	0.0327(6)
C6A	0.84124(15)	0.31129(18)	0.92436(10)	0.0374(7)
C7A	0.83842(15)	0.38274(17)	0.92055(10)	0.0370(7)
C8A	0.83144(14)	0.41674(16)	0.87772(10)	0.0319(6)
C9A	0.82585(16)	0.25953(16)	0.79732(10)	0.0343(7)
C10A	0.8466(2)	0.2752(2)	0.97098(13)	0.0603(11)
C11A	0.82529(18)	0.49470(16)	0.87455(11)	0.0408(7)
C12A	0.78316(13)	0.49183(15)	0.66311(9)	0.0257(6)
C13A	0.76620(14)	0.44731(16)	0.62504(10)	0.0323(6)
C14A	0.75096(16)	0.47837(19)	0.58142(11)	0.0398(7)
C15A	0.75085(16)	0.54958(19)	0.57502(11)	0.0409(8)
C16A	0.76697(14)	0.59110(17)	0.61442(11)	0.0362(7)
C17A	0.78352(13)	0.56348(15)	0.65883(10)	0.0280(6)
C18A	0.76129(18)	0.36998(17)	0.63039(12)	0.0433(8)
C19A	0.7322(2)	0.5810(2)	0.52690(13)	0.0630(11)
C20A	0.79996(16)	0.60963(16)	0.70082(11)	0.0367(7)
Pd2	0.5000	0.70989(2)	0.7500	0.02370(6)
I1B	0.45069(2)	0.80402(2)	0.69072(2)	0.03423(5)
N1B	0.46238(11)	0.62680(12)	0.70775(7)	0.0244(5)
C1B	0.47798(13)	0.56732(15)	0.72689(9)	0.0253(5)
C2B	0.41771(13)	0.62932(14)	0.66235(9)	0.0251(5)
C3B	0.44963(15)	0.63653(15)	0.62315(10)	0.0304(6)
C4B	0.40508(16)	0.64023(16)	0.58045(10)	0.0375(7)

C5B	0.33193(16)	0.63813(17)	0.57605(10)	0.0372(7)
C6B	0.30333(15)	0.63195(16)	0.61609(10)	0.0335(6)
C7B	0.34484(13)	0.62701(14)	0.65993(9)	0.0257(5)
C8B	0.52834(15)	0.64235(19)	0.62673(11)	0.0405(8)
C9B	0.2847(2)	0.6439(2)	0.52914(12)	0.0637(12)
C10B	0.31223(14)	0.62050(17)	0.70278(10)	0.0339(7)
Pd3	1.0000	0.66003(2)	0.7500	0.02416(6)
I1C	0.98018(2)	0.56584(2)	0.80874(2)	0.03392(5)
N1C	0.98459(11)	0.74305(12)	0.79207(8)	0.0251(5)
C1C	0.99042(13)	0.80200(14)	0.77319(9)	0.0270(6)
C2C	0.96584(14)	0.74040(14)	0.83768(9)	0.0267(6)
C3C	1.01963(15)	0.73342(16)	0.87636(10)	0.0322(6)
C4C	0.99920(17)	0.72997(17)	0.91950(11)	0.0392(7)
C5C	0.92964(18)	0.73080(17)	0.92513(11)	0.0416(7)
C6C	0.87795(16)	0.73621(16)	0.88576(11)	0.0361(7)
C7C	0.89447(14)	0.74149(15)	0.84165(10)	0.0299(6)
C8C	1.09604(15)	0.72793(19)	0.87147(12)	0.0427(8)
C9C	0.9101(2)	0.7242(2)	0.97309(13)	0.0650(11)
C10C	0.83808(14)	0.74695(18)	0.79885(11)	0.0380(7)
O1S	0.88366(18)	0.46415(17)	0.50487(10)	0.0808(9)
C1S	0.9230(2)	0.4776(2)	0.54076(14)	0.0572(10)
C2S	0.9526(3)	0.5480(3)	0.55049(18)	0.0910(17)
C3S	0.9423(3)	0.4235(3)	0.57738(17)	0.0816(14)
O2S	0.46528(17)	0.38283(19)	0.50471(11)	0.0826(10)
C4S	0.4881(2)	0.4125(2)	0.54049(14)	0.0582(10)
C5S	0.4446(3)	0.4231(3)	0.57740(17)	0.0847(15)
C6S	0.5615(3)	0.4387(3)	0.55054(18)	0.0931(17)
H1A	0.9199	0.4080	0.7901	0.032
H2A	0.9002	0.4627	0.7132	0.032
H5A	0.8387	0.2225	0.8862	0.039
H7A	0.8413	0.4099	0.9480	0.044
H9A1	0.8262	0.2100	0.8055	0.051
H9A2	0.8662	0.2698	0.7820	0.051
H9A3	0.7818	0.2706	0.7762	0.051

H10A	0.8804	0.2366	0.9727	0.091
H10B	0.8001	0.2571	0.9744	0.091
H10C	0.8629	0.3085	0.9960	0.091
H11A	0.8616	0.5130	0.8580	0.061
H11B	0.8320	0.5145	0.9059	0.061
H11C	0.7783	0.5073	0.8576	0.061
H14A	0.7401	0.4493	0.5548	0.048
H16A	0.7666	0.6402	0.6108	0.043
H18A	0.7487	0.3484	0.5997	0.065
H18B	0.7249	0.3591	0.6490	0.065
H18C	0.8070	0.3519	0.6460	0.065
H19A	0.6818	0.5930	0.5206	0.094
H19B	0.7423	0.5473	0.5038	0.094
H19C	0.7604	0.6232	0.5252	0.094
H20A	0.7689	0.5976	0.7229	0.055
H20B	0.7923	0.6584	0.6914	0.055
H20C	0.8494	0.6031	0.7156	0.055
H1B	0.4616	0.5252	0.7117	0.030
H4B	0.4253	0.6444	0.5532	0.045
H6B	0.2533	0.6310	0.6135	0.040
H8B1	0.5449	0.6854	0.6431	0.061
H8B2	0.5403	0.6431	0.5955	0.061
H8B3	0.5512	0.6023	0.6439	0.061
H9B1	0.2633	0.6903	0.5257	0.096
H9B2	0.2474	0.6086	0.5266	0.096
H9B3	0.3128	0.6365	0.5046	0.096
H10D	0.2606	0.6208	0.6940	0.051
H10E	0.3273	0.6597	0.7236	0.051
H10F	0.3275	0.5768	0.7187	0.051
H1C	0.9827	0.8442	0.7885	0.032
H4C	1.0349	0.7269	0.9464	0.047
H6C	0.8297	0.7363	0.8892	0.043
H8C1	1.1032	0.6855	0.8543	0.064
H8C2	1.1256	0.7261	0.9024	0.064

H8C3	1.1092	0.7686	0.8546	0.064
H9C1	0.9012	0.6752	0.9794	0.097
H9C2	0.8675	0.7515	0.9744	0.097
H9C3	0.9491	0.7416	0.9965	0.097
H10G	0.8424	0.7917	0.7835	0.057
H10H	0.7913	0.7437	0.8078	0.057
H10I	0.8438	0.7090	0.7774	0.057
H2S1	0.9373	0.5667	0.5783	0.137
H2S2	0.9359	0.5785	0.5240	0.137
H2S3	1.0044	0.5457	0.5557	0.137
H3S1	0.9165	0.3804	0.5677	0.122
H3S2	0.9296	0.4399	0.6066	0.122
H3S3	0.9932	0.4146	0.5818	0.122
H5S1	0.4011	0.3956	0.5701	0.127
H5S2	0.4326	0.4725	0.5790	0.127
H5S3	0.4715	0.4081	0.6074	0.127
H6S1	0.5833	0.4338	0.5228	0.140
H6S2	0.5887	0.4117	0.5761	0.140
H6S3	0.5614	0.4878	0.5594	0.140

Table A2.9 Bond lengths for **2-4**.

Pd1-N1A	2.065(2)	C4B-C5B	1.389(4)
Pd1-N2A	2.069(2)	C4B-H4B	0.9500
Pd1-I2A	2.5668(5)	C5B-C6B	1.382(4)
Pd1-I1A	2.5700(5)	C5B-C9B	1.510(4)
N1A-C1A	1.279(3)	C6B-C7B	1.389(4)
N1A-C3A	1.444(3)	C6B-H6B	0.9500
N2A-C2A	1.284(3)	C7B-C10B	1.500(4)
N2A-C12A	1.444(3)	C8B-H8B1	0.9800
C1A-C2A	1.459(4)	C8B-H8B2	0.9800
C1A-H1A	0.9500	C8B-H8B3	0.9800
C2A-H2A	0.9500	C9B-H9B1	0.9800
C3A-C4A	1.395(4)	C9B-H9B2	0.9800
C3A-C8A	1.397(4)	C9B-H9B3	0.9800
C4A-C5A	1.384(4)	C10B-H10D	0.9800

C4A-C9A	1.502(4)	C10B-H10E	0.9800
C5A-C6A	1.394(4)	C10B-H10F	0.9800
C5A-H5A	0.9500	Pd3-N1C	2.067(2)
C6A-C7A	1.378(5)	Pd3-N1C	2.067(2)
C6A-C10A	1.516(4)	Pd3-I1C	2.5682(5)
C7A-C8A	1.398(4)	Pd3-I1C	2.5682(4)
C7A-H7A	0.9500	N1C-C1C	1.273(3)
C8A-C11A	1.504(4)	N1C-C2C	1.442(3)
C9A-H9A1	0.9800	C1C-C1C	1.466(6)
C9A-H9A2	0.9800	C1C-H1C	0.9500
C9A-H9A3	0.9800	C2C-C7C	1.396(4)
C10A-H10A	0.9800	C2C-C3C	1.398(4)
C10A-H10B	0.9800	C3C-C4C	1.386(4)
C10A-H10C	0.9800	C3C-C8C	1.503(4)
C11A-H11A	0.9800	C4C-C5C	1.375(5)
C11A-H11B	0.9800	C4C-H4C	0.9500
C11A-H11C	0.9800	C5C-C6C	1.386(5)
C12A-C17A	1.382(4)	C5C-C9C	1.518(5)
C12A-C13A	1.396(4)	C6C-C7C	1.384(4)
C13A-C14A	1.392(4)	C6C-H6C	0.9500
C13A-C18A	1.499(4)	C7C-C10C	1.508(4)
C14A-C15A	1.381(5)	C8C-H8C1	0.9800
C14A-H14A	0.9500	C8C-H8C2	0.9800
C15A-C16A	1.391(5)	C8C-H8C3	0.9800
C15A-C19A	1.515(5)	C9C-H9C1	0.9800
C16A-C17A	1.387(4)	C9C-H9C2	0.9800
C16A-H16A	0.9500	C9C-H9C3	0.9800
C17A-C20A	1.502(4)	C10C-H10G	0.9800
C18A-H18A	0.9800	C10C-H10H	0.9800
C18A-H18B	0.9800	C10C-H10I	0.9800
C18A-H18C	0.9800	O1S-C1S	1.209(4)
C19A-H19A	0.9800	C1S-C2S	1.476(6)
C19A-H19B	0.9800	C1S-C3S	1.492(6)
C19A-H19C	0.9800	C2S-H2S1	0.9800

C20A-H20A	0.9800	C2S-H2S2	0.9800
C20A-H20B	0.9800	C2S-H2S3	0.9800
C20A-H20C	0.9800	C3S-H3S1	0.9800
Pd2-N1B	2.070(2)	C3S-H3S2	0.9800
Pd2-N1B	2.070(2)	C3S-H3S3	0.9800
Pd2-I1B	2.5682(5)	O2S-C4S	1.204(5)
Pd2-I1B	2.5682(4)	C4S-C6S	1.478(6)
N1B-C1B	1.285(3)	C4S-C5S	1.489(6)
N1B-C2B	1.450(3)	C5S-H5S1	0.9800
C1B-C1B	1.463(5)	C5S-H5S2	0.9800
C1B-H1B	0.9500	C5S-H5S3	0.9800
C2B-C7B	1.390(4)	C6S-H6S1	0.9800
C2B-C3B	1.398(4)	C6S-H6S2	0.9800
C3B-C4B	1.386(4)	C6S-H6S3	0.9800
C3B-C8B	1.501(4)		

Table A2.10 Bond angles for **2-4**.

N1A-Pd1-N2A	79.03(9)	C3B-C4B-C5B	122.5(3)
N1A-Pd1-I2A	95.27(6)	C3B-C4B-H4B	118.7
N2A-Pd1-I2A	174.20(6)	C5B-C4B-H4B	118.7
N1A-Pd1-I1A	174.22(6)	C6B-C5B-C4B	118.0(3)
N2A-Pd1-I1A	95.28(6)	C6B-C5B-C9B	120.7(3)
I2A-Pd1-I1A	90.437(17)	C4B-C5B-C9B	121.3(3)
C1A-N1A-C3A	118.9(2)	C5B-C6B-C7B	122.5(3)
C1A-N1A-Pd1	113.37(18)	C5B-C6B-H6B	118.7
C3A-N1A-Pd1	127.55(16)	C7B-C6B-H6B	118.7
C2A-N2A-C12A	119.0(2)	C6B-C7B-C2B	117.1(3)
C2A-N2A-Pd1	113.17(19)	C6B-C7B-C10B	121.3(2)
C12A-N2A-Pd1	127.75(16)	C2B-C7B-C10B	121.6(2)
N1A-C1A-C2A	117.3(2)	C3B-C8B-H8B1	109.5
N1A-C1A-H1A	121.4	C3B-C8B-H8B2	109.5
C2A-C1A-H1A	121.4	H8B1-C8B-H8B2	109.5
N2A-C2A-C1A	117.1(2)	C3B-C8B-H8B3	109.5
N2A-C2A-H2A	121.5	H8B1-C8B-H8B3	109.5

C1A-C2A-H2A	121.5	H8B2-C8B-H8B3	109.5
C4A-C3A-C8A	122.2(3)	C5B-C9B-H9B1	109.5
C4A-C3A-N1A	118.9(2)	C5B-C9B-H9B2	109.5
C8A-C3A-N1A	118.9(3)	H9B1-C9B-H9B2	109.5
C5A-C4A-C3A	118.0(3)	C5B-C9B-H9B3	109.5
C5A-C4A-C9A	121.2(3)	H9B1-C9B-H9B3	109.5
C3A-C4A-C9A	120.8(2)	H9B2-C9B-H9B3	109.5
C4A-C5A-C6A	121.7(3)	C7B-C10B-H10D	109.5
C4A-C5A-H5A	119.1	C7B-C10B-H10E	109.5
C6A-C5A-H5A	119.1	H10D-C10B-H10E	109.5
C7A-C6A-C5A	118.5(3)	C7B-C10B-H10F	109.5
C7A-C6A-C10A	121.6(3)	H10D-C10B-H10F	109.5
C5A-C6A-C10A	119.9(3)	H10E-C10B-H10F	109.5
C6A-C7A-C8A	122.3(3)	N1C-Pd3-N1C	78.97(13)
C6A-C7A-H7A	118.8	N1C-Pd3-I1C	95.32(6)
C8A-C7A-H7A	118.8	N1C-Pd3-I1C	174.25(6)
C3A-C8A-C7A	117.2(3)	N1C-Pd3-I1C	174.25(6)
C3A-C8A-C11A	121.8(3)	N1C-Pd3-I1C	95.32(6)
C7A-C8A-C11A	121.0(3)	I1C ² -Pd3-I1C	90.40(2)
C4A-C9A-H9A1	109.5	C1C-N1C-C2C	119.2(2)
C4A-C9A-H9A2	109.5	C1C-N1C-Pd3	113.34(19)
H9A1-C9A-H9A2	109.5	C2C-N1C-Pd3	127.44(18)
C4A-C9A-H9A3	109.5	N1C-C1C-C1C	117.14(16)
H9A1-C9A-H9A3	109.5	N1C-C1C-H1C	121.4
H9A2-C9A-H9A3	109.5	C1C ² -C1C-H1C	121.4
C6A-C10A-H10A	109.5	C7C-C2C-C3C	122.1(3)
C6A-C10A-H10B	109.5	C7C-C2C-N1C	118.9(2)
H10A-C10A-H10B	109.5	C3C-C2C-N1C	118.8(2)
C6A-C10A-H10C	109.5	C4C-C3C-C2C	117.0(3)
H10A-C10A-H10C	109.5	C4C-C3C-C8C	121.3(3)
H10B-C10A-H10C	109.5	C2C-C3C-C8C	121.7(3)
C8A-C11A-H11A	109.5	C5C-C4C-C3C	122.9(3)
C8A-C11A-H11B	109.5	C5C-C4C-H4C	118.5
H11A-C11A-H11B	109.5	C3C-C4C-H4C	118.5

C8A-C11A-H11C	109.5	C4C-C5C-C6C	118.2(3)
H11A-C11A-H11C	109.5	C4C-C5C-C9C	120.8(3)
H11B-C11A-H11C	109.5	C6C-C5C-C9C	121.1(3)
C17A-C12A-C13A	122.8(3)	C7C-C6C-C5C	122.1(3)
C17A-C12A-N2A	119.1(2)	C7C-C6C-H6C	119.0
C13A-C12A-N2A	118.0(3)	C5C-C6C-H6C	119.0
C14A-C13A-C12A	116.7(3)	C6C-C7C-C2C	117.7(3)
C14A-C13A-C18A	120.9(3)	C6C-C7C-C10C	121.9(3)
C12A-C13A-C18A	122.3(3)	C2C-C7C-C10C	120.4(3)
C15A-C14A-C13A	123.0(3)	C3C-C8C-H8C1	109.5
C15A-C14A-H14A	118.5	C3C-C8C-H8C2	109.5
C13A-C14A-H14A	118.5	H8C1-C8C-H8C2	109.5
C14A-C15A-C16A	117.5(3)	C3C-C8C-H8C3	109.5
C14A-C15A-C19A	121.0(3)	H8C1-C8C-H8C3	109.5
C16A-C15A-C19A	121.5(3)	H8C2-C8C-H8C3	109.5
C17A-C16A-C15A	122.5(3)	C5C-C9C-H9C1	109.5
C17A-C16A-H16A	118.8	C5C-C9C-H9C2	109.5
C15A-C16A-H16A	118.8	H9C1-C9C-H9C2	109.5
C12A-C17A-C16A	117.5(3)	C5C-C9C-H9C3	109.5
C12A-C17A-C20A	121.2(3)	H9C1-C9C-H9C3	109.5
C16A-C17A-C20A	121.3(3)	H9C2-C9C-H9C3	109.5
C13A-C18A-H18A	109.5	C7C-C10C-H10G	109.5
C13A-C18A-H18B	109.5	C7C-C10C-H10H	109.5
H18A-C18A-H18B	109.5	H10G-C10C-H10H	109.5
C13A-C18A-H18C	109.5	C7C-C10C-H10I	109.5
H18A-C18A-H18C	109.5	H10G-C10C-H10I	109.5
H18B-C18A-H18C	109.5	H10H-C10C-H10I	109.5
C15A-C19A-H19A	109.5	O1S-C1S-C2S	121.6(4)
C15A-C19A-H19B	109.5	O1S-C1S-C3S	120.8(4)
H19A-C19A-H19B	109.5	C2S-C1S-C3S	117.5(4)
C15A-C19A-H19C	109.5	C1S-C2S-H2S1	109.5
H19A-C19A-H19C	109.5	C1S-C2S-H2S2	109.5
H19B-C19A-H19C	109.5	H2S1-C2S-H2S2	109.5
C17A-C20A-H20A	109.5	C1S-C2S-H2S3	109.5

C17A-C20A-H20B	109.5	H2S1-C2S-H2S3	109.5
H20A-C20A-H20B	109.5	H2S2-C2S-H2S3	109.5
C17A-C20A-H20C	109.5	C1S-C3S-H3S1	109.5
H20A-C20A-H20C	109.5	C1S-C3S-H3S2	109.5
H20B-C20A-H20C	109.5	H3S1-C3S-H3S2	109.5
N1B-Pd2-N1B	79.05(12)	C1S-C3S-H3S3	109.5
N1B-Pd2-I1B	95.25(6)	H3S1-C3S-H3S3	109.5
N1B-Pd2-I1B	174.14(6)	H3S2-C3S-H3S3	109.5
N1B-Pd2-I1B	174.14(6)	O2S-C4S-C6S	121.6(4)
N1B-Pd2-I1B	95.25(6)	O2S-C4S-C5S	121.9(4)
I1B-Pd2-I1B	90.48(2)	C6S-C4S-C5S	116.5(4)
C1B-N1B-C2B	119.0(2)	C4S-C5S-H5S1	109.5
C1B-N1B-Pd2	113.32(18)	C4S-C5S-H5S2	109.5
C2B-N1B-Pd2	127.55(17)	H5S1-C5S-H5S2	109.5
N1B-C1B-C1B	117.08(15)	C4S-C5S-H5S3	109.5
N1B-C1B-H1B	121.5	H5S1-C5S-H5S3	109.5
C1B-C1B-H1B	121.5	H5S2-C5S-H5S3	109.5
C7B-C2B-C3B	122.9(2)	C4S-C6S-H6S1	109.5
C7B-C2B-N1B	118.4(2)	C4S-C6S-H6S2	109.5
C3B-C2B-N1B	118.7(2)	H6S1-C6S-H6S2	109.5
C4B-C3B-C2B	116.9(3)	C4S-C6S-H6S3	109.5
C4B-C3B-C8B	121.0(3)	H6S1-C6S-H6S3	109.5
C2B-C3B-C8B	122.1(3)	H6S2-C6S-H6S3	109.5

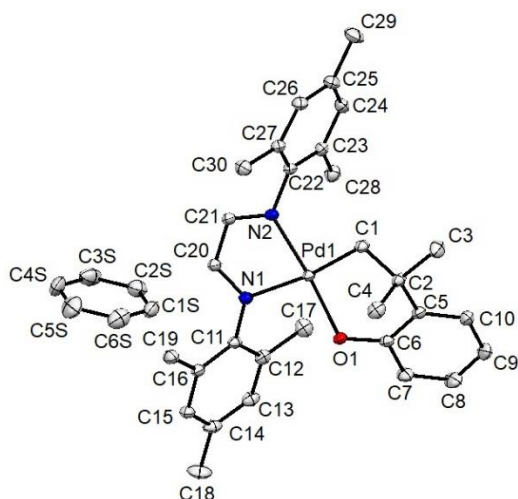


Figure A2.11 Displacement ellipsoid plot of **2-5** co-crystallized with a benzene molecule showing naming and numbering scheme. Ellipsoids are drawn at the 50% probability level and hydrogen atoms are omitted for clarity.

Table A2.11 Atomic coordinates for **2-5**.

Atom	x	y	z	$U_{\text{iso/equiv}}$
Pd1	0.59927(2)	0.33445(2)	0.41881(2)	0.01358(2)
O1	0.60930(9)	0.33516(4)	0.27694(6)	0.01661(14)
N1	0.44216(10)	0.26744(4)	0.41602(7)	0.01567(16)
N2	0.57067(10)	0.32759(4)	0.55976(7)	0.01515(16)
C1	0.74955(12)	0.39430(5)	0.44168(8)	0.01729(19)
C2	0.83109(12)	0.40891(5)	0.35675(8)	0.01692(19)
C3	0.93072(14)	0.45862(7)	0.39001(10)	0.0266(3)
C4	0.91552(13)	0.35513(6)	0.33093(10)	0.0232(2)
C5	0.73672(12)	0.42613(5)	0.26801(8)	0.01601(18)
C6	0.63319(12)	0.38586(5)	0.23296(8)	0.01567(18)
C7	0.55397(14)	0.39881(6)	0.14615(9)	0.0229(2)
C8	0.57353(17)	0.45017(6)	0.09574(10)	0.0299(3)
C9	0.67123(16)	0.49060(6)	0.13083(10)	0.0270(3)
C10	0.75179(14)	0.47793(6)	0.21653(9)	0.0210(2)
C11	0.36656(11)	0.23931(5)	0.33580(8)	0.01532(18)
C12	0.28007(12)	0.27510(6)	0.27409(8)	0.0179(2)
C13	0.19912(12)	0.24768(6)	0.19918(9)	0.0210(2)
C14	0.20538(13)	0.18685(6)	0.18376(9)	0.0216(2)

C15	0.29738(13)	0.15363(6)	0.24302(8)	0.0202(2)
C16	0.38053(12)	0.17889(5)	0.31928(8)	0.01690(19)
C17	0.27123(14)	0.34058(6)	0.28995(11)	0.0243(2)
C18	0.11519(16)	0.15830(8)	0.10288(11)	0.0334(3)
C19	0.48221(14)	0.14160(6)	0.37957(9)	0.0226(2)
C20	0.42369(12)	0.25103(5)	0.50204(8)	0.01767(19)
C21	0.49460(12)	0.28432(5)	0.58186(8)	0.01703(19)
C22	0.62379(12)	0.36794(5)	0.63359(8)	0.01557(18)
C23	0.56251(13)	0.42366(5)	0.63439(8)	0.0182(2)
C24	0.61726(14)	0.46463(6)	0.70190(9)	0.0219(2)
C25	0.73074(15)	0.45128(6)	0.76615(9)	0.0232(2)
C26	0.78821(14)	0.39525(6)	0.76299(9)	0.0212(2)
C27	0.73565(12)	0.35240(5)	0.69776(8)	0.01754(19)
C28	0.43983(14)	0.43843(6)	0.56566(9)	0.0231(2)
C29	0.78873(18)	0.49617(7)	0.83885(11)	0.0344(3)
C30	0.79684(14)	0.29164(6)	0.69658(10)	0.0233(2)
C1S	0.02508(16)	0.20220(7)	0.43243(10)	0.0301(3)
C2S	-0.09777(17)	0.21213(7)	0.46916(11)	0.0323(3)
C3S	-0.15116(18)	0.16995(8)	0.52567(13)	0.0384(4)
C4S	-0.0828(2)	0.11792(9)	0.54575(12)	0.0426(4)
C5S	0.0400(2)	0.10775(8)	0.50858(13)	0.0420(4)
C6S	0.09378(16)	0.15021(9)	0.45193(12)	0.0344(3)
H1A	0.7093	0.4315	0.4632	0.021
H1B	0.8141	0.3800	0.4956	0.021
H3A	0.8795	0.4942	0.4037	0.040
H3B	0.9894	0.4672	0.3390	0.040
H3C	0.9868	0.4462	0.4485	0.040
H4A	0.9690	0.3655	0.2778	0.035
H4B	0.8544	0.3223	0.3112	0.035
H4C	0.9769	0.3434	0.3873	0.035
H7	0.4856	0.3717	0.1216	0.028
H8	0.5196	0.4577	0.0367	0.036
H9	0.6833	0.5264	0.0972	0.032
H10	0.8191	0.5056	0.2404	0.025

H13	0.1384	0.2709	0.1577	0.025
H15	0.3041	0.1124	0.2315	0.024
H17A	0.2378	0.3481	0.3527	0.036
H17B	0.2085	0.3581	0.2388	0.036
H17C	0.3616	0.3582	0.2887	0.036
H18A	0.1685	0.1501	0.0488	0.050
H18B	0.0402	0.1850	0.0816	0.050
H18C	0.0784	0.1213	0.1258	0.050
H19A	0.4470	0.1324	0.4411	0.034
H19B	0.5681	0.1633	0.3916	0.034
H19C	0.4979	0.1048	0.3452	0.034
H20	0.3663	0.2186	0.5133	0.021
H21	0.4851	0.2745	0.6471	0.020
H24	0.5765	0.5025	0.7043	0.026
H26	0.8654	0.3860	0.8065	0.025
H28A	0.4030	0.4767	0.5831	0.035
H28B	0.3704	0.4078	0.5693	0.035
H28C	0.4662	0.4404	0.4998	0.035
H29A	0.7923	0.4793	0.9038	0.052
H29B	0.7309	0.5314	0.8352	0.052
H29C	0.8807	0.5070	0.8249	0.052
H30A	0.8856	0.2916	0.7349	0.035
H30B	0.8084	0.2804	0.6300	0.035
H30C	0.7364	0.2633	0.7241	0.035
H1S	0.0620	0.2314	0.3936	0.036
H2S	-0.1454	0.2481	0.4554	0.039
H3S	-0.2356	0.1769	0.5509	0.046
H4S	-0.1197	0.0890	0.5850	0.051
H5S	0.0873	0.0717	0.5220	0.050
H6S	0.1781	0.1434	0.4266	0.041

Table A2.12 Bond lengths for **2-5**.

Pd1-O1	1.9900(10)	C17-H17B	0.9800
Pd1-C1	2.0124(12)	C17-H17C	0.9800
Pd1-N2	2.0187(11)	C18-H18A	0.9800

Pd1-N1	2.1685(10)	C18-H18B	0.9800
O1-C6	1.3339(14)	C18-H18C	0.9800
N1-C20	1.2856(15)	C19-H19A	0.9800
N1-C11	1.4309(14)	C19-H19B	0.9800
N2-C21	1.2907(15)	C19-H19C	0.9800
N2-C22	1.4358(14)	C20-C21	1.4635(16)
C1-C2	1.5331(16)	C20-H20	0.9500
C1-H1A	0.9900	C21-H21	0.9500
C1-H1B	0.9900	C22-C27	1.3959(16)
C2-C5	1.5237(16)	C22-C23	1.4003(17)
C2-C3	1.5363(17)	C23-C24	1.3920(17)
C2-C4	1.5392(18)	C23-C28	1.5058(18)
C3-H3A	0.9800	C24-C25	1.3966(19)
C3-H3B	0.9800	C24-H24	0.9500
C3-H3C	0.9800	C25-C26	1.3927(19)
C4-H4A	0.9800	C25-C29	1.5077(19)
C4-H4B	0.9800	C26-C27	1.3943(17)
C4-H4C	0.9800	C26-H26	0.9500
C5-C10	1.3909(17)	C27-C30	1.5039(18)
C5-C6	1.4202(17)	C28-H28A	0.9800
C6-C7	1.4049(16)	C28-H28B	0.9800
C7-C8	1.382(2)	C28-H28C	0.9800
C7-H7	0.9500	C29-H29A	0.9800
C8-C9	1.384(2)	C29-H29B	0.9800
C8-H8	0.9500	C29-H29C	0.9800
C9-C10	1.3976(19)	C30-H30A	0.9800
C9-H9	0.9500	C30-H30B	0.9800
C10-H10	0.9500	C30-H30C	0.9800
C11-C16	1.3969(17)	C1S-C6S	1.373(2)
C11-C12	1.4074(16)	C1S-C2S	1.382(2)
C12-C13	1.3961(17)	C1S-H1S	0.9500
C12-C17	1.5031(18)	C2S-C3S	1.376(2)
C13-C14	1.397(2)	C2S-H2S	0.9500
C13-H13	0.9500	C3S-C4S	1.373(3)

C14-C15	1.3874(19)	C3S-H3S	0.9500
C14-C18	1.5109(18)	C4S-C5S	1.386(3)
C15-C16	1.3993(16)	C4S-H4S	0.9500
C15-H15	0.9500	C5S-C6S	1.383(3)
C16-C19	1.5035(18)	C5S-H5S	0.9500
C17-H17A	0.9800	C6S-H6S	0.9500

Table A2.13 Bond angles for **2-5**.

O1-Pd1-C1	92.45(4)	C12-C17-H17C	109.5
O1-Pd1-N2	173.48(4)	H17A-C17-H17C	109.5
C1-Pd1-N2	94.04(4)	H17B-C17-H17C	109.5
O1-Pd1-N1	95.41(4)	C14-C18-H18A	109.5
C1-Pd1-N1	171.84(4)	C14-C18-H18B	109.5
N2-Pd1-N1	78.12(4)	H18A-C18-H18B	109.5
C6-O1-Pd1	119.50(7)	C14-C18-H18C	109.5
C20-N1-C11	119.25(10)	H18A-C18-H18C	109.5
C20-N1-Pd1	110.70(8)	H18B-C18-H18C	109.5
C11-N1-Pd1	129.99(7)	C16-C19-H19A	109.5
C21-N2-C22	119.47(10)	C16-C19-H19B	109.5
C21-N2-Pd1	115.60(8)	H19A-C19-H19B	109.5
C22-N2-Pd1	124.88(8)	C16-C19-H19C	109.5
C2-C1-Pd1	117.35(8)	H19A-C19-H19C	109.5
C2-C1-H1A	108.0	H19B-C19-H19C	109.5
Pd1-C1-H1A	108.0	N1-C20-C21	117.29(11)
C2-C1-H1B	108.0	N1-C20-H20	121.4
Pd1-C1-H1B	108.0	C21-C20-H20	121.4
H1A-C1-H1B	107.2	N2-C21-C20	117.11(10)
C5-C2-C1	110.85(9)	N2-C21-H21	121.4
C5-C2-C3	112.30(10)	C20-C21-H21	121.4
C1-C2-C3	107.19(10)	C27-C22-C23	122.51(10)
C5-C2-C4	108.35(10)	C27-C22-N2	120.56(10)
C1-C2-C4	110.41(10)	C23-C22-N2	116.86(10)
C3-C2-C4	107.72(11)	C24-C23-C22	117.84(11)
C2-C3-H3A	109.5	C24-C23-C28	121.07(11)
C2-C3-H3B	109.5	C22-C23-C28	121.09(11)

H3A-C3-H3B	109.5	C23-C24-C25	121.48(12)
C2-C3-H3C	109.5	C23-C24-H24	119.3
H3A-C3-H3C	109.5	C25-C24-H24	119.3
H3B-C3-H3C	109.5	C26-C25-C24	118.74(11)
C2-C4-H4A	109.5	C26-C25-C29	120.45(13)
C2-C4-H4B	109.5	C24-C25-C29	120.80(13)
H4A-C4-H4B	109.5	C25-C26-C27	121.89(12)
C2-C4-H4C	109.5	C25-C26-H26	119.1
H4A-C4-H4C	109.5	C27-C26-H26	119.1
H4B-C4-H4C	109.5	C26-C27-C22	117.53(11)
C10-C5-C6	118.33(11)	C26-C27-C30	121.33(11)
C10-C5-C2	123.11(11)	C22-C27-C30	121.14(11)
C6-C5-C2	118.46(10)	C23-C28-H28A	109.5
O1-C6-C7	117.82(11)	C23-C28-H28B	109.5
O1-C6-C5	123.30(10)	H28A-C28-H28B	109.5
C7-C6-C5	118.85(11)	C23-C28-H28C	109.5
C8-C7-C6	121.28(12)	H28A-C28-H28C	109.5
C8-C7-H7	119.4	H28B-C28-H28C	109.5
C6-C7-H7	119.4	C25-C29-H29A	109.5
C7-C8-C9	120.33(12)	C25-C29-H29B	109.5
C7-C8-H8	119.8	H29A-C29-H29B	109.5
C9-C8-H8	119.8	C25-C29-H29C	109.5
C8-C9-C10	118.94(12)	H29A-C29-H29C	109.5
C8-C9-H9	120.5	H29B-C29-H29C	109.5
C10-C9-H9	120.5	C27-C30-H30A	109.5
C5-C10-C9	122.21(12)	C27-C30-H30B	109.5
C5-C10-H10	118.9	H30A-C30-H30B	109.5
C9-C10-H10	118.9	C27-C30-H30C	109.5
C16-C11-C12	121.84(10)	H30A-C30-H30C	109.5
C16-C11-N1	120.82(10)	H30B-C30-H30C	109.5
C12-C11-N1	117.33(10)	C6S-C1S-C2S	120.10(14)
C13-C12-C11	117.94(12)	C6S-C1S-H1S	119.9
C13-C12-C17	120.77(11)	C2S-C1S-H1S	119.9
C11-C12-C17	121.26(11)	C3S-C2S-C1S	120.00(16)

C12-C13-C14	121.54(12)	C3S-C2S-H2S	120.0
C12-C13-H13	119.2	C1S-C2S-H2S	120.0
C14-C13-H13	119.2	C4S-C3S-C2S	120.23(16)
C15-C14-C13	118.66(11)	C4S-C3S-H3S	119.9
C15-C14-C18	120.99(13)	C2S-C3S-H3S	119.9
C13-C14-C18	120.34(12)	C3S-C4S-C5S	119.86(15)
C14-C15-C16	122.06(12)	C3S-C4S-H4S	120.1
C14-C15-H15	119.0	C5S-C4S-H4S	120.1
C16-C15-H15	119.0	C6S-C5S-C4S	119.88(17)
C11-C16-C15	117.74(11)	C6S-C5S-H5S	120.1
C11-C16-C19	121.98(10)	C4S-C5S-H5S	120.1
C15-C16-C19	120.27(11)	C1S-C6S-C5S	119.93(16)
C12-C17-H17A	109.5	C1S-C6S-H6S	120.0
C12-C17-H17B	109.5	C5S-C6S-H6S	120.0
H17A-C17-H17B	109.5		

Appendix B: Supplementary Information for Chapter 3

Representative procedure for deuterium labeling to give **3-1-*d*₂** and **3-2-*d*₂**:

3-L1H (0.009 g, 0.046 mmol) was dissolved in CD₃OD (1.5 mL) and stirred for 3 minutes. Then the solution was dried under vacuum to give a yellow powder, **3-L1D**. Next, **3-L1D** was dissolved in CD₂Cl₂ (0.3 mL) and was added to a solution of [Pd(CH₂CMe₂C₆H₄)(COD)], **2-1**, (0.016 g, 0.046 mmol) in CD₂Cl₂ (0.3 mL) and D₂O (140 μL), while stirring. An immediate color change from yellow to dark purple was observed. After 10 minutes, a ¹H NMR experiment was performed of the purple solution identified as **3-1-*d*₂**. Then, the solution was fully dried under vacuum to give **3-1-*d*₂** as a purple powder. Next, **3-1-*d*₂** was dissolved in acetone to analyze by ²H NMR spectroscopy. ²H NMR for **3-1-*d*₂** ((CH₃)₂CO, 92.0 MHz): δ 7.66 (br, *D*₅ and *D*₉). **3-1-*d*₂** was dried under vacuum and dissolved in dry CD₂Cl₂ while stirring. To perform ²H NMR spectroscopy after 5 days, the solution was fully dried and dissolved in acetone. ²H NMR for **3-2-*d*₂** ((CH₃)₂CO, 92.0 MHz): δ 7.17(br, *D*₄), 1.69 (br, *D*₁).

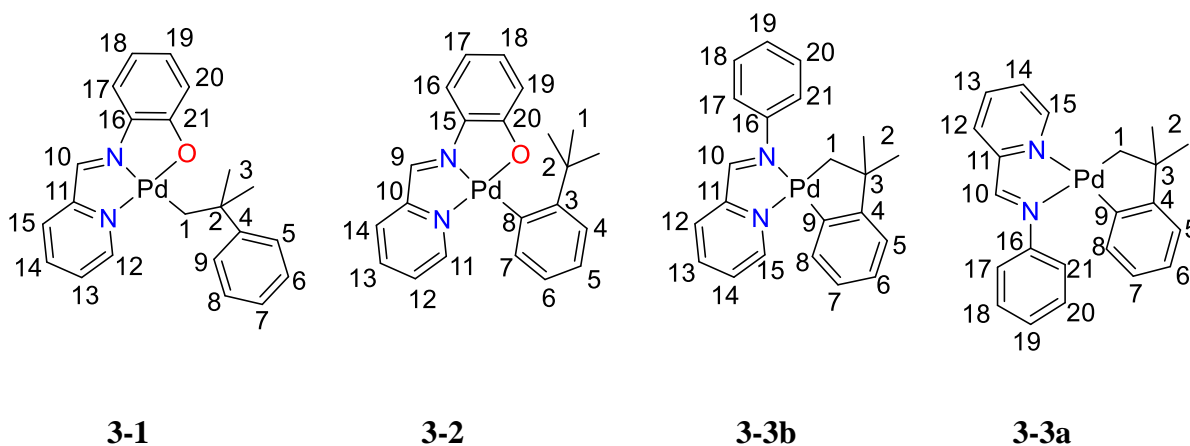


Chart A3.1 Atom labeling scheme for the reported compounds **3-1**, **3-2**, **3-3a** and **3-3b** used for NMR spectroscopy signal assignment.

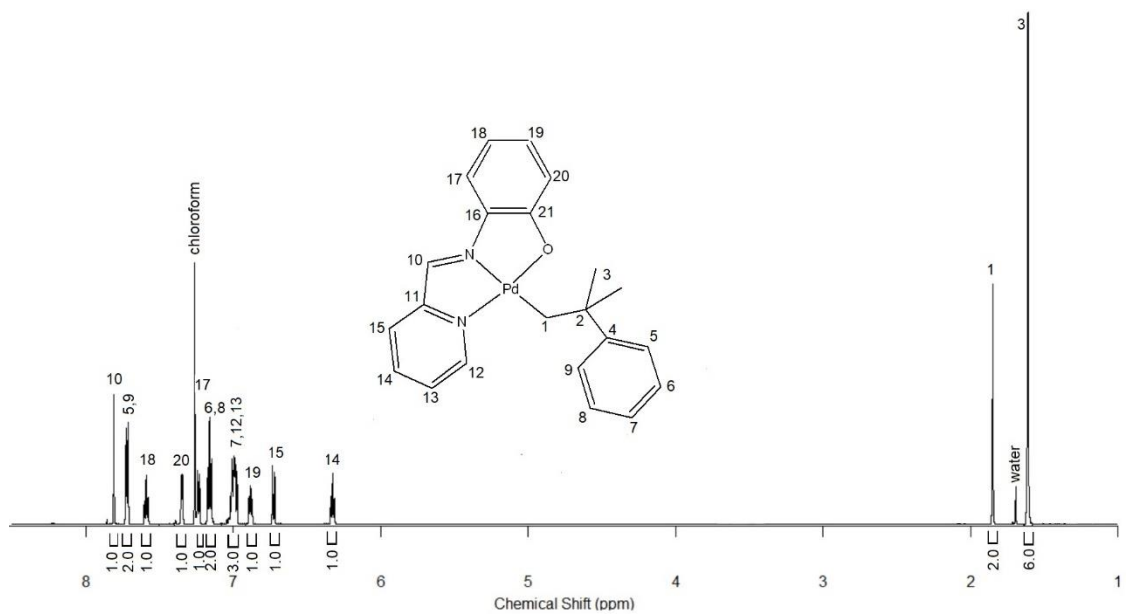


Figure A3.1 ^1H NMR spectrum (CDCl_3 , at 25°C) of **3-1** at 600 MHz.

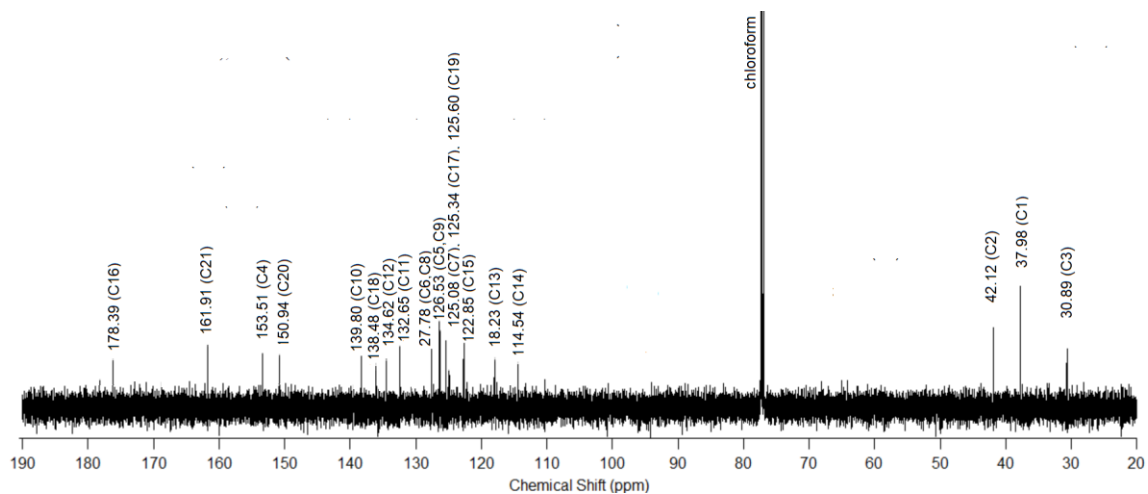


Figure A3.2 $^{13}\text{C}\{^1\text{H}\}$ NMR spectrum (CDCl_3) of **3-1**, at 25°C , 151 MHz.

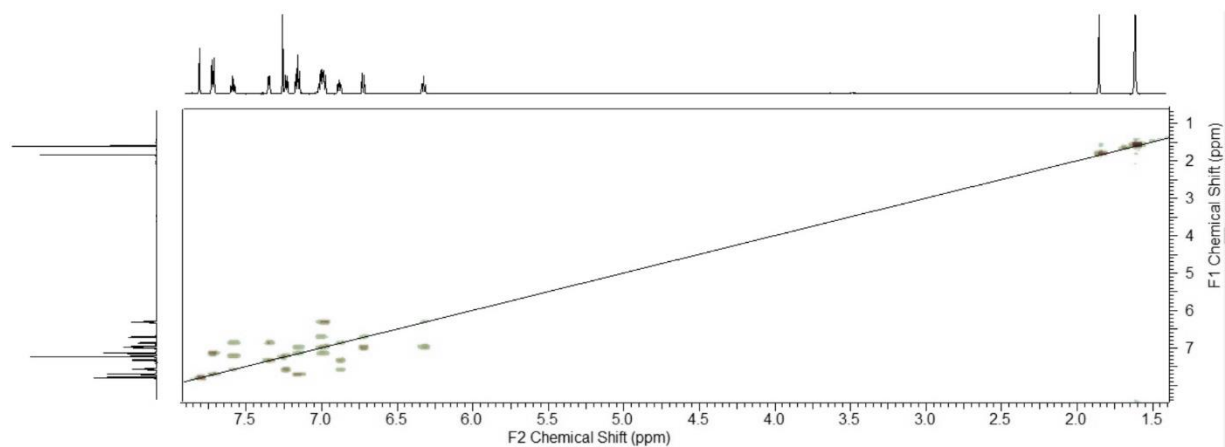


Figure A3.3 ^1H - ^1H gCOSY spectrum (CDCl_3) of **3-1**, at 25°C .

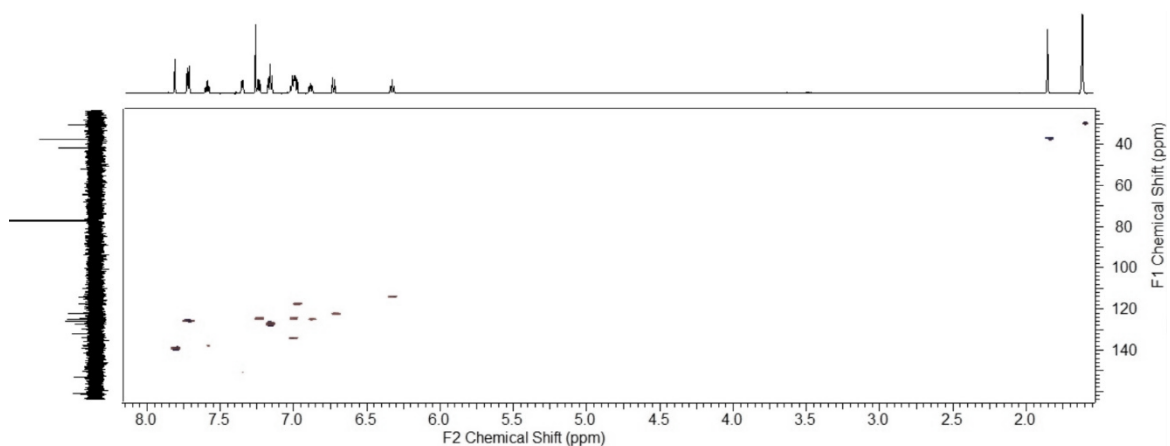


Figure A3.4 ^1H - $^{13}\text{C}\{^1\text{H}\}$ HSQC spectrum (CDCl_3) of **3-1**, at 25°C .

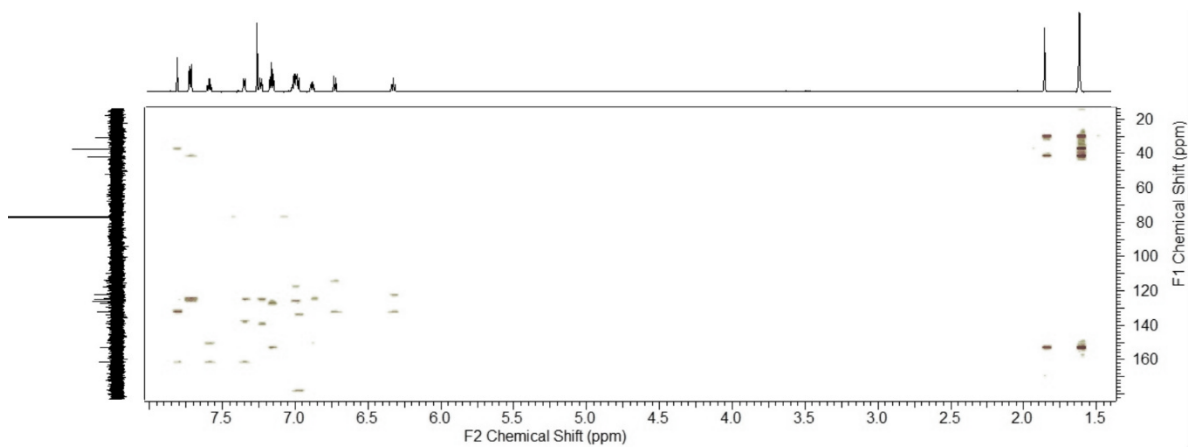


Figure A3.5 ^1H - $^{13}\text{C}\{^1\text{H}\}$ HMBC spectrum (CDCl_3) of **3-1**, at 25°C .

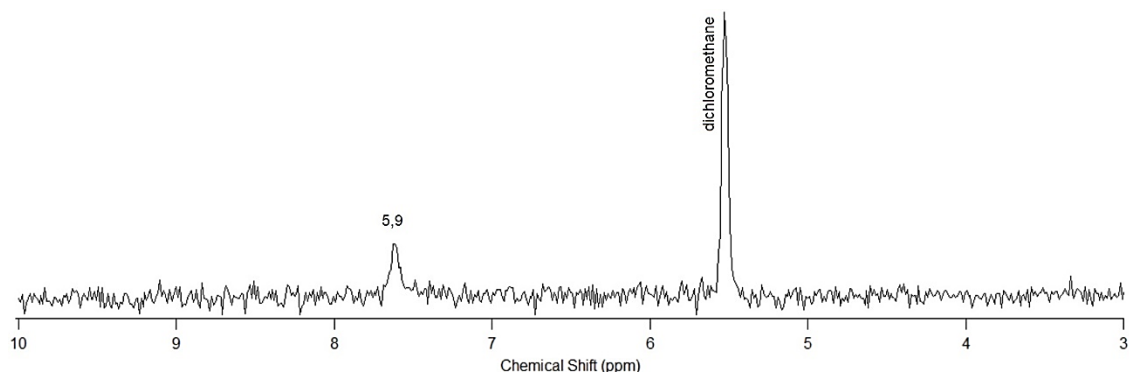


Figure A3.6 ^2H NMR Spectrum of **3-1-*d*₁** in CH_2Cl_2 .

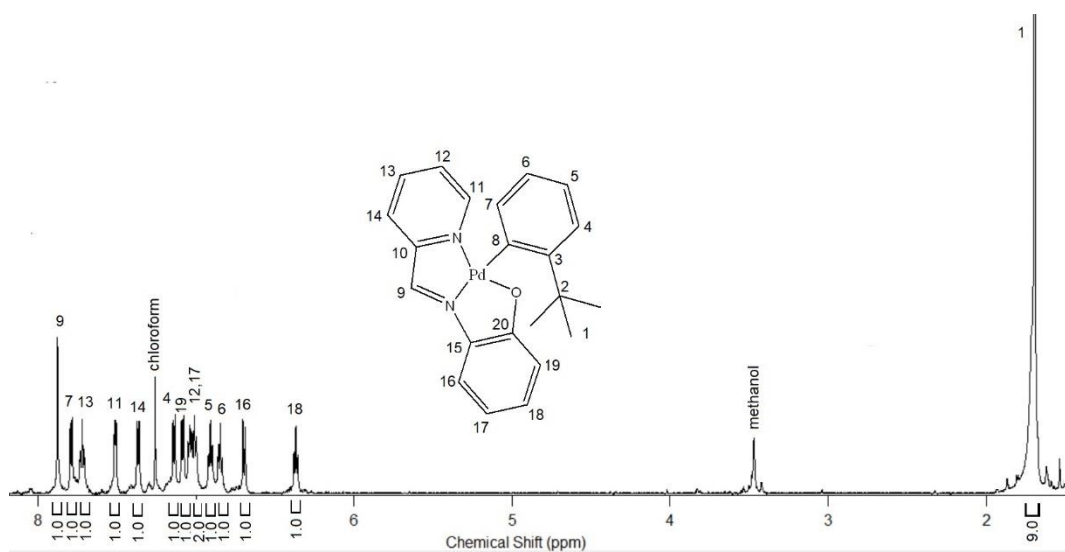


Figure AS.7 ^1H NMR spectrum (CDCl_3 , at 25°C) of **3-2** at 600 MHz.

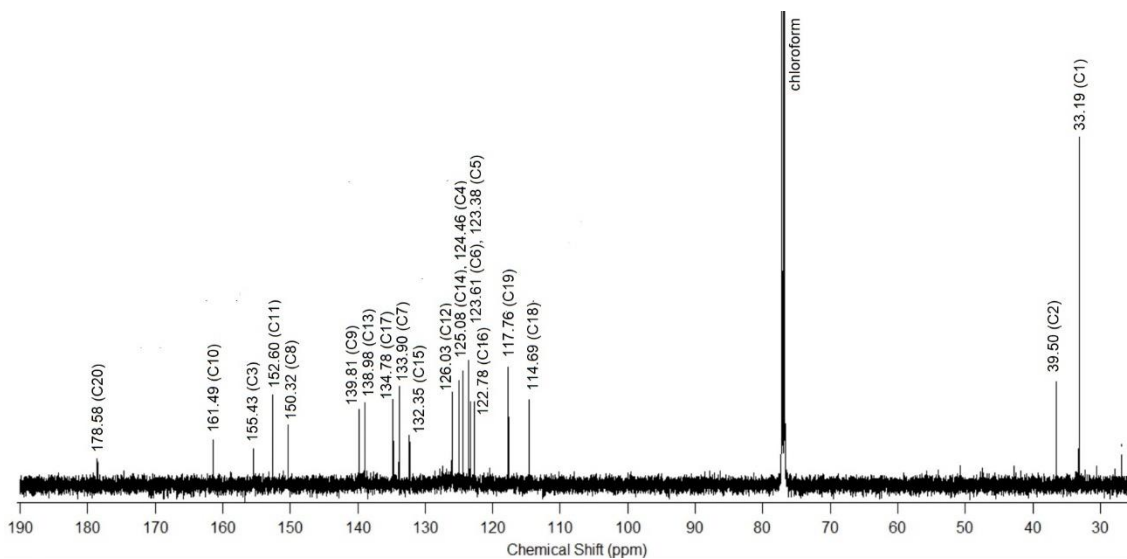


Figure A3.8 $^{13}\text{C}\{^1\text{H}\}$ NMR spectrum (CDCl_3) of **3-2**, at 25°C , 151 MHz.

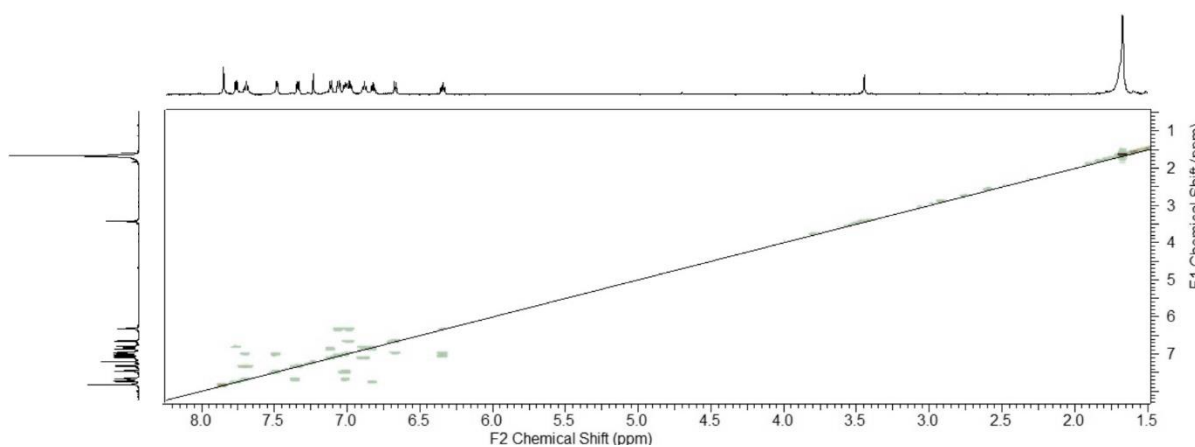


Figure A3.9 $^1\text{H}-^1\text{H}$ gCOSY spectrum (CDCl_3) of **3-2**, at 25°C .

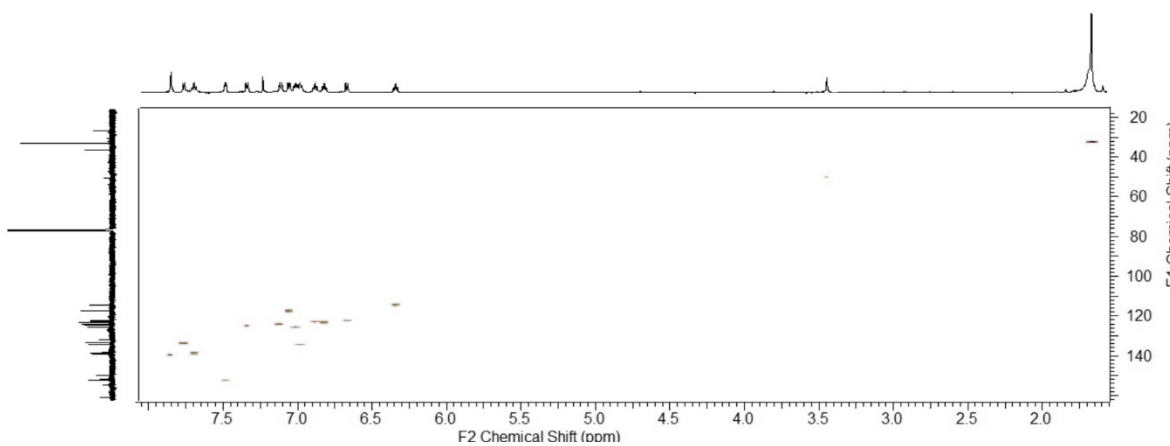


Figure A3.10 $^1\text{H}-^{13}\text{C}\{^1\text{H}\}$ HSQC spectrum (CDCl_3) of **3-2**, at 25°C .

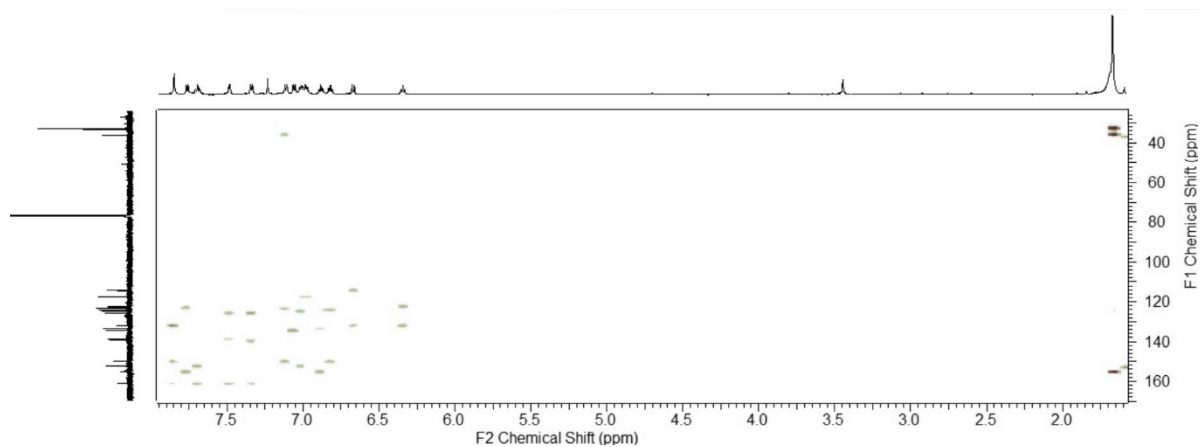


Figure A3.11 $^1\text{H}-^{13}\text{C}\{^1\text{H}\}$ HMBC spectrum (CDCl_3) of **3-2**, at 25°C .

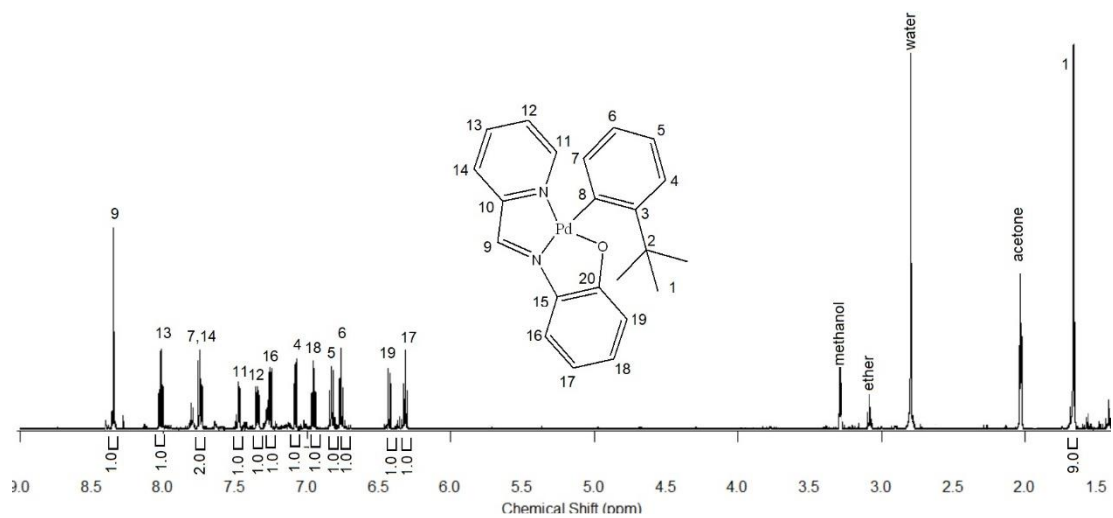


Figure A3.12 ^1H NMR spectrum ($(\text{CD}_3)_2\text{CO}$, at 25°C) of **3-2** at 600 MHz.

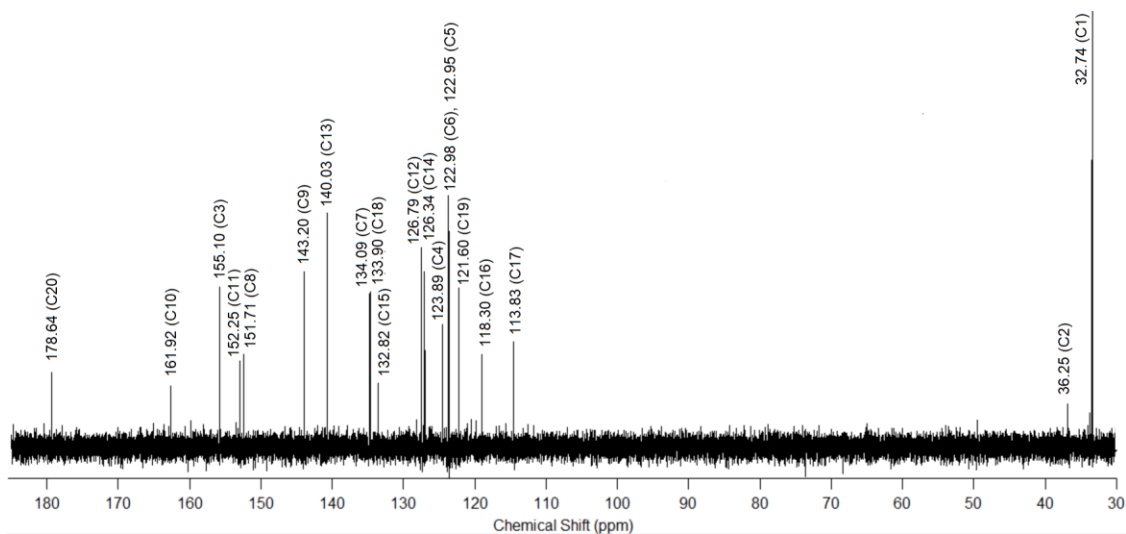


Figure A3.13 $^{13}\text{C}\{^1\text{H}\}$ NMR spectrum ($(\text{CD}_3)_2\text{CO}$) of **3-2**, at 25°C , 151 MHz..

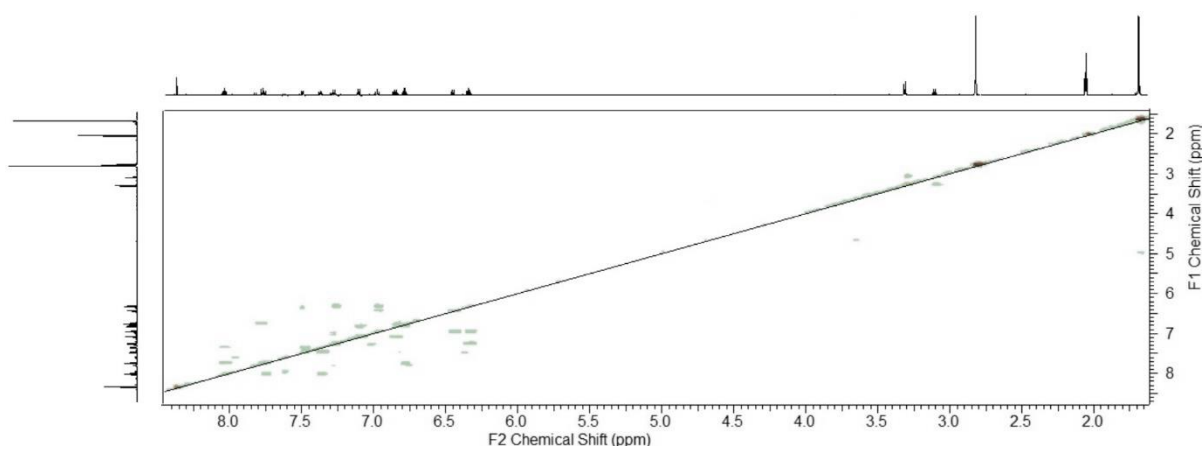


Figure A3.14 $^1\text{H}-^1\text{H}$ gCOSY spectrum ($(\text{CD}_3)_2\text{CO}$) of **3-2**, at 25°C .

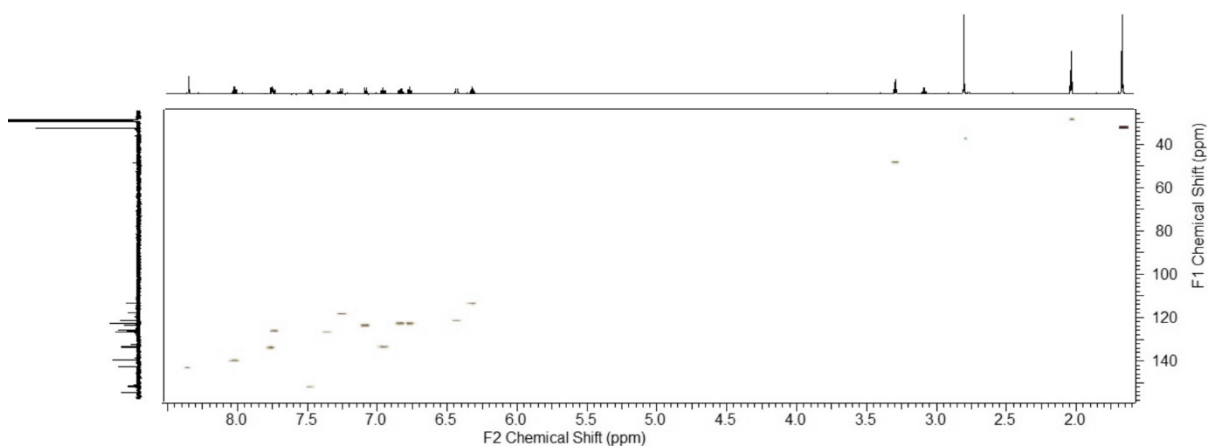


Figure A3.15 $^1\text{H}-^{13}\text{C}\{^1\text{H}\}$ HSQC spectrum ($(\text{CD}_3)_2\text{CO}$) of **3-2**, at 25°C .

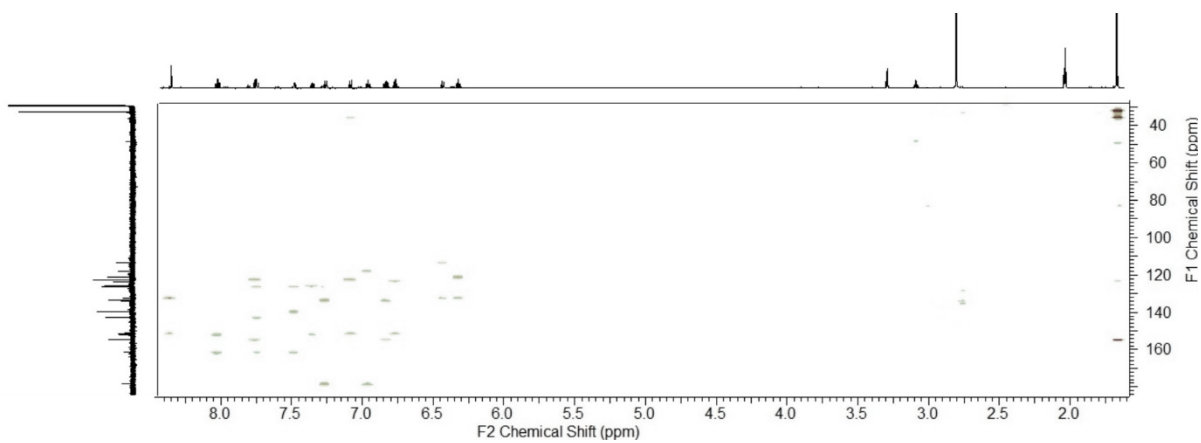


Figure A3.16 $^1\text{H}-^{13}\text{C}\{^1\text{H}\}$ HMBC spectrum ($(\text{CD}_3)_2\text{CO}$) of **3-2**, at 25°C .

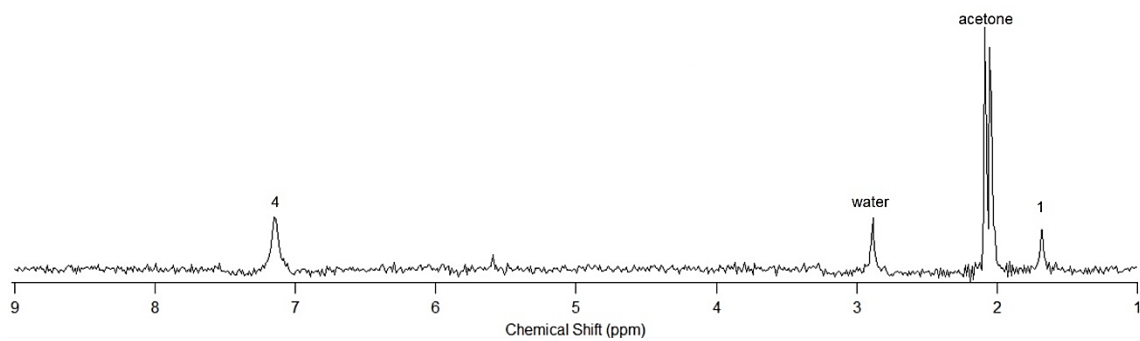


Figure A3.17 ^2H NMR spectrum ($(\text{CH}_3)_2\text{CO}$) of **3-2-*d*₂**, at 25°C .

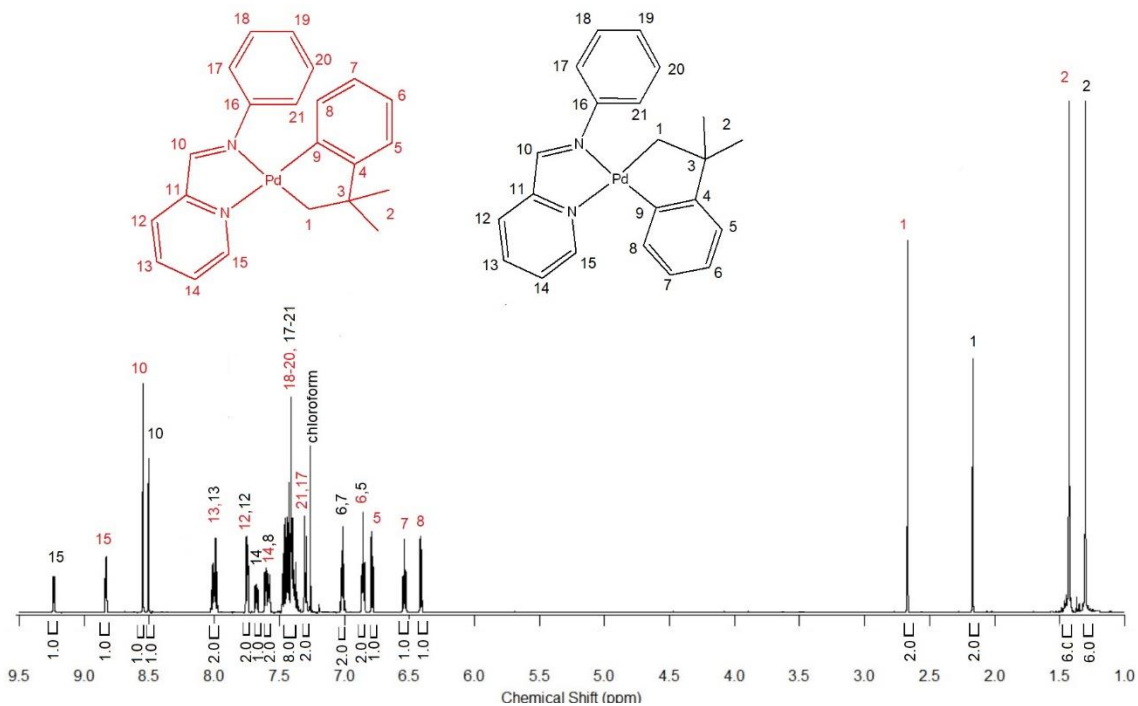


Figure A3.18 ^1H NMR spectrum (CDCl_3 , at 25°C) of 3-3a/3-3b at 600 MHz.

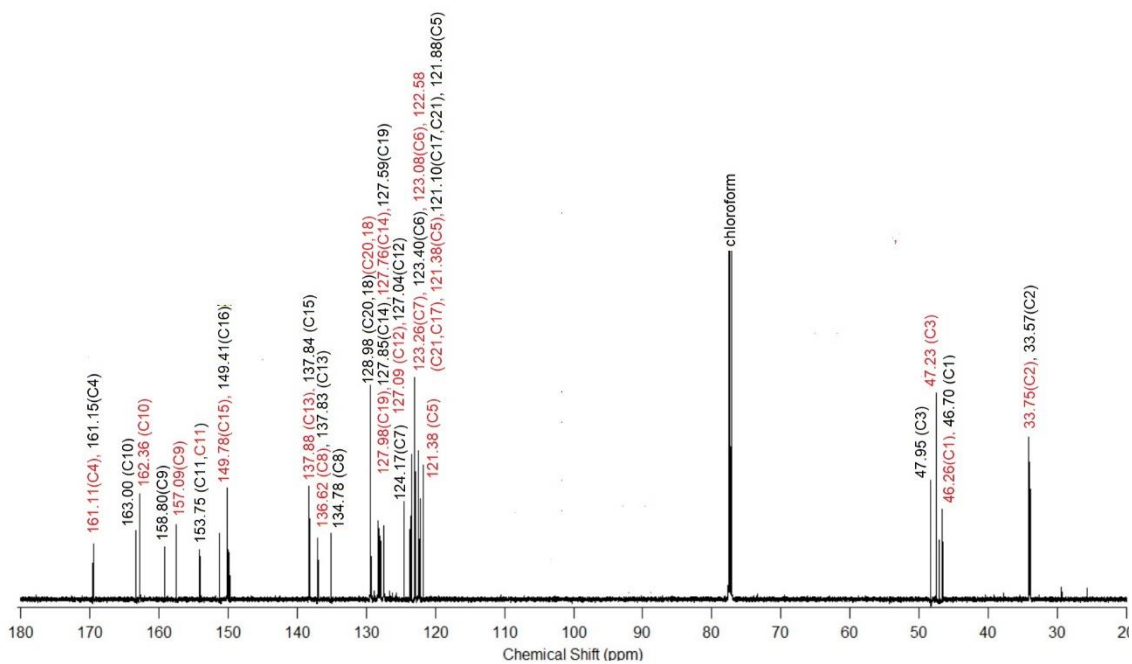


Figure A3.19 $^{13}\text{C}\{^1\text{H}\}$ NMR spectrum (CDCl_3) of 3-3a/3-3b, at 25°C , 151 MHz..

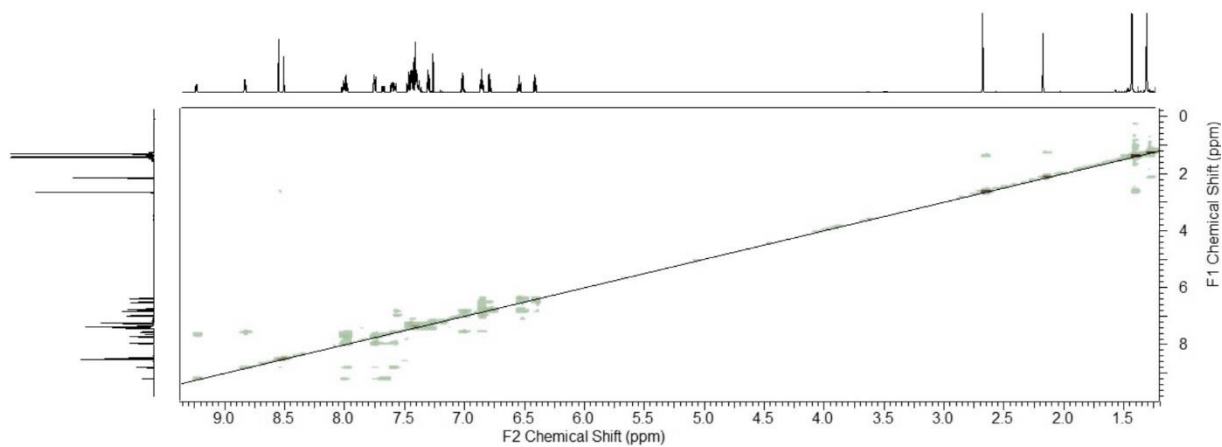


Figure A3.20 ^1H - ^1H gCOSY spectrum (CDCl_3) of **3-3a/3-3b**, at 25°C .

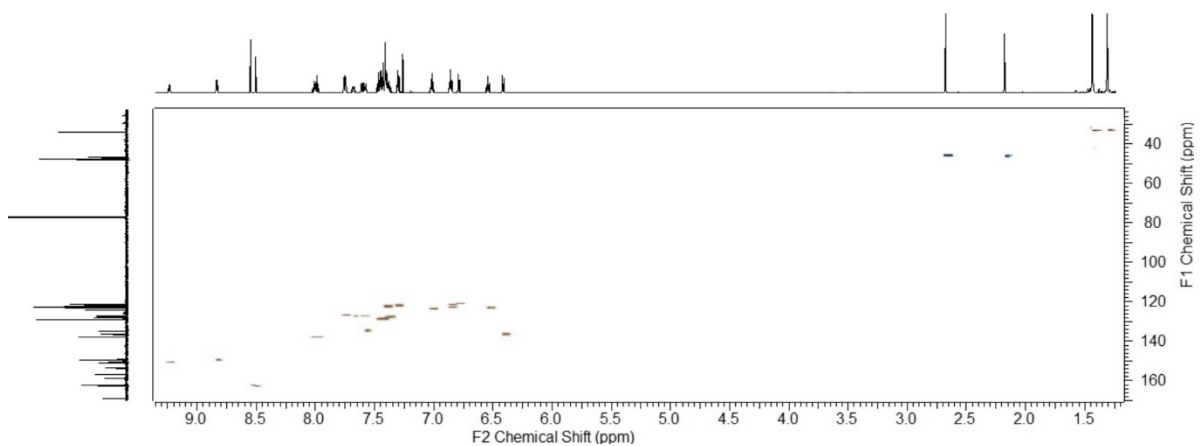


Figure A3.21 ^1H - $^{13}\text{C}\{^1\text{H}\}$ HSQC spectrum (CDCl_3) of **3-3a/3-3b**, at 25°C .

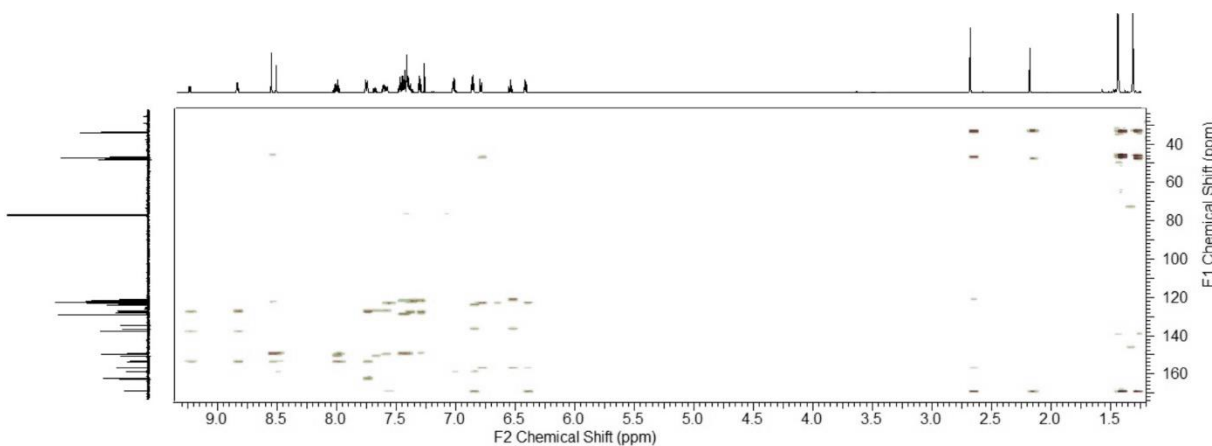


Figure AS.22 ^1H - $^{13}\text{C}\{^1\text{H}\}$ HMBC spectrum (CDCl_3) of **3-3a/3-3b**, at 25°C .

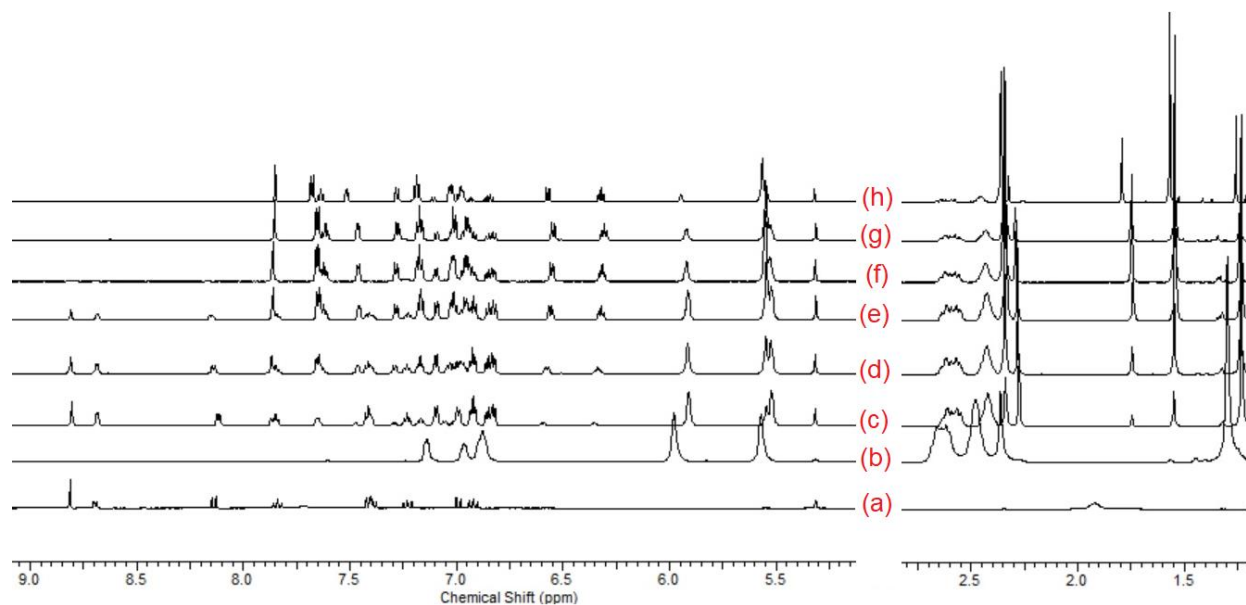


Figure A3.23 ^1H NMR spectra (CD_2Cl_2 , at 600 MHz) of a) **3-L1H** at 25°C ; b) $[\text{Pd}(\text{CH}_2\text{CMe}_2\text{C}_6\text{H}_4)(\text{COD})]$, **2-1**, at -20°C ; and a 1:1 mixture of pre-cooled **3-L1H** (-35°C) and $[\text{Pd}(\text{CH}_2\text{CMe}_2\text{C}_6\text{H}_4)(\text{COD})]$, **2-1**, (-20°C) at c) -20°C ; d) -10°C ; e) -5°C ; f) 0°C ; g) 5°C ; and h) 25°C .

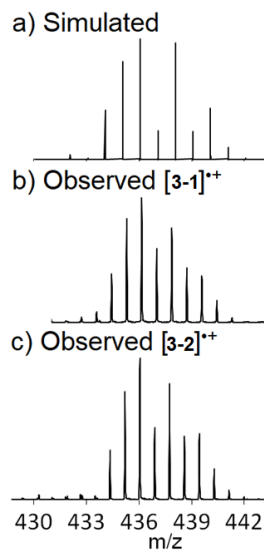


Figure A3.24 The MALDI MS isotope patterns for $[\mathbf{3-1}]^{++}$ and $[\mathbf{3-2}]^{++}$ obtained using anthracene matrix: (a) simulated, (b) observed $[\mathbf{3-1}]^{++}$ and (c) observed $[\mathbf{3-2}]^{++}$.

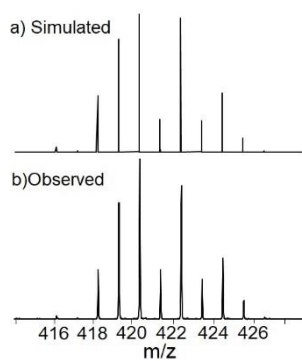


Figure A3.25 The MALDI MS isotope patterns for **[3-3a/3-3b]⁺** obtained using anthracene matrix: (a) simulated and (b) observed.

UV-VIS Study

Experimental Procedure

A solution of complex **3-1** (8.58×10^{-5} M, 3.0 mL) was prepared in different solvents (methanol, acetonitrile, dichloromethane, chloroform and benzene) and placed into a 4 mL cuvette (optical path length 1 cm) at room temperature.

Table A3.1 UV-Vis absorption spectroscopy data for **3-1** in different solvents.

Solvent	ϵ^a	$E_T^{N^b}$	λ_{\max} (nm)	$1/\lambda_{\max}$ (10^3 cm^{-1})	ϵ^c
MeOH	33.6	55.5	525	19.04	1375
CH ₃ CN	37.5	46	555	18.02	940
CH ₂ Cl ₂	8.9	41.1	570	17.54	1904
CHCl ₃	4.8	39.1	580	17.24	1652
C ₆ H ₆	2.2	34.5	585	17.09	1525

^a Dielectric constant. ^b Normalized Reichardt solvent polarity factor (kcal mol⁻¹ at 25°C).¹⁻³ ^c Molar absorptivity (cm⁻¹ mol⁻¹ L).

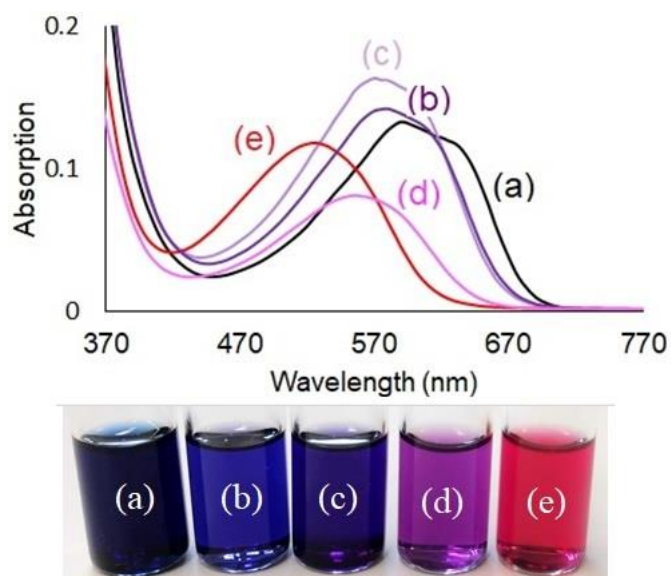


Figure A3.26 Top: UV-Visible absorption spectra of **3-1** (8.58×10^{-5} M) in (a) C_6H_6 , (c) CH_2Cl_2 and (e) CH_3OH . Bottom: photograph of solutions of **3-1** (8.58×10^{-5} M) in (a) C_6H_6 ; (b) $CHCl_3$; (c) CH_2Cl_2 ; (d) CH_3CN ; (e) CH_3OH .

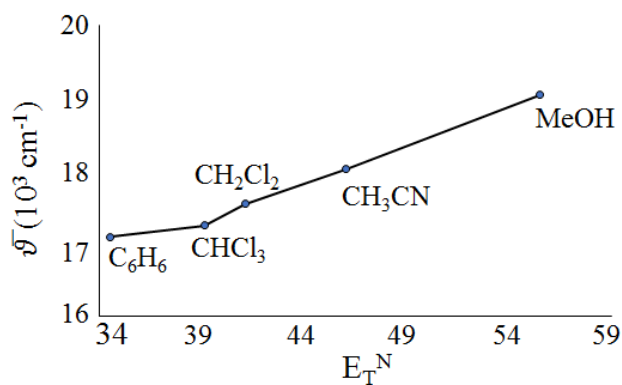


Figure A3.27 Correlation of wavenumber ($\bar{\nu}$) with the solvent Normalized Reichardt polarity factor (E_T^N) value.

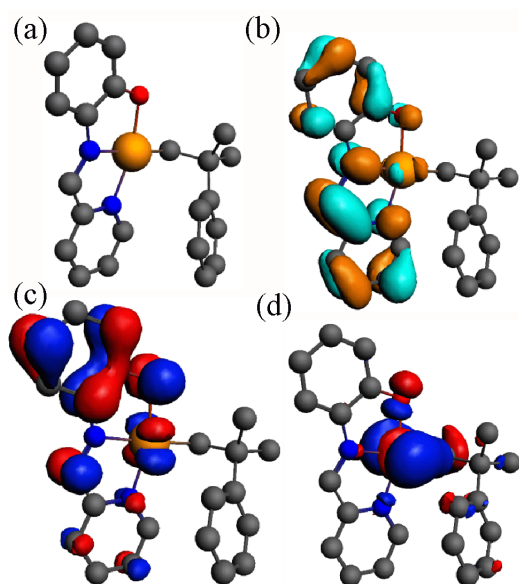


Figure A3.28 Calculated structure and frontier orbitals for complex **3-1**; (a) structure, (b) LUMO, (c) HOMO, (d) HOMO-1.

Efforts toward Mechanism Characterization

General Procedure for the Isomerization of **3-1** to **3-2**

All reactions were carried out under air and on an NMR scale. Internal standard, (1,3,5-trimethoxybenzene) (0.002 g, 0.012 mmol) was added to a solution of **3-1** (0.016 g, 0.036 mmol) in an appropriate solvent (1.5 mL) and the reaction was stirred in a 4 mL vial. At specific time points, reactions were monitored by ^1H NMR spectroscopy. More details are included in the tables (Table A3.2-A3.8).

Table A3.2 Solvent effect study for the isomerization reaction.

Entry	Solvent	ϵ^b	3-1 (%)	3-2 (%)	By-product (%)
1	CD ₃ CN	37.5	67	33	0

2	DMF	36.7	48	35	17
3	CH ₃ OH	33.6	42	58	0
4	Isopropanol	17.9	95	5	0
5	CD ₂ Cl ₂	8.9	70	30	0
6	2,2,2- trifluoroethanol	8.55	0	0	100
7	THF	7.58	92	8	0
8	CDCl ₃	4.8	68	32	0
9	CS ₂	2.6	0	0	100
10	1,4-Dioxane	2.25	100	0	0
11	CCl ₄	2.24	100	0	0
12	C ₆ D ₆	2.2	98	2	0

Conditions: [3-1] = 0.72 mM. Time = 22h. ^b Dielectric constant.

Table A3.3 Concentration study for the isomerization reaction.

Entry	Solvent	ϵ^b	[3-1] (mM)	3-1 (%)	3-2 (%)	BP (%)
1	CDCl ₃	4.8	0.72	68	32	0
2	CDCl ₃	4.8	3.33	70	30	0
3	CDCl ₃	4.8	5	74	26	0
4	CDCl ₃	4.8	10	70	30	0

Condition: Time = 22h. ^b Dielectric constant

Table A3.4 Time study for the isomerization reaction.

Entry	Solvent	ϵ^b	Time (h)	3-1 (%)	3-2 (%)	BP (%)
1	CDCl ₃	4.8	22	68	32	0
2	CDCl ₃	4.8	44	55	45	0
3	CDCl ₃	4.8	66	43	57	0
4	CDCl ₃	4.8	154	27	58	15
5	CH ₃ OH	33.6	22	42	58	0
6	CH ₃ OH	33.6	154	10	90	0

Condition: [**3-1**] = 0.72 mM. ^b Dielectric constant.

Table A3.5 Light effect study for the isomerization reaction.

Entry	Solvent	ϵ^b	Condition	Time (h)	3-1 (%)	3-2 (%)	BP (%)
1	CDCl ₃	4.8	Light	22	68	32	0
2	CDCl ₃	4.8	Light	44	55	45	0
3	CDCl ₃	4.8	Light	66	43	57	0
4	CDCl ₃	4.8	Dark ^c	22	65	35	0
5	CDCl ₃	4.8	Dark	44	60	50	0
6	CDCl ₃	4.8	Dark	66	40	60	0

Condition: [**3-1**] = 0.72 Mm, Time = 22 h. ^b Dielectric constant. ^c The vial was wrapped in an aluminum foil.

Table A3.6 Heating effect study for isomerization reaction.

entry	Solvent	ϵ^b	Time (h)	Temperature ^c	3-1 (%)	3-2 (%)	BP (%)
1	CH ₃ OH	33.6	22	43°C	25	75	0
2	CH ₃ OH	33.6	44	43°C	8	80	12
3	CH ₃ OH	33.6	66	43°C	4	30	66

Condition: [3-1] = 0.72 mM. ^b Dielectric constant. ^c The vial was heated in an oil bath.

Table A3.7 Deuterium effect study for the isomerization reaction.

Entry	Solvent	ϵ^b	Time (min)	3-1 (%)	3-2 (%)	BP (%)
1	CH ₃ OH	33.6	60	93	7	0
2	CH ₃ OH	33.6	120	89	11	0
3	CH ₃ OH	33.6	180	85	15	0
4	CH ₃ OH	33.6	240	80	20	0
5	CH ₃ OH	33.6	300	78	22	0
6	CH ₃ OH	33.6	1320	42	58	0
7	CH ₃ OH	33.6	2640	34	66	0
8	CH ₃ OH	33.6	6600	10	90	0
9	CD ₃ OD	33.6	60	100	0	0
10	CD ₃ OD	33.6	120	100	0	0
11	CD ₃ OD	33.6	180	100	0	0

12	CD ₃ OD	33.6	240	100	0	0
13	CD ₃ OD	33.6	300	100	0	0
14	CD ₃ OD	33.6	1320	97	3	0
15	CD ₃ OD	33.6	2640	95	5	0
16	CD ₃ OD	33.6	6600	0	0	100
17	CHCl ₃	4.8	1320	70	30	0
18	CDCl ₃	4.8	1320	68	32	0
19	CH ₂ Cl ₂	8.9	1320	72	28	0
20	CD ₂ Cl ₂	8.9	1320	70	30	0

Condition: [3-1] = 0.72 mM. ^b Dielectric constant.

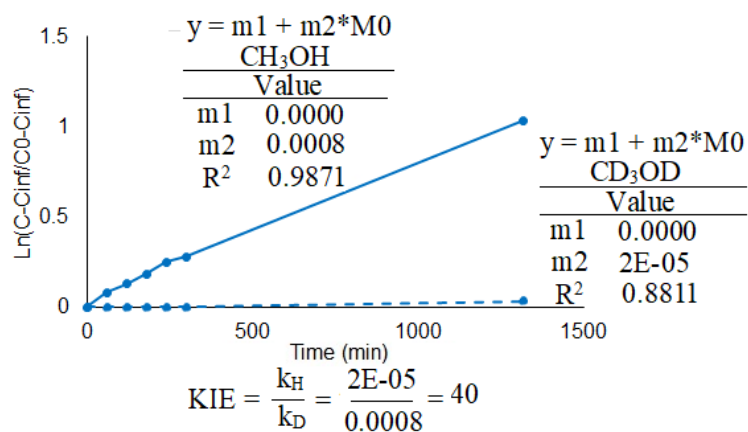


Figure A3.29 Isomerization reaction of 3-1 to 3-2 in protonated- and deuterated-methanol. Plot of

$\text{Ln} \frac{([3-2] - [3-2]_{\infty})}{([3-2]_0 - [3-2]_{\infty})}$ versus time (min). solid line: CH₃OH. Dash line: CD₃OD, both fit to

$$y = (m1) + (m2) * (M0) \text{ where } y = \text{Ln} \frac{([3-2] - [3-2]_{\infty})}{([3-2]_0 - [3-2]_{\infty})} \text{ and } M0 = \text{time.}$$

Table A3.8 Water effect study for the isomerization study.

Entry	Solvent	ϵ^b	Condition	Time (h)	3-1 (%)	3-2 (%)	BP (%)
1	CH ₃ OH	33.6	----	22	42	58	0
2	CH ₃ OH	33.6	H ₂ O (10 μ L)	22	46	54	0
3	CH ₃ OH	33.6	H ₂ O (50 μ L)	22	44	56	0
4	CH ₃ OH	33.6	H ₂ O (100 μ L)	22	46	54	0
5	CDCl ₃	4.8	Dry ^c	22	66	34	0
6	CDCl ₃	4.8	Dry ^c	44	48	52	0
7	CDCl ₃	4.8	H ₂ O (100 μ L)	22	67	33	0
8	CDCl ₃	4.8	H ₂ O (100 μ L)	44	46	54	0
9	CDCl ₃	4.8	D ₂ O (100 μ L)	22	93	7	0
10	CDCl ₃	4.8	D ₂ O (100 μ L)	44	86	14	0
11	CDCl ₃	4.8	CH ₃ OH (0.5 mL)	22	37	63	0
12	CDCl ₃	4.8	CH ₃ OH (0.5 mL)	44	32	68	0
13	CDCl ₃	4.8	CD ₃ OD (0.5 mL)	22	91	9	0
14	CDCl ₃	4.8	CD ₃ OD (0.5 mL)	44	83	17	0
15	CD ₂ Cl ₂	8.9	Dry ^c	22	74	26	0
16	CD ₂ Cl ₂	8.9	H ₂ O (100 μ L)	22	82	18	0
17	CD ₂ Cl ₂	8.9	D ₂ O (100 μ L)	22	100	0	0
18	CH ₃ CN	37.5	Dry ^c	22	66	34	0

19	CH ₃ CN	37.5	H ₂ O (100 μL)	22	70	30	0
20	CH ₃ CN	37.5	D ₂ O (100 μL)	22	100	0	0

Condition: [3-1] = 0.72 mM. ^b Dielectric constant. ^c Dry solvents (1 mL ampules) were purchased from Sigma-Aldrich and stored on 4 Å sieves in the dry-box for three days before usage.

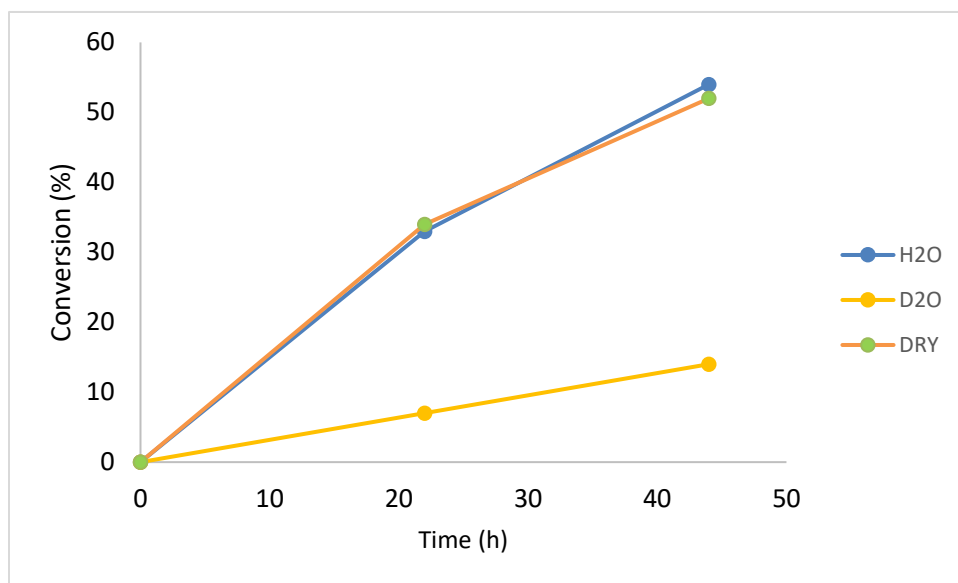


Figure A3.30 Isomerization of 3-1 to 3-2 in dry CHCl₃ (green), dry CHCl₃ with 10 equiv. H₂O (blue) and dry CHCl₃ with 10 equiv. D₂O (orange) Reactions were carried out in the presence of an internal standard (1,3,5-trimethoxybenzene).

X-ray Structure Determinations.⁴⁻⁷

Data Collection and Processing. A crystal was mounted on a Mitegen polyimide micromount with a small amount of Paratone N oil. All X-ray measurements were made using a Bruker Kappa Axis Apex2 diffractometer at a temperature of 110 K. The frame integration was performed using SAINT, and the resulting raw data were scaled and absorption corrected using a multiscan averaging of symmetry equivalent data using SADABS.

Structure Solution and Refinement. The structures were solved by using the SHELXT program. All non-hydrogen atoms were obtained from the initial solution. The hydrogen atoms were introduced at idealized positions and were allowed to ride on the parent atom. The structural model was fit to the data using full-matrix least squares based on F². The calculated structure factors included corrections for

anomalous dispersion from the usual tabulation. The structure was refined using the SHELXL-2014 program from the SHELX suite of crystallographic software.⁴⁻⁷ Details are given in Table A3.9.

Table A3.9 Crystallographic data and parameters for compounds **3-1**, **3-2** and **3-3b**

	3-1	3-2	3-3b
Formula	C ₂₂ H ₂₂ N ₂ OPd.C ₆ H ₆	C ₂₂ H ₂₂ N ₂ OPd.C ₆ H ₆	C ₂₂ H ₂₂ N ₂ Pd
Formula weight	514.92	514.92	420.81
Crystal system	monoclinic	monoclinic	monoclinic
Space group	P 2 ₁ /c	P 2 ₁	P 2 ₁ /c
<i>a</i> [Å]	6.515(2)	8.509(4)	11.322(4)
<i>b</i> [Å]	18.388(7)	9.397(4)	17.535(5)
<i>c</i> [Å]	18.995(7)	14.443(7)	9.999(2)
α [°]	90	90	90
β [°]	91.858(10)	91.146(17)	112.549(9)
γ [°]	90	90	90
<i>V</i> [Å ³]	2274.4(14)	1154.6(9)	1833.3(9)
<i>Z</i>	4	2	4
ρ_{cal} [g cm ⁻³]	1.504	1.481	1.525
λ , Å, (MoK α)	0.71073	0.71073	0.71073
<i>F</i> (000)	1056	528	856
Temperature [K]	110	110	110
θ_{min} , θ_{max} [°]	6.16, 57.24	5.18, 65.18	3.03, 38.30
Total reflns	60652	24450	10890
Unique reflns	5850	3724	9155
<i>R</i> ₁	0.0493	0.0372	0.0236
w <i>R</i> ₂ [<i>I</i> ≥ 2σ(<i>I</i>)]	0.1046	0.0910	0.0628
<i>R</i> ₁ (all data)	0.0952	0.0431	0.0337
w <i>R</i> ₂ (all data)	0.1252	0.0948	0.0726

GOF	1.003	1.011	1.095
Maximum shift/error	0.001	0.001	0.001
Min & Max peak heights on final ΔF Map ($e^{-}/\text{\AA}$)	-1.247, 1.614	-0.354, 0.826	-0.597, 1.018

Where: $R_1 = \Sigma(|F_o| - |F_c|) / \Sigma F_o$; $wR_2 = [\Sigma(w(F_o^2 - F_c^2)^2) / \Sigma(wF_o^4)]^{1/2}$; $GOF = [\Sigma(w(F_o^2 - F_c^2)^2) / (\text{No. of reflns.} - \text{No. of params.})]^{1/2}$

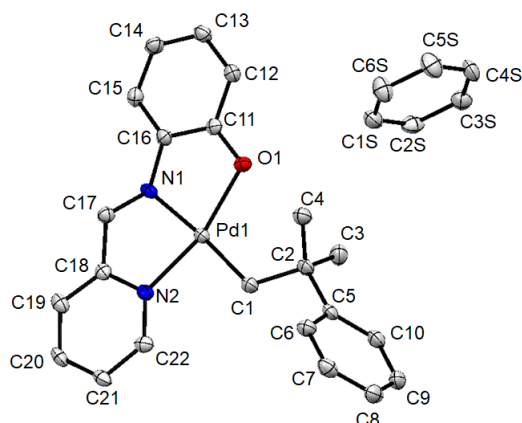


Figure A3. 31 Displacement ellipsoid plot of **3-1** co-crystallized with a benzene molecule showing naming and numbering scheme. Ellipsoids are drawn at the 50% probability level and hydrogen atoms are omitted for clarity.

Table A3.10 Atomic coordinates for **3-1**.

Atom	x	y	z	$U_{\text{iso/equiv}}$
Pd1	0.76493(4)	0.57891(2)	0.55298(2)	0.01729(11)
O1	0.7587(4)	0.55165(15)	0.65833(14)	0.0209(6)
N1	0.7425(4)	0.46928(18)	0.54232(16)	0.0176(7)
N2	0.7602(4)	0.57129(18)	0.44560(16)	0.0184(7)
C1	0.7991(6)	0.6895(2)	0.5555(2)	0.0222(9)
C2	0.7864(6)	0.7328(2)	0.6249(2)	0.0208(8)
C3	0.5734(7)	0.7200(2)	0.6541(2)	0.0302(10)
C4	0.9506(7)	0.7063(2)	0.6799(2)	0.0262(9)
C5	0.8262(6)	0.8135(2)	0.6095(2)	0.0213(9)
C6	1.0148(6)	0.8362(2)	0.5846(2)	0.0244(9)
C7	1.0577(7)	0.9085(2)	0.5706(2)	0.0268(10)

C8	0.9096(7)	0.9608(2)	0.5809(2)	0.0294(10)
C9	0.7210(7)	0.9403(2)	0.6040(2)	0.0289(10)
C10	0.6802(7)	0.8675(2)	0.6190(2)	0.0262(10)
C11	0.7542(5)	0.4798(2)	0.6652(2)	0.0183(8)
C12	0.7622(6)	0.4478(2)	0.7328(2)	0.0223(9)
C13	0.7554(6)	0.3731(2)	0.7407(2)	0.0231(9)
C14	0.7383(6)	0.3275(2)	0.6824(2)	0.0252(9)
C15	0.7333(6)	0.3566(2)	0.6158(2)	0.0212(9)
C16	0.7419(6)	0.4318(2)	0.6065(2)	0.0187(8)
C17	0.7417(6)	0.4451(2)	0.4786(2)	0.0197(8)
C18	0.7481(5)	0.5004(2)	0.4233(2)	0.0179(8)
C19	0.7440(6)	0.4830(2)	0.3523(2)	0.0226(9)
C20	0.7488(6)	0.5379(2)	0.3021(2)	0.0215(9)
C21	0.7567(6)	0.6094(2)	0.3243(2)	0.0221(9)
C22	0.7632(6)	0.6233(2)	0.3962(2)	0.0207(9)
C1S	0.5070(7)	0.6096(2)	0.8088(2)	0.0284(10)
C2S	0.3113(7)	0.6248(2)	0.8286(2)	0.0285(10)
C3S	0.2774(7)	0.6499(2)	0.8964(2)	0.0287(10)
C4S	0.4408(7)	0.6594(3)	0.9435(2)	0.0328(11)
C5S	0.6382(7)	0.6444(3)	0.9240(2)	0.0375(12)
C6S	0.6701(7)	0.6189(3)	0.8563(2)	0.0335(11)
H1A	0.9344	0.7004	0.5358	0.027
H1B	0.6940	0.7100	0.5223	0.027
H3A	0.5596	0.7482	0.6975	0.045
H3B	0.5560	0.6682	0.6643	0.045
H3C	0.4682	0.7356	0.6193	0.045
H4A	0.9474	0.7373	0.7218	0.039
H4B	1.0867	0.7090	0.6596	0.039
H4C	0.9213	0.6559	0.6930	0.039
H6	1.1177	0.8007	0.5769	0.029
H7	1.1883	0.9220	0.5541	0.032
H8	0.9382	1.0105	0.5721	0.035
H9	0.6173	0.9760	0.6098	0.035
H10	0.5497	0.8545	0.6361	0.031

H12	0.7723	0.4779	0.7734	0.027
H13	0.7625	0.3527	0.7867	0.028
H14	0.7302	0.2763	0.6887	0.030
H15	0.7239	0.3255	0.5759	0.025
H17	0.7372	0.3946	0.4682	0.024
H19	0.7379	0.4336	0.3379	0.027
H20	0.7467	0.5264	0.2533	0.026
H21	0.7577	0.6481	0.2912	0.026
H22	0.7702	0.6725	0.4112	0.025
H1S	0.5306	0.5926	0.7626	0.034
H2S	0.1989	0.6182	0.7961	0.034
H3S	0.1418	0.6604	0.9103	0.034
H4S	0.4170	0.6765	0.9897	0.039
H5S	0.7509	0.6513	0.9563	0.045
H6S	0.8054	0.6079	0.8425	0.040

Table A3.11 Bond lengths for **3-1**.

Pd1-N1	2.031(3)	C11-C12	1.413(6)
Pd1-N2	2.044(3)	C11-C16	1.423(5)
Pd1-C1	2.046(4)	C12-C13	1.382(6)
Pd1-O1	2.064(3)	C12-H12	0.9500
O1-C11	1.328(5)	C13-C14	1.390(6)
N1-C17	1.289(5)	C13-H13	0.9500
N1-C16	1.401(5)	C14-C15	1.375(6)
N2-C22	1.341(5)	C14-H14	0.9500
N2-C18	1.373(5)	C15-C16	1.394(5)
C1-C2	1.545(5)	C15-H15	0.9500
C1-H1A	0.9900	C17-C18	1.463(6)
C1-H1B	0.9900	C17-H17	0.9500
C2-C3	1.529(6)	C18-C19	1.385(5)
C2-C5	1.536(6)	C19-C20	1.389(6)
C2-C4	1.549(6)	C19-H19	0.9500
C3-H3A	0.9800	C20-C21	1.381(6)

C3-H3B	0.9800	C20-H20	0.9500
C3-H3C	0.9800	C21-C22	1.388(6)
C4-H4A	0.9800	C21-H21	0.9500
C4-H4B	0.9800	C22-H22	0.9500
C4-H4C	0.9800	C1S-C2S	1.370(6)
C5-C10	1.390(6)	C1S-C6S	1.382(6)
C5-C6	1.394(6)	C1S-H1S	0.9500
C6-C7	1.387(6)	C2S-C3S	1.393(6)
C6-H6	0.9500	C2S-H2S	0.9500
C7-C8	1.380(6)	C3S-C4S	1.379(6)
C7-H7	0.9500	C3S-H3S	0.9500
C8-C9	1.370(6)	C4S-C5S	1.378(7)
C8-H8	0.9500	C4S-H4S	0.9500
C9-C10	1.398(6)	C5S-C6S	1.390(6)
C9-H9	0.9500	C5S-H5S	0.9500
C10-H10	0.9500	C6S-H6S	0.9500

Table A3.12 Bond angles for **3-1**.

N1-Pd1-N2	80.43(13)	O1-C11-C12	120.3(4)
N1-Pd1-C1	175.08(14)	O1-C11-C16	122.8(3)
N2-Pd1-C1	95.14(14)	C12-C11-C16	116.9(4)
N1-Pd1-O1	81.49(11)	C13-C12-C11	120.8(4)
N2-Pd1-O1	161.91(12)	C13-C12-H12	119.6
C1-Pd1-O1	102.95(13)	C11-C12-H12	119.6
C11-O1-Pd1	109.8(2)	C12-C13-C14	121.0(4)
C17-N1-C16	130.3(4)	C12-C13-H13	119.5
C17-N1-Pd1	115.7(3)	C14-C13-H13	119.5
C16-N1-Pd1	113.9(2)	C15-C14-C13	119.8(4)
C22-N2-C18	117.6(3)	C15-C14-H14	120.1
C22-N2-Pd1	130.6(3)	C13-C14-H14	120.1
C18-N2-Pd1	111.8(2)	C14-C15-C16	120.2(4)
C2-C1-Pd1	121.6(3)	C14-C15-H15	119.9

C2-C1-H1A	106.9	C16-C15-H15	119.9
Pd1-C1-H1A	106.9	C15-C16-N1	126.8(4)
C2-C1-H1B	106.9	C15-C16-C11	121.2(4)
Pd1-C1-H1B	106.9	N1-C16-C11	112.0(3)
H1A-C1-H1B	106.7	N1-C17-C18	115.9(4)
C3-C2-C5	112.3(3)	N1-C17-H17	122.1
C3-C2-C1	107.7(3)	C18-C17-H17	122.1
C5-C2-C1	108.8(3)	N2-C18-C19	121.2(4)
C3-C2-C4	108.8(3)	N2-C18-C17	116.1(3)
C5-C2-C4	108.4(3)	C19-C18-C17	122.7(4)
C1-C2-C4	110.9(3)	C18-C19-C20	120.1(4)
C2-C3-H3A	109.5	C18-C19-H19	119.9
C2-C3-H3B	109.5	C20-C19-H19	119.9
H3A-C3-H3B	109.5	C21-C20-C19	118.9(4)
C2-C3-H3C	109.5	C21-C20-H20	120.6
H3A-C3-H3C	109.5	C19-C20-H20	120.6
H3B-C3-H3C	109.5	C20-C21-C22	118.4(4)
C2-C4-H4A	109.5	C20-C21-H21	120.8
C2-C4-H4B	109.5	C22-C21-H21	120.8
H4A-C4-H4B	109.5	N2-C22-C21	123.8(4)
C2-C4-H4C	109.5	N2-C22-H22	118.1
H4A-C4-H4C	109.5	C21-C22-H22	118.1
H4B-C4-H4C	109.5	C2S-C1S-C6S	119.9(4)
C10-C5-C6	116.5(4)	C2S-C1S-H1S	120.0
C10-C5-C2	122.9(4)	C6S-C1S-H1S	120.0
C6-C5-C2	120.6(4)	C1S-C2S-C3S	119.9(4)
C7-C6-C5	122.4(4)	C1S-C2S-H2S	120.1
C7-C6-H6	118.8	C3S-C2S-H2S	120.1
C5-C6-H6	118.8	C4S-C3S-C2S	120.0(4)
C8-C7-C6	119.7(4)	C4S-C3S-H3S	120.0
C8-C7-H7	120.2	C2S-C3S-H3S	120.0
C6-C7-H7	120.2	C5S-C4S-C3S	120.5(4)
C9-C8-C7	119.5(4)	C5S-C4S-H4S	119.7
C9-C8-H8	120.2	C3S-C4S-H4S	119.7
C7-C8-H8	120.2	C4S-C5S-C6S	119.0(4)

C8-C9-C10	120.5(4)	C4S-C5S-H5S	120.5
C8-C9-H9	119.8	C6S-C5S-H5S	120.5
C10-C9-H9	119.8	C1S-C6S-C5S	120.7(4)
C5-C10-C9	121.4(4)	C1S-C6S-H6S	119.6
C5-C10-H10	119.3	C5S-C6S-H6S	119.6
C9-C10-H10	119.3		

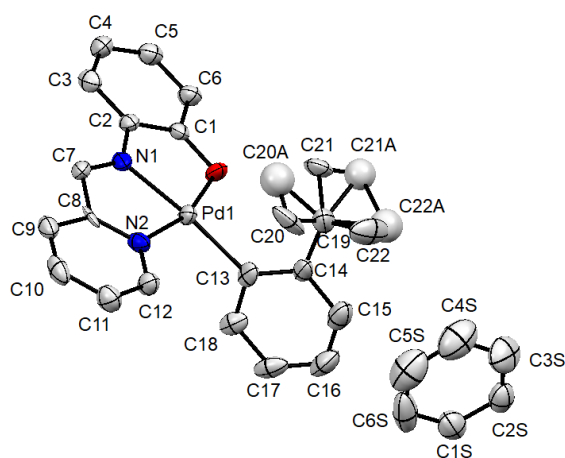


Figure A3. 32 Displacement ellipsoid plot of **3-2** co-crystallized with a benzene molecule showing naming and numbering scheme. Ellipsoids are drawn at the 50% probability level and hydrogen atoms are omitted for clarity.

Table A3.13 Atomic coordinates for **3-2**.

Atom	x	y	z	$U_{\text{iso/equiv}}$
Pd1	0.48061(5)	0.23739(11)	0.14562(4)	0.02933(18)
O1	0.3896(7)	0.4216(7)	0.0893(4)	0.0366(14)
N1	0.3209(8)	0.1438(8)	0.0603(5)	0.0308(16)
N2	0.5263(7)	0.0288(7)	0.1742(5)	0.0306(15)
C1	0.2732(9)	0.3868(10)	0.0295(6)	0.0282(18)
C2	0.2294(7)	0.2463(14)	0.0091(5)	0.0288(15)
C3	0.1102(9)	0.2106(9)	-0.0552(6)	0.035(2)
C4	0.0328(10)	0.3197(9)	-0.1003(7)	0.040(2)
C5	0.0724(10)	0.4594(9)	-0.0832(6)	0.038(2)
C6	0.1913(9)	0.4955(9)	-0.0188(6)	0.0364(19)

C7	0.3269(10)	0.0103(10)	0.0557(6)	0.0334(19)
C8	0.4436(8)	-0.0597(7)	0.1238(5)	0.0234(17)
C9	0.4528(10)	-0.2065(9)	0.1240(7)	0.038(2)
C10	0.5620(9)	-0.2640(16)	0.1847(5)	0.0433(18)
C11	0.6509(11)	-0.1771(9)	0.2416(7)	0.043(2)
C12	0.6315(10)	-0.0284(8)	0.2323(6)	0.0365(19)
C13	0.6575(10)	0.3287(8)	0.2196(6)	0.036(2)
C14	0.6497(10)	0.3949(9)	0.3080(6)	0.038(2)
C15	0.7859(12)	0.4654(10)	0.3408(7)	0.053(3)
C16	0.9230(12)	0.4723(10)	0.2912(8)	0.053(3)
C17	0.9304(10)	0.4035(9)	0.2082(8)	0.046(2)
C18	0.7984(9)	0.3342(8)	0.1731(7)	0.037(2)
C19	0.5055(11)	0.3896(11)	0.3697(7)	0.049(3)
C20	0.4819(19)	0.240(3)	0.3914(10)	0.059(4)
C21	0.3692(16)	0.4554(16)	0.3167(12)	0.044(4)
C22	0.530(2)	0.391(3)	0.4778(12)	0.073(7)
C20A	0.373(4)	0.265(4)	0.352(2)	0.072(8)
C21A	0.395(3)	0.531(3)	0.364(2)	0.059(7)
C22A	0.529(3)	0.483(3)	0.4540(18)	0.069(9)
C1S	1.0859(13)	0.5005(12)	0.5748(7)	0.054(3)
C2S	1.0165(12)	0.5864(11)	0.6383(6)	0.052(3)
C3S	0.8874(15)	0.5402(16)	0.6848(7)	0.074(4)
C4S	0.8267(19)	0.4082(18)	0.6682(10)	0.088(4)
C5S	0.9033(19)	0.3213(15)	0.6071(10)	0.086(4)
C6S	1.0295(18)	0.3669(14)	0.5586(8)	0.078(4)
H3A	0.0838	0.1140	-0.0673	0.041
H4A	-0.0490	0.2983	-0.1438	0.048
H5A	0.0180	0.5329	-0.1157	0.046
H6A	0.2166	0.5926	-0.0076	0.044
H7A	0.2639	-0.0431	0.0132	0.040
H9A	0.3880	-0.2639	0.0849	0.046
H10A	0.5760	-0.3643	0.1874	0.052
H11A	0.7232	-0.2158	0.2859	0.052
H12A	0.6960	0.0329	0.2690	0.044

H15A	0.7835	0.5101	0.3998	0.064
H16A	1.0109	0.5243	0.3146	0.063
H17A	1.0254	0.4030	0.1747	0.055
H18A	0.8047	0.2885	0.1146	0.045
H20A	0.3884	0.2295	0.4294	0.088
H20B	0.5740	0.2035	0.4257	0.088
H20C	0.4674	0.1858	0.3339	0.088
H21A	0.3594	0.4109	0.2555	0.067
H21B	0.3875	0.5577	0.3096	0.067
H21C	0.2721	0.4402	0.3508	0.067
H22A	0.5544	0.2945	0.4995	0.110
H22B	0.4336	0.4243	0.5069	0.110
H22C	0.6170	0.4549	0.4945	0.110
H20D	0.2846	0.2812	0.3929	0.108
H20E	0.4200	0.1721	0.3649	0.108
H20F	0.3362	0.2689	0.2873	0.108
H21D	0.3031	0.5180	0.4021	0.089
H21E	0.3614	0.5467	0.2991	0.089
H21F	0.4556	0.6137	0.3857	0.089
H22D	0.4353	0.4785	0.4924	0.104
H22E	0.6208	0.4507	0.4899	0.104
H22F	0.5454	0.5820	0.4342	0.104
H1SA	1.1740	0.5340	0.5418	0.065
H2SA	1.0578	0.6786	0.6502	0.062
H3SA	0.8398	0.6006	0.7289	0.089
H4SA	0.7342	0.3771	0.6979	0.106
H5SA	0.8671	0.2265	0.5984	0.103
H6SB	1.0773	0.3068	0.5144	0.093

Table A3.14 Bond lengths for **3-2**.

Pd1-N1	2.018(8)	C17-H17A	0.9500
Pd1-C13	2.019(8)	C18-H18A	0.9500
Pd1-N2	2.039(7)	C19-C20	1.46(3)

Pd1-O1	2.057(7)	C19-C22A	1.51(3)
O1-C1	1.342(10)	C19-C21	1.509(17)
N1-C7	1.257(12)	C19-C22	1.570(19)
N1-C2	1.434(13)	C19-C21A	1.63(3)
N2-C8	1.303(10)	C19-C20A	1.64(3)
N2-C12	1.328(11)	C20-H20A	0.9800
C1-C2	1.401(16)	C20-H20B	0.9800
C1-C6	1.413(13)	C20-H20C	0.9800
C2-C3	1.402(11)	C21-H21A	0.9800
C3-C4	1.376(12)	C21-H21B	0.9800
C3-H3A	0.9500	C21-H21C	0.9800
C4-C5	1.376(12)	C22-H22A	0.9800
C4-H4A	0.9500	C22-H22B	0.9800
C5-C6	1.403(12)	C22-H22C	0.9800
C5-H5A	0.9500	C20A-H20D	0.9800
C6-H6A	0.9500	C20A-H20E	0.9800
C7-C8	1.532(13)	C20A-H20F	0.9800
C7-H7A	0.9500	C21A-H21D	0.9800
C8-C9	1.382(12)	C21A-H21E	0.9800
C9-C10	1.375(13)	C21A-H21F	0.9800
C9-H9A	0.9500	C22A-H22D	0.9800
C10-C11	1.375(14)	C22A-H22E	0.9800
C10-H10A	0.9500	C22A-H22F	0.9800
C11-C12	1.413(12)	C1S-C2S	1.365(14)
C11-H11A	0.9500	C1S-C6S	1.362(18)
C12-H12A	0.9500	C1S-H1SA	0.9500
C13-C18	1.387(13)	C2S-C3S	1.370(16)
C13-C14	1.424(13)	C2S-H2SA	0.9500
C14-C15	1.409(13)	C3S-C4S	1.36(2)
C14-C19	1.532(13)	C3S-H3SA	0.9500
C15-C16	1.382(15)	C4S-C5S	1.38(2)
C15-H15A	0.9500	C4S-H4SA	0.9500
C16-C17	1.365(15)	C5S-C6S	1.36(2)
C16-H16A	0.9500	C5S-H5SA	0.9500

C17-C18 | 1.385(12)

C6S-H6SB | 0.9500

Table A3.15 Bond angles for **3-2**.

N1-Pd1-C13	173.7(3)	C20-C19-C21	113.4(11)
N1-Pd1-N2	80.1(3)	C20-C19-C14	105.8(8)
C13-Pd1-N2	99.4(3)	C22A-C19-C14	110.8(9)
N1-Pd1-O1	83.2(3)	C21-C19-C14	107.9(10)
C13-Pd1-O1	97.0(3)	C20-C19-C22	79.0(13)
N2-Pd1-O1	163.3(2)	C21-C19-C22	125.9(12)
C1-O1-Pd1	108.4(5)	C14-C19-C22	119.1(9)
C7-N1-C2	131.7(9)	C22A-C19-C21A	68.5(17)
C7-N1-Pd1	116.1(7)	C14-C19-C21A	114.1(13)
C2-N1-Pd1	111.9(6)	C22A-C19-C20A	128.3(14)
C8-N2-C12	116.4(7)	C14-C19-C20A	119.2(12)
C8-N2-Pd1	113.7(5)	C21A-C19-C20A	100.4(17)
C12-N2-Pd1	129.8(6)	C19-C20-H20A	109.5
O1-C1-C2	123.7(8)	C19-C20-H20B	109.5
O1-C1-C6	119.4(8)	H20A-C20-H20B	109.5
C2-C1-C6	116.8(8)	C19-C20-H20C	109.5
C1-C2-C3	123.4(9)	H20A-C20-H20C	109.5
C1-C2-N1	112.7(7)	H20B-C20-H20C	109.5
C3-C2-N1	123.9(10)	C19-C21-H21A	109.5
C4-C3-C2	117.9(8)	C19-C21-H21B	109.5
C4-C3-H3A	121.0	H21A-C21-H21B	109.5
C2-C3-H3A	121.0	C19-C21-H21C	109.5
C3-C4-C5	120.9(8)	H21A-C21-H21C	109.5
C3-C4-H4A	119.6	H21B-C21-H21C	109.5
C5-C4-H4A	119.6	C19-C22-H22A	109.5
C4-C5-C6	121.3(8)	C19-C22-H22B	109.5
C4-C5-H5A	119.3	H22A-C22-H22B	109.5
C6-C5-H5A	119.3	C19-C22-H22C	109.5
C5-C6-C1	119.6(8)	H22A-C22-H22C	109.5
C5-C6-H6A	120.2	H22B-C22-H22C	109.5
C1-C6-H6A	120.2	C19-C20A-H20D	109.5

N1-C7-C8	114.9(8)	C19-C20A-H20E	109.5
N1-C7-H7A	122.5	H20D-C20A-H20E	109.5
C8-C7-H7A	122.5	C19-C20A-H20F	109.5
N2-C8-C9	127.3(8)	H20D-C20A-H20F	109.5
N2-C8-C7	114.9(7)	H20E-C20A-H20F	109.5
C9-C8-C7	117.8(8)	C19-C21A-H21D	109.5
C10-C9-C8	115.6(10)	C19-C21A-H21E	109.5
C10-C9-H9A	122.2	H21D-C21A-H21E	109.5
C8-C9-H9A	122.2	C19-C21A-H21F	109.5
C9-C10-C11	120.3(13)	H21D-C21A-H21F	109.5
C9-C10-H10A	119.9	H21E-C21A-H21F	109.5
C11-C10-H10A	119.9	C19-C22A-H22D	109.5
C10-C11-C12	117.9(10)	C19-C22A-H22E	109.5
C10-C11-H11A	121.0	H22D-C22A-H22E	109.5
C12-C11-H11A	121.0	C19-C22A-H22F	109.5
N2-C12-C11	122.4(8)	H22D-C22A-H22F	109.5
N2-C12-H12A	118.8	H22E-C22A-H22F	109.5
C11-C12-H12A	118.8	C2S-C1S-C6S	120.3(12)
C18-C13-C14	118.3(8)	C2S-C1S-H1SA	119.8
C18-C13-Pd1	113.7(6)	C6S-C1S-H1SA	119.8
C14-C13-Pd1	127.8(7)	C1S-C2S-C3S	120.3(11)
C15-C14-C13	117.0(9)	C1S-C2S-H2SA	119.9
C15-C14-C19	118.9(8)	C3S-C2S-H2SA	119.9
C13-C14-C19	124.0(7)	C4S-C3S-C2S	120.5(12)
C16-C15-C14	123.0(9)	C4S-C3S-H3SA	119.8
C16-C15-H15A	118.5	C2S-C3S-H3SA	119.8
C14-C15-H15A	118.5	C3S-C4S-C5S	118.0(14)
C17-C16-C15	119.2(9)	C3S-C4S-H4SA	121.0
C17-C16-H16A	120.4	C5S-C4S-H4SA	121.0
C15-C16-H16A	120.4	C6S-C5S-C4S	122.1(13)
C16-C17-C18	119.5(9)	C6S-C5S-H5SA	119.0
C16-C17-H17A	120.2	C4S-C5S-H5SA	119.0
C18-C17-H17A	120.2	C5S-C6S-C1S	118.7(12)
C17-C18-C13	122.9(9)	C5S-C6S-H6SB	120.7

C17-C18-H18A | 118.6
C13-C18-H18A | 118.6

C1S-C6S-H6SB | 120.7

References

1. A. Marini, A. Muñoz-Losa, A. Biancardi and B. Mennucci, *J. Phys. Chem. B*, 2010, **114**, 17128-17135.
2. N. Chaudhury and R. J. Puddephatt, *J. Organomet. Chem.*, 1975, **84**, 105-115.
3. T. Yamamoto, A. Yamamoto and S. Ikeda, *J. Am. Chem. Soc.*, 1971, **93**, 3350-3359.
4. SAINT version 2013.8; Bruker-AXS, Madison, WI 53711, USA, 2013.
5. SADABS version 2012.1; Bruker-AXS, Madison, WI53711, USA, 2012.
6. G. M. Sheldrick, *Acta Cryst. A.*, **2015**, 71, 3-8.
7. G. M. Sheldrick, *Acta Cryst.*, 2015, **C71**, 3-8.

Appendix C: Supplementary Information for Chapter 4

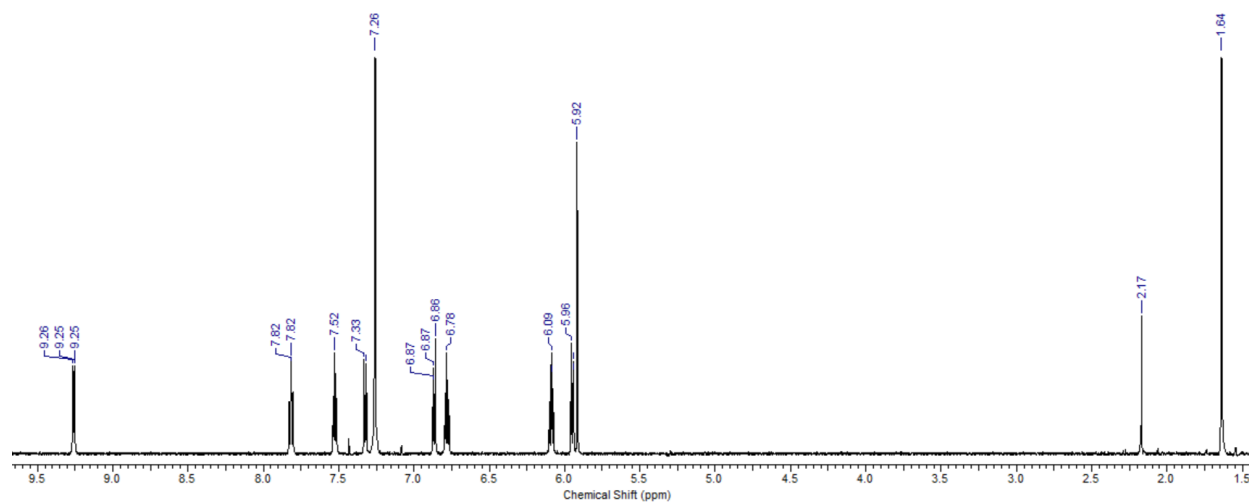


Figure A4.1 ^1H NMR spectrum of **4-1** in CDCl_3 at 600 MHz.

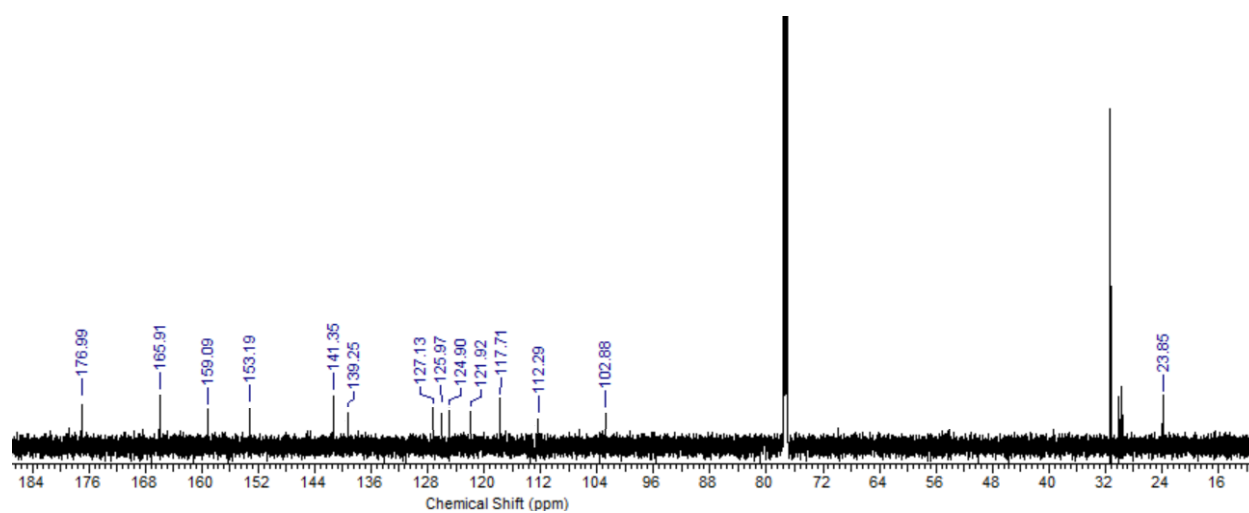


Figure A4.2 $^{13}\text{C}\{^1\text{H}\}$ NMR spectrum of **4-1** in CDCl_3 at 151 MHz.

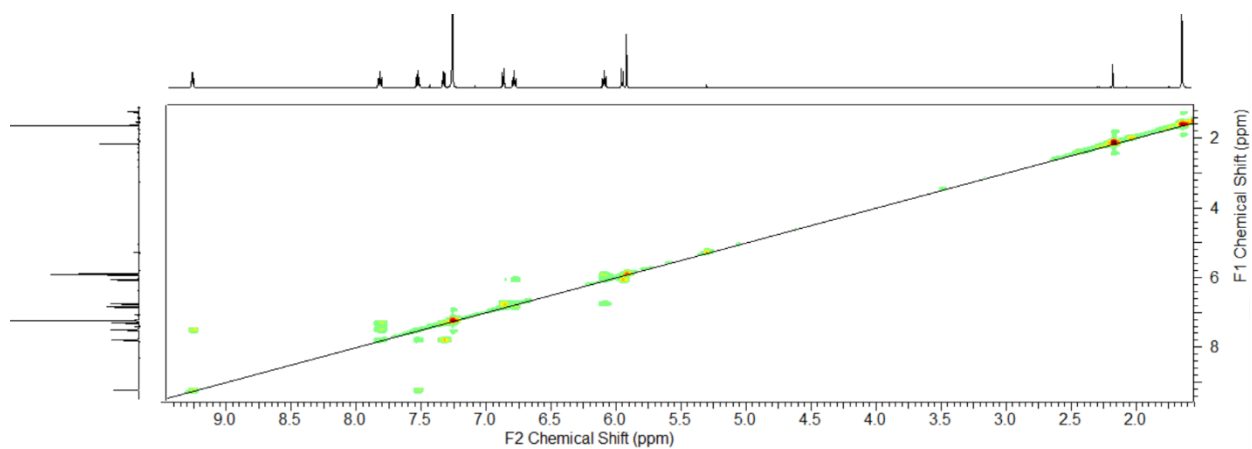


Figure A4.3 ^1H - ^1H gCOSY spectrum of **4-1** in CDCl_3 .

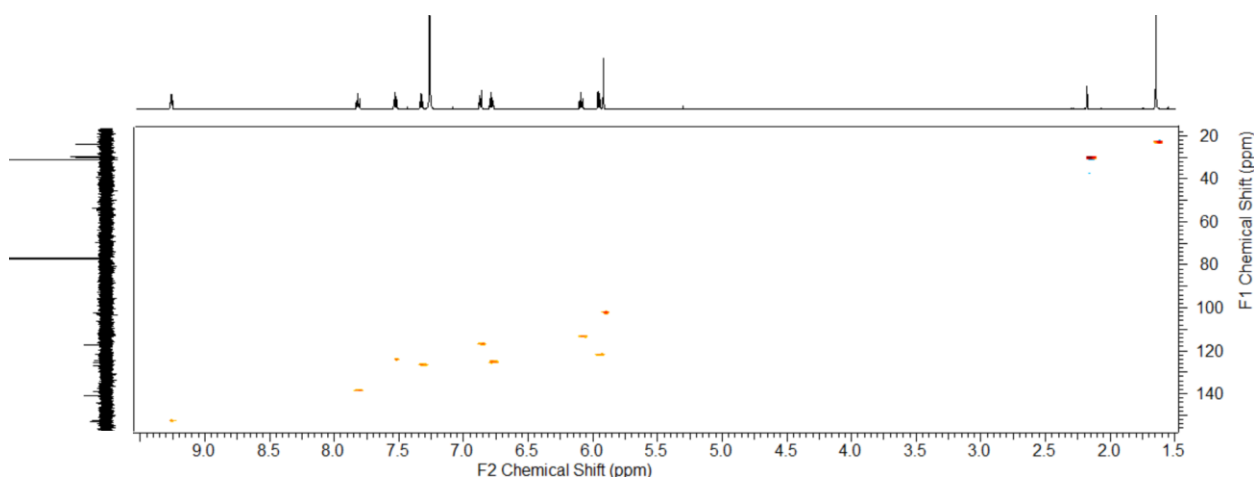


Figure A4.4 ^1H - $^{13}\text{C}\{^1\text{H}\}$ HSQC spectrum (CDCl_3) of **4-1**.

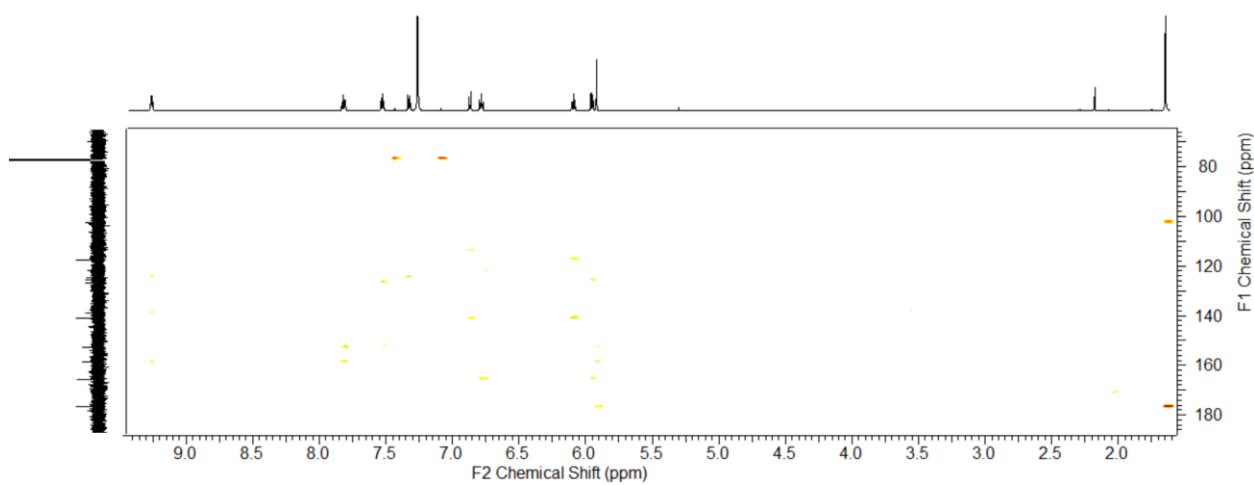


Figure A4.5 ^1H - $^{13}\text{C}\{^1\text{H}\}$ HMBC spectrum (CDCl_3) of **4-1**.

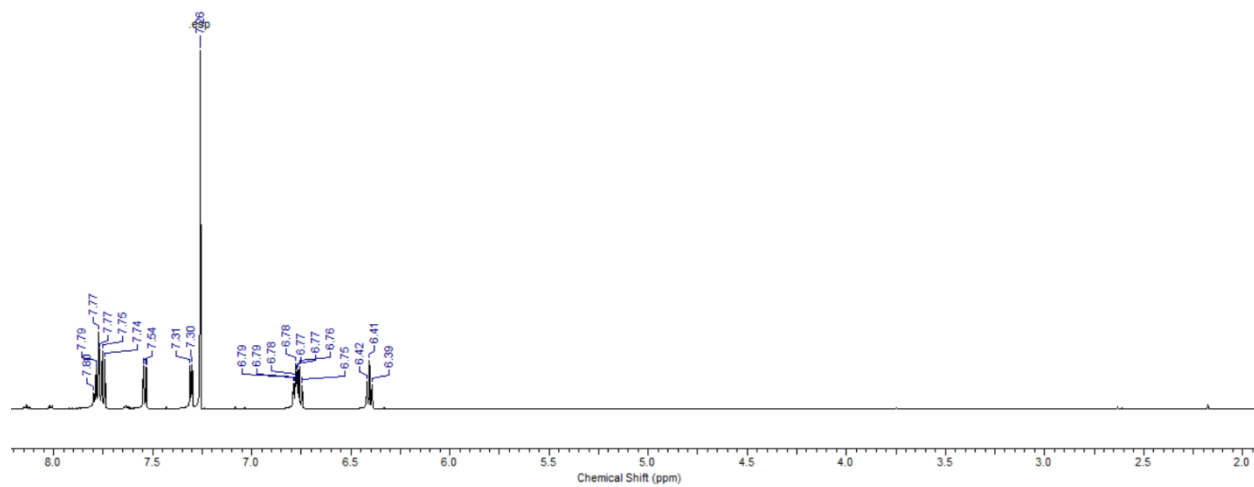


Figure A4.6 ^1H NMR spectrum of **4-2** in CDCl_3 at 600 MHz.

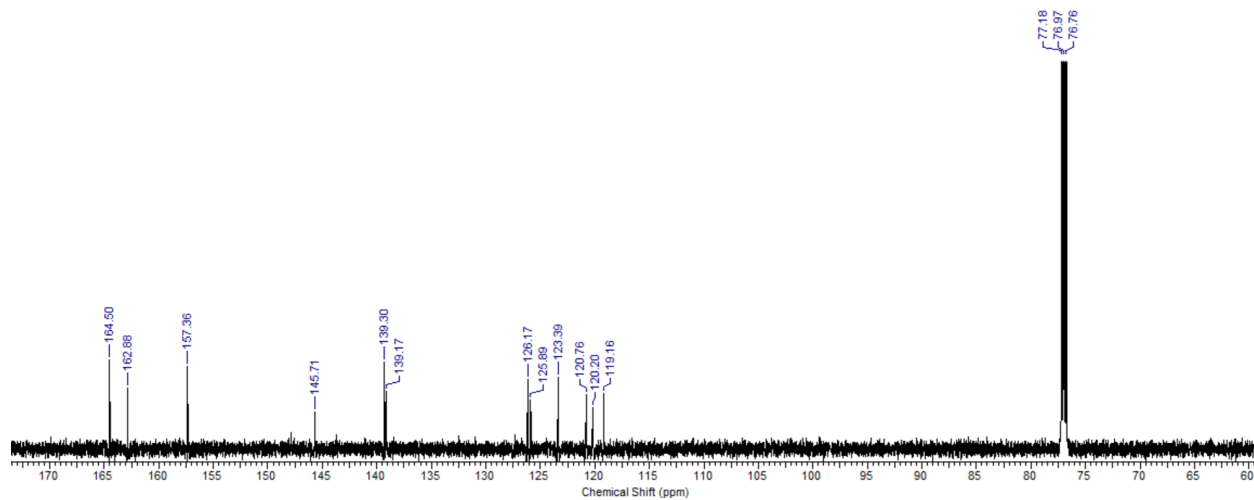


Figure A4.7 $^{13}\text{C}\{^1\text{H}\}$ NMR spectrum (CDCl_3) of **4-2** at 151 MHz.

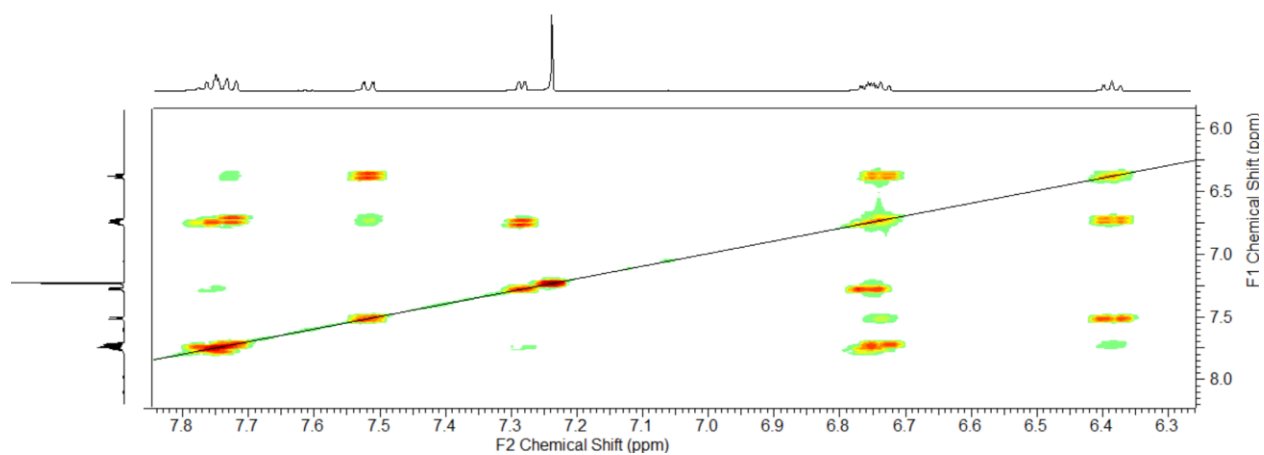


Figure A4.8 ^1H - ^1H gCOSY spectrum of **4-2** in CDCl_3 .

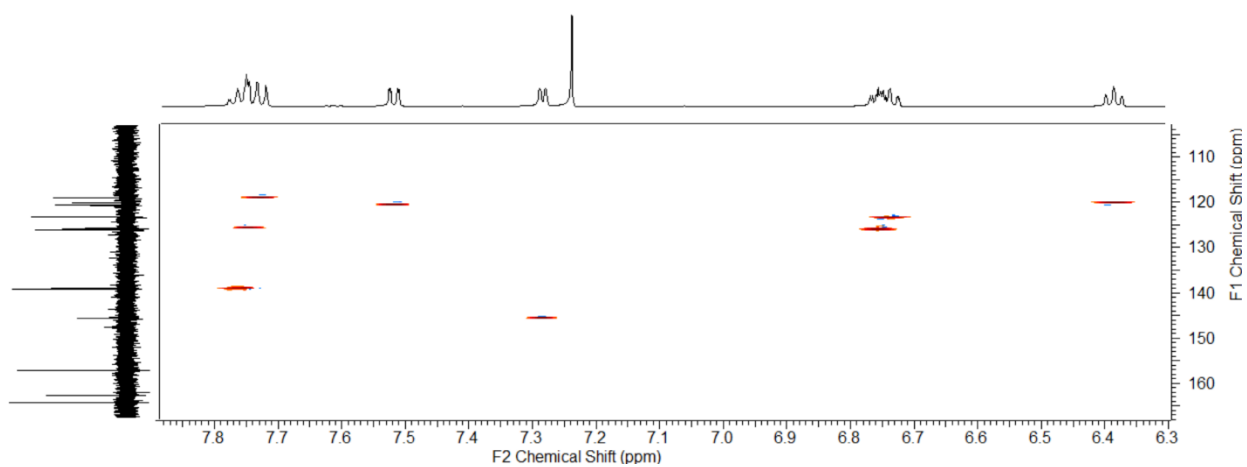


Figure A4.9 ^1H - $^{13}\text{C}\{^1\text{H}\}$ HSQC spectrum (CDCl_3) of **4-2**.

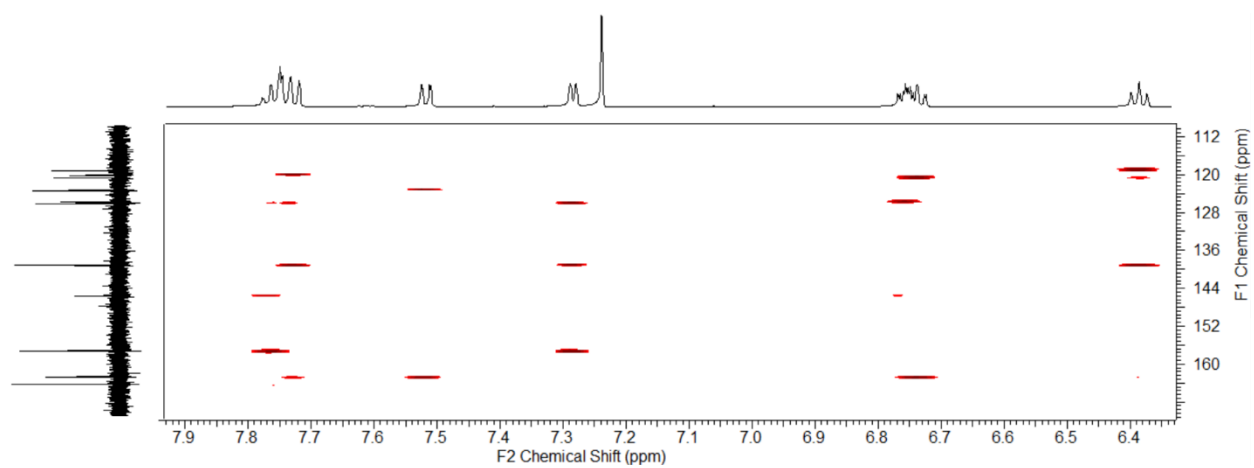


Figure A4.10 ^1H - $^{13}\text{C}\{^1\text{H}\}$ HMBC spectrum (CDCl_3) of **4-2**.

Table A4.1 Crystallographic data and parameters for compounds **4-1**, **4-2** and **4-3**.

	4-1	4-2	4-3
Formula	C ₆₃ H ₅₄ N ₈ O ₉ Pd ₄	C ₄₉ H ₃₃ Cl ₃ N ₈ O ₈ Pd ₄	C ₁₃ H ₁₀ Cl ₄ N ₂ OPd
Formula weight	1492.74	1393.78	458.43
Crystal system	monoclinic	triclinic	monoclinic
Space group	P 2/n	P -1	P 2 ₁ /n
<i>a</i> [Å]	13.327(4)	12.412(4)	12.823(3)
<i>b</i> [Å]	8.686(3)	13.358(3)	7.1043(14)
<i>c</i> [Å]	25.305(7)	17.436(4)	16.997(6)
α [°]	90	111.520(7)	90
β [°]	102.658(11)	106.400(11)	90.137(16)
γ [°]	90	91.530(15)	90
<i>V</i> [Å ³]	2857.9(16)	2552.3(11)	1548.4(7)
<i>Z</i>	2	2	4
d(calc.) (Mg/m ³)	1.735	1.814	1.966
λ , Å, (MoKa)	0.71073	0.71073	0.71073
<i>F</i> (000)	1488	1480	896
Temperature [K]	110	110	110
θ_{\min} , θ_{\max} [°]	2.486, 33.196	2.667, 43.313	3.108, 24.491
Total reflns	88521	179839	32693
Unique reflns	10882	37874	2574
<i>R</i> ₁	0.0509	0.0429	0.0228
w <i>R</i> ₂ [<i>I</i> ≥ 2σ(<i>I</i>)]	0.1101	0.1037	0.0727
<i>R</i> ₁ (all data)	0.0847	0.0676	0.0254
w <i>R</i> ₂ (all data)	0.1228	0.1177	0.0748
GOF	1.060	1.022	0.948
Maximum shift/error	0.003	0.002	0.001

Min & Max peak
heights on final
 ΔF Map ($e^{-}/\text{\AA}$)

-1.601, 1.100

-2.402, 3.008

-0.911, 0.807

Where: $R_1 = \Sigma(|F_o| - |F_c|) / \Sigma F_o$; $wR_2 = [\Sigma(w(F_o^2 - F_c^2)^2) / \Sigma(wF_o^4)]^{1/2}$; $GOF = [\Sigma(w(F_o^2 - F_c^2)^2) / (\text{No. of reflns.} - \text{No. of params.})]^{1/2}$

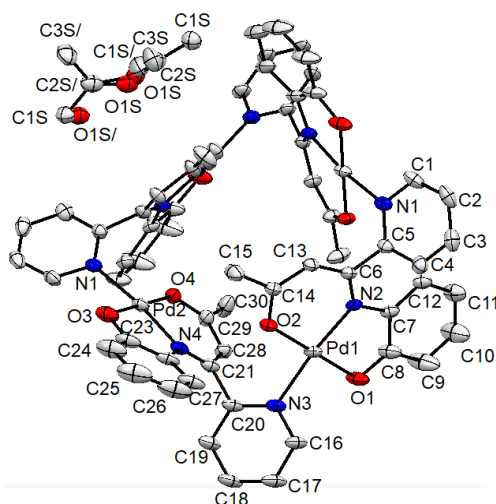


Figure A4.11 Displacement ellipsoid plot of **4-1** co-crystallized with acetone molecules showing naming and numbering scheme. Ellipsoids are drawn at the 50% probability level and hydrogen atoms are omitted for clarity.

Table A4.2 Atomic coordinates for **4-1**.

Atom	x	y	z	$U_{\text{iso/equiv}}$
Pd1	0.46687(2)	0.61042(3)	0.76290(2)	0.02367(7)
Pd2	0.82857(2)	0.40877(3)	0.90408(2)	0.02548(8)
O1	0.4010(3)	0.8105(3)	0.74083(11)	0.0386(7)
O2	0.5324(2)	0.4095(3)	0.78511(10)	0.0292(6)
O3	0.8062(3)	0.2154(3)	0.94061(11)	0.0386(7)
O4	0.8525(2)	0.6029(3)	0.86842(10)	0.0269(6)
N1	0.5153(3)	0.3731(4)	0.57658(11)	0.0257(7)
N2	0.4631(2)	0.5857(4)	0.68564(11)	0.0225(6)
N3	0.4543(3)	0.6457(4)	0.84171(12)	0.0285(7)
N4	0.6791(3)	0.4362(4)	0.89522(11)	0.0264(7)
C1	0.4769(4)	0.3172(5)	0.52581(14)	0.0348(10)

C2	0.3746(4)	0.3096(5)	0.50256(14)	0.0380(11)
C3	0.3043(4)	0.3619(5)	0.53114(16)	0.0370(10)
C4	0.3416(4)	0.4141(5)	0.58386(15)	0.0322(9)
C5	0.4471(3)	0.4173(4)	0.60608(13)	0.0245(7)
C6	0.4845(3)	0.4531(4)	0.66502(13)	0.0247(7)
C7	0.4282(3)	0.7217(4)	0.65639(14)	0.0244(7)
C8	0.3969(4)	0.8360(5)	0.68851(17)	0.0379(10)
C9	0.3616(6)	0.9766(6)	0.6643(2)	0.071(2)
C10	0.3621(5)	1.0042(6)	0.6108(2)	0.0649(18)
C11	0.3975(4)	0.8946(5)	0.57970(18)	0.0406(11)
C12	0.4315(3)	0.7552(5)	0.60249(15)	0.0274(8)
C13	0.5302(3)	0.3281(5)	0.69504(13)	0.0278(8)
C14	0.5554(3)	0.3126(5)	0.75158(14)	0.0301(9)
C15	0.6111(4)	0.1720(5)	0.77659(16)	0.0443(12)
C16	0.3646(3)	0.7020(5)	0.84879(16)	0.0327(9)
C17	0.3430(4)	0.7172(5)	0.89982(17)	0.0382(11)
C18	0.4150(4)	0.6729(6)	0.94447(16)	0.0405(12)
C19	0.5074(4)	0.6170(5)	0.93723(16)	0.0365(10)
C20	0.5270(3)	0.6057(5)	0.88564(15)	0.0295(9)
C21	0.6336(3)	0.5682(5)	0.87914(14)	0.0266(8)
C22	0.6335(4)	0.3025(5)	0.91206(15)	0.0344(10)
C23	0.7065(4)	0.1928(5)	0.93726(17)	0.0387(11)
C24	0.6729(5)	0.0554(6)	0.9572(2)	0.0553(15)
C25	0.5699(6)	0.0258(6)	0.9499(2)	0.0656(19)
C26	0.4976(5)	0.1305(7)	0.9224(2)	0.0617(18)
C27	0.5287(4)	0.2674(6)	0.90279(17)	0.0427(12)
C28	0.6803(3)	0.6933(5)	0.85821(14)	0.0272(8)
C29	0.7812(3)	0.7036(5)	0.85240(14)	0.0278(8)
C30	0.8165(4)	0.8453(5)	0.8272(2)	0.0414(11)
O1S	0.249(5)	0.354(3)	0.743(2)	0.0400(17)
C1S	0.193(4)	0.329(6)	0.6576(19)	0.038(8)
C2S	0.2057(8)	0.2782(12)	0.7084(4)	0.0400(17)
C3S	0.1595(9)	0.1228(12)	0.7074(4)	0.049(2)
O1S'	0.2092(11)	0.3558(17)	0.6692(6)	0.0400(17)
C1S'	0.249(2)	0.334(3)	0.7695(10)	0.062(7)

C2S'	0.2057(8)	0.2782(12)	0.7084(4)	0.0400(17)
C3S'	0.1595(9)	0.1228(12)	0.7074(4)	0.049(2)
H1	0.5242	0.2814	0.5055	0.042
H2	0.3520	0.2689	0.4671	0.046
H3	0.2327	0.3622	0.5154	0.044
H4	0.2948	0.4479	0.6048	0.039
H9	0.3371	1.0536	0.6850	0.085
H10	0.3377	1.1001	0.5950	0.078
H11	0.3984	0.9155	0.5429	0.049
H12	0.4575	0.6806	0.5815	0.033
H13	0.5462	0.2427	0.6749	0.033
H15A	0.6783	0.2016	0.7986	0.066
H15B	0.6208	0.1012	0.7480	0.066
H15C	0.5706	0.1210	0.7995	0.066
H16	0.3141	0.7325	0.8179	0.039
H17	0.2788	0.7580	0.9037	0.046
H18	0.4014	0.6806	0.9797	0.049
H19	0.5584	0.5858	0.9678	0.044
H24	0.7216	-0.0168	0.9758	0.066
H25	0.5475	-0.0668	0.9636	0.079
H26	0.4264	0.1078	0.9171	0.074
H27	0.4791	0.3368	0.8832	0.051
H28	0.6378	0.7802	0.8468	0.033
H30A	0.8657	0.9023	0.8548	0.062
H30B	0.7571	0.9110	0.8126	0.062
H30C	0.8497	0.8148	0.7979	0.062
H1S1	0.1549	0.2520	0.6327	0.057
H1S2	0.1551	0.4259	0.6536	0.057
H1S3	0.2608	0.3451	0.6491	0.057
H3S1	0.1281	0.0945	0.6700	0.074
H3S2	0.2131	0.0480	0.7227	0.074
H3S3	0.1067	0.1232	0.7290	0.074
H1S4	0.2384	0.2530	0.7946	0.093
H1S5	0.3232	0.3552	0.7749	0.093
H1S6	0.2135	0.4278	0.7763	0.093

H3S4	0.1667	0.0853	0.7446	0.074
H3S5	0.0864	0.1281	0.6897	0.074
H3S6	0.1948	0.0523	0.6873	0.074

Table A4.3 Bond lengths for **4-1**.

Pd1-N2	1.957(3)	C15-H15C	0.9800
Pd1-O1	1.971(3)	C16-C17	1.389(5)
Pd1-O2	1.977(3)	C16-H16	0.9500
Pd1-N3	2.061(3)	C17-C18	1.367(7)
Pd2-N4	1.970(3)	C17-H17	0.9500
Pd2-O3	1.971(3)	C18-C19	1.372(6)
Pd2-O4	1.971(3)	C18-H18	0.9500
Pd2-N1	2.054(4)	C19-C20	1.390(5)
O1-C8	1.332(5)	C19-H19	0.9500
O2-C14	1.279(4)	C20-C21	1.502(6)
O3-C23	1.327(6)	C21-C28	1.411(5)
O4-C29	1.290(5)	C22-C27	1.398(7)
N1-C5	1.352(5)	C22-C23	1.411(7)
N1-C1	1.364(5)	C23-C24	1.407(6)
N1-Pd2	2.054(4)	C24-C25	1.368(9)
N2-C6	1.321(5)	C24-H24	0.9500
N2-C7	1.417(5)	C25-C26	1.395(9)
N3-C16	1.339(5)	C25-H25	0.9500
N3-C20	1.351(5)	C26-C27	1.386(7)
N4-C21	1.319(5)	C26-H26	0.9500
N4-C22	1.419(5)	C27-H27	0.9500
C1-C2	1.363(7)	C28-C29	1.387(5)
C1-H1	0.9500	C28-H28	0.9500
C2-C3	1.379(7)	C29-C30	1.508(5)
C2-H2	0.9500	C30-H30A	0.9800
C3-C4	1.394(5)	C30-H30B	0.9800
C3-H3	0.9500	C30-H30C	0.9800
C4-C5	1.394(6)	O1S-C2S	1.15(5)
C4-H4	0.9500	C1S-C2S	1.33(5)
C5-C6	1.498(5)	C1S-H1S1	0.9800

C6-C13	1.387(5)	C1S-H1S2	0.9800
C7-C8	1.404(5)	C1S-H1S3	0.9800
C7-C12	1.404(5)	C2S-C3S	1.481(15)
C8-C9	1.401(7)	C3S-H3S1	0.9800
C9-C10	1.376(7)	C3S-H3S2	0.9800
C9-H9	0.9500	C3S-H3S3	0.9800
C10-C11	1.382(7)	O1S'-C2S'	1.210(17)
C10-H10	0.9500	C1S'-C2S'	1.60(3)
C11-C12	1.374(6)	C1S'-H1S4	0.9800
C11-H11	0.9500	C1S'-H1S5	0.9800
C12-H12	0.9500	C1S'-H1S6	0.9800
C13-C14	1.402(5)	C2S'-C3S'	1.481(15)
C13-H13	0.9500	C3S'-H3S4	0.9800
C14-C15	1.496(6)	C3S'-H3S5	0.9800
C15-H15A	0.9800	C3S'-H3S6	0.9800
C15-H15B	0.9800		

Table A4.4 Bond angles for **4-1**.

N2-Pd1-O1	84.34(12)	N3-C16-H16	118.9
N2-Pd1-O2	95.74(11)	C17-C16-H16	118.9
O1-Pd1-O2	179.78(13)	C18-C17-C16	119.4(4)
N2-Pd1-N3	173.59(14)	C18-C17-H17	120.3
O1-Pd1-N3	91.01(13)	C16-C17-H17	120.3
O2-Pd1-N3	88.90(12)	C17-C18-C19	118.5(4)
N4-Pd2-O3	84.46(14)	C17-C18-H18	120.8
N4-Pd2-O4	96.06(12)	C19-C18-H18	120.8
O3-Pd2-O4	179.18(14)	C18-C19-C20	120.6(4)
N4-Pd2-N1	172.69(11)	C18-C19-H19	119.7
O3-Pd2-N1	90.54(13)	C20-C19-H19	119.7
O4-Pd2-N1	88.89(12)	N3-C20-C19	120.4(4)
C8-O1-Pd1	110.4(2)	N3-C20-C21	119.4(3)
C14-O2-Pd1	123.2(2)	C19-C20-C21	119.7(4)
C23-O3-Pd2	110.4(3)	N4-C21-C28	125.1(4)

C29-O4-Pd2	122.8(2)	N4-C21-C20	122.4(3)
C5-N1-C1	117.5(4)	C28-C21-C20	112.3(4)
C5-N1-Pd2	126.5(3)	C27-C22-C23	119.6(4)
C1-N1-Pd2	115.4(3)	C27-C22-N4	127.3(4)
C6-N2-C7	126.5(3)	C23-C22-N4	112.9(4)
C6-N2-Pd1	122.0(2)	O3-C23-C24	119.7(5)
C7-N2-Pd1	111.3(2)	O3-C23-C22	120.7(4)
C16-N3-C20	119.0(3)	C24-C23-C22	119.5(5)
C16-N3-Pd1	116.6(3)	C25-C24-C23	120.0(6)
C20-N3-Pd1	124.2(3)	C25-C24-H24	120.0
C21-N4-C22	127.3(4)	C23-C24-H24	120.0
C21-N4-Pd2	121.7(3)	C24-C25-C26	120.5(5)
C22-N4-Pd2	110.8(3)	C24-C25-H25	119.7
C2-C1-N1	123.8(4)	C26-C25-H25	119.7
C2-C1-H1	118.1	C27-C26-C25	120.7(6)
N1-C1-H1	118.1	C27-C26-H26	119.7
C1-C2-C3	119.2(4)	C25-C26-H26	119.7
C1-C2-H2	120.4	C26-C27-C22	119.5(6)
C3-C2-H2	120.4	C26-C27-H27	120.2
C2-C3-C4	117.9(4)	C22-C27-H27	120.2
C2-C3-H3	121.0	C29-C28-C21	127.4(4)
C4-C3-H3	121.0	C29-C28-H28	116.3
C3-C4-C5	120.6(4)	C21-C28-H28	116.3
C3-C4-H4	119.7	O4-C29-C28	126.0(4)
C5-C4-H4	119.7	O4-C29-C30	114.1(4)
N1-C5-C4	120.8(3)	C28-C29-C30	119.8(4)
N1-C5-C6	119.4(3)	C29-C30-H30A	109.5
C4-C5-C6	119.5(3)	C29-C30-H30B	109.5
N2-C6-C13	125.0(3)	H30A-C30-H30B	109.5
N2-C6-C5	121.3(3)	C29-C30-H30C	109.5
C13-C6-C5	113.2(3)	H30A-C30-H30C	109.5
C8-C7-C12	119.5(4)	H30B-C30-H30C	109.5
C8-C7-N2	113.1(3)	C2S-C1S-H1S1	109.5
C12-C7-N2	127.1(3)	C2S-C1S-H1S2	109.5
O1-C8-C9	121.2(4)	H1S1-C1S-H1S2	109.5

O1-C8-C7	120.3(4)	C2S-C1S-H1S3	109.5
C9-C8-C7	118.5(4)	H1S1-C1S-H1S3	109.5
C10-C9-C8	120.6(4)	H1S2-C1S-H1S3	109.5
C10-C9-H9	119.7	O1S-C2S-C1S	119(3)
C8-C9-H9	119.7	O1S-C2S-C3S	133(2)
C9-C10-C11	121.1(5)	C1S-C2S-C3S	109(3)
C9-C10-H10	119.4	C2S-C3S-H3S1	109.5
C11-C10-H10	119.4	C2S-C3S-H3S2	109.5
C12-C11-C10	119.3(4)	H3S1-C3S-H3S2	109.5
C12-C11-H11	120.3	C2S-C3S-H3S3	109.5
C10-C11-H11	120.3	H3S1-C3S-H3S3	109.5
C11-C12-C7	120.9(4)	H3S2-C3S-H3S3	109.5
C11-C12-H12	119.6	C2S'-C1S'-H1S4	109.5
C7-C12-H12	119.6	C2S'-C1S'-H1S5	109.5
C6-C13-C14	127.7(3)	H1S4-C1S'-H1S5	109.5
C6-C13-H13	116.1	C2S'-C1S'-H1S6	109.5
C14-C13-H13	116.1	H1S4-C1S'-H1S6	109.5
O2-C14-C13	125.1(4)	H1S5-C1S'-H1S6	109.5
O2-C14-C15	115.2(3)	O1S'-C2S'-C3S'	125.7(13)
C13-C14-C15	119.7(3)	O1S'-C2S'-C1S'	123.5(12)
C14-C15-H15A	109.5	C3S'-C2S'-C1S'	110.8(12)
C14-C15-H15B	109.5	C2S'-C3S'-H3S4	109.5
H15A-C15-H15B	109.5	C2S'-C3S'-H3S5	109.5
C14-C15-H15C	109.5	H3S4-C3S'-H3S5	109.5
H15A-C15-H15C	109.5	C2S'-C3S'-H3S6	109.5
H15B-C15-H15C	109.5	H3S4-C3S'-H3S6	109.5
N3-C16-C17	122.1(4)	H3S5-C3S'-H3S6	109.5

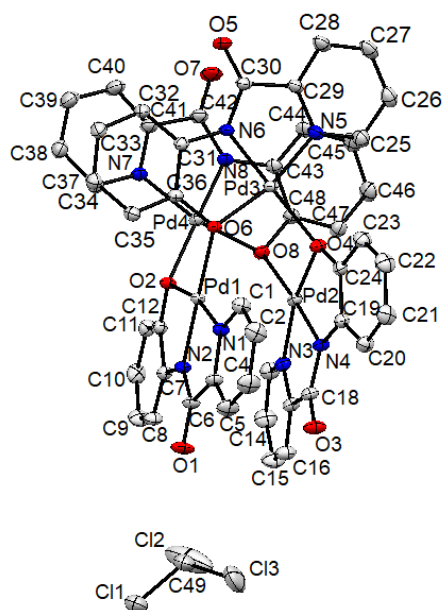


Figure A4.12 Displacement ellipsoid plot of **4-2** co-crystallized with a chloroform molecule showing naming and numbering scheme. Ellipsoids are drawn at the 50% probability level and hydrogen atoms are omitted for clarity.

Table A4.5 Atomic coordinates for **4-2**.

Atom	x	y	z	$U_{\text{iso/equiv}}$
Pd1	0.72729(2)	0.38288(2)	0.27222(2)	0.01306(2)
Pd2	0.58758(2)	0.13927(2)	0.16750(2)	0.01464(2)
Pd3	0.52709(2)	0.29943(2)	0.35746(2)	0.01486(2)
Pd4	0.77048(2)	0.20504(2)	0.37546(2)	0.01473(2)
O1	0.82543(15)	0.40511(15)	0.07742(11)	0.0269(3)
O2	0.83503(11)	0.29077(11)	0.31756(9)	0.0162(2)
O3	0.55251(15)	0.24179(14)	-0.02612(10)	0.0246(3)
O4	0.47274(12)	0.21096(12)	0.22467(9)	0.0188(2)
O5	0.54297(14)	0.39102(15)	0.60828(10)	0.0263(3)
O6	0.63899(12)	0.41372(11)	0.35911(9)	0.0171(2)
O7	0.69295(19)	0.14106(16)	0.56372(12)	0.0358(4)
O8	0.67272(12)	0.08686(12)	0.26307(9)	0.0184(2)
N1	0.64543(14)	0.47018(13)	0.21059(10)	0.0167(2)
N2	0.80827(13)	0.35702(13)	0.18859(10)	0.0153(2)
N3	0.67554(14)	0.07634(13)	0.08538(10)	0.0170(2)

N4	0.51728(14)	0.19735(13)	0.08196(10)	0.0166(2)
N5	0.42672(14)	0.20956(14)	0.38599(11)	0.0186(3)
N6	0.57688(13)	0.38071(14)	0.48167(10)	0.0169(2)
N7	0.85163(14)	0.30308(13)	0.49882(10)	0.0174(2)
N8	0.70216(14)	0.13056(14)	0.43008(10)	0.0186(3)
C1	0.55957(17)	0.52376(17)	0.22739(14)	0.0214(3)
C2	0.5105(2)	0.5828(2)	0.17900(17)	0.0282(4)
C3	0.5503(2)	0.5862(2)	0.11347(17)	0.0299(4)
C4	0.6390(2)	0.5298(2)	0.09675(15)	0.0266(4)
C5	0.68521(17)	0.47169(15)	0.14630(12)	0.0180(3)
C6	0.78116(16)	0.40780(15)	0.13298(12)	0.0174(3)
C7	0.88802(15)	0.28555(14)	0.19463(11)	0.0155(3)
C8	0.95493(18)	0.24858(18)	0.14026(13)	0.0218(3)
C9	1.0237(2)	0.1709(2)	0.15001(16)	0.0272(4)
C10	1.02695(19)	0.12969(19)	0.21282(15)	0.0258(4)
C11	0.96266(17)	0.16757(16)	0.26877(13)	0.0202(3)
C12	0.89511(15)	0.24674(15)	0.26120(11)	0.0158(3)
C13	0.74398(18)	0.00096(17)	0.08499(14)	0.0224(3)
C14	0.7944(2)	-0.0397(2)	0.01988(16)	0.0283(4)
C15	0.7758(2)	0.0028(2)	-0.04321(16)	0.0304(5)
C16	0.70658(19)	0.08284(19)	-0.04159(13)	0.0238(4)
C17	0.65565(16)	0.11622(15)	0.02239(11)	0.0172(3)
C18	0.57017(16)	0.19381(15)	0.02365(11)	0.0173(3)
C19	0.42835(15)	0.25536(15)	0.09907(11)	0.0167(3)
C20	0.36057(17)	0.30238(18)	0.04631(14)	0.0218(3)
C21	0.27155(19)	0.3527(2)	0.06967(16)	0.0277(4)
C22	0.2494(2)	0.3557(2)	0.14420(17)	0.0302(4)
C23	0.31618(18)	0.30863(19)	0.19647(15)	0.0250(4)
C24	0.40633(16)	0.25975(16)	0.17474(12)	0.0180(3)
C25	0.35338(18)	0.12024(18)	0.33105(15)	0.0233(3)
C26	0.28724(19)	0.0655(2)	0.36020(17)	0.0269(4)
C27	0.29817(19)	0.1057(2)	0.44782(17)	0.0281(4)
C28	0.37503(18)	0.1987(2)	0.50486(15)	0.0246(4)
C29	0.43897(16)	0.24892(17)	0.47219(13)	0.0186(3)
C30	0.52569(16)	0.34881(17)	0.52947(12)	0.0188(3)

C31	0.65892(15)	0.47115(15)	0.50987(11)	0.0164(3)
C32	0.71096(16)	0.54337(17)	0.59592(12)	0.0203(3)
C33	0.79281(18)	0.62951(18)	0.61457(14)	0.0234(3)
C34	0.82251(18)	0.64527(17)	0.54830(14)	0.0223(3)
C35	0.77177(17)	0.57319(16)	0.46224(13)	0.0197(3)
C36	0.69100(15)	0.48614(14)	0.44306(11)	0.0156(3)
C37	0.92916(16)	0.39045(16)	0.52781(13)	0.0198(3)
C38	0.97606(19)	0.45421(18)	0.61618(14)	0.0248(4)
C39	0.9403(2)	0.4265(2)	0.67501(15)	0.0316(5)
C40	0.8590(2)	0.3347(2)	0.64431(14)	0.0309(5)
C41	0.81655(19)	0.27445(17)	0.55590(13)	0.0218(3)
C42	0.72946(19)	0.17428(17)	0.51739(13)	0.0227(3)
C43	0.62121(16)	0.04030(15)	0.37045(12)	0.0185(3)
C44	0.55483(19)	-0.02627(18)	0.39026(14)	0.0232(3)
C45	0.4798(2)	-0.11496(19)	0.32336(16)	0.0280(4)
C46	0.4709(2)	-0.13708(19)	0.23765(16)	0.0282(4)
C47	0.53536(19)	-0.06974(17)	0.21703(14)	0.0241(4)
C48	0.60888(16)	0.01939(15)	0.28273(12)	0.0180(3)
C49	0.90872(19)	0.3261(2)	-0.08897(16)	0.0396(6)
C11	1.01538(6)	0.40565(7)	-0.09801(5)	0.04040(15)
C12	0.95039(17)	0.19948(10)	-0.09494(12)	0.1026(6)
C13	0.78146(15)	0.3438(5)	-0.1589(2)	0.0638(11)
C49'	0.90872(19)	0.3261(2)	-0.08897(16)	0.0396(6)
C11'	1.01538(6)	0.40565(7)	-0.09801(5)	0.04040(15)
C12'	0.95039(17)	0.19948(10)	-0.09494(12)	0.1026(6)
C13'	0.7877(2)	0.2726(7)	-0.1802(2)	0.0656(17)
C50	0.8545(4)	-0.1031(5)	0.3339(4)	0.58(3)
C14	0.7983(8)	-0.2208(6)	0.3383(7)	0.279(6)
C15	0.9847(11)	-0.0920(10)	0.4085(12)	0.517(14)
C16	0.8453(8)	-0.1573(7)	0.2261(5)	0.433(9)
C50'	0.8545(4)	-0.1031(5)	0.3339(4)	0.58(3)
C14'	0.9974(3)	-0.0856(3)	0.3380(3)	0.0777(13)
C15'	0.8026(4)	-0.2058(4)	0.2279(5)	0.181(5)
C16'	0.8751(11)	-0.1880(6)	0.3923(6)	0.170(5)
H1	0.5323	0.5214	0.2725	0.026

H2	0.4497	0.6207	0.1909	0.034
H3	0.5174	0.6267	0.0803	0.036
H4	0.6675	0.5310	0.0519	0.032
H8	0.9534	0.2763	0.0971	0.026
H9	1.0692	0.1457	0.1131	0.033
H10	1.0732	0.0754	0.2177	0.031
H11	0.9651	0.1394	0.3118	0.024
H13	0.7587	-0.0256	0.1300	0.027
H14	0.8406	-0.0954	0.0189	0.034
H15	0.8103	-0.0228	-0.0877	0.037
H16	0.6946	0.1140	-0.0838	0.029
H20	0.3753	0.2999	-0.0049	0.026
H21	0.2256	0.3852	0.0345	0.033
H22	0.1882	0.3900	0.1595	0.036
H23	0.3000	0.3100	0.2469	0.030
H25	0.3461	0.0935	0.2710	0.028
H26	0.2356	0.0017	0.3207	0.032
H27	0.2533	0.0700	0.4689	0.034
H28	0.3834	0.2271	0.5651	0.029
H32	0.6905	0.5337	0.6416	0.024
H33	0.8287	0.6779	0.6731	0.028
H34	0.8774	0.7051	0.5615	0.027
H35	0.7924	0.5836	0.4169	0.024
H37	0.9530	0.4098	0.4873	0.024
H38	1.0318	0.5158	0.6357	0.030
H39	0.9707	0.4693	0.7355	0.038
H40	0.8334	0.3141	0.6836	0.037
H44	0.5606	-0.0114	0.4490	0.028
H45	0.4344	-0.1605	0.3367	0.034
H46	0.4206	-0.1985	0.1926	0.034
H47	0.5288	-0.0849	0.1581	0.029
H49	0.9053	0.3639	-0.0286	0.047
H49'	0.8888	0.3644	-0.0348	0.047
H50	0.8126	-0.0398	0.3509	0.690
H50'	0.8144	-0.0385	0.3513	0.690

Table A4.6 Bond lengths for **4-2**.

Pd1-N2	1.9320(15)	C16-H16	0.9500
Pd1-N1	1.9782(16)	C17-C18	1.502(3)
Pd1-O2	2.0326(14)	C19-C20	1.401(3)
Pd1-O6	2.0422(13)	C19-C24	1.402(3)
Pd1-Pd2	3.2375(9)	C20-C21	1.390(3)
Pd2-N4	1.9335(15)	C20-H20	0.9500
Pd2-N3	1.9994(16)	C21-C22	1.390(4)
Pd2-O4	2.0291(15)	C21-H21	0.9500
Pd2-O8	2.0700(14)	C22-C23	1.391(3)
Pd3-N6	1.9326(16)	C22-H22	0.9500
Pd3-N5	1.9872(16)	C23-C24	1.385(3)
Pd3-O6	2.0229(14)	C23-H23	0.9500
Pd3-O4	2.0689(14)	C25-C26	1.394(3)
Pd4-N8	1.9293(16)	C25-H25	0.9500
Pd4-N7	1.9989(17)	C26-C27	1.385(4)
Pd4-O8	2.0224(15)	C26-H26	0.9500
Pd4-O2	2.0564(13)	C27-C28	1.391(4)
O1-C6	1.232(2)	C27-H27	0.9500
O2-C12	1.371(2)	C28-C29	1.383(3)
O3-C18	1.233(2)	C28-H28	0.9500
O4-C24	1.379(2)	C29-C30	1.508(3)
O5-C30	1.229(2)	C31-C32	1.399(3)
O6-C36	1.375(2)	C31-C36	1.409(2)
O7-C42	1.230(2)	C32-C33	1.392(3)
O8-C48	1.378(2)	C32-H32	0.9500
N1-C1	1.341(2)	C33-C34	1.389(3)
N1-C5	1.353(2)	C33-H33	0.9500
N2-C6	1.351(2)	C34-C35	1.396(3)
N2-C7	1.403(2)	C34-H34	0.9500
N3-C13	1.334(3)	C35-C36	1.390(3)
N3-C17	1.354(2)	C35-H35	0.9500
N4-C18	1.345(2)	C37-C38	1.394(3)
N4-C19	1.404(2)	C37-H37	0.9500
N5-C25	1.335(3)	C38-C39	1.383(3)

N5-C29	1.358(3)	C38-H38	0.9500
N6-C30	1.351(2)	C39-C40	1.399(4)
N6-C31	1.398(2)	C39-H39	0.9500
N7-C37	1.333(3)	C40-C41	1.382(3)
N7-C41	1.357(2)	C40-H40	0.9500
N8-C42	1.349(3)	C41-C42	1.505(3)
N8-C43	1.404(3)	C43-C44	1.391(3)
C1-C2	1.388(3)	C43-C48	1.412(3)
C1-H1	0.9500	C44-C45	1.395(3)
C2-C3	1.381(4)	C44-H44	0.9500
C2-H2	0.9500	C45-C46	1.384(3)
C3-C4	1.389(3)	C45-H45	0.9500
C3-H3	0.9500	C46-C47	1.392(3)
C4-C5	1.383(3)	C46-H46	0.9500
C4-H4	0.9500	C47-C48	1.383(3)
C5-C6	1.505(3)	C47-H47	0.9500
C7-C8	1.398(2)	C49-C11	1.753(2)
C7-C12	1.418(2)	C49-C12	1.757(3)
C8-C9	1.389(3)	C49-C13	1.784(3)
C8-H8	0.9500	C49-H49	1.0000
C9-C10	1.387(3)	C49'-C13'	1.749(3)
C9-H9	0.9500	C49'-C11'	1.753(2)
C10-C11	1.394(3)	C49'-C12'	1.757(3)
C10-H10	0.9500	C49'-H49'	1.0000
C11-C12	1.388(3)	C50-C16	1.716(5)
C11-H11	0.9500	C50-C15	1.728(5)
C13-C14	1.394(3)	C50-C14	1.740(5)
C13-H13	0.9500	C50-H50	1.0000
C14-C15	1.381(3)	C50'-C14'	1.760(5)
C14-H14	0.9500	C50'-C16'	1.763(5)
C15-C16	1.386(3)	C50'-C15'	1.770(5)
C15-H15	0.9500	C50'-H50'	1.0000
C16-C17	1.375(3)		

Table A4.7 Bond angles for **4-2**.

N2-Pd1-N1	82.84(6)	C16-C17-C18	122.11(16)
N2-Pd1-O2	83.71(6)	O3-C18-N4	127.88(18)
N1-Pd1-O2	166.44(6)	O3-C18-C17	121.52(16)
N2-Pd1-O6	178.12(6)	N4-C18-C17	110.55(15)
N1-Pd1-O6	95.29(6)	C20-C19-C24	120.01(17)
O2-Pd1-O6	98.15(6)	C20-C19-N4	125.91(17)
N2-Pd1-Pd2	90.48(5)	C24-C19-N4	114.02(16)
N1-Pd1-Pd2	104.99(5)	C21-C20-C19	119.30(19)
O2-Pd1-Pd2	76.86(5)	C21-C20-H20	120.3
O6-Pd1-Pd2	90.18(4)	C19-C20-H20	120.3
N4-Pd2-N3	81.92(7)	C22-C21-C20	120.4(2)
N4-Pd2-O4	83.60(6)	C22-C21-H21	119.8
N3-Pd2-O4	165.15(6)	C20-C21-H21	119.8
N4-Pd2-O8	175.66(6)	C21-C22-C23	120.4(2)
N3-Pd2-O8	97.50(6)	C21-C22-H22	119.8
O4-Pd2-O8	97.19(6)	C23-C22-H22	119.8
N4-Pd2-Pd1	82.95(5)	C24-C23-C22	119.8(2)
N3-Pd2-Pd1	99.80(5)	C24-C23-H23	120.1
O4-Pd2-Pd1	81.60(5)	C22-C23-H23	120.1
O8-Pd2-Pd1	92.93(4)	O4-C24-C23	120.97(17)
N6-Pd3-N5	82.66(7)	O4-C24-C19	118.94(16)
N6-Pd3-O6	83.62(6)	C23-C24-C19	120.04(18)
N5-Pd3-O6	166.21(6)	N5-C25-C26	121.2(2)
N6-Pd3-O4	179.32(6)	N5-C25-H25	119.4
N5-Pd3-O4	96.67(7)	C26-C25-H25	119.4
O6-Pd3-O4	97.05(6)	C27-C26-C25	118.8(2)
N8-Pd4-N7	82.26(7)	C27-C26-H26	120.6
N8-Pd4-O8	84.73(7)	C25-C26-H26	120.6
N7-Pd4-O8	166.98(6)	C26-C27-C28	119.76(19)
N8-Pd4-O2	176.24(6)	C26-C27-H27	120.1
N7-Pd4-O2	97.58(6)	C28-C27-H27	120.1
O8-Pd4-O2	95.44(6)	C29-C28-C27	118.8(2)
C12-O2-Pd1	109.30(10)	C29-C28-H28	120.6

C12-O2-Pd4	122.99(11)	C27-C28-H28	120.6
Pd1-O2-Pd4	114.53(6)	N5-C29-C28	121.05(19)
C24-O4-Pd2	109.33(11)	N5-C29-C30	116.62(15)
C24-O4-Pd3	116.18(12)	C28-C29-C30	122.33(18)
Pd2-O4-Pd3	118.49(7)	O5-C30-N6	127.9(2)
C36-O6-Pd3	109.86(10)	O5-C30-C29	121.71(17)
C36-O6-Pd1	118.69(11)	N6-C30-C29	110.42(16)
Pd3-O6-Pd1	123.14(7)	N6-C31-C32	126.17(16)
C48-O8-Pd4	108.39(11)	N6-C31-C36	114.48(15)
C48-O8-Pd2	116.77(12)	C32-C31-C36	119.34(17)
Pd4-O8-Pd2	115.52(7)	C33-C32-C31	119.87(18)
C1-N1-C5	121.05(16)	C33-C32-H32	120.1
C1-N1-Pd1	126.38(13)	C31-C32-H32	120.1
C5-N1-Pd1	112.58(12)	C34-C33-C32	120.58(19)
C6-N2-C7	129.07(15)	C34-C33-H33	119.7
C6-N2-Pd1	117.30(12)	C32-C33-H33	119.7
C7-N2-Pd1	113.63(11)	C33-C34-C35	120.03(19)
C13-N3-C17	119.83(17)	C33-C34-H34	120.0
C13-N3-Pd2	128.12(14)	C35-C34-H34	120.0
C17-N3-Pd2	112.00(12)	C36-C35-C34	119.82(18)
C18-N4-C19	127.82(15)	C36-C35-H35	120.1
C18-N4-Pd2	117.02(12)	C34-C35-H35	120.1
C19-N4-Pd2	114.09(11)	O6-C36-C35	121.47(16)
C25-N5-C29	120.42(17)	O6-C36-C31	118.18(16)
C25-N5-Pd3	127.32(14)	C35-C36-C31	120.34(17)
C29-N5-Pd3	112.26(13)	N7-C37-C38	121.61(18)
C30-N6-C31	128.04(16)	N7-C37-H37	119.2
C30-N6-Pd3	117.98(14)	C38-C37-H37	119.2
C31-N6-Pd3	113.85(11)	C39-C38-C37	119.1(2)
C37-N7-C41	119.93(17)	C39-C38-H38	120.5
C37-N7-Pd4	127.67(13)	C37-C38-H38	120.5
C41-N7-Pd4	112.36(13)	C38-C39-C40	119.1(2)
C42-N8-C43	128.31(16)	C38-C39-H39	120.4
C42-N8-Pd4	118.17(14)	C40-C39-H39	120.4
C43-N8-Pd4	113.28(12)	C41-C40-C39	118.9(2)

N1-C1-C2	120.10(19)	C41-C40-H40	120.5
N1-C1-H1	120.0	C39-C40-H40	120.5
C2-C1-H1	120.0	N7-C41-C40	121.3(2)
C3-C2-C1	119.9(2)	N7-C41-C42	116.25(17)
C3-C2-H2	120.0	C40-C41-C42	122.41(18)
C1-C2-H2	120.0	O7-C42-N8	127.9(2)
C2-C3-C4	119.16(19)	O7-C42-C41	121.24(19)
C2-C3-H3	120.4	N8-C42-C41	110.81(16)
C4-C3-H3	120.4	C44-C43-N8	126.44(18)
C5-C4-C3	119.1(2)	C44-C43-C48	119.53(18)
C5-C4-H4	120.5	N8-C43-C48	114.03(16)
C3-C4-H4	120.5	C43-C44-C45	119.6(2)
N1-C5-C4	120.69(18)	C43-C44-H44	120.2
N1-C5-C6	116.30(15)	C45-C44-H44	120.2
C4-C5-C6	123.01(17)	C46-C45-C44	120.5(2)
O1-C6-N2	127.22(18)	C46-C45-H45	119.7
O1-C6-C5	121.87(17)	C44-C45-H45	119.7
N2-C6-C5	110.91(14)	C45-C46-C47	120.3(2)
C8-C7-N2	126.08(16)	C45-C46-H46	119.8
C8-C7-C12	119.54(16)	C47-C46-H46	119.8
N2-C7-C12	114.34(15)	C48-C47-C46	119.7(2)
C9-C8-C7	119.38(19)	C48-C47-H47	120.2
C9-C8-H8	120.3	C46-C47-H47	120.1
C7-C8-H8	120.3	O8-C48-C47	120.21(17)
C10-C9-C8	120.98(19)	O8-C48-C43	119.53(17)
C10-C9-H9	119.5	C47-C48-C43	120.25(17)
C8-C9-H9	119.5	C11-C49-C12	109.86(14)
C9-C10-C11	120.27(19)	C11-C49-C13	103.62(17)
C9-C10-H10	119.9	C12-C49-C13	124.6(3)
C11-C10-H10	119.9	C11-C49-H49	105.8
C12-C11-C10	119.63(19)	C12-C49-H49	105.8
C12-C11-H11	120.2	C13-C49-H49	105.8
C10-C11-H11	120.2	C13'-C49'-C11'	115.57(17)
O2-C12-C11	121.84(16)	C13'-C49'-C12'	95.4(3)
O2-C12-C7	118.06(15)	C11'-C49'-C12'	109.86(14)

C11-C12-C7	120.09(16)	Cl3'-C49'-H49'	111.7
N3-C13-C14	121.37(19)	Cl1'-C49'-H49'	111.7
N3-C13-H13	119.3	Cl2'-C49'-H49'	111.7
C14-C13-H13	119.3	Cl6-C50-Cl5	117.3(9)
C15-C14-C13	118.6(2)	Cl6-C50-Cl4	97.2(5)
C15-C14-H14	120.7	Cl5-C50-Cl4	94.2(7)
C13-C14-H14	120.7	Cl6-C50-H50	114.9
C14-C15-C16	119.9(2)	Cl5-C50-H50	114.9
C14-C15-H15	120.0	Cl4-C50-H50	114.9
C16-C15-H15	120.0	Cl4'-C50'-Cl6'	94.8(5)
C17-C16-C15	118.61(19)	Cl4'-C50'-Cl5'	97.3(4)
C17-C16-H16	120.7	Cl6'-C50'-Cl5'	98.0(6)
C15-C16-H16	120.7	Cl4'-C50'-H50'	120.4
N3-C17-C16	121.62(17)	Cl6'-C50'-H50'	120.4
N3-C17-C18	116.19(15)	Cl5'-C50'-H50'	120.4

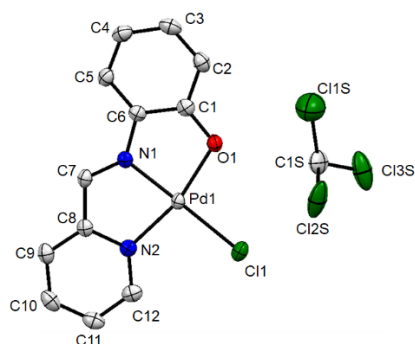


Figure A4.13 Displacement ellipsoid plot of **4-3** co-crystallized with a chloroform molecule showing naming and numbering scheme. Ellipsoids are drawn at the 50% probability level and hydrogen atoms are omitted for clarity.

Table A4.8 Atomic coordinates for **4-3**.

Atom	x	y	z	$U_{\text{iso/equiv}}$
Pd1	0.43430(2)	0.71415(3)	0.48073(2)	0.01920(11)
Cl1	0.41633(6)	0.60984(10)	0.35310(4)	0.02974(18)
O1	0.28175(16)	0.7034(3)	0.50753(12)	0.0252(5)
N1	0.44879(18)	0.8213(3)	0.58585(14)	0.0202(5)

N2	0.59047(19)	0.7485(3)	0.48184(14)	0.0215(5)
C1	0.2676(2)	0.7764(4)	0.57878(18)	0.0237(6)
C2	0.1671(2)	0.7922(4)	0.6122(2)	0.0297(7)
C3	0.1549(2)	0.8774(4)	0.68447(19)	0.0325(7)
C4	0.2397(2)	0.9491(4)	0.72693(18)	0.0303(7)
C5	0.3389(2)	0.9298(4)	0.69705(16)	0.0259(6)
C6	0.3526(2)	0.8433(4)	0.62434(17)	0.0224(6)
C7	0.5418(2)	0.8695(4)	0.60706(16)	0.0231(6)
C8	0.6241(2)	0.8282(4)	0.55143(16)	0.0222(6)
C9	0.7282(2)	0.8629(4)	0.56477(18)	0.0281(6)
C10	0.8001(2)	0.8139(4)	0.5073(2)	0.0322(7)
C11	0.7659(2)	0.7340(4)	0.4386(2)	0.0302(7)
C12	0.6603(2)	0.7034(4)	0.42715(18)	0.0264(7)
C1S	0.1348(3)	0.6276(6)	0.3585(2)	0.0450(9)
Cl1S	0.8406(5)	1.1934(11)	0.7171(4)	0.071(2)
Cl2S	0.0403(3)	0.7661(7)	0.4156(2)	0.0906(11)
Cl3S	0.6028(6)	1.0675(11)	0.8223(4)	0.0714(19)
C2S	0.1348(3)	0.6276(6)	0.3585(2)	0.0450(9)
Cl4S	0.8830(3)	1.1831(7)	0.7001(3)	0.0644(12)
Cl5S	0.03395(10)	0.6061(3)	0.42921(10)	0.0501(4)
Cl6S	0.6277(4)	1.0854(7)	0.7982(2)	0.0452(8)
H2	0.1081	0.7441	0.5850	0.036
H3	0.0869	0.8878	0.7061	0.039
H4	0.2290	1.0106	0.7759	0.036
H5	0.3973	0.9750	0.7258	0.031
H7A	0.5555	0.9284	0.6562	0.028
H9	0.7506	0.9196	0.6125	0.034
H10	0.8724	0.8356	0.5155	0.039
H11	0.8144	0.6997	0.3990	0.036
H12	0.6372	0.6488	0.3792	0.032
H1S	0.1995	0.6106	0.3907	0.054
H2S	0.2041	0.6353	0.3854	0.054

Table A4.9 Bond lengths for **4-3**.

Pd1-N1	1.951(2)	C8-C9	1.376(4)
Pd1-O1	2.011(2)	C9-C10	1.390(5)
Pd1-N2	2.017(3)	C9-H9	0.9500
Pd1-Cl1	2.3034(10)	C10-C11	1.369(5)
O1-C1	1.330(4)	C10-H10	0.9500
N1-C7	1.292(4)	C11-C12	1.384(5)
N1-C6	1.406(4)	C11-H11	0.9500
N2-C12	1.332(4)	C12-H12	0.9500
N2-C8	1.379(4)	ClS-Cl3S	1.570(8)
C1-C2	1.414(4)	ClS-Cl1S	1.835(8)
C1-C6	1.418(4)	ClS-Cl2S	1.839(5)
C2-C3	1.378(5)	ClS-H1S	1.0000
C2-H2	0.9500	Cl1S-C1S	1.835(8)
C3-C4	1.400(5)	Cl3S-C1S	1.570(8)
C3-H3	0.9500	C2S-Cl4S	1.688(6)
C4-C5	1.377(4)	C2S-Cl5S	1.774(4)
C4-H4	0.9500	C2S-Cl6S	1.829(6)
C5-C6	1.392(4)	C2S-H2S	1.0000
C5-H5	0.9500	Cl4S-C2S	1.688(6)
C7-C8	1.448(4)	Cl6S-C2S	1.830(6)
C7-H7A	0.9500		

Table A4.10 Bond angles for **4-3**.

N1-Pd1-O1	84.14(9)	N1-C7-C8	116.0(3)
N1-Pd1-N2	81.48(10)	N1-C7-H7A	122.0
O1-Pd1-N2	165.60(9)	C8-C7-H7A	122.0
N1-Pd1-Cl1	175.80(7)	C9-C8-N2	121.1(3)
O1-Pd1-Cl1	96.08(6)	C9-C8-C7	124.3(3)
N2-Pd1-Cl1	98.33(7)	N2-C8-C7	114.6(2)
C1-O1-Pd1	109.02(18)	C8-C9-C10	119.0(3)
C7-N1-C6	130.6(3)	C8-C9-H9	120.5
C7-N1-Pd1	116.4(2)	C10-C9-H9	120.5

C6-N1-Pd1	112.82(18)	C11-C10-C9	119.4(3)
C12-N2-C8	119.2(3)	C11-C10-H10	120.3
C12-N2-Pd1	129.3(2)	C9-C10-H10	120.3
C8-N2-Pd1	111.47(18)	C10-C11-C12	119.8(3)
O1-C1-C2	121.5(3)	C10-C11-H11	120.1
O1-C1-C6	121.5(3)	C12-C11-H11	120.1
C2-C1-C6	117.0(3)	N2-C12-C11	121.5(3)
C3-C2-C1	119.9(3)	N2-C12-H12	119.2
C3-C2-H2	120.1	C11-C12-H12	119.2
C1-C2-H2	120.1	Cl3S-C1S-Cl1S	112.5(4)
C2-C3-C4	122.0(3)	Cl3S-C1S-Cl2S	120.5(4)
C2-C3-H3	119.0	Cl1S-C1S-Cl2S	96.5(3)
C4-C3-H3	119.0	Cl3S-C1S-H1S	108.8
C5-C4-C3	119.3(3)	Cl1S-C1S-H1S	108.8
C5-C4-H4	120.3	Cl2S-C1S-H1S	108.8
C3-C4-H4	120.3	Cl4S-C2S-Cl5S	111.7(3)
C4-C5-C6	119.4(3)	Cl4S-C2S-Cl6S	108.8(3)
C4-C5-H5	120.3	Cl5S-C2S-Cl6S	105.8(3)
C6-C5-H5	120.3	Cl4S-C2S-H2S	110.1
C5-C6-N1	125.1(3)	Cl5S-C2S-H2S	110.1
C5-C6-C1	122.3(3)	Cl6S-C2S-H2S	110.1
N1-C6-C1	112.5(2)		

Appendix D. Supplementary Information for Chapter 5

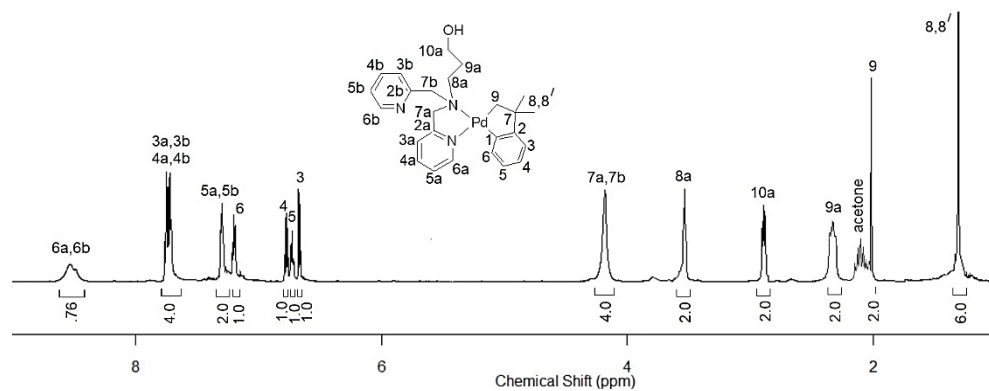


Figure A5.1 ¹H NMR Spectrum of [Pd(CH₂CMe₂C₆H₄)(κ²-5-L1)], **5-1**, in (CD₃)₂CO at 25°C, 600 MHz.

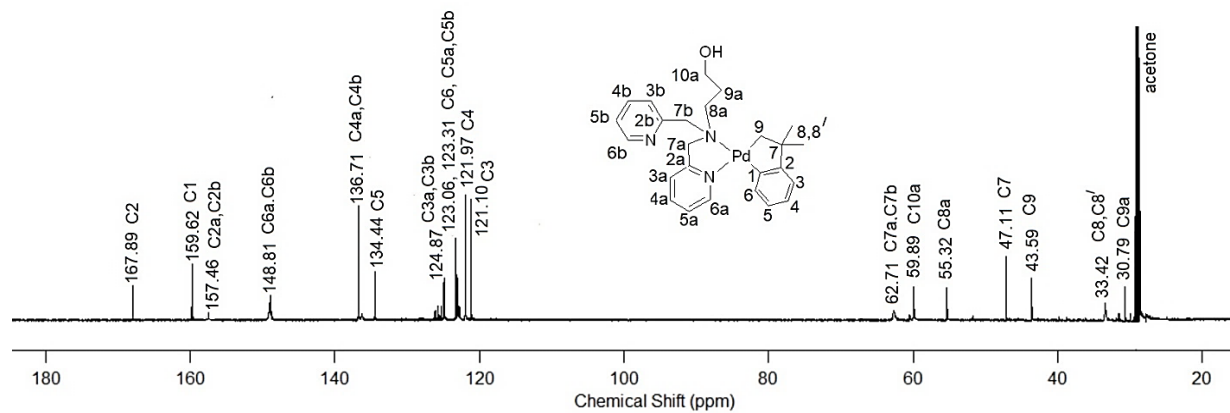


Figure A5.2 ¹³C{¹H} NMR Spectrum of [Pd(CH₂CMe₂C₆H₄)(κ²-5-L1)], **5-1**, in (CD₃)₂CO at 25°C, 151 MHz.

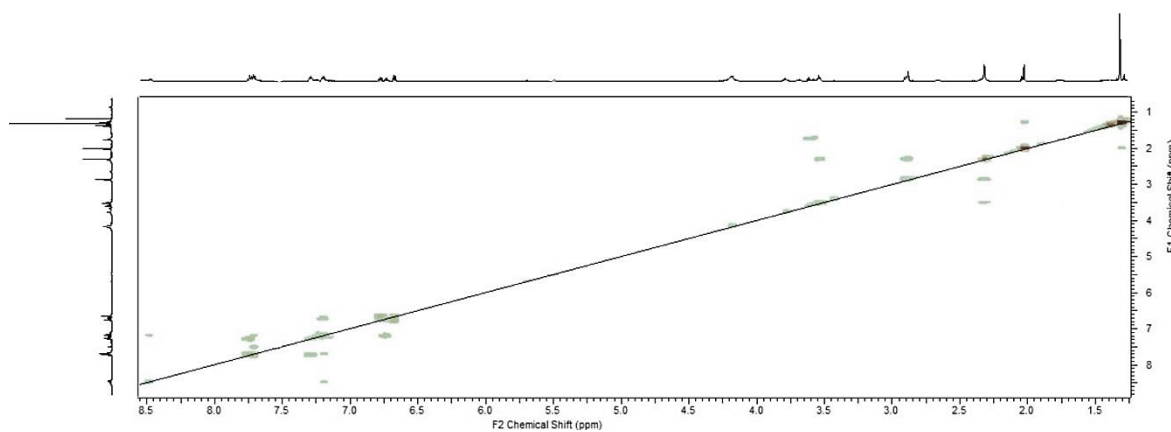


Figure A5.3 ^1H - ^1H gCOSY Spectrum of $[\text{Pd}(\text{CH}_2\text{CMe}_2\text{C}_6\text{H}_4)(\kappa^2\text{-5-L1})]$, **5-1**, in $(\text{CD}_3)_2\text{CO}$ at 25°C .

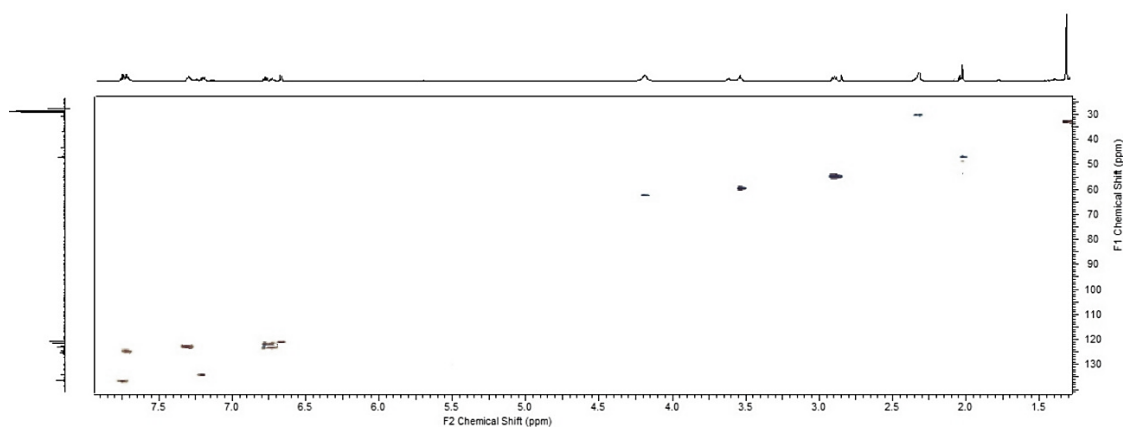


Figure A5.4 ^1H - $^{13}\text{C}\{^1\text{H}\}$ HSQC Spectrum of $[\text{Pd}(\text{CH}_2\text{CMe}_2\text{C}_6\text{H}_4)(\kappa^2\text{-5-L1})]$, **5-1**, in $(\text{CD}_3)_2\text{CO}$ at 25°C .

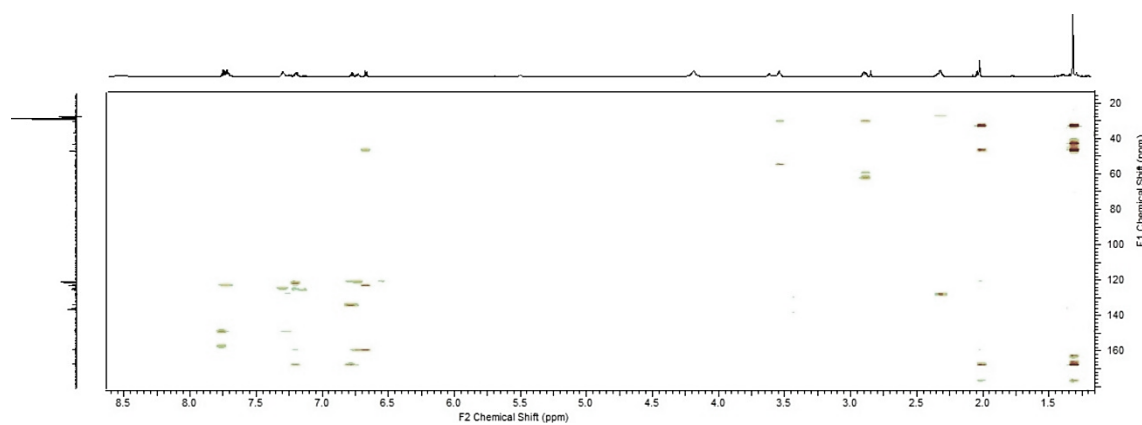


Figure A5.5 ^1H - $^{13}\text{C}\{^1\text{H}\}$ HMBC Spectrum of $[\text{Pd}(\text{CH}_2\text{CMe}_2\text{C}_6\text{H}_4)(\kappa^2\text{-5-L1})]$, **5-1**, in $(\text{CD}_3)_2\text{CO}$ at 25°C .

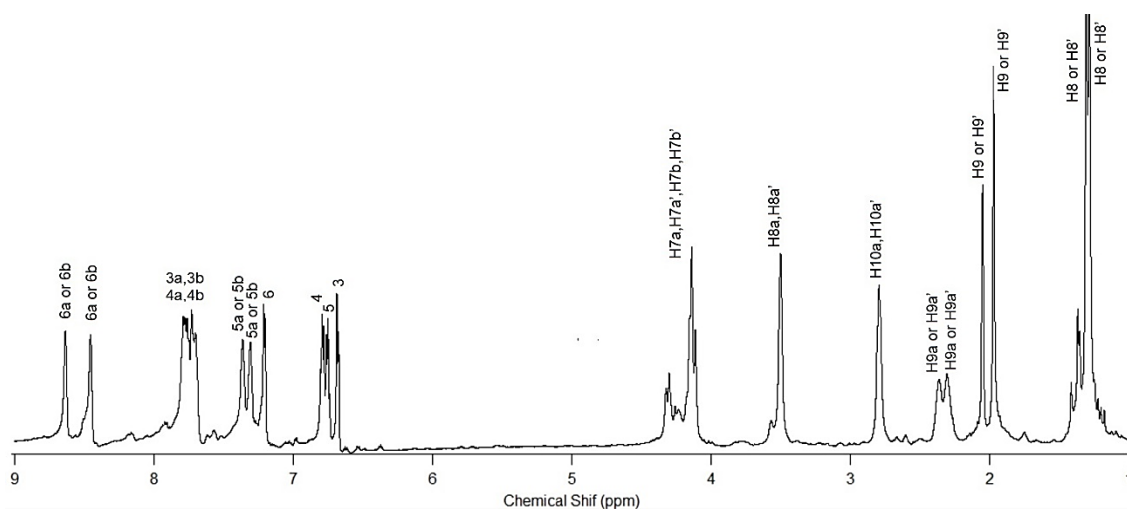


Figure A5.6 ^1H NMR Spectrum of of $[\text{Pd}(\text{CH}_2\text{CMe}_2\text{C}_6\text{H}_4)(\kappa^2\text{-5-L1})]$, **5-1**, in $(\text{CD}_3)_2\text{CO}$ at -25°C , 600 MHz.

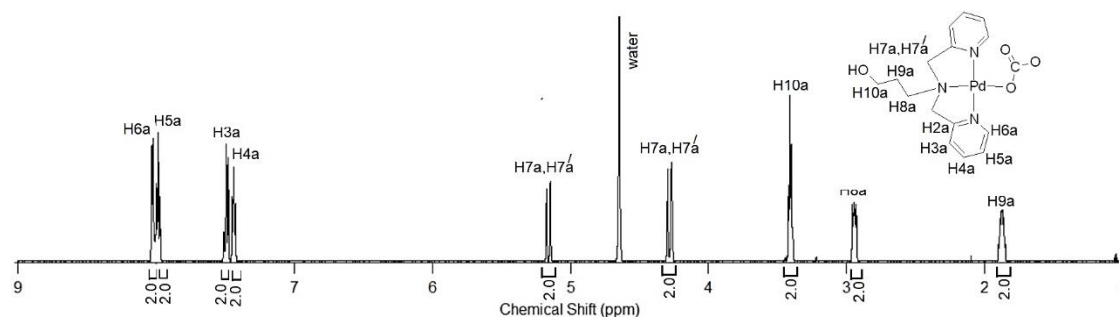


Figure A5.7 ^1H NMR Spectrum of $[\text{Pd}(\text{CO}_3)(\kappa^3\text{-5-L1})]$, **5-2**, in D_2O at 25°C , 600 MHz.

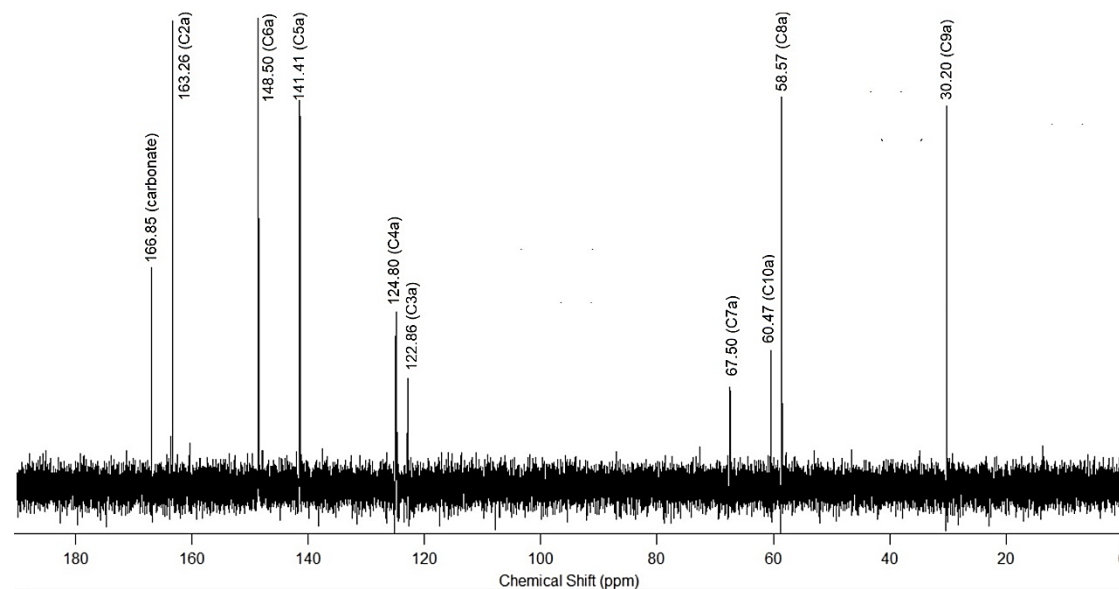


Figure A5.8 $^{13}\text{C}\{^1\text{H}\}$ NMR Spectrum of $[\text{Pd}(\text{CO}_3)(\kappa^3\text{-5-L1})]$, **5-2**, in D_2O at 25°C , 151 MHz.

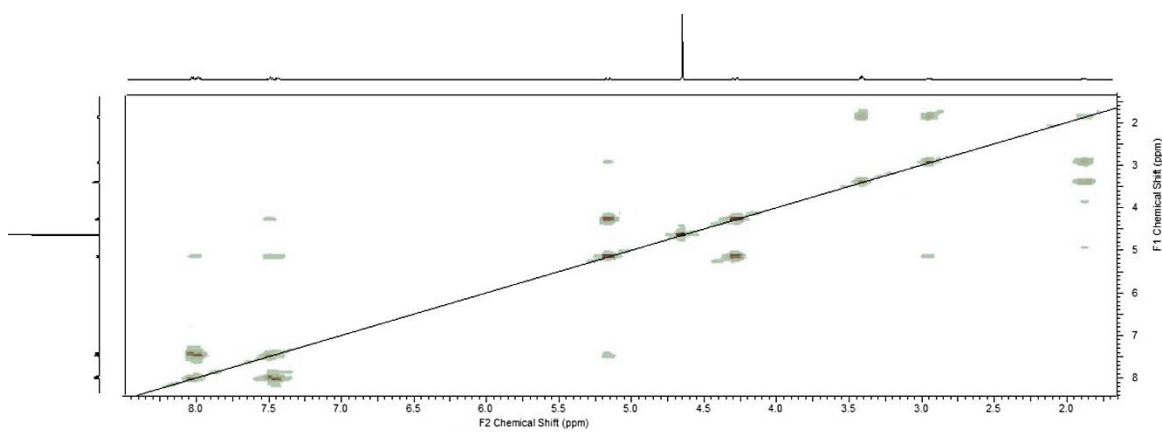


Figure A5.9 ^1H - ^1H gCOSY Spectrum of $[\text{Pd}(\text{CO}_3)(\kappa^3\text{-5-L1})]$, **5-2**, in D_2O at 25°C .

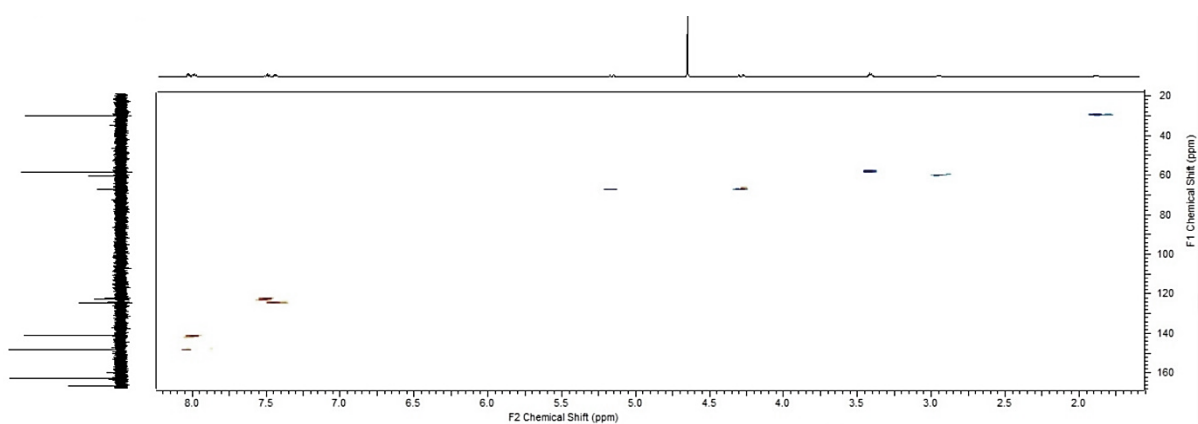


Figure A5.10 ^1H - $^{13}\text{C}\{^1\text{H}\}$ HSQC Spectrum of $[\text{Pd}(\text{CO}_3)(\kappa^3\text{-5-L1})]$, **5-2**, in D_2O at 25°C .

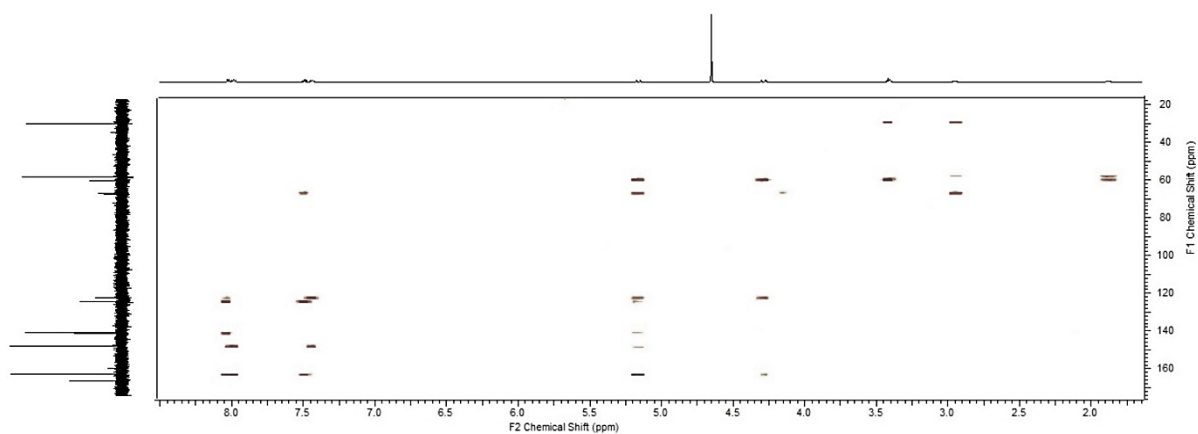


Figure A5.11 ^1H - $^{13}\text{C}\{^1\text{H}\}$ HMBC Spectrum of $[\text{Pd}(\text{CO}_3)(\kappa^3\text{-5-L1})]$, **5-2**, in D_2O at 25°C .

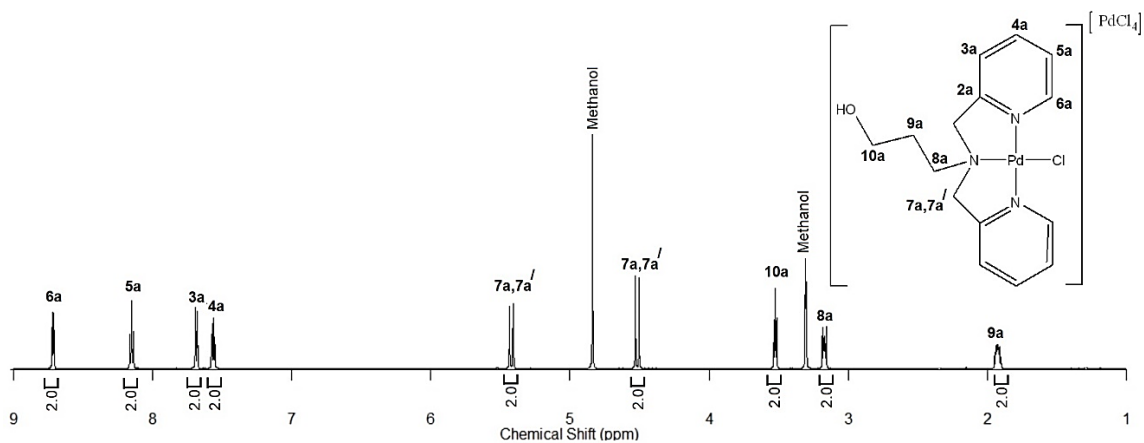


Figure A5.12 ^1H NMR Spectrum of $[\text{PdCl}(\kappa^3\text{-5-L1})]_2[\text{PdCl}_4]$, 5-3, in CD_3OD at 25°C , 600 MHz.

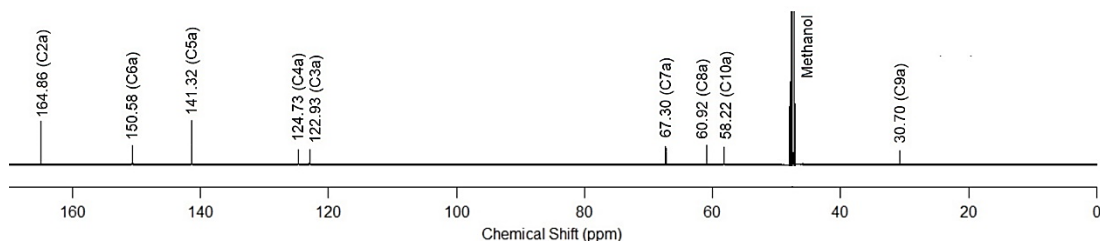


Figure A5.13 $^{13}\text{C}\{^1\text{H}\}$ NMR Spectrum of $[\text{PdCl}(\kappa^3\text{-5-L1})]_2[\text{PdCl}_4]$, 5-3, in CD_3OD at 25°C , 151 MHz.

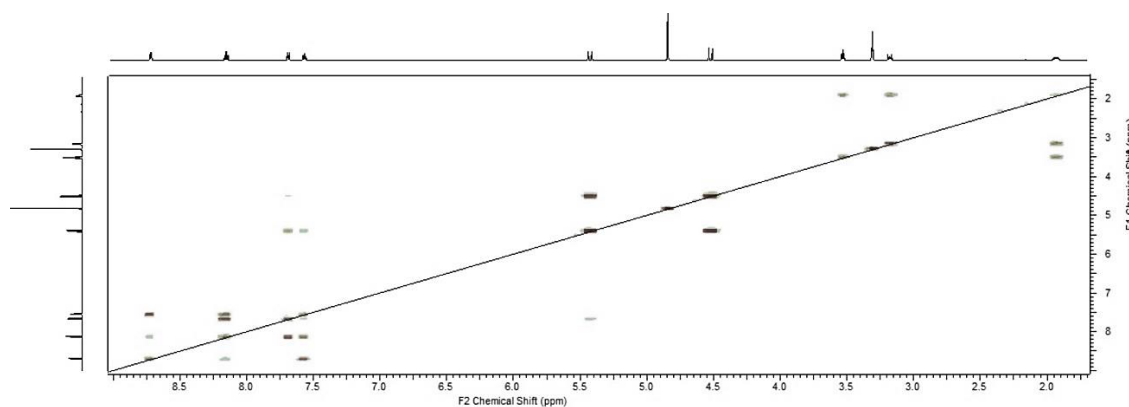


Figure A5.14 $^1\text{H}-^1\text{H}$ gCOSY Spectrum of $[\text{PdCl}(\kappa^3\text{-5-L1})]_2[\text{PdCl}_4]$, 5-3, in CD_3OD at 25°C .

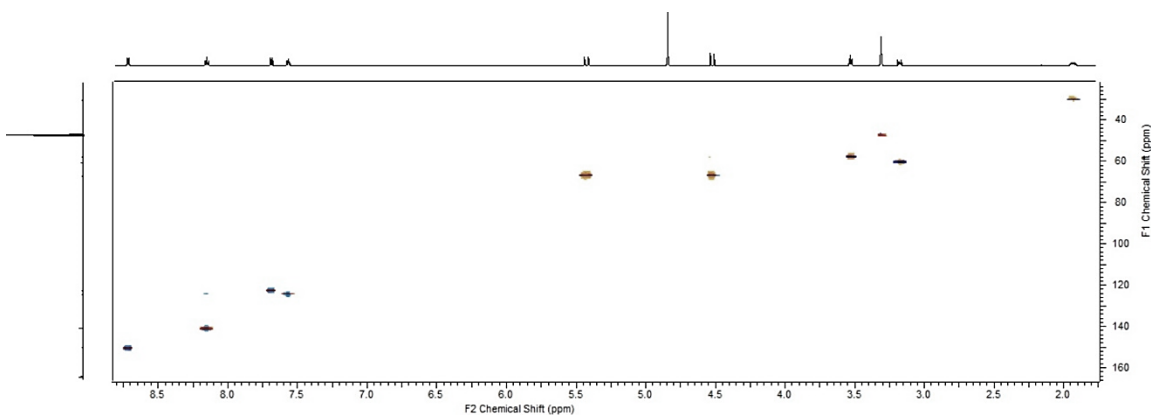


Figure A5.15 ^1H - $^{13}\text{C}\{^1\text{H}\}$ HSQC Spectrum of $[\text{PdCl}(\kappa^3\text{-5-L1})]_2[\text{PdCl}_4]$, **5-3**, in CD_3OD at 25°C .

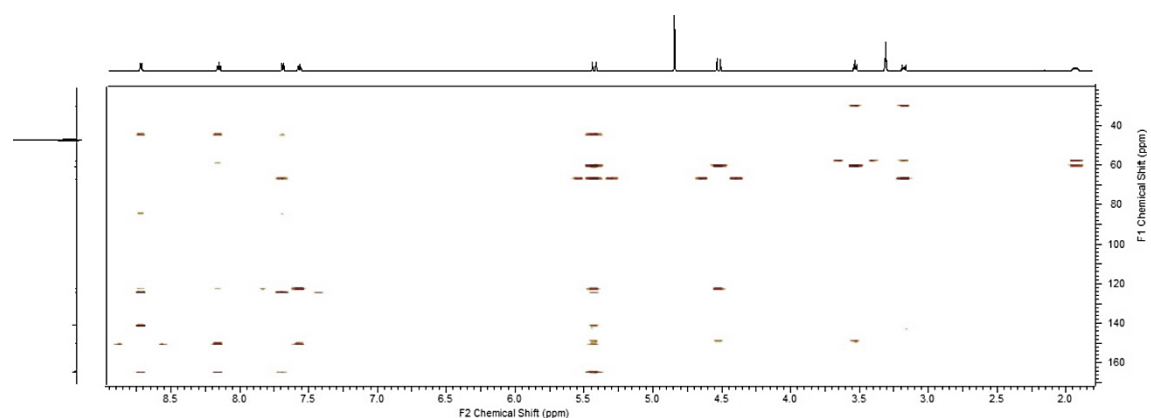


Figure A5.16 ^1H - $^{13}\text{C}\{^1\text{H}\}$ HMBC Spectrum of $[\text{PdCl}(\kappa^3\text{-5-L1})]_2[\text{PdCl}_4]$, **5-3**, in CD_3OD at 25°C .

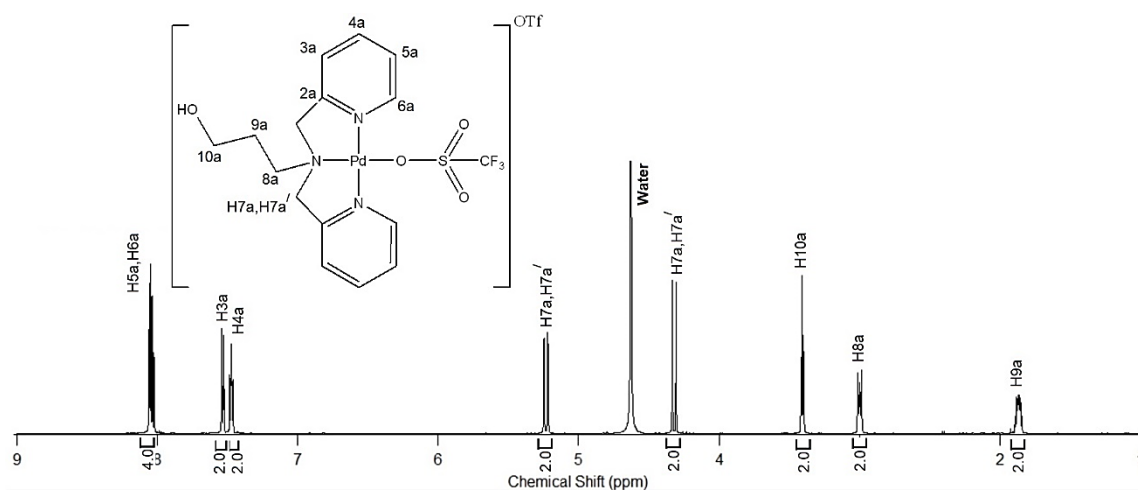


Figure A5.17 ^1H NMR Spectrum of $[\text{Pd}(\text{OTf})(\kappa^3\text{-5-L1})](\text{OTf})$, **5-4**, in D_2O at 25°C , 600 MHz.

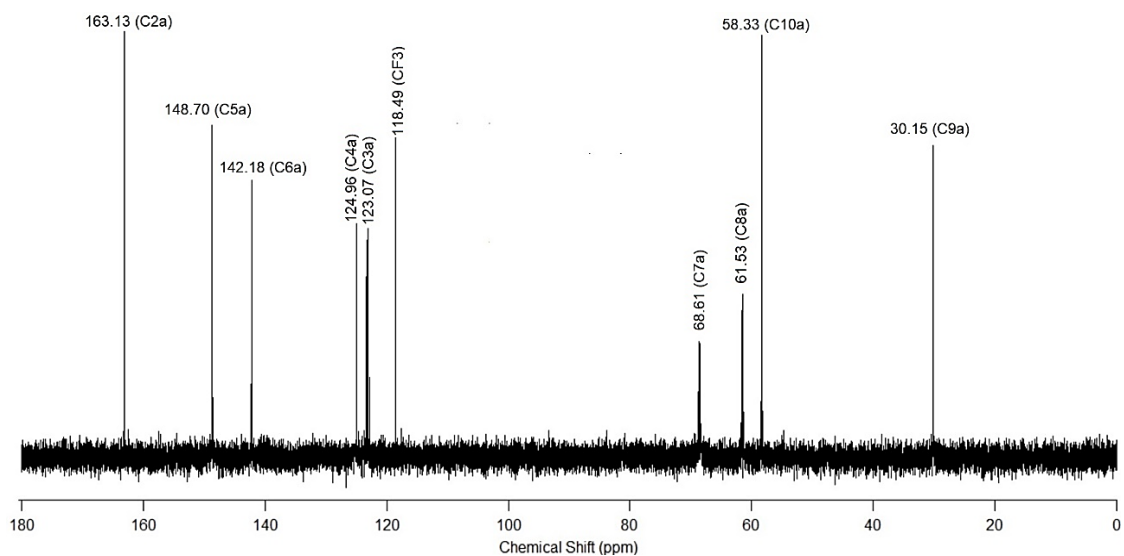


Figure A5.18 $^{13}\text{C}\{^1\text{H}\}$ NMR Spectrum of $[\text{Pd}(\text{OTf})(\kappa^3\text{-5-L1})](\text{OTf})$, **5-4**, in D_2O at 25°C , 151 MHz.

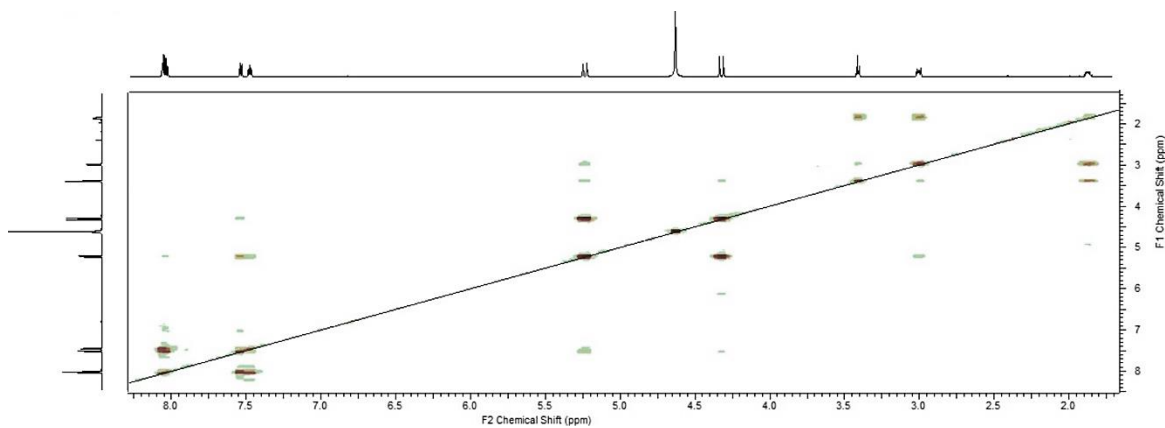


Figure A5.19 $^1\text{H}-^1\text{H}$ gCOSY Spectrum of $[\text{Pd}(\text{OTf})(\kappa^3\text{-5-L1})](\text{OTf})$, **5-4**, in D_2O at 25°C .

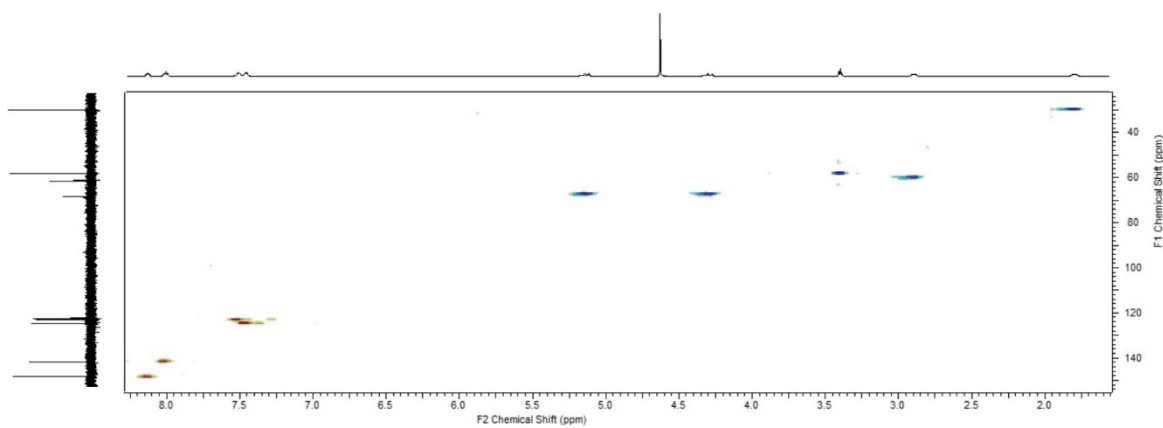


Figure A5.20 $^1\text{H}-^{13}\text{C}\{^1\text{H}\}$ HSQC Spectrum of $[\text{Pd}(\text{OTf})(\kappa^3\text{-5-L1})](\text{OTf})$, **5-4**, in D_2O at 25°C .

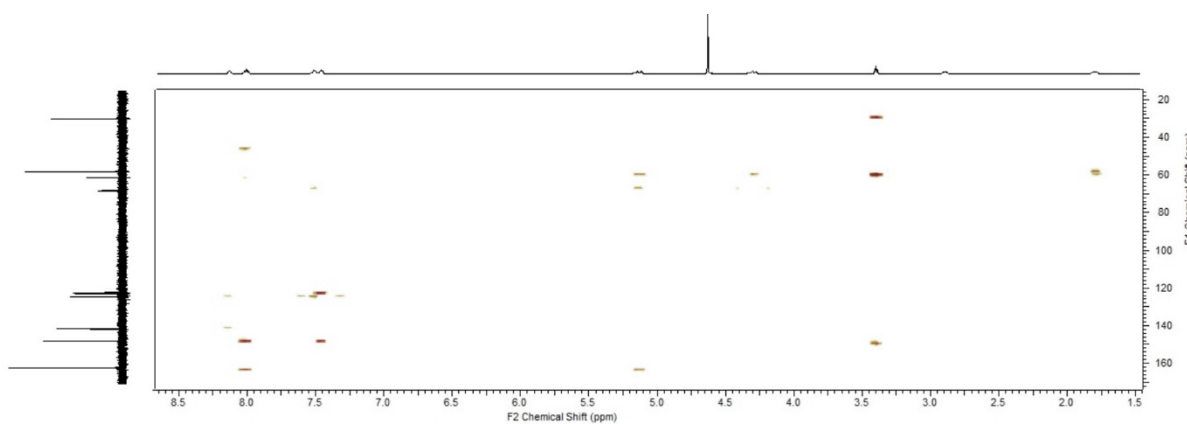


Figure A5.21 $^1\text{H}-^{13}\text{C}\{^1\text{H}\}$ HMBC Spectrum of $[\text{Pd}(\text{OTf})(\kappa^3\text{-5-L1})](\text{OTf})$, **5-4**, in D_2O at 25°C .

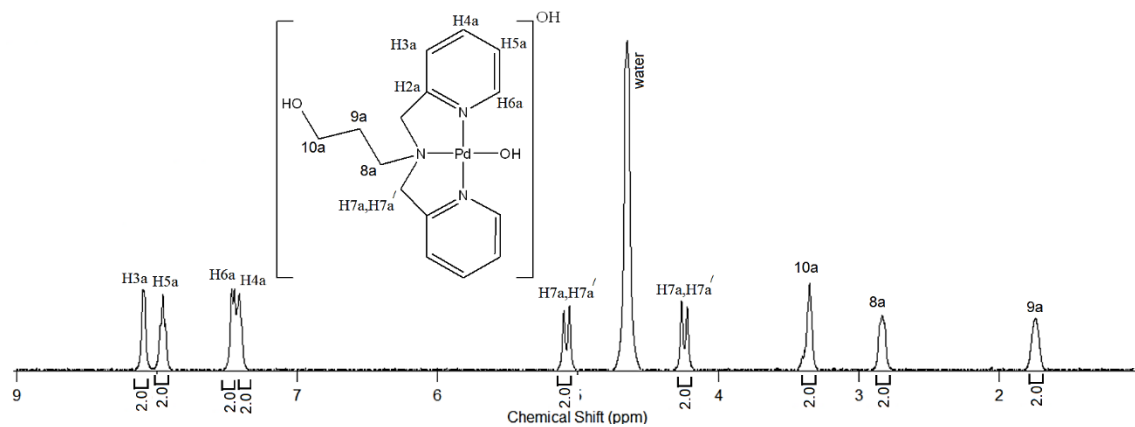


Figure A5.22 ^1H NMR Spectrum of $[\text{Pd}(\text{OH})(\kappa^3\text{-5-L1})](\text{OH})$, **5-5**, in D_2O at 25°C , at 600 MHz.

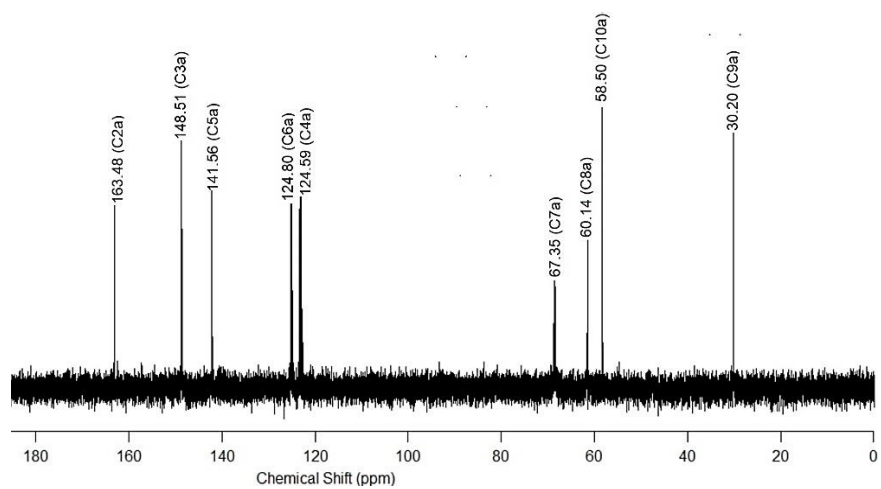


Figure A5.23 $^{13}\text{C}\{^1\text{H}\}$ NMR Spectrum of $[\text{Pd}(\text{OH})(\kappa^3\text{-5-L1})](\text{OH})$, **5-5**, in D_2O at 25°C , 151 MHz.

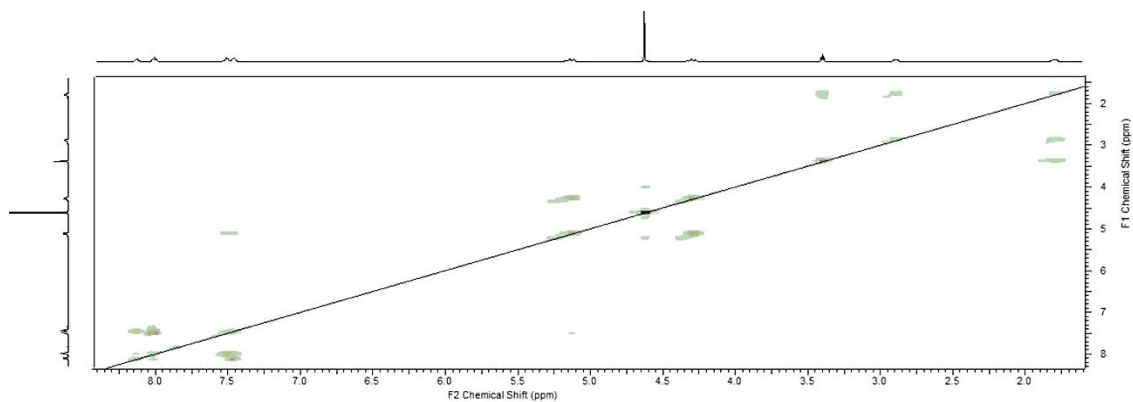


Figure A5.24 ^1H - ^1H gCOSY Spectrum of $[\text{Pd}(\text{OH})(\kappa^3\text{-5-L1})](\text{OH})$, **5-5**, in D_2O at 25°C .

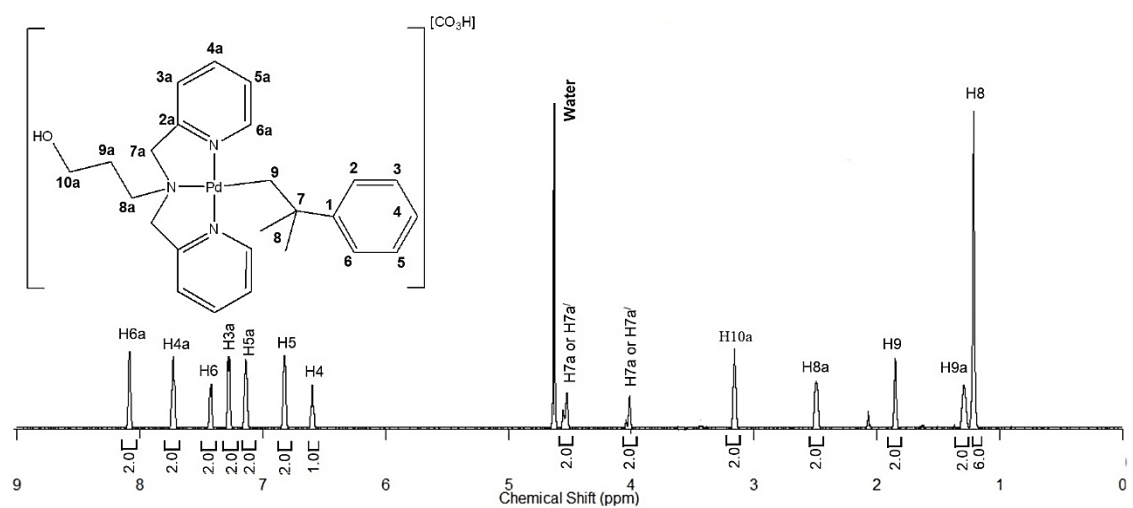


Figure A5.25 ^1H NMR Spectrum of $[\text{Pd}(\text{CH}_2\text{CMe}_2\text{Ph})(\kappa^3\text{-5-L1})](\text{HCO}_3)$, **5-6**, in D_2O at 25°C , at 600 MHz.

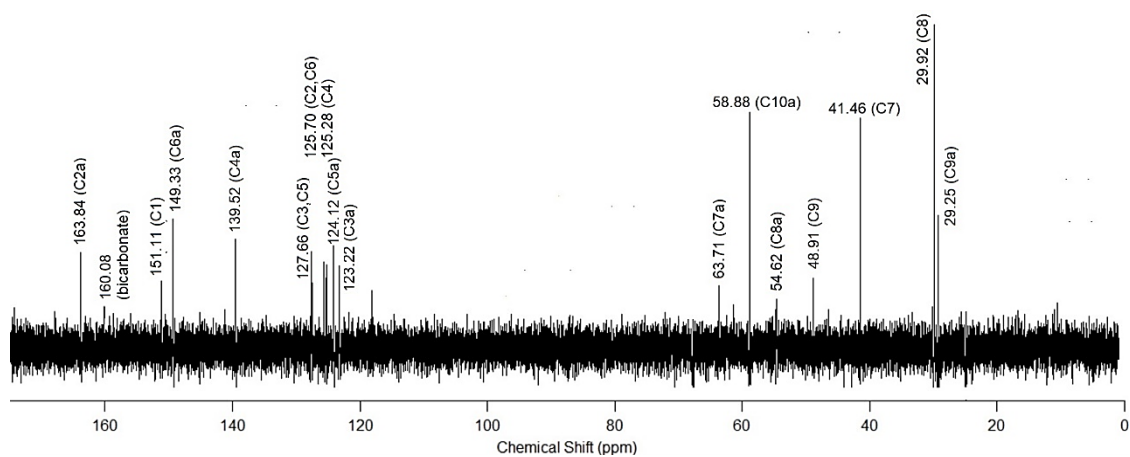


Figure A5.26 $^{13}\text{C}\{^1\text{H}\}$ NMR Spectrum of $[\text{Pd}(\text{CH}_2\text{CMe}_2\text{Ph})(\kappa^3\text{-5-L1})][\text{HCO}_3]$, **5-6**, in D_2O at 25°C , 151 MHz.

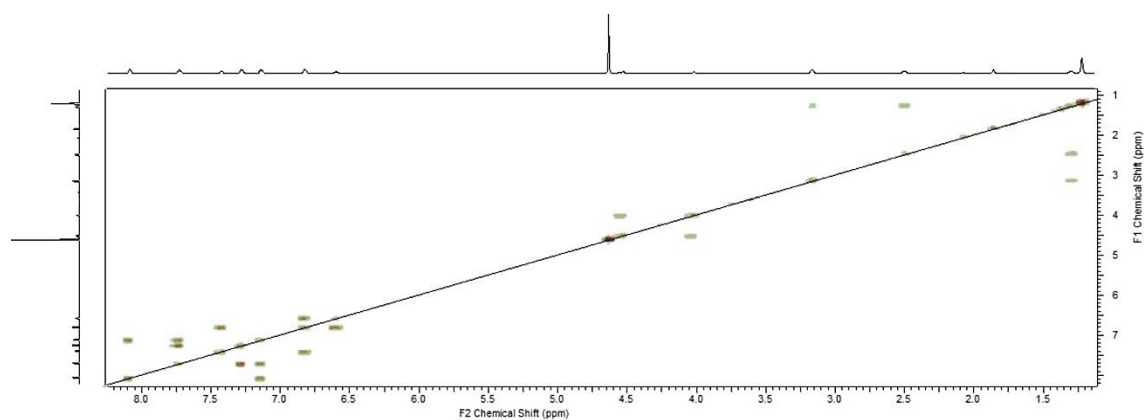


Figure A5.27 $^1\text{H}\text{-}^1\text{H}$ gCOSY Spectrum of $[\text{Pd}(\text{CH}_2\text{CMe}_2\text{Ph})(\kappa^3\text{-5-L1})][\text{HCO}_3]$, **5-6**, in D_2O at 25°C .

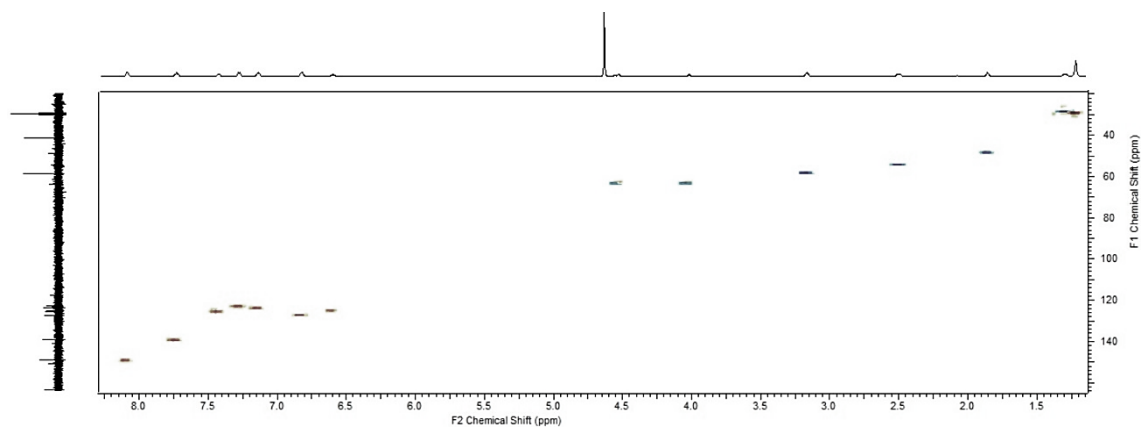


Figure A5.28 $^1\text{H}-^{13}\text{C}\{^1\text{H}\}$ HSQC Spectrum of $[\text{Pd}(\text{CH}_2\text{CMe}_2\text{Ph})(\kappa^3\text{-5-L1})][\text{HCO}_3]$, **5-6**, in D_2O at 25°C .

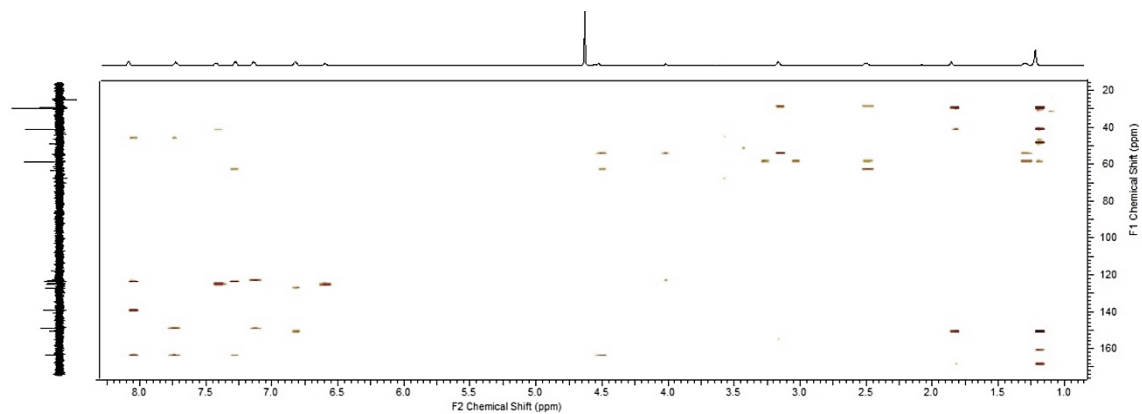


Figure A5.29 $^1\text{H}-^{13}\text{C}\{^1\text{H}\}$ HMBC Spectrum of $[\text{Pd}(\text{CH}_2\text{CMe}_2\text{Ph})(\kappa^3\text{-5-L1})][\text{HCO}_3]$, **5-6**, in D_2O at 25°C .

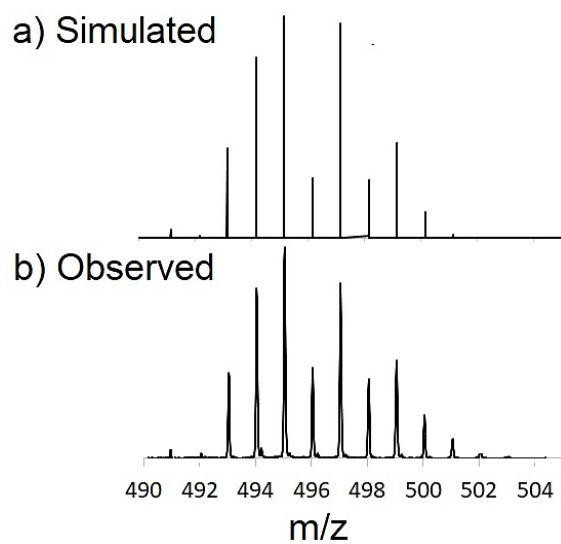


Figure A5.30 The MALDI MS isotope patterns for $[5-1]^{*+}$ obtained using pyrene matrix: (a) simulated and (b) observed.

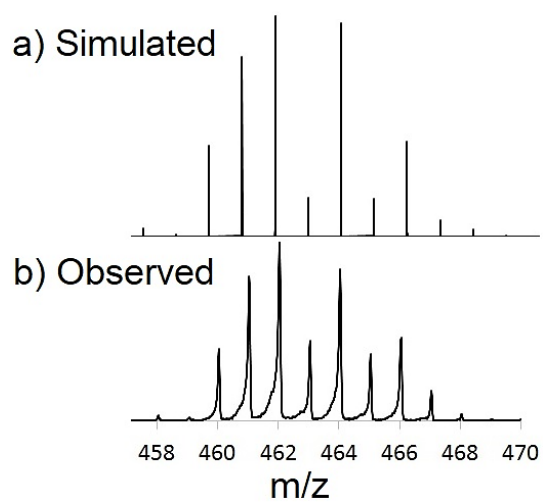


Figure A5.31 The MALDI MS isotope patterns for $[5-2+K]^{*+}$ obtained using anthracene matrix: (a) simulated and (b) observed.

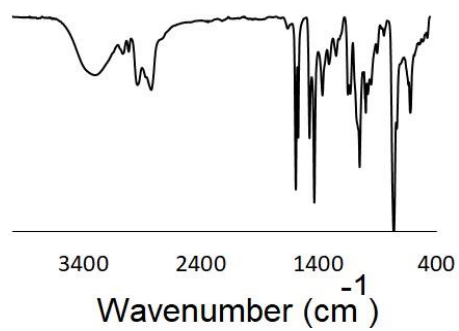


Figure A5.32 IR Spectrum of free ligand, **5-L1**.

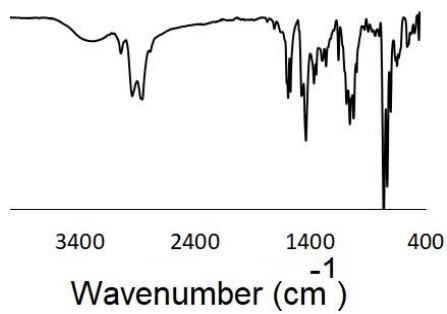


Figure A5.33 IR Spectrum of $[\text{Pd}(\text{CH}_2\text{CMe}_2\text{C}_6\text{H}_4)(\kappa^2\text{-5-L1})]$, **5-1**.

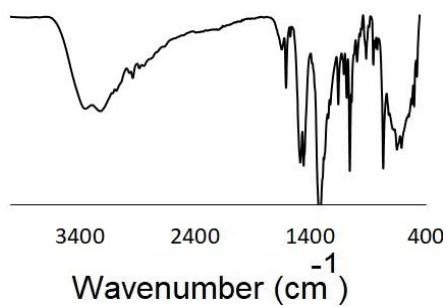


Figure A5.34 IR Spectrum of $[\text{Pd}(\text{CO}_3)(\kappa^3\text{-5-L1})]$, **5-2**.

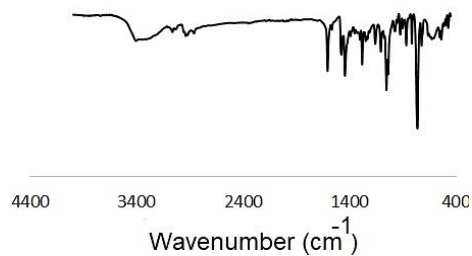


Figure A5.35 IR spectrum of $[\text{PdCl}(\kappa^3\text{-5-L1})]_2[\text{PdCl}_4]$, **5-3**.

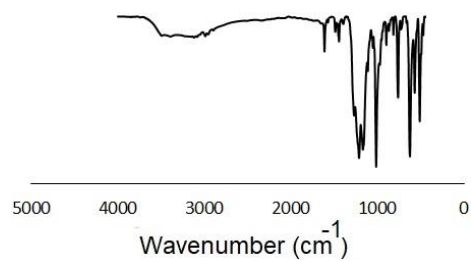


Figure A5.36 IR spectrum of $[\text{Pd}(\text{OTf})(\kappa^3\text{-5-L1})](\text{OTf})$, **5-4**.

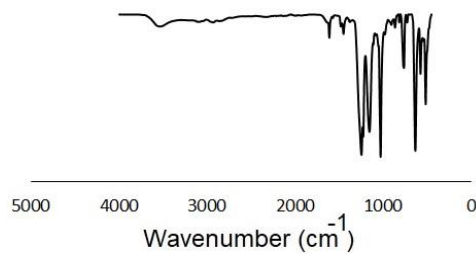


Figure A5.37 IR spectrum of $[\text{Pd}(\text{OH})(\kappa^3\text{-5-L1})](\text{OH})$, **5-5**.

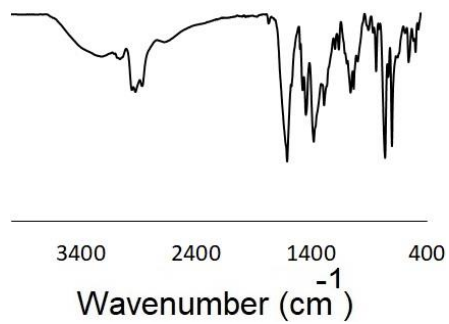


Figure A5.38 IR spectrum of $[\text{Pd}(\text{CH}_2\text{CMe}_2\text{Ph})(\kappa^3\text{-5-L1})][\text{HCO}_3]$, **5-6**.

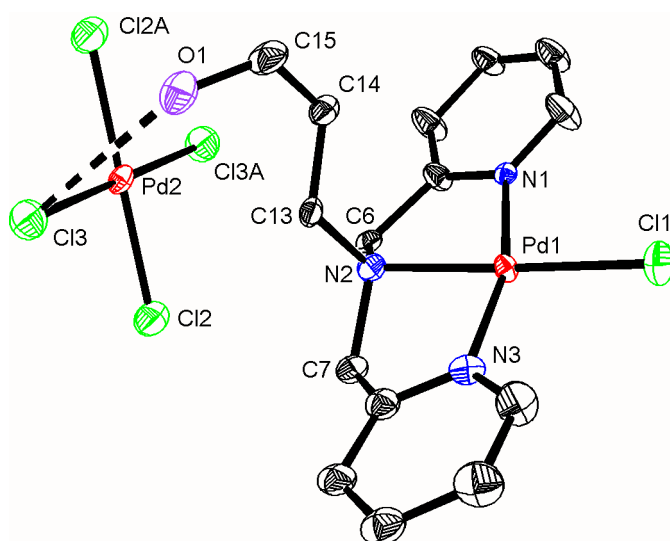


Figure A5.39 Structure of complex **5-3a**, showing the atom connectivity. The cif file has been deposited as CCDC 1570681.

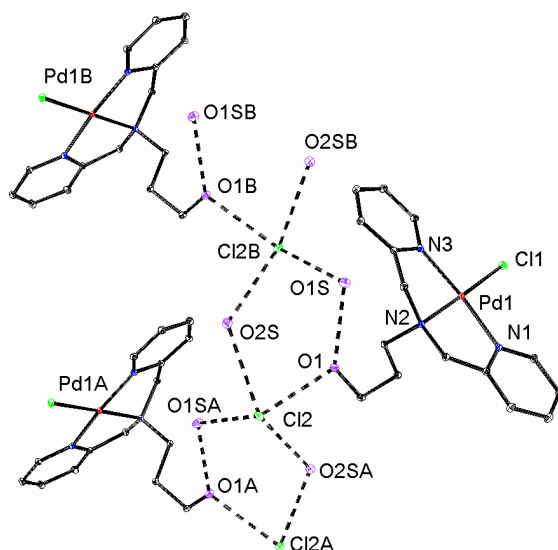


Figure A5.40 Part of the supramolecular polymeric structure of complex **5-3b** formed by hydrogen bonding. Selected distances (Å): O(1)..O(1S) 2.81; O(1)..Cl(2) 3.10; Cl(2)..O(1SA) 3.19; Cl(2)..O(2S) 3.26; Cl(2)..O(2SA) 3.25. Symmetry equivalent atoms: A, $3/2 - x, 1/2 + y, 3/2 - z$; B, $3/2 - x, -1/2 + y, 3/2 - z$.

Table A5.1 Crystallographic data and parameters for compounds **5-2**, **5-3a** and **5-3b**

	5-2a	5-2b	5-3b
Formula	C ₁₆ H ₁₈ N ₃ O ₂ Pd.6H ₂ O	C ₁₆ H ₁₈ N ₃ O ₂ Pd.5H ₂ O.MeOH	C ₁₅ H ₁₈ Cl ₂ N ₃ OPd ·2H ₂ O
Formula weight	513.82	527.85	451.65
Crystal system	triclinic	orthorhombic	monoclinic
Space group	P -1	P bca	P ₂ ₁ /n
<i>a</i> [Å]	9.699(7)	13.717(5)	12.494(3)
<i>b</i> [Å]	10.044(8)	14.238(7)	10.586(3)
<i>c</i> [Å]	11.540(9)	21.945(7)	15.101(5)
α [°]	80.300(13)	90	90
β [°]	85.154(12)	90	112.943(14)
γ [°]	66.605(13)	90	90
<i>V</i> [Å ³]	1016.9(13)	4286(3)	1839.28(9)

Z	2	8	4
ρ_{cal} [g cm ⁻³]	1.678	1.636	1.700
λ , Å, (MoK α)	0.71073	1.54178	0.71073
$F(000)$	528	2176	952
Temperature [K]	110	273	110
$\theta_{\text{min}}, \theta_{\text{max}}$ [°]	5.0, 44.48	12.44, 128.58	5.22, 84.56
Total reflns	21518	2414	96125
Unique reflns	3357	3675	13048
R_1	0.0776	0.0322	0.0236
wR_2 [$I \geq 2\sigma(I)$]	0.1776	0.0900	0.0609
R_1 (all data)	0.1168	0.0388	0.0302
wR_2 (all data)	0.1973	0.0968	0.0642
GOF	1.061	0.959	1.080
Maximum shift/error	0.000	0.005	0.005
Min & Max peak heights on final ΔF Map (e ⁻ /Å)	-0.914, 2.529	-0.692, 1.257	-0.827, 1.128

Where: $R_1 = \Sigma(|F_o| - |F_c|) / \Sigma F_o$; $wR_2 = [\Sigma(w(F_o^2 - F_c^2)^2) / \Sigma(wF_o^4)]^{1/2}$; $GOF = [\Sigma(w(F_o^2 - F_c^2)^2) / (\text{No. of reflns.} - \text{No. of params.})]^{1/2}$

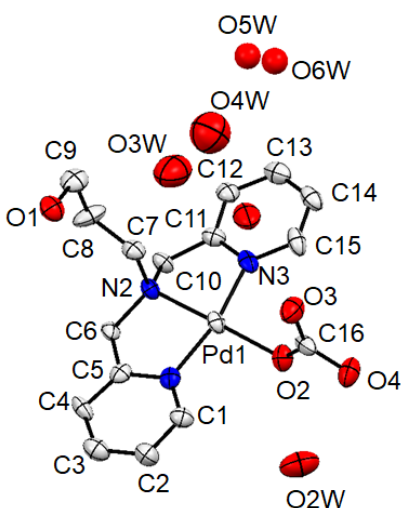


Figure A5.41 Displacement ellipsoid plot of **5-2a** co-crystallized with water molecules showing naming and numbering scheme. Ellipsoids are drawn at the 50% probability level and hydrogen atoms are omitted for clarity.

Table A5.2 Atomic coordinates for **5-2a**.

Atom	x	y	z	$U_{\text{iso/equiv}}$
Pd1	0.49424(9)	0.17947(9)	0.45192(7)	0.0281(3)
N1	0.2822(9)	0.2421(9)	0.5139(8)	0.031(2)
N2	0.3982(9)	0.2440(9)	0.2938(7)	0.0289(19)
N3	0.6849(9)	0.1199(9)	0.3550(8)	0.032(2)
O1	0.1931(8)	0.7090(9)	0.1477(7)	0.0435(19)
O2	0.5901(8)	0.1059(8)	0.6106(6)	0.0388(18)
O3	0.6311(10)	0.3056(9)	0.6100(7)	0.051(2)
O4	0.6937(9)	0.1274(9)	0.7647(7)	0.049(2)
C1	0.2311(12)	0.2593(11)	0.6234(9)	0.033(2)
C2	0.0820(12)	0.3001(12)	0.6569(10)	0.038(3)
C3	-0.0196(13)	0.3262(12)	0.5696(10)	0.041(3)
C4	0.0280(11)	0.3137(10)	0.4540(10)	0.033(2)
C5	0.1820(11)	0.2677(10)	0.4287(9)	0.028(2)
C6	0.2459(10)	0.2357(11)	0.3101(9)	0.029(2)
C7	0.3842(12)	0.3988(11)	0.2479(9)	0.033(2)
C8	0.3362(16)	0.4556(12)	0.1232(10)	0.050(3)
C9	0.3174(14)	0.6157(12)	0.0896(11)	0.045(3)

C10	0.5038(10)	0.1384(11)	0.2179(9)	0.029(2)
C11	0.6605(11)	0.1138(10)	0.2420(9)	0.030(2)
C12	0.7774(11)	0.0805(11)	0.1603(10)	0.034(2)
C13	0.9226(12)	0.0500(11)	0.1927(11)	0.041(3)
C14	0.9452(12)	0.0570(11)	0.3079(11)	0.039(3)
C15	0.8275(11)	0.0937(11)	0.3872(11)	0.038(3)
C16	0.6364(11)	0.1812(11)	0.6559(11)	0.038(3)
O1W	0.6533(10)	0.4662(10)	0.4007(9)	0.069(3)
O2W	0.4069(13)	0.2026(11)	0.9014(8)	0.073(3)
O3W	0.7601(14)	-0.1028(14)	-0.0560(10)	0.103(4)
O4W	0.7149(13)	0.5002(15)	0.1778(12)	0.120(5)
O5W	0.9810(17)	0.3264(17)	0.0104(13)	0.049(5)
O6W	1.0007(14)	0.4111(17)	0.1031(13)	0.050(6)
H1	0.2227	0.7444	0.1968	0.065
H16	0.3018	0.2423	0.6820	0.040
H2	0.0501	0.3100	0.7363	0.046
H3	-0.1232	0.3530	0.5895	0.049
H4	-0.0419	0.3357	0.3936	0.040
H6A	0.1774	0.3073	0.2493	0.034
H6B	0.2550	0.1365	0.3005	0.034
H7A	0.3112	0.4652	0.2990	0.039
H7B	0.4827	0.4041	0.2558	0.039
H8A	0.2398	0.4473	0.1128	0.060
H8B	0.4123	0.3950	0.0703	0.060
H9A	0.4093	0.6263	0.1102	0.054
H9B	0.3045	0.6444	0.0036	0.054
H10A	0.4905	0.0443	0.2347	0.035
H10B	0.4820	0.1785	0.1340	0.035
H12	0.7582	0.0785	0.0814	0.040
H13	1.0040	0.0251	0.1375	0.049
H14	1.0437	0.0361	0.3324	0.046
H15	0.8448	0.1010	0.4653	0.046
H1WA	0.5671	0.5359	0.3977	0.103
H1WB	0.6471	0.4162	0.4655	0.103

H2WA	0.4891	0.1806	0.8621	0.110
H2WB	0.3672	0.2933	0.8786	0.110
H3WA	0.7399	-0.0324	-0.1113	0.154
H3WB	0.7134	-0.1310	-0.0130	0.154
H4WA	0.6959	0.4921	0.2378	0.180
H4WB	0.7849	0.4787	0.1605	0.180
H5WB	1.0496	0.2669	0.0223	0.073
H5WA	0.9278	0.3153	-0.0380	0.073
H6WB	1.0103	0.5029	0.0616	0.075
H6WA	0.9783	0.3962	0.0727	0.075

Table A5.3 Bond lengths for **5-2a**.

Pd1-N1	2.003(9)	C7-H7B	0.9900
Pd1-N2	2.007(8)	C8-C9	1.530(15)
Pd1-N3	2.007(9)	C8-H8A	0.9900
Pd1-O2	2.012(7)	C8-H8B	0.9900
N1-C1	1.331(13)	C9-H9A	0.9900
N1-C5	1.362(12)	C9-H9B	0.9900
N2-C10	1.496(12)	C10-C11	1.482(14)
N2-C6	1.506(12)	C10-H10A	0.9900
N2-C7	1.511(12)	C10-H10B	0.9900
N3-C11	1.361(13)	C11-C12	1.382(14)
N3-C15	1.373(13)	C12-C13	1.387(15)
O1-C9	1.400(14)	C12-H12	0.9500
O1-H1	0.8400	C13-C14	1.383(16)
O2-C16	1.221(13)	C13-H13	0.9500
O3-C16	1.256(12)	C14-C15	1.371(16)
O4-C16	1.352(13)	C14-H14	0.9500
C1-C2	1.377(15)	C15-H15	0.9500
C1-H16	0.9500	O1W-H1WA	0.8500
C2-C3	1.389(15)	O1W-H1WB	0.8400
C2-H2	0.9500	O2W-H2WA	0.8500
C3-C4	1.383(16)	O2W-H2WB	0.8400
C3-H3	0.9500	O3W-H3WA	0.8401

C4-C5	1.397(14)	O3W-H3WB	0.7399
C4-H4	0.9500	O4W-H4WA	0.7000
C5-C6	1.485(14)	O4W-H4WB	0.6499
C6-H6A	0.9900	O5W-H5WB	0.6999
C6-H6B	0.9900	O5W-H5WA	0.8400
C7-C8	1.497(15)	O6W-H6WB	1.0000
C7-H7A	0.9900	O6W-H6WA	0.4999

Table A5.4 Bond angles for **5-2a**.

N1-Pd1-N2	84.3(3)	N2-C7-H7B	108.2
N1-Pd1-N3	166.9(3)	H7A-C7-H7B	107.4
N2-Pd1-N3	83.0(3)	C7-C8-C9	111.3(10)
N1-Pd1-O2	95.5(3)	C7-C8-H8A	109.4
N2-Pd1-O2	177.4(3)	C9-C8-H8A	109.4
N3-Pd1-O2	97.1(3)	C7-C8-H8B	109.4
C1-N1-C5	118.7(9)	C9-C8-H8B	109.4
C1-N1-Pd1	128.9(7)	H8A-C8-H8B	108.0
C5-N1-Pd1	112.5(7)	O1-C9-C8	111.3(10)
C10-N2-C6	113.5(7)	O1-C9-H9A	109.4
C10-N2-C7	110.8(8)	C8-C9-H9A	109.4
C6-N2-C7	111.0(7)	O1-C9-H9B	109.4
C10-N2-Pd1	104.5(6)	C8-C9-H9B	109.4
C6-N2-Pd1	107.1(6)	H9A-C9-H9B	108.0
C7-N2-Pd1	109.6(6)	C11-C10-N2	109.3(8)
C11-N3-C15	119.2(10)	C11-C10-H10A	109.8
C11-N3-Pd1	112.2(6)	N2-C10-H10A	109.8
C15-N3-Pd1	128.5(8)	C11-C10-H10B	109.8
C9-O1-H1	109.5	N2-C10-H10B	109.8
C16-O2-Pd1	120.4(7)	H10A-C10-H10B	108.3
N1-C1-C2	124.0(10)	N3-C11-C12	120.7(9)
N1-C1-H16	118.0	N3-C11-C10	114.7(9)
C2-C1-H16	118.0	C12-C11-C10	124.5(9)

C1-C2-C3	117.1(11)	C11-C12-C13	120.5(10)
C1-C2-H2	121.5	C11-C12-H12	119.7
C3-C2-H2	121.5	C13-C12-H12	119.7
C4-C3-C2	120.9(10)	C14-C13-C12	117.9(10)
C4-C3-H3	119.5	C14-C13-H13	121.1
C2-C3-H3	119.5	C12-C13-H13	121.1
C3-C4-C5	118.0(10)	C15-C14-C13	120.9(10)
C3-C4-H4	121.0	C15-C14-H14	119.5
C5-C4-H4	121.0	C13-C14-H14	119.5
N1-C5-C4	121.3(10)	C14-C15-N3	120.7(11)
N1-C5-C6	116.5(9)	C14-C15-H15	119.7
C4-C5-C6	122.1(9)	N3-C15-H15	119.7
C5-C6-N2	110.7(8)	O2-C16-O3	124.7(11)
C5-C6-H6A	109.5	O2-C16-O4	117.2(9)
N2-C6-H6A	109.5	O3-C16-O4	118.1(10)
C5-C6-H6B	109.5	H1WA-O1W-H1WB	101.2
N2-C6-H6B	109.5	H2WA-O2W-H2WB	100.5
H6A-C6-H6B	108.1	H3WA-O3W-H3WB	133.5
C8-C7-N2	116.3(9)	H4WA-O4W-H4WB	120.6
C8-C7-H7A	108.2	H5WB-O5W-H5WA	114.5
N2-C7-H7A	108.2	H6WB-O6W-H6WA	102.9
C8-C7-H7B	108.2		

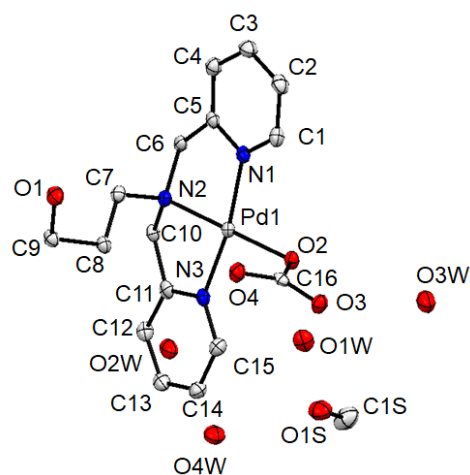


Figure A5.42 Displacement ellipsoid plot of **5-2b** co-crystallized with water molecules and a methanol molecule showing naming and numbering scheme. Ellipsoids are drawn at the 50% probability level and hydrogen atoms are omitted for clarity.

Table A5.5 Atomic coordinates for **5-2b**

Atom	x	y	z	$U_{\text{iso/equiv}}$
Pd1	0.47832(2)	0.37727(2)	0.50312(2)	0.01348(12)
O2	0.38902(14)	0.41433(13)	0.57226(8)	0.0181(4)
O1	0.49720(14)	0.04598(14)	0.41944(9)	0.0234(4)
O3	0.35992(14)	0.26062(13)	0.58015(8)	0.0221(4)
O4	0.29911(15)	0.36141(13)	0.64897(8)	0.0219(4)
N1	0.38016(17)	0.39597(16)	0.43643(10)	0.0164(5)
N3	0.59963(18)	0.36213(15)	0.55393(10)	0.0169(5)
N2	0.56622(16)	0.33914(15)	0.43371(9)	0.0149(5)
C15	0.6064(2)	0.35485(19)	0.61539(12)	0.0193(6)
C6	0.52999(19)	0.39303(19)	0.37907(12)	0.0160(6)
C8	0.5736(2)	0.17127(18)	0.47363(11)	0.0174(6)
C12	0.7728(2)	0.34796(18)	0.54641(12)	0.0201(6)
C1	0.2826(2)	0.40409(19)	0.44279(12)	0.0204(6)
C13	0.7794(2)	0.34414(19)	0.60937(12)	0.0222(6)
C16	0.34866(19)	0.34215(18)	0.60086(11)	0.0158(6)
C7	0.5595(2)	0.23647(18)	0.41934(11)	0.0175(6)
C14	0.6951(2)	0.3462(2)	0.64420(12)	0.0225(6)

C2	0.2220(2)	0.4085(2)	0.39297(12)	0.0241(6)
C5	0.4204(2)	0.39323(18)	0.38011(12)	0.0168(6)
C9	0.58311(19)	0.07055(17)	0.45193(12)	0.0185(6)
C10	0.6680(2)	0.36707(18)	0.45182(12)	0.0166(6)
C11	0.6819(2)	0.35720(18)	0.51981(13)	0.0181(6)
C3	0.2615(2)	0.4030(2)	0.33522(12)	0.0241(6)
C4	0.3619(2)	0.39513(18)	0.32856(12)	0.0211(6)
C1S	0.4554(3)	0.4461(2)	0.76050(14)	0.0377(8)
O1S	0.40844(17)	0.35806(15)	0.75427(10)	0.0343(5)
O1W	0.20751(14)	0.21828(14)	0.70761(8)	0.0282(5)
O2W	0.44912(16)	0.11675(13)	0.63788(9)	0.0287(5)
O3W	0.22716(16)	0.53581(14)	0.68498(9)	0.0349(5)
O4W	0.53223(15)	0.20805(15)	0.73431(9)	0.0297(5)
H1A	0.5064	-0.0030	0.4007	0.035
H15A	0.5497	0.3557	0.6386	0.023
H6A	0.5543	0.4570	0.3803	0.019
H6B	0.5532	0.3637	0.3419	0.019
H8A	0.6318	0.1893	0.4958	0.021
H8B	0.5183	0.1767	0.5010	0.021
H12A	0.8286	0.3444	0.5224	0.024
H1B	0.2558	0.4068	0.4817	0.025
H13A	0.8401	0.3402	0.6282	0.027
H7A	0.6084	0.2215	0.3889	0.021
H7B	0.4961	0.2240	0.4015	0.021
H14A	0.6985	0.3419	0.6864	0.027
H2A	0.1551	0.4151	0.3981	0.029
H9A	0.6396	0.0643	0.4256	0.022
H9B	0.5915	0.0290	0.4865	0.022
H10A	0.6797	0.4317	0.4399	0.020
H10B	0.7147	0.3276	0.4307	0.020
H3A	0.2214	0.4045	0.3011	0.029
H4A	0.3896	0.3912	0.2900	0.025
H1S1	0.4115	0.4953	0.7485	0.057
H1S2	0.5122	0.4477	0.7350	0.057

H1S3	0.4744	0.4551	0.8022	0.057
H1S	0.3754	0.3580	0.7231	0.052
H1W1	0.2357	0.2635	0.6895	0.042
H1W2	0.2270	0.1626	0.7007	0.042
H2W1	0.4212	0.1619	0.6195	0.043
H2W2	0.4753	0.1451	0.6678	0.043
H3W1	0.2494	0.4827	0.6741	0.052
H3W2	0.1752	0.5606	0.6714	0.052
H4W1	0.4938	0.2540	0.7401	0.045
H4W2	0.5869	0.2105	0.7525	0.045

Table A5.6 Bond lengths for **5-2b**.

Pd1-N1	2.007(2)	C13-C14	1.387(4)
Pd1-N3	2.015(2)	C13-H13A	0.9300
Pd1-N2	2.017(2)	C7-H7A	0.9700
Pd01-O2	2.0202(18)	C7-H7B	0.9700
O2-C16	1.325(3)	C14-H14A	0.9300
O1-C9	1.421(3)	C2-C3	1.381(4)
O1-H1A	0.8200	C2-H2A	0.9300
O3-C16	1.256(3)	C5-C4	1.387(4)
O4-C16	1.285(3)	C9-H9A	0.9700
N1-C1	1.351(4)	C9-H9B	0.9700
N1-C5	1.354(3)	C10-C11	1.511(4)
N3-C15	1.356(3)	C10-H10A	0.9700
N3-C11	1.357(4)	C10-H10B	0.9700
N2-C7	1.498(3)	C3-C4	1.389(4)
N2-C10	1.505(3)	C3-H3A	0.9300
N2-C6	1.508(3)	C4-H4A	0.9300
C15-C14	1.378(4)	C1S-O1S	1.416(4)
C15-H15A	0.9300	C1S-H1S1	0.9600
C6-C5	1.504(4)	C1S-H1S2	0.9600
C6-H6A	0.9700	C1S-H1S3	0.9600
C6-H6B	0.9700	O1S-H1S	0.8200

C8-C9	1.517(4)	O1W-H1W1	0.8500
C8-C7	1.523(3)	O1W-H1W2	0.8500
C8-H8A	0.9700	O2W-H2W1	0.8501
C8-H8B	0.9700	O2W-H2W2	0.8500
C12-C11	1.383(4)	O3W-H3W1	0.8500
C12-C13	1.386(4)	O3W-H3W2	0.8500
C12-H12A	0.9300	O4W-H4W1	0.8501
C1-C2	1.374(4)	O4W-H4W2	0.8499
C1-H1B	0.9300		

Table A5.7 Bond angles for **5-2b**.

N1-Pd01-N3	166.45(10)	N2-C7-C8	115.0(2)
N1-Pd01-N2	83.45(9)	N2-C7-H7A	108.5
N3-Pd01-N2	84.00(9)	C8-C7-H7A	108.5
N1-Pd01-O2	96.10(9)	N2-C7-H7B	108.5
N3-Pd01-O2	96.50(8)	C8-C7-H7B	108.5
N2-Pd01-O2	179.28(8)	H7A-C7-H7B	107.5
C16-O2-Pd01	113.98(16)	C15-C14-C13	119.1(3)
C9-O1-H1A	109.5	C15-C14-H14A	120.5
C1-N1-C5	120.0(2)	C13-C14-H14A	120.5
C1-N1-Pd01	126.94(19)	C1-C2-C3	119.3(3)
C5-N1-Pd01	112.88(19)	C1-C2-H2A	120.3
C15-N3-C11	119.2(2)	C3-C2-H2A	120.3
C15-N3-Pd01	127.9(2)	N1-C5-C4	120.6(3)
C11-N3-Pd01	112.80(18)	N1-C5-C6	114.9(2)
C7-N2-C10	111.7(2)	C4-C5-C6	124.5(2)
C7-N2-C6	107.99(19)	O1-C9-C8	108.6(2)
C10-N2-C6	112.4(2)	O1-C9-H9A	110.0
C7-N2-Pd01	112.65(16)	C8-C9-H9A	110.0
C10-N2-Pd01	106.49(15)	O1-C9-H9B	110.0
C6-N2-Pd01	105.46(16)	C8-C9-H9B	110.0
N3-C15-C14	121.6(3)	H9A-C9-H9B	108.3
N3-C15-H15A	119.2	N2-C10-C11	110.7(2)
C14-C15-H15A	119.2	N2-C10-H10A	109.5
C5-C6-N2	108.6(2)	C11-C10-H10A	109.5
C5-C6-H6A	110.0	N2-C10-H10B	109.5
N2-C6-H6A	110.0	C11-C10-H10B	109.5
C5-C6-H6B	110.0	H10A-C10-H10B	108.1
N2-C6-H6B	110.0	N3-C11-C12	121.5(3)
H6A-C6-H6B	108.4	N3-C11-C10	115.8(2)
C9-C8-C7	110.0(2)	C12-C11-C10	122.7(3)
C9-C8-H8A	109.7	C2-C3-C4	119.4(3)

C7-C8-H8A	109.7	C2-C3-H3A	120.3
C9-C8-H8B	109.7	C4-C3-H3A	120.3
C7-C8-H8B	109.7	C5-C4-C3	119.3(3)
H8A-C8-H8B	108.2	C5-C4-H4A	120.4
C11-C12-C13	118.9(3)	C3-C4-H4A	120.4
C11-C12-H12A	120.5	O1S-C1S-H1S1	109.5
C13-C12-H12A	120.5	O1S-C1S-H1S2	109.5
N1-C1-C2	121.4(3)	H1S1-C1S-H1S2	109.5
N1-C1-H1B	119.3	O1S-C1S-H1S3	109.5
C2-C1-H1B	119.3	H1S1-C1S-H1S3	109.5
C12-C13-C14	119.6(3)	H1S2-C1S-H1S3	109.5
C12-C13-H13A	120.2	C1S-O1S-H1S	109.5
C14-C13-H13A	120.2	H1W1-O1W-H1W2	118.7
O3-C16-O4	124.0(2)	H2W1-O2W-H2W2	101.4
O3-C16-O2	119.6(2)	H3W1-O3W-H3W2	124.9
O4-C16-O2	116.4(2)	H4W1-O4W-H4W2	116.5

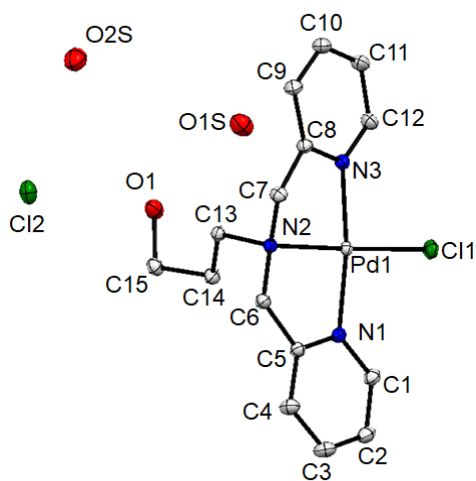


Figure A5.43 Displacement ellipsoid plot of **5-3b** co-crystallized with two water molecules showing naming and numbering scheme. Ellipsoids are drawn at the 50% probability level and hydrogen atoms are omitted for clarity.

Table A5.8 Atomic coordinates for **5-3b**.

Atom	x	y	z	U _{iso} /equiv
Pd1	0.14862(2)	0.41443(2)	0.56005(2)	0.01050(2)
Cl1	0.09579(2)	0.48089(2)	0.68250(2)	0.01716(4)
O1	0.51714(7)	0.16383(8)	0.64395(7)	0.02303(15)
N1	0.03274(6)	0.27232(7)	0.51172(6)	0.01298(11)
N2	0.20379(6)	0.35536(7)	0.45740(5)	0.01123(10)
N3	0.26312(7)	0.55462(7)	0.57551(6)	0.01310(11)
C1	-0.04151(8)	0.22941(9)	0.55023(7)	0.01597(14)
C2	-0.12495(9)	0.13935(10)	0.50434(8)	0.01938(16)
C3	-0.13288(9)	0.09305(10)	0.41583(9)	0.02099(17)
C4	-0.05531(9)	0.13512(10)	0.37683(7)	0.01826(15)
C5	0.02709(7)	0.22533(8)	0.42653(6)	0.01331(12)
C6	0.10906(7)	0.27904(8)	0.38495(6)	0.01353(12)
C7	0.22740(8)	0.47632(8)	0.41639(6)	0.01396(13)
C8	0.29220(8)	0.56360(8)	0.49823(7)	0.01365(12)
C9	0.37398(8)	0.65078(9)	0.49577(8)	0.01774(15)
C10	0.42529(9)	0.73056(9)	0.57424(8)	0.01980(16)
C11	0.39471(9)	0.72094(10)	0.65268(8)	0.01961(16)
C12	0.31346(8)	0.63116(9)	0.65157(7)	0.01645(14)
C13	0.31501(7)	0.28164(8)	0.49840(6)	0.01307(12)
C14	0.30967(8)	0.16981(9)	0.55966(7)	0.01549(13)
C15	0.41857(9)	0.08907(8)	0.58878(7)	0.01662(14)
O1S	0.51295(9)	0.42151(9)	0.68685(7)	0.02833(18)
Cl2	0.73144(2)	-0.00157(3)	0.66871(2)	0.02267(5)
O2S	0.84101(9)	0.28265(10)	0.71169(8)	0.03198(19)
H1A	0.578251	0.123213	0.652900	0.039(5)
H1B	-0.036255	0.261952	0.610409	0.019
H2A	-0.175943	0.109654	0.532790	0.023
H3A	-0.191035	0.032979	0.382208	0.025
H4A	-0.058501	0.102764	0.317174	0.022
H6A	0.144017	0.209082	0.361823	0.016
H6B	0.064921	0.333098	0.329109	0.016

H7A	0.153287	0.515710	0.373866	0.017
H7B	0.274397	0.459192	0.377958	0.017
H9A	0.394519	0.655884	0.441564	0.021
H10A	0.481073	0.791362	0.573934	0.024
H11A	0.428913	0.775105	0.706567	0.024
H12A	0.292923	0.623537	0.705644	0.020
H13A	0.378153	0.338904	0.538058	0.016
H13B	0.334855	0.250529	0.444848	0.016
H14A	0.300579	0.201000	0.618147	0.019
H14B	0.240927	0.117456	0.523072	0.019
H15A	0.412048	0.016087	0.627361	0.020
H15B	0.427704	0.056433	0.530680	0.020
H1S	0.528626	0.334933	0.682267	0.042
H2S	0.594255	0.465210	0.729590	0.042
H3S	0.804032	0.202340	0.713623	0.048
H4S	0.812696	0.319688	0.751055	0.048

Table A5.9 Bond lengths for **5-3b**.

Pd1-N3	2.0107(8)	C7-C8	1.5022(13)
Pd1-N1	2.0170(8)	C7-H7A	0.9900
Pd1-N2	2.0254(8)	C7-H7B	0.9900
Pd1-C11	2.3024(6)	C8-C9	1.3881(13)
O1-C15	1.4274(13)	C9-C10	1.3916(15)
O1-H1A	0.8400	C9-H9A	0.9500
N1-C1	1.3511(12)	C10-C11	1.3828(16)
N1-C5	1.3553(12)	C10-H10A	0.9500
N2-C6	1.4969(12)	C11-C12	1.3859(14)
N2-C13	1.5008(11)	C11-H11A	0.9500
N2-C7	1.5010(12)	C12-H12A	0.9500
N3-C12	1.3447(13)	C13-C14	1.5200(13)
N3-C8	1.3540(12)	C13-H13A	0.9900
C1-C2	1.3830(14)	C13-H13B	0.9900
C1-H1B	0.9500	C14-C15	1.5194(13)
C2-C3	1.3905(17)	C14-H14A	0.9900
C2-H2A	0.9500	C14-H14B	0.9900
C3-C4	1.3890(15)	C15-H15A	0.9900
C3-H3A	0.9500	C15-H15B	0.9900
C4-C5	1.3903(13)	O1S-H1S	0.9454
C4-H4A	0.9500	O1S-H2S	1.0730
C5-C6	1.5059(12)	O2S-H3S	0.9735
C6-H6A	0.9900	O2S-H4S	0.8923
C6-H6B	0.9900		

Table 5A.10 Bond angles for **5-3b**.

N1-Pd1-N3	166.45(10)	N2-C7-C8	115.0(2)
N1-Pd1-N2	83.45(9)	N2-C7-H7A	108.5
N3-Pd1-N2	84.00(9)	C8-C7-H7A	108.5
N1-Pd1-O2	96.10(9)	N2-C7-H7B	108.5

N3-Pd1-O2	96.50(8)	C8-C7-H7B	108.5
N2-Pd1-O2	179.28(8)	H7A-C7-H7B	107.5
C16-O2-Pd1	113.98(16)	C15-C14-C13	119.1(3)
C9-O1-H1A	109.5	C15-C14-H14A	120.5
C1-N1-C5	120.0(2)	C13-C14-H14A	120.5
C1-N1-Pd1	126.94(19)	C1-C2-C3	119.3(3)
C5-N1-Pd1	112.88(19)	C1-C2-H2A	120.3
C15-N3-C11	119.2(2)	C3-C2-H2A	120.3
C15-N3-Pd1	127.9(2)	N1-C5-C4	120.6(3)
C11-N3-Pd1	112.80(18)	N1-C5-C6	114.9(2)
C7-N2-C10	111.7(2)	C4-C5-C6	124.5(2)
C7-N2-C6	107.99(19)	O1-C9-C8	108.6(2)
C10-N2-C6	112.4(2)	O1-C9-H9A	110.0
C7-N2-Pd1	112.65(16)	C8-C9-H9A	110.0
C10-N2-Pd1	106.49(15)	O1-C9-H9B	110.0
C6-N2-Pd1	105.46(16)	C8-C9-H9B	110.0
N3-C15-C14	121.6(3)	H9A-C9-H9B	108.3
N3-C15-H15A	119.2	N2-C10-C11	110.7(2)
C14-C15-H15A	119.2	N2-C10-H10A	109.5
C5-C6-N2	108.6(2)	C11-C10-H10A	109.5
C5-C6-H6A	110.0	N2-C10-H10B	109.5
N2-C6-H6A	110.0	C11-C10-H10B	109.5
C5-C6-H6B	110.0	H10A-C10-H10B	108.1
N2-C6-H6B	110.0	N3-C11-C12	121.5(3)
H6A-C6-H6B	108.4	N3-C11-C10	115.8(2)
C9-C8-C7	110.0(2)	C12-C11-C10	122.7(3)
C9-C8-H8A	109.7	C2-C3-C4	119.4(3)
C7-C8-H8A	109.7	C2-C3-H3A	120.3
C9-C8-H8B	109.7	C4-C3-H3A	120.3
C7-C8-H8B	109.7	C5-C4-C3	119.3(3)
H8A-C8-H8B	108.2	C5-C4-H4A	120.4
C11-C12-C13	118.9(3)	C3-C4-H4A	120.4
C11-C12-H12A	120.5	O1S-C1S-H1S1	109.5
C13-C12-H12A	120.5	O1S-C1S-H1S2	109.5

N1-C1-C2	121.4(3)	H1S1-C1S-H1S2	109.5
N1-C1-H1B	119.3	O1S-C1S-H1S3	109.5
C2-C1-H1B	119.3	H1S1-C1S-H1S3	109.5
C12-C13-C14	119.6(3)	H1S2-C1S-H1S3	109.5
C12-C13-H13A	120.2	C1S-O1S-H1S	109.5
C14-C13-H13A	120.2	H1W1-O1W-H1W2	118.7
O3-C16-O4	124.0(2)	H2W1-O2W-H2W2	101.4
O3-C16-O2	119.6(2)	H3W1-O3W-H3W2	124.9
O4-C16-O2	116.4(2)	H4W1-O4W-H4W2	116.5

Appendix E. Supplementary Information for Chapter 6

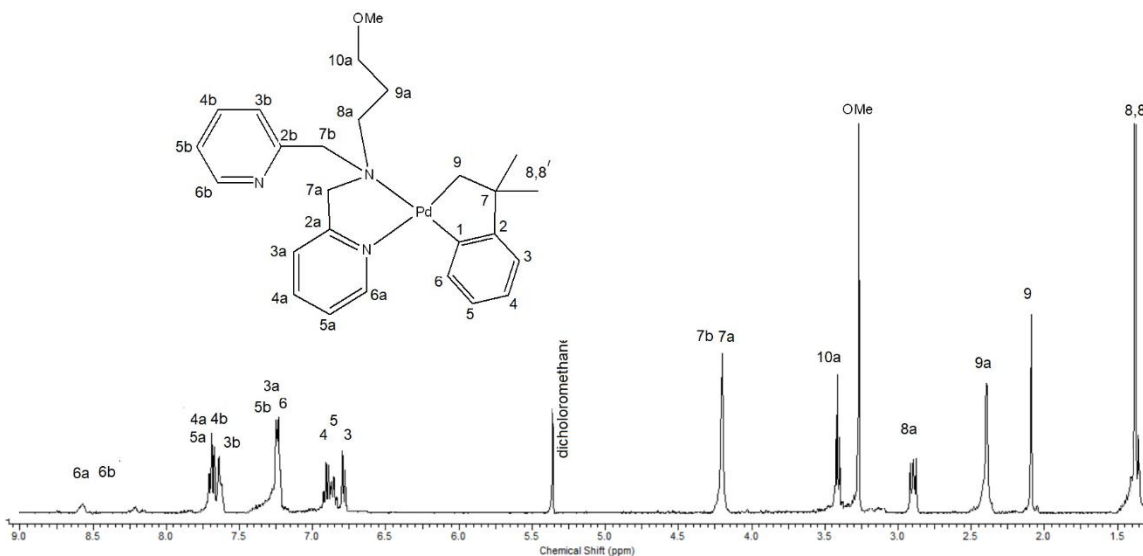


Figure A6.1 ^1H NMR Spectrum of $[\text{Pd}^{\text{III}}(\text{CH}_2\text{CMe}_2\text{C}_6\text{H}_4)(\kappa^2\text{-N,N}'\text{-6-L1})]$, **6-1**, in CD_2Cl_2 at RT, 600 MHz.

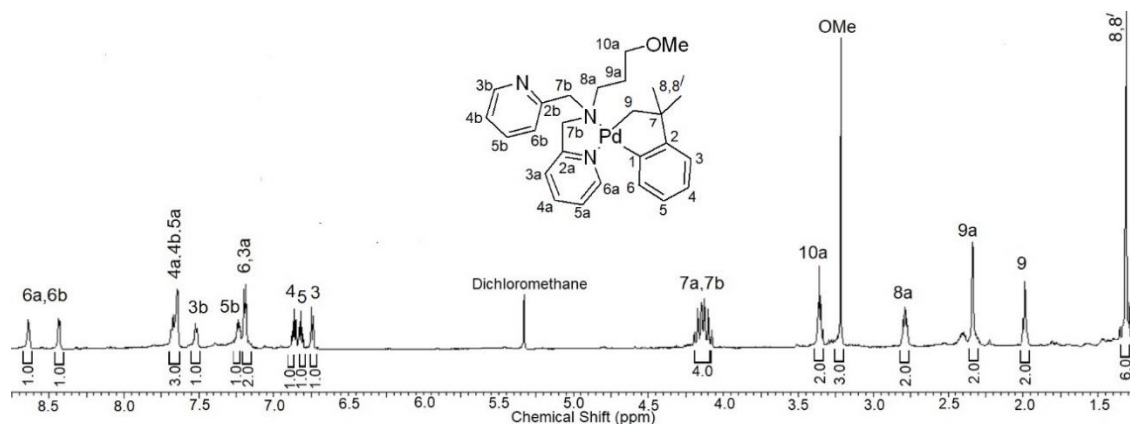


Figure A6.2 ^1H NMR Spectrum of $[\text{Pd}^{\text{II}}(\text{CH}_2\text{CMe}_2\text{C}_6\text{H}_4)(\kappa^2\text{-N,N}'\text{-6-L1})]$, **6-1**, in CD_2Cl_2 at -30°C , at 600 MHz.

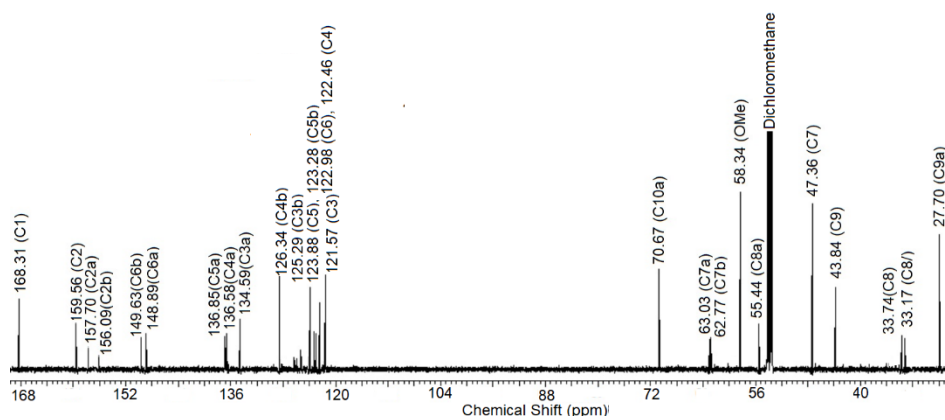


Figure A6.3 $^{13}\text{C}\{^1\text{H}\}$ NMR Spectrum of $[\text{Pd}^{\text{II}}(\text{CH}_2\text{CMe}_2\text{C}_6\text{H}_4)(\kappa^2\text{-N,N}'\text{-6-L1})]$, **6-1**, in CD_2Cl_2 at -30°C , 151 MHz.

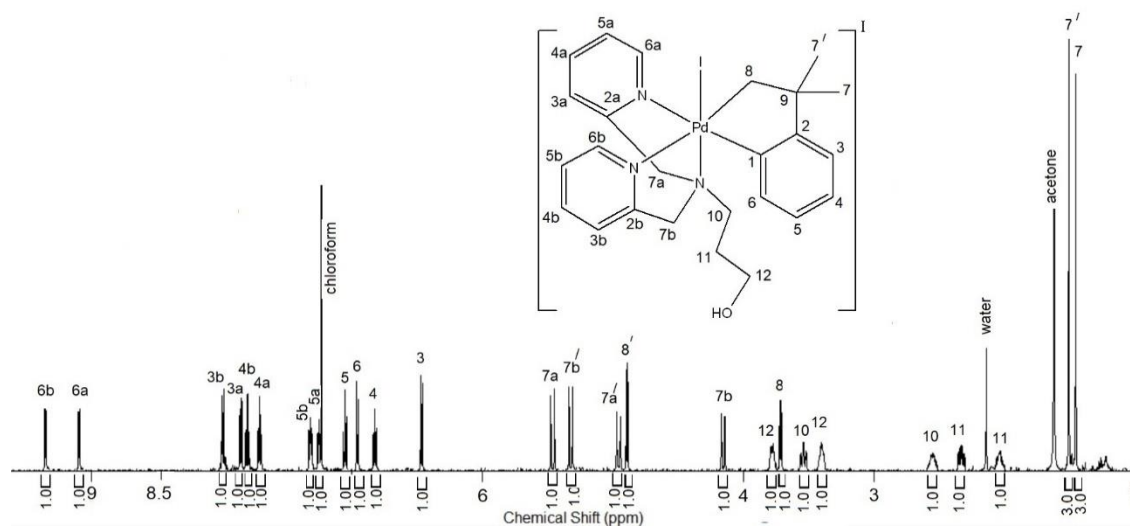


Figure A6.4 ^1H NMR Spectrum of $[\text{Pd}^{\text{IV}}(\text{CH}_2\text{CMe}_2\text{C}_6\text{H}_4)(\kappa^3\text{-N,N',N''}\text{-5-L1})\text{I}][\text{I}]$, **6-2**, in CDCl_3 at 25°C , 600 MHz.

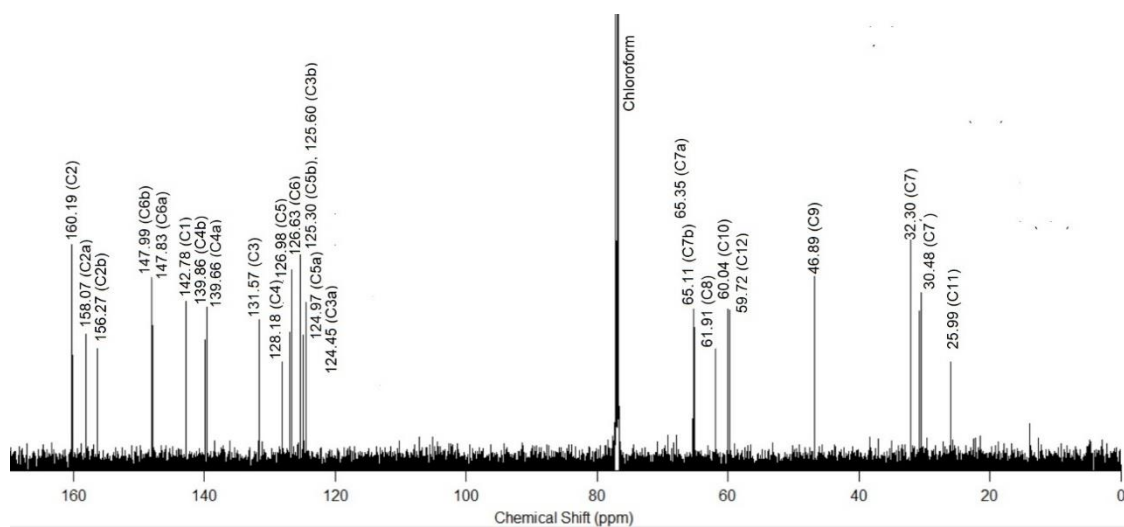


Figure A6.5 $^{13}\text{C}\{^1\text{H}\}$ NMR Spectrum of $[\text{Pd}^{\text{IV}}(\text{CH}_2\text{CMe}_2\text{C}_6\text{H}_4)(\kappa^3\text{-N,N',N''-5-L1})\text{I}][\text{I}]$, **6-2**, in CDCl_3 at 25°C , 151 MHz.

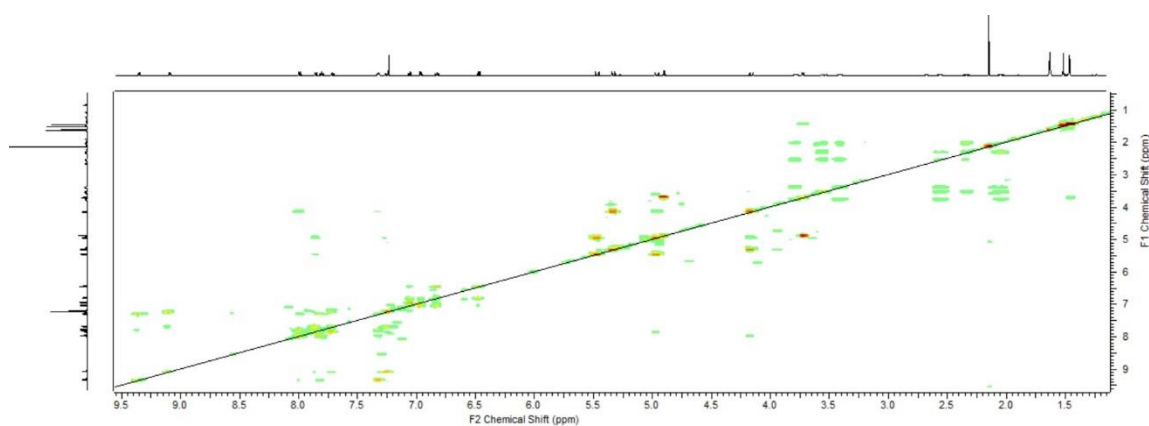


Figure A6.6 $^1\text{H}\text{-}^1\text{H}$ gCOSY Spectrum of $[\text{Pd}^{\text{IV}}(\text{CH}_2\text{CMe}_2\text{C}_6\text{H}_4)(\kappa^3\text{-N,N',N''-5-L1})\text{I}][\text{I}]$, **6-2**, in CDCl_3 at 25°C .

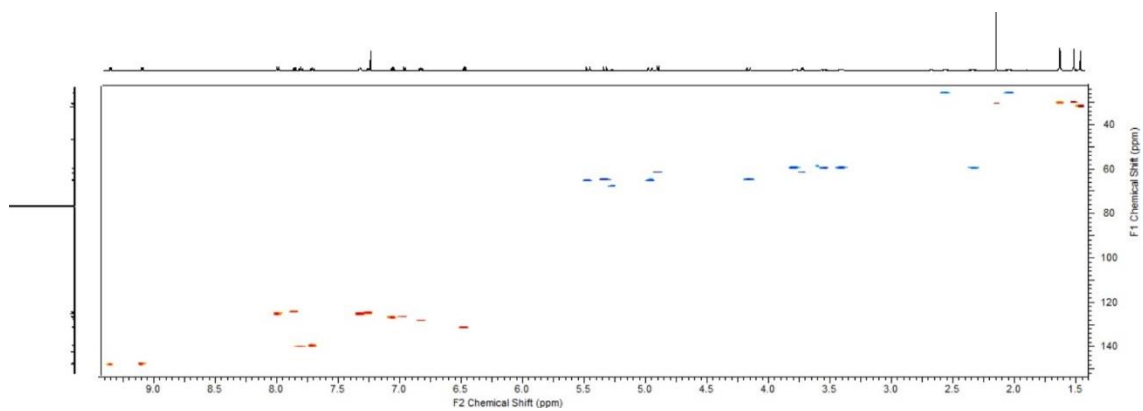


Figure A6.7 ^1H - $^{13}\text{C}\{^1\text{H}\}$ HSQC Spectrum of $[\text{Pd}^{\text{IV}}(\text{CH}_2\text{CMe}_2\text{C}_6\text{H}_4)(\kappa^3\text{-N,N',N''-5-L1})\text{I}][\text{I}]$, **6-2**, in CDCl_3 at 25°C .

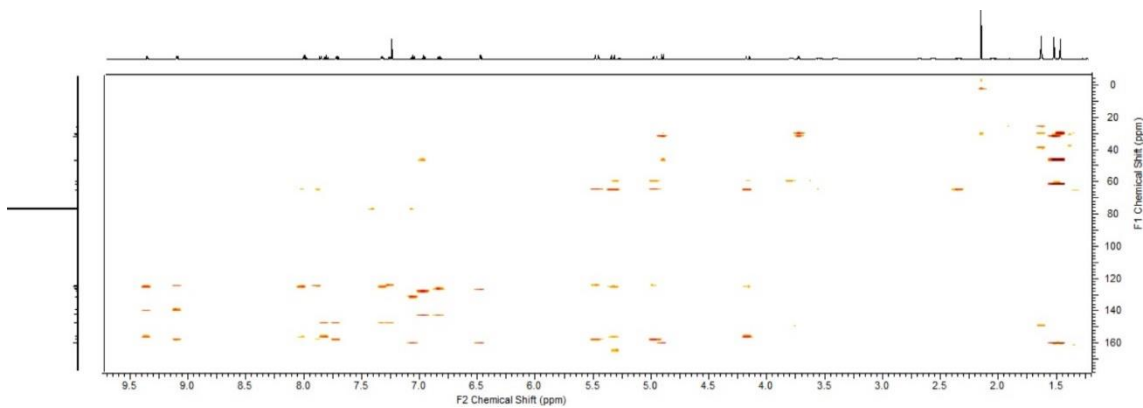


Figure A6.8 ^1H - $^{13}\text{C}\{^1\text{H}\}$ HMBC Spectrum of $[\text{Pd}^{\text{IV}}(\text{CH}_2\text{CMe}_2\text{C}_6\text{H}_4)(\kappa^3\text{-N,N',N''-5-L1})\text{I}][\text{I}]$, **6-2**, in CDCl_3 at 25°C .

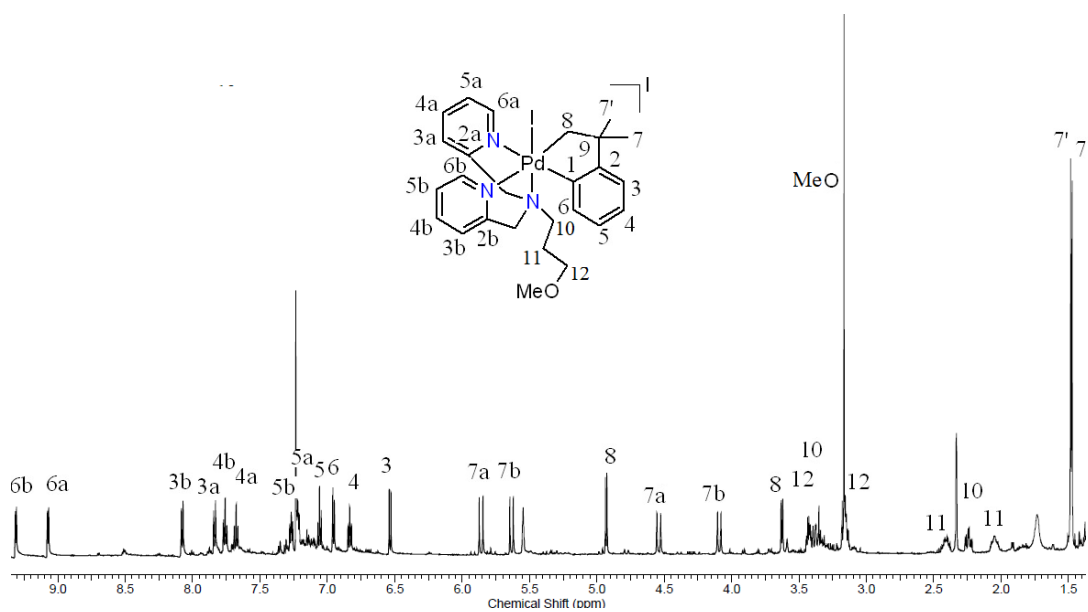


Figure A6.9 ¹H NMR Spectrum of [Pd^{IV}(CH₂CMe₂C₆H₄)(κ³-N,N',N''-6-L1)I][I], 6-3, in CDCl₃ at 25°C, 600 MHz.

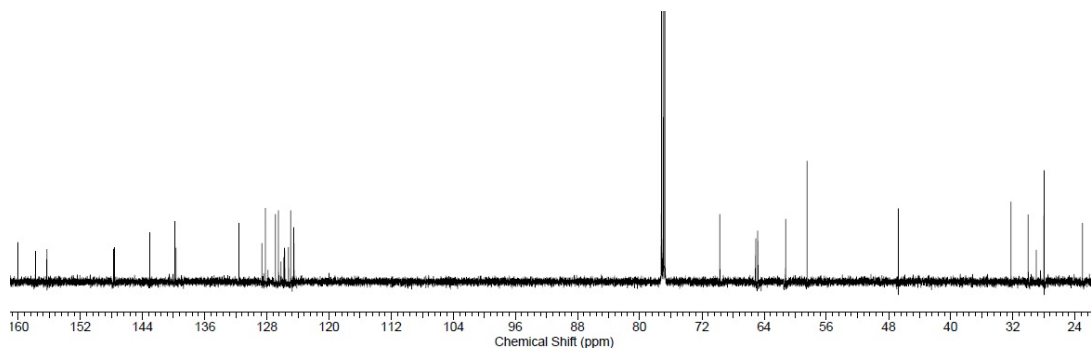


Figure A6.10 ¹³C{¹H} NMR Spectrum of [Pd^{IV}(CH₂CMe₂C₆H₄)(κ³-N,N',N''-6-L1)I][I], 6-3, in CDCl₃ at 25°C, 151 MHz.

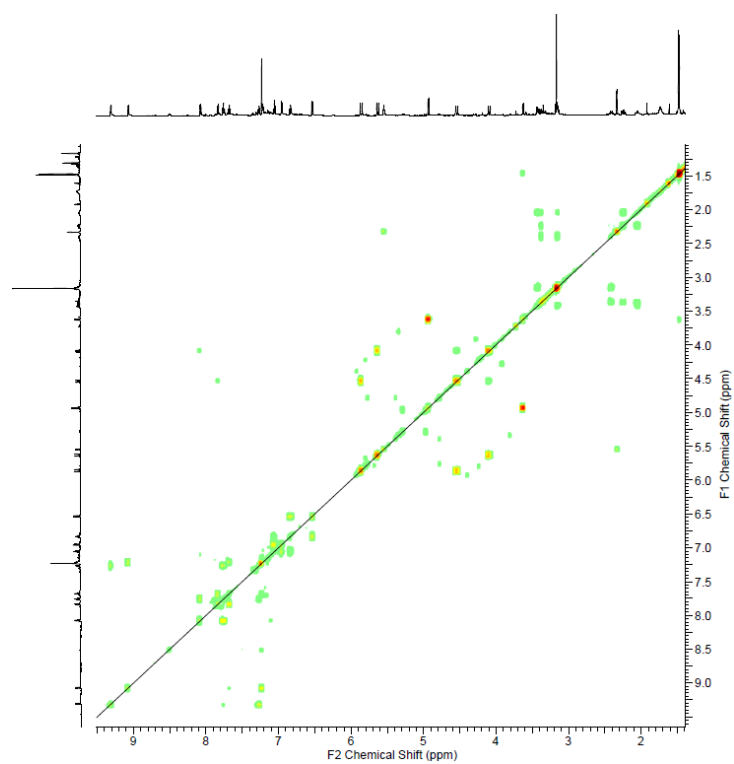


Figure A6.11 ^1H - ^1H gCOSY Spectrum of $[\text{Pd}^{\text{IV}}(\text{CH}_2\text{CMe}_2\text{C}_6\text{H}_4)(\kappa^3\text{-}N,N',N''\text{-6-L1})\text{I}][\text{I}]$, **6-3**, in CDCl_3 at 25°C

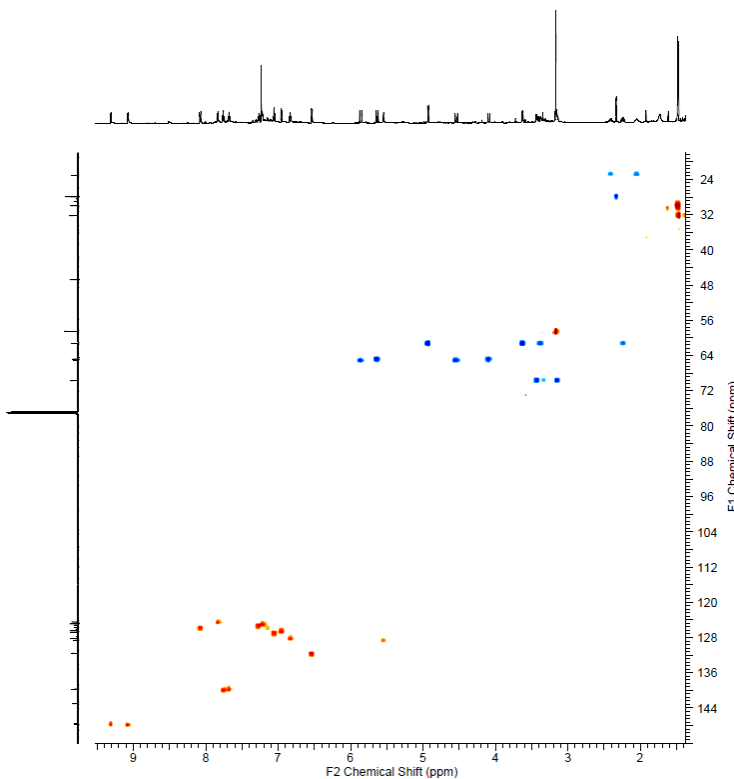


Figure A6.12 ^1H - $^{13}\text{C}\{^1\text{H}\}$ HSQC Spectrum of $[\text{Pd}^{\text{IV}}(\text{CH}_2\text{CMe}_2\text{C}_6\text{H}_4)(\kappa^3\text{-}N,N',N''\text{-6-L1})\text{I}][\text{I}]$, **6-3**, in CDCl_3 at 25°C

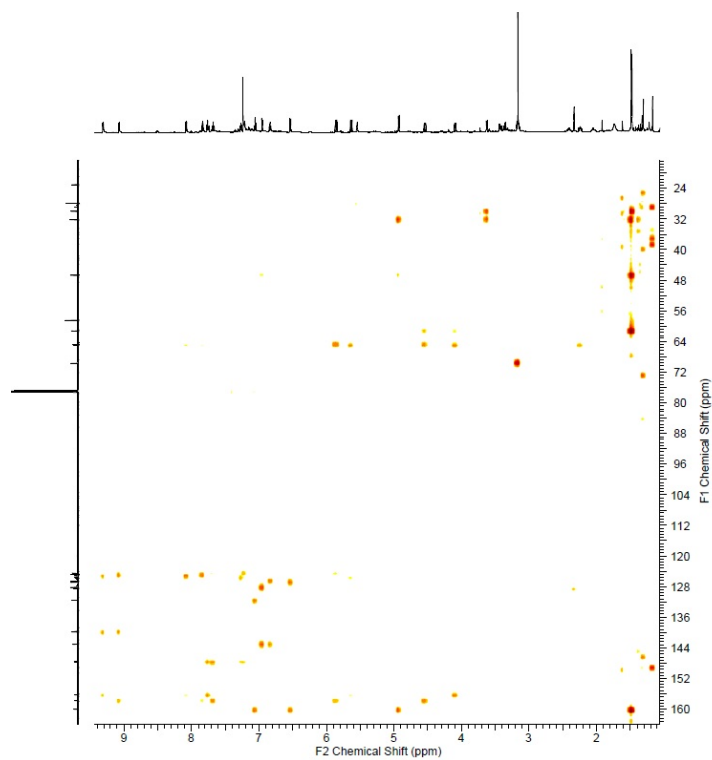


Figure A6.13 $^1\text{H}-^{13}\text{C}\{^1\text{H}\}$ HMBC Spectrum of $[\text{Pd}^{\text{IV}}(\text{CH}_2\text{CMe}_2\text{C}_6\text{H}_4)(\kappa^3\text{-N,N',N''-6-L1})\text{I}][\text{I}]$, **6-3**, in CDCl_3 at 25°C

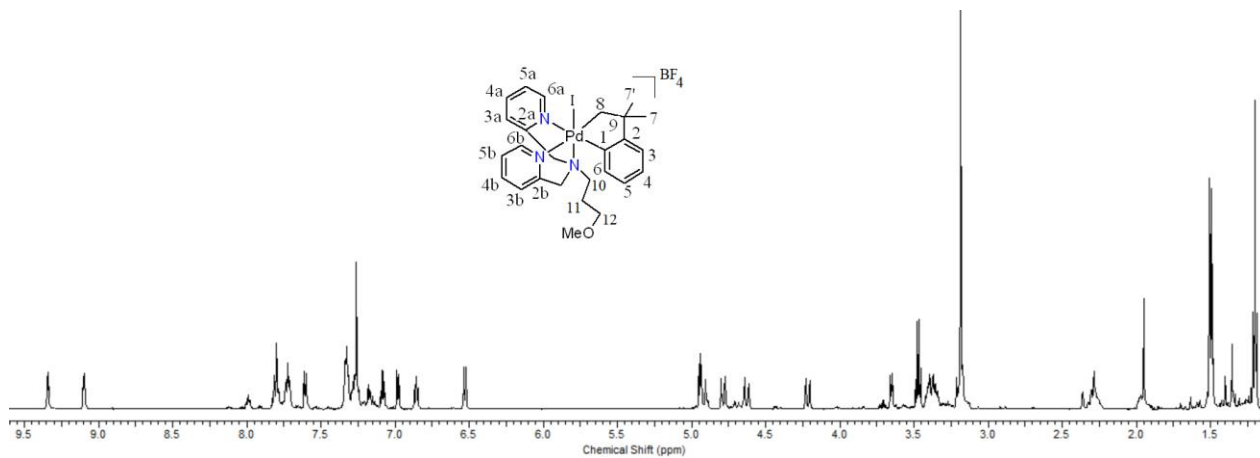


Figure A6.14 ^1H NMR Spectrum of $[\text{Pd}^{\text{IV}}(\text{CH}_2\text{CMe}_2\text{C}_6\text{H}_4)(\kappa^3\text{-N,N',N''-6-L1})\text{I}][\text{BF}_4]$, **6-3a**, in CDCl_3 at 25°C , 600 MHz.

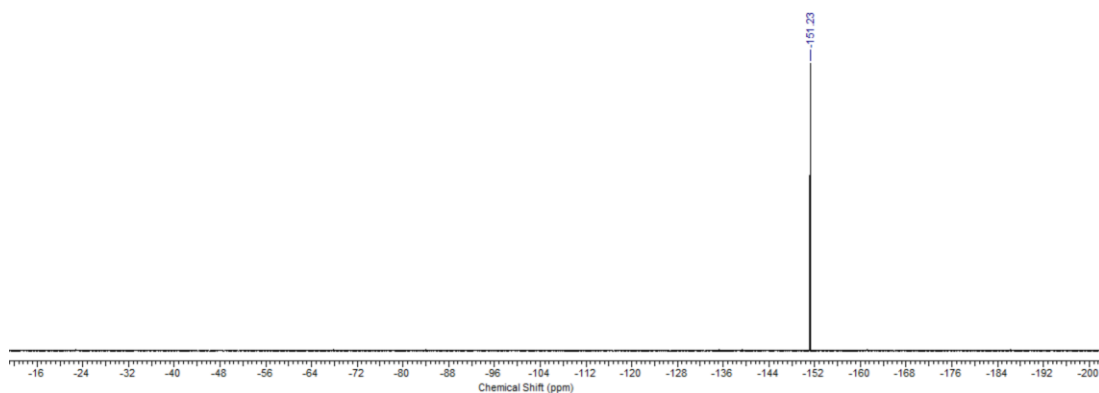


Figure A6.15 ^{19}F NMR Spectrum of $[\text{Pd}^{\text{IV}}(\text{CH}_2\text{CMe}_2\text{C}_6\text{H}_4)(\kappa^3\text{-N,N',N''-6-L1)I}][\text{BF}_4]$, **6-3a**, in CDCl_3 at 25°C

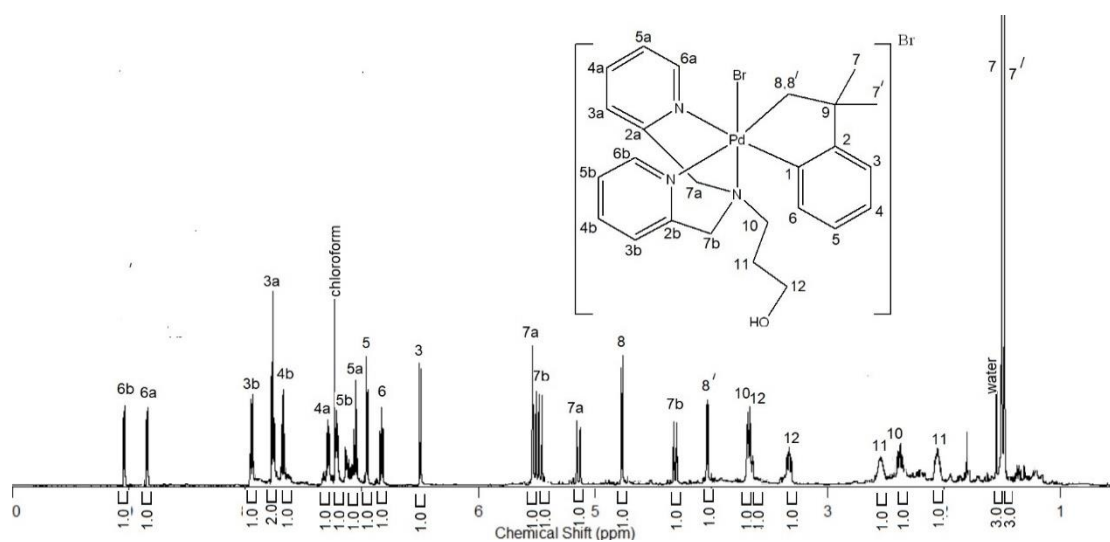


Figure A6.16 ^1H NMR Spectrum of $[\text{Pd}^{\text{IV}}(\text{CH}_2\text{CMe}_2\text{C}_6\text{H}_4)(\kappa^3\text{-N,N',N''-5-L1)Br}][\text{Br}]$, **6-4**, in CDCl_3 at 25°C , 600 MHz.

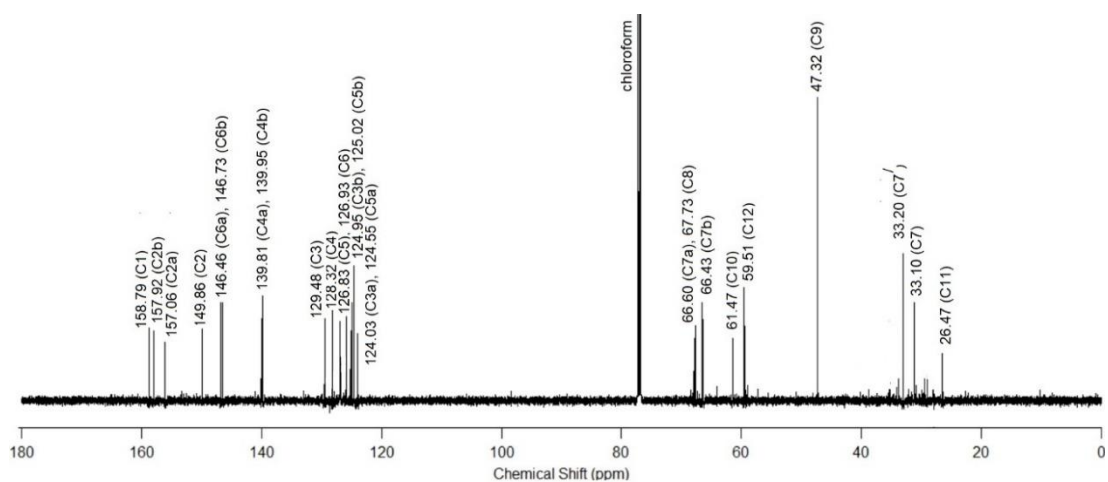


Figure A6.17 $^{13}\text{C}\{^1\text{H}\}$ NMR Spectrum of $[\text{Pd}^{\text{IV}}(\text{CH}_2\text{CMe}_2\text{C}_6\text{H}_4)(\kappa^3\text{-}N,N',N''\text{-}5\text{-L1})\text{Br}][\text{Br}]$, **6-4**, in CDCl_3 at 25°C , 151 MHz.

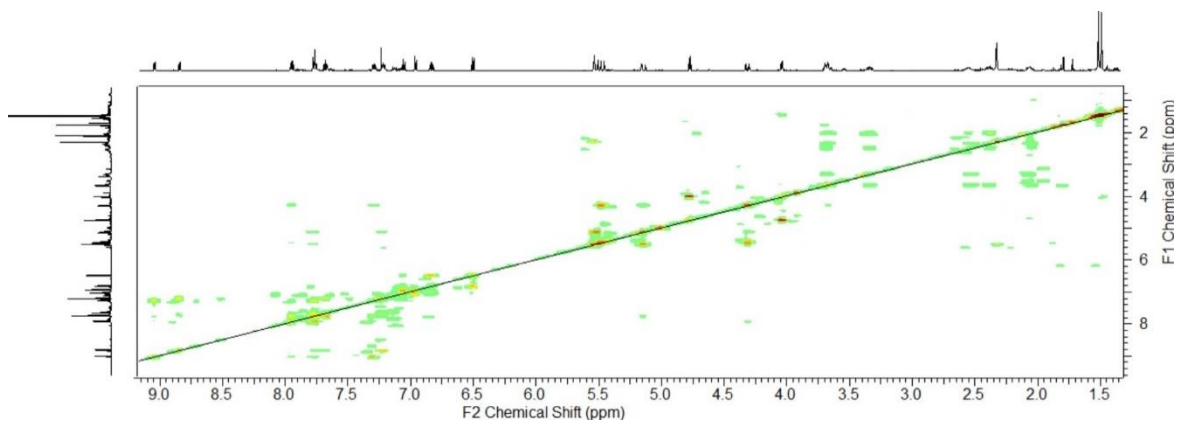


Figure A6.18 $^1\text{H}\text{-}^1\text{H}$ gCOSY Spectrum of $[\text{Pd}^{\text{IV}}(\text{CH}_2\text{CMe}_2\text{C}_6\text{H}_4)(\kappa^3\text{-}N,N',N''\text{-}5\text{-L1})\text{Br}][\text{Br}]$, **6-4**, in CDCl_3 at 25°C .

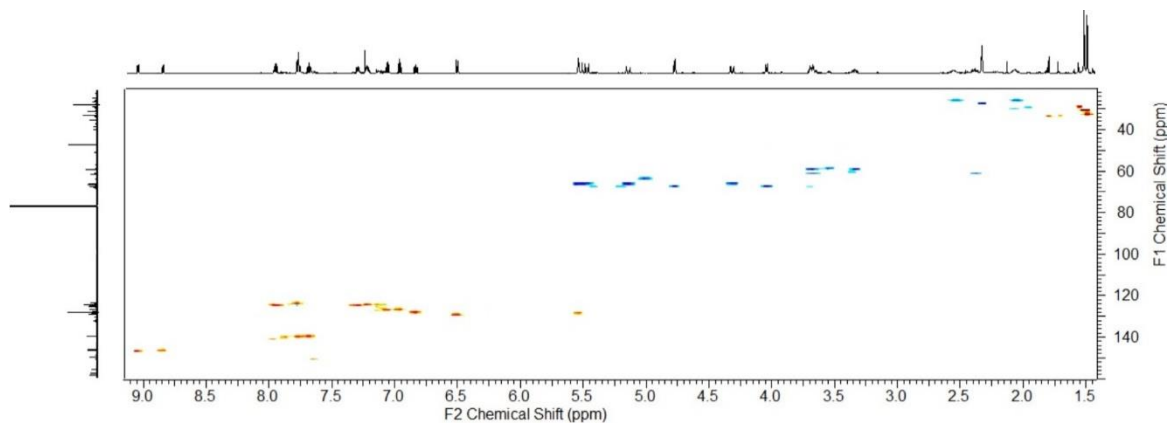


Figure A6.19 $^1\text{H}\text{-}^{13}\text{C}\{^1\text{H}\}$ HSQC Spectrum of $[\text{Pd}^{\text{IV}}(\text{CH}_2\text{CMe}_2\text{C}_6\text{H}_4)(\kappa^3\text{-}N,N',N''\text{-}5\text{-L1})\text{Br}][\text{Br}]$, **6-4**, in CDCl_3 at 25°C .

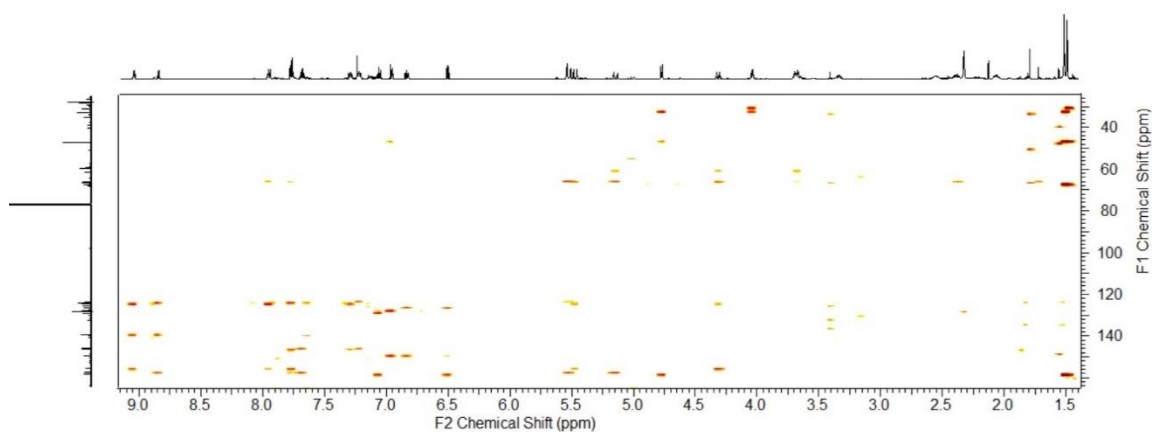


Figure A6.20 $^1\text{H}-^{13}\text{C}\{^1\text{H}\}$ HMBC Spectrum of $[\text{Pd}^{\text{IV}}(\text{CH}_2\text{CMe}_2\text{C}_6\text{H}_4)(\kappa^3\text{-}N,N',N''\text{-5-L1})\text{Br}][\text{Br}]$, **6-4**, in CDCl_3 at 25°C .

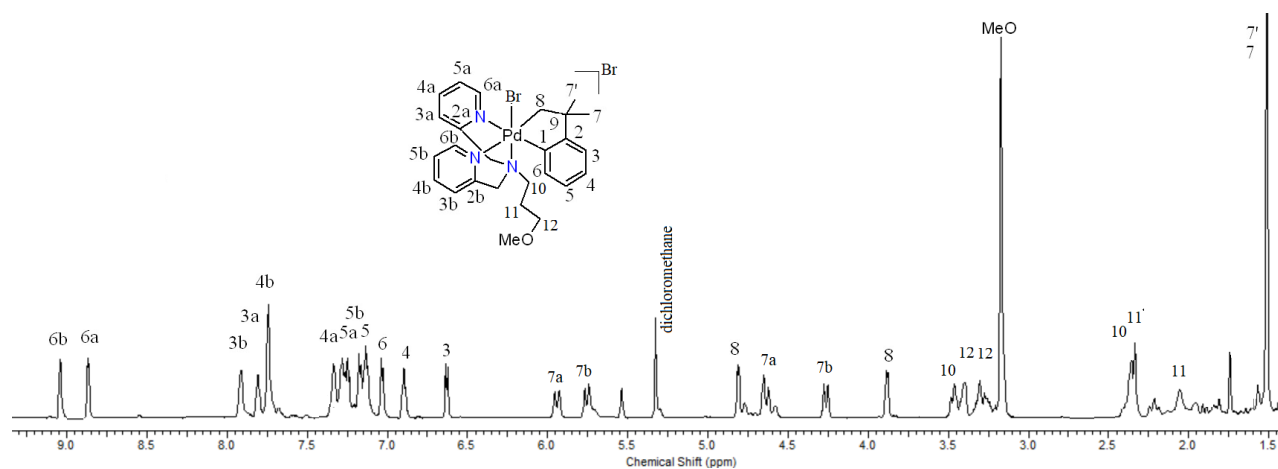


Figure A6.21 ^1H NMR Spectrum of $[\text{Pd}^{\text{IV}}(\text{CH}_2\text{CMe}_2\text{C}_6\text{H}_4)(\kappa^3\text{-}N,N',N''\text{-5-L1})\text{Br}][\text{Br}]$, **6-5**, in CD_2Cl_2 at -8°C , 600 MHz.

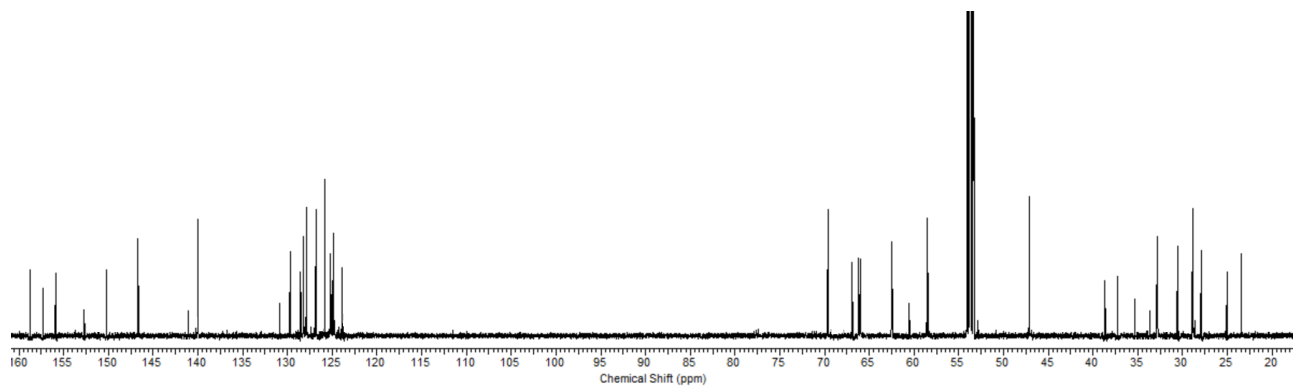


Figure A6.22 $^{13}\text{C}\{^1\text{H}\}$ NMR Spectrum of $[\text{Pd}^{\text{IV}}(\text{CH}_2\text{CMe}_2\text{C}_6\text{H}_4)(\kappa^3\text{-}N,N',N''\text{-5-L1})\text{Br}][\text{Br}]$, **6-5**, in CD_2Cl_2 at -8°C , 151 MHz.

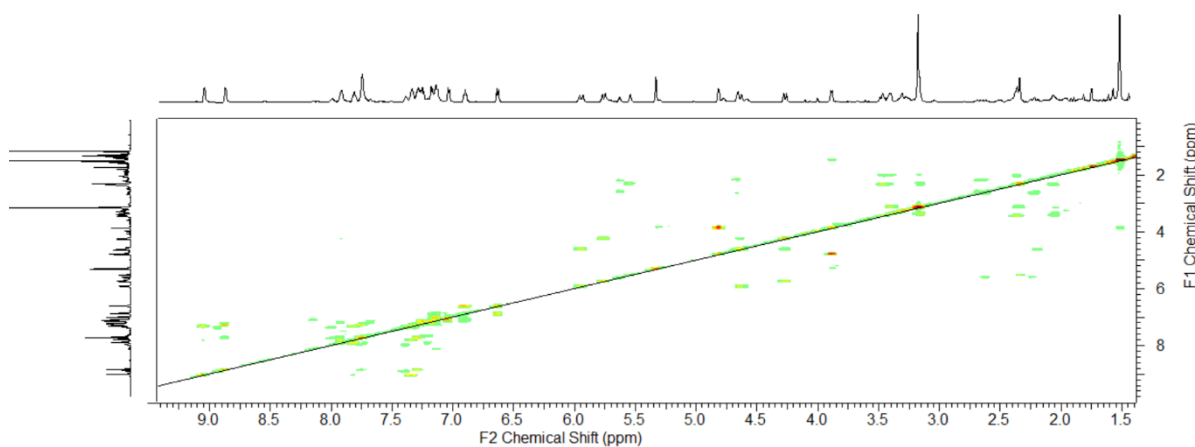


Figure A6.23 ^1H - ^1H COSY Spectrum of $[\text{Pd}^{\text{IV}}(\text{CH}_2\text{CMe}_2\text{C}_6\text{H}_4)(\kappa^3\text{-}N,N',N''\text{-}5\text{-L1})\text{Br}][\text{Br}]$, **6-5**, in CD_2Cl_2 at -8°C .

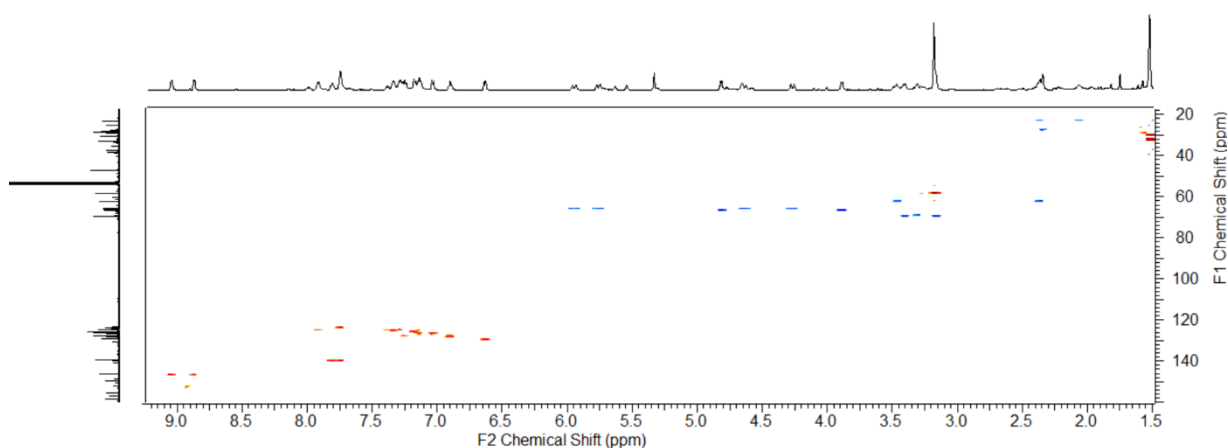


Figure A6.24 ^1H - $^{13}\text{C}\{^1\text{H}\}$ HSQC Spectrum of $[\text{Pd}^{\text{IV}}(\text{CH}_2\text{CMe}_2\text{C}_6\text{H}_4)(\kappa^3\text{-}N,N',N''\text{-}5\text{-L1})\text{Br}][\text{Br}]$, **6-5**, in CD_2Cl_2 at -8°C .

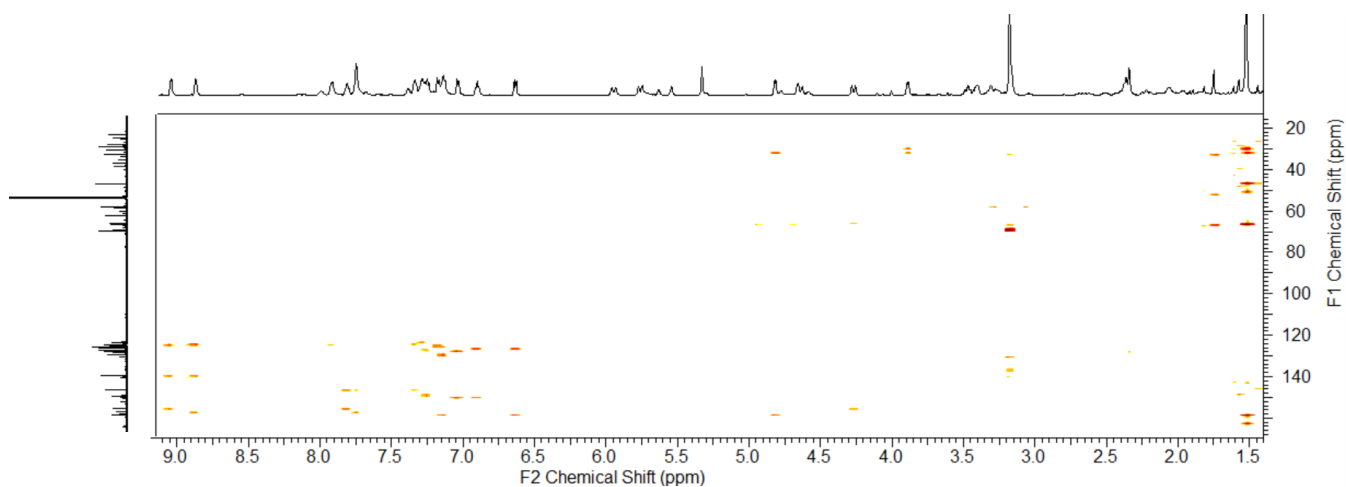


Figure A6.25 $^1\text{H}-^{13}\text{C}\{^1\text{H}\}$ HMBC Spectrum of $[\text{Pd}^{\text{IV}}(\text{CH}_2\text{CMe}_2\text{C}_6\text{H}_4)(\kappa^3\text{-}N,N',N''\text{-}5\text{-L1})\text{Br}][\text{Br}]$, **6-5**, in CD_2Cl_2 at -8°C .

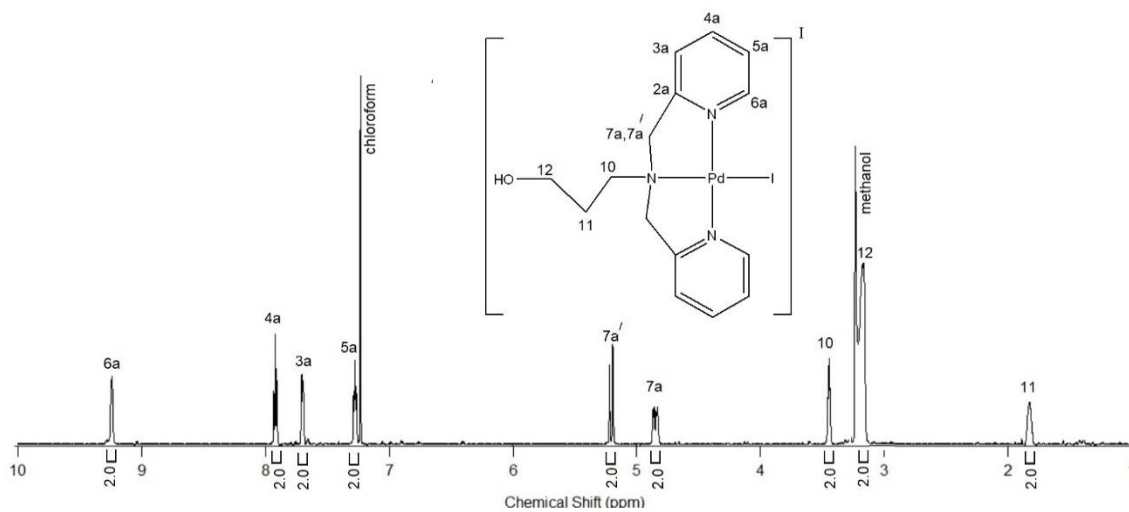


Figure A6.26 ^1H NMR Spectrum of $[\text{Pd}^{\text{II}}(\kappa^3\text{-}N,N',N''\text{-}5\text{-L1})\text{I}][\text{I}]$, **6-6**, in $\text{CDCl}_3:\text{CD}_3\text{OD}$, 1:0.3 at 25°C , 600 MHz.

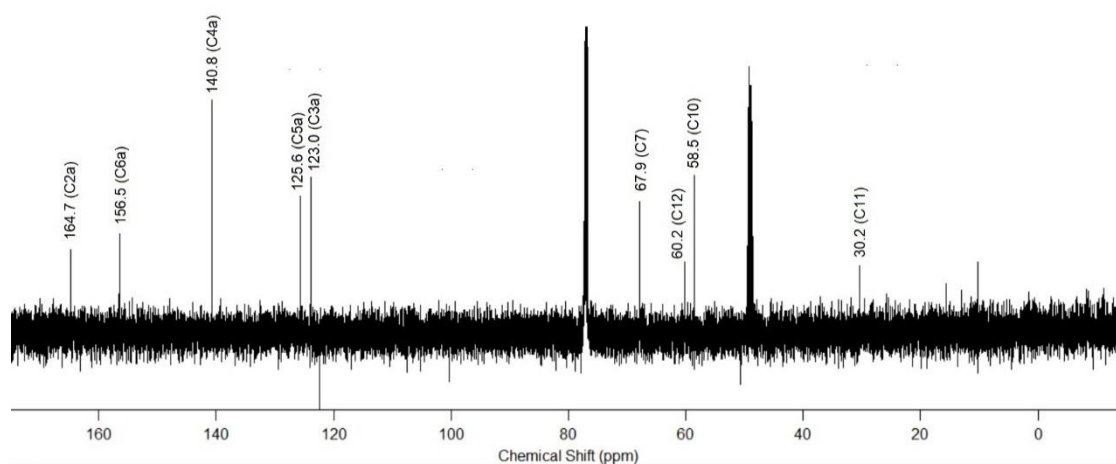


Figure A6.27 $^{13}\text{C}\{^1\text{H}\}$ NMR Spectrum of $[\text{Pd}^{\text{II}}(\kappa^3\text{-}N,N',N''\text{-}5\text{-L1})\text{I}][\text{I}]$, **6-6**, in $\text{CDCl}_3:\text{CD}_3\text{OD}$, 1:0.3 at 25°C , 151 MHz.

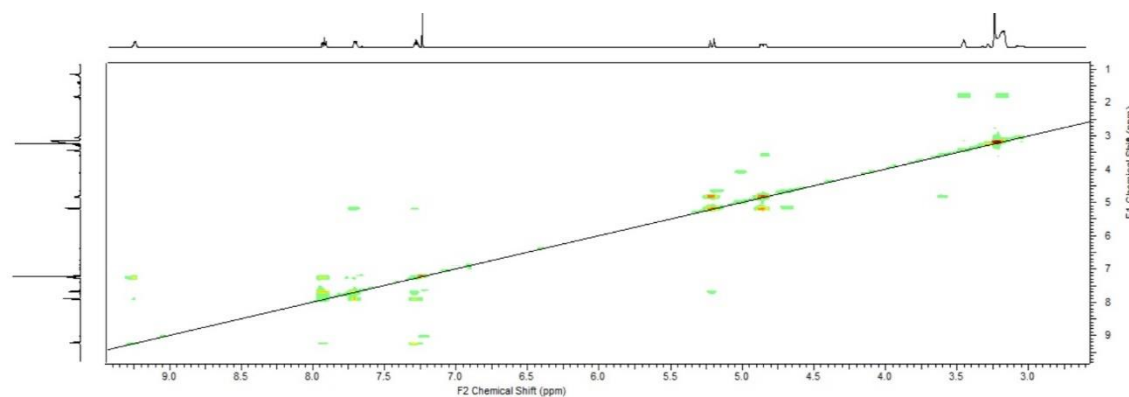


Figure A6.28 $^1\text{H}\text{-}^1\text{H}$ COSY Spectrum of $[\text{Pd}^{\text{II}}(\kappa^3\text{-}N,N',N''\text{-}5\text{-L1})\text{I}][\text{I}]$, **6-6**, in $\text{CDCl}_3:\text{CD}_3\text{OD}$, 1:0.3 at 25°C .

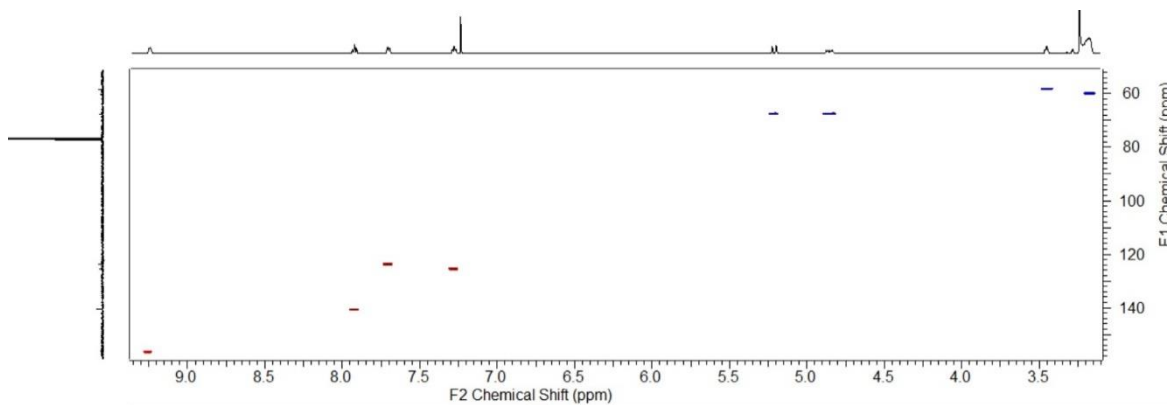


Figure A6.29 $^1\text{H}\text{-}^{13}\text{C}\{^1\text{H}\}$ HSQC Spectrum of $[\text{Pd}^{\text{II}}(\kappa^3\text{-}N,N',N''\text{-}5\text{-L1})\text{I}][\text{I}]$, **6-6**, in $\text{CDCl}_3:\text{CD}_3\text{OD}$, 1:0.3 at 25°C .

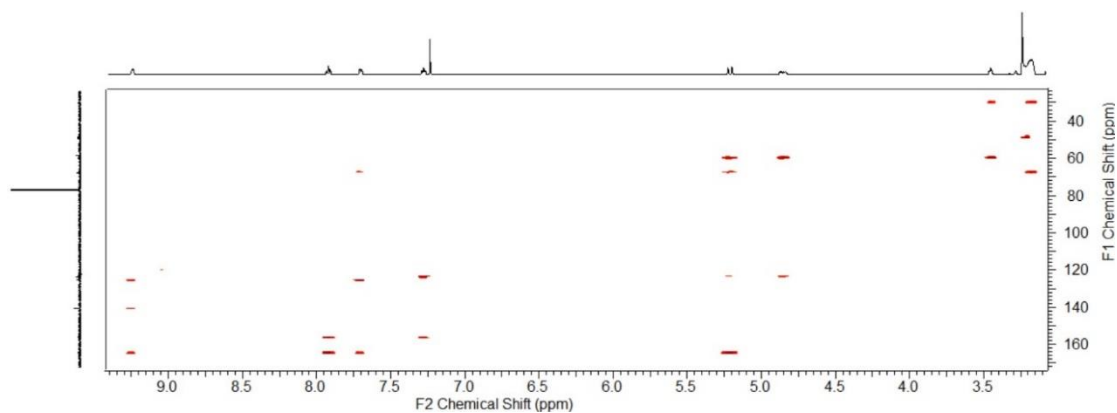


Figure A6.30 ^1H - $^{13}\text{C}\{^1\text{H}\}$ HMBC Spectrum of $[\text{Pd}^{\text{II}}(\kappa^3\text{-}N,N',N''\text{-}5\text{-L1})\text{I}][\text{I}]$, **6-6**, in $\text{CDCl}_3:\text{CD}_3\text{OD}$, 1:0.3 at 25°C .

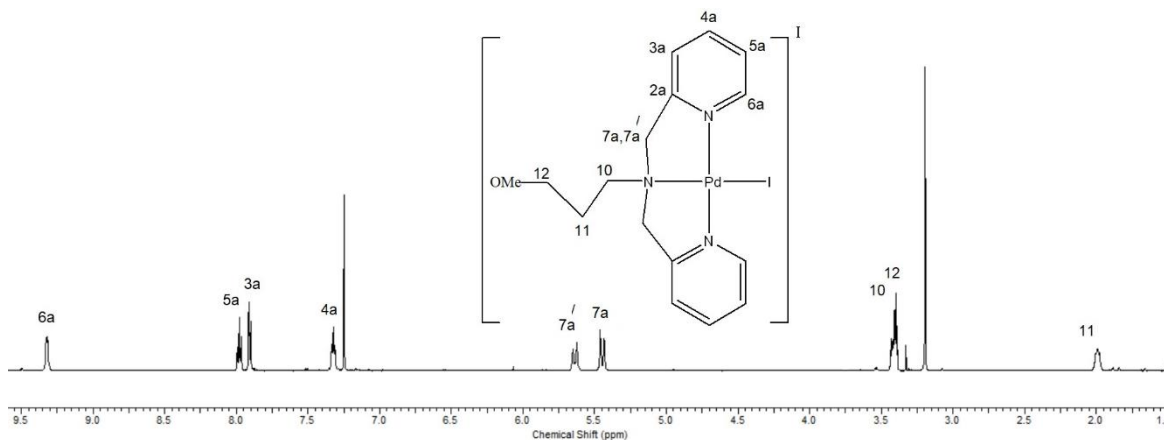


Figure A6.31 ^1H NMR Spectrum of $[\text{Pd}^{\text{II}}(\kappa^3\text{-}N,N',N''\text{-}5\text{-L1})\text{I}][\text{I}]$, **6-7**, in CDCl_3 at 25°C , 600 MHz.

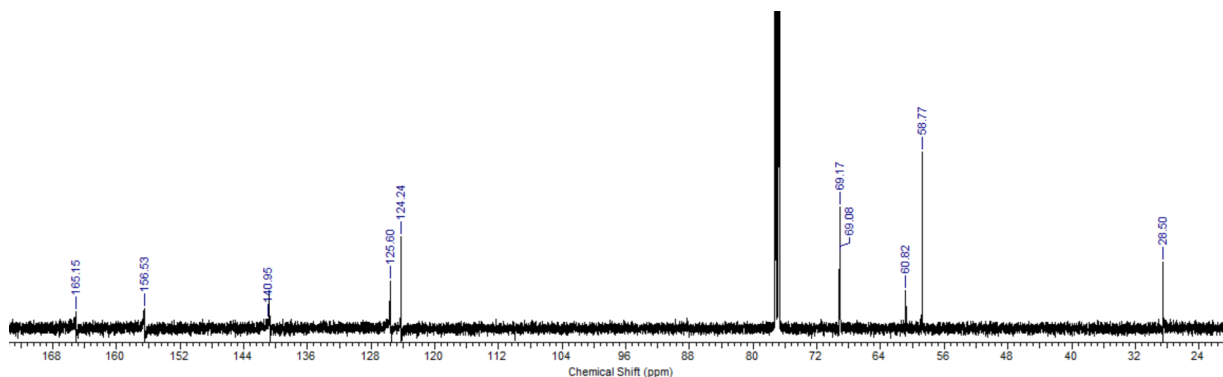


Figure A6.32 $^{13}\text{C}\{^1\text{H}\}$ spectrum of $[\text{Pd}^{\text{II}}(\kappa^3\text{-}N,N',N''\text{-}5\text{-L1})\text{I}][\text{I}]$, **6-7**, in CDCl_3 at 25°C , 151 MHz.

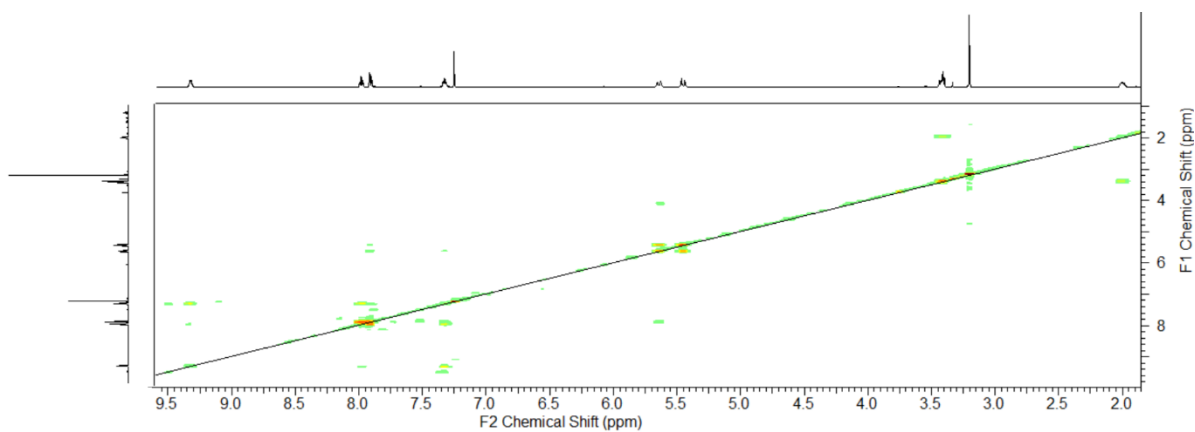


Figure A6.33 ^1H - ^1H COSY Spectrum of $[\text{Pd}^{\text{II}}(\kappa^3\text{-}N,N',N''\text{-}5\text{-L1})\text{I}][\text{I}]$, **6-7**, in CDCl_3 at 25°C .

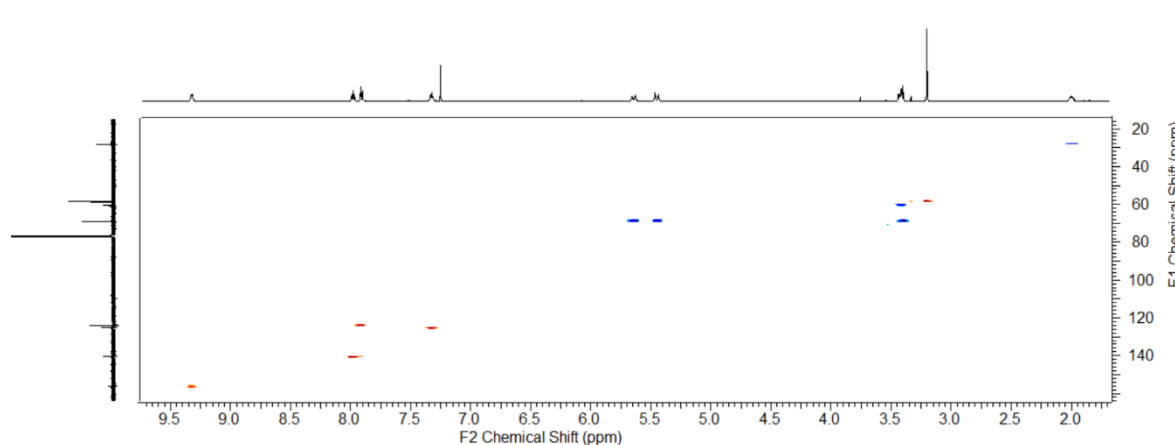


Figure A6.34 ^1H - $^{13}\text{C}\{^1\text{H}\}$ HSQC spectrum of $[\text{Pd}^{\text{II}}(\kappa^3\text{-}N,N',N''\text{-}5\text{-L1})\text{I}][\text{I}]$, **6-7**, CDCl_3 at 25°C .

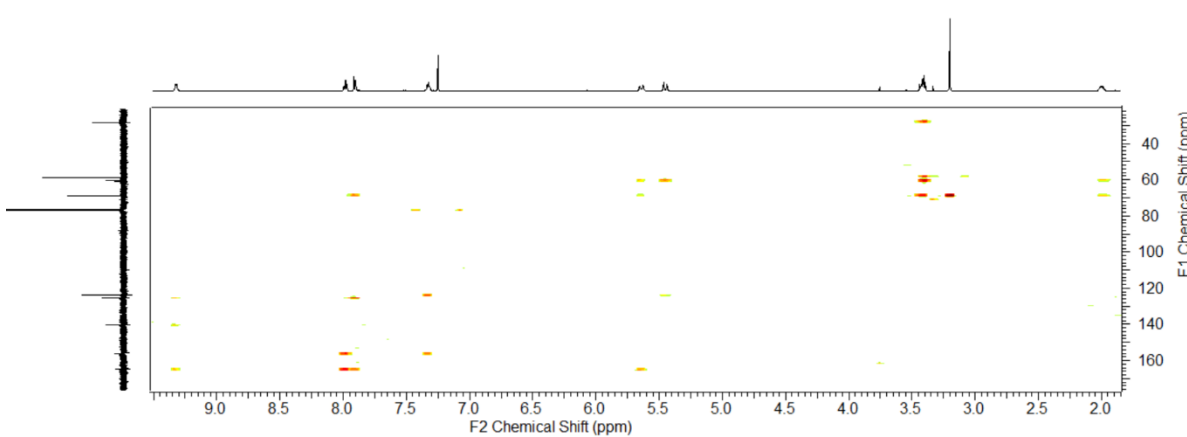


Figure A6.35 ^1H - $^{13}\text{C}\{^1\text{H}\}$ HMBC spectrum of $[\text{Pd}^{\text{II}}(\kappa^3\text{-}N,N',N''\text{-}5\text{-L1})\text{I}][\text{I}]$, **6-7**, CDCl_3 at 25°C .

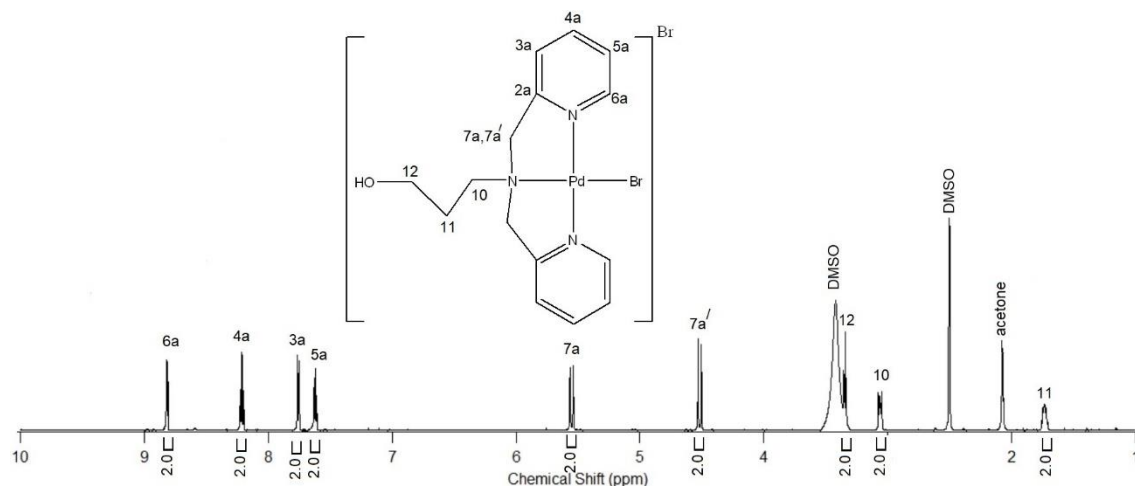


Figure A6.36 ^1H Spectrum of $[\text{Pd}^{\text{II}}(\kappa^3\text{-}N,N',N''\text{-}5\text{-L1})\text{Br}][\text{Br}]$, **6-8**, in $(\text{CD}_3)_2\text{SO}$, at 25°C , 600 MHz.

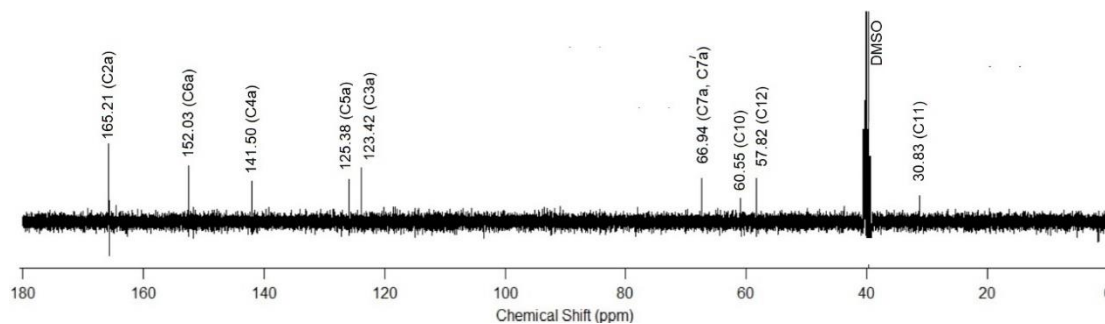


Figure A6.37 $^{13}\text{C}\{^1\text{H}\}$ spectrum of $[\text{Pd}^{\text{II}}(\kappa^3\text{-}N,N',N''\text{-}5\text{-L1})\text{Br}][\text{Br}]$, **6-8**, in $(\text{CD}_3)_2\text{SO}$, at 25°C , 151 MHz.

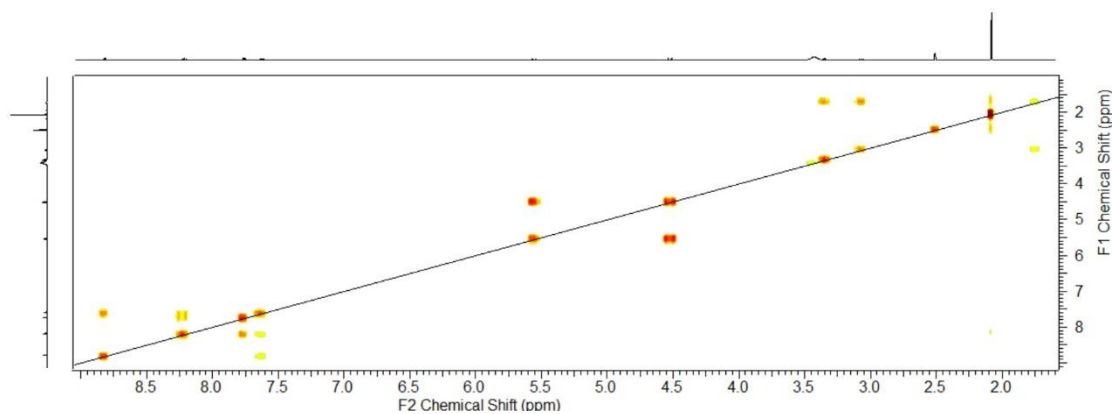


Figure A6.38 $^1\text{H}\text{-}^1\text{H}$ COSY spectrum of $[\text{Pd}^{\text{II}}(\kappa^3\text{-}N,N',N''\text{-}5\text{-L1})\text{Br}][\text{Br}]$, **6-8**, in $(\text{CD}_3)_2\text{SO}$, at 25°C .

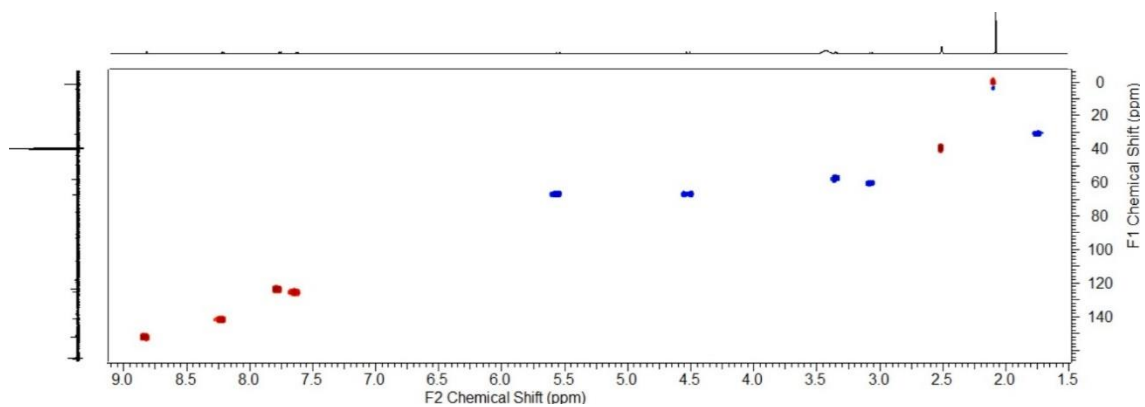


Figure A6.39 $^1\text{H}-^{13}\text{C}\{^1\text{H}\}$ HSQC spectrum of $[\text{Pd}^{\text{II}}(\kappa^3\text{-}N,N',N''\text{-5-L1})\text{Br}][\text{Br}]$, **6-8**, in $(\text{CD}_3)_2\text{SO}$, at 25°C .

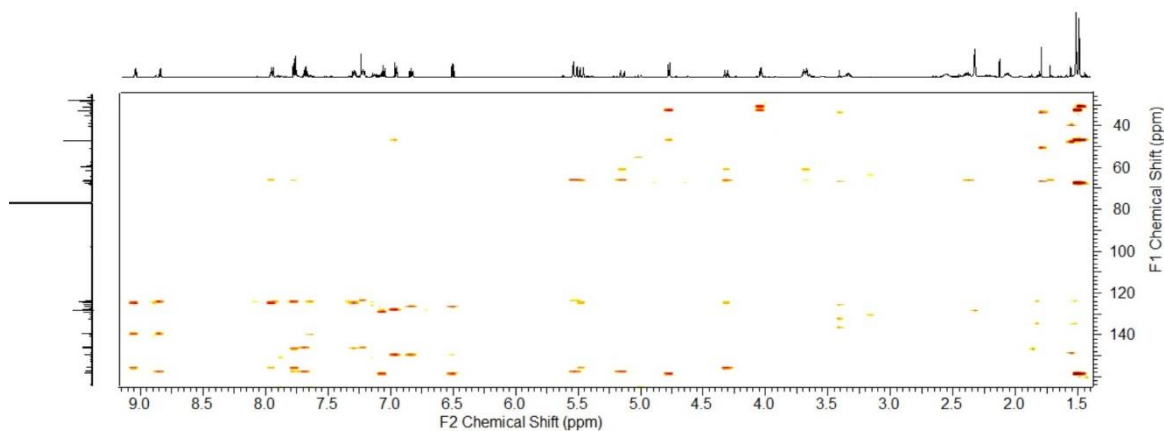


Figure A6.40 $^1\text{H}-^{13}\text{C}\{^1\text{H}\}$ HMBC spectrum of $[\text{Pd}^{\text{II}}(\kappa^3\text{-}N,N',N''\text{-5-L1})\text{Br}][\text{Br}]$, **6-8**, in $(\text{CD}_3)_2\text{SO}$, at 25°C .

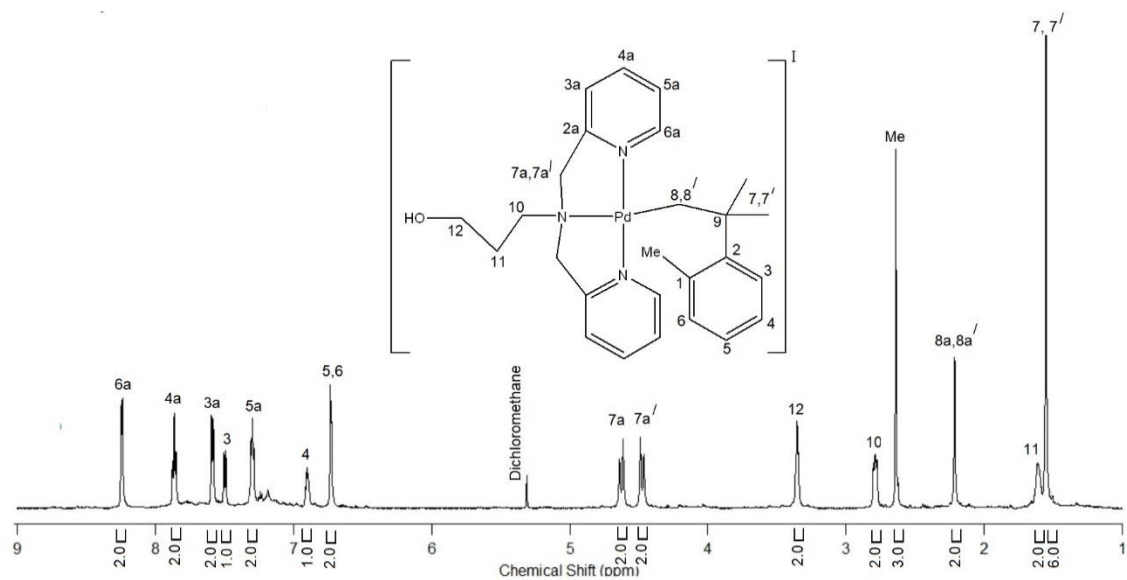


Figure A6.41 ¹H Spectrum of [Pd^{II}(CH₂CMe₂C₆H₄-CH₃)(κ²-N,N'-5-L1)][I], **6-12**, in CD₂Cl₂, at 25°C, 600 MHz.

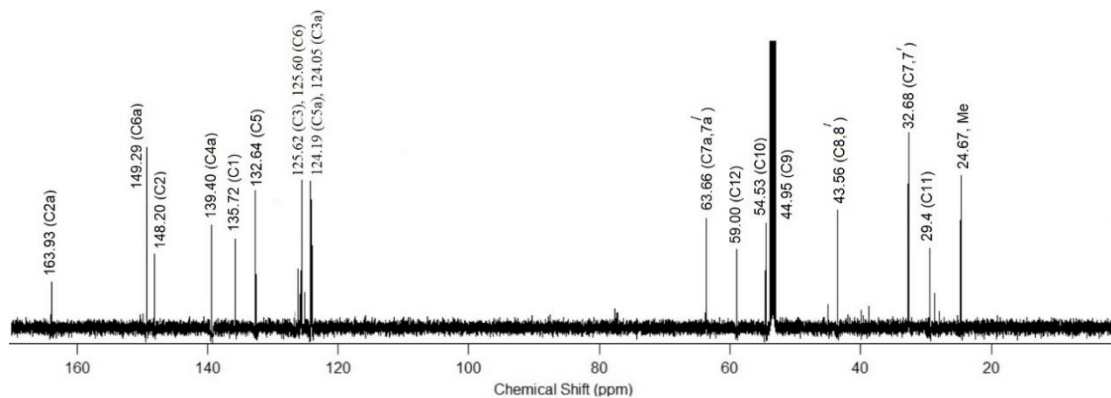


Figure A6.42 ¹³C{¹H} spectrum [Pd^{II}(CH₂CMe₂C₆H₄-CH₃)(κ²-N,N'-5-L1)][I], **6-12**, in CD₂Cl₂, at 25°C, 151 MHz.

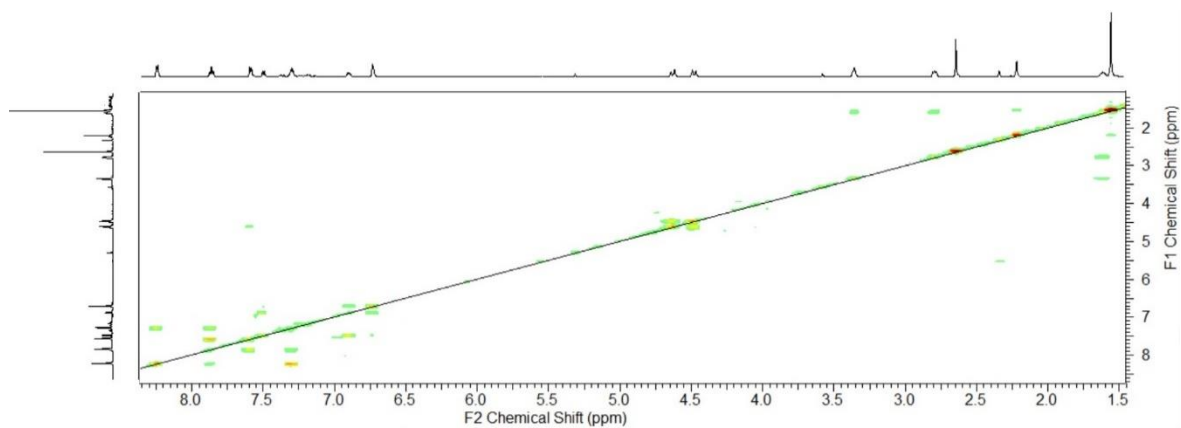


Figure A.643 ^1H - ^1H COSY Spectrum of $[\text{Pd}^{\text{II}}(\text{CH}_2\text{CMe}_2\text{C}_6\text{H}_4\text{-CH}_3)(\kappa^2\text{-}N,N'\text{-5-L1})][\text{I}]$, **6-12**, in CD_2Cl_2 , at 25°C .

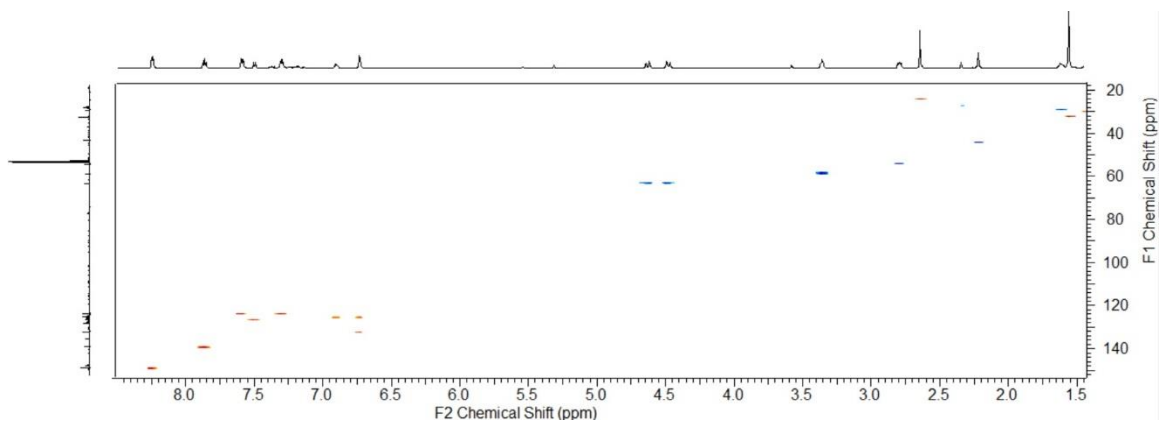


Figure A6.44 ^1H - $^{13}\text{C}\{^1\text{H}\}$ HSQC spectrum of $[\text{Pd}^{\text{II}}(\text{CH}_2\text{CMe}_2\text{C}_6\text{H}_4\text{-CH}_3)(\kappa^2\text{-}N,N'\text{-5-L1})][\text{I}]$, **6-12**, in CD_2Cl_2 , at 25°C .

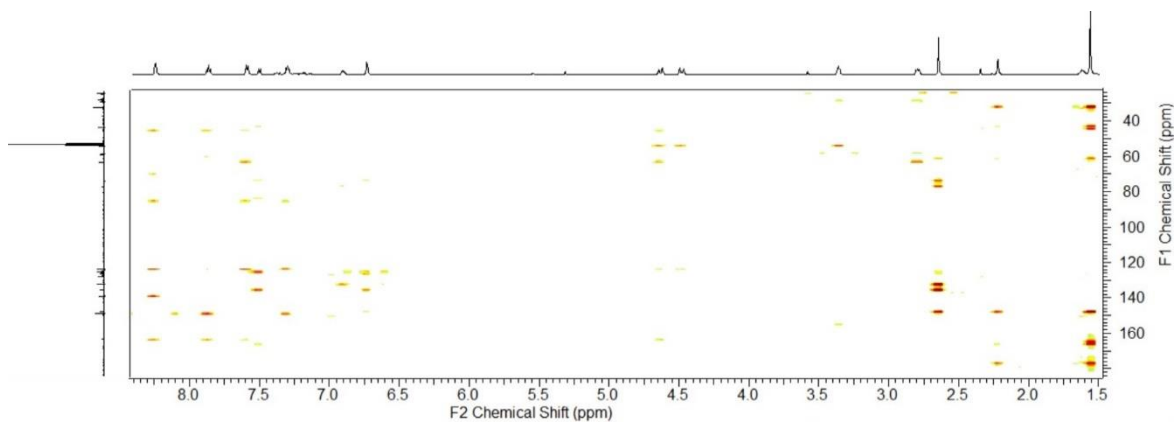


Figure A6.45 ^1H - $^{13}\text{C}\{^1\text{H}\}$ HMBC spectrum of $[\text{Pd}^{\text{II}}(\text{CH}_2\text{CMe}_2\text{C}_6\text{H}_4\text{-CH}_3)(\kappa^2\text{-}N,N'\text{-5-L1})][\text{I}]$, **6-12**, in CD_2Cl_2 , at 25°C .

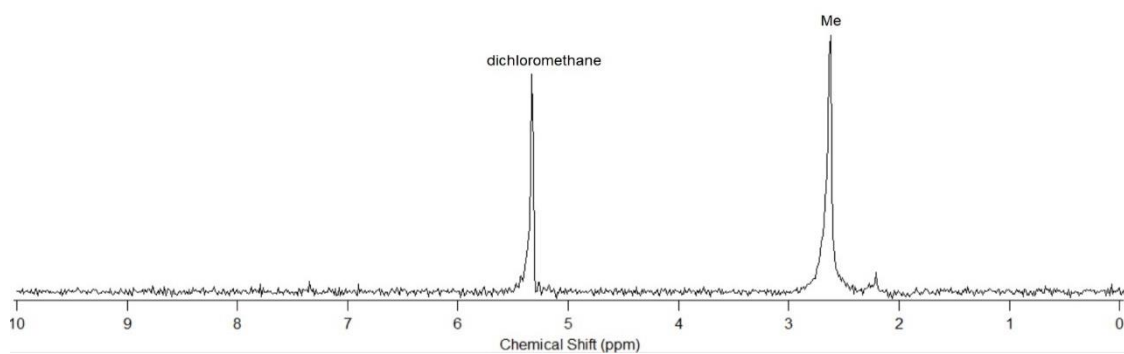


Figure A6.46 ^2H NMR Spectrum of $[\text{Pd}^{\text{II}}(\text{CH}_2\text{CMe}_2\text{C}_6\text{H}_4\text{-CH}_3)(\kappa^2\text{-N,N}'\text{-5-L1})][\text{I}]$, **6-12-d**, in CH_2Cl_2 , at 25°C .

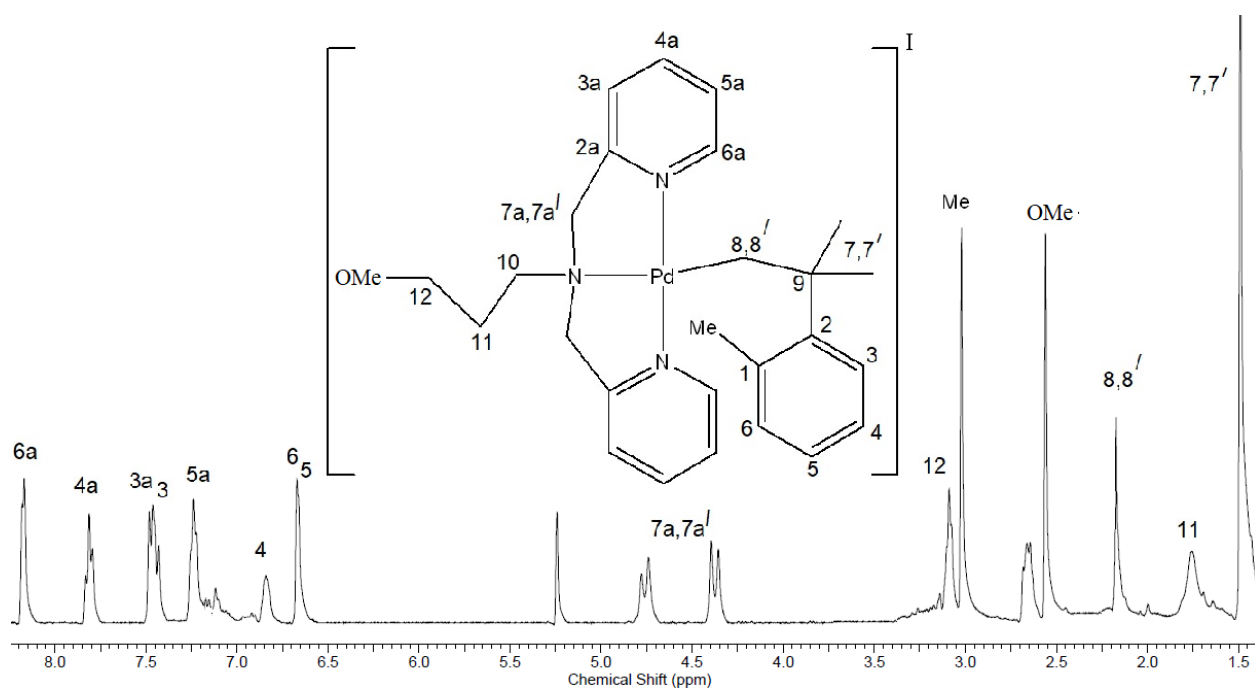


Figure A6.47 ^1H NMR Spectrum of $[\text{Pd}^{\text{II}}(\text{CH}_2\text{CMe}_2\text{C}_6\text{H}_4\text{-CD}_3)(\kappa^2\text{-N,N}'\text{-6-L1})][\text{I}]$, **6-13**, in CH_2Cl_2 , at 25°C , 600 MHz.

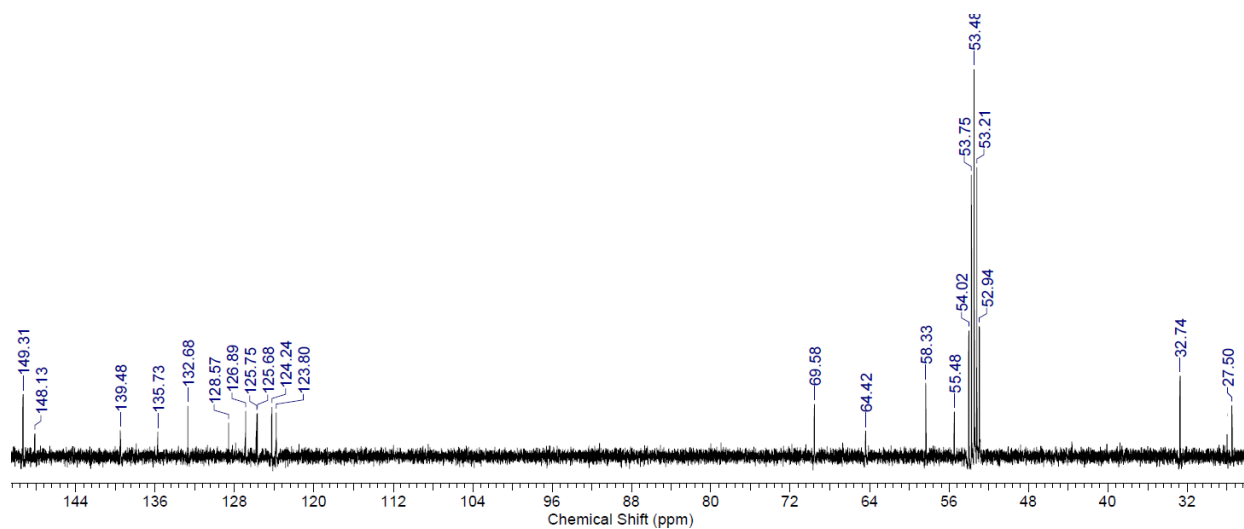


Figure A6.48 $^{13}\text{C}\{^1\text{H}\}$ NMR spectrum of $[\text{Pd}^{\text{II}}(\text{CH}_2\text{CMe}_2\text{C}_6\text{H}_4\text{-CD}_3)(\kappa^2\text{-N,N}'\text{-6-L1})][\text{I}]$, **6-13**, in CH_2Cl_2 , at 25°C , 151 MHz.

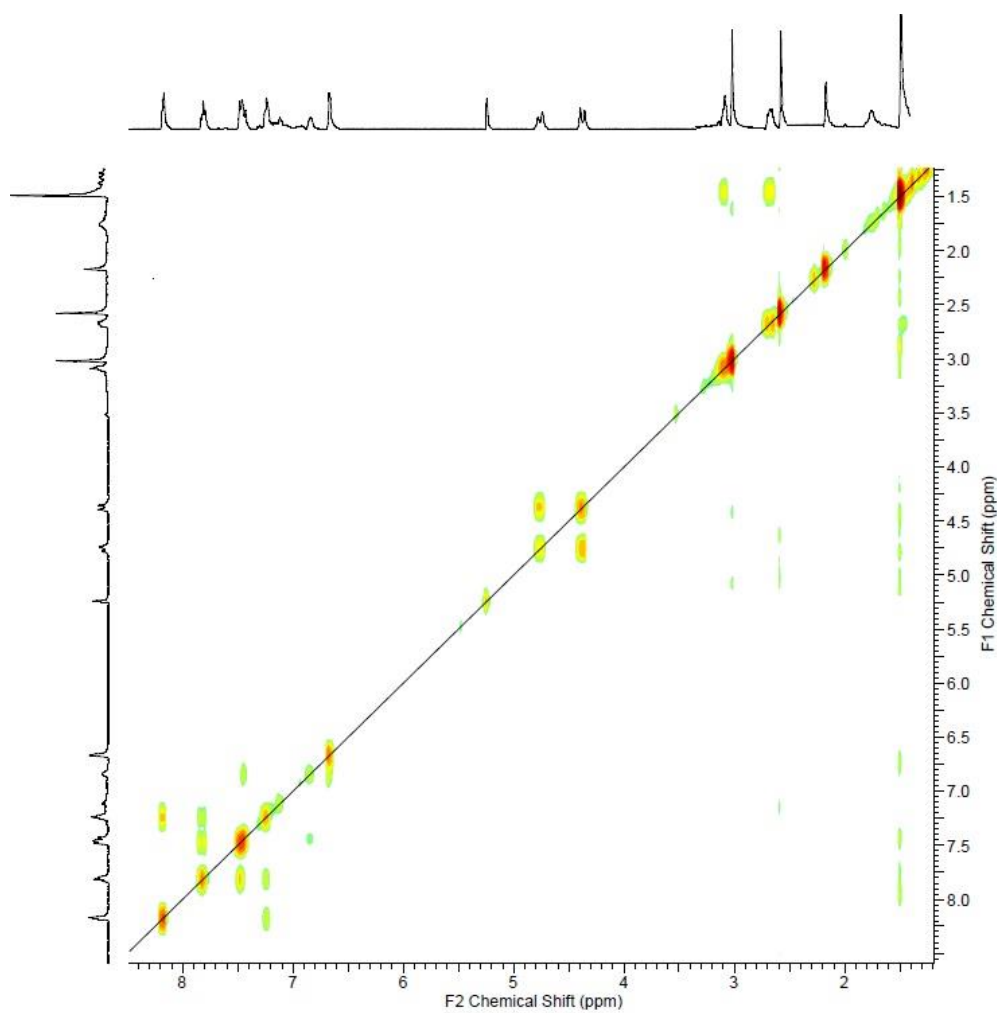


Figure A6.49 ^1H - ^1H COSY Spectrum of $[\text{Pd}^{\text{II}}(\text{CH}_2\text{CMe}_2\text{C}_6\text{H}_4\text{-CD}_3)(\kappa^2\text{-N,N}'\text{-6-L1})][\text{I}]$, **6-13**, in CH_2Cl_2 , at 25°C .

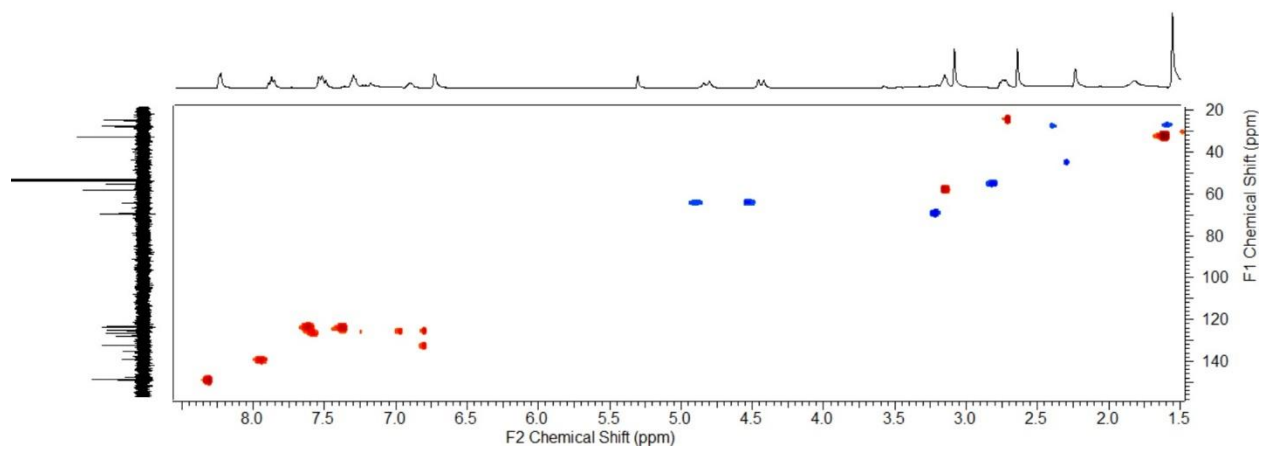


Figure A6.50 ^1H - $^{13}\text{C}\{^1\text{H}\}$ HSQC spectrum of $[\text{Pd}^{\text{II}}(\text{CH}_2\text{CMe}_2\text{C}_6\text{H}_4\text{-CD}_3)(\kappa^2\text{-N,N}'\text{-6-L1})][\text{I}]$, **6-13**, in CH_2Cl_2 , at 25°C .

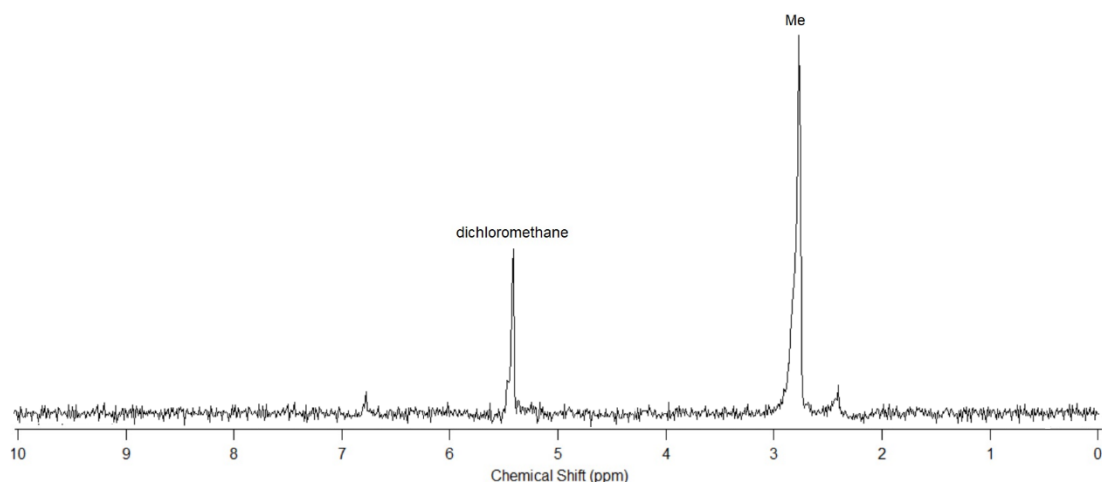


Figure A6.51 ^2H NMR Spectrum of $[\text{Pd}^{\text{II}}(\text{CH}_2\text{CMe}_2\text{C}_6\text{H}_4\text{-CD}_3)(\kappa^2\text{-N,N}'\text{-6-L1})][\text{I}]$, **6-13-d**, in CH_2Cl_2 .

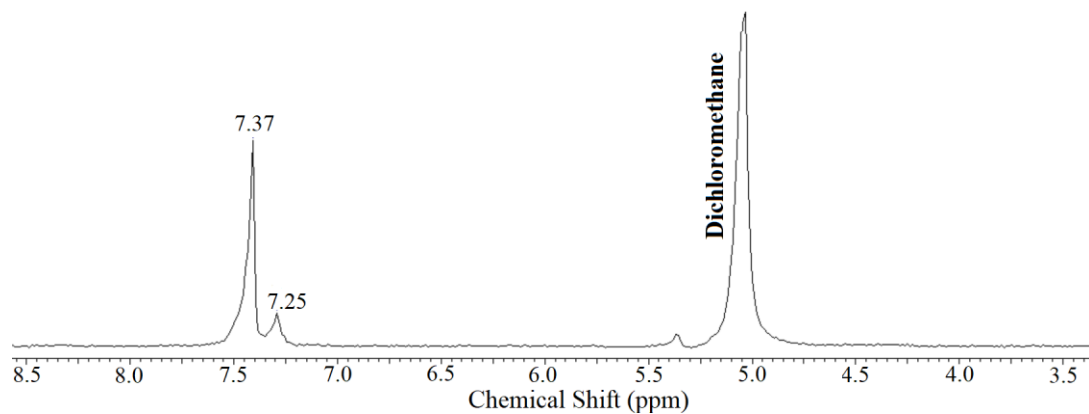


Figure A6.52 ^2H NMR spectrum (CH_2Cl_2) of reductive elimination reaction from **6-3** in $\text{CDCl}_3:\text{D}_2\text{O}$, at 25°C .

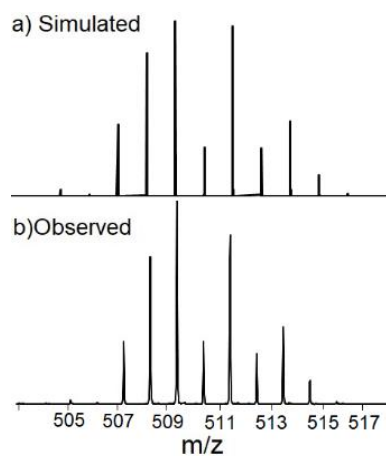


Figure A6.53 The MALDI MS isotope patterns for [6-1]•+ obtained using anthracene matrix: (a) simulated and (b) observed.

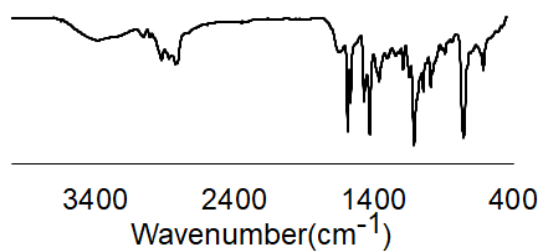


Figure A6.54 IR Spectrum of free ligand, 6-L1.

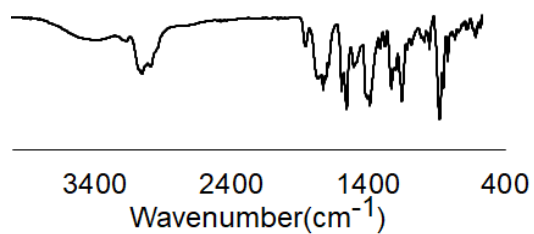


Figure A6.55 IR Spectrum of [Pd^{II}(CH₂CMe₂C₆H₄)(κ²-N,N'-6-L1)], 6-1.

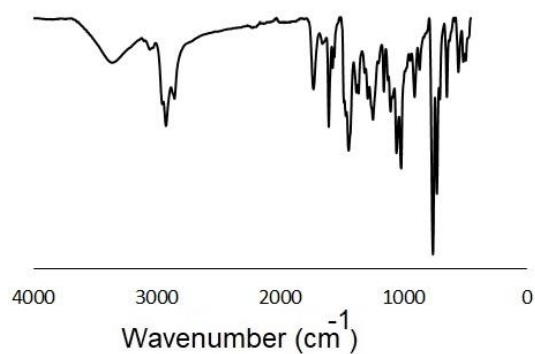


Figure A6.56 IR spectrum of $[\text{Pd}^{\text{IV}}(\text{CH}_2\text{CMe}_2\text{C}_6\text{H}_4)(\kappa^3\text{-N,N',N''-5-L1})\text{I}][\text{I}]$, **6-2**.

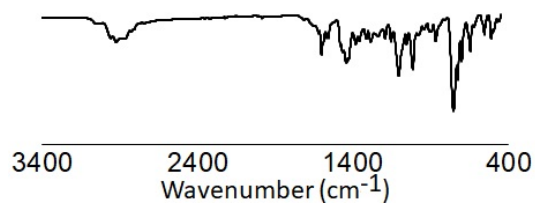


Figure A6.57 IR spectrum of $[\text{Pd}^{\text{IV}}(\text{CH}_2\text{CMe}_2\text{C}_6\text{H}_4)(\kappa^3\text{-N,N',N''-6-L1})\text{I}][\text{I}]$, **6-3**.

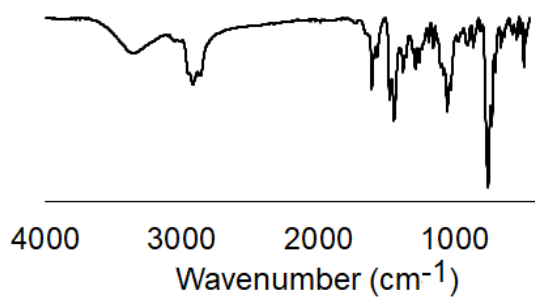


Figure A6.58 IR spectrum of $[\text{Pd}^{\text{IV}}(\text{CH}_2\text{CMe}_2\text{C}_6\text{H}_4)(\kappa^3\text{-N,N',N''-5-L1})\text{Br}][\text{Br}]$, **6-4**.

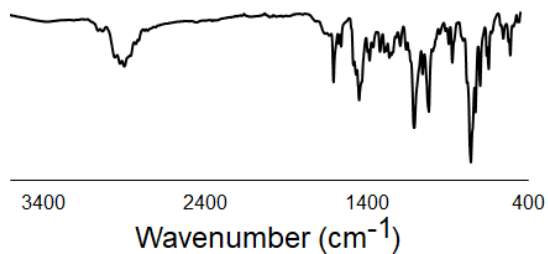


Figure A6.59 IR spectrum of $[\text{Pd}^{\text{IV}}(\text{CH}_2\text{CMe}_2\text{C}_6\text{H}_4)(\kappa^3\text{-N,N',N''-6-L1})\text{Br}][\text{Br}]$, **6-5**.

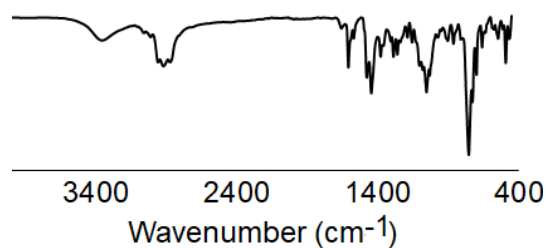


Figure A6.60 IR spectrum of $[\text{Pd}^{\text{II}}(\text{CH}_2\text{CMe}_2\text{C}_6\text{H}_4\text{-CH}_3)(\kappa^2\text{-N,N}'\text{-5-L1})][\text{I}]$, **6-12**.

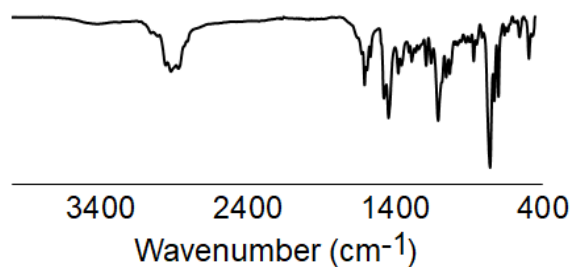


Figure A6.61 IR spectrum of $[\text{Pd}^{\text{II}}(\text{CH}_2\text{CMe}_2\text{C}_6\text{H}_4\text{-CH}_3)(\kappa^2\text{-N,N}'\text{-6-L1})][\text{I}]$, **6-13**.

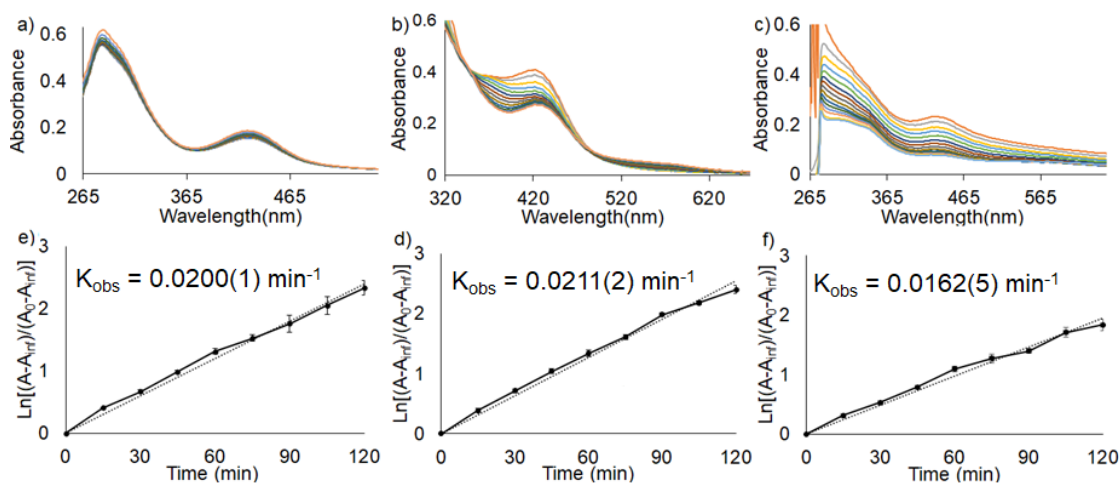


Figure A6.62 Above, UV-visible absorption spectra of complex **6-2** in a) methanol b) chloroform c) benzene (8.33×10^{-3} M, 50°C) during the reductive elimination reaction. Below, the corresponding first order plot of $\ln[(A-A_\infty)/(A_0-A_\infty)]$ versus time for e) methanol d) chloroform f) benzene.

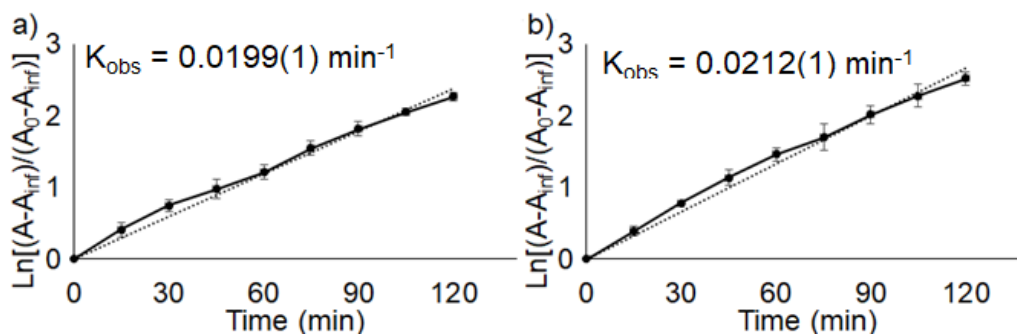


Figure A6.63 First order plot of $\ln[A-A_\infty]/[A_0-A_\infty]$ versus time for **6-2** in methanol (8.33×10^{-3} M) in the presence of excess a) sodium iodide b) pyridine.

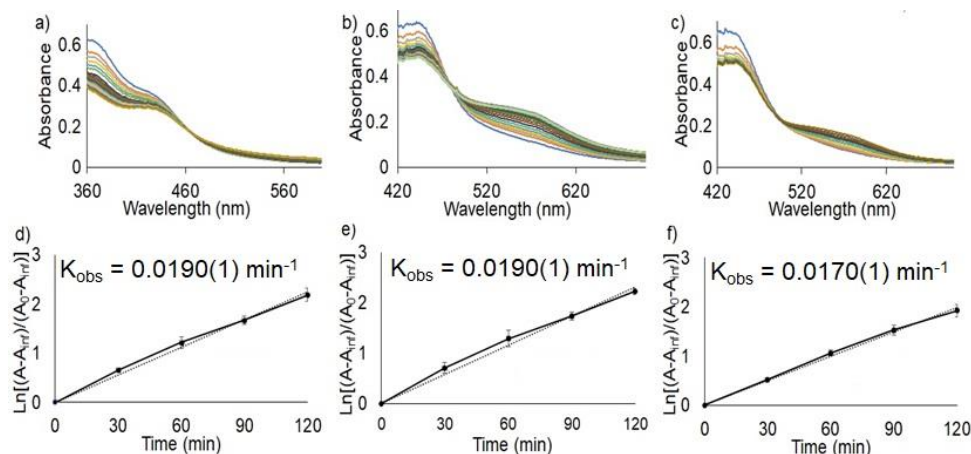


Figure A6.64 Above, UV-visible absorption spectra of complex **6-3** in a) methanol (8.33×10^{-3} M, 50°C) b) chloroform (8.33×10^{-3} M, 50°C) c) benzene (1.30×10^{-3} M, 50°C) during the reductive elimination reaction. Below, the corresponding first order plot of $\ln[A-A_\infty]/[A_0-A_\infty]$ versus time for e) methanol d) chloroform f) benzene.

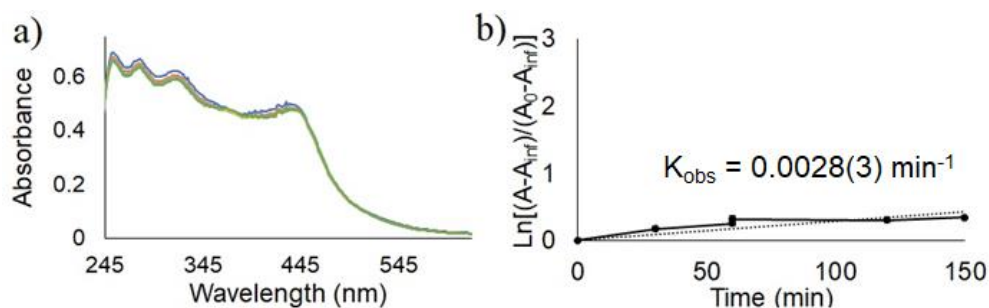


Figure A6.65 (a) UV-visible absorption spectra of complex **6-3a** in chloroform (4.33×10^{-3} M). (b) Corresponding first order plot of $\ln[A-A_\infty]/[A_0-A_\infty]$ versus time.

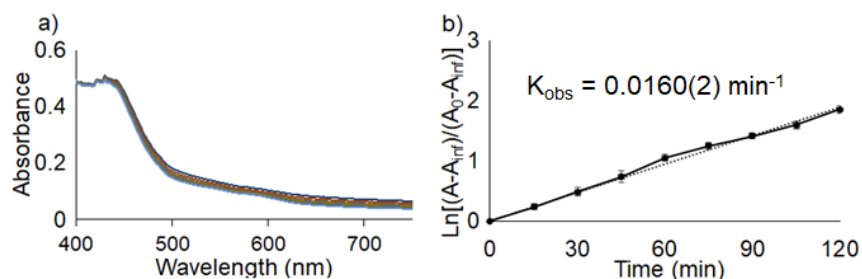


Figure A6.66 (a) UV-visible absorption spectra of complex **6-4** in chloroform (8.33×10^{-3} M). (b) Corresponding first order plot of $\ln[A-A_\infty]/[A_0-A_\infty]$ versus time.

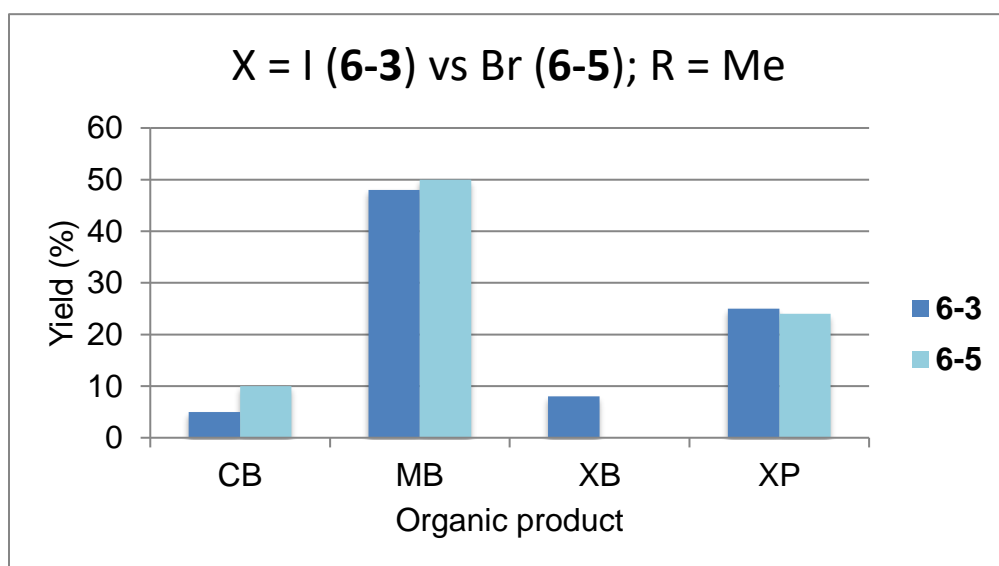


Figure A6.67 Observed products after reductive elimination from complexes **6-3** and **6-5** in CDCl_3 solution.

Table A6.1 Crystallographic data and parameters for compounds **6-2**, **6-4** and **6-6**, **6-7**, **6-8**, and **6-**

9.

	6-2 and 6-6	6-4	6-8	6-7	6-9
Formula	$\text{C}_{43}\text{H}_{56}\text{Br}_5\text{N}$ $6\text{O}_3\text{Pd}_2$	$\text{C}_{28}\text{H}_{37}\text{Br}_2\text{N}_3$ O_2Pd	$\text{C}_{15}\text{H}_{19}\text{Br}_2\text{N}_3$ OPd	$\text{C}_{17}\text{H}_{23}\text{Cl}_2\text{I}_2\text{N}_3$ OPd	$\text{C}_{16}\text{H}_{21}\text{Br}_2\text{N}_3\text{OPd}$ $\cdot\text{H}_2\text{O}$

	$\cdot\text{CO}(\text{CH}_3)_2$	$\cdot(\text{CH}_3)_2\text{CO}$			
Formula weight	1552.32	771.9	523.57	716.48	555.61
Crystal system	Triclinic	Orthorhombic	Monoclinic	Orthorhombic	Monoclinic
Space group	$P-1$	$Pca2_1$	$P2_1/c$	$Pbca$	$P2_1/c$
a [Å]	9.125(3)	18.365(4)	18.484(5)	11.291(11)	8.8407(12)
b [Å]	16.078(6)	8.298(2)	9.302(4)	15.345(11)	16.336(2)
c [Å]	17.370(7)	38.438(10)	21.445(8)	26.52(2)	26.695(3)
α [°]	74.749 (13)	90	90	90	90
β [°]	80.804 (11)	90	112.647(8)	90	91.781(2)
γ [°]	84.646 (17)	90	90	90	90
V [Å ³]	2423.9 (16)	5858(2)	3403(2)	4595(7)	3853.5(9)
Z	4	8	8	8	8
ρ_{cal} [g cm ⁻³]	1.953	1.619	2.044	2.071	1.884
μ (MoKa)	0.71073	0.71073	0.71073	0.71073	1.54178
$F(000)$	1368	2864	2032	2720	2136
T [K]	110	110	110	110	110
$\theta_{\text{min}}, \theta_{\text{max}}$ [°]	1.227, 24.749	2.455, 24.864	2.494, 24.750	3.80, 35.98	3.172, 58.964
Total reflns	41867	100603	54489	36363	22008
Unique reflns	8302	10094	5814	10622	5511

R_1	0.0335	0.0513	0.0458	0.0313	0.0389
$wR_2 [I \geq 2\sigma(I)]$	0.0885	0.1001	0.1232	0.0636	0.0905
R_1 (all data)	0.0386	0.0955	1.055	1.086	1.083
wR_2 (all data)	0.0967	0.1162	0.1285	0.0666	0.0919
GOF	1.112	1.027	1.055	1.086	1.083
Maximum shift/error	0.0001	0.001	0.001	0.003	0.002
Min & Max peak heights on final ΔF Map ($e^-/\text{\AA}$)	-1.253, 3.080	-1.128, 1.075	-1.128, 1.075	-1.066, 1.926	-0.711, 4.444

Where: $R_1 = \sum(|F_o| - |F_c|) / \sum F_o$; $wR_2 = [\sum(w(F_o^2 - F_c^2)^2) / \sum(wF_o^4)]^{1/2}$; $GOF = [\sum(w(F_o^2 - F_c^2)^2) / (\text{No. of reflns.} - \text{No. of params.})]^{1/2}$

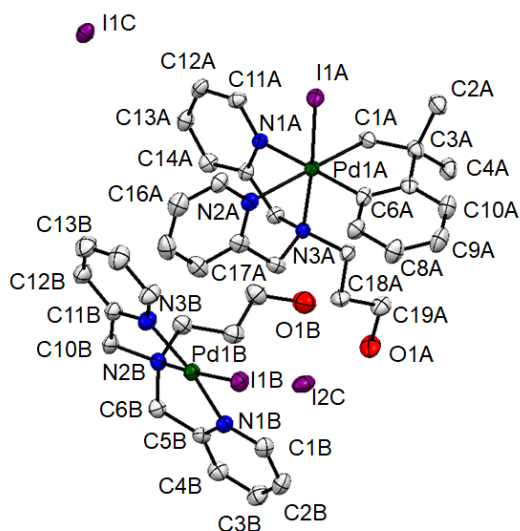


Figure A6.68 Displacement ellipsoid plot of 6-6 co-crystalized with 6-2 showing naming and numbering scheme. Ellipsoids are drawn at the 50% probability level and hydrogen atoms are omitted for clarity.

Table A6.2 Atomic coordinates for **6-2** and **6-6**.

Atom	x	y	z	U _{iso} /equiv
I1A	0.73514(4)	0.84294(3)	0.10168(2)	0.02850(11)
Pd1A	0.57361(4)	0.78078(3)	0.23732(2)	0.01992(11)
O1A	-0.0147(5)	0.6613(3)	0.5345(3)	0.0445(12)
N1A	0.6745(5)	0.8423(3)	0.3100(3)	0.0212(9)
N2A	0.4538(5)	0.7200(3)	0.3561(3)	0.0213(9)
N3A	0.7354(5)	0.6721(3)	0.2801(3)	0.0248(10)
C1A	0.4182(6)	0.8821(4)	0.2077(3)	0.0265(12)
C2A	0.3137(6)	0.8681(4)	0.1521(3)	0.0292(13)
C3A	0.1521(6)	0.8862(4)	0.1887(4)	0.0365(15)
C4A	0.3433(7)	0.9311(5)	0.0682(4)	0.0388(15)
C5A	0.3384(6)	0.7758(4)	0.1454(3)	0.0265(12)
C6A	0.4582(6)	0.7260(4)	0.1774(3)	0.0257(12)
C7A	0.4852(7)	0.6414(4)	0.1734(4)	0.0309(13)
C8A	0.3907(7)	0.6043(5)	0.1372(4)	0.0381(15)
C9A	0.2717(7)	0.6531(5)	0.1050(4)	0.0410(16)
C10A	0.2451(7)	0.7386(5)	0.1091(4)	0.0372(15)
C11A	0.7900(6)	0.8936(4)	0.2860(4)	0.0265(12)
C12A	0.8573(6)	0.9214(4)	0.3403(4)	0.0305(13)
C13A	0.8064(6)	0.8947(4)	0.4215(4)	0.0303(13)
C14A	0.6883(6)	0.8415(4)	0.4469(3)	0.0262(12)
C15A	0.6233(6)	0.8177(3)	0.3894(3)	0.0216(11)
C16A	0.4846(6)	0.7682(4)	0.4137(3)	0.0236(11)
C17A	0.2881(6)	0.7189(4)	0.3605(3)	0.0266(12)
C18A	0.2079(6)	0.6703(4)	0.4422(4)	0.0321(13)
C19A	0.0487(7)	0.7045(4)	0.4550(4)	0.0335(14)
C20A	0.5174(7)	0.6286(4)	0.3773(3)	0.0267(12)
C21A	0.6816(7)	0.6197(4)	0.3508(3)	0.0265(12)
C22A	0.7716(7)	0.5560(4)	0.3946(4)	0.0336(14)
C23A	0.9199(8)	0.5449(4)	0.3643(4)	0.0404(16)
C24A	0.9743(7)	0.5986(4)	0.2909(4)	0.0382(15)
C25A	0.8801(7)	0.6619(4)	0.2513(4)	0.0298(13)
I1B	0.97420(4)	0.10932(3)	0.08593(2)	0.03057(11)

Pd1B	1.00018(5)	0.17106(3)	0.20648(2)	0.02343(11)
O1B	0.6182(6)	0.4453(3)	0.2049(3)	0.0470(12)
N1B	0.8005(5)	0.1350(3)	0.2704(3)	0.0240(10)
N2B	1.0100(5)	0.2277(3)	0.2985(3)	0.0263(10)
N3B	1.2102(6)	0.2123(3)	0.1687(3)	0.0308(11)
C1B	0.6858(7)	0.1056(4)	0.2462(4)	0.0289(13)
C2B	0.5568(7)	0.0805(4)	0.2988(4)	0.0339(14)
C3B	0.5452(7)	0.0880(4)	0.3765(4)	0.0355(14)
C4B	0.6595(7)	0.1200(4)	0.4011(4)	0.0322(13)
C5B	0.7876(6)	0.1429(4)	0.3472(3)	0.0254(12)
C6B	0.9198(7)	0.1748(4)	0.3705(3)	0.0280(12)
C7B	0.9555(7)	0.3211(4)	0.2783(4)	0.0311(13)
C8B	0.8023(7)	0.3368(4)	0.2544(4)	0.0353(14)
C9B	0.7569(8)	0.4324(4)	0.2316(4)	0.0388(15)
C10B	1.1711(7)	0.2240(4)	0.3066(4)	0.0299(13)
C11B	1.2629(7)	0.2408(4)	0.2255(4)	0.0300(13)
C12B	1.3969(7)	0.2801(4)	0.2084(4)	0.0370(15)
C13B	1.4807(8)	0.2884(5)	0.1328(4)	0.0452(17)
C14B	1.4291(8)	0.2566(5)	0.0769(4)	0.0453(17)
C15B	1.2925(7)	0.2197(4)	0.0958(4)	0.0365(15)
O1S	1.0703(9)	0.4162(5)	0.0875(4)	0.098(3)
C1S	1.2732(11)	0.4771(6)	-0.0070(6)	0.069(2)
C2S	1.1420(9)	0.4218(5)	0.0221(5)	0.053(2)
C3S	1.1018(10)	0.3765(6)	-0.0348(6)	0.062(2)
I2C	0.38444(5)	0.39920(3)	0.39173(2)	0.03731(12)
I1C	1.19990(4)	0.97100(2)	0.39933(2)	0.03006(11)
H1AA	-0.103653	0.679221	0.543187	0.067
H1AB	0.357972	0.890917	0.257978	0.032
H1AC	0.471089	0.935480	0.181131	0.032
H3AA	0.138827	0.946280	0.192479	0.055
H3AB	0.083719	0.876334	0.154328	0.055
H3AC	0.131276	0.847492	0.242707	0.055
H4AA	0.326920	0.990598	0.073308	0.058
H4AB	0.446279	0.921732	0.044222	0.058

H4AC	0.275490	0.920931	0.033539	0.058
H7AA	0.567742	0.608349	0.195145	0.037
H8AA	0.408386	0.545813	0.134746	0.046
H9AA	0.207934	0.628214	0.079991	0.049
H10A	0.162954	0.771752	0.087118	0.045
H11A	0.826687	0.911294	0.230203	0.032
H12A	0.937632	0.958517	0.321668	0.037
H13A	0.851922	0.912713	0.459537	0.036
H14A	0.652251	0.821525	0.502623	0.031
H16A	0.491383	0.726608	0.466484	0.028
H16B	0.398872	0.809205	0.421261	0.028
H17A	0.266859	0.692258	0.318460	0.032
H17B	0.246497	0.779313	0.347845	0.032
H18A	0.210295	0.608080	0.444377	0.038
H18B	0.259982	0.676933	0.485849	0.038
H19A	0.044660	0.767561	0.449050	0.040
H19B	-0.007081	0.693148	0.414687	0.040
H20A	0.497149	0.605182	0.436493	0.032
H20B	0.465891	0.593255	0.352160	0.032
H22A	0.731542	0.520364	0.444987	0.040
H23A	0.982831	0.501418	0.393147	0.048
H24A	1.075194	0.592083	0.268084	0.046
H25A	0.918874	0.699674	0.201744	0.036
H1BA	0.551002	0.435990	0.244841	0.070
H1BB	0.693587	0.102092	0.191900	0.035
H2BA	0.478288	0.058622	0.281288	0.041
H3BA	0.458083	0.071091	0.413407	0.043
H4BA	0.650877	0.126335	0.454523	0.039
H6BA	0.885299	0.209945	0.409645	0.034
H6BB	0.982005	0.124933	0.396873	0.034
H7BA	0.956247	0.344368	0.325621	0.037
H7BB	1.025898	0.353695	0.233520	0.037
H8BA	0.730240	0.306887	0.299877	0.042
H8BB	0.799567	0.312178	0.208124	0.042

H9BA	0.752499	0.456408	0.278938	0.047
H9BB	0.831950	0.463135	0.188439	0.047
H10B	1.188947	0.267665	0.334501	0.036
H10C	1.200362	0.166345	0.339398	0.036
H12B	1.431498	0.301237	0.248004	0.044
H13B	1.572498	0.315736	0.120065	0.054
H14B	1.486495	0.259912	0.025615	0.054
H15A	1.256060	0.198975	0.056432	0.044
H1SA	1.316387	0.473033	-0.061319	0.103
H1SB	1.241086	0.537284	-0.008097	0.103
H1SC	1.347917	0.457261	0.029578	0.103
H3SA	1.172833	0.388847	-0.084496	0.093
H3SB	1.104439	0.314219	-0.010249	0.093
H3SC	1.001495	0.396538	-0.047261	0.093

Table A6.3 Bond lengths for **6-2** and **6-6**.

I1A-Pd1A	2.5785(9)	C22A-C23A	1.385(10)
Pd1A-C6A	1.994(6)	C22A-H22A	0.9500
Pd1A-C1A	2.072(5)	C23A-C24A	1.384(10)
Pd1A-N1A	2.150(4)	C23A-H23A	0.9500
Pd1A-N2A	2.197(4)	C24A-C25A	1.380(9)
Pd1A-N3A	2.229(5)	C24A-H24A	0.9500
O1A-C19A	1.428(7)	C25A-H25A	0.9500
O1A-H1AA	0.8400	I1B-Pd1B	2.5928(10)
N1A-C11A	1.343(7)	Pd1B-N1B	2.025(5)
N1A-C15A	1.348(7)	Pd1B-N3B	2.037(5)
N2A-C16A	1.490(7)	Pd1B-N2B	2.055(5)
N2A-C20A	1.502(7)	O1B-C9B	1.395(8)
N2A-C17A	1.503(7)	O1B-H1BA	0.8400
N3A-C21A	1.343(7)	N1B-C1B	1.354(7)
N3A-C25A	1.346(8)	N1B-C5B	1.358(7)
C1A-C2A	1.530(8)	N2B-C6B	1.486(7)
C1A-H1AB	0.9900	N2B-C10B	1.493(7)
C1A-H1AC	0.9900	N2B-C7B	1.505(7)
C2A-C5A	1.513(8)	N3B-C15B	1.347(8)
C2A-C4A	1.540(8)	N3B-C11B	1.358(8)
C2A-C3A	1.543(8)	C1B-C2B	1.391(9)
C3A-H3AA	0.9800	C1B-H1BB	0.9500
C3A-H3AB	0.9800	C2B-C3B	1.374(9)
C3A-H3AC	0.9800	C2B-H2BA	0.9500
C4A-H4AA	0.9800	C3B-C4B	1.375(9)
C4A-H4AB	0.9800	C3B-H3BA	0.9500
C4A-H4AC	0.9800	C4B-C5B	1.389(8)
C5A-C6A	1.393(8)	C4B-H4BA	0.9500
C5A-C10A	1.395(9)	C5B-C6B	1.505(8)
C6A-C7A	1.377(9)	C6B-H6BA	0.9900

C7A-C8A	1.401(9)	C6B-H6BB	0.9900
C7A-H7AA	0.9500	C7B-C8B	1.501(9)
C8A-C9A	1.383(10)	C7B-H7BA	0.9900
C8A-H8AA	0.9500	C7B-H7BB	0.9900
C9A-C10A	1.392(10)	C8B-C9B	1.518(9)
C9A-H9AA	0.9500	C8B-H8BA	0.9900
C10A-H10A	0.9500	C8B-H8BB	0.9900
C11A-C12A	1.387(8)	C9B-H9BA	0.9900
C11A-H11A	0.9500	C9B-H9BB	0.9900
C12A-C13A	1.378(9)	C10B-C11B	1.491(8)
C12A-H12A	0.9500	C10B-H10B	0.9900
C13A-C14A	1.383(8)	C10B-H10C	0.9900
C13A-H13A	0.9500	C11B-C12B	1.383(9)
C14A-C15A	1.389(8)	C12B-C13B	1.390(10)
C14A-H14A	0.9500	C12B-H12B	0.9500
C15A-C16A	1.501(8)	C13B-C14B	1.370(10)
C16A-H16A	0.9900	C13B-H13B	0.9500
C16A-H16B	0.9900	C14B-C15B	1.385(9)
C17A-C18A	1.534(8)	C14B-H14B	0.9500
C17A-H17A	0.9900	C15B-H15A	0.9500
C17A-H17B	0.9900	O1S-C2S	1.203(9)
C18A-C19A	1.507(8)	C1S-C2S	1.499(13)
C18A-H18A	0.9900	C1S-H1SA	0.9800
C18A-H18B	0.9900	C1S-H1SB	0.9800
C19A-H19A	0.9900	C1S-H1SC	0.9800
C19A-H19B	0.9900	C2S-C3S	1.478(12)
C20A-C21A	1.501(8)	C3S-H3SA	0.9800
C20A-H20A	0.9900	C3S-H3SB	0.9800
C20A-H20B	0.9900	C3S-H3SC	0.9800
C21A-C22A	1.390(9)		

Table A6.4 Bond angles for **6-2** and **6-6**.

C6A-Pd1A-C1A	82.4(2)	C21A-C20A-H20B	108.8
C6A-Pd1A-N1A	173.51(19)	N2A-C20A-H20B	108.8
C1A-Pd1A-N1A	93.7(2)	H20A-C20A-H20B	107.7
C6A-Pd1A-N2A	94.24(19)	N3A-C21A-C22A	121.6(6)
C1A-Pd1A-N2A	96.3(2)	N3A-C21A-C20A	116.7(5)
N1A-Pd1A-N2A	80.97(16)	C22A-C21A-C20A	121.5(5)
C6A-Pd1A-N3A	100.4(2)	C23A-C22A-C21A	119.7(6)
C1A-Pd1A-N3A	175.1(2)	C23A-C22A-H22A	120.2
N1A-Pd1A-N3A	83.11(17)	C21A-C22A-H22A	120.2
N2A-Pd1A-N3A	79.57(17)	C22A-C23A-C24A	118.4(6)
C6A-Pd1A-I1A	87.51(16)	C22A-C23A-H23A	120.8
C1A-Pd1A-I1A	88.84(16)	C24A-C23A-H23A	120.8
N1A-Pd1A-I1A	97.64(12)	C25A-C24A-C23A	119.1(6)
N2A-Pd1A-I1A	174.73(12)	C25A-C24A-H24A	120.4
N3A-Pd1A-I1A	95.24(12)	C23A-C24A-H24A	120.4
C19A-O1A-H1AA	109.5	N3A-C25A-C24A	122.6(6)
C11A-N1A-C15A	118.5(5)	N3A-C25A-H25A	118.7
C11A-N1A-Pd1A	127.2(4)	C24A-C25A-H25A	118.7
C15A-N1A-Pd1A	114.0(3)	N1B-Pd1B-N3B	165.67(19)
C16A-N2A-C20A	111.1(4)	N1B-Pd1B-N2B	83.15(19)
C16A-N2A-C17A	108.2(4)	N3B-Pd1B-N2B	83.18(19)
C20A-N2A-C17A	108.9(4)	N1B-Pd1B-I1B	95.89(13)
C16A-N2A-Pd1A	107.3(3)	N3B-Pd1B-I1B	98.07(14)
C20A-N2A-Pd1A	105.7(3)	N2B-Pd1B-I1B	175.63(13)
C17A-N2A-Pd1A	115.6(3)	C9B-O1B-H1BA	109.5
C21A-N3A-C25A	118.6(5)	C1B-N1B-C5B	119.3(5)
C21A-N3A-Pd1A	112.1(4)	C1B-N1B-Pd1B	128.7(4)
C25A-N3A-Pd1A	128.4(4)	C5B-N1B-Pd1B	112.0(4)
C2A-C1A-Pd1A	113.8(4)	C6B-N2B-C10B	113.1(4)
C2A-C1A-H1AB	108.8	C6B-N2B-C7B	112.8(5)
Pd1A-C1A-H1AB	108.8	C10B-N2B-C7B	108.0(5)
C2A-C1A-H1AC	108.8	C6B-N2B-Pd1B	105.6(3)
Pd1A-C1A-H1AC	108.8	C10B-N2B-Pd1B	105.3(3)

H1AB-C1A-H1AC	107.7	C7B-N2B-Pd1B	111.8(3)
C5A-C2A-C1A	108.3(5)	C15B-N3B-C11B	119.4(5)
C5A-C2A-C4A	110.3(5)	C15B-N3B-Pd1B	128.5(4)
C1A-C2A-C4A	110.8(5)	C11B-N3B-Pd1B	111.9(4)
C5A-C2A-C3A	111.0(5)	N1B-C1B-C2B	121.6(5)
C1A-C2A-C3A	108.5(5)	N1B-C1B-H1BB	119.2
C4A-C2A-C3A	108.0(5)	C2B-C1B-H1BB	119.2
C2A-C3A-H3AA	109.5	C3B-C2B-C1B	118.7(6)
C2A-C3A-H3AB	109.5	C3B-C2B-H2BA	120.7
H3AA-C3A-H3AB	109.5	C1B-C2B-H2BA	120.7
C2A-C3A-H3AC	109.5	C2B-C3B-C4B	120.1(6)
H3AA-C3A-H3AC	109.5	C2B-C3B-H3BA	119.9
H3AB-C3A-H3AC	109.5	C4B-C3B-H3BA	119.9
C2A-C4A-H4AA	109.5	C3B-C4B-C5B	119.4(6)
C2A-C4A-H4AB	109.5	C3B-C4B-H4BA	120.3
H4AA-C4A-H4AB	109.5	C5B-C4B-H4BA	120.3
C2A-C4A-H4AC	109.5	N1B-C5B-C4B	120.8(5)
H4AA-C4A-H4AC	109.5	N1B-C5B-C6B	116.7(5)
H4AB-C4A-H4AC	109.5	C4B-C5B-C6B	122.5(5)
C6A-C5A-C10A	118.9(6)	N2B-C6B-C5B	110.7(4)
C6A-C5A-C2A	118.6(5)	N2B-C6B-H6BA	109.5
C10A-C5A-C2A	122.5(5)	C5B-C6B-H6BA	109.5
C7A-C6A-C5A	121.0(5)	N2B-C6B-H6BB	109.5
C7A-C6A-Pd1A	122.7(4)	C5B-C6B-H6BB	109.5
C5A-C6A-Pd1A	116.1(4)	H6BA-C6B-H6BB	108.1
C6A-C7A-C8A	119.8(6)	C8B-C7B-N2B	114.5(5)
C6A-C7A-H7AA	120.1	C8B-C7B-H7BA	108.6
C8A-C7A-H7AA	120.1	N2B-C7B-H7BA	108.6
C9A-C8A-C7A	119.8(6)	C8B-C7B-H7BB	108.6
C9A-C8A-H8AA	120.1	N2B-C7B-H7BB	108.6
C7A-C8A-H8AA	120.1	H7BA-C7B-H7BB	107.6
C8A-C9A-C10A	120.1(6)	C7B-C8B-C9B	111.7(5)
C8A-C9A-H9AA	119.9	C7B-C8B-H8BA	109.3
C10A-C9A-H9AA	119.9	C9B-C8B-H8BA	109.3

C9A-C10A-C5A	120.4(6)	C7B-C8B-H8BB	109.3
C9A-C10A-H10A	119.8	C9B-C8B-H8BB	109.3
C5A-C10A-H10A	119.8	H8BA-C8B-H8BB	107.9
N1A-C11A-C12A	122.0(5)	O1B-C9B-C8B	110.4(6)
N1A-C11A-H11A	119.0	O1B-C9B-H9BA	109.6
C12A-C11A-H11A	119.0	C8B-C9B-H9BA	109.6
C13A-C12A-C11A	119.4(5)	O1B-C9B-H9BB	109.6
C13A-C12A-H12A	120.3	C8B-C9B-H9BB	109.6
C11A-C12A-H12A	120.3	H9BA-C9B-H9BB	108.1
C12A-C13A-C14A	119.1(5)	C11B-C10B-N2B	110.2(5)
C12A-C13A-H13A	120.5	C11B-C10B-H10B	109.6
C14A-C13A-H13A	120.5	N2B-C10B-H10B	109.6
C13A-C14A-C15A	118.7(5)	C11B-C10B-H10C	109.6
C13A-C14A-H14A	120.6	N2B-C10B-H10C	109.6
C15A-C14A-H14A	120.6	H10B-C10B-H10C	108.1
N1A-C15A-C14A	122.3(5)	N3B-C11B-C12B	120.8(6)
N1A-C15A-C16A	117.3(5)	N3B-C11B-C10B	116.1(5)
C14A-C15A-C16A	120.3(5)	C12B-C11B-C10B	123.0(5)
N2A-C16A-C15A	115.7(4)	C11B-C12B-C13B	119.6(6)
N2A-C16A-H16A	108.4	C11B-C12B-H12B	120.2
C15A-C16A-H16A	108.4	C13B-C12B-H12B	120.2
N2A-C16A-H16B	108.4	C14B-C13B-C12B	119.1(6)
C15A-C16A-H16B	108.4	C14B-C13B-H13B	120.5
H16A-C16A-H16B	107.4	C12B-C13B-H13B	120.5
N2A-C17A-C18A	114.8(5)	C13B-C14B-C15B	119.5(7)
N2A-C17A-H17A	108.6	C13B-C14B-H14B	120.3
C18A-C17A-H17A	108.6	C15B-C14B-H14B	120.3
N2A-C17A-H17B	108.6	N3B-C15B-C14B	121.6(6)
C18A-C17A-H17B	108.6	N3B-C15B-H15A	119.2
H17A-C17A-H17B	107.6	C14B-C15B-H15A	119.2
C19A-C18A-C17A	110.8(5)	C2S-C1S-H1SA	109.5
C19A-C18A-H18A	109.5	C2S-C1S-H1SB	109.5
C17A-C18A-H18A	109.5	H1SA-C1S-H1SB	109.5
C19A-C18A-H18B	109.5	C2S-C1S-H1SC	109.5

O1A	0.4356(6)	0.1726(12)	0.2954(3)	0.050(3)
O1B	0.6604(6)	0.6671(12)	0.7054(3)	0.047(3)
O1S	0.3834(6)	-0.0388(13)	0.4498(3)	0.059(3)
N1A	0.7739(6)	0.2991(13)	0.3505(3)	0.028(3)
N1B	0.9975(6)	0.7981(14)	0.6483(3)	0.025(3)
C1A	0.6414(7)	0.1315(15)	0.3842(4)	0.026(3)
C1B	0.8651(7)	0.6408(15)	0.6161(4)	0.030(3)
C1S	0.2967(10)	0.081(2)	0.4856(5)	0.058(5)
Br2C	0.79691(8)	0.42891(18)	0.71547(4)	0.0326(4)
O2S	0.6024(6)	0.4663(15)	0.5589(4)	0.065(4)
N2A	0.6376(6)	0.4004(14)	0.3287(3)	0.025(3)
N2B	0.8600(6)	0.9041(12)	0.6717(3)	0.023(2)
C2A	0.5707(8)	0.1182(19)	0.4053(4)	0.030(3)
C2B	0.7947(7)	0.6258(17)	0.5941(4)	0.025(3)
C2S	0.3472(9)	-0.0463(19)	0.4764(5)	0.038(4)
N3A	0.7200(6)	0.6120(14)	0.3704(3)	0.026(3)
N3B	0.9460(7)	1.1160(14)	0.6302(3)	0.023(3)
C3A	0.5166(7)	0.0098(17)	0.3849(4)	0.033(4)
C3B	0.7407(7)	0.5202(15)	0.6142(4)	0.028(3)
C3S	0.3521(11)	-0.1849(19)	0.5007(5)	0.057(5)
C4A	0.5889(8)	0.0354(18)	0.4397(4)	0.033(4)
C4B	0.8099(8)	0.5455(16)	0.5590(4)	0.030(3)
C4S	0.5161(17)	0.590(3)	0.5218(7)	0.150(14)
C5A	0.5418(8)	0.2819(17)	0.4120(4)	0.023(3)
C5B	0.7644(8)	0.7995(16)	0.5887(4)	0.021(3)
C5S	0.5734(10)	0.467(3)	0.5309(6)	0.064(6)
C6A	0.5841(8)	0.4161(18)	0.4034(4)	0.026(3)
C6B	0.8076(8)	0.9258(17)	0.5970(4)	0.023(3)
C6S	0.5850(11)	0.346(2)	0.5046(5)	0.066(6)
C7A	0.5619(9)	0.5711(19)	0.4095(4)	0.032(4)
C7B	0.7841(8)	1.0853(17)	0.5911(4)	0.025(3)
C8A	0.4910(8)	0.5996(18)	0.4244(4)	0.034(4)
C8B	0.7168(7)	1.1115(17)	0.5767(4)	0.024(3)
C9A	0.4484(8)	0.4664(17)	0.4318(4)	0.028(3)

C9B	0.6727(8)	0.9810(17)	0.5674(4)	0.036(4)
C10A	0.4722(8)	0.3098(18)	0.4262(4)	0.031(4)
C10B	0.6962(7)	0.8255(17)	0.5740(4)	0.027(4)
C11A	0.8427(8)	0.2817(16)	0.3625(4)	0.031(3)
C11B	1.0663(7)	0.7854(16)	0.6360(4)	0.029(3)
C12A	0.8999(8)	0.2568(16)	0.3406(5)	0.036(4)
C12B	1.1237(7)	0.7571(15)	0.6587(4)	0.028(3)
C13A	0.8855(8)	0.2463(17)	0.3052(4)	0.035(4)
C13B	1.1113(8)	0.7428(17)	0.6939(4)	0.034(4)
C14A	0.8153(8)	0.2600(16)	0.2930(4)	0.034(4)
C14B	1.0411(8)	0.7614(17)	0.7067(4)	0.032(4)
C15A	0.7590(8)	0.2852(16)	0.3162(4)	0.030(3)
C15B	0.9859(7)	0.7890(16)	0.6828(4)	0.022(3)
C16A	0.6827(7)	0.2978(18)	0.3048(4)	0.026(3)
C16B	0.9079(7)	0.7964(17)	0.6944(4)	0.026(3)
C17A	0.5579(7)	0.3606(18)	0.3236(4)	0.028(3)
C17B	0.7824(7)	0.8584(17)	0.6771(4)	0.026(3)
C18A	0.5287(7)	0.3859(17)	0.2870(4)	0.033(4)
C18B	0.7542(7)	0.8840(16)	0.7136(4)	0.028(3)
C19A	0.4484(8)	0.3366(17)	0.2840(5)	0.036(4)
C19B	0.6748(8)	0.8348(18)	0.7155(5)	0.042(4)
C20A	0.6462(8)	0.5776(17)	0.3190(4)	0.032(4)
C20B	0.8699(8)	1.0767(16)	0.6808(4)	0.028(3)
C21A	0.7080(7)	0.6569(17)	0.3380(5)	0.025(3)
C21B	0.9330(8)	1.1583(18)	0.6635(4)	0.030(4)
C22A	0.7475(8)	0.7819(16)	0.3230(4)	0.033(4)
C22B	0.9700(8)	1.2809(17)	0.6796(4)	0.036(4)
C23A	0.7986(8)	0.8640(18)	0.3420(5)	0.037(4)
C23B	1.0225(8)	1.3623(17)	0.6602(4)	0.037(4)
C24A	0.8061(7)	0.8206(17)	0.3769(5)	0.036(4)
C24B	1.0354(8)	1.3231(17)	0.6268(4)	0.036(4)
C25A	0.7670(8)	0.6915(17)	0.3901(4)	0.034(4)
C25B	0.9967(8)	1.1951(17)	0.6127(4)	0.029(3)
H1AA	0.472977	0.116888	0.291725	0.070

H1BA	0.697997	0.611480	0.708761	0.066
H1AB	0.633158	0.087198	0.360598	0.031
H1AC	0.679589	0.065615	0.395518	0.031
H1BB	0.903630	0.573398	0.605462	0.036
H1BC	0.855580	0.598561	0.639738	0.036
H1SA	0.272705	0.054677	0.507652	0.087
H1SB	0.323384	0.183099	0.488195	0.087
H1SC	0.259989	0.092888	0.467298	0.087
H3AA	0.538478	-0.096582	0.381253	0.050
H3AB	0.471542	-0.001757	0.398327	0.050
H3AC	0.505766	0.059348	0.362383	0.050
H3BA	0.730287	0.569769	0.636810	0.042
H3BB	0.695445	0.510156	0.600885	0.042
H3BC	0.761861	0.413016	0.617817	0.042
H3SA	0.318833	-0.167540	0.520312	0.085
H3SB	0.338617	-0.284162	0.488528	0.085
H3SC	0.402079	-0.194261	0.509442	0.085
H4AA	0.608028	-0.072808	0.435151	0.050
H4AB	0.625644	0.098746	0.452211	0.050
H4AC	0.544800	0.027241	0.453974	0.050
H4BA	0.844415	0.611411	0.545747	0.045
H4BB	0.830748	0.438254	0.562879	0.045
H4BC	0.764332	0.535394	0.545947	0.045
H4SA	0.498944	0.570845	0.498006	0.226
H4SB	0.475188	0.580099	0.538013	0.226
H4SC	0.537026	0.698082	0.523460	0.226
H6SA	0.555546	0.372173	0.484062	0.099
H6SB	0.636614	0.344544	0.498116	0.099
H6SC	0.570775	0.240620	0.513625	0.099
H7AA	0.592977	0.658979	0.404092	0.038
H7BA	0.814616	1.173702	0.596977	0.031
H8AA	0.474225	0.705883	0.428869	0.041
H8BA	0.700122	1.218561	0.573074	0.029
H9AA	0.400967	0.482859	0.441059	0.034

H9BA	0.626876	0.999059	0.556639	0.043
H10A	0.441693	0.221383	0.432039	0.037
H10B	0.665775	0.736487	0.568483	0.033
H11A	0.851282	0.286883	0.386831	0.037
H11B	1.075257	0.795950	0.611752	0.035
H12A	0.948129	0.246858	0.349310	0.043
H12B	1.171811	0.747517	0.649845	0.034
H13A	0.924379	0.229621	0.289272	0.042
H13B	1.150497	0.720309	0.709275	0.041
H14A	0.805636	0.252207	0.268820	0.041
H14B	1.031234	0.755521	0.730883	0.038
H16A	0.661274	0.188518	0.303631	0.031
H16B	0.681299	0.344466	0.281090	0.031
H16C	0.906226	0.836848	0.718619	0.031
H16D	0.887461	0.686000	0.694353	0.031
H17A	0.528857	0.427469	0.339777	0.034
H17B	0.550085	0.246417	0.330072	0.034
H17C	0.776501	0.743197	0.671022	0.031
H17D	0.751902	0.921674	0.660843	0.031
H18A	0.557974	0.321594	0.270383	0.039
H18B	0.533844	0.500934	0.280561	0.039
H18C	0.759294	0.998944	0.720102	0.034
H18D	0.783115	0.818930	0.730194	0.034
H19A	0.418430	0.410797	0.298204	0.043
H19B	0.432643	0.347590	0.259465	0.043
H19C	0.657262	0.851280	0.739566	0.050
H19D	0.646185	0.906718	0.700118	0.050
H20A	0.654879	0.586173	0.293600	0.039
H20B	0.600447	0.635488	0.324322	0.039
H20C	0.876314	1.085093	0.706337	0.034
H20D	0.824887	1.135708	0.674675	0.034
H22A	0.738865	0.810575	0.299471	0.040
H22B	0.960237	1.309268	0.703042	0.043
H23A	0.827567	0.946488	0.331852	0.044

H23B	1.049608	1.446782	0.670755	0.044
H24A	0.837991	0.879532	0.391617	0.043
H24B	1.069932	1.381138	0.613340	0.043
H25A	0.774007	0.659593	0.413580	0.041
H25B	1.007069	1.162979	0.589477	0.035

Table A6.6 Bond lengths for **6-4**.

Pd1A-C6A	1.985(15)	C6S-H6SB	0.9800
Pd1A-C1A	2.075(13)	C6S-H6SC	0.9800
Pd1A-N2A	2.121(12)	C7A-C8A	1.44(2)
Pd1A-N1A	2.171(12)	C7A-H7AA	0.9500
Pd1A-N3A	2.203(12)	C7B-C8B	1.371(19)
Pd1A-Br1A	2.420(2)	C7B-H7BA	0.9500
Pd1B-C6B	1.996(15)	C8A-C9A	1.385(19)
Pd1B-C1B	2.049(12)	C8A-H8AA	0.9500
Pd1B-N2B	2.147(12)	C8B-C9B	1.399(18)
Pd1B-N1B	2.154(12)	C8B-H8BA	0.9500
Pd1B-N3B	2.206(12)	C9A-C10A	1.389(19)
Pd1B-Br1B	2.4272(19)	C9A-H9AA	0.9500
O1A-C19A	1.449(17)	C9B-C10B	1.385(19)
O1A-H1AA	0.8400	C9B-H9BA	0.9500
O1B-C19B	1.468(18)	C10A-H10A	0.9500
O1B-H1BA	0.8400	C10B-H10B	0.9500
O1S-C2S	1.221(18)	C11A-C12A	1.362(19)
N1A-C15A	1.353(19)	C11A-H11A	0.9500
N1A-C11A	1.352(17)	C11B-C12B	1.39(2)
N1B-C15B	1.342(18)	C11B-H11B	0.9500
N1B-C11B	1.354(17)	C12A-C13A	1.39(2)
C1A-C2A	1.535(19)	C12A-H12A	0.9500
C1A-H1AB	0.9900	C12B-C13B	1.38(2)
C1A-H1AC	0.9900	C12B-H12B	0.9500
C1B-C2B	1.550(19)	C13A-C14A	1.38(2)
C1B-H1BB	0.9900	C13A-H13A	0.9500
C1B-H1BC	0.9900	C13B-C14B	1.389(19)

C1S-C2S	1.45(2)	C13B-H13B	0.9500
C1S-H1SA	0.9800	C14A-C15A	1.38(2)
C1S-H1SB	0.9800	C14A-H14A	0.9500
C1S-H1SC	0.9800	C14B-C15B	1.386(19)
O2S-C5S	1.20(2)	C14B-H14B	0.9500
N2A-C16A	1.503(17)	C15A-C16A	1.472(19)
N2A-C17A	1.514(17)	C15B-C16B	1.503(18)
N2A-C20A	1.526(18)	C16A-H16A	0.9900
N2B-C20B	1.486(17)	C16A-H16B	0.9900
N2B-C17B	1.489(17)	C16B-H16C	0.9900
N2B-C16B	1.528(17)	C16B-H16D	0.9900
C2A-C5A	1.48(2)	C17A-C18A	1.52(2)
C2A-C4A	1.53(2)	C17A-H17A	0.9900
C2A-C3A	1.550(19)	C17A-H17B	0.9900
C2B-C4B	1.53(2)	C17B-C18B	1.51(2)
C2B-C3B	1.534(18)	C17B-H17C	0.9900
C2B-C5B	1.559(19)	C17B-H17D	0.9900
C2S-C3S	1.49(2)	C18A-C19A	1.535(18)
N3A-C25A	1.322(18)	C18A-H18A	0.9900
N3A-C21A	1.319(19)	C18A-H18B	0.9900
N3B-C25B	1.323(18)	C18B-C19B	1.517(19)
N3B-C21B	1.350(19)	C18B-H18C	0.9900
C3A-H3AA	0.9800	C18B-H18D	0.9900
C3A-H3AB	0.9800	C19A-H19A	0.9900
C3A-H3AC	0.9800	C19A-H19B	0.9900
C3B-H3BA	0.9800	C19B-H19C	0.9900
C3B-H3BB	0.9800	C19B-H19D	0.9900
C3B-H3BC	0.9800	C20A-C21A	1.50(2)
C3S-H3SA	0.9800	C20A-H20A	0.9900
C3S-H3SB	0.9800	C20A-H20B	0.9900
C3S-H3SC	0.9800	C20B-C21B	1.50(2)
C4A-H4AA	0.9800	C20B-H20C	0.9900
C4A-H4AB	0.9800	C20B-H20D	0.9900
C4A-H4AC	0.9800	C21A-C22A	1.390(19)

C4B-H4BA	0.9800	C21B-C22B	1.37(2)
C4B-H4BB	0.9800	C22A-C23A	1.37(2)
C4B-H4BC	0.9800	C22A-H22A	0.9500
C4S-C5S	1.51(3)	C22B-C23B	1.39(2)
C4S-H4SA	0.9800	C22B-H22B	0.9500
C4S-H4SB	0.9800	C23A-C24A	1.40(2)
C4S-H4SC	0.9800	C23A-H23A	0.9500
C5A-C6A	1.397(19)	C23B-C24B	1.35(2)
C5A-C10A	1.409(19)	C23B-H23B	0.9500
C5B-C6B	1.353(19)	C24A-C25A	1.39(2)
C5B-C10B	1.391(19)	C24A-H24A	0.9500
C5S-C6S	1.44(2)	C24B-C25B	1.389(19)
C6A-C7A	1.37(2)	C24B-H24B	0.9500
C6B-C7B	1.411(19)	C25A-H25A	0.9500
C6S-H6SA	0.9800	C25B-H25B	0.9500

Table A6.7 Bond angles for **6-4**.

C6A-Pd1A-C1A	82.9(6)	H6SB-C6S-H6SC	109.5
C6A-Pd1A-N2A	95.3(5)	C6A-C7A-C8A	119.5(15)
C1A-Pd1A-N2A	94.7(5)	C6A-C7A-H7AA	120.3
C6A-Pd1A-N1A	174.0(5)	C8A-C7A-H7AA	120.3
C1A-Pd1A-N1A	93.2(5)	C8B-C7B-C6B	119.3(14)
N2A-Pd1A-N1A	80.4(5)	C8B-C7B-H7BA	120.3
C6A-Pd1A-N3A	101.1(5)	C6B-C7B-H7BA	120.3
C1A-Pd1A-N3A	174.6(5)	C9A-C8A-C7A	117.5(14)
N2A-Pd1A-N3A	81.4(4)	C9A-C8A-H8AA	121.3
N1A-Pd1A-N3A	82.4(4)	C7A-C8A-H8AA	121.3
C6A-Pd1A-Br1A	88.1(4)	C7B-C8B-C9B	120.2(13)
C1A-Pd1A-Br1A	89.4(4)	C7B-C8B-H8BA	119.9
N2A-Pd1A-Br1A	174.9(3)	C9B-C8B-H8BA	119.9
N1A-Pd1A-Br1A	96.4(3)	C8A-C9A-C10A	122.4(14)
N3A-Pd1A-Br1A	94.3(3)	C8A-C9A-H9AA	118.8
C6B-Pd1B-C1B	83.4(6)	C10A-C9A-H9AA	118.8
C6B-Pd1B-N2B	93.9(5)	C10B-C9B-C8B	119.6(13)

C1B-Pd1B-N2B	93.5(5)	C10B-C9B-H9BA	120.2
C6B-Pd1B-N1B	173.7(5)	C8B-C9B-H9BA	120.2
C1B-Pd1B-N1B	92.0(5)	C9A-C10A-C5A	120.0(14)
N2B-Pd1B-N1B	81.9(4)	C9A-C10A-H10A	120.0
C6B-Pd1B-N3B	101.3(5)	C5A-C10A-H10A	120.0
C1B-Pd1B-N3B	173.5(6)	C9B-C10B-C5B	120.0(13)
N2B-Pd1B-N3B	81.8(4)	C9B-C10B-H10B	120.0
N1B-Pd1B-N3B	82.9(4)	C5B-C10B-H10B	120.0
C6B-Pd1B-Br1B	87.2(4)	N1A-C11A-C12A	121.8(15)
C1B-Pd1B-Br1B	90.7(5)	N1A-C11A-H11A	119.1
N2B-Pd1B-Br1B	175.7(3)	C12A-C11A-H11A	119.1
N1B-Pd1B-Br1B	97.2(3)	N1B-C11B-C12B	120.1(15)
N3B-Pd1B-Br1B	93.9(3)	N1B-C11B-H11B	119.9
C19A-O1A-H1AA	109.5	C12B-C11B-H11B	119.9
C19B-O1B-H1BA	109.5	C11A-C12A-C13A	117.9(15)
C15A-N1A-C11A	120.7(13)	C11A-C12A-H12A	121.1
C15A-N1A-Pd1A	111.5(9)	C13A-C12A-H12A	121.1
C11A-N1A-Pd1A	127.6(10)	C13B-C12B-C11B	120.4(14)
C15B-N1B-C11B	119.3(13)	C13B-C12B-H12B	119.8
C15B-N1B-Pd1B	112.8(9)	C11B-C12B-H12B	119.8
C11B-N1B-Pd1B	127.1(11)	C14A-C13A-C12A	120.3(15)
C2A-C1A-Pd1A	112.5(9)	C14A-C13A-H13A	119.8
C2A-C1A-H1AB	109.1	C12A-C13A-H13A	119.8
Pd1A-C1A-H1AB	109.1	C12B-C13B-C14B	119.4(14)
C2A-C1A-H1AC	109.1	C12B-C13B-H13B	120.3
Pd1A-C1A-H1AC	109.1	C14B-C13B-H13B	120.3
H1AB-C1A-H1AC	107.8	C13A-C14A-C15A	119.7(16)
C2B-C1B-Pd1B	113.1(9)	C13A-C14A-H14A	120.1
C2B-C1B-H1BB	109.0	C15A-C14A-H14A	120.1
Pd1B-C1B-H1BB	109.0	C15B-C14B-C13B	117.6(15)
C2B-C1B-H1BC	109.0	C15B-C14B-H14B	121.2
Pd1B-C1B-H1BC	109.0	C13B-C14B-H14B	121.2
H1BB-C1B-H1BC	107.8	N1A-C15A-C14A	119.4(14)
C2S-C1S-H1SA	109.5	N1A-C15A-C16A	118.4(13)

C2S-C1S-H1SB	109.5	C14A-C15A-C16A	122.2(15)
H1SA-C1S-H1SB	109.5	N1B-C15B-C14B	123.2(13)
C2S-C1S-H1SC	109.5	N1B-C15B-C16B	116.2(13)
H1SA-C1S-H1SC	109.5	C14B-C15B-C16B	120.5(14)
H1SB-C1S-H1SC	109.5	C15A-C16A-N2A	112.6(12)
C16A-N2A-C17A	109.3(10)	C15A-C16A-H16A	109.1
C16A-N2A-C20A	109.8(11)	N2A-C16A-H16A	109.1
C17A-N2A-C20A	106.2(12)	C15A-C16A-H16B	109.1
C16A-N2A-Pd1A	107.6(9)	N2A-C16A-H16B	109.1
C17A-N2A-Pd1A	115.5(8)	H16A-C16A-H16B	107.8
C20A-N2A-Pd1A	108.4(8)	C15B-C16B-N2B	113.7(12)
C20B-N2B-C17B	109.3(11)	C15B-C16B-H16C	108.8
C20B-N2B-C16B	110.9(11)	N2B-C16B-H16C	108.8
C17B-N2B-C16B	108.7(10)	C15B-C16B-H16D	108.8
C20B-N2B-Pd1B	106.9(8)	N2B-C16B-H16D	108.8
C17B-N2B-Pd1B	116.4(8)	H16C-C16B-H16D	107.7
C16B-N2B-Pd1B	104.6(8)	N2A-C17A-C18A	115.5(12)
C5A-C2A-C4A	109.9(13)	N2A-C17A-H17A	108.4
C5A-C2A-C1A	109.2(12)	C18A-C17A-H17A	108.4
C4A-C2A-C1A	107.7(12)	N2A-C17A-H17B	108.4
C5A-C2A-C3A	112.9(12)	C18A-C17A-H17B	108.4
C4A-C2A-C3A	108.5(12)	H17A-C17A-H17B	107.5
C1A-C2A-C3A	108.5(12)	N2B-C17B-C18B	115.0(12)
C4B-C2B-C3B	108.3(12)	N2B-C17B-H17C	108.5
C4B-C2B-C1B	111.4(12)	C18B-C17B-H17C	108.5
C3B-C2B-C1B	108.1(12)	N2B-C17B-H17D	108.5
C4B-C2B-C5B	110.6(12)	C18B-C17B-H17D	108.5
C3B-C2B-C5B	111.3(11)	H17C-C17B-H17D	107.5
C1B-C2B-C5B	107.2(11)	C17A-C18A-C19A	111.8(13)
O1S-C2S-C1S	121.0(17)	C17A-C18A-H18A	109.3
O1S-C2S-C3S	122.3(16)	C19A-C18A-H18A	109.3
C1S-C2S-C3S	116.6(16)	C17A-C18A-H18B	109.3
C25A-N3A-C21A	120.5(14)	C19A-C18A-H18B	109.3
C25A-N3A-Pd1A	126.5(11)	H18A-C18A-H18B	107.9

C21A-N3A-Pd1A	111.0(10)	C17B-C18B-C19B	109.6(13)
C25B-N3B-C21B	118.6(13)	C17B-C18B-H18C	109.7
C25B-N3B-Pd1B	128.3(10)	C19B-C18B-H18C	109.7
C21B-N3B-Pd1B	110.0(10)	C17B-C18B-H18D	109.7
C2A-C3A-H3AA	109.5	C19B-C18B-H18D	109.7
C2A-C3A-H3AB	109.5	H18C-C18B-H18D	108.2
H3AA-C3A-H3AB	109.5	O1A-C19A-C18A	112.6(12)
C2A-C3A-H3AC	109.5	O1A-C19A-H19A	109.1
H3AA-C3A-H3AC	109.5	C18A-C19A-H19A	109.1
H3AB-C3A-H3AC	109.5	O1A-C19A-H19B	109.1
C2B-C3B-H3BA	109.5	C18A-C19A-H19B	109.1
C2B-C3B-H3BB	109.5	H19A-C19A-H19B	107.8
H3BA-C3B-H3BB	109.5	O1B-C19B-C18B	114.5(12)
C2B-C3B-H3BC	109.5	O1B-C19B-H19C	108.6
H3BA-C3B-H3BC	109.5	C18B-C19B-H19C	108.6
H3BB-C3B-H3BC	109.5	O1B-C19B-H19D	108.6
C2S-C3S-H3SA	109.5	C18B-C19B-H19D	108.6
C2S-C3S-H3SB	109.5	H19C-C19B-H19D	107.6
H3SA-C3S-H3SB	109.5	C21A-C20A-N2A	112.4(13)
C2S-C3S-H3SC	109.5	C21A-C20A-H20A	109.1
H3SA-C3S-H3SC	109.5	N2A-C20A-H20A	109.1
H3SB-C3S-H3SC	109.5	C21A-C20A-H20B	109.1
C2A-C4A-H4AA	109.5	N2A-C20A-H20B	109.1
C2A-C4A-H4AB	109.5	H20A-C20A-H20B	107.9
H4AA-C4A-H4AB	109.5	N2B-C20B-C21B	115.2(13)
C2A-C4A-H4AC	109.5	N2B-C20B-H20C	108.5
H4AA-C4A-H4AC	109.5	C21B-C20B-H20C	108.5
H4AB-C4A-H4AC	109.5	N2B-C20B-H20D	108.5
C2B-C4B-H4BA	109.5	C21B-C20B-H20D	108.5
C2B-C4B-H4BB	109.5	H20C-C20B-H20D	107.5
H4BA-C4B-H4BB	109.5	N3A-C21A-C22A	121.0(15)
C2B-C4B-H4BC	109.5	N3A-C21A-C20A	117.6(13)
H4BA-C4B-H4BC	109.5	C22A-C21A-C20A	121.2(15)
H4BB-C4B-H4BC	109.5	N3B-C21B-C22B	122.2(15)

C5S-C4S-H4SA	109.5	N3B-C21B-C20B	116.2(13)
C5S-C4S-H4SB	109.5	C22B-C21B-C20B	121.3(15)
H4SA-C4S-H4SB	109.5	C23A-C22A-C21A	120.6(16)
C5S-C4S-H4SC	109.5	C23A-C22A-H22A	119.7
H4SA-C4S-H4SC	109.5	C21A-C22A-H22A	119.7
H4SB-C4S-H4SC	109.5	C21B-C22B-C23B	117.6(16)
C6A-C5A-C10A	117.7(14)	C21B-C22B-H22B	121.2
C6A-C5A-C2A	119.4(13)	C23B-C22B-H22B	121.2
C10A-C5A-C2A	122.9(13)	C22A-C23A-C24A	116.7(15)
C6B-C5B-C10B	120.3(13)	C22A-C23A-H23A	121.6
C6B-C5B-C2B	118.3(13)	C24A-C23A-H23A	121.6
C10B-C5B-C2B	121.3(13)	C24B-C23B-C22B	120.9(14)
O2S-C5S-C6S	124(2)	C24B-C23B-H23B	119.5
O2S-C5S-C4S	121(2)	C22B-C23B-H23B	119.5
C6S-C5S-C4S	114.3(19)	C25A-C24A-C23A	120.0(15)
C7A-C6A-C5A	122.8(14)	C25A-C24A-H24A	120.0
C7A-C6A-Pd1A	121.8(12)	C23A-C24A-H24A	120.0
C5A-C6A-Pd1A	115.3(11)	C23B-C24B-C25B	117.9(15)
C5B-C6B-C7B	120.6(14)	C23B-C24B-H24B	121.0
C5B-C6B-Pd1B	116.4(11)	C25B-C24B-H24B	121.0
C7B-C6B-Pd1B	122.9(11)	N3A-C25A-C24A	121.0(16)
C5S-C6S-H6SA	109.5	N3A-C25A-H25A	119.5
C5S-C6S-H6SB	109.5	C24A-C25A-H25A	119.5
H6SA-C6S-H6SB	109.5	N3B-C25B-C24B	122.7(15)
C5S-C6S-H6SC	109.5	N3B-C25B-H25B	118.7
H6SA-C6S-H6SC	109.5	C24B-C25B-H25B	118.7

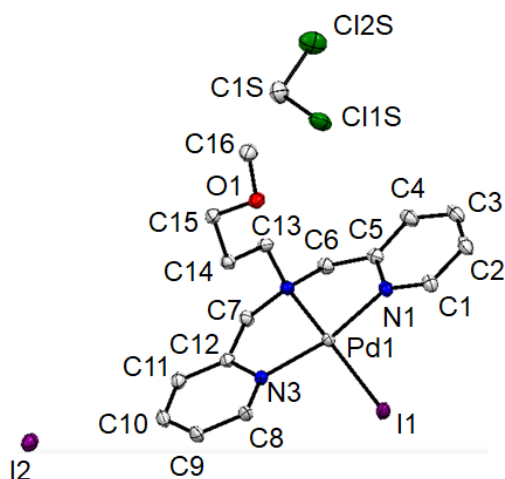


Figure A6.70 Displacement ellipsoid plot of **6-7** co-crystallized with a dichloromethane molecule showing naming and numbering scheme. Ellipsoids are drawn at the 50% probability level and hydrogen atoms are omitted for clarity.

Table A6.8 Atomic coordinates for **6-7**.

Atom	x	y	z	$U_{\text{iso/equiv}}$
Pd1	0.62340(2)	0.61593(2)	0.57239(2)	0.01309(3)
I1	0.75179(2)	0.61892(2)	0.49142(2)	0.02024(3)
I2	0.59261(2)	1.10793(2)	0.70975(2)	0.02364(4)
O1	0.20253(15)	0.61383(11)	0.56909(6)	0.0203(3)
N1	0.59967(16)	0.48503(11)	0.57496(7)	0.0166(3)
N2	0.54039(16)	0.61181(11)	0.64071(7)	0.0149(3)
N3	0.62523(16)	0.74529(11)	0.58587(7)	0.0153(3)
C1	0.6010(2)	0.42693(14)	0.53694(9)	0.0199(4)
C2	0.5831(2)	0.33860(15)	0.54561(10)	0.0244(5)
C3	0.5640(2)	0.30986(15)	0.59431(11)	0.0253(5)
C4	0.5580(2)	0.36988(15)	0.63331(10)	0.0234(4)
C5	0.57676(19)	0.45769(14)	0.62268(9)	0.0171(4)
C6	0.5794(2)	0.52676(14)	0.66272(9)	0.0188(4)
C7	0.5874(2)	0.68835(14)	0.66977(8)	0.0177(4)
C8	0.6353(2)	0.81032(13)	0.55211(9)	0.0181(4)
C9	0.6278(2)	0.89708(14)	0.56643(10)	0.0220(4)
C10	0.6112(2)	0.91724(14)	0.61667(10)	0.0232(4)

C11	0.5980(2)	0.85045(15)	0.65137(9)	0.0199(4)
C12	0.60332(18)	0.76451(14)	0.63513(8)	0.0164(4)
C13	0.40749(18)	0.61249(14)	0.63690(8)	0.0173(4)
C16	0.0820(2)	0.58846(17)	0.56724(10)	0.0252(5)
C14	0.35467(19)	0.69235(14)	0.61161(9)	0.0179(4)
C15	0.22181(19)	0.68063(14)	0.60552(9)	0.0187(4)
C1S	0.1895(3)	0.44027(19)	0.70954(11)	0.0322(6)
C11S	0.17103(8)	0.33758(6)	0.73971(3)	0.04044(17)
C12S	0.22732(7)	0.42447(5)	0.64540(3)	0.03454(15)
H1A	0.614441	0.446720	0.503480	0.024
H2A	0.584022	0.298418	0.518362	0.029
H3A	0.554959	0.249411	0.601026	0.030
H4A	0.541273	0.351406	0.666758	0.028
H6A	0.526066	0.510191	0.690766	0.023
H6B	0.660676	0.532440	0.676320	0.023
H7A	0.531322	0.703867	0.697038	0.021
H7B	0.664212	0.672943	0.685371	0.021
H8A	0.647799	0.796465	0.517601	0.022
H9A	0.633923	0.942075	0.541967	0.026
H10A	0.608952	0.976317	0.627340	0.028
H11A	0.585353	0.863342	0.685993	0.024
H13A	0.374184	0.607825	0.671328	0.021
H13B	0.382165	0.560157	0.617920	0.021
H16A	0.071906	0.542593	0.541892	0.038
H16B	0.057692	0.566396	0.600332	0.038
H16C	0.033094	0.638849	0.558210	0.038
H14A	0.391676	0.700883	0.578125	0.021
H14B	0.370857	0.744691	0.632312	0.021
H15A	0.185736	0.663975	0.638155	0.022
H15B	0.185162	0.735818	0.594103	0.022
H1SA	0.115046	0.474125	0.711880	0.039
H1SB	0.252783	0.473695	0.726651	0.039

Table A6.9 Bond lengths for **6-7**.

Pd1-N3	2.017(2)	C7-H7A	0.9900
Pd1-N1	2.028(2)	C7-H7B	0.9900
Pd1-N2	2.041(2)	C8-C9	1.387(3)
Pd1-I1	2.5911(19)	C8-H8A	0.9500
O1-C16	1.416(3)	C9-C10	1.380(4)
O1-C15	1.425(3)	C9-H9A	0.9500
N1-C1	1.346(3)	C10-C11	1.386(4)
N1-C5	1.358(3)	C10-H10A	0.9500
N2-C6	1.496(3)	C11-C12	1.389(3)
N2-C7	1.502(3)	C11-H11A	0.9500
N2-C13	1.504(3)	C13-C14	1.519(3)
N3-C8	1.346(3)	C13-H13A	0.9900
N3-C12	1.362(3)	C13-H13B	0.9900
C1-C2	1.390(3)	C16-H16A	0.9800
C1-H1A	0.9500	C16-H16B	0.9800
C2-C3	1.382(4)	C16-H16C	0.9800
C2-H2A	0.9500	C14-C15	1.519(3)
C3-C4	1.387(4)	C14-H14A	0.9900
C3-H3A	0.9500	C14-H14B	0.9900
C4-C5	1.393(3)	C15-H15A	0.9900
C4-H4A	0.9500	C15-H15B	0.9900
C5-C6	1.501(3)	C1S-C12S	1.770(3)
C6-H6A	0.9900	C1S-C11S	1.779(3)
C6-H6B	0.9900	C1S-H1SA	0.9900
C7-C12	1.497(3)	C1S-H1SB	0.9900

Table A6.10 Bond angles for **6-7**.

N3-Pd1-N1	166.00(8)	N3-C8-C9	121.6(2)
N3-Pd1-N2	82.99(7)	N3-C8-H8A	119.2
N1-Pd1-N2	83.03(7)	C9-C8-H8A	119.2
N3-Pd1-I1	97.11(5)	C10-C9-C8	119.2(2)
N1-Pd1-I1	96.86(5)	C10-C9-H9A	120.4
N2-Pd1-I1	173.29(5)	C8-C9-H9A	120.4

C16-O1-C15	111.59(18)	C9-C10-C11	119.3(2)
C1-N1-C5	119.7(2)	C9-C10-H10A	120.3
C1-N1-Pd1	129.01(16)	C11-C10-H10A	120.3
C5-N1-Pd1	111.26(14)	C10-C11-C12	119.5(2)
C6-N2-C7	112.22(17)	C10-C11-H11A	120.3
C6-N2-C13	109.03(17)	C12-C11-H11A	120.3
C7-N2-C13	112.42(17)	N3-C12-C11	120.7(2)
C6-N2-Pd1	103.79(13)	N3-C12-C7	116.19(19)
C7-N2-Pd1	105.61(13)	C11-C12-C7	123.1(2)
C13-N2-Pd1	113.48(14)	N2-C13-C14	115.28(17)
C8-N3-C12	119.55(19)	N2-C13-H13A	108.5
C8-N3-Pd1	127.78(16)	C14-C13-H13A	108.5
C12-N3-Pd1	112.41(14)	N2-C13-H13B	108.5
N1-C1-C2	121.4(2)	C14-C13-H13B	108.5
N1-C1-H1A	119.3	H13A-C13-H13B	107.5
C2-C1-H1A	119.3	O1-C16-H16A	109.5
C3-C2-C1	119.3(2)	O1-C16-H16B	109.5
C3-C2-H2A	120.4	H16A-C16-H16B	109.5
C1-C2-H2A	120.4	O1-C16-H16C	109.5
C2-C3-C4	119.5(2)	H16A-C16-H16C	109.5
C2-C3-H3A	120.2	H16B-C16-H16C	109.5
C4-C3-H3A	120.2	C13-C14-C15	109.82(18)
C3-C4-C5	118.9(2)	C13-C14-H14A	109.7
C3-C4-H4A	120.5	C15-C14-H14A	109.7
C5-C4-H4A	120.5	C13-C14-H14B	109.7
N1-C5-C4	121.1(2)	C15-C14-H14B	109.7
N1-C5-C6	115.94(19)	H14A-C14-H14B	108.2
C4-C5-C6	122.9(2)	O1-C15-C14	107.93(18)
N2-C6-C5	109.52(18)	O1-C15-H15A	110.1
N2-C6-H6A	109.8	C14-C15-H15A	110.1
C5-C6-H6A	109.8	O1-C15-H15B	110.1
N2-C6-H6B	109.8	C14-C15-H15B	110.1
C5-C6-H6B	109.8	H15A-C15-H15B	108.4
H6A-C6-H6B	108.2	Cl2S-C1S-C11S	109.82(16)

C12-C7-N2	109.76(18)	C12S-C1S-H1SA	109.7
C12-C7-H7A	109.7	C11S-C1S-H1SA	109.7
N2-C7-H7A	109.7	C12S-C1S-H1SB	109.7
C12-C7-H7B	109.7	C11S-C1S-H1SB	109.7
N2-C7-H7B	109.7	H1SA-C1S-H1SB	108.2
H7A-C7-H7B	108.2		

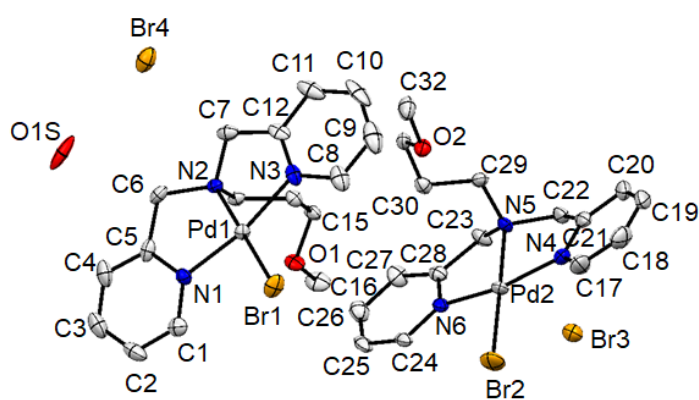


Figure A6.71 Displacement ellipsoid plot of **6-9** co-crystallized with a water molecule showing naming and numbering scheme. Ellipsoids are drawn at the 50% probability level and hydrogen atoms are omitted for clarity.

Table A6.11 Atomic coordinates for **6-9**.

Atom	x	y	z	$U_{\text{iso/equiv}}$
Pd1	0.57011(5)	0.39755(2)	0.23566(2)	0.01553(12)
Br1	0.52517(8)	0.25973(4)	0.26378(2)	0.02958(18)
O1	0.8362(5)	0.5864(3)	0.34550(15)	0.0239(10)
N1	0.7823(6)	0.3799(3)	0.21122(18)	0.0196(11)
N2	0.6054(5)	0.5121(3)	0.21063(17)	0.0168(10)
N3	0.3635(6)	0.4426(3)	0.25261(18)	0.0231(12)
C1	0.8823(7)	0.3211(4)	0.2245(2)	0.0253(15)
C2	1.0233(8)	0.3179(4)	0.2040(3)	0.0335(17)
C3	1.0640(8)	0.3751(4)	0.1696(3)	0.0347(17)

C4	0.9638(8)	0.4378(4)	0.1571(2)	0.0330(17)
C5	0.8252(7)	0.4394(4)	0.1786(2)	0.0218(14)
C6	0.7072(7)	0.5035(4)	0.1672(2)	0.0220(14)
C7	0.4536(7)	0.5451(4)	0.1951(2)	0.0241(14)
C8	0.2663(7)	0.4112(5)	0.2860(3)	0.0333(17)
C9	0.1397(8)	0.4556(6)	0.2980(3)	0.048(2)
C10	0.1099(8)	0.5305(5)	0.2753(3)	0.044(2)
C11	0.2088(8)	0.5604(5)	0.2412(3)	0.0382(18)
C12	0.3364(7)	0.5163(4)	0.2306(2)	0.0233(14)
C13	0.6831(7)	0.5644(3)	0.2499(2)	0.0173(12)
C14	0.6036(7)	0.5696(4)	0.2991(2)	0.0191(13)
C15	0.6908(7)	0.6223(4)	0.3369(2)	0.0211(13)
C16	0.9143(8)	0.6247(4)	0.3867(3)	0.0329(16)
Br3	0.92110(8)	0.79235(4)	0.67448(3)	0.03078(18)
Pd2	0.72026(5)	0.66747(3)	0.55388(2)	0.02114(13)
Br2	0.78986(9)	0.52428(4)	0.56039(3)	0.0420(2)
O2	0.4341(5)	0.7159(3)	0.40989(15)	0.0236(10)
N4	0.5109(6)	0.6569(3)	0.58291(19)	0.0251(12)
N5	0.6561(6)	0.7865(3)	0.54619(18)	0.0207(11)
N6	0.9172(6)	0.7082(3)	0.52518(18)	0.0204(11)
C17	0.4247(9)	0.5903(4)	0.5871(3)	0.0389(18)
C18	0.2798(8)	0.5942(5)	0.6048(3)	0.0397(19)
C19	0.2194(8)	0.6696(5)	0.6166(2)	0.0352(17)
C20	0.3067(8)	0.7389(4)	0.6115(2)	0.0295(16)
C21	0.4531(7)	0.7315(4)	0.5949(2)	0.0251(15)
C22	0.5613(7)	0.8016(4)	0.5903(2)	0.0253(14)
C23	0.7973(7)	0.8368(4)	0.5474(2)	0.0249(14)
C24	1.0287(7)	0.6634(4)	0.5058(2)	0.0230(14)
C25	1.1496(7)	0.6999(4)	0.4836(2)	0.0293(16)
C26	1.1556(8)	0.7842(4)	0.4797(3)	0.0321(16)
C27	1.0412(7)	0.8302(4)	0.5000(3)	0.0314(16)
C28	0.9229(7)	0.7909(4)	0.5228(2)	0.0222(14)
C29	0.5624(7)	0.7998(4)	0.4990(2)	0.0213(13)
C30	0.6420(7)	0.7828(4)	0.4507(2)	0.0222(14)

C31	0.5294(7)	0.7858(4)	0.4067(2)	0.0225(14)
C32	0.3229(8)	0.7131(5)	0.3703(2)	0.0347(17)
Br4	0.28354(9)	0.50668(4)	0.06967(2)	0.0364(2)
O1S	0.6632(7)	0.4665(3)	0.05008(16)	0.0488(16)
H1A	0.855722	0.281945	0.247923	0.030
H2A	1.090854	0.276713	0.213635	0.040
H3A	1.157565	0.372082	0.154728	0.042
H4A	0.990328	0.478126	0.134406	0.040
H6A	0.755910	0.555516	0.160778	0.026
H6B	0.648208	0.488098	0.137493	0.026
H7A	0.426952	0.526792	0.161402	0.029
H7B	0.456797	0.604478	0.194964	0.029
H8A	0.284797	0.360337	0.300655	0.040
H9A	0.073937	0.435227	0.321523	0.057
H10A	0.023808	0.560116	0.283056	0.053
H11A	0.189784	0.610173	0.225389	0.046
H13A	0.693531	0.619306	0.236615	0.021
H13B	0.784230	0.542985	0.256331	0.021
H14A	0.592070	0.514933	0.312651	0.023
H14B	0.503291	0.592428	0.293244	0.023
H15A	0.701314	0.677477	0.323985	0.025
H15B	0.637114	0.625062	0.367985	0.025
H16A	1.011701	0.599554	0.391832	0.049
H16B	0.927001	0.681853	0.379731	0.049
H16C	0.856701	0.618356	0.416387	0.049
H17A	0.463426	0.539824	0.577813	0.047
H18A	0.223461	0.546720	0.608651	0.048
H19A	0.121169	0.673552	0.627925	0.042
H20A	0.267748	0.790125	0.619107	0.035
H22A	0.505835	0.852495	0.585945	0.030
H22B	0.624922	0.805937	0.620461	0.030
H23A	0.826956	0.849232	0.581858	0.030
H23B	0.778816	0.888091	0.529939	0.030
H24A	1.023855	0.606614	0.507410	0.028

H25A	1.227157	0.667914	0.471288	0.035
H26A	1.234894	0.809503	0.463637	0.039
H27A	1.043882	0.887016	0.498396	0.038
H29A	0.527588	0.856076	0.498490	0.026
H29B	0.473630	0.764951	0.500141	0.026
H30A	0.689255	0.729209	0.452388	0.027
H30B	0.720681	0.823254	0.446127	0.027
H31A	0.469627	0.835487	0.407914	0.027
H31B	0.582210	0.785080	0.375348	0.027
H32A	0.261306	0.665166	0.373956	0.052
H32B	0.260420	0.761047	0.371545	0.052
H32C	0.371877	0.711057	0.338757	0.052
H1S	0.677334	0.473256	0.019385	0.073
H2S	0.570394	0.476266	0.054975	0.073

Table A6.12 Bond lengths for **6-9**.

Pd1-N2	2.014(5)	Pd2-N6	2.035(5)
Pd1-N1	2.026(5)	Pd2-N4	2.036(5)
Pd1-N3	2.034(5)	Pd2-Br2	2.4237(9)
Pd1-Br1	2.4101(8)	O2-C32	1.421(8)
O1-C15	1.425(7)	O2-C31	1.423(7)
O1-C16	1.425(8)	N4-C17	1.334(9)
N1-C1	1.345(8)	N4-C21	1.362(8)
N1-C5	1.366(8)	N5-C22	1.487(8)
N2-C7	1.493(8)	N5-C23	1.494(8)
N2-C6	1.495(8)	N5-C29	1.501(8)
N2-C13	1.502(7)	N6-C24	1.344(8)
N3-C12	1.357(8)	N6-C28	1.354(8)
N3-C8	1.359(8)	C17-C18	1.380(10)
C1-C2	1.378(9)	C17-H17A	0.9300
C1-H1A	0.9300	C18-C19	1.383(10)
C2-C3	1.367(10)	C18-H18A	0.9300
C2-H2A	0.9300	C19-C20	1.379(10)
C3-C4	1.388(10)	C19-H19A	0.9300

C3-H3A	0.9300	C20-C21	1.386(9)
C4-C5	1.369(9)	C20-H20A	0.9300
C4-H4A	0.9300	C21-C22	1.501(9)
C5-C6	1.502(9)	C22-H22A	0.9700
C6-H6A	0.9700	C22-H22B	0.9700
C6-H6B	0.9700	C23-C28	1.507(8)
C7-C12	1.502(9)	C23-H23A	0.9700
C7-H7A	0.9700	C23-H23B	0.9700
C7-H7B	0.9700	C24-C25	1.374(9)
C8-C9	1.380(11)	C24-H24A	0.9300
C8-H8A	0.9300	C25-C26	1.383(10)
C9-C10	1.388(12)	C25-H25A	0.9300
C9-H9A	0.9300	C26-C27	1.384(10)
C10-C11	1.371(11)	C26-H26A	0.9300
C10-H10A	0.9300	C27-C28	1.384(9)
C11-C12	1.375(9)	C27-H27A	0.9300
C11-H11A	0.9300	C29-C30	1.515(8)
C13-C14	1.511(8)	C29-H29A	0.9700
C13-H13A	0.9700	C29-H29B	0.9700
C13-H13B	0.9700	C30-C31	1.518(9)
C14-C15	1.519(8)	C30-H30A	0.9700
C14-H14A	0.9700	C30-H30B	0.9700
C14-H14B	0.9700	C31-H31A	0.9700
C15-H15A	0.9700	C31-H31B	0.9700
C15-H15B	0.9700	C32-H32A	0.9600
C16-H16A	0.9600	C32-H32B	0.9600
C16-H16B	0.9600	C32-H32C	0.9600
C16-H16C	0.9600	O1S-H1S	0.8400
Pd2-N5	2.034(5)	O1S-H2S	0.8500

Table A6.13 Bond angles for **6-9**.

N2-Pd1-N1	82.57(19)	N5-Pd2-N4	82.3(2)
N2-Pd1-N3	83.5(2)	N6-Pd2-N4	165.8(2)
N1-Pd1-N3	166.0(2)	N5-Pd2-Br2	177.78(15)

N2-Pd1-Br1	178.69(14)	N6-Pd2-Br2	97.12(14)
N1-Pd1-Br1	97.50(14)	N4-Pd2-Br2	97.05(15)
N3-Pd1-Br1	96.37(15)	C32-O2-C31	112.3(5)
C15-O1-C16	110.9(5)	C17-N4-C21	119.3(6)
C1-N1-C5	118.9(5)	C17-N4-Pd2	129.0(5)
C1-N1-Pd1	128.6(4)	C21-N4-Pd2	111.4(4)
C5-N1-Pd1	112.4(4)	C22-N5-C23	112.5(5)
C7-N2-C6	112.1(4)	C22-N5-C29	109.2(5)
C7-N2-C13	112.1(4)	C23-N5-C29	112.2(5)
C6-N2-C13	108.7(4)	C22-N5-Pd2	104.0(4)
C7-N2-Pd1	106.3(4)	C23-N5-Pd2	107.1(4)
C6-N2-Pd1	105.9(3)	C29-N5-Pd2	111.6(4)
C13-N2-Pd1	111.7(3)	C24-N6-C28	119.7(6)
C12-N3-C8	120.9(6)	C24-N6-Pd2	127.9(4)
C12-N3-Pd1	111.8(4)	C28-N6-Pd2	112.2(4)
C8-N3-Pd1	126.9(5)	N4-C17-C18	122.0(7)
N1-C1-C2	121.2(6)	N4-C17-H17A	119.0
N1-C1-H1A	119.4	C18-C17-H17A	119.0
C2-C1-H1A	119.4	C17-C18-C19	119.3(7)
C3-C2-C1	120.0(6)	C17-C18-H18A	120.4
C3-C2-H2A	120.0	C19-C18-H18A	120.4
C1-C2-H2A	120.0	C20-C19-C18	119.1(6)
C2-C3-C4	119.1(6)	C20-C19-H19A	120.5
C2-C3-H3A	120.4	C18-C19-H19A	120.5
C4-C3-H3A	120.4	C19-C20-C21	119.4(6)
C5-C4-C3	119.1(7)	C19-C20-H20A	120.3
C5-C4-H4A	120.5	C21-C20-H20A	120.3
C3-C4-H4A	120.5	N4-C21-C20	120.9(6)
N1-C5-C4	121.5(6)	N4-C21-C22	114.8(5)
N1-C5-C6	114.8(5)	C20-C21-C22	124.3(6)
C4-C5-C6	123.6(6)	N5-C22-C21	108.3(5)
N2-C6-C5	109.8(5)	N5-C22-H22A	110.0
N2-C6-H6A	109.7	C21-C22-H22A	110.0
C5-C6-H6A	109.7	N5-C22-H22B	110.0

N2-C6-H6B	109.7	C21-C22-H22B	110.0
C5-C6-H6B	109.7	H22A-C22-H22B	108.4
H6A-C6-H6B	108.2	N5-C23-C28	110.0(5)
N2-C7-C12	110.1(5)	N5-C23-H23A	109.7
N2-C7-H7A	109.6	C28-C23-H23A	109.7
C12-C7-H7A	109.6	N5-C23-H23B	109.7
N2-C7-H7B	109.6	C28-C23-H23B	109.7
C12-C7-H7B	109.6	H23A-C23-H23B	108.2
H7A-C7-H7B	108.2	N6-C24-C25	121.4(6)
N3-C8-C9	119.2(7)	N6-C24-H24A	119.3
N3-C8-H8A	120.4	C25-C24-H24A	119.3
C9-C8-H8A	120.4	C24-C25-C26	119.8(6)
C8-C9-C10	120.5(7)	C24-C25-H25A	120.1
C8-C9-H9A	119.8	C26-C25-H25A	120.1
C10-C9-H9A	119.8	C25-C26-C27	118.7(6)
C11-C10-C9	119.1(7)	C25-C26-H26A	120.6
C11-C10-H10A	120.4	C27-C26-H26A	120.6
C9-C10-H10A	120.4	C26-C27-C28	119.5(7)
C10-C11-C12	119.7(7)	C26-C27-H27A	120.3
C10-C11-H11A	120.1	C28-C27-H27A	120.3
C12-C11-H11A	120.2	N6-C28-C27	120.9(6)
N3-C12-C11	120.6(6)	N6-C28-C23	116.6(6)
N3-C12-C7	115.8(5)	C27-C28-C23	122.5(6)
C11-C12-C7	123.6(6)	N5-C29-C30	115.4(5)
N2-C13-C14	115.0(5)	N5-C29-H29A	108.4
N2-C13-H13A	108.5	C30-C29-H29A	108.4
C14-C13-H13A	108.5	N5-C29-H29B	108.4
N2-C13-H13B	108.5	C30-C29-H29B	108.4
C14-C13-H13B	108.5	H29A-C29-H29B	107.5
H13A-C13-H13B	107.5	C29-C30-C31	110.0(5)
C13-C14-C15	111.6(5)	C29-C30-H30A	109.7
C13-C14-H14A	109.3	C31-C30-H30A	109.7
C15-C14-H14A	109.3	C29-C30-H30B	109.7
C13-C14-H14B	109.3	C31-C30-H30B	109.7

C15-C14-H14B	109.3	H30A-C30-H30B	108.2
H14A-C14-H14B	108.0	O2-C31-C30	107.6(5)
O1-C15-C14	108.1(5)	O2-C31-H31A	110.2
O1-C15-H15A	110.1	C30-C31-H31A	110.2
C14-C15-H15A	110.1	O2-C31-H31B	110.2
O1-C15-H15B	110.1	C30-C31-H31B	110.2
C14-C15-H15B	110.1	H31A-C31-H31B	108.5
H15A-C15-H15B	108.4	O2-C32-H32A	109.5
O1-C16-H16A	109.5	O2-C32-H32B	109.5
O1-C16-H16B	109.5	H32A-C32-H32B	109.5
H16A-C16-H16B	109.5	O2-C32-H32C	109.5
O1-C16-H16C	109.5	H32A-C32-H32C	109.5
H16A-C16-H16C	109.5	H32B-C32-H32C	109.5
H16B-C16-H16C	109.5	H1S-O1S-H2S	107.4
N5-Pd2-N6	83.6(2)		

Appendix F. Supplementary Information for Chapter 7

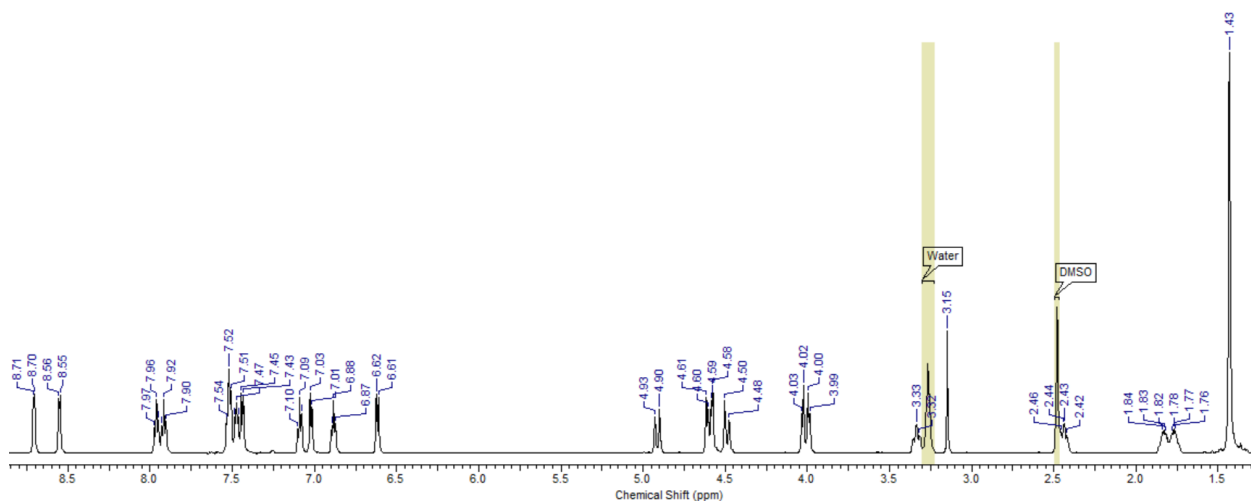


Figure A7.1 ^1H NMR spectrum of $[\text{Pd}^{\text{IV}}(\text{CH}_2\text{CMe}_2\text{C}_6\text{H}_4)(\kappa^3\text{-N,N',N''-5-L1})\text{OH}][\text{PF}_6]$, **7-1**, in $(\text{CD}_3)_2\text{SO}$, at 25°C , 600 MHz.

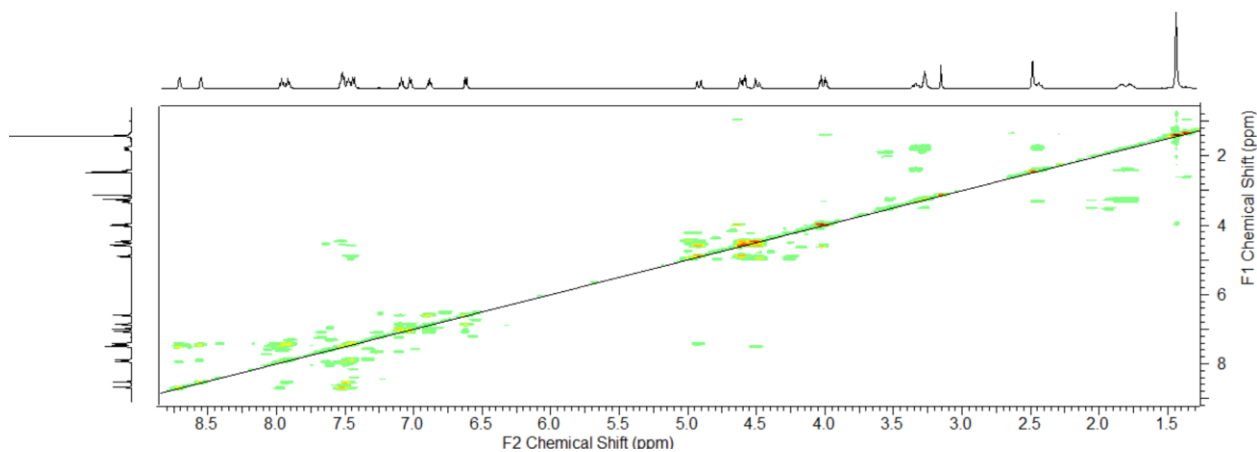


Figure A7.2 ^1H - ^1H COSY spectrum of $[\text{Pd}^{\text{IV}}(\text{CH}_2\text{CMe}_2\text{C}_6\text{H}_4)(\kappa^3\text{-N,N',N''-5-L1})\text{OH}][\text{PF}_6]$, **7-1**, in $(\text{CD}_3)_2\text{SO}$, at 25°C .

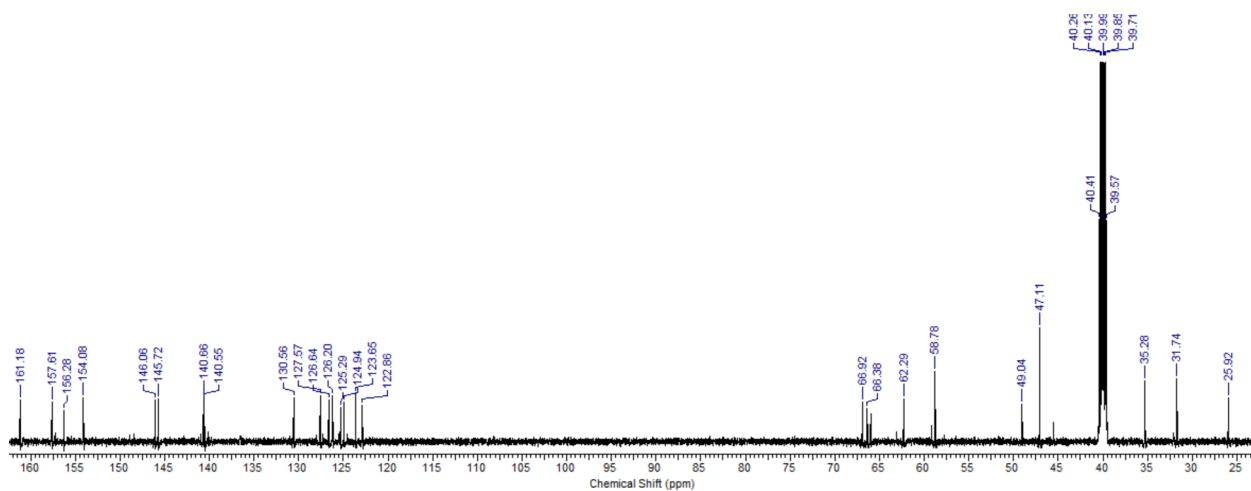


Figure A7.3 $^{13}\text{C}\{^1\text{H}\}$ NMR spectrum of $[\text{Pd}^{\text{IV}}(\text{CH}_2\text{CMe}_2\text{C}_6\text{H}_4)(\kappa^3\text{-}N,N',N''\text{-}5\text{-L1})\text{OH}][\text{PF}_6]$, **7-1**, in $(\text{CD}_3)_2\text{SO}$, at 25°C , 151 MHz.

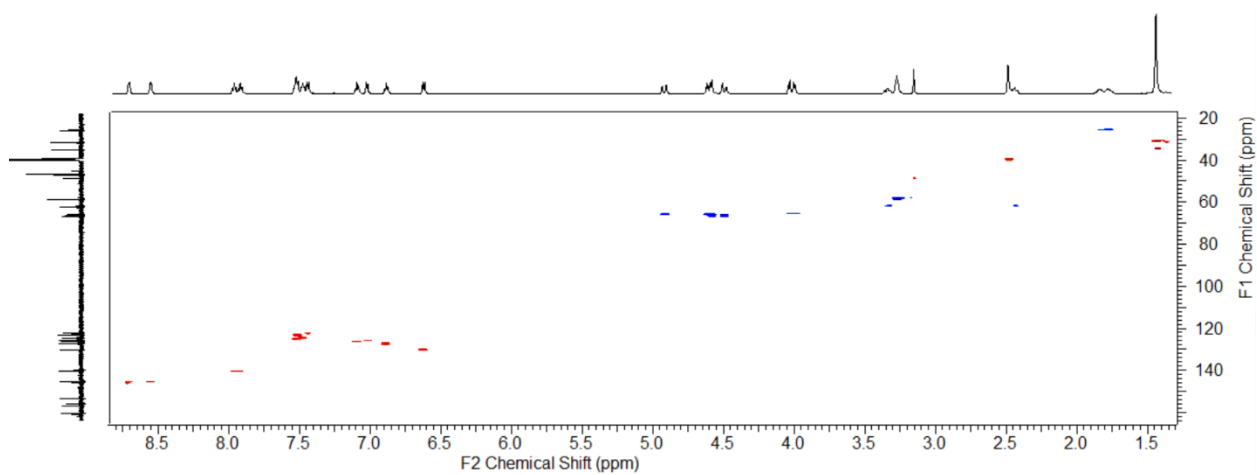


Figure A7.4 $^1\text{H}\text{-}^{13}\text{C}\{^1\text{H}\}$ HSQC spectrum of $[\text{Pd}^{\text{IV}}(\text{CH}_2\text{CMe}_2\text{C}_6\text{H}_4)(\kappa^3\text{-}N,N',N''\text{-}5\text{-L1})\text{OH}][\text{PF}_6]$, **7-1**, in $(\text{CD}_3)_2\text{SO}$, at 25°C .

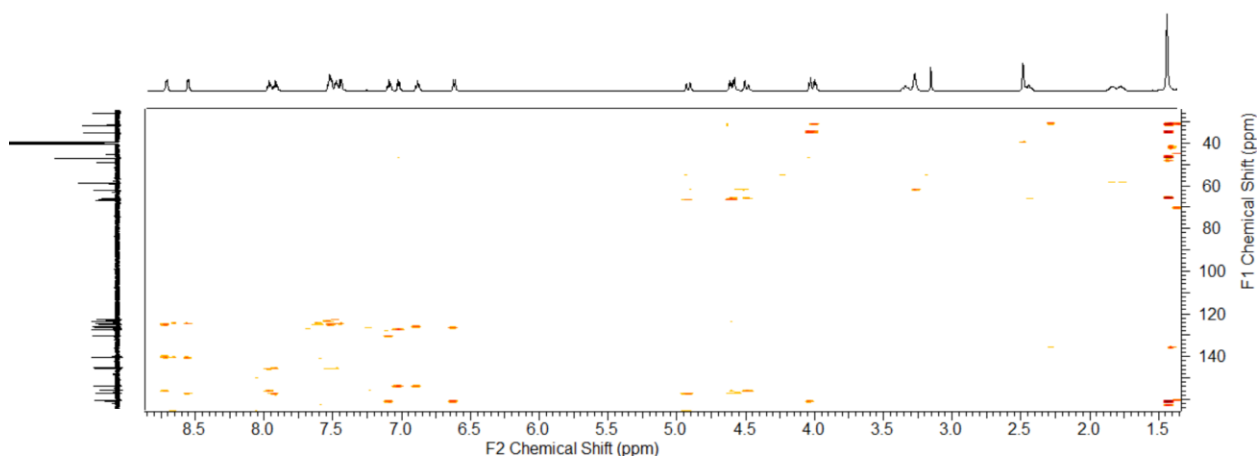


Figure A7.5 $^1\text{H}\text{-}^{13}\text{C}\{^1\text{H}\}$ HMBC spectrum of $[\text{Pd}^{\text{IV}}(\text{CH}_2\text{CMe}_2\text{C}_6\text{H}_4)(\kappa^3\text{-}N,N',N''\text{-}5\text{-L1})\text{OH}][\text{PF}_6]$, **7-1**, in $(\text{CD}_3)_2\text{SO}$, at 25°C .

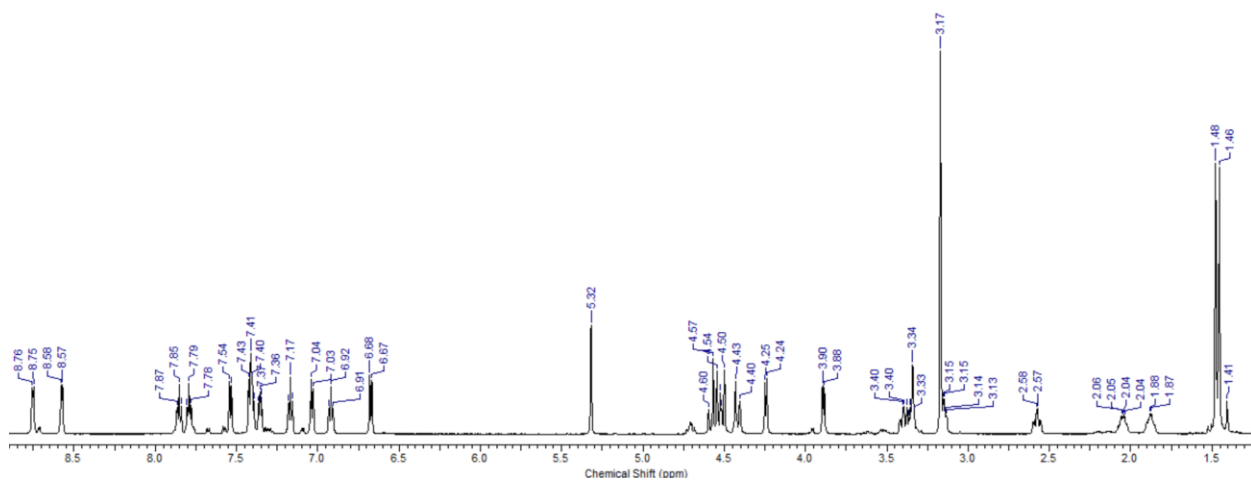


Figure A7.6 ^1H NMR spectrum of $[\text{Pd}^{\text{IV}}(\text{CH}_2\text{CMe}_2\text{C}_6\text{H}_4)(\kappa^3\text{-}N,N',N''\text{-}6\text{-L1})\text{OH}][\text{PF}_6]$, **7-2**, in CD_2Cl_2 , at -10°C , 600 MHz.

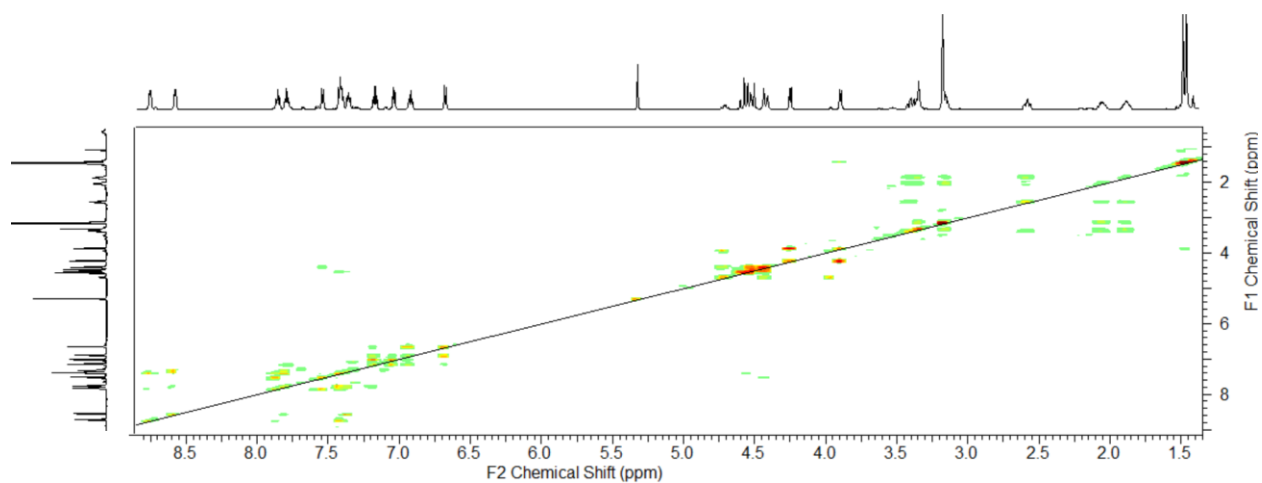


Figure A7.7 ^1H - ^1H COSY spectrum of $[\text{Pd}^{\text{IV}}(\text{CH}_2\text{CMe}_2\text{C}_6\text{H}_4)(\kappa^3\text{-}N,N',N''\text{-}6\text{-L1})\text{OH}][\text{PF}_6]$, **7-2**, in CD_2Cl_2 , at -10°C .

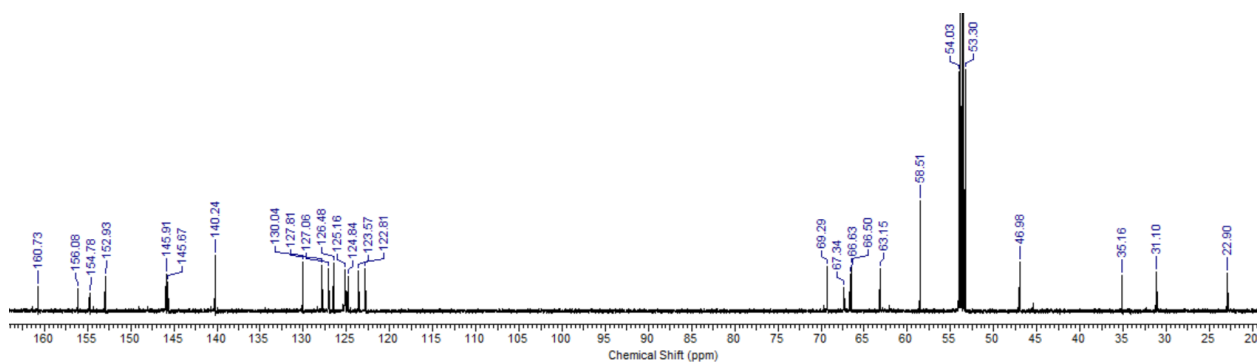


Figure A7.8 $^{13}\text{C}\{^1\text{H}\}$ spectrum of $[\text{Pd}^{\text{IV}}(\text{CH}_2\text{CMe}_2\text{C}_6\text{H}_4)(\kappa^3\text{-}N,N',N''\text{-}6\text{-L1})\text{OH}][\text{PF}_6]$, **7-2**, in CD_2Cl_2 , at -10°C , 151 MHz.

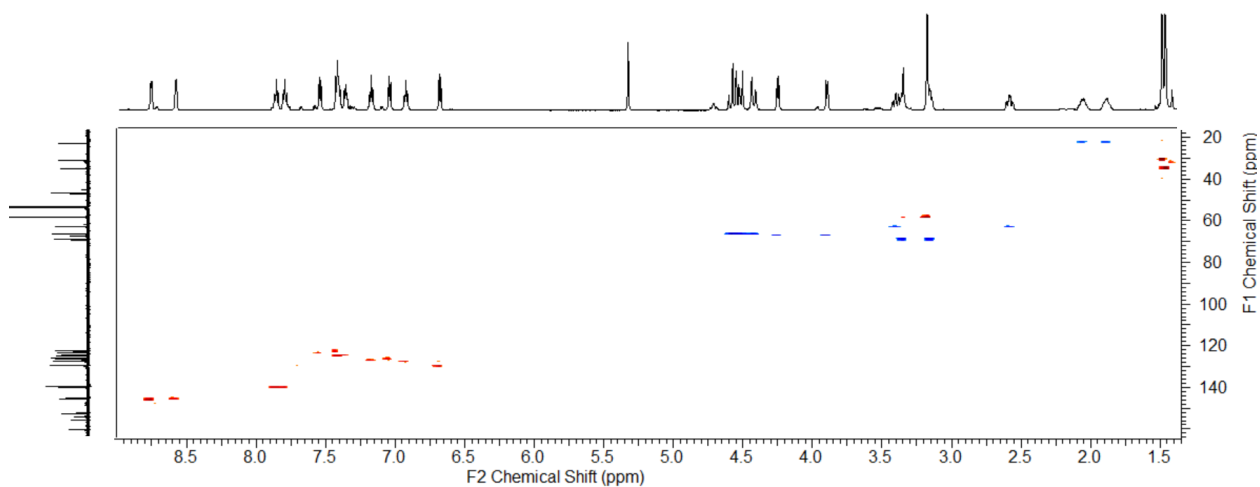


Figure A7.9 $^1\text{H}-^{13}\text{C}\{^1\text{H}\}$ HSQC spectrum of $[\text{Pd}^{\text{IV}}(\text{CH}_2\text{CMe}_2\text{C}_6\text{H}_4)(\kappa^3\text{-N,N',N''-6-L1})\text{OH}][\text{PF}_6]$, **7-2**, in CD_2Cl_2 , at -10°C .

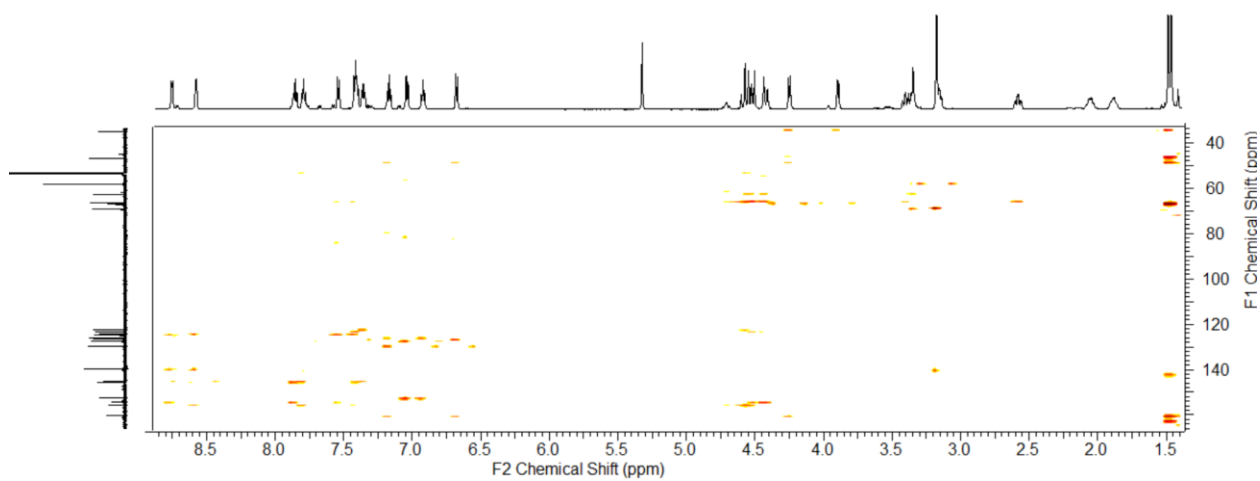


Figure A7.10 $^1\text{H}-^{13}\text{C}\{^1\text{H}\}$ HMBC spectrum of $[\text{Pd}^{\text{IV}}(\text{CH}_2\text{CMe}_2\text{C}_6\text{H}_4)(\kappa^3\text{-N,N',N''-6-L1})\text{OH}][\text{PF}_6]$, **7-2**, in CD_2Cl_2 , at -10°C .

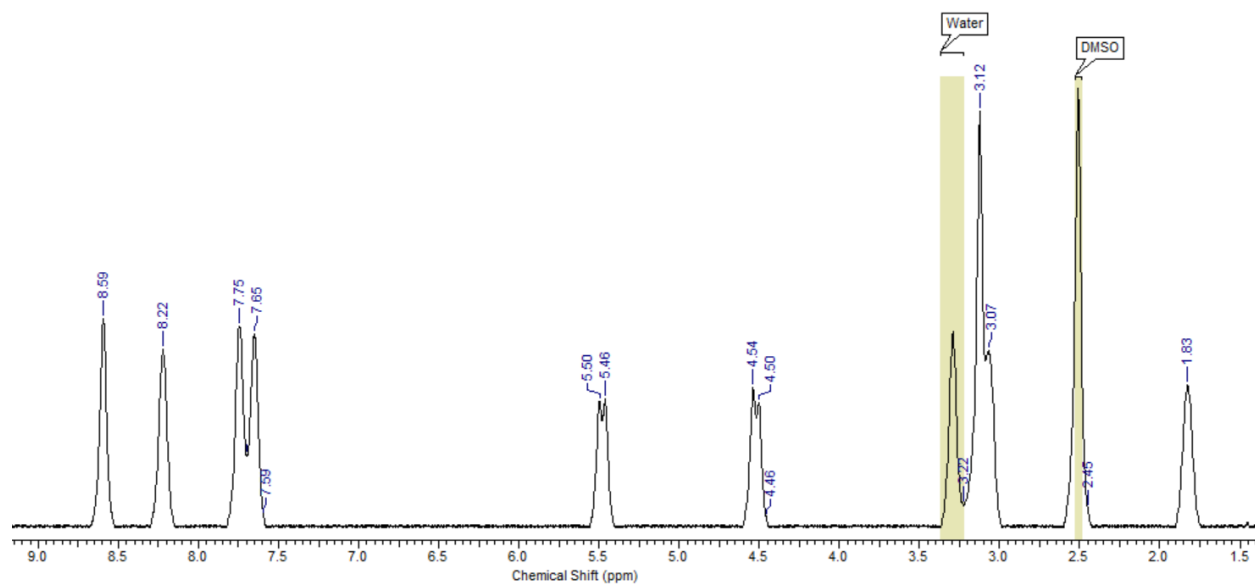


Figure A7.11 ^1H NMR spectrum of $[\text{Pd}^{\text{II}}(\kappa^3\text{-}N,N',N''\text{-6-L1})][\text{PF}_6]$, **7-3**, in $(\text{CD}_3)_2\text{SO}$, at 25°C , 600 MHz.

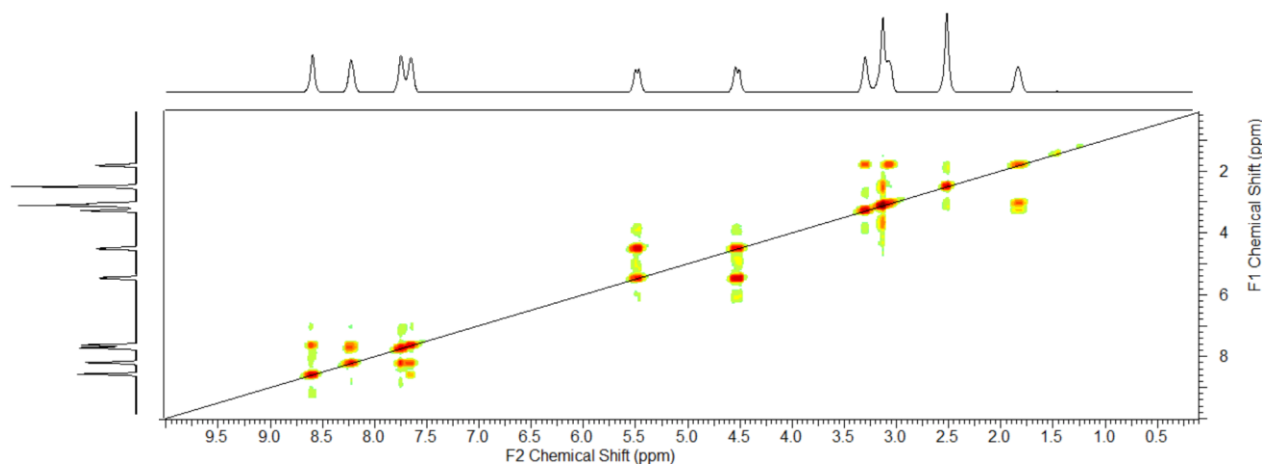


Figure A7.12 ^1H - ^1H COSY spectrum of $[\text{Pd}^{\text{II}}(\kappa^3\text{-}N,N',N''\text{-6-L1})][\text{PF}_6]$, **7-3**, in $(\text{CD}_3)_2\text{SO}$, at 25°C .

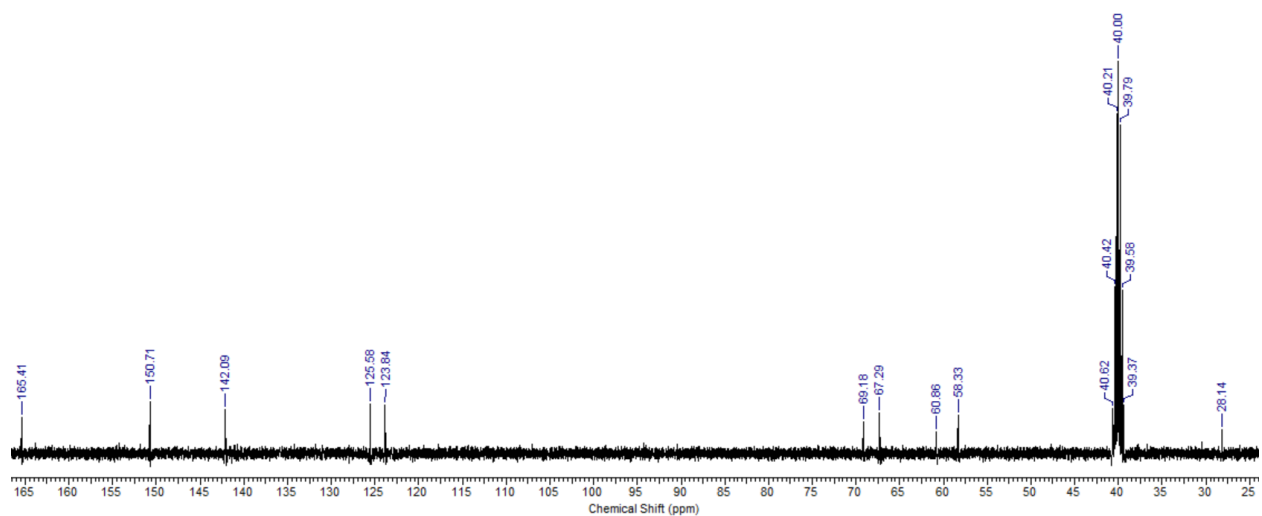


Figure A7.13 $^{13}\text{C}\{^1\text{H}\}$ NMR spectrum of $[\text{Pd}^{\text{II}}(\kappa^3\text{-}N,N',N''\text{-}6\text{-L1})][\text{PF}_6]$, **7-3**, in $(\text{CD}_3)_2\text{SO}$, at 25°C , 151 MHz.

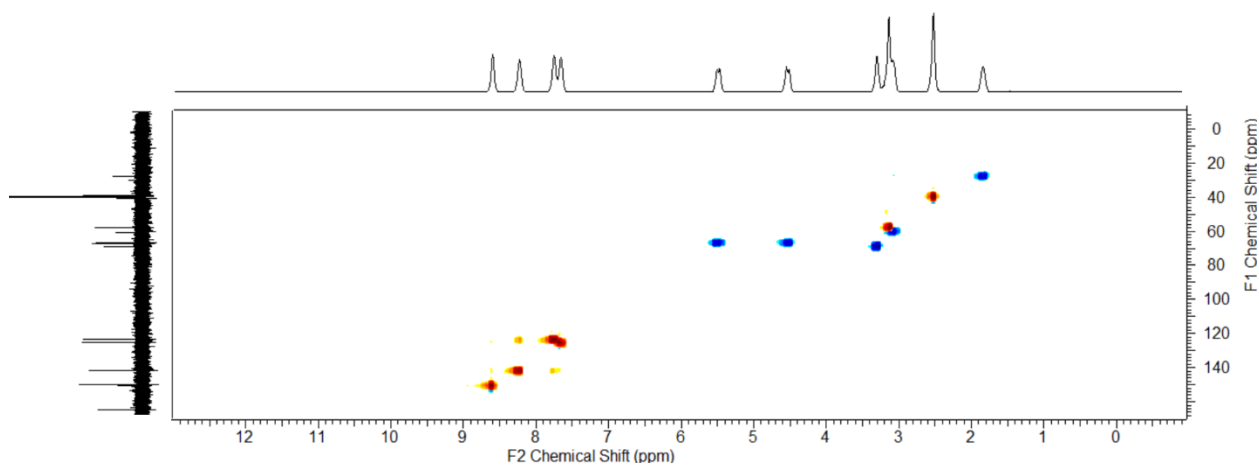


Figure A7.14 $^1\text{H}\text{-}^{13}\text{C}\{^1\text{H}\}$ HSQC spectrum of $[\text{Pd}^{\text{II}}(\kappa^3\text{-}N,N',N''\text{-}6\text{-L1})][\text{PF}_6]$, **7-3**, in $(\text{CD}_3)_2\text{SO}$, at 25°C .

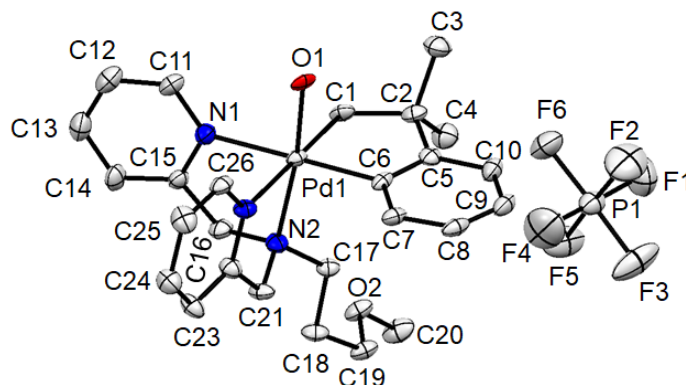
Table A7.1 Crystallographic data and parameters for compounds **7-2**.

7-2	
Formula	$\text{C}_{26}\text{H}_{34}\text{N}_3\text{O}_2\text{PPd}$
Formula weight	557.95
Crystal system	Orthorhombic

Space group	P 2 ₁ 2 ₁ 2 ₁
<i>a</i> [Å]	10.060(4)
<i>b</i> [Å]	13.2520(6)
<i>c</i> [Å]	20.6558(9)
α [°]	90
β [°]	90
γ [°]	90
<i>V</i> [Å ³]	2753.9 (16)
<i>Z</i>	4
ρ_{cal} [g cm ⁻³]	1.621
μ (MoK α)	0.71073
<i>F</i> (000)	1368
<i>T</i> [K]	110
$\theta_{\text{min}}, \theta_{\text{max}}$ [°]	2.50, 31.67
Total reflns	70130
Unique reflns	9305
<i>R</i> ₁	0.0800
w <i>R</i> ₂ [<i>I</i> ≥ 2σ(<i>I</i>)]	0.1959
<i>R</i> ₁ (all data)	0.0979
w <i>R</i> ₂ (all data)	0.2080

GOF	1.024
Maximum shift/error	0.0001
Min & Max peak heights on final ΔF Map ($e^-/\text{\AA}$)	-2.056, 3.465

Where: $R_1 = \sum(|F_o| - |F_c|) / \sum F_o$; $wR_2 = [\sum(w(F_o^2 - F_c^2)^2) / \sum(wF_o^4)]^{1/2}$; $GOF = [\sum(w(F_o^2 - F_c^2)^2) / (\text{No. of reflns.} - \text{No. of params.})]^{1/2}$



Scheme A7.15 Displacement ellipsoid plot of **7-2** co-crystallized with a PF_6 molecule showing naming and numbering scheme. Ellipsoids are drawn at the 50% probability level and hydrogen atoms are omitted for clarity.

Table A8.2 Atomic coordinates for **7-2**.

Atom	x	y	z	$U_{\text{iso/equiv}}$
Pd1	0.70164(6)	0.07491(5)	0.55059(3)	0.01741(17)
O1	0.8922(5)	0.1148(4)	0.5535(4)	0.0205(11)
O2	0.2057(6)	-0.0696(5)	0.6658(3)	0.0274(12)
N1	0.7429(8)	-0.0627(6)	0.5006(4)	0.0231(14)
N2	0.5000(7)	0.0296(7)	0.5320(4)	0.0230(14)
N3	0.6784(6)	0.1348(5)	0.4527(4)	0.0208(13)
C1	0.7172(9)	0.0135(7)	0.6408(4)	0.0214(16)
C2	0.7038(9)	0.0913(7)	0.6962(4)	0.0248(16)
C3	0.8399(10)	0.1037(9)	0.7304(5)	0.033(2)
C4	0.6017(11)	0.0565(8)	0.7458(5)	0.032(2)

C5	0.6638(8)	0.1916(7)	0.6662(5)	0.0220(15)
C6	0.6591(8)	0.1995(6)	0.5992(4)	0.0183(14)
C7	0.6333(8)	0.2908(7)	0.5691(5)	0.0222(16)
C8	0.6127(9)	0.3759(7)	0.6067(5)	0.0259(17)
C9	0.6138(9)	0.3711(8)	0.6726(5)	0.0275(18)
C10	0.6385(9)	0.2783(8)	0.7034(5)	0.0262(18)
C11	0.8641(9)	-0.0904(7)	0.4783(5)	0.0255(18)
C12	0.8783(11)	-0.1691(8)	0.4355(5)	0.033(2)
C13	0.7666(11)	-0.2180(9)	0.4138(5)	0.034(2)
C14	0.6417(11)	-0.1884(7)	0.4363(5)	0.0285(19)
C15	0.6339(9)	-0.1103(7)	0.4805(4)	0.0208(16)
C16	0.5060(8)	-0.0798(9)	0.5119(5)	0.0253(16)
C17	0.4053(8)	0.0399(7)	0.5873(4)	0.0197(15)
C18	0.2600(9)	0.0196(8)	0.5698(5)	0.0251(18)
C19	0.1724(8)	0.0166(7)	0.6289(5)	0.0247(18)
C20	0.1144(10)	-0.0832(10)	0.7177(5)	0.035(2)
C21	0.4507(8)	0.0934(8)	0.4782(4)	0.0242(18)
C22	0.5537(9)	0.1253(8)	0.4296(4)	0.0226(16)
C23	0.5216(10)	0.1496(8)	0.3660(5)	0.0274(19)
C24	0.6218(10)	0.1844(8)	0.3259(5)	0.029(2)
C25	0.7520(10)	0.1938(8)	0.3499(5)	0.030(2)
C26	0.7755(8)	0.1675(7)	0.4131(5)	0.0227(16)
P1	0.7557(3)	0.6831(2)	0.64712(15)	0.0319(6)
F1	0.7532(11)	0.6578(9)	0.7233(4)	0.073(3)
F2	0.8700(9)	0.7630(8)	0.6612(6)	0.077(3)
F3	0.6445(8)	0.7682(6)	0.6551(6)	0.075(3)
F4	0.7609(12)	0.7080(9)	0.5738(4)	0.084(3)
F5	0.6399(8)	0.6027(6)	0.6399(5)	0.062(2)
F6	0.8654(7)	0.5967(6)	0.6373(4)	0.0481(18)
H3A	0.864415	0.040070	0.751485	0.0490
H4A	0.626205	0.010511	0.761949	0.0480
H7A	0.629902	0.295039	0.523199	0.0270
H8A	0.597375	0.438953	0.586098	0.0310
H10A	0.638045	0.274264	0.749274	0.0310

H11A	0.940748	-0.054758	0.492439	0.0310
H12A	0.964036	-0.189295	0.421173	0.0390
H13A	0.774274	-0.271801	0.383619	0.040
H14A	0.563511	-0.221253	0.421418	0.0340
H16A	0.491850	-0.122423	0.550701	0.030
H17A	0.412471	0.109213	0.604947	0.0240
H18A	0.228095	0.073033	0.540194	0.030
H19A	0.185732	0.078387	0.655048	0.030
H20A	0.128826	-0.149384	0.737562	0.053
H21A	0.409824	0.154761	0.496909	0.029
H23A	0.433230	0.142480	0.350428	0.033
H24A	0.602633	0.202001	0.282312	0.035
H25A	0.821851	0.217716	0.323013	0.036
H26A	0.863521	0.172544	0.429500	0.027
H1B	0.647336	-0.038487	0.646028	0.0260
H3B	0.833725	0.157188	0.763030	0.0490
H4B	0.513828	0.053275	0.725451	0.0480
H16B	0.432183	-0.093447	0.481467	0.030
H17B	0.432231	-0.007439	0.621987	0.0240
H18B	0.253691	-0.045769	0.546774	0.030
H19B	0.077848	0.013455	0.615750	0.030
H20B	0.023308	-0.079220	0.701025	0.053
H21B	0.379854	0.055958	0.455182	0.029
H1C	0.804431	-0.020542	0.644632	0.0260
H3C	0.907777	0.121598	0.698375	0.049
H4C	0.599301	0.104340	0.781986	0.0480
H20C	0.128117	-0.030215	0.750098	0.053

Table A8.3 Bond angles for **7-2**.

C6-Pd1-O1	88.3(3)	C1-Pd1-N1	94.9(3)
C6-Pd1-C1	83.4(4)	C6-Pd1-N2	96.9(3)
O1-Pd1-C1	90.2(3)	O1-Pd1-N2	171.4(3)
C6-Pd1-N1	177.8(3)	C1-Pd1-N2	97.1(3)
O1-Pd1-N1	93.1(3)	N1-Pd1-N2	81.9(3)

C6-Pd1-N3	98.2(3)	C21-N2-C16	110.8(7)
O1-Pd1-N3	92.0(3)	C17-N2-C16	108.9(7)
C1-Pd1-N3	177.3(3)	C21-N2-Pd1	106.9(5)
N1-Pd1-N3	83.4(3)	C17-N2-Pd1	116.1(5)
N2-Pd1-N3	80.5(3)	C16-N2-Pd1	106.2(5)
Pd1-O1-H1A	109.5	C26-N3-C22	119.4(8)
C19-O2-C20	110.8(7)	C26-N3-Pd1	127.0(6)
C15-N1-C11	120.5(8)	C22-N3-Pd1	113.1(6)
C15-N1-Pd1	113.3(6)	C2-C1-Pd1	113.8(6)
C11-N1-Pd1	124.8(7)	Pd1-C1-H1B	108.8
C21-N2-C17	107.9(7)	C2-C1-H1C	108.8
Pd1-C1-H1C	108.8	H1B-C1-H1C	107.7
C5-C2-C4	111.1(8)	C5-C2-C1	107.7(7)
C4-C2-C1	110.8(8)	C5-C2-C3	109.1(8)
C4-C2-C3	108.8(8)	C1-C2-C3	109.3(8)
C2-C3-H3A	109.5	C2-C3-H3B	109.5
H3A-C3-H3B	109.5	C2-C3-H3C	109.5
H3A-C3-H3C	109.5	H3B-C3-H3C	109.5
C2-C4-H4A	109.5	C2-C4-H4B	109.5
H4A-C4-H4B	109.5	C2-C4-H4C	109.5
H4A-C4-H4C	109.5	H4B-C4-H4C	109.5
C6-C5-C10	118.5(9)	C6-C5-C2	118.8(8)
C10-C5-C2	122.7(8)	C7-C6-C5	121.3(8)
C7-C6-Pd1	122.8(7)	C5-C6-Pd1	115.8(6)
C8-C7-C6	119.2(9)	C8-C-H7A	120.4
C6-C7-H7A	120.4	C9-C8-C7	121.4(9)
C9-C8-H8A	119.3	C7-C8-H8A	119.3
C8-C9-C10	119.6(9)	C8-C9-H9A	120.2
C10-C9-H9A	120.2	C5-C10-C9	120.1(9)
C5-C10-H10A	120.0	C9-C10-H10A	120.0
N1-C11-C12	121.2(9)	N1-C11-H11A	119.4
C12-C11-H11A	119.4	C13-C12-C11	118.9(10)
C13-C12-H12A	120.6	C11-C12-H12A	120.6
C12-C13-C14	119.7(9)	C12-C13-H13A	120.1

C14-C13-H13A	120.1	C15-C14-C13	118.8(10)
C15-C14-H14A	120.6	C13-C14-H14A	120.6
N1-C15-C14	120.9(8)	N1-C15-C16	116.5(8)
C14-C15-C16	122.5(9)	C15-C16-N2	114.4(8)
C15-C16-H16A	108.7	N2-C16-H16A	108.7
C15-C16-H16B	108.7	N2-C16-H16B	108.7
H16A-C16-H16B	107.6	N2-C17-C18	114.3(7)
N2-C17-H17A	108.7	N2-C17-H17B	108.7
C18-C17-H17A	108.7	C18-C17-H17B	108.7
C19-C18-C17	111.9(8)	H17A-C17-H17B	107.6
C19-C18-H18A	109.2	C17-C18-H18A	109.2
C19-C18-H18B	109.2	C17-C18-H18B	109.2
H18A-C18-H18B	107.9	O2-C19-C18	108.6(7)
O2-C19-H19A	110.0	C18-C19-H19A	110.0
O2-C19-H19B	110.0	C18-C19-H19B	110.0
H19A-C19-H19B	108.4	H20-C20-H20A	109.5
O2-C20-H20B	109.5	H20A-C20-H20B	109.5
O2-C20-H20C	109.5	H20A-C20-H20C	109.5
H20B-C20-H20C	109.5	N2 -C21-C22	115.5(7)
N2-C21-H21A	108.4	C22-C21-H21A	108.4
N2-C21-H21B	108.4	C22-C21-H21B	108.4
H21A-C21-H21B	107.5	N3-C22-C23	121.9(8)
N3-C22-C21	115.5(8)	C23-C22-C21	122.4(8)
C24-C23-C22	118.3(9)	C24-C23-H23A	120.9
C22-C23-H23A	120.9	C23-C24-C25	119.9(9)
C23-C24-H24A	120.1	C25-C24-H24A	120.1
C26-C25-C24	118.3(9)	C26-C25-H25A	120.9
C24-C25-H25A	120.9	N3-C26-C25	122.3(8)
N3-C26-H26A	118.8	C25-C26-H26A	118.8
F4-P1-F5	94.4(7)	F4-P1-F2	90.7(7)
F5-P1-F2	74.8(6)	F4-P1-F3	88.5(6)
F5-P1-F3	88.3(4)	F2-P1-F3	91.0(5)
F4-P1-F6	90.3(5)	F2-P1-F6	90.1(5)
F5-P1-F6	90.8(4)	F4-P1-F1	78.9(7)

F3-P1-F6	178.5(6)
F5-P1-F1	86.6(6)
F3-P1-F1	92.0(6)

F2-P1-F1	88.3(6)
F6-P1-F1	89.2(5)

Appendix G. Copyright Material and Permissions

Chapter 2 and Chapter 5- American Chemical Society's Policy on Theses and Dissertations

Title: Selective Oxygen Atom Insertion into an Aryl-Palladium Bond

Author: Ava Behnia, Paul D. Boyle, Johanna M. Blacquiere, Richard J. Puddephatt

Publication: Organometallics

Publisher: American Chemical Society

Date: Aug 1, 2016

Copyright © 2016, American Chemical Society

PERMISSION/LICENSE IS GRANTED FOR YOUR ORDER AT NO CHARGE

This type of permission/license, instead of the standard Terms & Conditions, is sent to you because no fee is being charged for your order. Please note the following:

- Permission is granted for your request in both print and electronic formats, and translations.
- If figures and/or tables were requested, they may be adapted or used in part.
- Please print this page for your records and send a copy of it to your publisher/graduate school.
- Appropriate credit for the requested material should be given as follows: "Reprinted (adapted) with permission from (COMPLETE REFERENCE CITATION). Copyright (YEAR) American Chemical Society." Insert appropriate information in place of the capitalized words.
- One-time permission is granted only for the use specified in your request. No additional uses are granted (such as derivative works or other editions). For any other uses, please submit a new request.

Title: Reactivity of a Palladacyclic Complex: A Monodentate Carbonate Complex and the Remarkable Selectivity and Mechanism of a Neophyl Rearrangement

Author: Ava Behnia, Mahmood A. Fard, Johanna M. Blacquiere, Richard J. Puddephatt

Publication: Organometallics

Publisher: American Chemical Society

Date: Dec 1, 2017

Copyright © 2017, American Chemical Society

PERMISSION/LICENSE IS GRANTED FOR YOUR ORDER AT NO CHARGE

This type of permission/license, instead of the standard Terms & Conditions, is sent to you because no fee is being charged for your order. Please note the following:

- Permission is granted for your request in both print and electronic formats, and translations.
- If figures and/or tables were requested, they may be adapted or used in part.

- Please print this page for your records and send a copy of it to your publisher/graduate school.
- Appropriate credit for the requested material should be given as follows: "Reprinted (adapted) with permission from (COMPLETE REFERENCE CITATION). Copyright (YEAR) American Chemical Society." Insert appropriate information in place of the capitalized words.
- One-time permission is granted only for the use specified in your request. No additional uses are granted (such as derivative works or other editions). For any other uses, please submit a new request.

Chapter 3 and Chapter 4- Royal Society of Chemistry Reproduction Permission

A. Behnia, M. A. Fard, J. M. Blacquiere and R. J. Puddephatt, *Dalton Trans.*, 2018, **47**, 3538-3548 -
Reproduced by permission of The Royal Society of Chemistry.

A. Behnia, P. D. Boyle, M. A. Fard, J. M. Blacquiere and R. J. Puddephatt, *Dalton Trans.*, 2016, **45**,
19485-19490 - Reproduced by permission of The Royal Society of Chemistry.

Appendix H. Curriculum Vitae

Name: Ava Behnia

Post-secondary Education and Degrees: The University of Western Ontario
London, Ontario, Canada
2014-2018 Ph.D.

University of Tehran
Tehran, Iran
2012-2014 M.Sc.

K. N. Toosi University and Technology
Tehran, Iran
2007-2012 B.Sc.

Related Work Experience

Teaching Assistant
The University of Western Ontario
2014-2018

Crystallography Lab Technician
The University of Western Ontario
2016-2018

Publications:

- 7.** Behnia, A.; Fard, M. A.; *Blacquiere, J. M.; *Puddephatt, R. J. Mild and selective Pd–Ar Protonolysis and C–H Activation Promoted by a Ligand Aryloxy Group. *Dalton Trans* **2018**, 47, 3538-3548.
- 6.** Behnia, A.; Fard, M. A.; *Blacquiere, J. M.; *Puddephatt, R. J. Reactivity of a Palladacyclic Complex: A Monodentate Carbonate Complex and the Remarkable Selectivity and Mechanism of a Neophyl Rearrangement. *Organometallics* **2017**, 36, 4759–4769.
- 5.** Fard, M. A.; Behnia, A.; *Puddephatt, R. J. Activation of Dioxygen by Dimethylplatinum(II) Complexes. *Organometallics*, **2017**, 36, 4169-4178.
- 4.** Fard, M. A.; Behnia, A.; *Puddephatt, R. J. Coordination Chemistry of Mercury(II) with 2-Pyridylnitrones: Monomers to Polymers. *Dalton Trans*, **2017**, 46, 3579-3587.
- 3.** Behnia, A.; Boyle, P. D.; Fard, M. A.; *Blacquiere, J. M.; *Puddephatt, R. J. Pincer-Plus-One Ligands in Self-Assembly with Palladium(II): A Molecular Square and a Molecular Tetrahedron. *Dalton Trans.*, **2016**, 45, 19485-19490.
- 2.** Behnia, A.; Boyle, P. D.; *Blacquiere, J. M.; *Puddephatt, R. J. Selective Oxygen Atom Insertion into an Aryl–Palladium Bond. *Organometallics* **2016**, 35, 2645–2654.

1. Behnia, A.; Tammadoni, B.; *Nemati, A. Tail-to-tail Dimerization of Methyl Acrylate in the Presence of Triphenylarsine Ruthenium Complexes. *J. Coord. Chem.*, **2014**, *67*, 3018-3025.

Conferences:

- 3- Oral Presentation.** Behnia, A.; Blacquiere, J. M.; Puddephatt, R. J. 'Palladacyclic Complexes Containing *N*-donor Ligands: From Oxidation Chemistry to C-H Activation, 101th CSC Conference
- Edmonton, AB
May 2018
- 3- Poster Presentation.** Behnia, A.; Blacquiere, J. M.; Puddephatt, R. J. Palladacyclic Complexes Containing *N*-donor Ligands: From Oxidation Chemistry to C-H Activation. Fallona family research day, Western University
- London, ON
April 2018
- 2-Poster Presentation.** Behnia, A.; Blacquiere, J. M.; Puddephatt, R. J. Atmospheric Carbon Dioxide Transformation into Carbonate at a Pd(II) Center. 100th CSC Conference
- Toronto, ON,
May 2017
- 2-Oral Presentation.** Behnia, A.; Blacquiere, J. M.; Puddephatt, R. J. 'Selective Oxygen Atom Insertion into an Aryl-Palladium Bond', 99th CSC Conference
- Halifax, NS,
June 2016
- 1-Oral Presentation.** Behnia, A.; Blacquiere, J. M.; Puddephatt, R. J. 'Selective C(sp²)-O Bond Formation from Palladium Complexes by Using a Green Oxidant, 48th IDW
- Kingston, ON,
May 2015
- 1-Poster Presentation.** Behnia, A.; Blacquiere, J. M.; Puddephatt, R. J. Ligand and Oxidant Effects on C-O Reductive Elimination at Palladium (IV), 98th CSC Conference
- Ottawa, ON,
June 2015